Hydromechanical Characteristics of a Single Rock Joint

by

Masahiro Iwano

B.E. in Civil Engineering, University of Tokyo
(1981)
M.S. in Civil Engineering, Massachusetts Institute of Technology
(1990)

Submitted to the Department of
Civil and Environmental Engineering in Partial Fulfillment of
the Requirements for the Degree of

DOCTOR OF PHILOSOPHY

in Geotechnical Engineering

at the

Massachusetts Institute of Technology

June 1995

Signature of Auther .....
Department of Civil and Environmental Engineering
April 5, 1995

Certified by.....
Herbert H. Einstein
Chairman, Thesis Committee
Department of Civil and Environmental Engineering

Accepted by.....
Joseph M. Sussman
Departmental Committee on Graduate Studies

Hydromechanical Characteristics of a Single Rock Joint

by

Masahiro Iwano

Submitted to the Department of Civil and Environmental Engineering
on April 5, 1995, in partial fulfillment of the requirements
for the Degree of Doctor of Philosophy
in Geotechnical Engineering

ABSTRACT

It is necessary to understand the stress-deformation-flow behavior of a single rock joint to understand the behavior of complex joint system in rock masses and to build predictive models. The objective of this research is to observe the surface roughness and aperture of a single joint in combination with the hydromechanical behavior of it and to draw general conclusions.

Sets of precise measurements of the surface roughness on natural and man-made joints in four rocks have been carried out by using a specially built non-contact optical system employing a laser beam profilometer. Surface roughness and fracture aperture are statistically analyzed, especially with respect to the spatial variation and correlation. The spatial distribution of aperture in a joint is observed to be almost homogeneous, isotropic and uncorrelated.

The stress effect on the joint hydraulic conductivity was observed by using the transient pulse method at pressures up to 40 MPa during both external confining pressurization and internal pore pressure cycling. It was observed that the hydraulic conductivity of jointed rock decreased more rapidly with pressure than that of intact rock and joint hydraulic conductivity was more sensitive to confining pressure than pore pressure. It was also observed that the stress dependency of joint hydraulic conductivity was getting smaller with cyclic loading. Effective pressure is not equal to the conventional effective pressure at least for the hydraulic conductivity of jointed rock.

The stress-flow experiments for six different joints have been carried out to obtain both simultaneously the deformability and hydraulic conductivity of joints at the confining pressures up to 20 MPa. It was observed that first cycle exhibited the largest flow rate hysteresis and the irrecoverable joint deformation. The hysteresis in both joint hydraulic conductivity and deformation decreased with successive test cycles and they were related to the amount of permanent joint deformation. Given the isotropic cyclic loading, the surface roughness of joints did not change significantly. Nevertheless the average aperture of joint decreased and aperture variation also decreased slightly. Aperture correlation was not sensitive to cyclic stress changes.

Thesis Supervisor: Dr. Herbert H. Einstein
Title: Professor of Civil and Environmental Engineering
Thesis Supervisor: Dr. Daniele Veneziano
Title: Professor of Civil and Environmental Engineering
Thesis Supervisor: Dr. Lynn W. Gelhar
Title: Professor of Civil and Environmental Engineering

Acknowledgments

I wish to express sincerest gratitude to :

Professor Herbert H. Einstein for providing constant guidance, technical comments and moral support throughout this research.

Professor Daniele Veneziano and Professor Lynn W. Gelhar for giving me their constant encouragement and valuable suggestions during the course of this study.

My friends in geotechnical engineering group in MIT for creating a friendly and pleasant work environment. Especially Mrs. Carloyn Comer for helping to communicate between Cambridge and Yokohama by using e-mail during my non-resident Ph.D. course work in Japan. Dante Lagaspi for reviewing this document. Dr. Hans Herda for giving valuable suggestions and discussions.

Dr. T. Maekawa for his witty suggestions and recommendations throughout my graduate studies at MIT. Mr. K. Tanaka for his help during my stay in Cambridge.

Extensive laboratory experiments were carried out in Soil & Rock Laboratory at Taisei Technology Research Center, Yokohama. I am deeply grateful to Taisei Corporation for providing the funds to support my four years study. I would like to especially thank to Mr. T. Ito and Mr. K. Kamemura in design department and Dr. T. Naitou and Dr. S. Iihoshi in the technology research center for encouraging me to study and giving me this chance. I wish to give my deepest gratitude to my hearty colleges in Rock Mechanics and Engineering Group in Taisei technology research center, Yokohama, Mr. M. Shimo, Dr. M. Sato, Dr. T. Ogawa, Mr. T. Aoki, Mr. Y. Ijiri and Mr. Y. Ohsato for their help, skill, patience and sympathy. Among them, I was able to encourage myself to continue and finish this work. I owe a great deal to Mr. S. Kubo, for his excellent programing skill and to Mr. M. Yokoyama, for his help with experimental tasks.

Finally, I would like to thank my wife, Ikuko, for her many many supports and great patiance and my sons, Takeshi and Tooru, for the active efforts of them who kept me in good humor and cheered me up with their sweet during most of the research.

To Sumiko

Table of Contents

List of Tables

List of Figures

Chapter 1 Introduction

Flow through jointed rock is important in many areas of the geosciences, such as oil recovery, geothermal energy extraction and underground disposal of nuclear waste. These fields require a detailed understanding of the ground water flow system in order to evaluate the performance of planned underground structures. The theory of flow through jointed rock is, however, not yet fully developed, mainly owing to the difficulty in defining the geometry of the joint system and understanding the flow mechanism through an individual joint.

Several questions have been pointed out by numerous previous workers. One of the most fundamental and serious questions is how does water conduct and transport occur in a single joint and what factors significantly affect conducting and transport properties? For example, surface roughness, variable fracture aperture and infilling material in a joint will control flow through a joint and can make the flow behavior complicated. It is necessary, at a minimum, to understand the deformation-flow behavior of a single rock joint to understand the behavior of complex joint system in rock masses and to build predictive models.

Joints are often visualized conceptually as parallel plates separated by some distance. In the parallel plate model as shown in Fig.1.1, an individual fracture is represented by two infinite smooth parallel plates, and the flow is assumed to be laminar with a parabolic velocity profile. This leads to the well-known "cubic law" relating fluid flux to aperture. The parallel plate representation, however, is too idealized since there are generally voids and contacts in the plane of a real joint. The conductivity of a rock joint is governed by both the geometry of void space and the distribution of contact areas between the opposing two joint surfaces. The voids of a joint create a complex interconnected network through which water must flow. This complex geometry makes flow through a joint tortuous. Therefore one needs to closely analyze the effect of both the void geometry and the contact area of a joint on the flow through a joint.

On the other hand, when a joint is stressed, the joint void space deforms and changes in the contact area occur. These changes significantly affect the hydraulic and mechanical properties of the joint. Several researchers have investigated the deformation characteristics of joints and the increase in contact area as a function of applied normal stress. Also several experimental investigations on flow through a single joint have been carried out. Iwai (1976) studied flow through a joint as a functions of deformation, contact area and stress up to 20 MPa. The results of his laboratory investigation on artificially induced tension joints showed that the cubic law was found to hold whether the joints are

open or closed and whether the flow path geometry is straight or radial regardless of both the loading path and loading cycle. Raven and Gale(1985) studied the effect of stress on radial flow through natural joints on samples of various sizes and stresses up to 30 MPa. They found that their results did not follow the cubic law and suggested that the change in the contact area with stress plays a major role in decreasing the joint flow and in deviating the flow from that predicted by the cubic law. There are, thus, several inconsistencies, such as the applicability of the cubic law to a joint flow and the effect of contact area in a rock joint on flow. More works on the measurement of joint surface geometry and thus aperture geometry in combination with stress-deformation and stress-conductivity testing using several different rock joints are required. These measurements not only confirm the observed trends that the hydromechanical characteristics of joints may be subject to the cyclic loading effects, but also provide a solid basis for stress-deformation-flow theory. It will lead to the development of a predictive model for stress-deformation-flow behavior of a single joint.

The objective of this research is to observe both the surface roughness and aperture of joints in combination with the hydromechanical behavior of a single joint and to draw general conclusions from the observation. The study was conducted as follows :

1) Previous work concentrating on the properties of a single joint is critically reviewed in Chapter 2. In the review, the previous work has been separated into four different themes.
   a)Joint roughness and aperture variation
   b)Flow behavior in a single joint
   c)Conductivity variation with pressure in rocks and rock joints
   d)Stress-flow models for a single joint
2) In Chapter 3, sets of precise measurements of the surface roughness on natural and artificial joints in four relatively impermeable rocks have been carried out by a specially built non-contact optical system employing the laser beam profilometer. Six joints were used, representing igneous, metamorphic and sedimentary rocks. The geometrical properties of joints such as surface roughness and aperture were statistically analyzed, especially with respect to the variation, distribution and correlation of joint aperture and are documented.
3) In Chapter 4, stress effect on joint conductivity is observed using the transient pulse method at pressures up to 40 MPa during both external confining pressurization and internal pore pressure cycles. The changes of joint conductivity of three different joints in granodiorite with respect to both external confining pressure and internal pore

pressure as well as stress history were analyzed. In particular the effective stress for hydraulic conductivity of joints are examined.

4) In Chapter 5, stress-flow experiments for the six different jointed rock specimens, whose geometrical properties have been obtained in Chapter 3, have been carried out to measure the joint deformability and conductivity simultaneously by changing the confining pressures up to 20 MPa. The high-pressure triaxial testing apparatus are used for these experiments. Each specimens are subjected to three cycles of incremental loading and unloading and the flow rate through each specimens are measured by steady-state straight flow test at each stress level. The hydromechanical characteristics of joints in terms of several conventionally used properties such as hydraulic conductivity, transmissivity, maximum closure, mechanical aperture and hydraulic aperture, are presented. In addition, similar measurements of the geometrical properties of joints such as surface roughness and joint aperture to those in Chapter 3 are conducted after stress-flow experiments. Then, the change of geometrical properties of joints due to the cyclic loading are obtained. The hydromechanical properties of joints in combination with their geometrical properties are closely examined and are presented.
5) Conclusions and recommendations for future study are then given in Chapter 6.

In this study, three different measurements and experiments have been conducted. Contents of research such as objectives, measurements and experiments, rocks and jointed specimens used, applied analysis and model, and main properties in each measurements and experiments are schematically illustrated in Fig.1.2.

Note:
In the following chapters of the thesis, the term "joint" and "fracture" are used interchangeably though the strict definitions of them are different. Also the term of "permeability" and "conductivity" are used interchangeably in this text, but those definitions are clearly distinguished in Chapter 4.

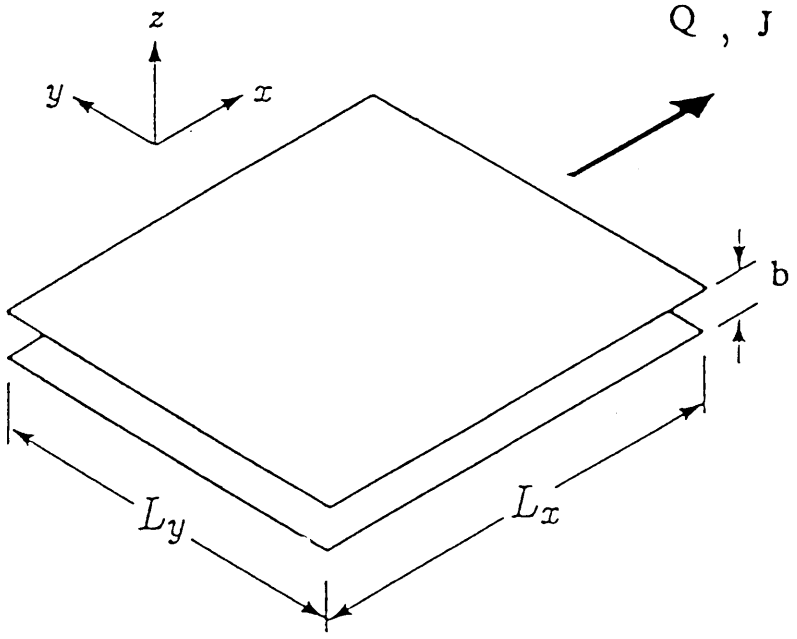

Fig. 1.1 Parallel Plate Representation

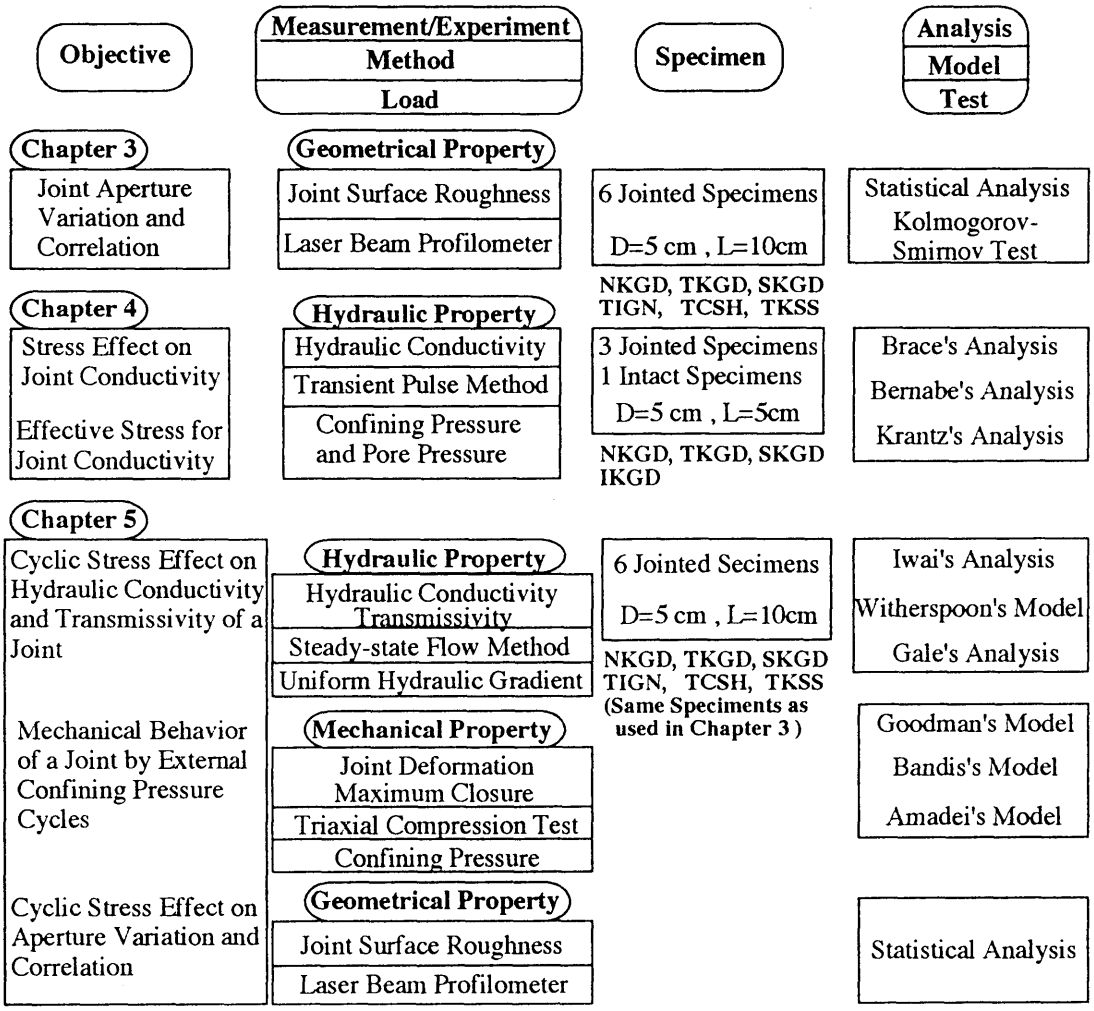

Note : NKGD : Natural Joint in Kikuma Granodiorite
TKGD : Tension Joint in Kikuma Granodiorite
SKGD : Sawed Joint in Kikuma Granodiorite
TIGN : Tension Joint in Inada Granite
TCSH : Tension Joint in Chichibu Schist
TKSS : Tension Joint in Kimachi Sandstone

Fig.1.2 Schematic view of content of research

Fig.5.5 Photographs on the procedure for the sample preparation
(a) Sealing both side ends of a joint with epoxy

the conductivity variation with pressure of a single joint are presented.

Note that scale effects of these characteristics are important especially when one applies all the results obtained in core or on the laboratory scale to the in-situ joint. The aim of this study is, however, much more fundamental. In this section, scale effects on the hydromechanical characteristics of a single joint is not reviewed since the following comprehensive reviews already exist, i.e. ; The ISRM Commission on Scale Effects in Rock Mechanics organized two specialty workshops : the first held in Loen, Norway in 1990 and the second held in Lisbon, Portugal in 1993.

The final section of this chapter describes existing stress-flow models both for rocks and for a rock joint. First of all, stress-flow model for intact rocks with distributed pores and cracks are reviewed. Second, stress-flow models for a single rock joint are described. There are numerous stress-flow models for a joint which have been developed during the last two decades, i.e.; the beds of nails model of Gangi(1978), the aperture frequency model of Neuzil and Tracy(1981), the void-asperity model of Tsang and Witherspoon(1981), the Helzian contact model of Walsh and Grosenbaugh(1979) and Swan(1981, 1983), and the JRC-JCS empirical model of Barton el al.(1985) and so on. Several models have been already reviewed by Iwano(1990). Therefore in this section, a couple of most relevant models are selected and are closely reviewed.

2.2 Joint roughness and aperture variation

To observe and characterize fracture aperture variation, several methods have been proposed using profilometers (Swan 1983, Brown et al. 1986, Gentier 1986) or injection and casting techniques (Gale et al. 1987, Pyrac-Nolte et al. 1987, Hakami 1988, Gentier et al. 1989) as well as optical techniques (Miller et al. 1990, Kimura and Esaki 1992 and Iwano and Einstein 1993). A critical review regarding these techniques will be presented by Hakami et al.(1995).

The measurement methods can be grouped into the following three categories according to the basic approach to the measurement :

1) Surface topography approach
2) Aperture replica approach
3) Surface replica approach

These three approaches will be simply reviewed below.

It is noted that, in this study, the optical technique, which belongs to the surface topography approach, has been utilized to measure the three dimensional surface height topography of joint surfaces. Details of my optical technique are presented in Chapter 3.

2.2.1 Surface topography approach

This approach has been used by Gentier(1986) to measure the aperture variations in natural granite joints. She measured the surface height and location along the joint profile on both opposing joint surfaces by using a profilemeter, which is a mechanical device having a stylus that moved along profiles on the surface. The corresponding profiles were put together to form the composite topography, i.e.: the aperture profile at zero normal stress. Examples of both the obtained joint profiles and the resulting frequency histograms over the joint aperture by Gentier are presented in Fig.2.2 and Fig.2.3 respectively. This approach was also used by Brown(1984) in the laboratory and the field to characterize the joint surface and to analyze the scaling function of the individual joint.

The advantage of this approach is that it utilizes surface roughness data which is the most easily obtainable data regarding the geometric properties of joints. The difficulty in this approach lies in matching of profiles since it is difficult to measure the exact relative positions of the profiles. Also one needs to infer the change of aperture from zero stress condition to non-zero stress condition by using appropriate mechanical models. Most of these measurements have been conducted in two dimensions, i.e. ; the measurable variable is the surface height along profile. One should, however, measure the surface height in three dimensions on a joint plane since the flow path through a joint is tortuous.

2.2.2 Aperture replica approach

Another approach to reveal the aperture inside a joint has been used by Gale(1987). The experiments involved the injection of an epoxy resin into a joint under a given normal load from a central hole in a joint. After hardening, the joint was cut into sections and the thickness of the resin and void along the sections were measured with the microscope. Fig.2.4 presents the distribution of pore space along four profiles in Stripa granite joint sample by Gale. Other injection materials for filling a joint have been used, e.g. ; Pyrak-Nolte et al.(1987) used Wood's metal, Gentier et al.(1989) used Silicon polymer resin and Hakami and Stephansson(1993) used cement grout for an in-situ joint.

Pyrak-Nolte et al.(1987) injected Wood's metal into the three natural fractures in Stripa granite (Quartz monzonite) to study the fracture void geometry and contact area as a

function of normal stress. Pyrak-Nolte et al. encountered the following problems. : Especially when the two surfaces were taken apart after hardening of Wood's metal, Wood's metal could break and parts of it stayed on each joint surface. Further, errors were also involved in the measurement of the thickness of Wood's metal. These errors were likely to cause a totally false image of the void space in a joint.

Gentier et al.(1989) made a transparent colored replica of joint aperture and developed a sophisticated procedure for determining the thickness of the produced replica. She used a silicone polymer resin as the casting material and it yielded precise reproductions of the void spaces of a joint. A digital image of the cast could then be recorded and processed using an image analyzer since the image of the replica had different gray-scales according to the thickness of the resin. Fig.2.5 shows an example of the gray-level pixel map of the cast in a granite joint under no stress. However, as Gentier mentioned, this technique might underestimate the size of the void in a joint since some air could stay trapped in a fracture.

This approach has the advantage that the replica of joint aperture under compressive load can be obtained and a replica is expected to give a realistic image of compressed joint aperture. Also the distributions of contact areas in a joint can be observed. On the other hand, the injecting materiel involves destroying the sample to retrieve the information and thus the same joint specimen cannot be used. There are another serious problems on resolution. The accuracy of the measurement seems inadequate to examine the aperture distribution. Further development for the measurement of the thickness of replica is strongly recommended.

2.2.3 Surface replica approach

Hakami & Barton(1990) used the surface replica approach. They made a transparent epoxy replica from each joint surface, matched the surface replicas of the two surfaces together and produced the realistic joint aperture. Then they performed flow experiments using the produced replica of a joint with the visible stream lines, which made the water drop area visible, and the aperture was measured by placing a small known volume of water drop between the two surfaces. The main advantage of this technique is that the flow path in a joint is visible and one can directly observe the flow behavior through a joint.

The disadvantage in this approach is that natural joints with very soft fillings cannot be studied as well as the aperture replica approach. Small differences between the original joint and the replicas can appear due to the imperfect copying procedure and hardening effects such as shrinking or warping of the specimen. Therefore this approach is not

appropriate for detailed study of aperture distribution.

Any of these techniques has advantages and disadvantages. Thus no technique has yet been developed which can provide not only complete descriptions but also general conclusions regarding the aperture variation of a single joint. In fact, the applicability of each technique depends on the type of join, the scale of measurement and the aim of the investigation. The amount of data on joint aperture is too limited to yield the general characteristics on the geometrical properties of joint apertures or to distinguish the differences in these properties between joints in different rock types.

2.3 Flow behavior in a single joint

The results by Abelin et al. (1985) and Hakami (1988) revealed tortuous flow behavior through a joint, the so-called channeling, both in the field and in the laboratory, respectively. Brown (1987), Tsang and Tsang (1987), Tsang et al. (1988) and Moreno et al. (1988, 1990) have all confirmed this behavior by numerical analysis using realistically generated joint apertures. Fig.2.6 shows an example presented by Brown(1987). Fig.2.6(a) is an aperture distribution formed by placing two surfaces together which have been created by using the fractal generation. Flat areas are regions of zero aperture or "contacts" defined by the overlap of the two surfaces. Surfaces are in intimate contact with a fractional contact area of about 7% in this simulation. Fig.2.6(b) is the flow field for the same fracture as in Fig.2.6(a). The channeling behavior of flow path through a fracture is clearly observed.

Also theoretical and experimental studies have been carried out to investigate the effect of the void geometry on flow through a single joint (Neuzil and Tracy 1981, Raven and Gale 1985, Schrauf and Evans 1986, Silliman 1989 and Brown 1989). Their results clearly suggested that the geometry of void space and contact area between two opposing joint surfaces, namely both of the variation and the correlation of joint aperture, may be important in describing the channeling nature of flow through a joint.

In addition, the effects of heterogeneity and anisotropy of aperture variation on flow in a joint are not well established. Tsang and Tsang (1989) used the simple negative exponential form for covariance functions to describe the correlation of aperture and Thompson and Brown(1991) used the anisotropic decaying power law functions as correlation functions in their numerical generation of heterogeneous joint aperture. In addition, Amadei and Illangasekare (1992, 1994) developed a closed-form analytical solution for flow and transport analysis in a joint with non-homogeneous hydraulic properties. Such approaches are often limited to joints with idealized geometry and cannot

be applied to all natural joints. One needs to examine additional cases with actual spatial variation and correlation of apertures to make the numerical generation of heterogeneous joint apertures more realistic. The details of aperture simulation techniques will be discussed in Section 2.6.

2.4 Hydraulic conductivity variation with pressure in rocks and rock joints

2.4.1 Hydraulic conductivity variation in rocks

As Walsh(1966) explained, nearly all rocks have some porosity, which varies widely from one rock to another, i.e. : 0.1 or 0.2 for sandstone and only 0.001 or 0.002 for diabase. Most other rocks fall between these limits. Not only porosity but also pore shape varies among rocks. In a rough way porosity and pore shape are related each other. Therefore high porosity rocks usually contain cavities of irregular shape which are more or less equidimensional. On the other hand, cavities in low porosity rocks are usually in the form of cracks. The cracks are situated along cleavages in the minerals or at grain boundaries. Walsh distinguished this difference between what one calls pores on the one hand and cracks on the other hand because of the way in which porosity is developed in rocks.

The conductivity of rocks strongly depends on both the volumes and the shape of pores and cracks as well as the interconnectivity of these cavities. Brace(1980) published an excellent review of the conductivity of rocks using readily available laboratory, in-situ and inferred values of permeability of crystalline and argillaceous rocks. His review showed that laboratory permeabilities of intact samples, which ranged in size from 25 to 150 mm, varied from 10^{-24} m^2 to 10^{-10} m^2. The wide range of permeabilities and the size of samples indicated that these measurement reflected the contributions to the permeability of pores and cracks, but not joints. He also showed that in situ permeabilities for crystalline rocks ranged from about 10^{-18} m^2 to 10^{-13} m^2 and those for argillaceous rocks ranged from 10^{-20} m^2 to 10^{-18} m^2. Given the length of brothel in well tests and the length of test intervals, these data must reflect the contributions to the permeability from joints, large fractures to shear zones which intersected the borehole.

He concluded that unfortunately these values ranged too widely to be of much practical use, that no systematic decrease in permeability with depth was evident and that many additional measurements are needed at various conditions and in a wide variety of geologic situations. Brace(1984) presented additional data on the permeability of crystalline rock which supported the general conclusions stated in his 1980 paper.

Fig.2.7(a) presents an example of variation of in-situ permeability of rocks. In this figure, the bars represent the range of values reported for one or more boreholes, the above two numbers over each bar give maximum depth and interval respectively and the numbers in parentheses are references in Brace's paper(1984).

Clauser(1992) updated Brace's (1980, 1984) compilation of permeability data. His extensive compilation of the permeability data of crystalline rocks was presented and evaluated by Gale(1993), as shown in Fig.2.7(b) which combines the laboratory data and in-situ data. Clauser's additional data confirmed Brace's conclusion that there were three orders of magnitude increases in the average permeability from the laboratory to borehole scales. He correctly related this increases to the lack of joints in intact samples and the presence of joints, fracture zones and shear zones in the intervals of borehole tests. The other effects on the permeability of intact and in-situ rocks, i.e.: scale, depth, the method of testing and stress etc., were presented and reviewed by Gale(1993).

In-situ, rocks are exposed to a wide variety of pressures, i.e.; lithostatic pressure and fluid pressure, thermal stress and deviatoric stress. These variable pressures can result in major changes in hydromechanical properties of rocks. Before going into details about the hydromechanical properties of a joint, first, the conductivity variation with pressure for intact rocks having different pores and cracks is reviewed here.

2.4.2 Stress effects on hydraulic conductivity of rocks

Increasing confining pressure reduces the conductivity by progressively closing cracks. Because cracks close easily when pressure is applied, pressure effects are very pronounced in rocks where conductivity is primarily due to cracks. For example cracks submitted to a pressure P will close easily if they are vary flat, that is, their aspect ratio, R, is small. The existing result emphasizes the importance of crack geometry. Elastic calculations show that for P < 100 MPa, it is possible to describe crack aperture changes by the following equation:

$$b = b_0\left[1 - \frac{2(1-\nu^2)}{RE}P\right] \qquad (2.1)$$

where b_0 is the aperture under zero pressure, ν is Poison's ratio and E is Young's modulus (Walsh, 1965). This equation implies that a crack of initial aspect ratio R_0 will close when the pressure reaches the closure pressure which is given by

$$P = \frac{RE}{2(1-\nu^2)} \tag{2.2}$$

For isotropic pores, in sandstones or other granular materials, pressure effects are very small. In the intermediate case where both pores and cracks coexist, the effects can be large or small depending on whether the cracks are required to maintain the interconnectivity of the pore network. For example, the porosity at grain contacts in sandstone can be viewed as a crack porosity. The comparison of the experimental results and models show that the closing of cracks is controlled by elastic processes up to a certain value of pressure. Above this value, the surface roughness controls further closure. Thus there are two ways that a non-negligible conductivity can be preserved at elevated pressures, the first is to have an interconnected porosity composed of "isotropic pores", the second is to have cracks with rough surfaces. In the second case, interconnection is more likely to be assured. The structure of void in a single joint is supposed the be similar to cracks with rough surfaces, but it will strongly depend on the texture of the intact rock and the multitude of joint genesis processes.

Gueguén and Palciauskas(1994) presented a good review on the conductivity variation for rocks having different pores and cracks in their book. Fig.2.8, Fig.2.9 and Fig.2.10 show examples the variation of conductivity with confining pressure for the isotropic pores (Fontainebleau sandstone, ϕ=12%, after David and Darot, 1989), for the isotropic pores plus crack gain porosity (Fontainebleau sandstone, ϕ=6%, after David and Darot, 1989) and for the crack porosity (Chelmsford granite and Barre granite, after Barnabe, 1986), respectively.

2.4.3 Stress effect on joint hydraulic conductivity

Flow through a joint depends on the state of stress in and on a joint. A single joint can be thought of as two opposing surfaces in contact. When a joint is stressed, the joint void space deforms and changes in the contact area occur. Since void spaces in a rock joint play a predominant role in controlling the joint conductivity, the change of void spaces and the interconnectivity in a joint due to the external stress change on a joint results in the change of the joint conductivity. Therefore, the stress dependency of the joint conductivity can be explained by the change of geometry of void spaces in a joint. Joint conductivity is also supposed to be changed by internal pore pressure in a joint due to the same reason as for the external stress. The changes of void spaces in a joint significantly affects not only

the hydraulic properties of a joint but also the mechanical properties of the joint. Several researchers (Goodman 1976, Swan 1983 , Bandis et al. 1983 and Brown & Scholz 1985) have investigated the deformation characteristics of joints and the increase in contact area as functions of applied normal stress. Brown and Scholz (1985) concluded from experimental and theoretical studies that joint deformation is not only a function of the elastic properties of the host rock but also depends on the way in which the surface topography affects the distribution of contact area.

Also several investigations on flow through a single joint have been carried out. Iwai (1976) studied flow through a joint as functions of deformation, contact area and stress up to 20 MPa. The results of his laboratory investigation on tension joints that were artificially induced in homogeneous samples of granite, basalt, and marble showed that the cubic law for flow in a joint was found to hold whether the joints are open or closed and whether the flow path geometry is straight or radial regardless of both the loading path and loading cycle. He also found that there is always a residual flow even under a high stress and that the cube of the aperture is proportional to flow when corrected by the residual flow. His study, in particular the procedure of the analysis on joint flow data, will be closely reviewed in Chapter 5 since his work is most relevant to this study.

Raven and Gale(1985) studied the effect of changes in specimen size on the normal stress-permeability properties of natural joints. They used five granite cores (10.0, 15.0, 19.3, 24.5 and 29.4 cm diameter) which contained the part of the same natural joint oriented normal to the core axis. Each joint specimen was subjected to three uniaxial compressive loading and unloading cycles with maximum normal stresses up to 30 MPa. In each cycle, joint deformation and steady-state flow rate through a joint from a central borehole were measured for specified levels of normal stress. As shown in Fig.2.11, they found that their results did not follow the cubic law and the deviation between their results and the theory increased with the number of loading cycles and specimen size. They suggested that the main reason for these deviations is that the change in the contact area with stress plays a major role in decreasing the joint flow.

Krantz et al. (1979) measured the hydraulic conductivity of artificial joints for pressures up to 200 MPa by changing the confining pressure and pore pressure individually. They found that the hydraulic conductivity decreased more rapidly with stress for jointed rock than for an intact rock and the joint hydraulic conductivity was more sensitive to the confining pressure than to pore pressure. The fact that the effects of both the confining pressure and pore pressure on the joint hydraulic conductivity were different was suggesting that one should be cautions when applying the term "effective pressure" or "effective stress" to jointed rock. It follows that effective pressure is not the conventional

effective pressure, which is defined as the pressure difference between confining stress and pore pressure, at least for the hydraulic properties of jointed rock. Note that, in general, effective pressure which produce the same effect irrespective of both of the confining pressure and pore pressure must be considered as a controlling variable for the joint conductivity. The definition of effective pressure for the hydraulic properties of jointed rock will be discussed in Chapter 4.

As one can understand from this review, there are still several inconsistencies such as the applicability of the cubic law in the stress-flow behavior of a single joint under pressure. As suggested by Raven and Gale (1985), more work on the measurement of joint roughness in combination with stress-deformation-flow tests using several different rock joints is required to confirm the trends pointed out by previous works, to provide a solid basis for stress - joint flow theory and to develop the predictable model for stress-deformation-flow behavior of a single joint.

2.5 Stress-flow model for a single joint

2.5.1 Stress-flow model for rocks

According to Scheidegger (1974), one can group the flow models for porous media with distributed pores and cracks into two categories : models containing networks of the capillary tubes and models utilizing the notion of hydraulic radius. In the first case (the capillary tube model), one attempts to describe conductivity in terms of capillaries with a distribution of radii and thus it is an approximation to the real system. In the second case (the hydraulic radius model), one introduces the notion of the equivalent porous medium (Walsh and Brace, 1984). Dullin(1979) also calls the first model "statistical model" and the second "geometrical model". Detailed explanation on two models can be found in a book written by Dulline(1979) and Gueguén and Palciauskas(1994).

For crystalline rocks, in the past decade, the so-called " equivalent channel model" (Walsh and Brace, 1984), which is a more comprehensive version of the hydraulic radius model, was extensively used and yielded satisfactory results for the analysis of hydraulic behavior of intact crystalline rocks. This model is extremely simple conceptually. The entire pore network of the rock is just replaced by a single equivalent conduit characterized by a number of geometrical parameters like tortuosity, hydraulic radius or aspect ratio. This model always involves the replacing operation, but it makes very little physical sense unless the equivalent channel is somehow the representative of the rock pore structure. The reason for this success is probably that the pore phase in

crystalline rocks is almost exclusively formed for low aspect ratio cracks. Hence, it is reasonable to think that the equivalent channel corresponds to an average of the cracks in the rock.

In the equivalent channel model, one can proceed by replacing the whole conducting pore network with a single equivalent conduit, the conductivity of which is given by the following equation

$$K = \frac{\langle m \rangle^2}{\langle s \rangle} \frac{\phi}{\langle \tau \rangle^2} = \frac{\langle m \rangle^2}{\langle s \rangle} \frac{1}{F} \tag{2.3}$$

where $<m>$ is the mean hydraulic radius, $<s>$ is a shape factor ranging from 2 to 3 when the aspect ratio varies from 1 to 0, ϕ is the conducting porosity (the ratio of conducting pore volume to the sample volume), $<\tau>$ is the tortuosity (the ratio of the equivalent channel length to the sample length) and F is called the resistivity formation factor. The symbol $< >$ will thus be used for an averaging operation. By assuming that wetted area of the equivalent channel is simply equal to, A_c, real wetted area of conducting pore space, the mean hydraulic radius is $<m>= F\,(V/A_c)$.

Walsh and Brace (1984) assumed that the aspect ratio of the equivalent channel is close to zero. Therefore a shape factor will be simply taken equal to 3. Walsh and Brace (1984) plotted the square root of $3KF$ against crack porosity for Westerly granite and Chelmsford granite and found fairly linear relationships. This implies that the wetted area remained nearly constant in the range of pressure investigated. Consequently, most of the deformation taking place at the surface of the pores are elastic. This is the point where one needs to introduce some elements of elastic joint deformation in hydraulic model. The hydraulic radius is identical to the crack half-aperture and one can write the following approximated equation to account for the effect of effective pressure.

$$d\langle m \rangle = -\frac{2h}{P_e} dP_e \tag{2.4}$$

where P_e is the effective pressure and h is the standard deviation of the asperity heights distribution.

By combining Eq.2.3 and Eq.2.4, stress-flow model for the crystalline rocks has been proposed.

In this model, an asperity is defined as a local maximum of the crack wall topography. Also, the interactions between asperities are excluded. Therefore one can deduce that the square root of 3KF should be proportional to the natural logarithm of pressure. Walsh and Brace (1984) verified this point on Westerly granite and Chelmsford granite. Bernabe(1985) extensively used the equivalent channel model to provide the appropriate means for interpreting the conductivity measurement of Chelmsford granite, Pottsville sandstone, Pigeon Cove granite and Westerly granite during cyclic incremental loading and unloading. He concluded that the conductivity in rocks is controlled by the hydraulic radius.

Another important point was raised by Walsh(1981). At different scales, micro cracks and joints or faults play very similar roles in the behavior of rock under pressure. It is therefore tempting to use the models for the mechanical and hydraulic properties of cracks or joints and is recently devised (Gangi, 1978, Walsh and Grosenbaugh, 1979, Tsang and Witherspoon, 1981, Walsh, 1981 and Brown and Scholz,1985), in which cracks or joints are always considered as rough surfaces in contact.

In the following section, several stress-deformation-flow models for joints are closely reviewed. In addition, stochastic model for joint flow proposed by Brown(1984), which does not account for the joint deformation, is reviewed since this model can represent a couple of existing models which vary from a simple parallel plate model, the frequency aperture model of Neuzil and Tracy(1981) to the quasi-two-dimensional asperity model of Tsang and Witherspoon(1981). Also, it can be implemented into existing joint system models like a discrete fracture network model or channel network model with taking in-plane anisotropy of joint conductivity into account. The versatility of the stochastic model will be demonstrated.

2.5.2 Beds of nails model

Gangi(1978) developed the asperity model, labeled a "beds of nails model", to determine the stress dependent conductivity of a joint subject to confining stress. Fig.2.12 shows the schematic representation of a joint as proposed by Gangi. In this figure, the asperities are indexed by j. At zero applied normal stress, each asperity is defined by the height hj, width aj and the corresponding aperture bj. Bo is the maximum aperture of a joint. In this model, the closure of a joint subject to normal stress is ascribed to the elastic compression of the asperities in a joint. Assuming that the asperities obey Hooke's law, the top surface of a joint displaces downward up to the displacement corresponding to the applied normal stress.

Therefore the deformability of a joint is said to result from the small number of asperities which are in contact. These contact areas sustain much higher stress than that measured by total load divided by the total joint area. As a result, the deformation of the asperities in contact is expected to be larger than the deformation in the intact rock under the same load.

In the beds of nails model, the conductivity variation of an individual rock joint was expressed as a function of the acting confining stress and the effective modulus of the joint asperities as follows.

$$K(P_e) = K_0\left[1-\left(\frac{P_e}{\sigma_M}\right)^m\right]^3 \qquad (2.5)$$

where P_e is the effective confining stress, σ_M is the effective modulus of the asperities in a joint, m is the material constant ($0<m<1$) which depend on the asperity distribution in a joint and K_0 is the conductivity at a zero pressure.

Gangi found that the effect of cyclic loading on conductivity could be expressed in terms of an increase in m values. He also demonstrated that conical or wedge-like asperities could be treated as the bed of nails model. With this model, Gangi obtained a very good result in the analysis of the flow data in a jointed sandstone.

Tsang and Witherspoon(1981) encountered some difficulties with the bed of nails model due to the discrepancy in contact at the same maximum stress when the beds of nails model was applied to both the flow data and the stress-strain measurements for a granite joint which were obtained by Iwai(1976). They found that, to force an agreement between the calculated and measured flow rates, adopting a value of Young's modulus for each asperity that was two orders of magnitude smaller than that of intact rock was required. Then they concluded that above result did not seem reasonable. Therefore they proceeded to seek an alternative physical model for the hydromechanical behavior of a single joint under normal stress.

2.5.3 Void asperity model

Tsang and Witherspoon(1981) considered the closure of a joint as resulting from the deformation of voids or cracks between the asperities. Geometrically, one may either envision a single joint as composed to a collection of voids or a distribution of asperities as

illustrated in Fig.2.13. Therefore the asperity model and the void model are interchangeable as far as the geometry of joint is concerned. They utilized the void model to describe the joint deformation under normal stress and the asperity model to describe the flow through a rough walled joint. They developed the mathematical correspondence between the void model and asperity model. This correspondence allowed the prediction of flow rate as a function of normal stress. The physical picture for the deformation of voids in a sequence of increasing normal stresses is also illustrated in Fig.2.13. The crack length 2d is defined as the distance between two adjacent areas where the two joint surfaces come into contact. These areas of contact are simply the asperities as shown in Fig.2.13. Under increasing load, the deformation of voids causes more asperities to come into contact and leads to a decrease in the average crack length. This process results in a gradual increase of the effective modulus with increasing normal stress to approach the intrinsic value of intact rock. The theory contains several simplifying assumptions, but no arbitrary adjustable parameter was used in the validation of their theory. Hence their model seems to contain the essential physics relevant to the problem of flow through a single joint coupled with stress. The lack of any fitting parameters in the interpretation of flow versus stress data is the key difference between this model and previous model (Iwai 1976 and Gangi 1978).

However, as Tsang and Witherspoon(1981) also pointed out, in general, all of the several physical assumptions and mathematical approximations in the void asperity model can contribute to errors in the calculated result for flow. Especially two functions : the number of asperities in contact function and the asperity height distribution function are involved in all phases of the computation. To determine these functions involves various fitting manipulations. Then it is likely that errors associated with these various manipulations and resulting quantities may play a greater roll in contributing to the discrepancy between the theoretical predictions of flow and the experimental measurements.

In fact, Tsang and Witherspoon(1981) obtained a very good fit to Iwai's deformation-flow data for joints in granite and basalt since they encountered no difficulty in choosing the analytical functions with excellent fit in treating the stress-deformation data to calculate the number of asperities in contact function. However the stress-displacement data for a joint in marble could not be fitted by an analytical function throughout the range of the measured stress due to the anomalous shape of the data. Therefore the resultant of the number of asperities in contact function was probably a poor representation of the actual roughness profile of the joint walls. Thus this error gave rise to the associating errors in the prediction of flow.

2.5.4 Hertzian contact model

For the case in which a joint is represented by asperities in contact, the geometry at the contact point can be represented by two spheres in contact. This is a Hertzian contact problem. For both the normal and shear stress of the Hertzian contact, solutions already exist. The Hertz theory of elastic contact is well documented in a book by Johnson(1985).

The key point on the application of the Hertzian contact theory to the joint deformation behavior is that each deformation at each Hertzian contact are combined to yield total joint deformation. The initial application of Hertzian contact theory to the joint deformation behavior was made by Swan(1981,1983). After comparing laboratory data with the theoretical prediction on the basis of tribology using the elastic Hertzian contact theory for joint stiffness, he concluded that the tribological approach was valid only qualitatively and empirical corrections to the surface topography terms had to be made to get quantitative agreement. Fig.2.14 describes the half-joint model, which was the first to receive an analytical treatment using the Hertzian contact theory by Greenwood and Williamson(1966) and was applied to the real joint contact problem by Swan.

Next, Swan carried out direct measurements of surface profiles using a simple profilometer to access statistically the topographic features of real fracture surfaces. The results from the statistical analysis of profiles clearly show that the peak height distribution of a fracture surface is found to be essentially a Gaussian distribution.

Finally, Swan developed a discrete numerical model using digital data provided by a profilometer to analyze the fracture contact problem for normal loading in comparison with the tribological model. This numerical simulation using the discrete model showed that the functional relation between normal stress, stiffness, true contact area and initial aperture are shown to be surprisingly simple, and this fact is attributed to the Gaussian type distribution of asperity height. Only the effect of applied normal stress on joint deformation is considered in the relatively simple theory and modeling discussed above but the effect of pore pressure must be considered in practical problems.

Walsh(1981) derived an analytical expression describing the variation of the rough-walled joint conductivity as a function of the confining stress and pore pressure on the basis of both the analogy to the heat conduction theory for flow and the contact theory for deformation. The stress dependent conductivity proposed by Walsh (1981) is expressed as the product of two factors, one giving the effect of aperture change and the other giving the effect of tortuosity due to applied effective confining stress, P_e, as follows.

$$\frac{K}{K_0} = \left[1 - \sqrt{2}\left(\frac{h}{b_{0\frac{1}{2}}}\right)\ln\left(\frac{P_e}{P_{e0}}\right)\right]^3 \left[\frac{1 - g(P_e - P_{e0})}{1 + g(P_e - P_{e0})}\right] \tag{2.6}$$

where K_0 and $b_{01/2}$are the joint conductivity (essentially joint transmissivity in his expression) and the half aperture at some reference effective stress P_{e0}. h is the r.m.s. value of the asperity height distribution. g is the first derivative of the contact area with the applied effective stress, which is expressed by Young's modulus, E, Poison's ratio, ν , of the country rock and the autocorrelation length of joint surface, f, (i.e. ; the distance a curve must be indexed relative to itself to become uncorrelated) as follows.

$$g = \sqrt{3}\frac{f}{hE(1-\nu^2)} \tag{2.7}$$

Once these parameters have been measured for a joint, Eq.2.6 can be used to show how flow through a joint responds to the changes in the applied effective stress. The first term in brackets in Eq.2.6 expresses the change of aperture and the second term in brackets describes the tortuosity. Walsh used the following expression as the effective stress, P_e , which was previously derived by Robin(1973) and it is a fundamental parameter in the poroelasticity theory initiated by Biot(1941).

$$P_e = P_c - \alpha P_p \tag{2.8}$$

where P_c is a confining pressure and P_p is pore pressure. Parameter α is a constant for materials which is called the effective stress coefficient. Note that Robin (1973) rightly pointed out that the parameter α is not necessarily constant for rocks. But the approximation that the parameter α is nearly constant is considered to be adequate at least over the range of pressures that one are interested.

The value of α is dependent on how the volume and shape of flow path changes with confining pressure when pore pressure is zero. From several experimental data, Walsh presented that the value of a was taken to be 1.0 in most presentations of data that were found in the resent literature. In this case, P_e is exactly same as the conventional effective stress. Note that detailed discussion on the definition of the effective confining stress for the joint conductivity will appear in Chapter 4.

Walsh(1980) also presented that if the tortuosity term were equal to unity, the conductivity would vary with the effective confining pressure according to the following relation:

$$K^{1/3} \cong C - D \ln P_e \tag{2.9}$$

where C and D are constants which depend on certain geometric parameters describing the microcracks and their surface topography.

One sees in Eq.2.9 that the cube-root of flow rate should vary linearly with lnP_e.. Walsh examined the validity of Eq.2.9 by using experimental data by Kranz et al.(1979), Brar & Stesky(1980) and Jones & Owens(1979) and concluded that the conductivity of a joint changes with effective pressure according to the law described by Eq.2.9.

Walsh used specific constant values of a with effective stress for several joints. The coefficient a for a joint with effective stress is considered not to be constant. It should be strongly stress history dependent and should decrease with increasing effective confining pressure since the coefficient a is closely related to the geometry of void spaces in a joint. A couple of experimental results showed that the coefficient a for intact rocks were almost constant with the effective confining stress and were dependent on the intrinsic structure of pores and cracks in rocks. It is also noted that the effective stress coefficient a for joint hydraulic conductivity will be discussed in Chapter 4.

Therefore in his conclusion, the joint conductivity (in fact joint transmissivity) is proportional to the product of two factors : aperture change and tortuosity, as given in Eq.2.6. He also suggested that the effect of tortuosity could be neglected for fluid flow since aperture term is raised to the third power and dominates the tortuosity term which is raised to only the first power. In contrast, the theoretical study by Tsang (1984) showed that tortuosity effect greatly affected a flow though a joint, especially when contact area was greater than 30 % of a total joint area.

2.5.5 Stochastic model

Gelhar(1979,1986) used the stochastic analysis for flow/transport problems in aquifers. Mizell et al.(1982) looked at a two-dimensional flow in a confined aquifer with variable transmissivity and Gelhar and Axness(1983) studied flow and mass transport for a multi-dimensional porous medium with variable hydraulic conductivity. They employed the spectral method. The spectral method has met with some success in two-dimensional

porous medium models of aquifer heterogeneity.

Brown(1984) assumed that aperture varies log-normally over a fracture and the logaperture variation was a two-dimensional stationary stochastic process. He applied a similar methodology to variable-aperture fracture in order to evaluate the effect of aperture variation on fracture flow and developed the stochastic method to define the effective aperture and equivalent anisotropic hydraulic conductivity tensor.

In his study, it was assumed that the aperture, b(x,y), varies continuously through a fracture and was a two-dimensional stochastic process. Fig.2.15 shows the definition of local aperture and mean aperture in a joint. From the result of laboratory measurements of apertures using natural joints, Gentier et al.(1987) described that aperture distribution could be modeled as lognormal distribution as shown in Fig.2.3. For convenience, the process was assumed to be second-order stationary and had the lognormal distribution, so that the natural logarithm of aperture variation was a Gaussian process.

The correlation structure of aperture distribution in a joint was assumed to be anisotropic, and could be represented by several autocovariance functions, i.e. : the negative exponential, the Whittle, the Whittle A and the Whittle B, based on the second-order stationarity. The exponential and the Whittle function had a monotonically declining autocovariance function. The Whittle A and B functions were proposed by Mizell et al. (1982) in order to produce a finite potential head variance due to variations in the transmissivity of a confined aquifer. These four functions are plotted in Fig.2.16. These autocovariance functions were also necessary to get a finite head variance in fracture modeling. The other basic assumption was that the cubic law holds at any point over the entire fracture domain. This assumption was still questionable. Schrauf and Evans(1986) showed that flow rate through a fracture was found to be inversely proportional to the fourth power of fracture aperture due to the nonlinear flow effect. Even though the transition between linear and fully nonlinear flow should be taken into account, the cubic law was used for simplicity because the main purpose of his study was to evaluate the effect of aperture variation on the flow and was not to discuss the validity of the cubic law for flow.

This stochastic model is closely examined since it can represent a couple of existing models which vary from a simple parallel plate model, the frequency aperture model of Neuzil and Tracy(1981) and the quasi-two-dimensional asperity model of Tsang and Witherspoon(1981).

1) General formulation

Consider laminar flow in a single variable fracture which is surrounded by a impermeable rock matrix. The cross-sectionally averaged velocity at any point is proportional to the square of the aperture at that point and is in the direction of the hydraulic gradient through a fracture. It can be described as follows.

$$u = -\frac{g}{12\nu} b^2 \nabla\phi \tag{2.10}$$

where
- u : averaged velocity
- ϕ : piezometric head
- b(x,y) : fracture aperture
- g : gravitational constant
- ν : kinematic viscosity

Then the fluid flux vector is given by

$$Q = -\frac{g}{12\nu} b^3 \nabla\phi \tag{2.11}$$

This is equivalent to Darcy's equation in porous media system.

Assuming a non-deformable fracture and an incompressible fluid, conservation of mass of fluid for steady-state flow in a fracture requires that

$$\nabla Q = \nabla(bu) = 0 \tag{2.12}$$

Substituting Eq.2.10 into Eq.2.11, Eq.2.12 can be written

$$\nabla^2\phi + 3\nabla\phi\nabla(\ln b) = 0 \tag{2.13}$$

This is in similar form to the equation used in Mizell et al. (1982) to analyze a two-dimensional vertically-averaged heterogeneous aquifer, with log-aperture taking the place of log-transmissivity.

First the variables in Eq.2.13 are represented by means and perturbations as follows

$$\ln b = B + \beta(x,y) : B = E[b],\ E[\beta] = 0 \tag{2.14}$$

$$\phi = H(x) + h(x,y) : E[h] = 0 \tag{2.15}$$

Next define the mean hydraulic gradient over the domain, *J*, as follows

$$J = -\frac{\partial H}{\partial x} \tag{2.16}$$

Note that the x-coordinate has been aligned with the direction of *J*.
Assuming that *J* and *B* are constant, substitution of Eq.2.14, 2.15 and 2.16 into Eq.2.13 gives

$$\nabla^2 h - 3J\frac{\partial \beta}{\partial x} + 3\nabla h \nabla \beta = 0 \tag{2.17}$$

Taking Eq.2.17 and subtracting its mean,

$$\overline{3\nabla h \nabla \beta} = 0 \tag{2.18}$$

where the overbar signifies the expected value.

Subtracting Eq.2.18 from Eq.2.17, one obtains the following perturbation equation.

$$\nabla^2 h - 3J\frac{\partial \beta}{\partial x} + 3(\nabla h \nabla \beta - \overline{\nabla h \nabla \beta}) = 0 \tag{2.19}$$

By assuming that the perturbations are small, the term in parentheses may be neglected. The first-order approximation of the perturbation equation is then

$$\nabla^2 h - 3J\frac{\partial \beta}{\partial x} = 0 \tag{2.20}$$

This equation can be solved for a stationary head field by using the spectral representation theorem. The assumption of stationarity allows to write the perturbations in terms of their

stochastic Fourier-Stieltjes representations (Lumpy and Panofsky, 1964) as follows.

$$h = \int_{\mathbf{k}} e^{i\mathbf{k}\cdot\mathbf{x}} dZ_h(\mathbf{k}) \tag{2.21}$$

$$\beta = \int_{\mathbf{k}} e^{i\mathbf{k}\cdot\mathbf{x}} dZ_\beta(\mathbf{k}) \tag{2.22}$$

where the vector $\mathbf{k}$ is the two-dimensional wave number and $dZ_h(\mathbf{k})$ and $dZ_\beta(\mathbf{k})$ are the complex Fourier amplitudes.

The integrals must be written in this peculiar way because it is much easier not to assume that $Z(\mathbf{k})$ has derivatives. This process $Z(\mathbf{k})$ has orthogonal increments in that non overlapping differences are uncorrelated as follows.

$$\overline{dZ(\mathbf{k}_1)dZ^*(\mathbf{k}_2)} = 0, \ \mathbf{k}_1 \neq \mathbf{k}_2 \quad dZ^* \text{is the complex conjugate} \tag{2.23}$$

Substituting Eq.2.21 and 2.22 into Eq.2.20 along with the uniqueness of these representations, it follows that

$$dZ_h(\mathbf{k}) = -\frac{3iJk_1}{k^2} dZ_\beta(\mathbf{k}) \tag{2.24}$$

where $k^2 = k_1^2 + k_2^2$

The relationship between the spectra of h and ß is given by

$$S_{hh}(\mathbf{k})d\mathbf{k} = \overline{dZ_h(\mathbf{k})dZ_h^*(\mathbf{k})} = \frac{9J^2k_1^2}{k^4}\overline{dZ_\beta(\mathbf{k})dZ_\beta^*(\mathbf{k})} = \frac{9J^2k_1^2}{k^4} S_{\beta\beta}(\mathbf{k})d\mathbf{k} \tag{2.25}$$

The variance of a process is equal to the integral of its spectrum over the entire wave number domain. Therefore,

$$\sigma_h^2 = \int_{\mathbf{k}} \frac{9J^2k_1^2}{k^4} S_{\beta\beta}(\mathbf{k})d\mathbf{k} \tag{2.26}$$

Four autocovariance/spectrum pairs can be chosen to represent the statistical properties of the logaperture process. The first is based on the exponential decline of correlation with lag. This exponential function is

$$R_{\beta\beta}(\xi) = \sigma_\beta^2 \exp\left[-(\xi/\lambda)\right] \tag{2.27}$$

where σ_β^2 is the variance of the logaperture process and λ_1 and λ_2 are the correlation scales in the directions of the directions of maximum and minimum correlation respectively. ξ_i is the component of lag vector in the direction of λ_i .

and $$\frac{\xi}{\lambda} = \left(\frac{\xi_1^2}{\lambda_1^2} + \frac{\xi_2^2}{\lambda_2^2}\right)^{1/2}$$

The spectrum for this covariance is

$$S_{\beta\beta}(\mathbf{k}) = \frac{\sigma_\beta^2 \lambda_1 \lambda_2}{2\pi(1+\lambda_1^2 k_1^2 + \lambda_2^2 k_2^2)^{3/2}} \tag{2.28}$$

where k_i is the component of lag vector in the direction of λ_i .

This pair of functions is attractive because of the simplicity of the exponential function, and in particular its monotonic decline in correlation with distance. Fig.2.17 shows the relationship between the orientation of correlation structure with respect to mean hydraulic gradient. Iwano (1990) found that the covariance functions of simulated apertures using three 50 cm JRC profiles became negative and approached zero from below. Hence, the simple negative exponential covariance function is not appropriate to represent the correlation structure of fracture aperture. On the other hand, Mizell et al. (1982) found that using the exponential covariance or the ordinary Whittle covariance for the perturbation of the log-transmissivity led to an infinite head variance and using the Whittle A or B led to a finite head variance. As might be expected, the same results occur here. Therefore the Whittle A or B is appropriate to represent the correlation structure of logaperture process. The Whittle A and B covariance functions are, respectively,

$$R_{(A)\beta\beta}(\xi) = \sigma_\beta^2\left[\left(\frac{\pi\xi}{4\lambda}\right)K_1\left(\frac{\pi\xi}{4\lambda}\right) - \frac{1}{2}\left(\frac{\pi\xi}{4\lambda}\right)^2 K_0\left(\frac{\pi\xi}{4\lambda}\right)\right] \tag{2.29}$$

and

$$R_{(B)\beta\beta}(\xi) = \sigma_\beta^2\left\{\left[1 + \frac{1}{8}\left(\frac{3\pi\xi}{16\lambda}\right)^2\right]\left(\frac{3\pi\xi}{16\lambda}\right)K_1\left(\frac{3\pi\xi}{16\lambda}\right) - \left(\frac{3\pi\xi}{16\lambda}\right)^2 K_0\left(\frac{3\pi\xi}{16\lambda}\right)\right\} \tag{2.30}$$

where K_0 is the zero order modified Bessel function and K_1 is the first order modified Bessel function.

The corresponding Whittle A and B spectra are, respectively,

$$S_{(A)\beta\beta}(\mathbf{k}) = \frac{2\sigma_\beta^2\eta^2\lambda_1\lambda_2\left(\lambda_1^2k_1^2+\lambda_2^2k_2^2\right)}{\pi(\eta^2+\lambda_1^2k_1^2+\lambda_2^2k_2^2)^3}, \quad \eta = \frac{\pi}{4} \tag{2.31}$$

and

$$S_{(B)\beta\beta}(\mathbf{k}) = \frac{3\sigma_\beta^2\eta^2\lambda_1\lambda_2\left(\lambda_1^2k_1^2+\lambda_2^2k_2^2\right)^2}{\pi(\eta^2+\lambda_1^2k_1^2+\lambda_2^2k_2^2)^4}, \quad \eta = \frac{3\pi}{16} \tag{2.32}$$

The head variance resulting from the Whittle A and B spectrum for β are, respectively,

$$\sigma_{(A)h}^2 = \frac{9J^2\lambda_1\lambda_2}{2\eta^2}\sigma_\beta^2, \quad \eta = \pi/4 \tag{2.33}$$

and

$$\sigma_{(B)h}^2 = \frac{9J^2\lambda_1\lambda_2}{4\eta^2}\sigma_\beta^2, \quad \eta = 3\pi/16 \tag{2.34}$$

For the isotropic case ($\lambda_1 = \lambda_2 = \lambda$), these results are exactly what Mizell et al. (1982) found, except for the factor of 9.

2) Effective aperture and equivalent permeability tensor

The effective aperture for flux is the equivalent homogeneous aperture which produces the same flux as the mean flux in the heterogeneous aperture system. The mean flux in the direction of x_i is

$$\overline{Q_i} = \overline{bu_i} = -\frac{g}{12\nu}\overline{b^3\frac{\partial\phi}{\partial x_i}} = -\frac{g}{12\nu}b_l^3\overline{e^{3\beta}\frac{\partial(H+h)}{\partial x_i}}\ ,\ b_l = e^B \tag{2.35}$$

Expanding the exponential into its Taylor series, retaining terms to second order in the perturbations and noting that

$$\overline{\beta^2} = \sigma_\beta^2 \tag{2.36}$$

give the second-order approximation as follows

$$\overline{Q_i} = -\frac{g}{12\nu}b_l^3\left[\left(1+\frac{9}{2}\sigma_\beta^2\right)J_i - 3E\left(\beta\frac{\partial h}{\partial x_i}\right)\right],\ b_l = e^B \tag{2.37}$$

The last term in this equation reflects the correlation between the aperture perturbation and the resulting head perturbation. This term can be evaluated by solving for the head perturbation in terms of the aperture perturbation as shown in Eq.2.20. Using Eq.2.21 and Eq.2.24, one obtains the following.

$$E\left[\beta\frac{\partial h}{\partial x_i}\right] = \int_{\mathbf{k}} E\left[dZ_\beta(\mathbf{k})\bullet(-ik_i)dZ_h(\mathbf{k})\right]d\mathbf{k} = \int_{\mathbf{k}} 3J_j\frac{k_jk_i}{k^2}S_{\beta\beta}(\mathbf{k})d\mathbf{k} \tag{2.38}$$

Therefore the mean flow is given by

$$\overline{Q_i} = \frac{g}{12\nu}b_l^3\left[\left(1+\frac{9}{2}\sigma_\beta^2\right)J_j\delta_{ij} - 9J_j\int_{\mathbf{k}}\frac{k_ik_j}{k^2}S_{\beta\beta}(\mathbf{k})\,d\mathbf{k}\right] = \frac{g}{12\nu}B_{ij}J_j = K_{ij}J_j \tag{2.39}$$

where

$$B_{ij} = b_l^3\left[\left(1+\frac{9}{2}\sigma_\beta^2\right)\delta_{ij} - 9\int_{\mathbf{k}}\frac{k_ik_j}{k^2}S_{\beta\beta}(\mathbf{k})\,d\mathbf{k}\right] : \text{Effective Aperture Cubed Tensor} \tag{2.40}$$

K_{ij} : Equivalent Hydraulic Conductivity Tensor

δ_{ij} : the Kronecker delta

For the exponential spectrum,

$$B_{11} = b_l^3\left\{1 + \sigma_\beta^2\left[\frac{9}{2} - 9\left(\frac{\rho\sin^2\alpha + \cos^2\alpha}{\rho + 1}\right)\right]\right\} \tag{2.41}$$

$$B_{22} = b_l^3\left\{1 + \sigma_\beta^2\left[\frac{9}{2} - 9\left(\frac{\rho\cos^2\alpha + \sin^2\alpha}{\rho + 1}\right)\right]\right\} \tag{2.42}$$

$$B_{12} = B_{21} = 9b_l^3\sigma_\beta^2\left(\frac{\rho - 1}{\rho + 1}\right)\sin\alpha\cos\alpha \tag{2.43}$$

and

$$K_{11} = \frac{g}{12\nu}b_l^3\left\{1 + \sigma_\beta^2\left[\frac{9}{2} - 9\left(\frac{\rho\sin^2\alpha + \cos^2\alpha}{\rho + 1}\right)\right]\right\} \tag{2.44}$$

$$K_{22} = \frac{g}{12\nu}b_l^3\left\{1 + \sigma_\beta^2\left[\frac{9}{2} - 9\left(\frac{\rho\cos^2\alpha + \sin^2\alpha}{\rho + 1}\right)\right]\right\} \tag{2.45}$$

$$K_{12} = K_{21} = \frac{9g}{12\nu}b_l^3\sigma_\beta^2\left(\frac{\rho - 1}{\rho + 1}\right)\sin\alpha\cos\alpha \tag{2.46}$$

where α is the angle between the mean hydraulic gradient and the maximum correlation scale direction and ρ is the ratio of the maximum and minimum correlation length as follows.

$$\rho = \frac{\lambda_1}{\lambda_2}$$

λ_i is the correlation scale for the two-dimensional statistically anisotropic process and indicates the average distance over which the logaperture is correlated.

$$\lambda = \int_0^\infty \frac{R_{\beta\beta}(\xi)}{\sigma_\beta^2}d\xi \tag{2.47}$$

Knowing the value of K_{11}, K_{12} and K_{22}, the values and directions of the principal hydraulic conductivity can be calculated with standard techniques of eigen value problem. The eigen value equation is

$$\Omega^2 - (K_{11} + K_{22})\,\Omega + K_{11}K_{22} - K_{12}^2 = 0 \tag{2.48}$$

So the principal hydraulic conductivities are

$$K_{max} = \Omega_1 = \frac{K_{11} + K_{22}}{2} + \frac{\sqrt{(K_{11} + K_{22})^2 - 4\left(K_{11}K_{22} - K_{12}^2\right)}}{2} \tag{2.49}$$

$$K_{min} = \Omega_2 = \frac{K_{11} + K_{22}}{2} - \frac{\sqrt{(K_{11} + K_{22})^2 - 4\left(K_{11}K_{22} - K_{12}^2\right)}}{2} \tag{2.50}$$

and the principal directions, $\mathbf{e_1}$ and $\mathbf{e_2}$, are

$$\mathbf{e}_1 = \left[\frac{K_{12}}{\sqrt{K_{12} + (\Omega_1 - K_{11})^2}}, \frac{\Omega_1 - K_{11}}{\sqrt{K_{12} + (\Omega_1 - K_{11})^2}}\right] \tag{2.51}$$

$$\mathbf{e}_2 = \left[\frac{K_{12}}{\sqrt{K_{12} + (\Omega_2 - K_{11})^2}}, \frac{\Omega_2 - K_{11}}{\sqrt{K_{12} + (\Omega_2 - K_{11})^2}}\right] \tag{2.52}$$

The principal directions of this tensor becomes α and $\alpha + \pi/2$.

3) Effective aperture for special cases

The mean flux in the direction of mean hydraulic gradient is

$$\overline{Q_1} = \frac{g}{12\nu} J b_l^3 \left\{1 + \sigma_\beta^2 \left[\frac{9}{2} - 9\left(\frac{\rho \sin^2\alpha + \cos^2\alpha}{\rho + 1}\right)\right]\right\} \tag{2.53}$$

For the special case of an isotropic logaperture autocovariance, $\rho = 1$,

$$\overline{Q_1} = \frac{g}{12\nu} b_l^3 J \tag{2.54}$$

so that the effective aperture is the geometric mean of the aperture process. The same result is had when the variance of logaperture is zero, since the geometric mean is trivially the parallel plate aperture.

When $\alpha = 0$ and $\rho = \infty$, one obtains the equivalent model as Neuzil and Tracy (1981) as shown in Fig.2.18. In this model, the direction of mean hydraulic conductivity is the same as the maximum correlation direction and the aperture is constant in the direction of mean hydraulic gradient. The mean flux in the direction of mean hydraulic gradient is

$$\overline{Q_1} = \frac{b_l^3 g J}{12\nu}\left(1 + \frac{9}{2}\sigma_\beta^2\right) \cong \frac{b_l^3 g J}{12\nu} \exp\left(\frac{9}{2}\sigma_\beta^2\right) \tag{2.55}$$

Therefore the effective aperture in the direction of mean hydraulic gradient is the arithmetic mean of b^3 as follows.

$$\widehat{b^3} = b_l^3 \exp\left(\frac{9}{2}\sigma_\beta^2\right) = \overline{b^3} \tag{2.56}$$

When $\alpha = \pi / 2$ and $\rho = \infty$, we have the equivalent model as Tsang and Witherspoon (1981) as shown in Fig.2.19. This model is the other quasi-two-dimensional model. The mean flux in the direction of mean hydraulic gradient is

$$\overline{Q_l} = \frac{b_l^3 gJ}{12\nu}\left(1 - \frac{9}{2}\sigma_\beta^2\right) \cong \frac{b_l^3 gJ}{12\nu}\exp\left(-\frac{9}{2}\sigma_\beta^2\right) \tag{2.57}$$

In this case, the effective aperture in the direction of mean hydraulic gradient is the harmonic mean of b^3 as follows.

$$\widehat{b^3} = b_l^3 \exp\left(-\frac{9}{2}\sigma_\beta^2\right) = \left[\overline{b^{-3}}\right]^{-1} \tag{2.58}$$

It is demonstrated the versatility of the stochastic model in that the stochastic model presented above can represent a couple of existing models which vary from a simple parallel plate model, the frequency aperture model of Neuzil and Tracy(1981) to the quasi-two-dimensional asperity model of Tsang and Witherspoon(1981).

The advantage of the stochastic model is that only four geometrical parameters, the mean of aperture, the variance of logaperture, the ratio of maximum correlation scale to minimum correlation scale and the angle between the mean hydraulic gradient and the maximum correlation scale direction, are required to express the anisotropic conductivity tensor in a joint plane. It can be implemented into existing joint system models like a discrete fracture network model or channel network model with taking in-plane anisotropy of joint conductivity into account.

The fundamental disadvantage of the stochastic model is that aperture distribution must obey the log-normal distribution. The other critical disadvantage is how to deal with contact areas in a rough-walled joint and how to modify the aperture distribution and its correlation structure when a joint is subjected to stress. Therefore the combinations of the stochastic model for flow and the mechanical model for joint deformation is recommended to represent a real joint behavior.

2.6 Summary and Discussion

To observe and characterize the geometrical properties of joint aperture, several methods have been developed. Any of these techniques has advantages and disadvantages. Thus no technique has yet been developed which can provide not only complete descriptions but also general conclusions regarding the aperture variation of a single joint. The applicability of each techniques depends on the type joint, the scale of the measurement and the aim of the investigation.

One promising method to overcome the disadvantages of surface topography approach is the probabilistic approach since the difficulty in this approach lies in matching of profiles. Roberds(1979) presented a unified systematic approach to the deterministic, statistical and probabilistic description of joint surfaces. In his method, joint surface geometry can be described deterministically, statistically and probabilistically using the same systematic approach. This is didactically interesting and also important when one wants to go from one description to the other. Particular emphasis related to this study is placed on the probabilistic approach which described the procedure to derive the statistical properties of the local apertures, which are defined as the distance between the two opposing surfaces at any points in a fracture, from the statistical properties of each opposing surfaces. Thus his method allows one to capture surface characteristics and their correlations within a single surface and between two surfaces. Such capabilities are advantageous when modeling the interaction of the joint surfaces be this in form of relative normal and shear displacement, fluid flow through the open space between the surfaces or coupled mechanics. Roberds et al.(1990) also mentioned the relations of probabilistic approach to other geometric models and the incorporation into solid and fluid mechanical models.

In fact, the amount of data on joint aperture is too limited to yield the general characteristics on the geometrical properties of joint apertures or to distinguish the differences in these properties between joints in different rock types. Also, the effects of heterogeneity and anisotropy of aperture variation on flow in a joint are not well established. The geometry of void space and contact area between two opposing joint surfaces, namely both of the variation and the correlation of joint aperture, may be important in describing the channeling nature of flow in a joint, which is clearly described by existing experimental, analytical and numerical researches. But one needs to examine not only additional cases with actual spatial variation and correlation of apertures to make the numerical generation of heterogeneous joint apertures more realistic, but also the simulation techniques for multidimensional numerical generation of joint apertures since

in-situ joints may have more spatial heterogeneity and more complex correlation structure in their aperture distributions than those observed in the laboratory.

A variety of the multidimensional simulation techniques have been proposed in the various field. The reader is referred to Mantoglou and Wilson (1981) for discussion on these techniques and a list of references. For example, two multi-dimensional simulation methods proposed by Media and Rodrigue-Iturbe (1974) and Shinozuka and Jan (1972). In both methods each simulated point value of the field is calculated by the superposition of a series of cosine functions. In the first method (Media and Rodriguez-Iturbe, 1974), the cosine functions have the same amplitude and random frequency vectors are sampled from the spectral density function of the process, while in the second method (Shinozuka and Jan, 1972), the cosine functions have weighted amplitudes and evenly spaced frequencies. In other words, both of them are based on the representation of random process as a weighted integral of the spectral density function of the process. They, however, differ in that the method of Media and Rodriguez-Iturbe is based on random sampling from the spectral density function, while the method by Shinozuka and Jan is based on the discretization of the spectral density function. In the simulation models, it is assumed that the statistical characteristics of the random fields, such as mean, variance and covariance function, are known. The simulation models use those characteristics and the obtained realization should preserve those statistics. Mantoglou and Wilson (1981) closely compared these two simulation methods with the turning bands method (TBM) in term of the cost and efficiency. Turning bands method (TBM) was first developed in a strict mathematical format by Matheron (1973) to generate a realization of a stationary correlated multi-dimensional random field from a normal distribution with zero mean and a specified covariance structure. Mantoglou and Wilson (1981) discussed in detail the use of a two dimensional simulator for hydrologic problem. Montoglou (1987) has extended the three dimensional algorithm for use in simulating anisotropic or cross-correlated fields. More recently, Tompson, Ababou and Gelhar (1989) provided some recommendation of the three dimensional algorithm.

Mantoglou and Wilson (1981) found that the cost of the turning bands method increases with the square root of the number of simulated points, while with above-mentioned two methods, the cost is proportional to the number of generated point values. They also concluded that the turning bands method is most efficient among three methods. Therefore, for recommendation, one had better adopt the turning bands method to generate the two dimensional aperture process in a single fracture.

From reviews on conductivity variation with pressure in rocks and rock joints and stress-flow models for a single joint, one of the main purposes of existing researches is to

postulate the behavior of joints, in particular joint aperture distributions, as they change when joints are subjected to different conditions of stress. Combined with the modified Poiseuille equation, it is then possible to relate changes in flow rate to changes in the mean apertures of joints. A simple model of aperture change in a joint under changing compressive stress and pore pressure is presented by Neuzil and Tracy, as shown in Fig.2.20. For external compression, which is illustrated in Fig.2.20(a), a change of stress normal to the joint will result in a reversible change of aperture at any location which is proportional to the original aperture at that location according to the model. This is a simplification of a complex process. It does not account for the crushing of asperities or the creation of new points of contact. However, the model should reasonably approximate changes in aperture between points of contact once it is established. For internal extension (Fig.2.20(b)), which can occur when internal pore pressure is increased, joint surfaces are moved apart and no deformation of the surfaces takes place. As the joint aperture increases, the unevenness of the surfaces become less relative to the opening. These simplification seems reasonable for the modeling a single joint behavior for ordinal investigations relating to rock mechanics. Further complicated models does exist and can be established, but the applicability of each models depend on the type of joint, the scale of the measurement, the level of applied stress and the aim of the investigation.

It was demonstrated that stochastic model developed by Brown(1984) was versatile. The advantage of the stochastic model is that only four geometrical parameters, the mean of aperture, the variance of logaperture, the ratio of maximum correlation scale to minimum correlation scale and the angle between the mean hydraulic gradient and the maximum correlation scale direction, are required to express the anisotropic conductivity tensor in a joint plane. It can be implemented into existing joint system models like a discrete fracture network model or channel network model with taking in-plane anisotropy of joint conductivity into account. The critical disadvantage is how to deal with contact areas in a rough-walled joint and how to modify the aperture distribution and its correlation structure when a joint is subjected to stress. Therefore the combinations of the stochastic model for flow and the mechanical model for joint deformation is recommended to represent a real joint behavior. These modeling can be possible and seems promising if one needs to deal with very large scale problem.

In the field, the stochastic nature of variable joint aperture is more complicated than one expects. Field evidences indicate that the bulk of water flow in jointed crystalline rock often occurs in preferred flow paths or channels. A theoretical approach was proposed by Tsang and Tsang (1987) to interpret flow and transport through a two or three dimensional jointed medium in terms of system of statistically equivalent one dimensional channels.

Tsang et al. (1988) suggested that both tracer breakthrough measurements and flow rate measurements were needed to obtain the aperture parameters of the flow system since the hydraulic conductivity measurements alone were controlled by the small constrictions along the flow paths and therefore did not yield a good measure of the mean aperture in channel. Moreno et al. (1990) used statistical model fractures with variable apertures to study the impact of the use of different injection flow rates and the different locations of injection and collection pints. Their results showed that the transport time, dispersion, and so-called mass balance joint aperture were very sensitive to the location of the injection point and the injection flow rate. They concluded that a point tracer test in a fracture was not sufficient to characterize the properties of the joint because of the stochastic nature of variable joint apertures and their hydraulic conductivities. They suggested that a line injection of tracer (multiple point injection on a line at a constant injection pressure) might avoid some of these problems and the line length should be of the order of 2 or 3 correlation lengths of a joint. This meant that the averaged variations, so that results were no longer sensitive to local effects, and interpretable results could be obtained.

Table 2.1 Friction laws for one-dimensional fissure percolation

Conditions	Friction Laws	acc. to	Remarks
hydraulically smooth	$\lambda = \frac{96}{Re}$	Poiseuille	laminar - A
	$\lambda = 0.316\ Re^{-1/4}$	Blasius	turbulent - C
completely rough $k/Dh \leq 0.032$	$\frac{1}{\sqrt{\lambda}} = -2 \log \frac{k/D_h}{3.7}$	Nikuradse	turbulent - D
non-parallel $k/Dh > 0.032$	$\lambda = \frac{96}{Re}\ [1+8.8(k/D_h)^{1.5}]$	Louis	laminar - B
	$\frac{1}{\sqrt{\lambda}} = -2 \log \frac{k/D_h}{1.9}$	Louis	turbulent - E

k : average wall roughness
D_h : hydraulic diameter
Re : Reynolds number

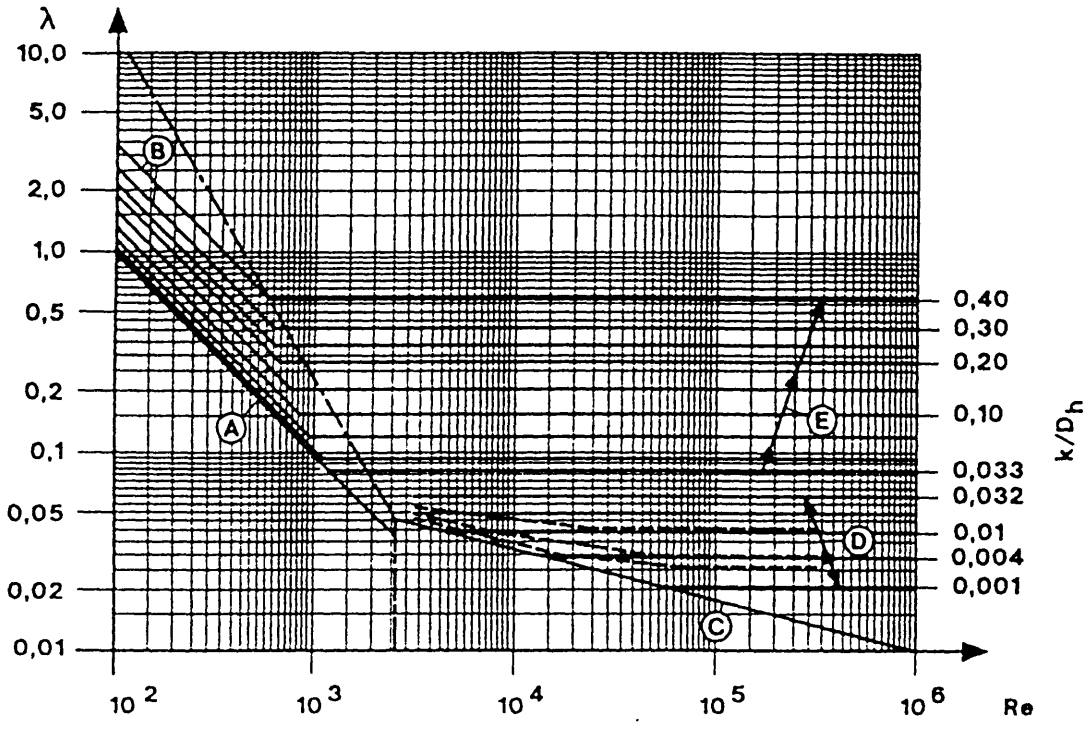

Fig. 2.1 Friction laws for one-dimensional fissure percolation (after Rißler, 1991)

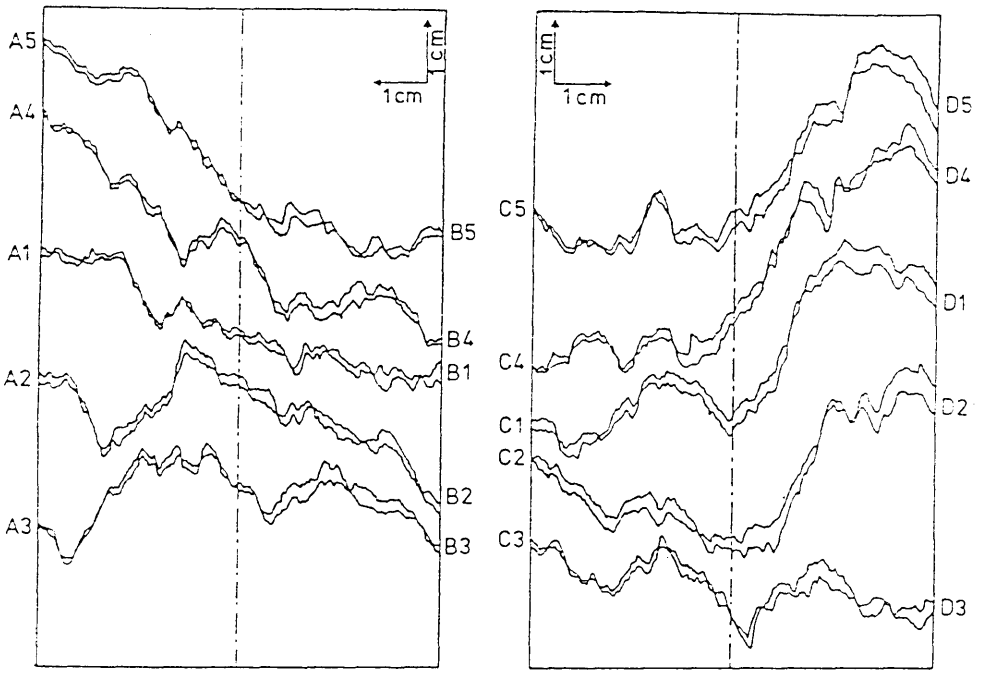

Fig. 2.2 10 sets of surface roughness profiles of granite fractures (after Gentier, 1986)

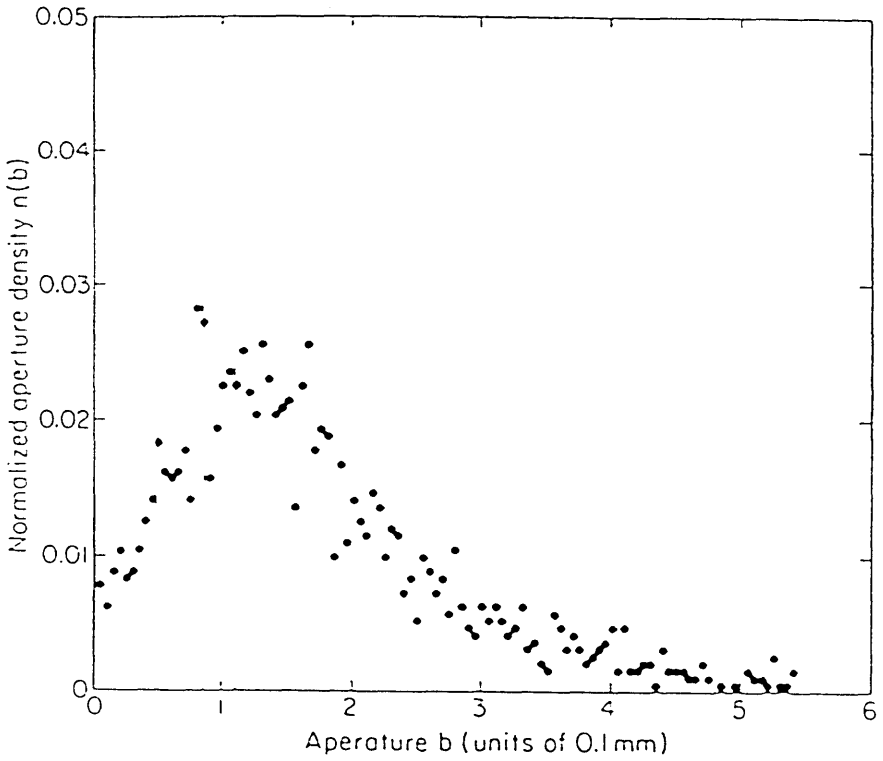

Fig. 2.3 Aperture distribution derived from 10 sets of surface roughness profiles of granite fractures (after Gentier, 1986)

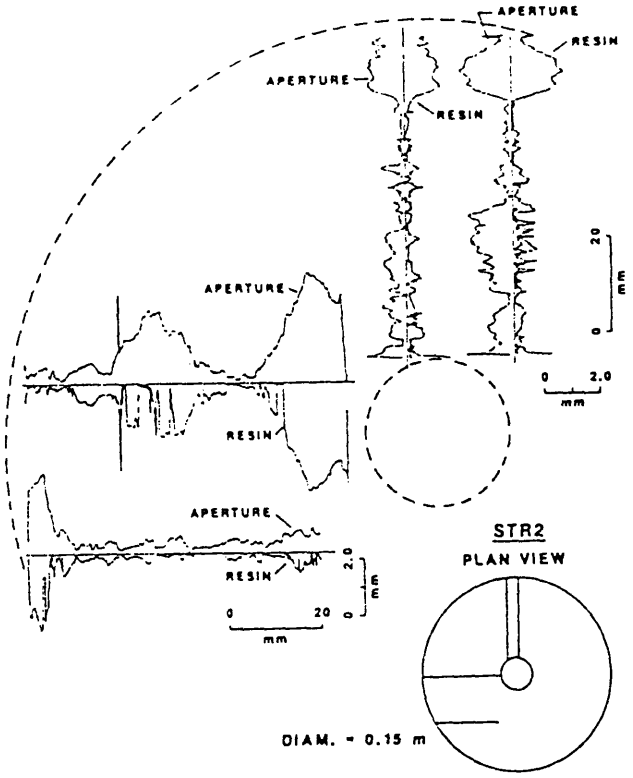

Fig. 2.4 Distribution of pore space along four profiles in STR2 (after Gale, 1987)

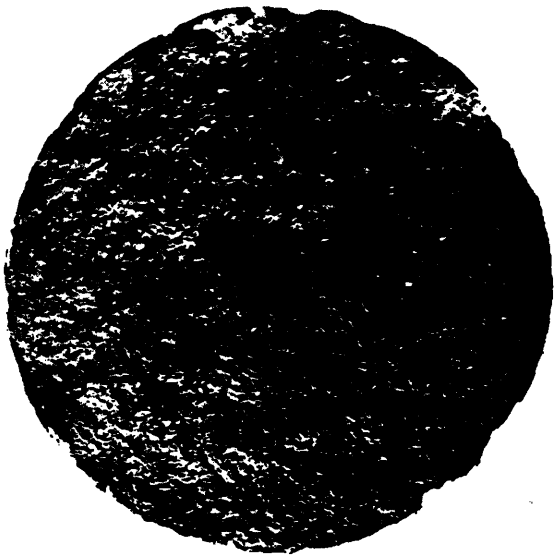

Fig. 2.5 Grey-level pixel map of a cast in a granite (after Gentier, Billaux and Vilet, 1989)

(a) Generated aperture disribution

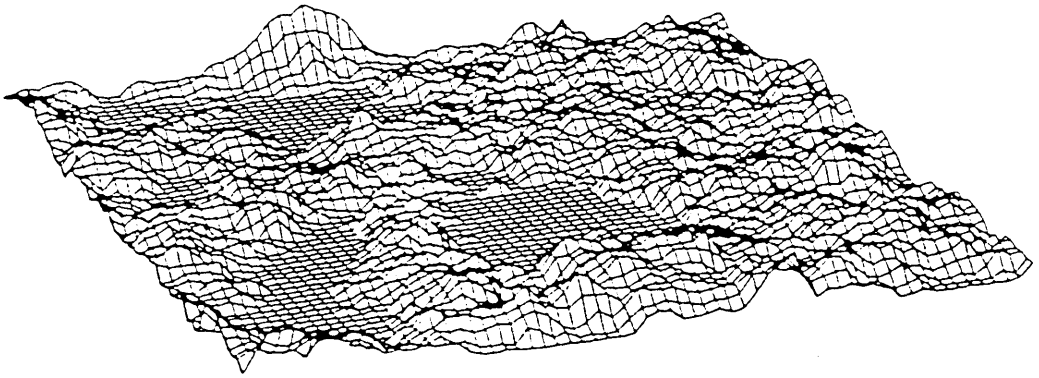

(b) Flow field resulting the finite difference analysis

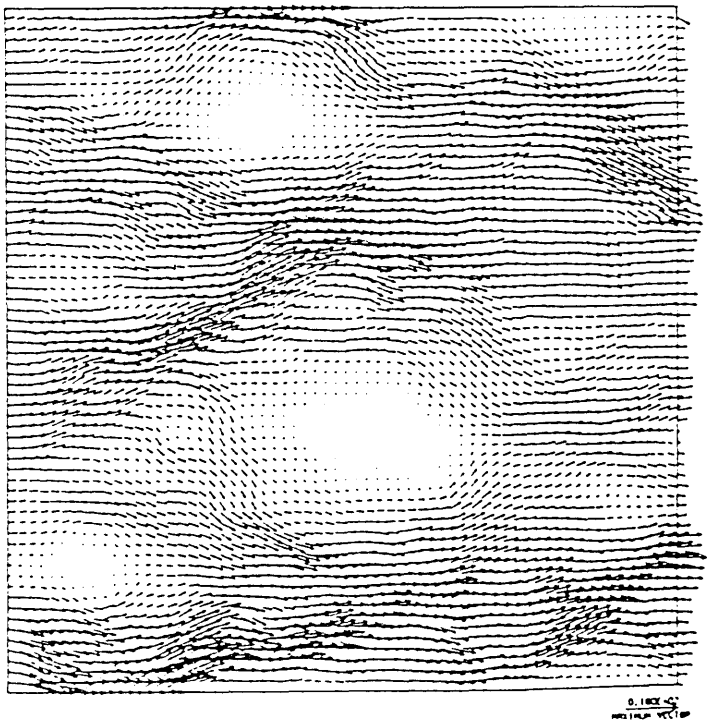

Fig. 2.6 Generated aperture distribution fromed by placing two fractal surfaces and its flow field (after Brown, 1987)

(a) Variation of in situ permeability (after Brace, 1984)

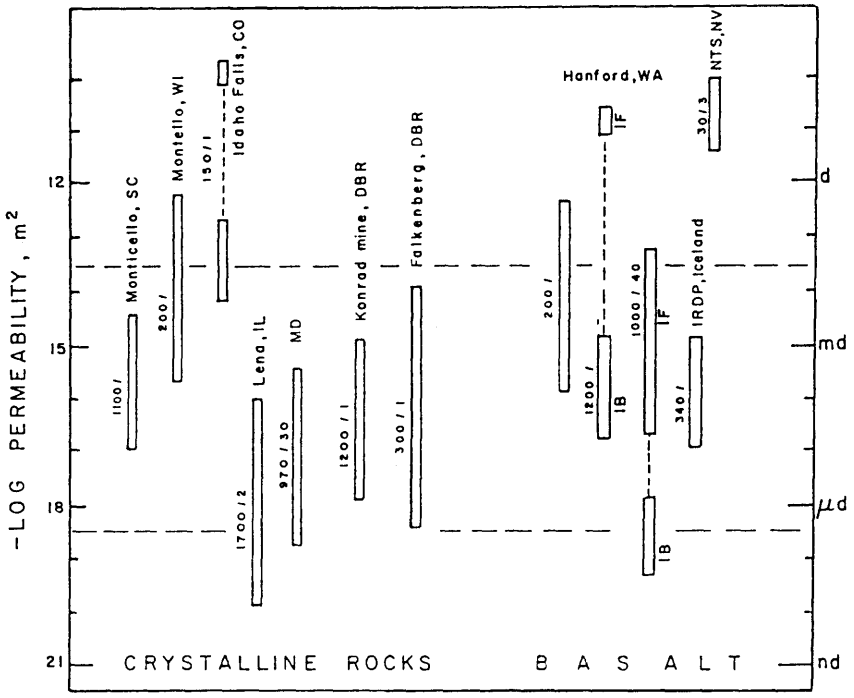

(b) Permeability of crystalline rocks and craracteric scale of measurement (after Clauser, 1992)

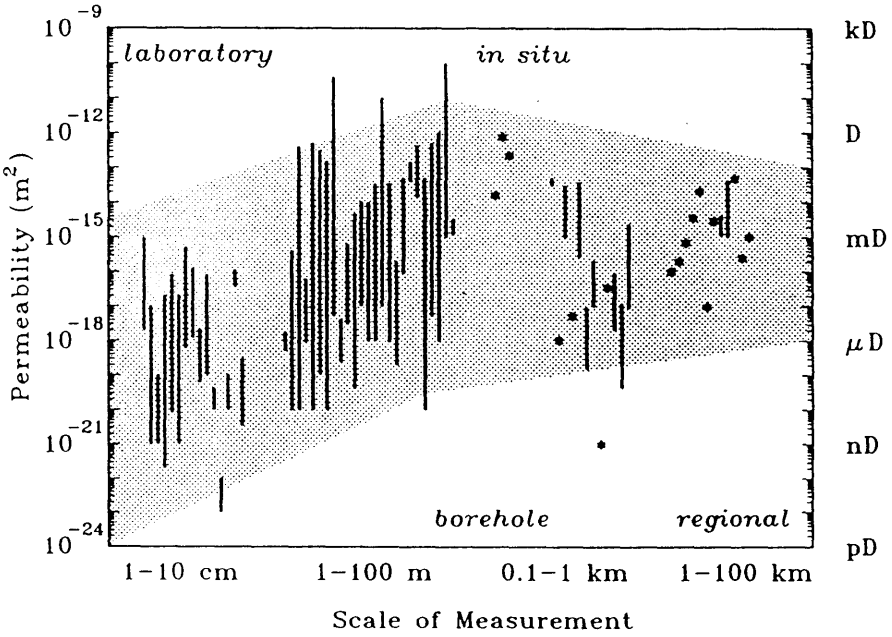

Fig. 2.7 Variation of permeability of rocks

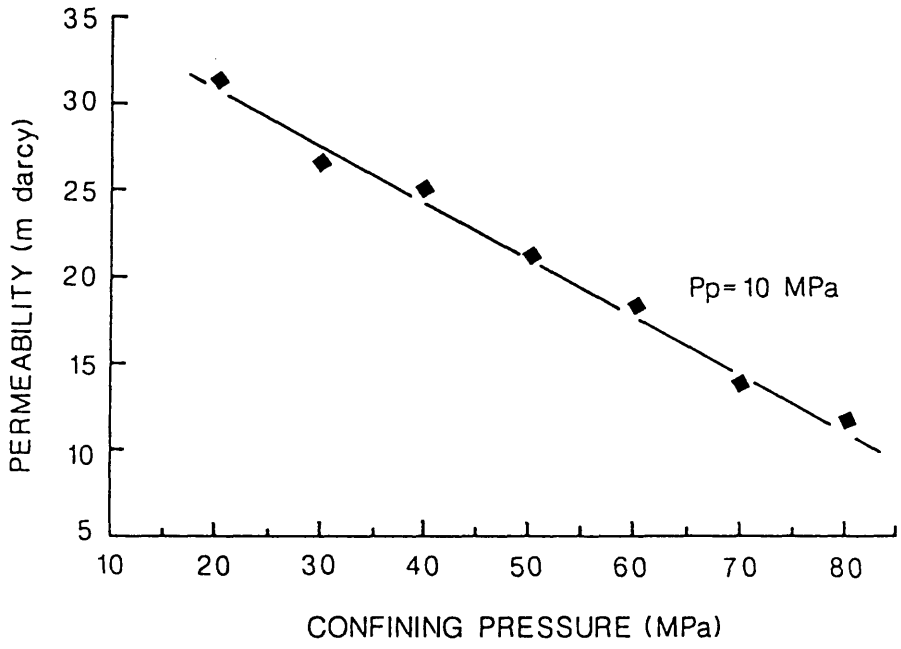

Fig. 2.8 Variation of permeability with confining pressure for Fontainebleau sandstone with isotropic pore (after David and Darot, 1989)

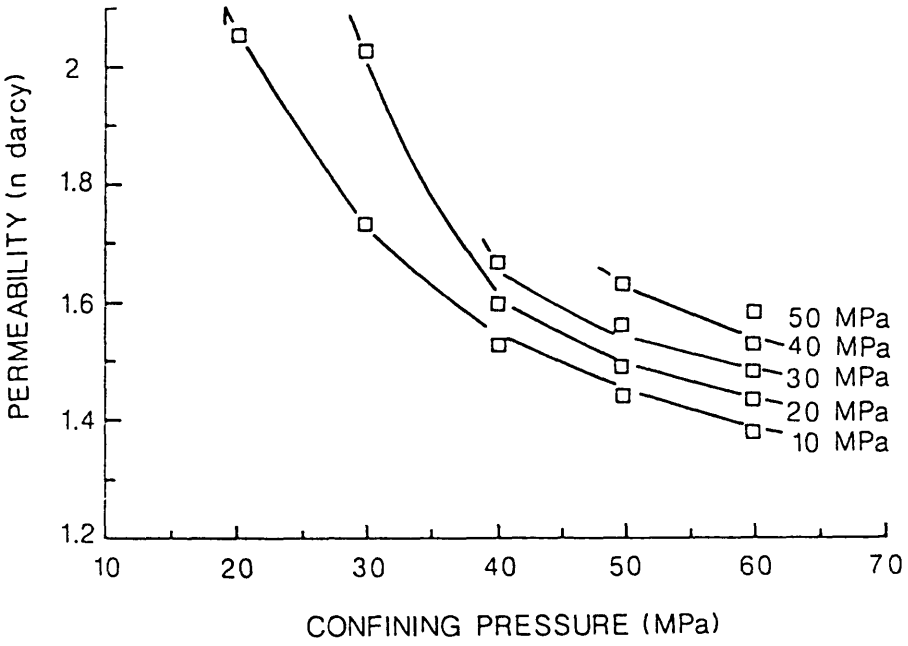

Fig. 2.9 Variation of permeability with confining pressure for Fontainebleau sandstone with isotropic pore and crack porosity (after David and Darot, 1989)

(a) Chelmsford granite

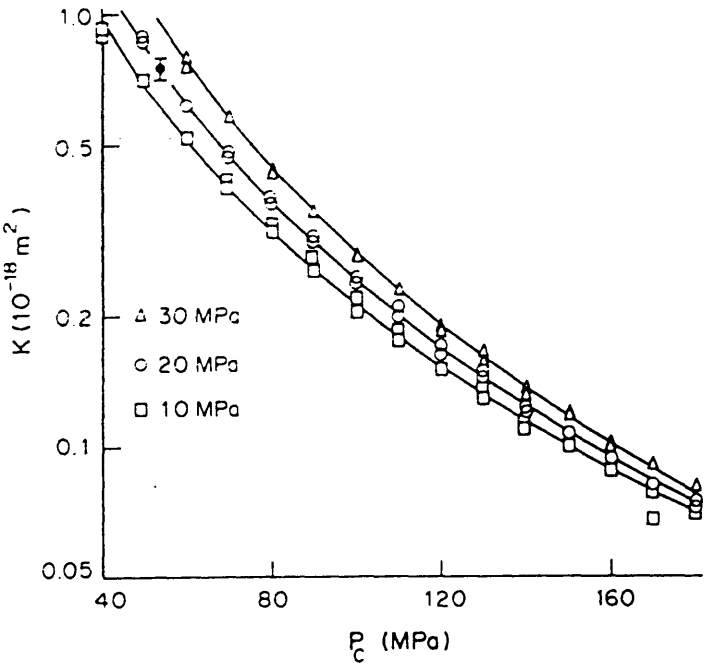

(b) Barre granite

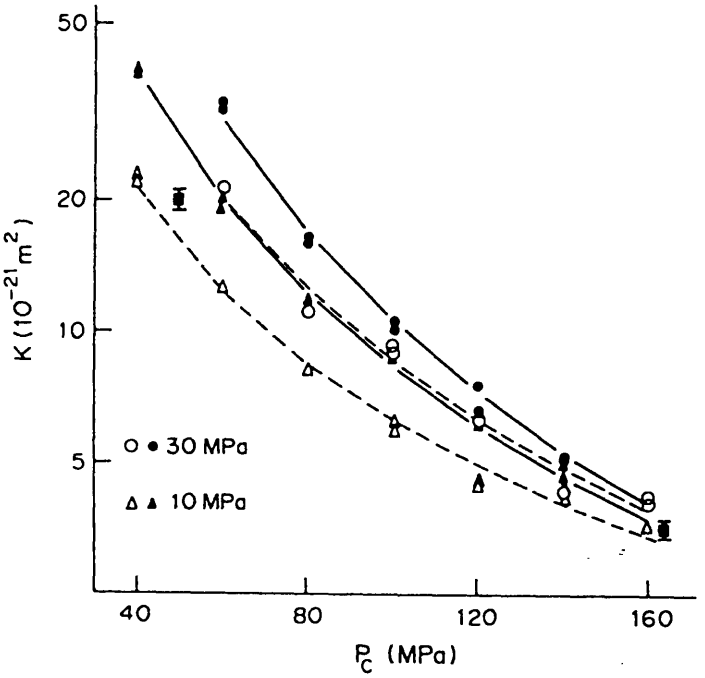

Fig. 2.10 Variation of permeability with confining pressure for Chelmsford granite and Barre granite with crack porosity

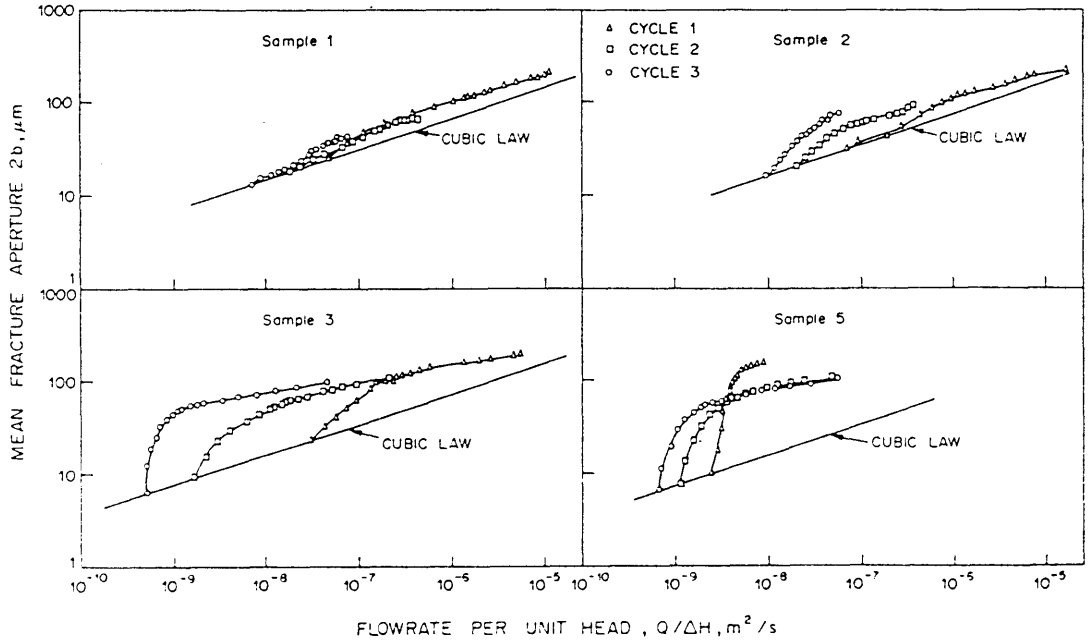

Fig. 2.11 Discrepancy between experimental results and theory of cubic law (after Raven and Gale, 1985)

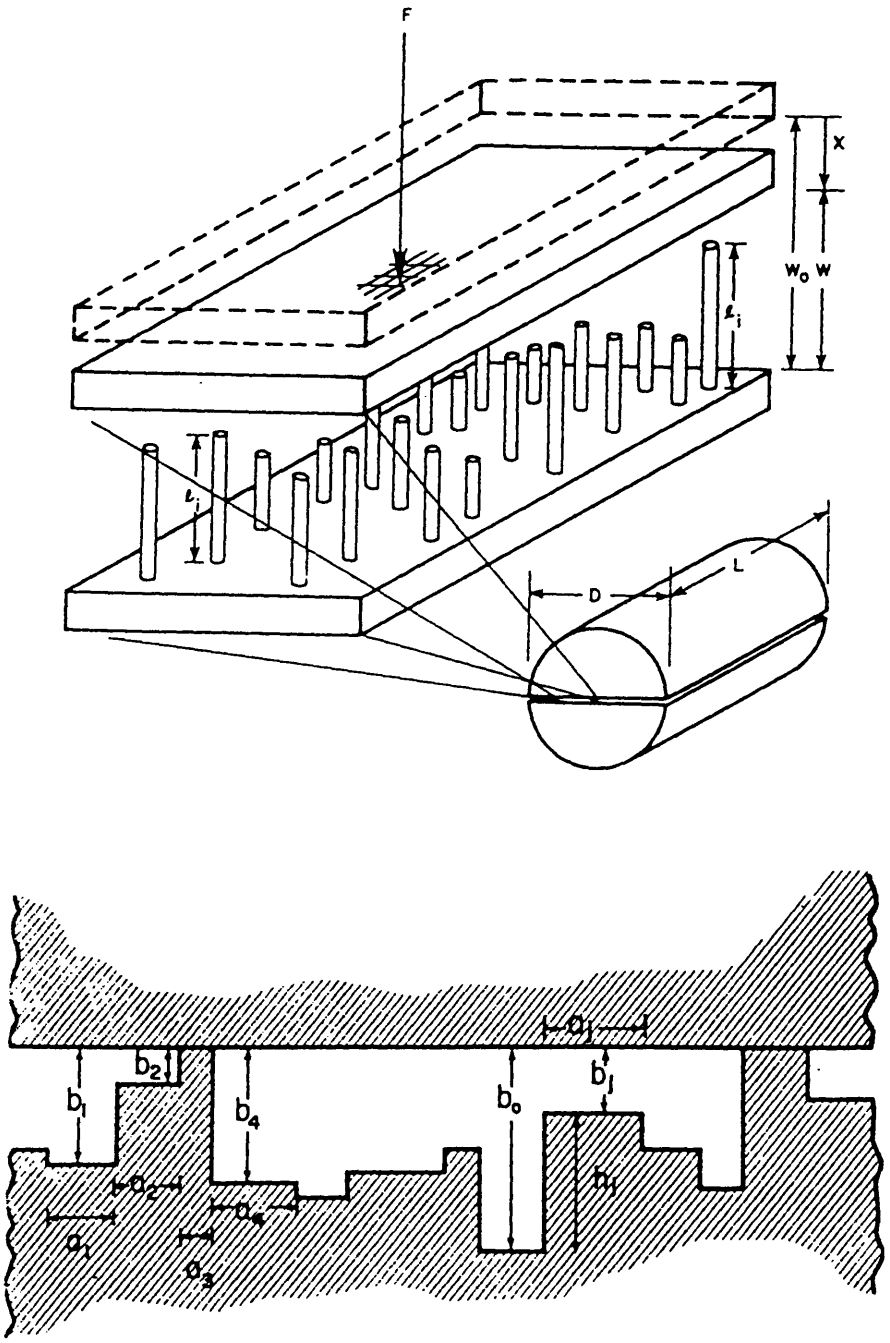

Fig. 2.12 Schematic representation of a joint by beds of nails model (after Gangi, 1978)

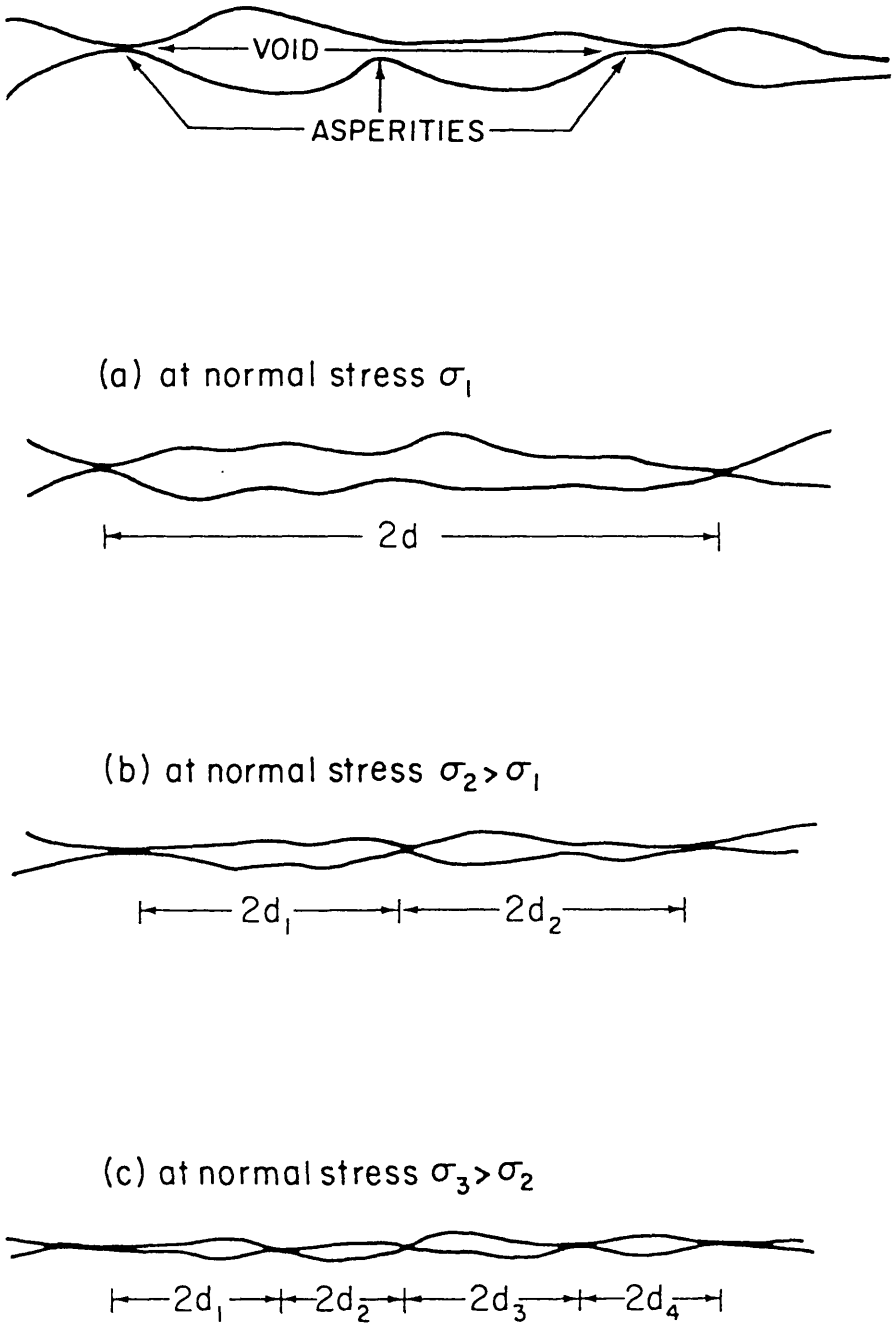

Fig. 2.13 Schematic representation of a joint by void and asperity model (after Tsang and Witherspoon, 1981)

(a) Unit Herzian contact between a plane and hemi-spherical peak

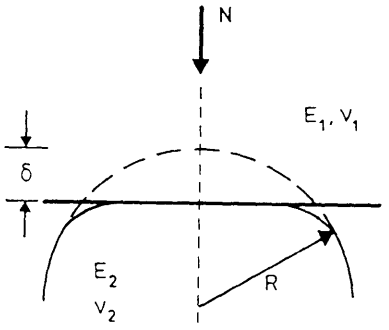

(b) Schematic of a half-joint contact

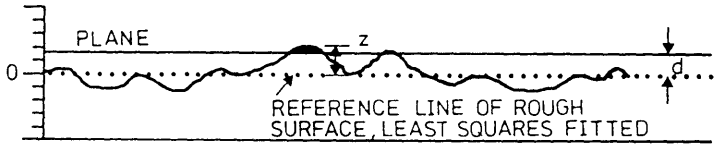

Fig. 2.14 Schematic representation of a half joint model (after Swan, 1983)

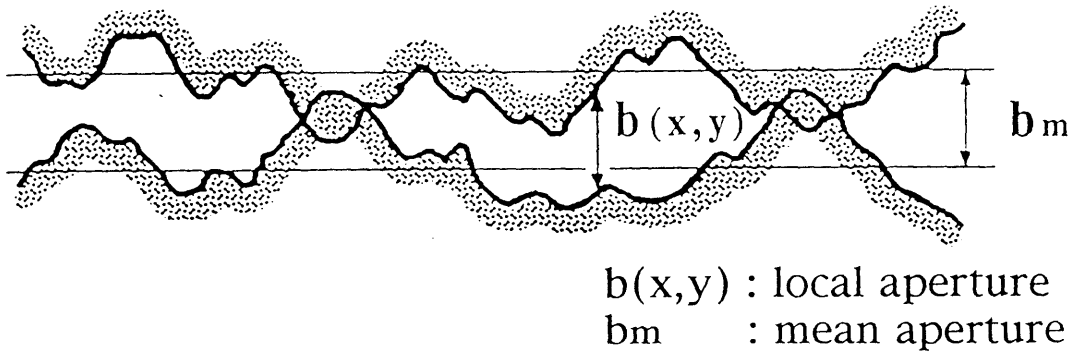

Fig. 2.15 Definition of aperture

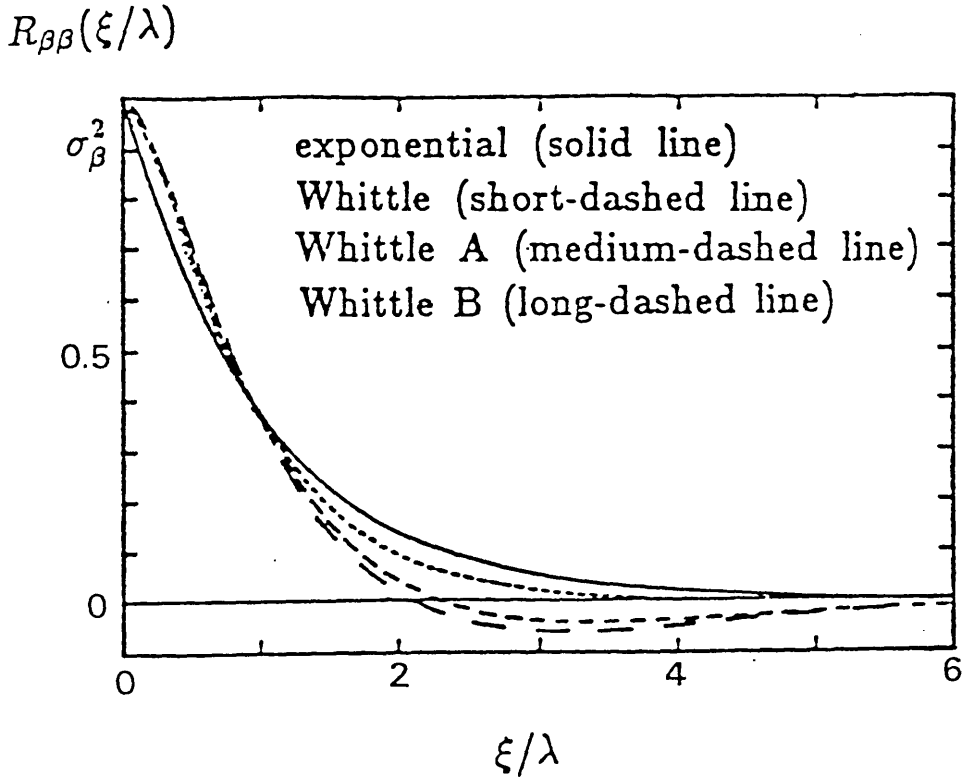

Fig. 2.16 Autocovariance functions used for stochastic model (after Brown, 1984)

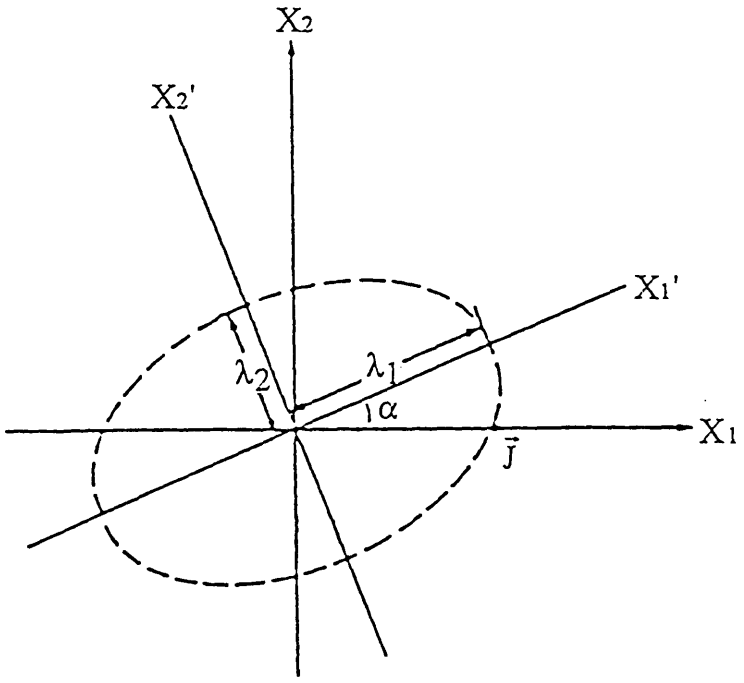

Fig. 2.17 Orientation of correlation structure with respect to mean hydraulic gradient (after Brown, 1984)

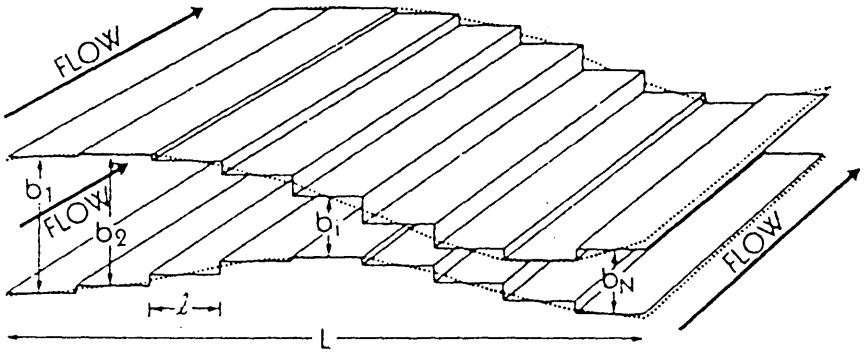

Fig. 2.18 Aperture frequency model
(after Neuzil and Tracy, 1981)

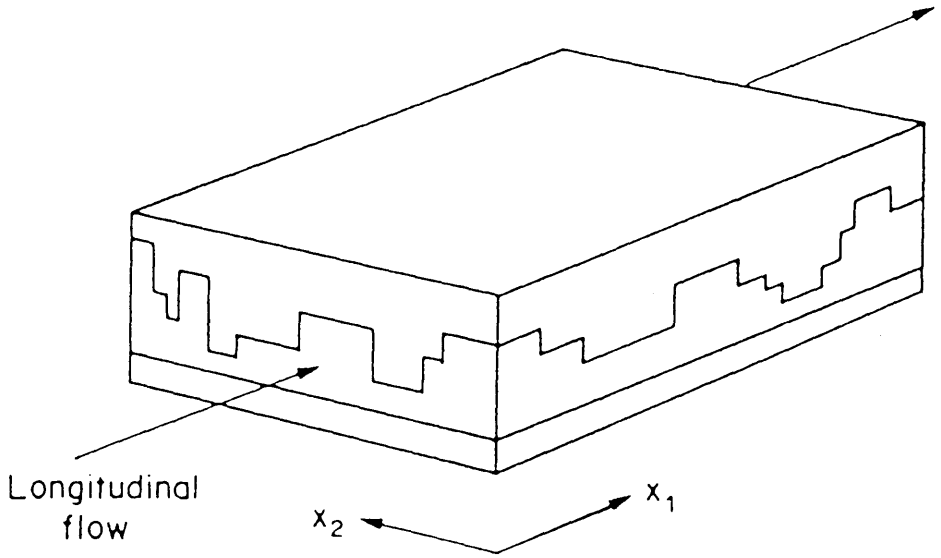

Fig. 2.19 Void and asperity model
(after Elsworth and Goodman, 1986)

(a) Compressional deformation

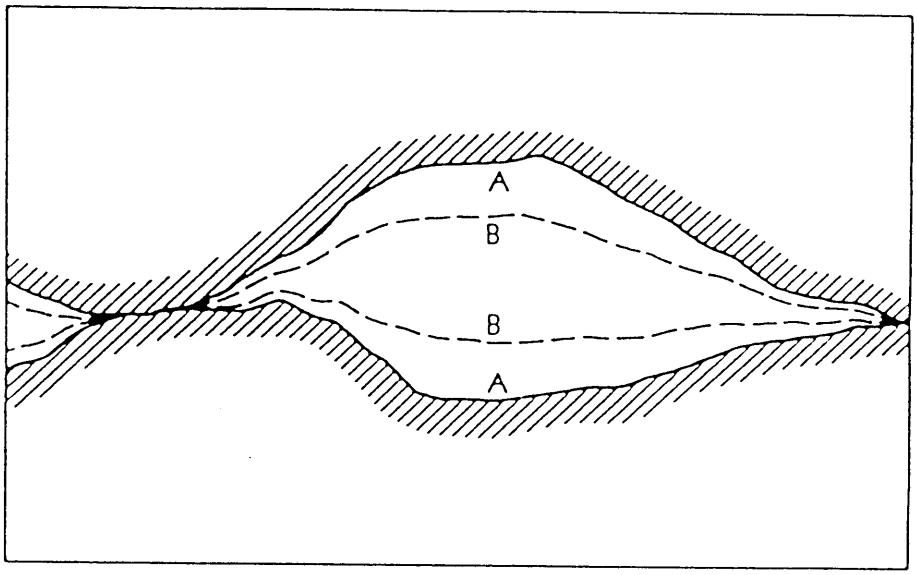

(b) Extensional deformation

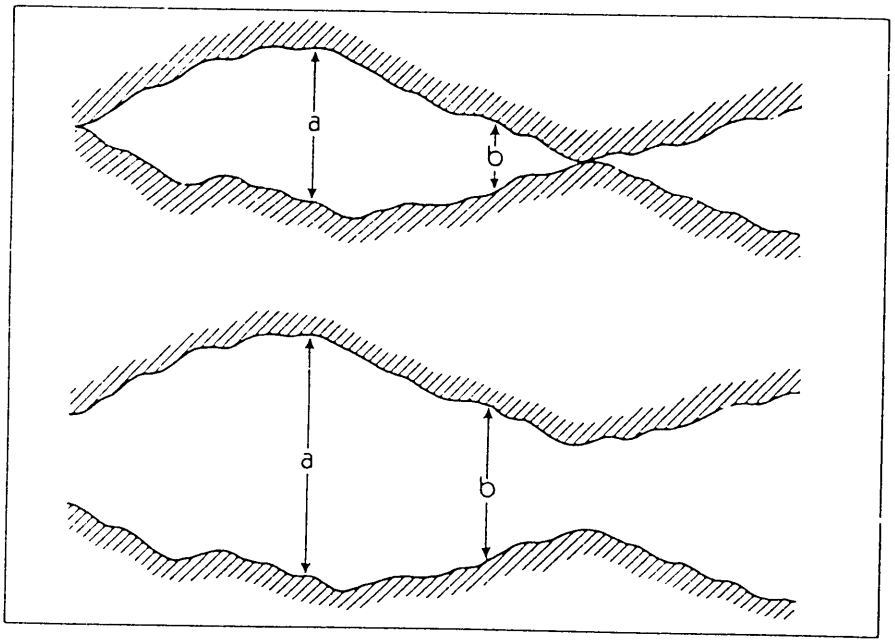

Fig.2.20 Model of aperture change due to compression and extension (after Neuzil and Tracy, 1981)

Chapter 3 Geometrical Property in a Single Joint

3.1 Introductory remarks

The measurement and description of surface roughness of materials has been extensively studied in the field of tribology. Thomas(1982) presents a complete review of surface roughness measurement. There are many surface roughness standards which have been developed from different applications and Thomas(1982) describes more than 20 of these standards such as the root-mean-square, the variances of height, slope and curvature and so on. In the field of rock mechanics, direct physical evidences for the influence of joint surface properties on the mechanical properties of joints such as the strength and deformability were obtained by Jaeger(1959), Patton(1966) and Barton(1971). These show that the mechanical properties of joints are highly dependent on joint surface characteristics such as surface roughness and wall strength and numerous investigations have been carried out to develop the methods of quantifying the influence of surface properties. Among them, extensive test series have been carried out by Barton and Choubey(1976), Barton(1977), Barton and Bandis(1980), Bandis et al.(1981, 1983), they developed the empirical method of quantifying surface roughness and wall strength and utilized them in shear strength, deformation and conductivity coupling relationship for joints (Barton et al., 1985 and Barton, 1986).

On the other hand, aperture variation and correlation may be important in describing the channeling nature of flow through a fracture. To observe and characterize the surface roughness of joint and fracture aperture variation, several methods have been proposed using profilometers (Swan 1983, Brown et al. 1986, Gentier 1986) or injection and casting techniques (Gale et. al, 1987, Pyrac-Nolte et al. 1987, Hakami 1988, Gentier 1989) or optical techniques (Miller et al., 1990 and Kimura and Esaki 1992). However, they could not draw general conclusions regarding the aperture variation in a fracture mainly due to the limited number of measurements. In addition, the effect of heterogeneity and anisotropy of aperture variation on flow in a fracture are not well examined. Tsang and Tsang (1989) used the specific form to describe the spatial correlation of aperture in their numerical generation of heterogeneous fracture aperture. Amadei and Illangasekare (1992, 1994) developed a closed-form analytical solution for flow analysis in a fracture with anisotropic and heterogeneous hydraulic properties. Such approaches, however, are often limited to joints with idealized geometries and cannot be generalized to all natural fractures. Therefore, one needs to examine more the real spatial variation and correlation of aperture in a fracture to make the numerical generation of heterogeneous fracture aperture much

more realistic.

First of all, in this study, a recently developed non-contact optical measurement system with laser beam profilometer is utilized to precisely measure the topography of real fracture surfaces. Next, after removing the trend of each of fracture surfaces, fracture aperture are calculated. Then, surface roughness and fracture aperture are statistically analyzed and tested to draw some conclusions regarding to the spatial variation, heterogeniety, anisotropy and correlation. Finally, based on observations, discussions, questions and comments on the geometrical properties of joints are presented.

3.2 Measurement of joint surface topography

3.2.1 Sample material and preparation

Six jointed specimens were used in this study, representing igneous, metamorphic and sedimentary rocks. Three rock specimens, Kikuma granodiorite, were chosen for their homogeneous structure, relatively large grain size and low intact rock permeability. Three specimens were cored as solid cylinders with 50 mm in diameter and were cut to 100 mm in length. One of these Kikuma granodiorite specimens includes a natural joint which is well matched and is almost parallel to an axial plane. The second one, which is initially an intact rock specimen, was fractured along the core axis by compressing the cylindrical specimen in a stiff press, in a so-called Brazilian test manner, as shown in Fig.3.1. In the third one, which is also initially an intact rock specimen, a joint was made along the core axis of the cylindrical rock specimen by cutting using a diamond saw and the surfaces were finished with #120 grit. In this study, these joints are named 'natural joint', 'tension joint' and 'sawed joint' in granodiorite, respectively. The other three rocks, Inada granite (with relatively small grain size), Chichibu schist and Kimachi sandstone were also fractured along the core axis using the same Brazilian technique. These specimens were also 50 mm in diameter and 100 mm in length. The core axis of the Chichibu muscovite schist specimen was parallel to its schistosity plane.

The basic properties of the four rocks are presented in Table 3.1. and the photographs were taken at low magnification to illustrate representative views of the constituent minerals and their sizes by using petrographic microscope, as shown in Fig.3.2. The representative size of minerals in granodiorite is relatively large than other three rocks and ranges from 0.1 mm to 2 mm. On the other hand, granite and schist have relatively small minerals less than 0.5 mm. Schistosity is clearly observed in Fig.3.2(c). There are almost equal size minerals in sandstone which ranges from 0.5 mm to 1mm.

Voids are composed mainly by cracks between minerals in granodiorite, granite and schist, but there are both cracks and pores in sandstone. The representative hydraulic conductivities of intact rocks are presented in Table 3.1, which range from 2.0 x 10-11 to 3.76 x 10-9. Thus, the conductivities of these rocks are very low. The effective porosity of Kikuma granodiorite is 0.59 %. An example of rock joints, natural joint in Kikuma granodiorite, is presented in Fig.3.3 and others are presented in Appendix A.

3.2.2 Apparatus and measurement techniques

Measuring the surface roughness is done with a non-contact optical system employing a semiconductor laser beam. This newly built system as shown in Fig.3.4 is capable of measuring objects without any damage which is difficult to achieve with conventional measuring instruments. The components include the detector head (laser beam profilometer : LI-1205, Mitsutoyo Corporation), connecting unit and display unit (200P, Mitsutoyo Corporation), cross-traveling cantilever arm (KR3306A+300LP, THK Co., Ltd.), multi servo controller (IA-C-SEL2-60, THK Co., Ltd.), core stage and personal computers. The dimensions and fundamental specifications of laser beam profilometer are presented in Fig.3.4. ; it has 20 mm measuring range (10 mm from the absolute zero position) and 5 μm resolution.

Measurements using this system are made by digitizing an object surface in three dimensions along a series of parallel trace lines on the object surface. The x coordinate is the direction of the trace line parallel to the core axis, the y coordinate is normal to the x coordinate and subparallel to the surface and the z coordinate is the direction normal to the surface. This elevation z is measured as a distance from an absolute zero position (mechanical zero position).

First, the origin on the surface is defined as well as both sets of trace lines along the x and y directions and also the sampling interval. The detector head measures the distance to the surface as it translates along the x direction. At the end of one x-trace, the position is stepped in the y-direction and a new trace along the x direction is begun. The entire process is automated and the maximum size of scanning area is 30 cm by 30 cm squares in our system. In this study, square areas ranging from 45 mm by 96 mm to 46 mm by 98 mm for the six fracture surfaces were scanned. 1 mm sampling interval (spacing between measurement points) was used in both x and y directions. To measure the roughness on one surface with 1 mm sampling interval needs about 2 hours in this system. Measurement time is simply proportional to the number of points. Therefore it depends on both the sampling interval and the scanning area. Measurement error can be $\pm$ 5 μm since

the resolution of laser beam profilometer is 5 μm. Note that observed value is an averaged height over the laser spot on the surface. Radius of laser spot is 0.1 mm in this profilometer.

From the point of view of digital imaging, the fracture aperture formed by two facing surfaces is the simple arithmetic difference between two fracture surfaces. However, the measurements of the fracture surfaces include a trend. This is caused by the handling of the specimens, which involves separation of the two fracture surfaces and then placing the specimens in the core stand. The associated rotation and translation is different for the two fracture surfaces producing different "trends". This trend was removed by multiple linear regression. With this technique, we first obtained the regression planes (trend surfaces) of the two surfaces and then computed the residuals with respect to the regression planes as digital surfaces.

To check the performance of this technique, the coefficient of curvilinear correlation was calculated. The coefficient of curvilinear correlation describes the degree of fit of the regression plane relative to the sample variable and ranges from zero to one (complete fitness). The coefficients of curvilinear correlation were, in general, greater than 0.75 for the two facing surfaces of each of the six fractures; the correlation was especially high (greater than 0.90) for the natural joint surfaces of Kikuma granodiorite.

3.2.3 Aperture derivation

The term aperture is often used in the description of joint void space. Assuming that joint surfaces lie parallel to a flat reference plane, the aperture (local aperture) is the physical difference between the two fracture surfaces at a certain point in the direction perpendicular to the reference plane at that point. It is illustrated in Fig.2.15. The aperture is defined at all points on the joint surface area, which can include the zero aperture (contact point) in a closed joint. In Fig.2.15, the average aperture in a joint is also illustrated, which describes the overall geometrical character of joint aperture.

To obtain aperture using two digitized surfaces, the opposing surfaces are matched together. Therefore it is requiring an exact definition of two facing positions on the two fracture surfaces. As mentioned in Chapter 2, The difficulty in surface topography method lies in the matching of surfaces since it is difficult to obtain the exact relative position of the surfaces if once a joint has been opened for the surface measurements. This is done by making special marks at the four corners of the square scanning area, whose positions are then precisely determined by a laser spot (radius : 0.1 mm). When relating the two fracture surfaces to each other, these spots must exactly coincide. In this study, the following

procedure has been used to obtain joint aperture.

1) It is considered that the residuals of the digitized surfaces with respect to the regression plane is the surface roughness.
2) The two surfaces is overlapped numerically to derive the joint aperture between surfaces ; a very simple procedure. If the two regression planes of two facing surfaces are made to coincide, some asperities will overlap. This is assumed to be physically impossible.
3) One assumes that the measuring point with maximum overlap between the two digitized surfaces should be the contact point. Then, the two surfaces are separated to the amount exactly equal to the maximum overlap in the direction perpendicular to the regression planes. Thus only one contact point in a joint is found out. In physical sense, there must be at least three points in contact in a joint. Therefore the joint aperture is correspondingly corrected to make three points in contact in a joint.
4) Some error will be involved in this procedure since exact peaks and valleys of asperities on the surfaces cannot be obtained in this measurements as well as other measurement techniques. The following several errors are anticipated. The simple mechanical measurement error on surface height is 10 μm on each surface due to the measurement resolution. Therefore maximum error for two surfaces can be 20 μm. In the derivation of aperture, also systematic 40 μm error will be involved due to the mismatching in relative positions between two surfaces. Thus the calculated aperture is larger than real aperture since only one point contact is assumed in this calculation. Error involved in this assumption is hard to be estimated since it depends on the distribution of asperities on the surface. In my estimation, total maximum error will be 60 μm and the real aperture has to be smaller than the calculated aperture.

3.2.4 Results of measurements

The digital surfaces of the six joints after linear trend removal are presented in Fig.3.7. In this study, the two opposing surfaces are named as the upper and lower surface individually. In these figures, nx and ny are the numbers of digitized points in x and y directions respectively. Xmax and Ymax show the length of scanning area in x and y directions respectively. The unit in these figures is mm. The elevation z is exaggerated 100 times real values and figures are drawn by the automatic scaling. Both Zmax and Zmin describe the maximum and minimum values of asperity heights, respectively. Zmean and Zvari are the mean and the variance of the elevation z. In general, Fig.3.7 clearly shows that the two digitized surfaces after linear trend removal are very similar to each other and

all surfaces look relatively smooth. In Fig.3.7(e), one can see that the surfaces of tension joint in schist are stepped surfaces due to the presence of the its schistosity. Fig.3.8 shows the histograms of residuals, i.e. the asperity heights with respect to the regression planes for the two surfaces of joints. The histogram of the digitized surface of the natural joint in Kikuma granodiorite (Fig.3.8(a)) has a distribution which is slightly skewed to the positive side and ranges between -3488 μm and 1860 μm in upper surface and between -3476 μm and 1849 μm in lower surface.

On the other hand, the histogram of the tension joint in Kikuma granodiorite (Fig.3.8(b)) has a relatively wide-spread distribution ranging from -3242 μm to 5079 μm and the histogram of the sawed joint in Kikuma granodiorite (Fig.3.8(c)) has a very narrow, peaked distribution ranging from -84 μm to 90 μm due to the polishing after cutting. The double amplitude (peak to peak amplitude) of asperity height of the sawed joint is about 175 μm and the surface is very close to planar. The histograms of the other three tension joints have nearly normal distributions with zero mean. Table 3.2 summarizes the statistics of the asperity heights relative to the regression planes. The most wide-spread is observed in tension joint in Kikuma granodiorite and the sharpest distribution is observed in sawed joint in Kikuma granodiorite.

To check the normality, the cumulative probability of asperity height of one surfaces for six fractures are plotted on probability paper shown as in Fig.3.9. In this figure, the following abbreviations of the names of joints are used and these abbreviations are also extensively used in the other figures, tables and texts.

NKGD : natural joint in Kikuma granodiorite
TKGD : tension joint in Kikuma granodiorite
SKGD : sawed joint in Kikuma granodiorite
TIGN : tension joint in Inada granite
TCSH : tension joint in Chichibu schist
TKSS : tension joint in Kimachi sandstone

The linearity can be clearly observed from 5% to 95% cumulative probability for five joints except a natural joint in granodiorite. These distributions would mostly depend on the grain size of materials in rock since four tension joints are newly created tensile joints and a sawed joint in granodiorite are polished. But for a natural joint, same distortion from the normal distribution is involved. As shown in Fig.3.8(a), the distributions of asperity heights of both surfaces are very close and show a negative skewness. In Fig.3.7(a), relatively large fluctuations of asperity heights of two surfaces to the scale of sample (100

mm in length and 50 mm in width) are observed. These fluctuations might be induced by the multitude of joint genesis processes including shearing processes. The shearing can distort the homogeneous isotropic distribution of asperities since it has the strong directional effect on aperture distributions. Therefore one explanation to these different fluctuations may come from the difference in shear displacement that the joints have experienced. Newly created tension joints have experienced little shearing, but a natural joint should have experienced some amount of shearing displacement. The other issue which should be considered is the scale effect. In-situ joints have relatively large extents i.e. ; from several meters to kilometers. Therefore they can show greater variations in their surface properties. Fluctuation discussed here is relatively large to the sample size, but quite shorter than the size of real in-situ joints. It cannot be concluded that any distribution can be best fitted for the natural joints since only one data for a natural joint has been measured.

3.3 Joint aperture variation and spatial correlation

3.3.1 Aperture variation

The basic statistics of six apertures are listed in Table 3.3. The mean, standard deviation and the coefficient of variation (C.O.V.) are often used as a measure of aperture variation. The means of apertures range from 101 μm to 650 μm and C.O.V. varies from 0.297 to 0.539. In terms of C.O.V., a sawed joint in granodiorite has the smallest variation and the tension joint in granite has the largest variation. Fig.3.10 shows the aperture distributions in joints and the histogram plots of the aperture of all six joints. The aperture distribution seem to widen with increasing average aperture. As well seen in these figures and also understood from the statistics of aperture distribution listed in Table 3.3, all aperture distributions have the positive skewness. These results are consistent with reported data (Gentier 1986 and Hakami 1992). Also the statistics of the transformed variable, log-aperture (lnb), since the transformed variable (lnb) instead of aperture (b) has been used in existing investigations (Gelhar 1987 and Gale 1990). As listed in Table 3.4, mean of log-aperture varies from 4.529 to 6.290 μm. Gale(1990) reported that the mean of log-aperture of aperture distributions along several profiles in natural joints in Stripa granite using the resin characterization approach varied from 5.2 to 6.0 μm. In this study, the mean of log-aperture in the natural joint in Kikuma granodiorite is 5.474 μm.

All of the histograms can be approximated by the normal or lognormal distribution. To confirm this, the cumulative frequencies of the six apertures are plotted on probability

paper as shown in Fig.3.11. It can be clearly seen that theses six joints can be categorized into three groups in terms of magnitude of aperture, i.e. ; very small aperture (SKGD), relatively small apertures (NKGD, TCSH and TKSS) and relatively large apertures (TKGD and TIGN). As shown in Table 3.3, mean apertures range from 101 μm to 650 μm. The explanation to this may lie in the differences of textures of host rocks, in particular their grain sizes, and the special treatment of surfaces like a sawed joint since most of jointed specimens used in this study are newly created tension joints. From Fig.3.11, the linearity of a line of a sawed joint is very clear in both the linear and log scale plots. In the linear scale plot shown in Fig.3.11(a), the linearity of three lines (NKGD, TCSH and TKSS) can be observed for more than 100 μm, but the linearity of other two lines (TKGD and TIGN) cannot be observed . On the other hand, in the log scale plot shown in Fig.3.11(b), the linearity of three lines (NKGD, TCSH and TKSS) can be observed for more than 100 μm, but the linearity of other two lines (TKGD and TIGN) can be observed for more than 200 μm. Therefore, in this study, the normal distribution will be more appropriate for the modeling of the aperture distributions of four joints with small apertures (NKGD, SKGD, TCSH and TKSS) and the lognormal distribution will be more appropriate for other two joints with relatively large apertures (TKGD and TIGN).

When a theoretical distribution has been assumed, perhaps determined on the basis of the general shape of the histogram or on the basis of the data plotted on a given probability paper, the validity of the assumed distribution may be verified or disposed statistically by the goodness-of-fit tests. The Kolmogorov-Smirnov (K-S) test is generally used to test the validity of an assumed distribution model and is applied to test the aperture distribution in this study. The basic procedure involves the comparison between the experimental cumulative frequency and an assumed theoretical distribution function. If the discrepancy is large with respect to what is normally expected from a given sample size, the theoretical model is rejected. The details of K-S test are well documented in many books on statistics, i.e.; Benjamin and Cornell(1970). In this study, two theoretical distribution functions, the normal and lognormal distribution, are used.

Fig.3.12 show the results of K-S test for the six observed apertures. The upper graph in Fig.3.12 show the comparison between a stepwise cumulative frequency function of aperture (Sn(x)), the normal distribution function (Fnor(x)) and lognormal distribution function (Flog(x)). To obtain two assumed functions, the statistical properties of apertures have been calculated using observed data. They are tabulated in Table 3.3 for the normal distribution and in Table 3.4 for the lognormal distribution. The lower graph in Fig.3.12 describes the differences between the stepwise cumulative frequency function of aperture (Sn(x))and the two proposed functions, which are indicated as Dnor(x) and Dlog(x) for

normal and lognormal, respectively.

In the K-S test, one has to compare the maximum difference (Dnor(max) for the normal distribution and Dlog(max) for the lognormal distribution) with the critical value (Dc) for a specified significant level. Theoretically, Dc is a random variable, whose distribution depends on the sample size and the specified significant level. In this study, the 5% significant level is used. If the observed maximum difference is less than the critical value, the assumed distribution is acceptable at the specified significant level, otherwise, the assumed distribution has to be rejected. All calculated values (Dc, Dnor(max), Dlog(max)) and test results for the six joint apertures are summarized in Table 3.5. All aperture distributions are rejected as both the normal distribution and the lognormal distribution. The positive skewness, however, is observed for all aperture distributions, suggesting that the lognormal distribution is more appropriate for aperture distribution.

In addition, our results do not agree with those from the observations on different size fractures using other techniques, i.e. in well logs by Bianchi and Snow (1968) and in cores by Gentier (1986). They suggested that the aperture distribution can be modeled by the lognormal distribution. The number of their observations, however, is very limited and the size of measurements is different. Therefore, we cannot draw a general conclusion regarding aperture distribution due to the limited number of measurements.

3.3.2 Spatial correlation

To analyze the aperture correlation in a joint, the correlation function which is defined as the auto-covariance function normalized by variance of the variable and is calculated as the central moment of the product of two different values with the distance separation is used in this study. The correlation function describes the general dependence of the variable at one point on the values at other points and their relative strength.

The correlation functions of the six apertures are presented in Fig.3.13. The calculations were performed along four lines in the x-y plane whose directions range from 0 degree (x direction) to 90 degrees (y direction) in 30 degree steps. The correlation functions are plotted with respect to the lag distance which is the separation length for calculating the covariance of two corresponding points. To clearly visualize these features, the 2-dimensional correlation functions of the six joint apertures are also presented in Fig.3.13.

From these figures, the following can be concluded:

a) The correlated aperture region in all joints is very small, namely less than 5 mm; in

sandstone it is a little bit greater but still quite small (less than 10 mm).
b) The correlations in six joints are almost isotropic, but are a little bit anisotropic in the two fractures (sawed joint in Kikuma granodiorite and tension joint in Chichibu schist) in that relatively high correlation is observed in the x direction (parallel to the core axis ; 0 degree in Fig.3.11). With a schist this is to be expected due to the schistosity. With a sawed joint, however, this is not to be expected and seems related to the textural anisotropy of the surfaces due to the polishing after being cut by a diamond saw. But in conclusion, the correlation is isotropic, particularly for the artificially induced tension joint.

3.4 Summary and discussion

The main objective of these measurements is to obtain some information on aperture variation and correlation in order to conceptually construct the fracture aperture model. The described method for measuring the surface roughness is relatively simple and produces results with sufficient accuracy. From the observed statistical values for the six joints, the sawed joint in Kikuma granodiorite has the smallest aperture variation and the tension joint in Inada granite has the largest. The means apertures of six joints range from 101 to 650 μm, the maximum apertures from 243 to 1990 μm and the coefficients of variation range from 0.297 to 0.539. The aperture distributions seem to widen with increasing average aperture. Positive skewness is observed for all aperture distributions. These results are consistent with those reported by Hakami (1988) and Hakami and Barton (1990). All of the histograms seem to have either a normal or a lognormal form. However, based on the Kolmogorov-Smirnov test, neither form fits the aperture distributions and this for all six joints. This contradicts observations made by others which state that aperture distributions are usually lognormal (Gentier, 1986 ; Gale, 1987 ; Hakami, 1988). However, since we have only a limited set of observations, one cannot draw any conclusions at this stage.

From an engineering point of view, this difference does not a matter since the aperture distributions may have an approximately normal, log-normal or similar form. However, actual size of the aperture is much more important. In particular for joint flow, a few flow channels with large apertures, named super-conductors by Long (1983), may conduct greater quantities of water than numerous flow channels with small apertures. Therefore, the distributional form of apertures greater than average apertures is much more important for joint flow than the over-all functional form of aperture distribution. On the other hand, relatively smaller apertures in a joint will mostly contribute to the mechanical properties of the joints such as the deformability, strength and dilatancy.

In this study, the correlation of apertures in the six joints were limited to very small

distances (less than 1 cm) ; in addition, these correlations are almost isotropic. These observations on the geometrical properties of joint aperture on small size joints (laboratory scale, i.e. ; less than 10 cm), cannot to be extrapolated to those on large size joints (e.g. ; in-situ scale) since larger size joints may have both more large scale variations and a more anisotropic correlation of apertures. Therefore one has to be cautious when applying results obtained on the lab scale to real engineering problems.

In this study, the surface topographies were first measured, the opposing topographies were matched and the resulting joint aperture was numerically calculated. The difficulty in obtaining aperture distributions with these procedures lies in the matching of surface topographies since it is difficult to determine the exact relative position of the surface topographies. In the aperture derivation, zero overlap between surfaces and three points in contact are assumed in a joint. These assumptions induce some error in aperture derivation. If one allows some non-zero overlap between surfaces and simply neglects the resulting negative aperture in a joint, the calculated aperture distribution will shift laterally to the negative side while the shape of aperture distribution will remain the same. These changes will cause the average aperture to decrease and the variance of aperture to slightly decrease. The reductions in aperture depend on the assumed threshold value of non-zero overlap between surfaces. The change in correlation and variance associated with non-zero overlap is small since these quantities are second order statistics.

In order to draw general conclusions, additional measurements and interpretations involving a wide variety of rock types, joint types and sizes, especially using natural joints would be needed. Nevertheless, a number of questions and comments can be crystallized from the present study :

a) Can joint apertures in rocks be modeled as an isotropic random (uncorrelated) process since observations in this study clearly show that aperture correlation is very small and isotropic ?

b) Will apertures of natural joints in sedimentary rocks show some correlation anisotropy ? Is this anisotropy related to the textural anisotropy of the intact rock ?

c) Will natural joints in-situ show greater anisotropy than those measured in the laboratory due to either their size or the multitude of joint genesis processes or both?

In Chapter 5, the similar measurements and analyses on surface roughness and joint aperture will be discussed using the same six joints but cyclic stress-deformation-flow

(hydromechanical) tests have been performed. Therefore recommendations for further studies to characterize the surface roughness and joint aperture will be also presented in Chapter 5.

Table 3.1 Bacis properties of rock samples

	Kikuma Granodiorite	Inada Granite	Chichibu Schist	Kimachi Sandstone
Young's Modulus (GPa)	32	35	27	9.2
Poisson Ratio	0.23	0.13	0.22	0.2
Vp (m/sec)	4,380	3,740	3,460	2,750
Vs (m/sec)	2,560	2,800	2,070	1,450
Uniaxial Strength (MPa)	120	150	220	50
Hydraulic Conductivity (cm/sec)	5.0 x 10-11	1.34 x 10-9	2.0 x 10-11	3.76 x 10-9

Table 3.2 Statistics of asperity heights of surfaces in six joints

			Mean (μm)	Standard Deviation (μm)	Maximum Asperity Hight (μm)	Minimum Asperity Hight (μm)	Double Amplitude (μm)
Kikuma Granodiorite	Natural Joint	Upper Surface	0.0	983	1860	-3488	5348
		Lower Surface	0.0	980	1849	-3476	5325
	Tension Joint	Upper Surface	0.0	1326	4449	-3416	7865
		Lower Surface	0.0	1334	5079	-3242	8321
	Sawed Joint	Upper Surface	0.0	21	77	-84	161
		Lower Surface	0.0	19	91	-81	172
Inada Granite	Tension Joint	Upper Surface	0.0	743	2265	-2496	4761
		Lower Surface	0.0	735	2548	-2358	4906
Chichibu Shist	Tension Joint	Upper Surface	0.0	398	1367	-1310	2677
		Lower Surface	0.0	395	1316	-1250	2566
Kimachi Sandstone	Tension Joint	Upper Surface	0.0	561	1844	-1508	3352
		Lower Surface	0.0	560	1851	-1495	3346

Table 3.3 Statistics of apertures in six joints

Joint	Points	Minimum (μm)	Maximum (μm)	Mean (μm)	Geometric Mean(μm)	Standard Dev.(μm)	C.O.V.	Standard Error(μm)	Skewness	Kurtosis
NKGD	4500	0	691	262	238	105	0.402	1.58	0.792	1.191
TKGD	4656	0	1874	627	536	311	0.497	4.60	0.767	0.855
SKGD	4653	0	243	101	93	30	0.297	0.45	0.285	0.284
TIGN	4462	0	1990	650	539	350	0.539	5.30	0.761	0.600
TCSH	4462	0	683	283	255	113	0.400	1.70	0.332	0.136
TKSS	4462	0	798	296	275	104	0.352	1.57	0.733	1.866

Table 3.4 Statistics of apertures in six joints for the lognormal distribution

Joint	Geometric Mean(μm)	Mean of log aperture(μm)	Standard dev. of log aperture (μm)
NKGD	238	5.474	0.504
TKGD	536	6.284	0.675
SKGD	93	4.529	0.471
TIGN	539	6.290	0.730
TCSH	255	5.540	0.562
TKSS	275	5.617	0.464

Table 3.5 Results of S-K goodness-of-fit test

	Points (n)	Critical Value Dc (μm)	Max. of Dnor(x) Dnor(max)	Max. of Dlog(x) Dlog(max)	Test Result Normal Dis.	Test Result Lognormal Dis.
NKGD	4500	0.0203	0.0629	0.0848	Reject	Reject
TKGD	4656	0.0199	0.0543	0.1005	Reject	Reject
SKGD	4653	0.0199	0.0271	0.0900	Reject	Reject
TIGN	4462	0.0204	0.0502	0.0499	Reject	Reject
TCSH	4462	0.0204	0.0252	0.1040	Reject	Reject
TKSS	4462	0.0204	0.0508	0.0994	Reject	Reject

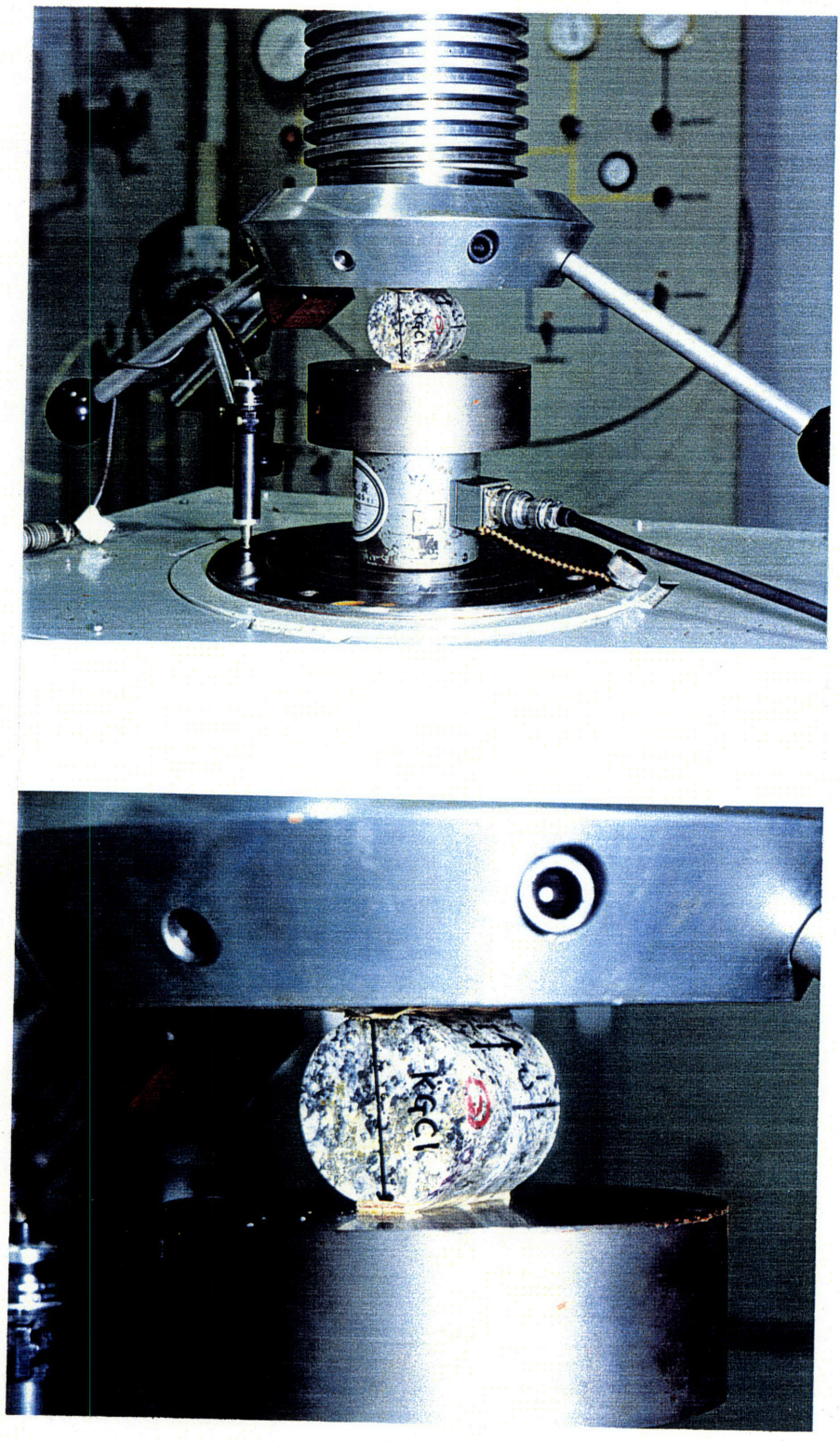

Fig. 3.1 A photograph of the Brazilian test

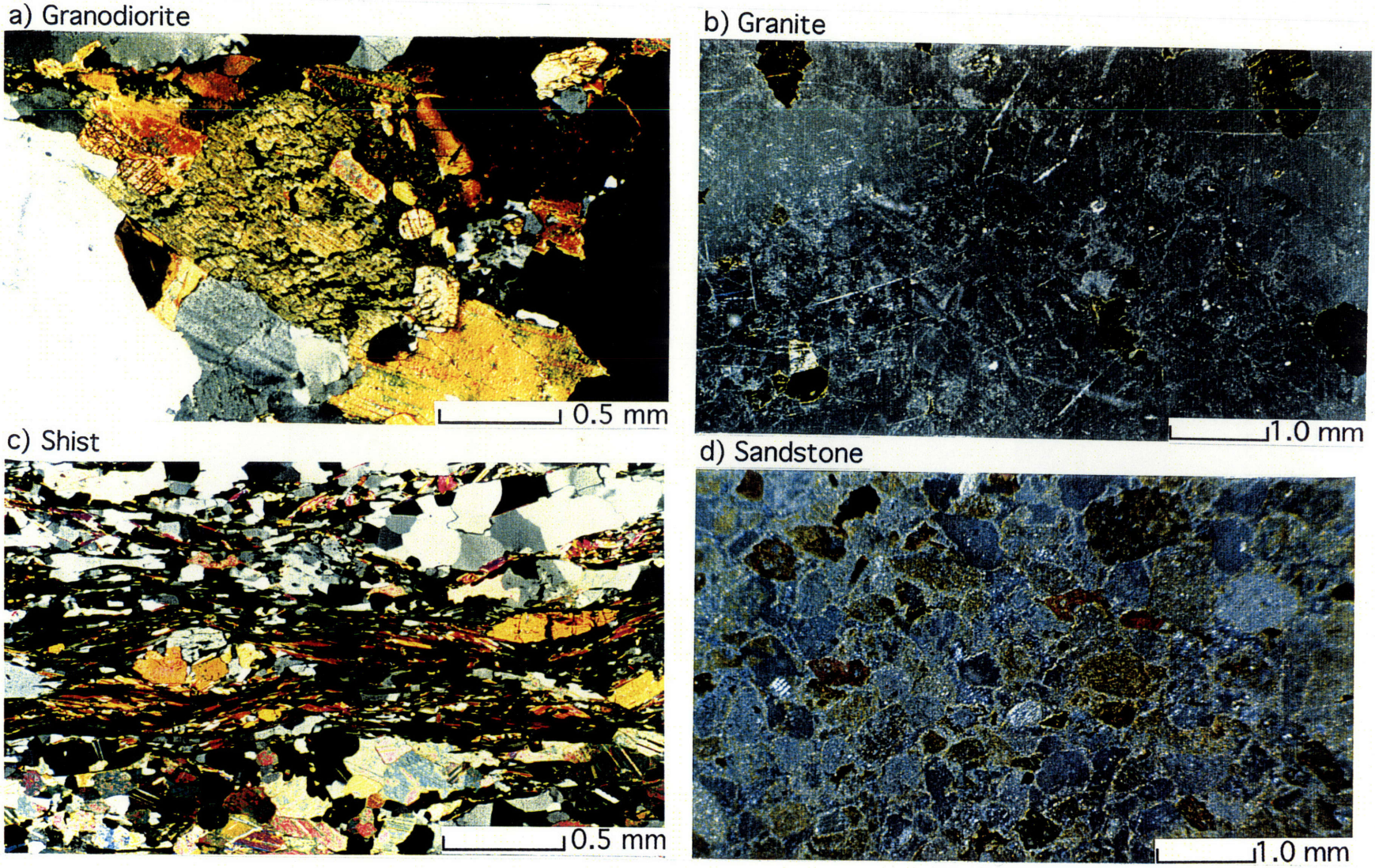

Fig. 3.2 Photographs of rocks using a petrographic microscope

Fig. 3.3 An example of rock joints
(Natural Joint in Kikum Granodiorite)

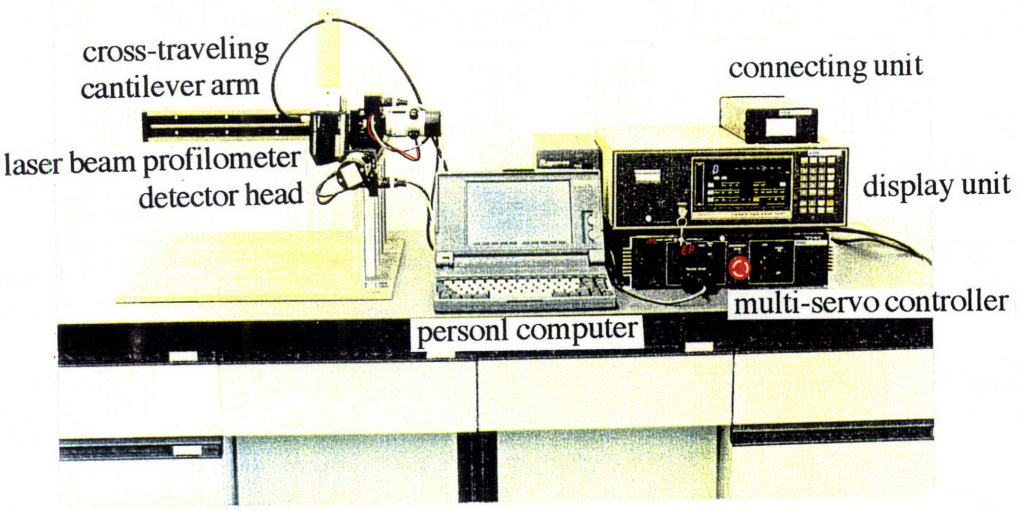

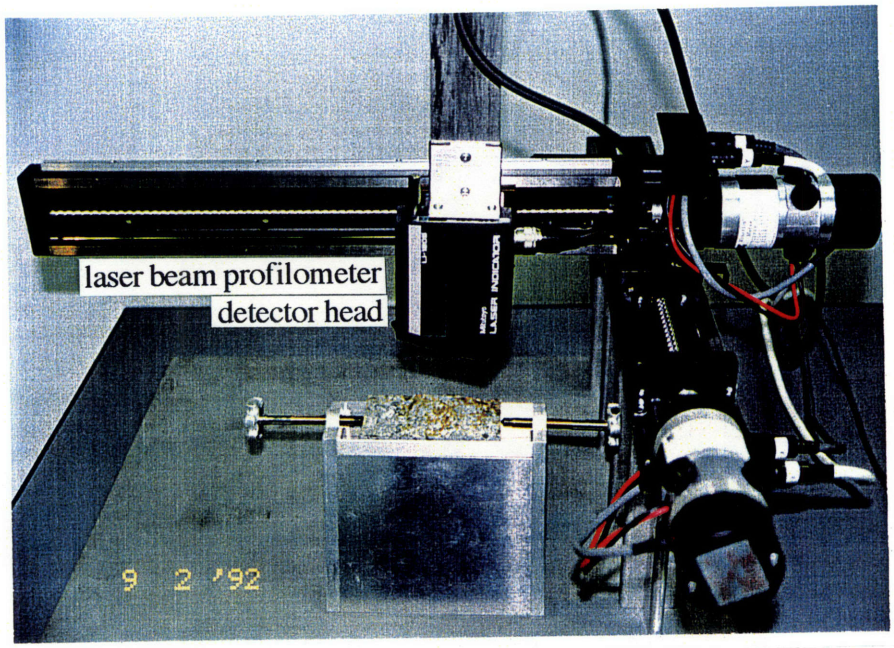

Fig. 3.4 A non-contact optical system employing a semiconductor laser beam profilometer

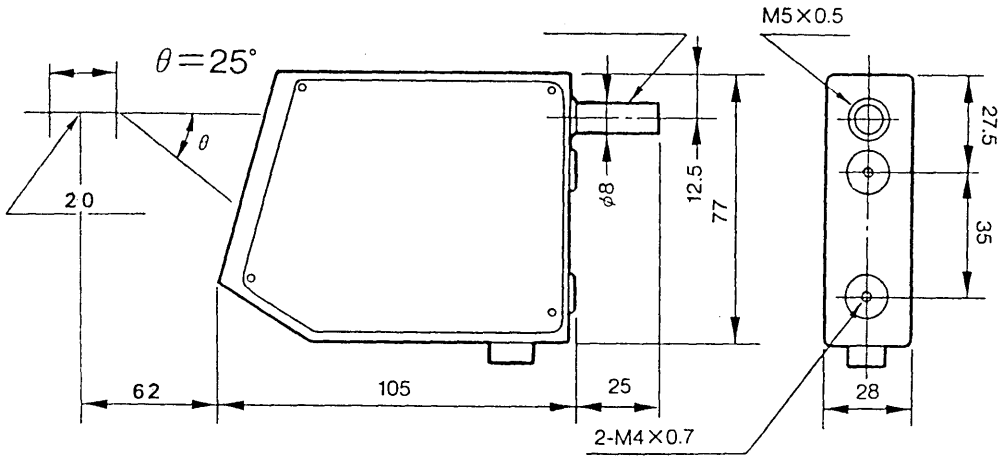

Laser beam profilometer(LI1205:Mitsutoyo Corporation)
Resolution : 0.005 mm (5 μm)
Range of measurement : ± 10 mm
Radius of laser spot : 0.1 mm

Fig. 3.5 Dimensions and fundamental specifications of the laser beam profilometer

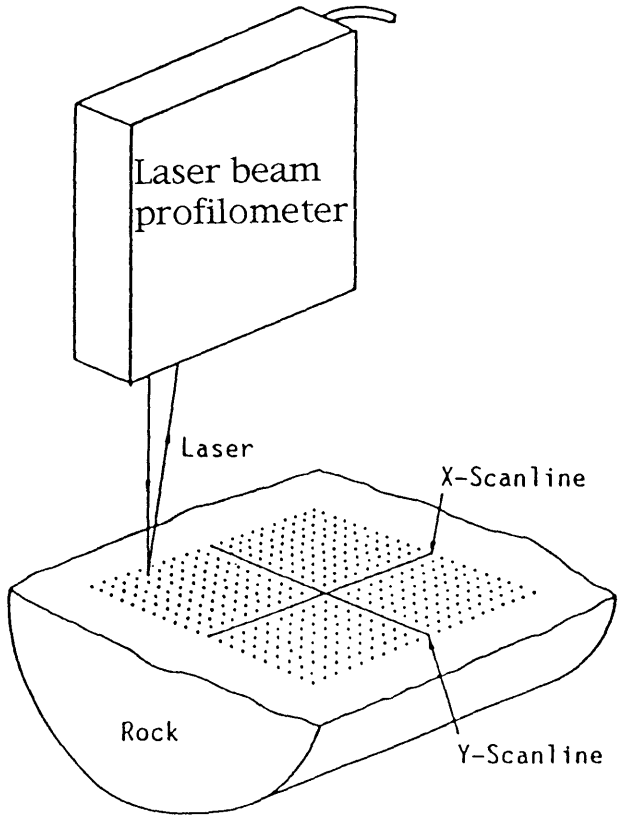

Fig. 3.6 Schematic view of the measurement of surface roughness

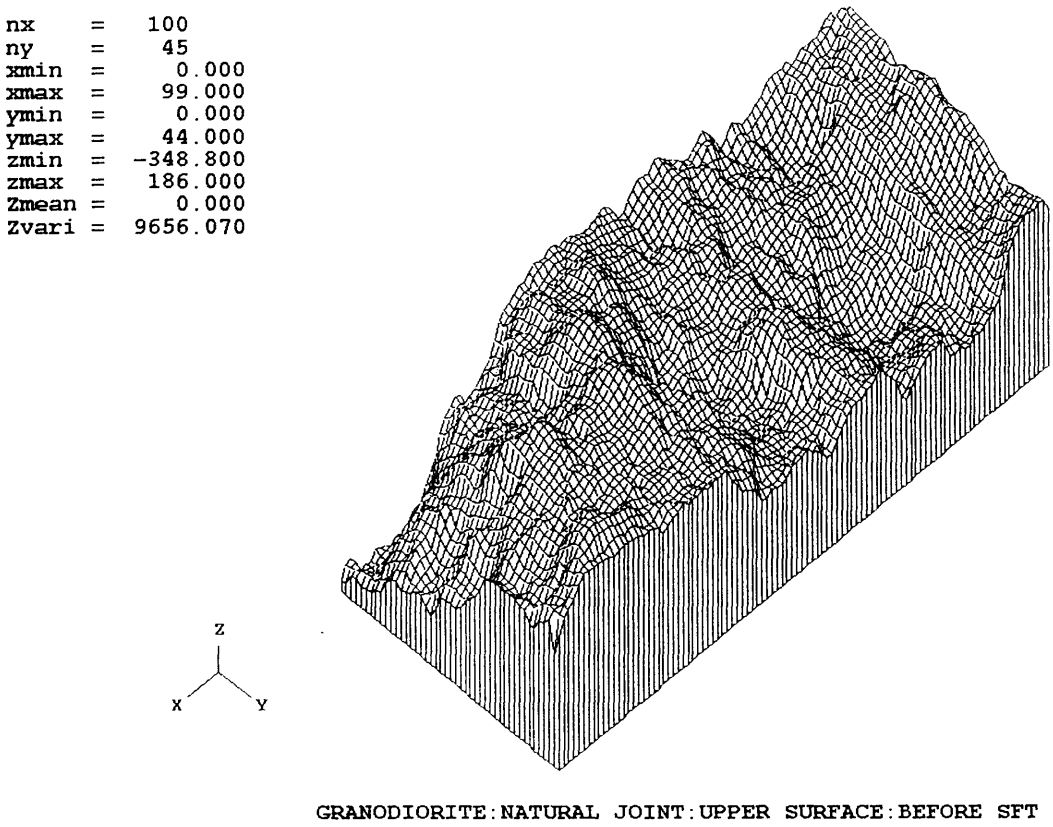

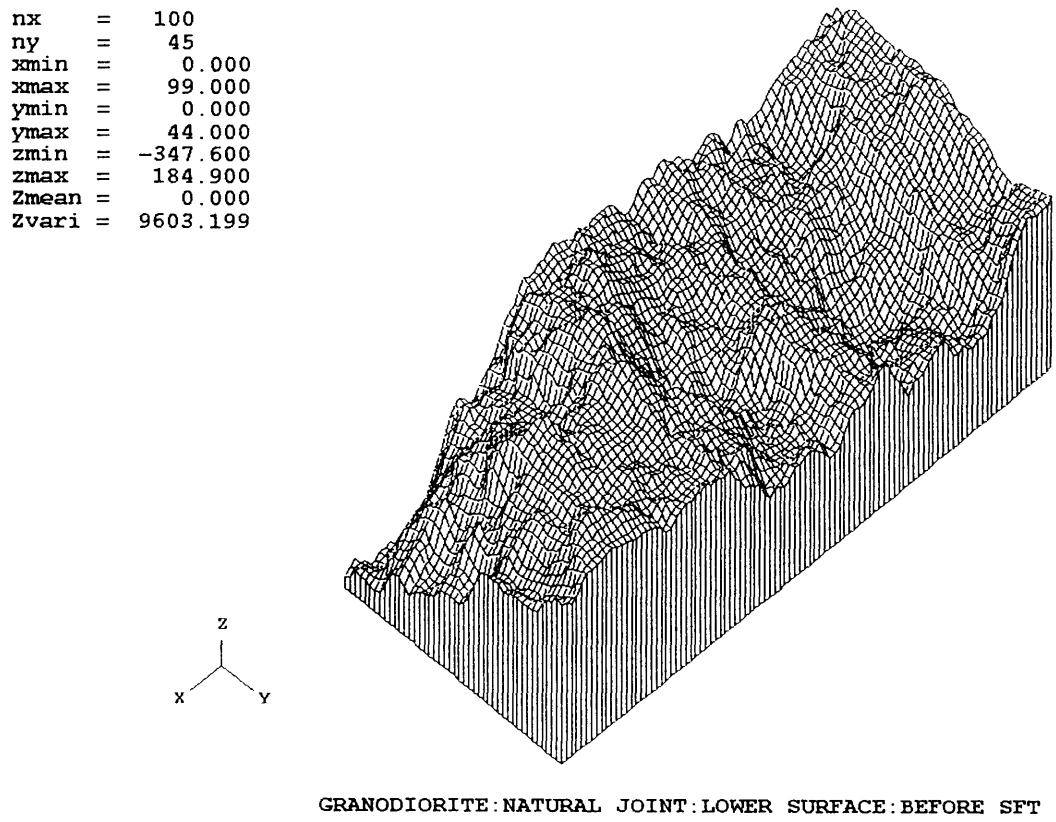

Fig. 3.7 Two digitized surfaces of a joint after linear trend removal (a) Natural joint in Kikuma granodiorite

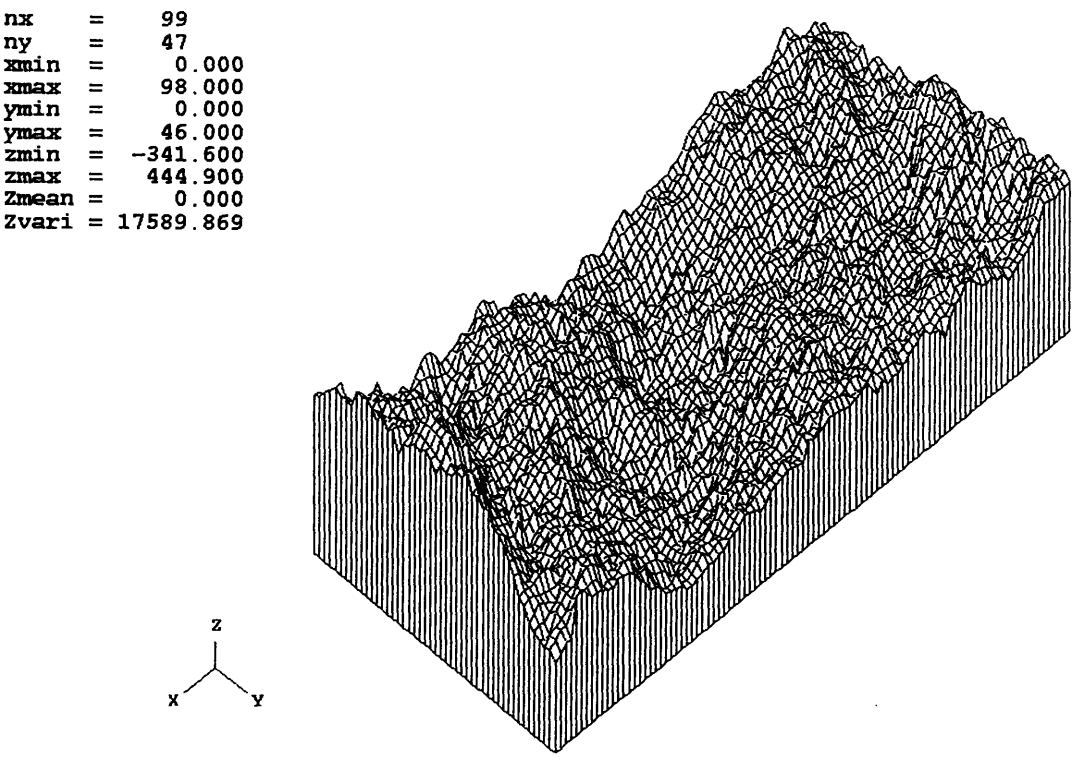

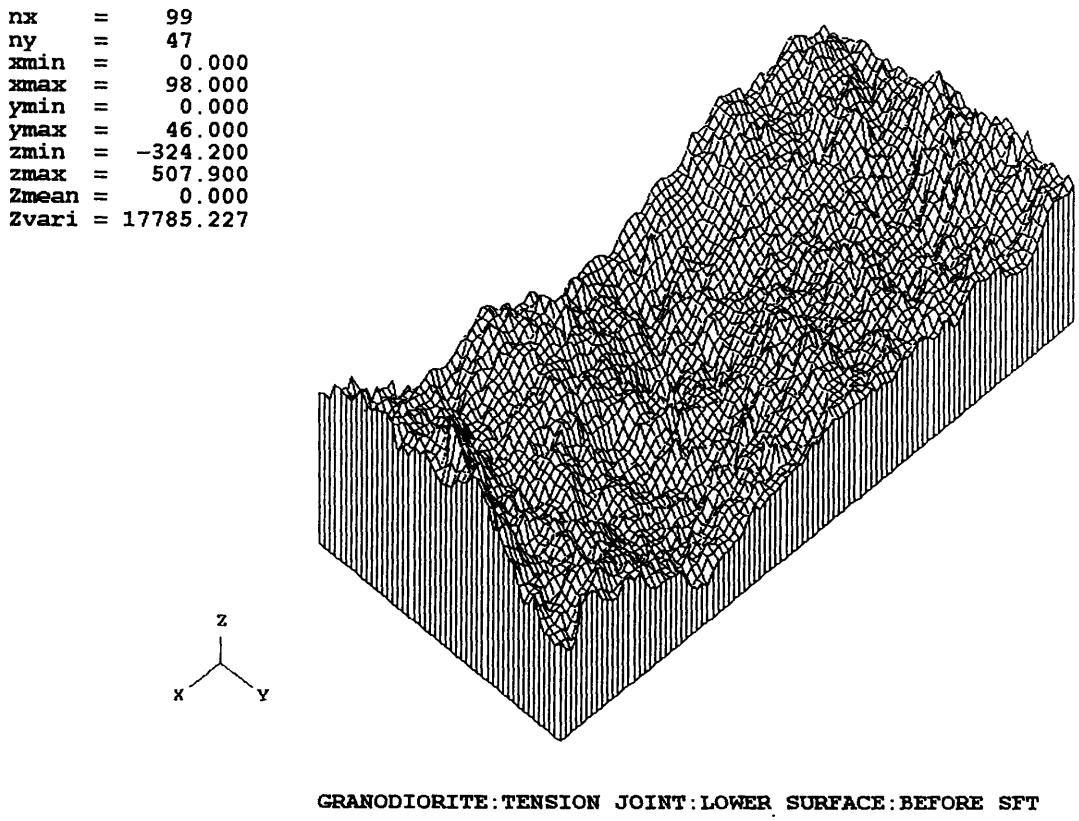

Fig. 3.7 Two digitized surfaces of a joint after linear trend removal (b) Tension joint in Kikuma granodiorite

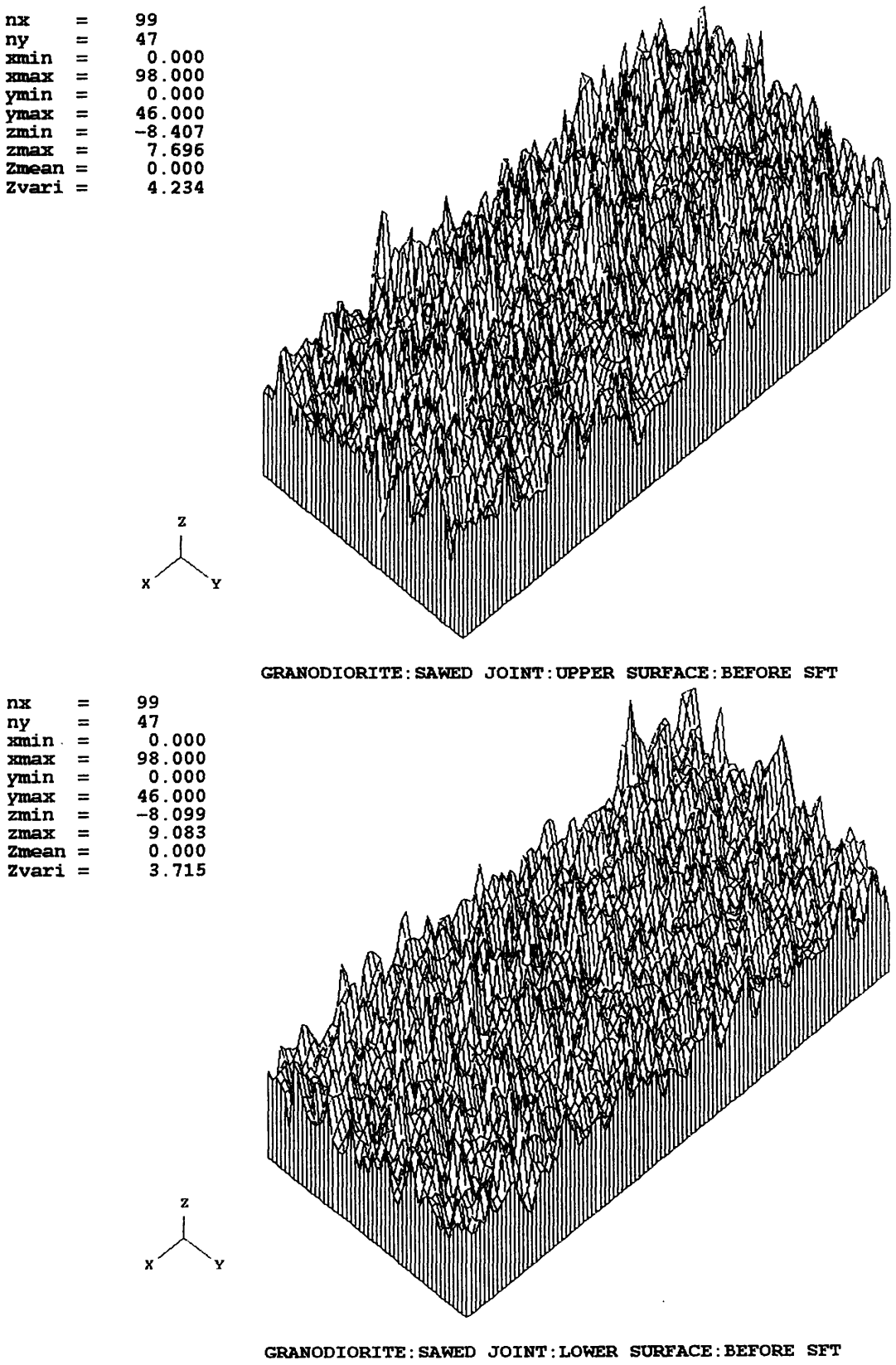

Fig. 3.7 Two digitized surfaces of a joint after linear trend removal (c) Sawed joint in Kikuma granodiorite

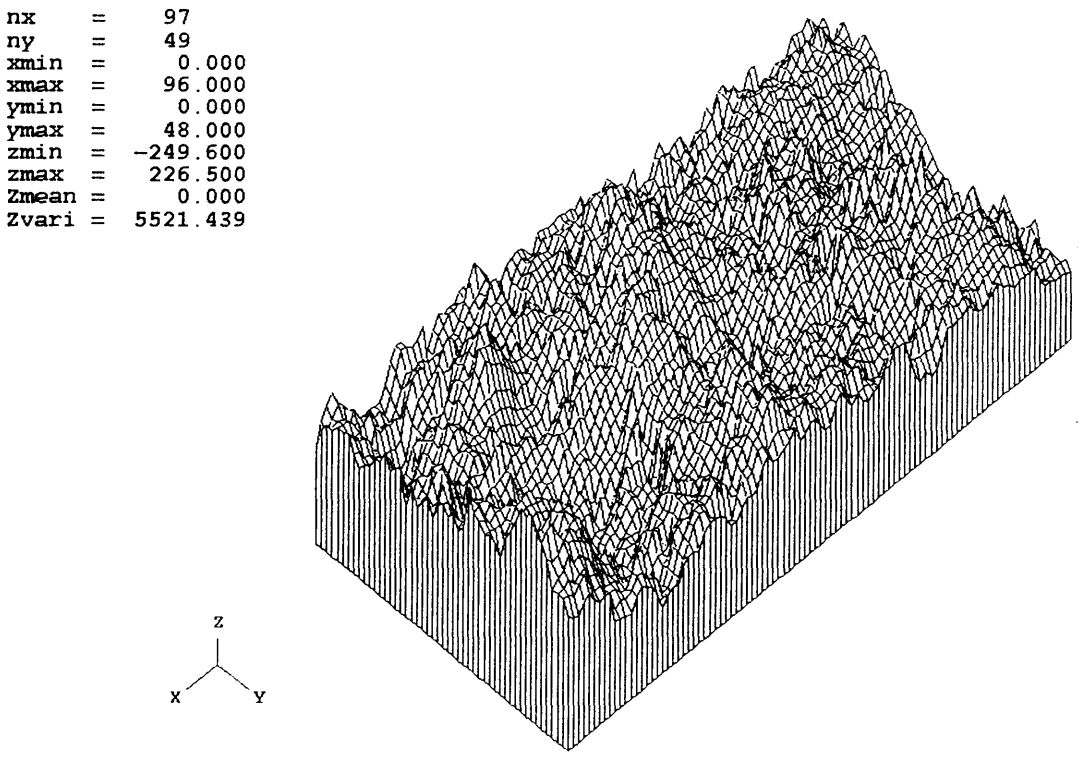

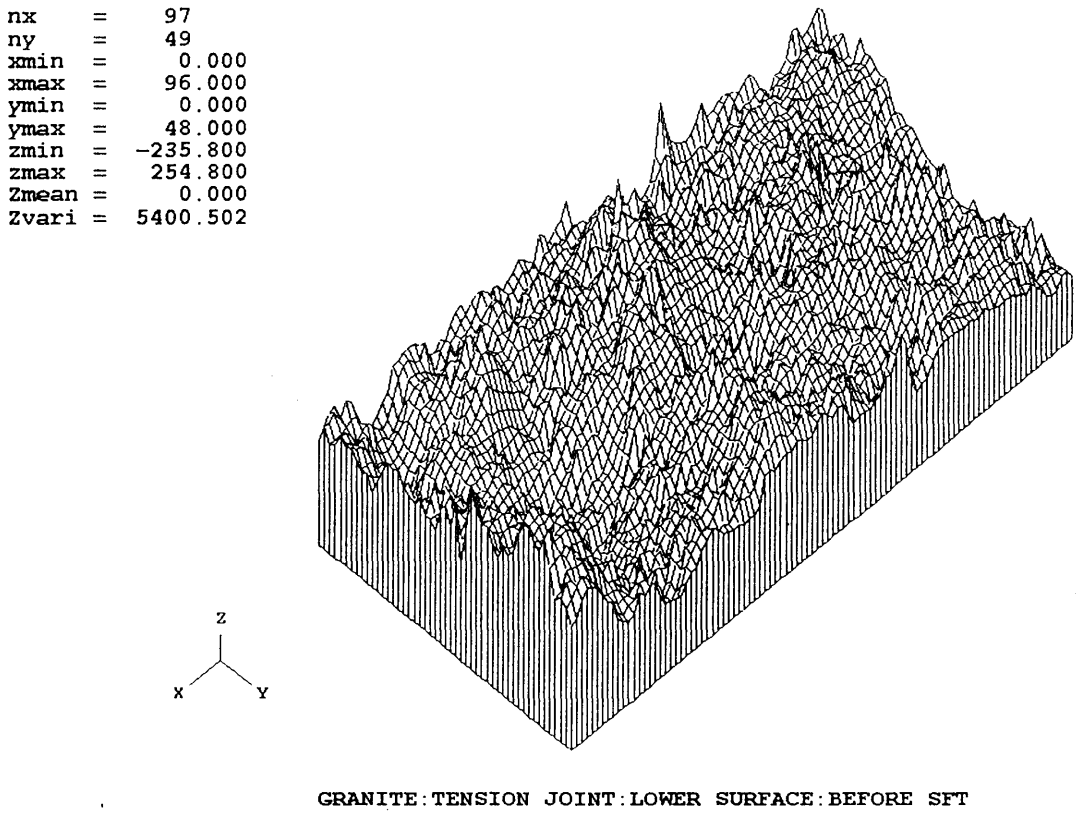

Fig. 3.7 Two digitized surfaces of a joint after linear trend removal (d) Tension joint in Inada granite

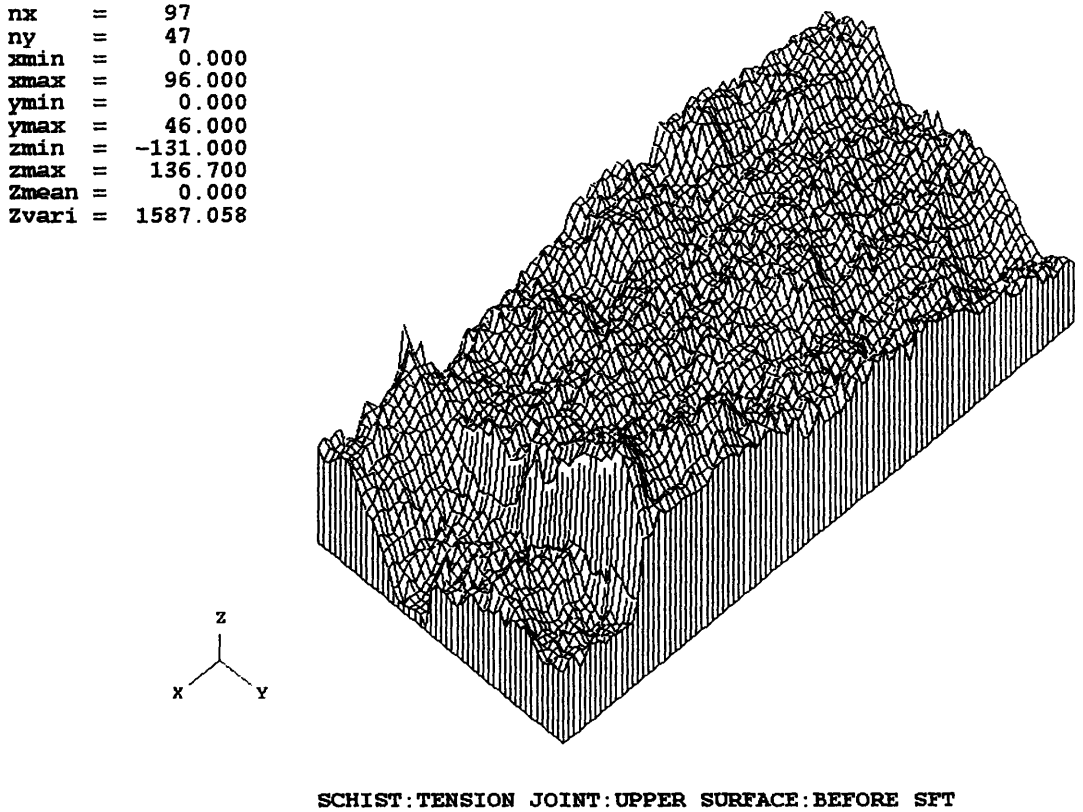

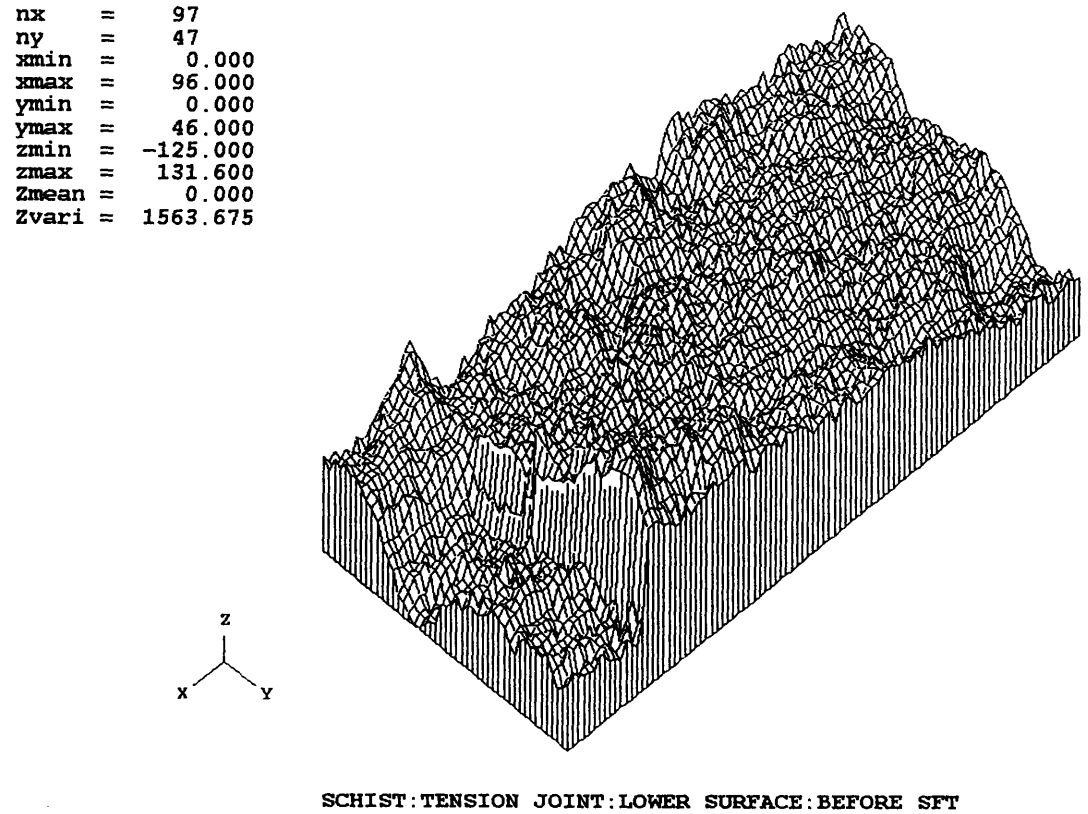

Fig. 3.7 Two digitized surfaces of a joint after linear trend removal
(e) Tension joint in Chichibu schist

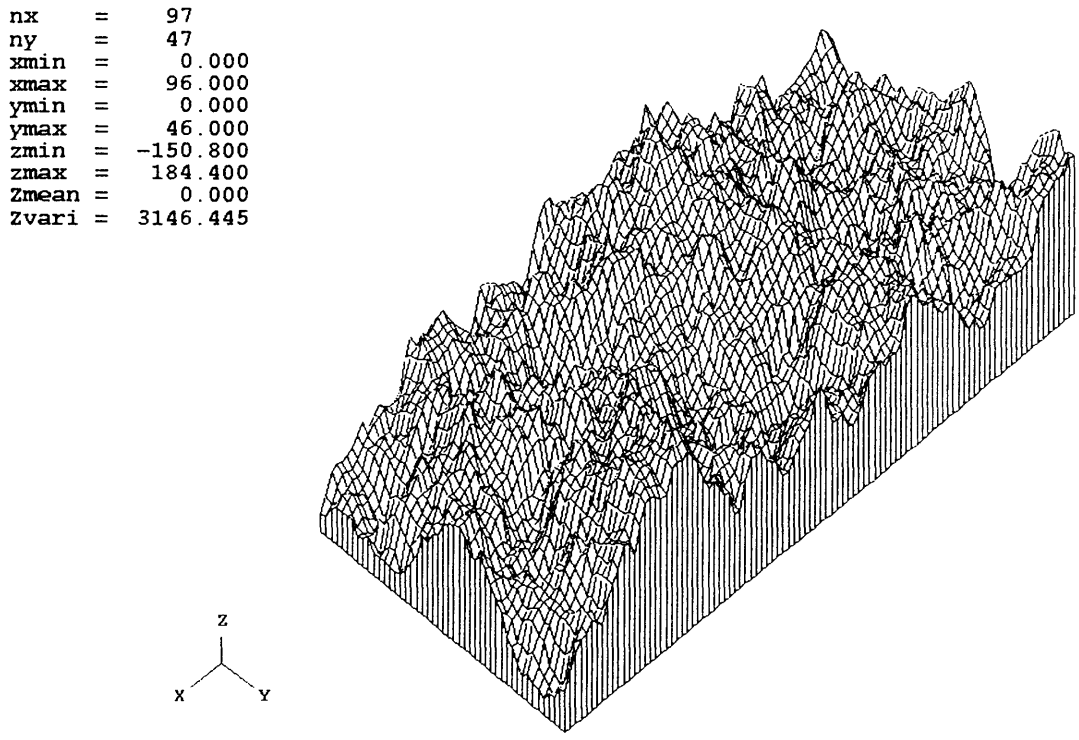

SANDSTONE:TENSION JOINT:UPPER SURFACE:BEFORE SFT

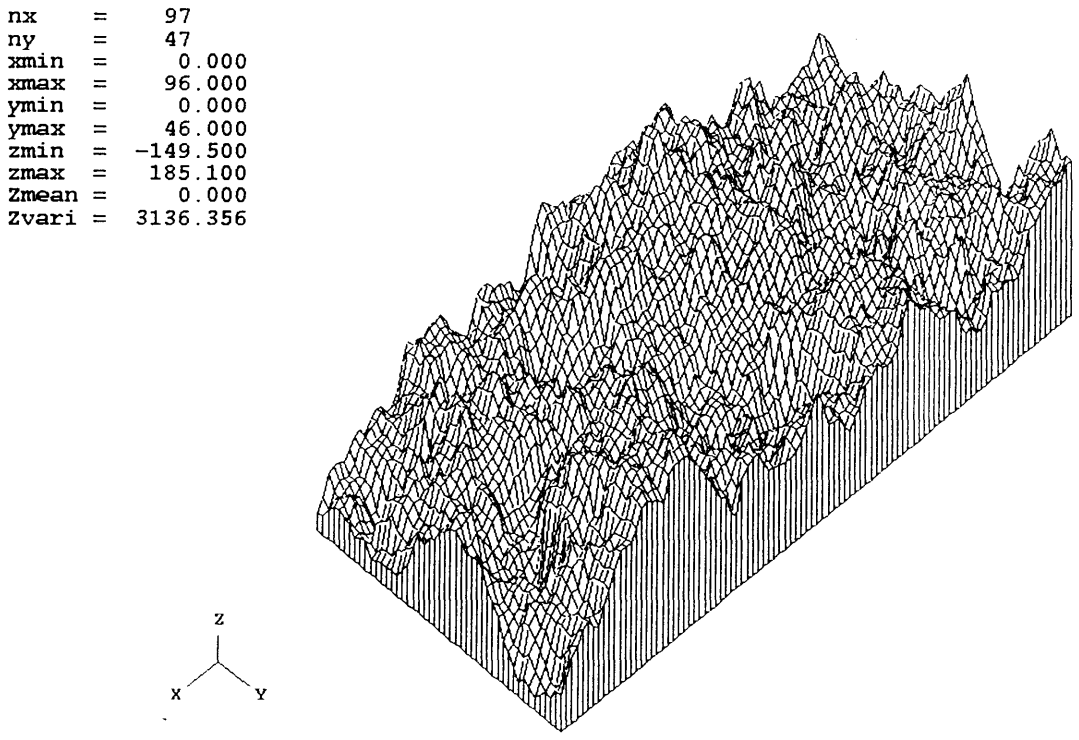

SANDSTONE:TENSION JOINT:LOWER SURFACE:BEFORE SFT

Fig. 3.7 Two digitized surfaces of a joint after linear trend removal (f) Tension joint in Kimachi sandstone

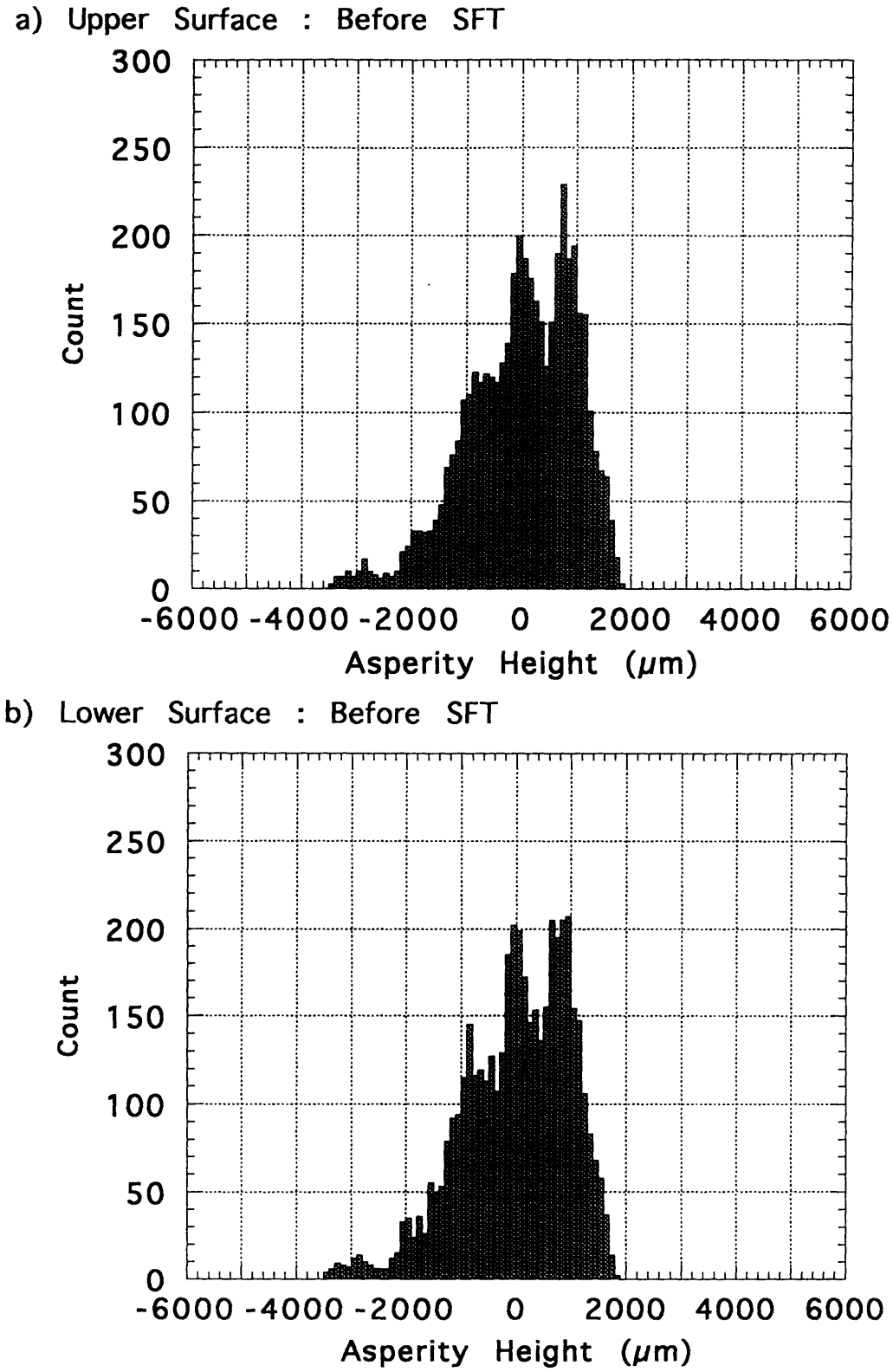

Fig. 3.8 Histogram plot for asperities of two digitized surfaces (a) Natural joint in Kikuma granodiorite

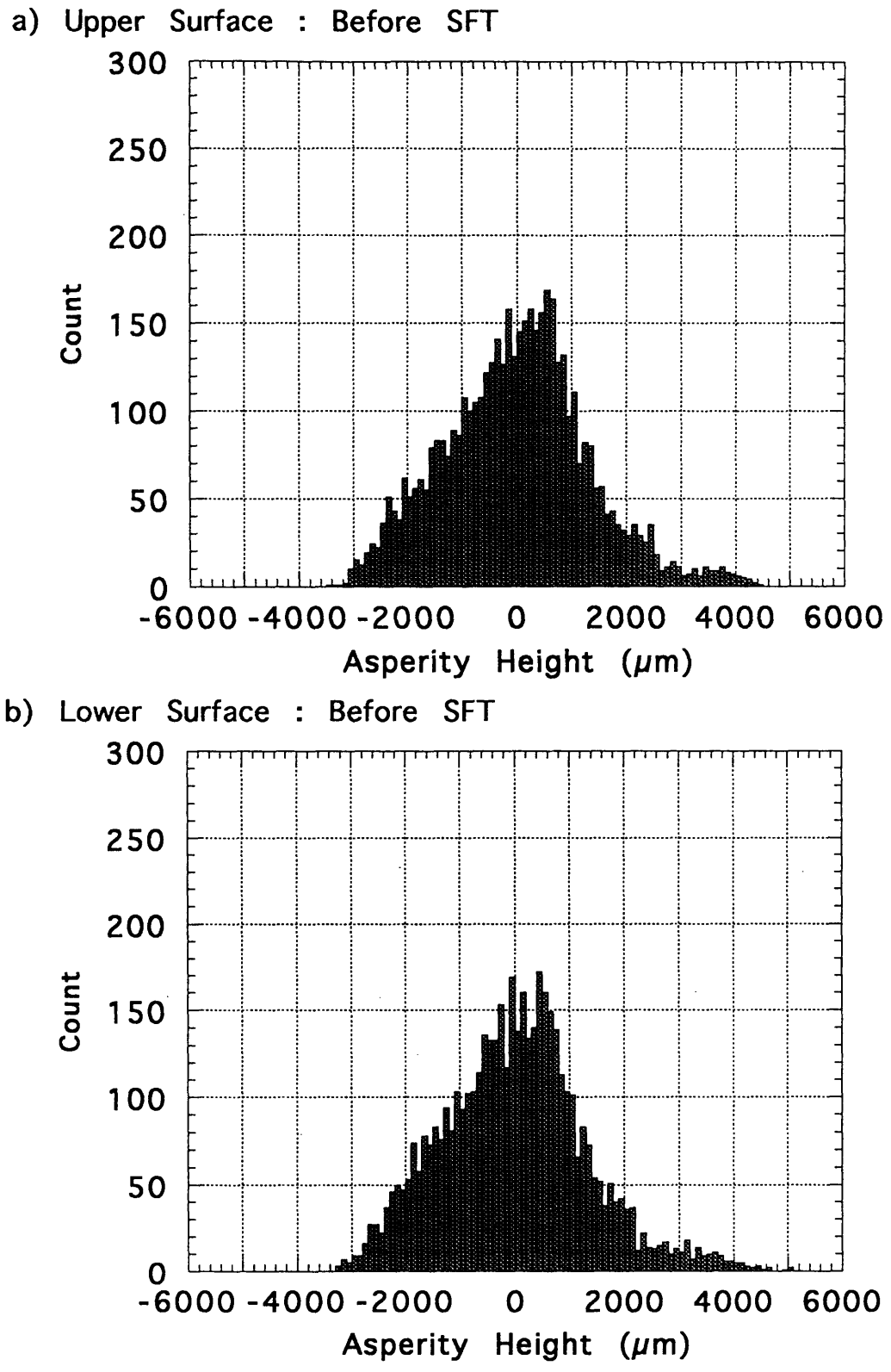

Fig. 3.8 Histogram plot for asperities of two digitized surfaces (b) Tension joint in Kikuma granodiorite

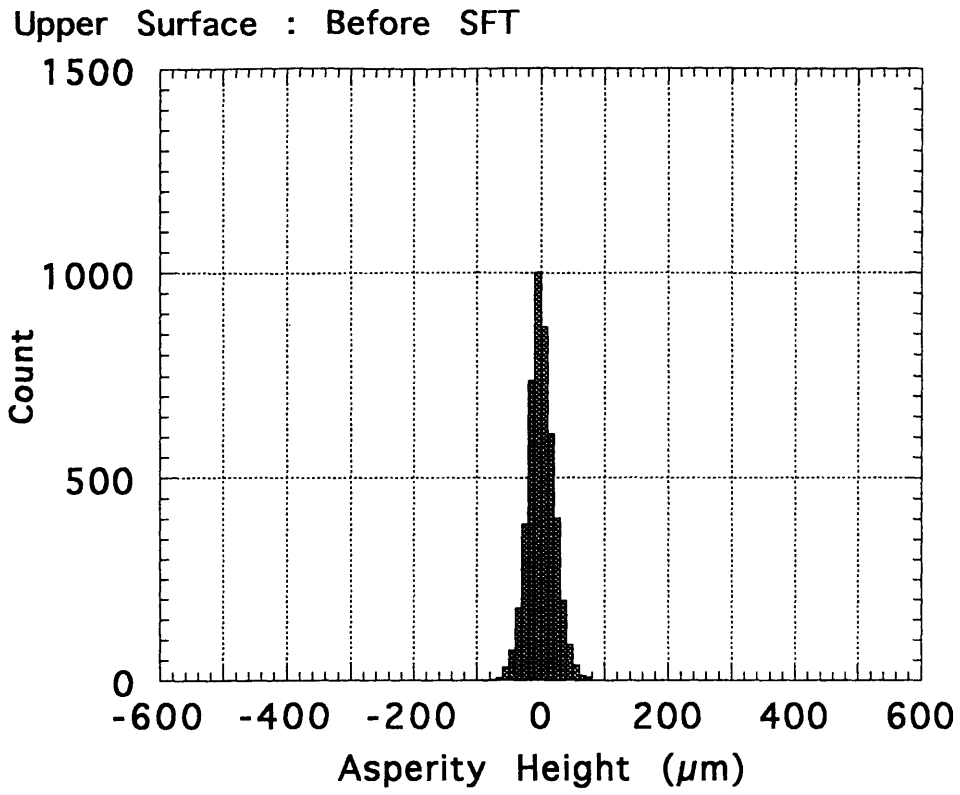

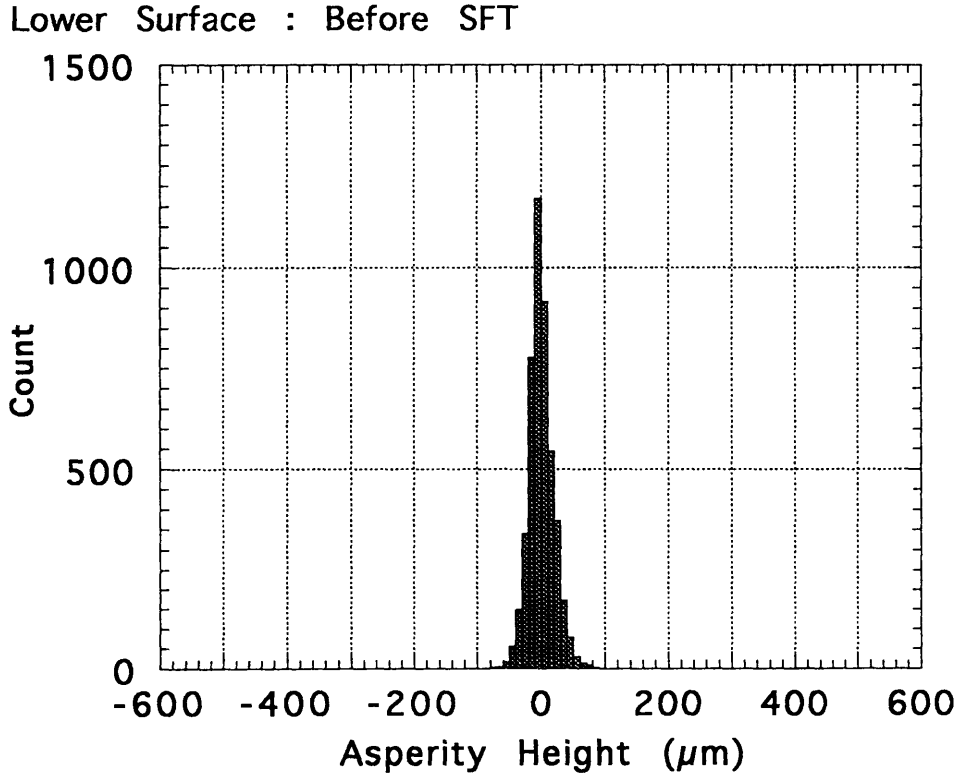

Fig. 3.8 Histogram plot for asperities of two digitized surfaces (c) Sawed joint in Kikuma granodiorite

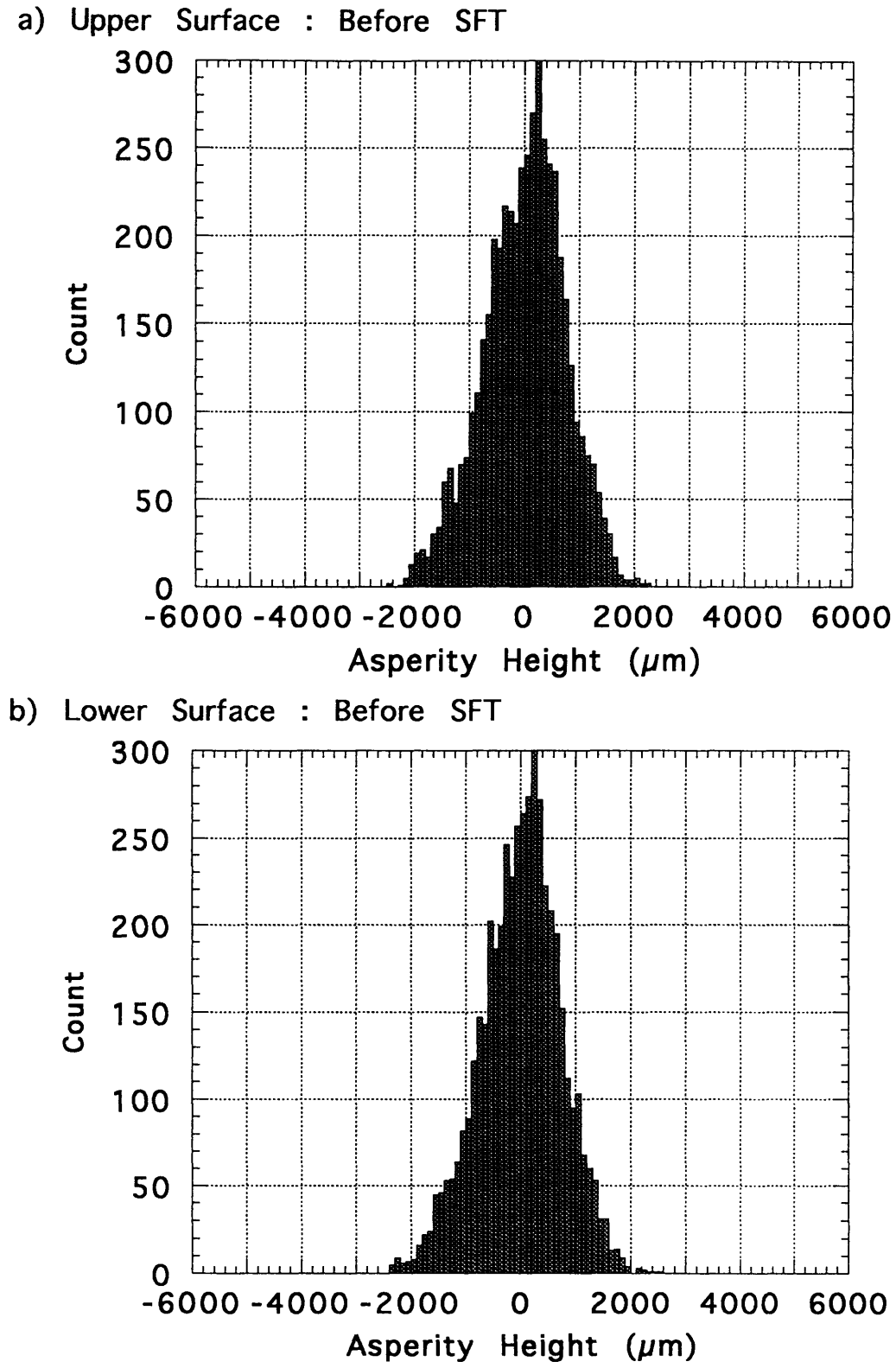

Fig. 3.8 Histogram plot for asperities of two digitized surfaces (d) Tension joint in Inada granite

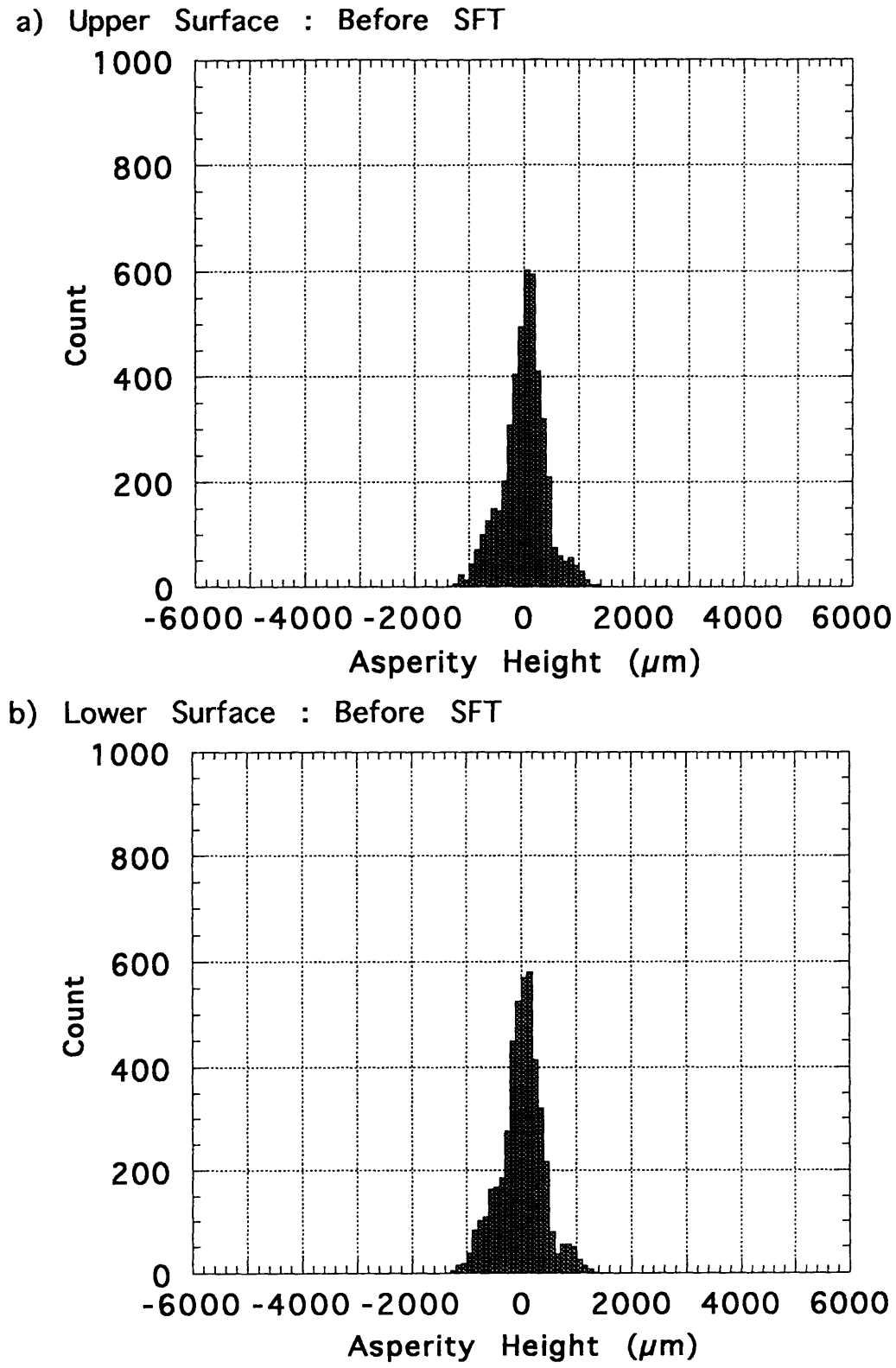

Fig. 3.8 Histogram plot for asperities of two digitized surfaces (e) Tension joint in Chichibu schist

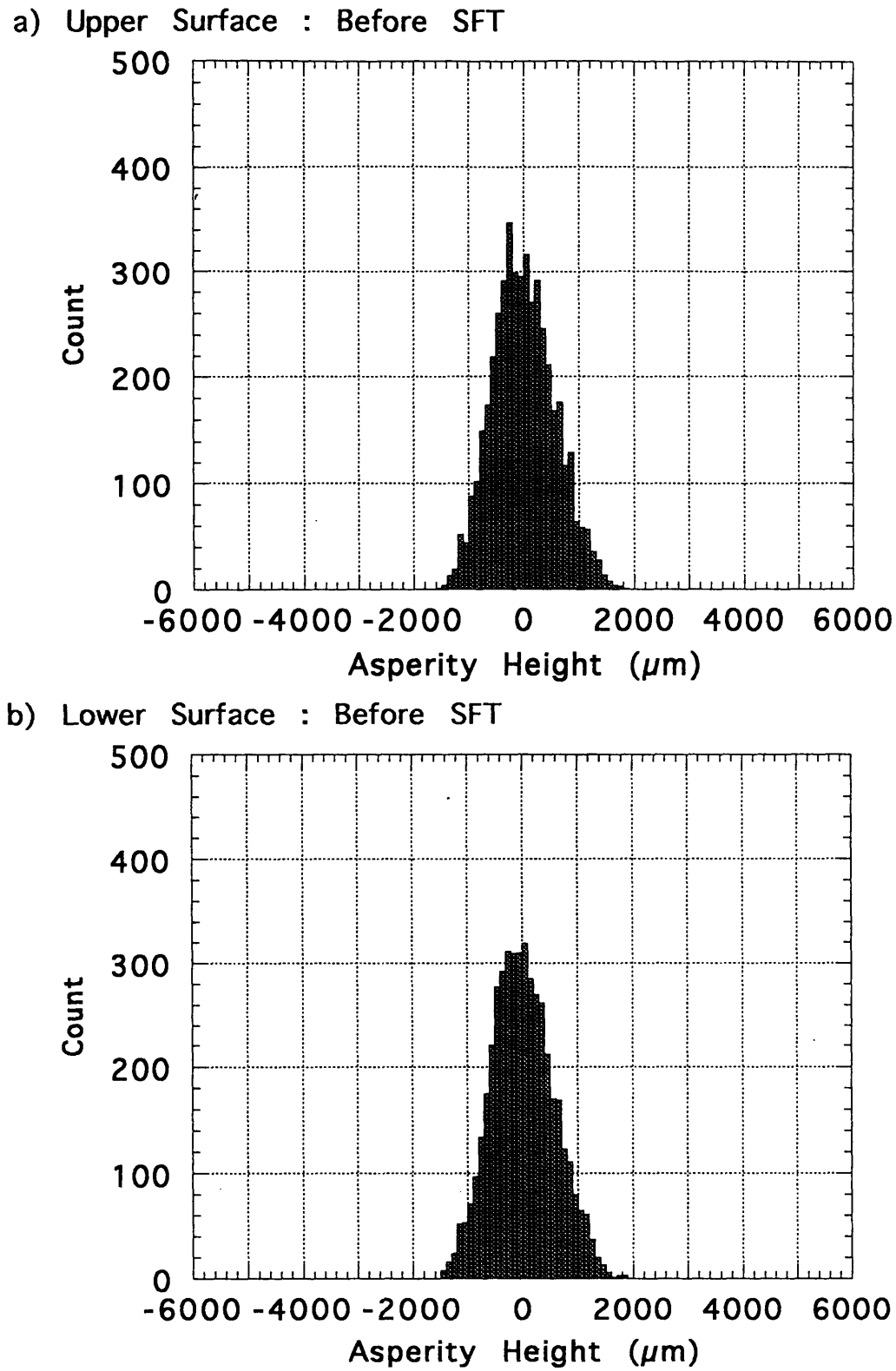

Fig. 3.8 Histogram plot for asperities of two digitized surfaces (f) Tension joint in Kimachi sandstone

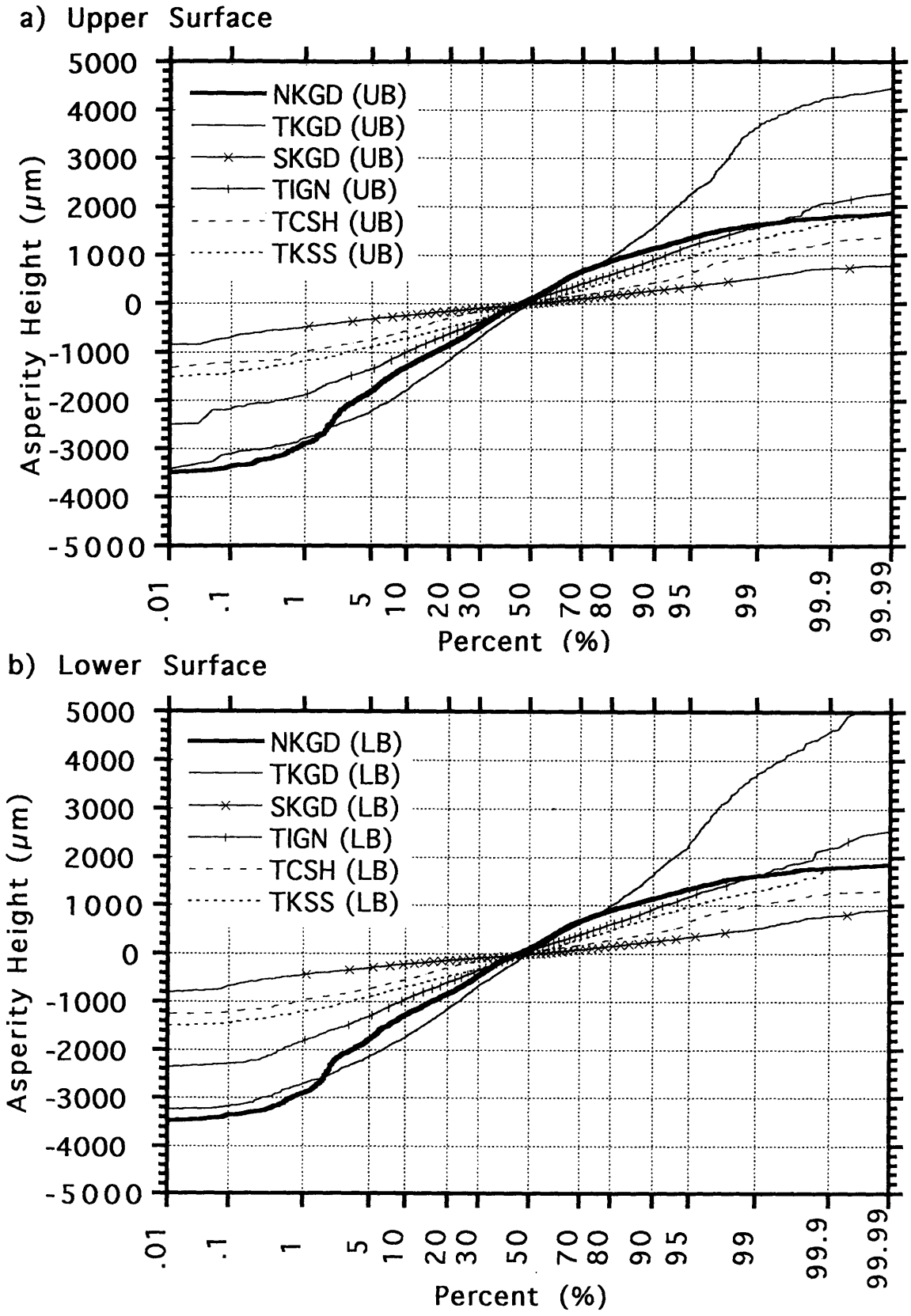

Fig.3.9 Cumulative probability plot of asperity height

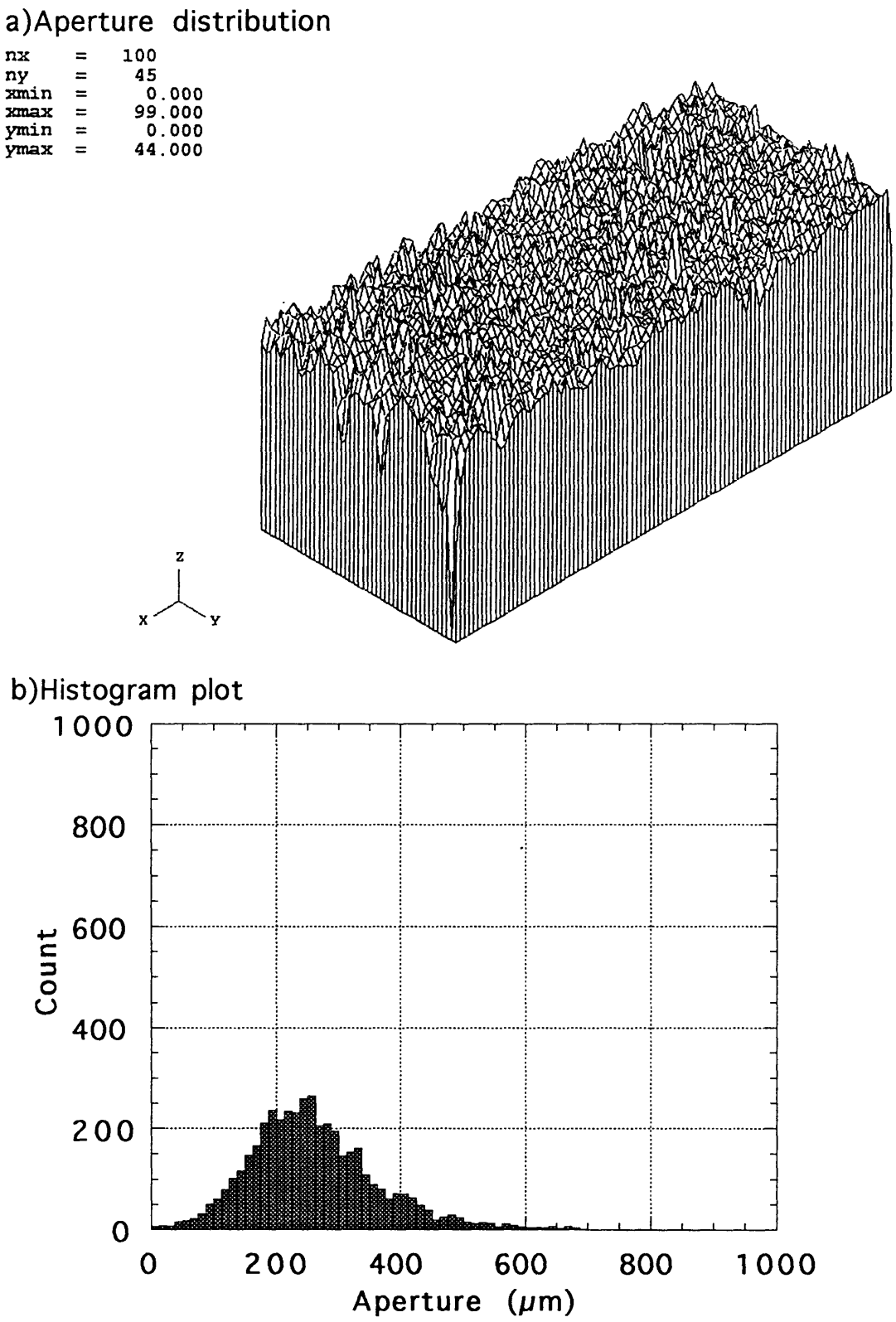

Fig. 3.10 Aperture distribution and its histogram plot
(a) Natural joint in Kikuma granodiorite

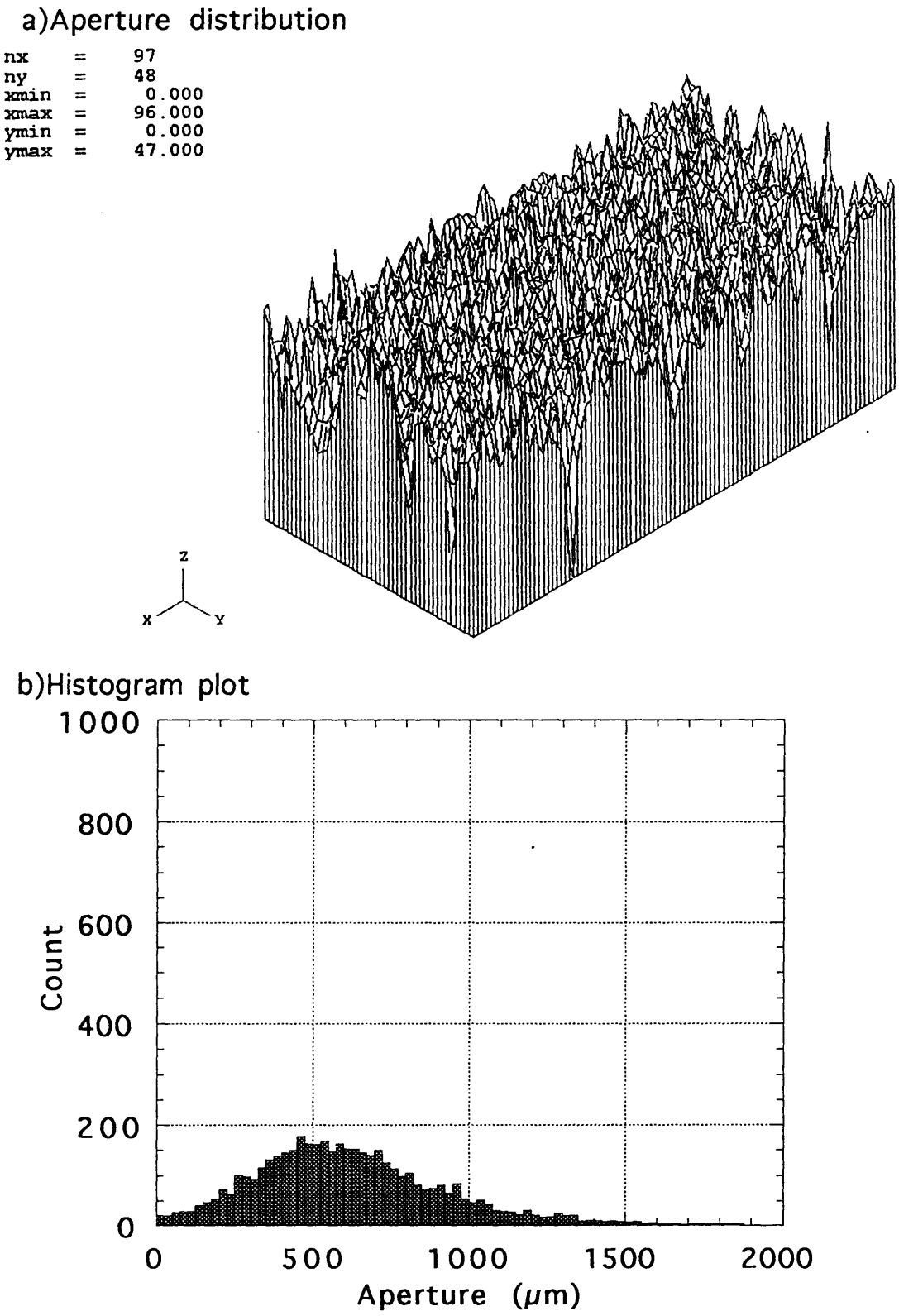

Fig. 3.10 Aperture distribution and its histogram plot
(b) Tension joint in Kikuma granodiorite

a)Aperture distribution

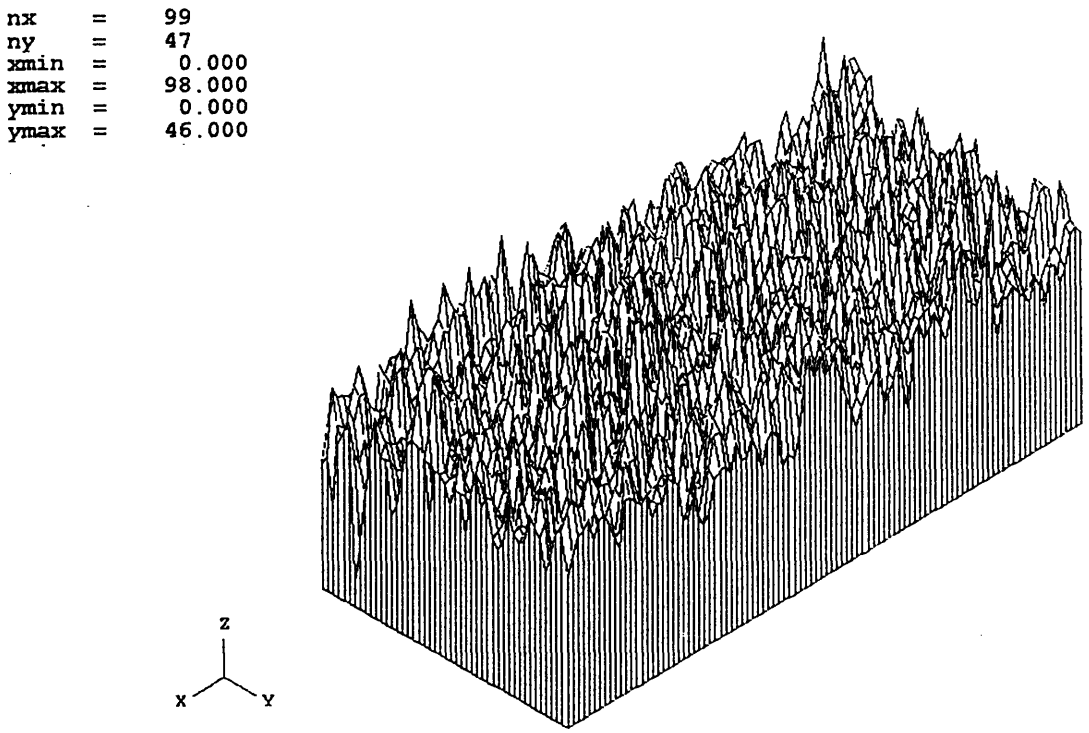

b)Histogram plot

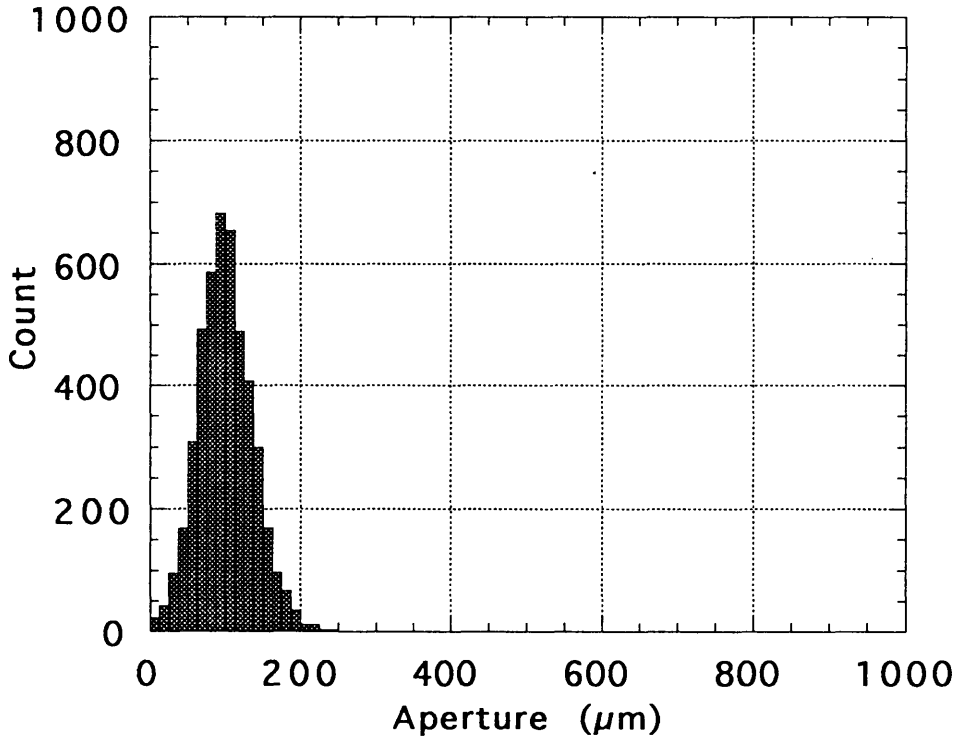

Fig. 3.10 Aperture distribution and its histogram plot
(c) Sawed joint in Kikuma granodiorite

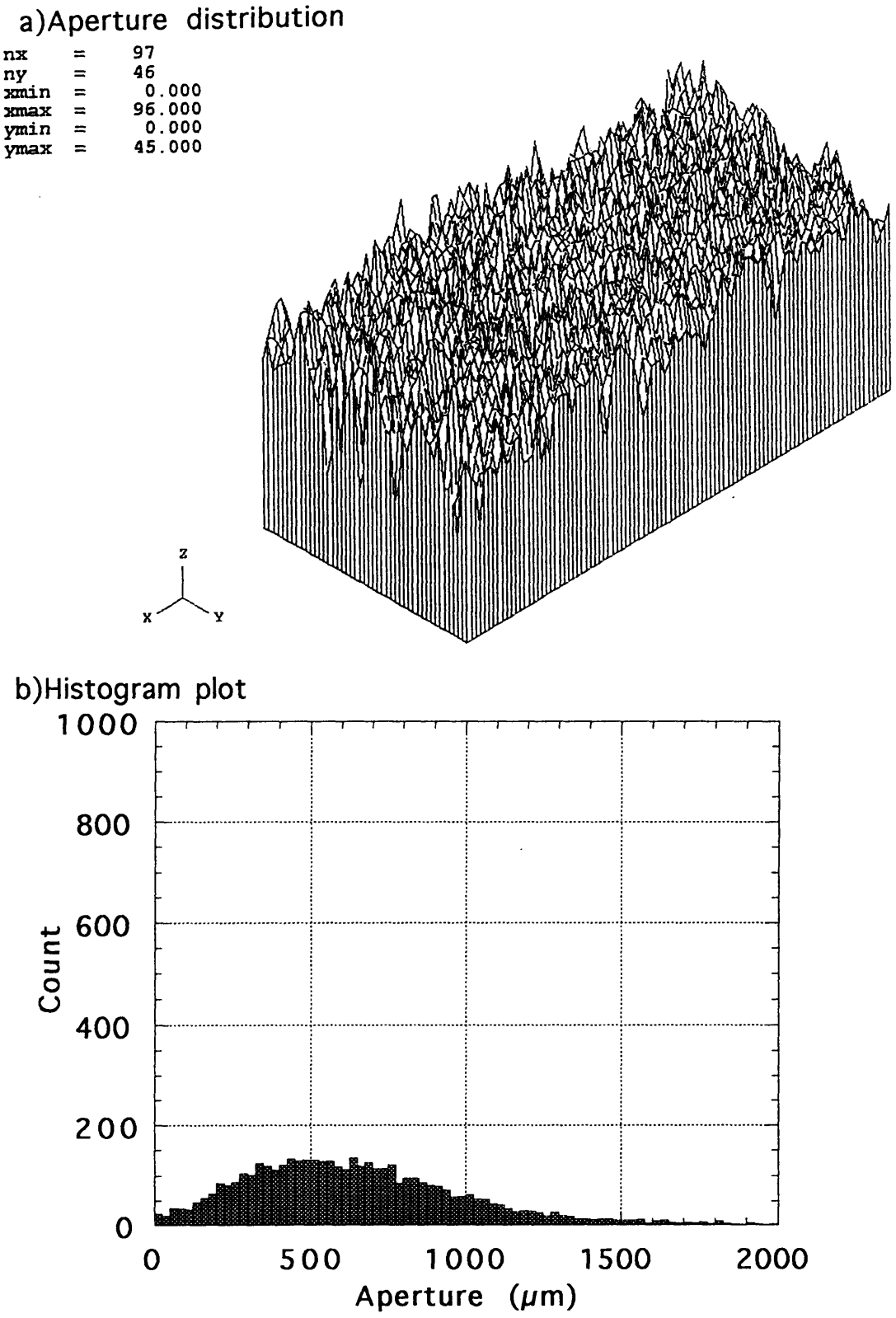

Fig. 3.10 Aperture distribution and its histogram plot
(d) Tension joint in Inada granite

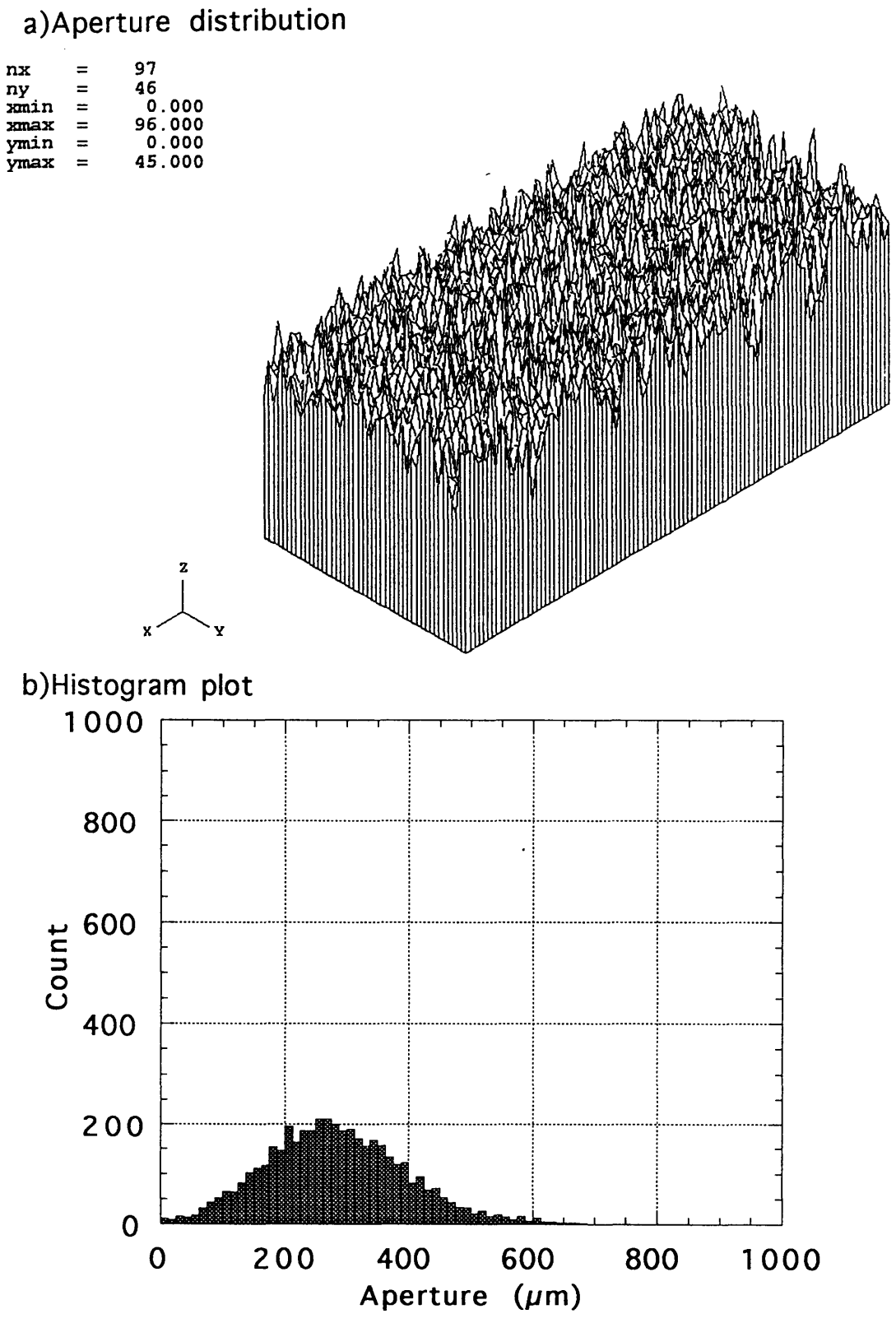

Fig. 3.10 Aperture distribution and its histogram plot
(e) Tension joint in Chichibu schist

a)Aperture distribution

nx = 97
ny = 46
xmin = 21.000
xmax = 117.000
ymin = 41.000
ymax = 86.000

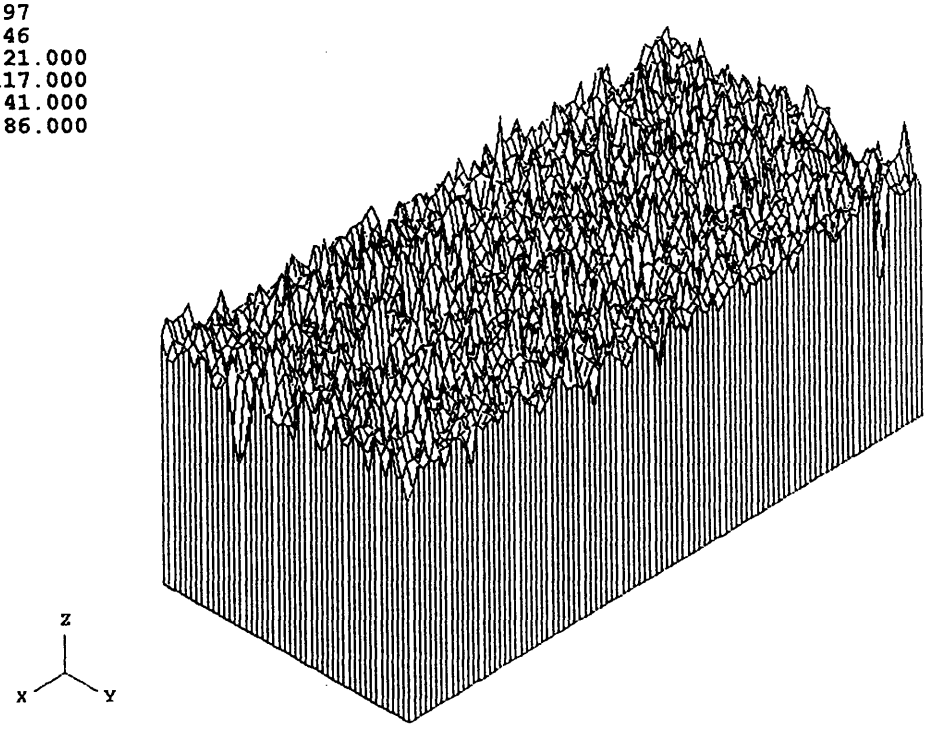

b)Histogram plot

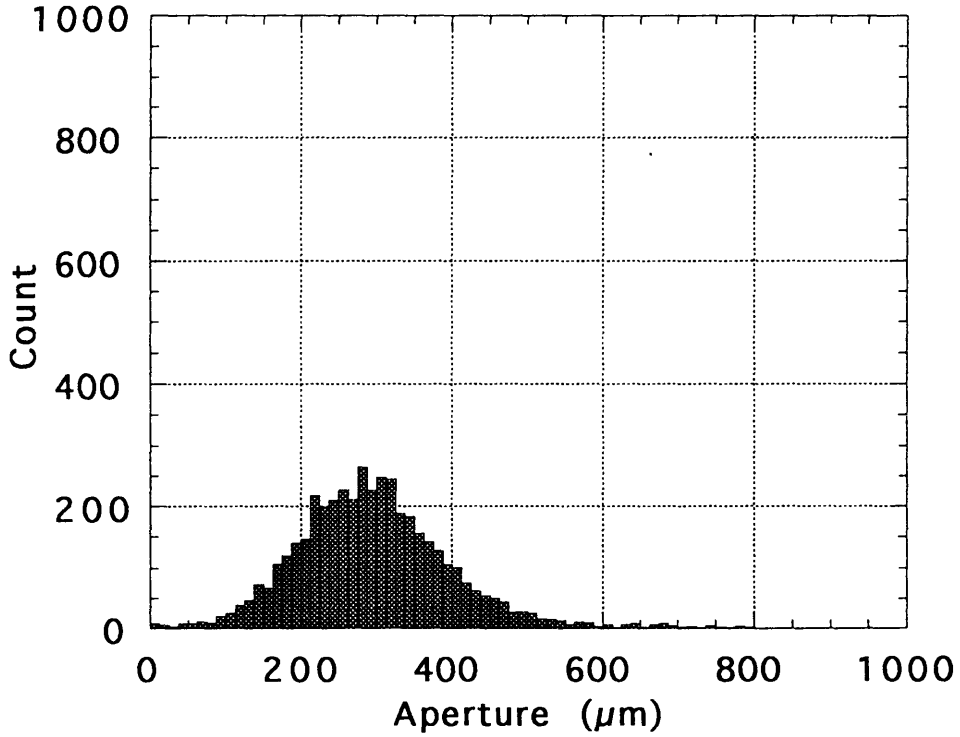

Fig. 3.10 Aperture distribution and its histogram plot
(f) Tension joint in Kimachi sandstone

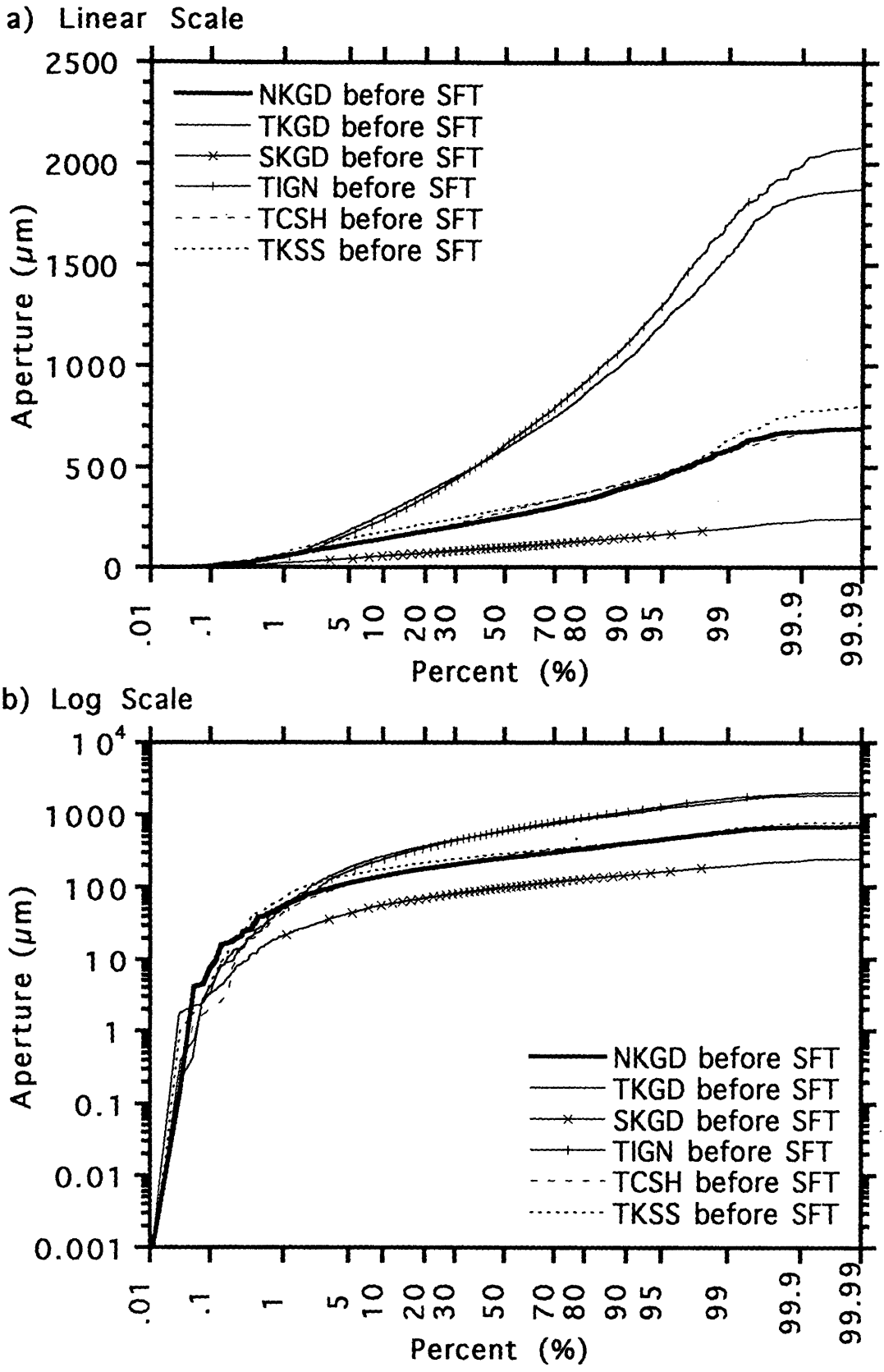

Fig. 3.11 Cumulative probability plot for aperture

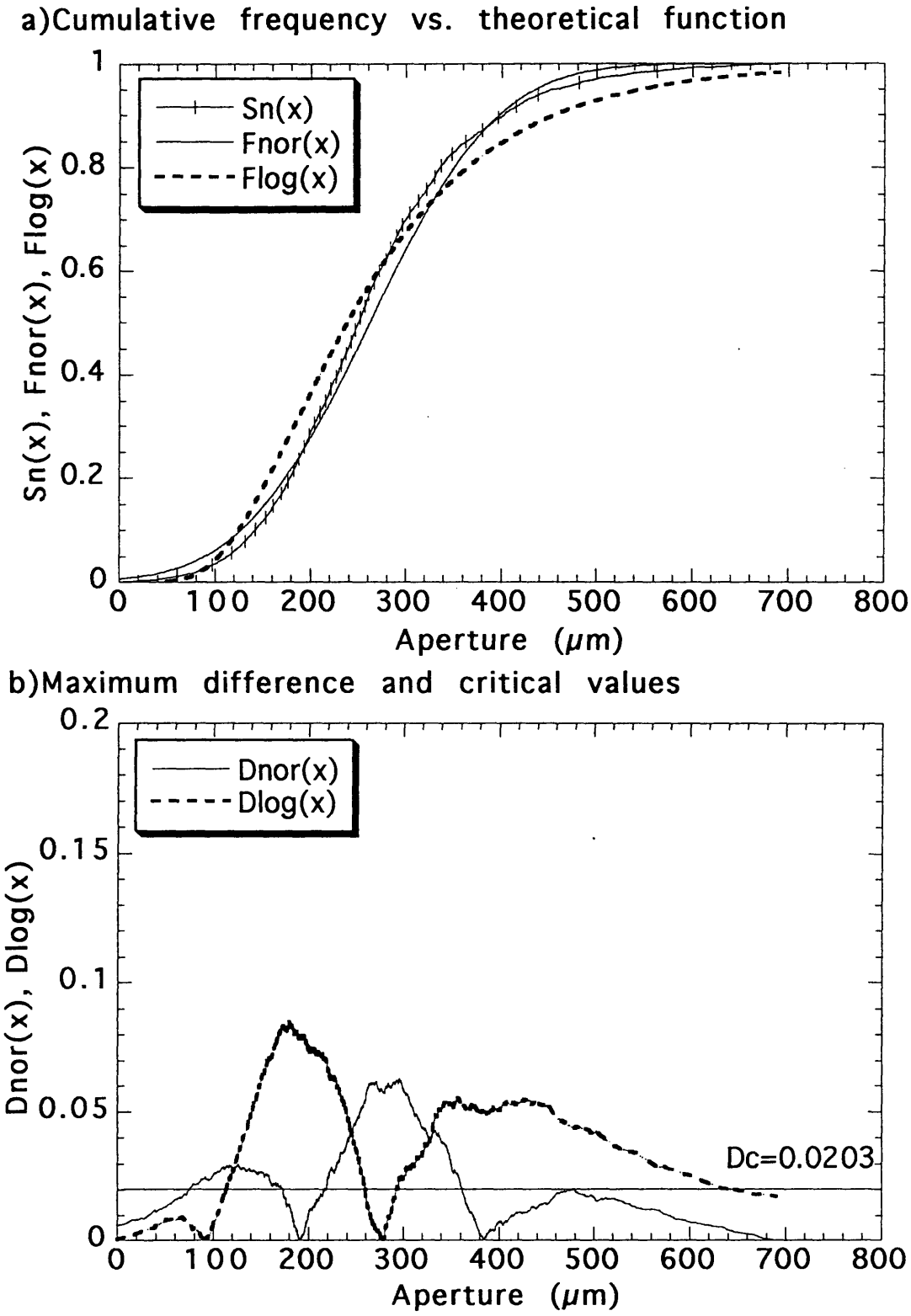

Fig. 3.12 Results of S-K goodness-of-fit test
(a) Natural joint in Kikuma granodiorite

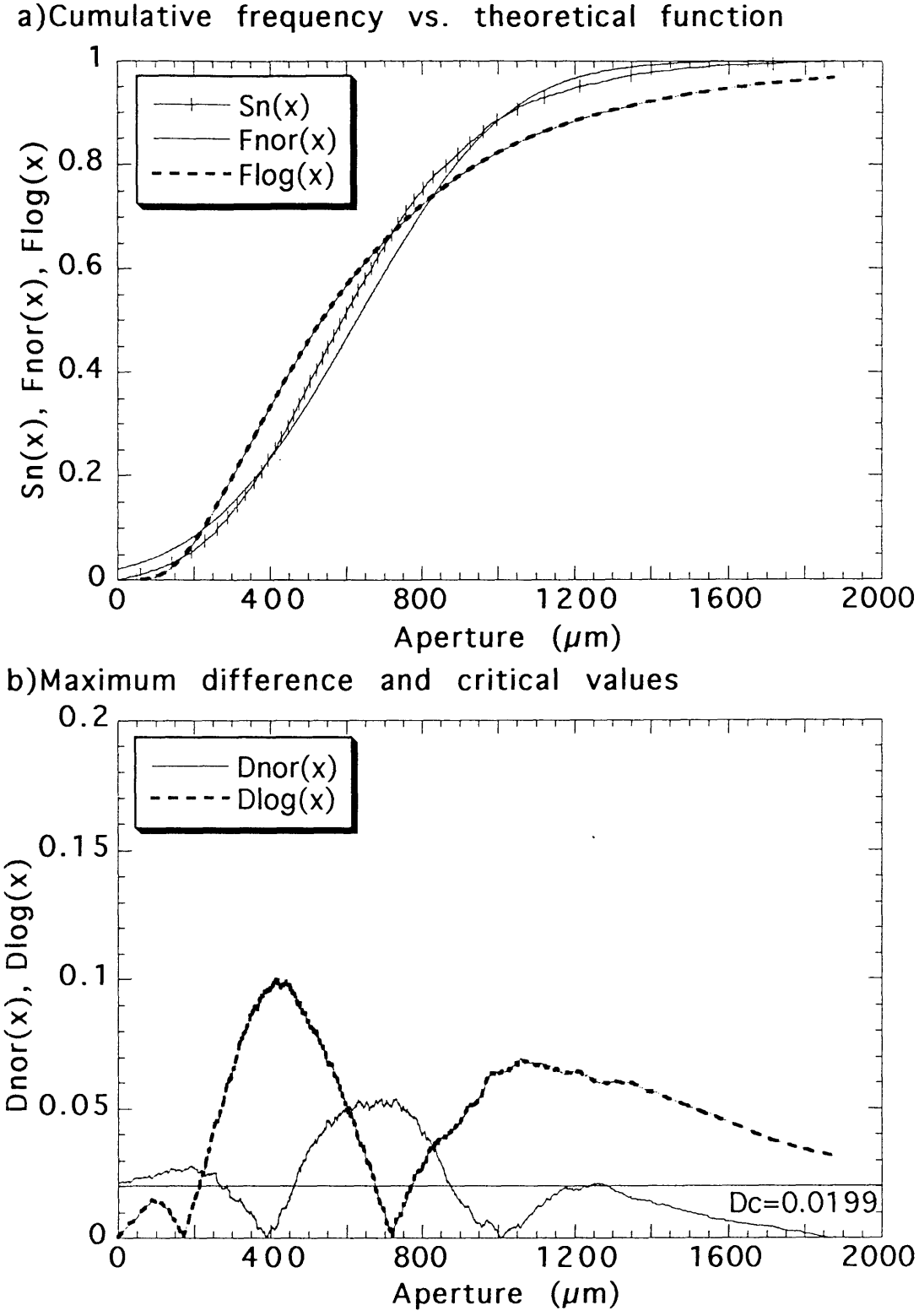

Fig. 3.12 Results of S-K goodness-of-fit test
(b) Tension joint in Kikuma granodiorite

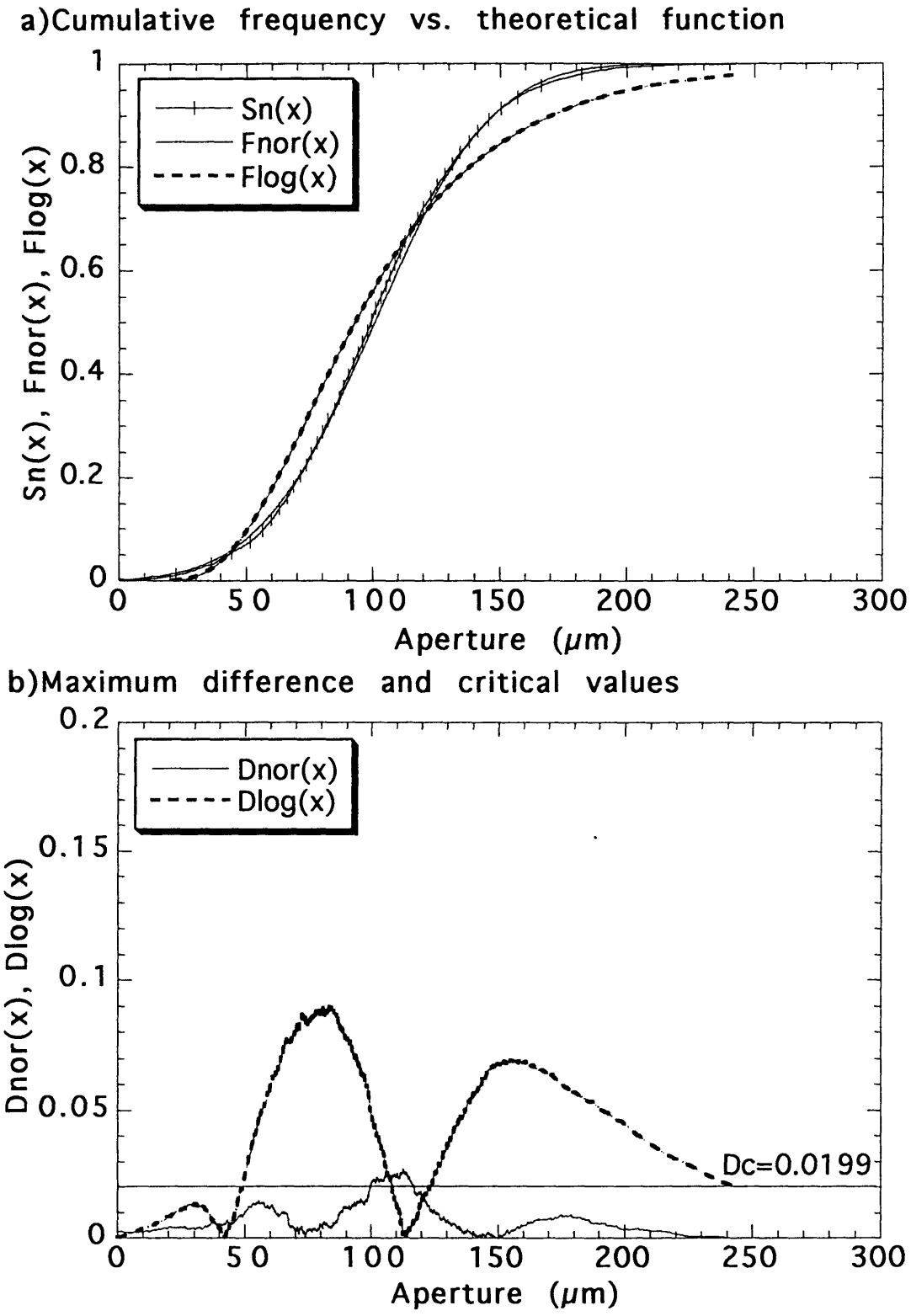

Fig. 3.12 Results of S-K goodness-of-fit test
(c) Sawed joint in Kikuma granodiorite

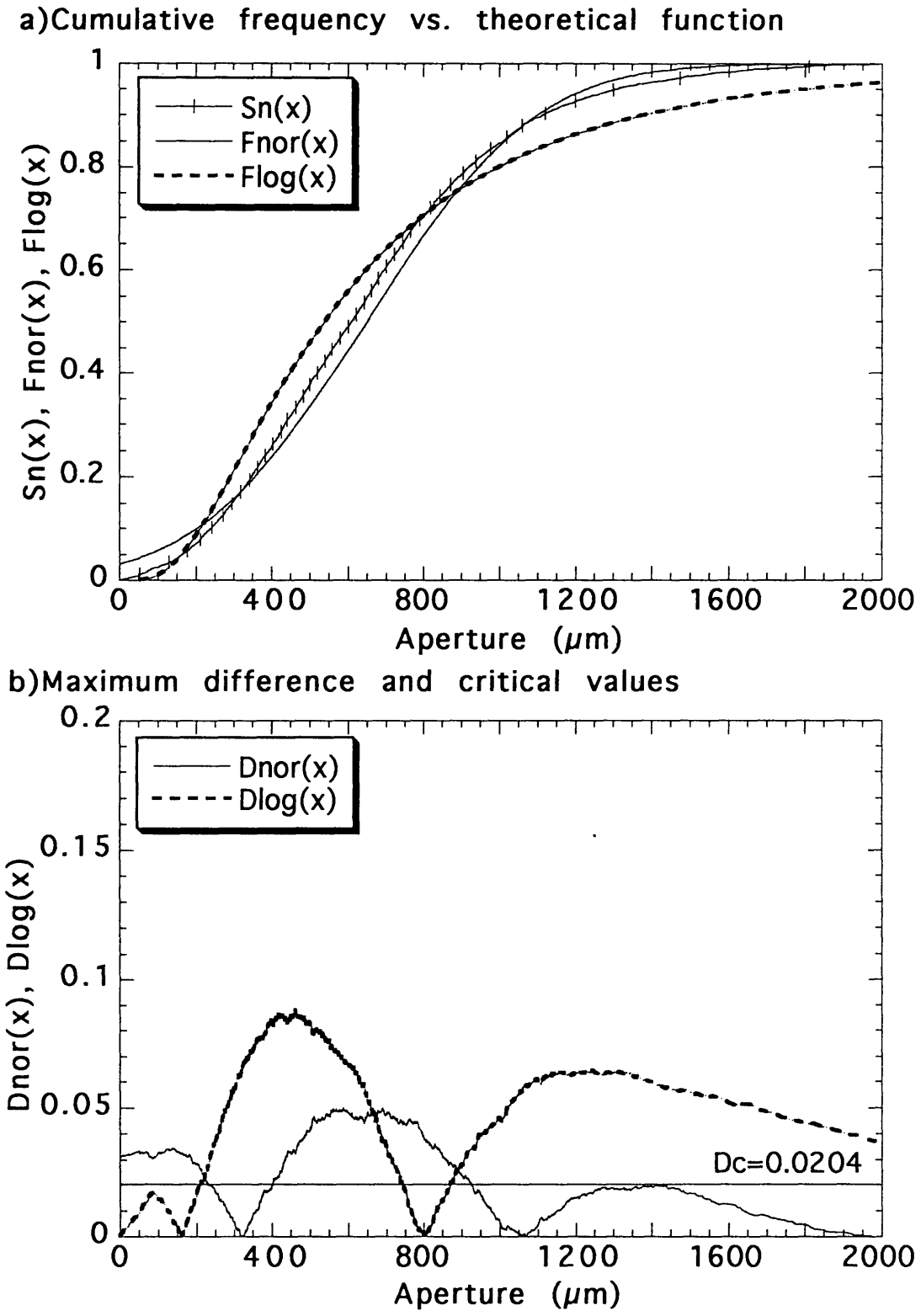

Fig. 3.12 Results of S-K goodness-of-fit test
(d) Tension joint in Inada granite

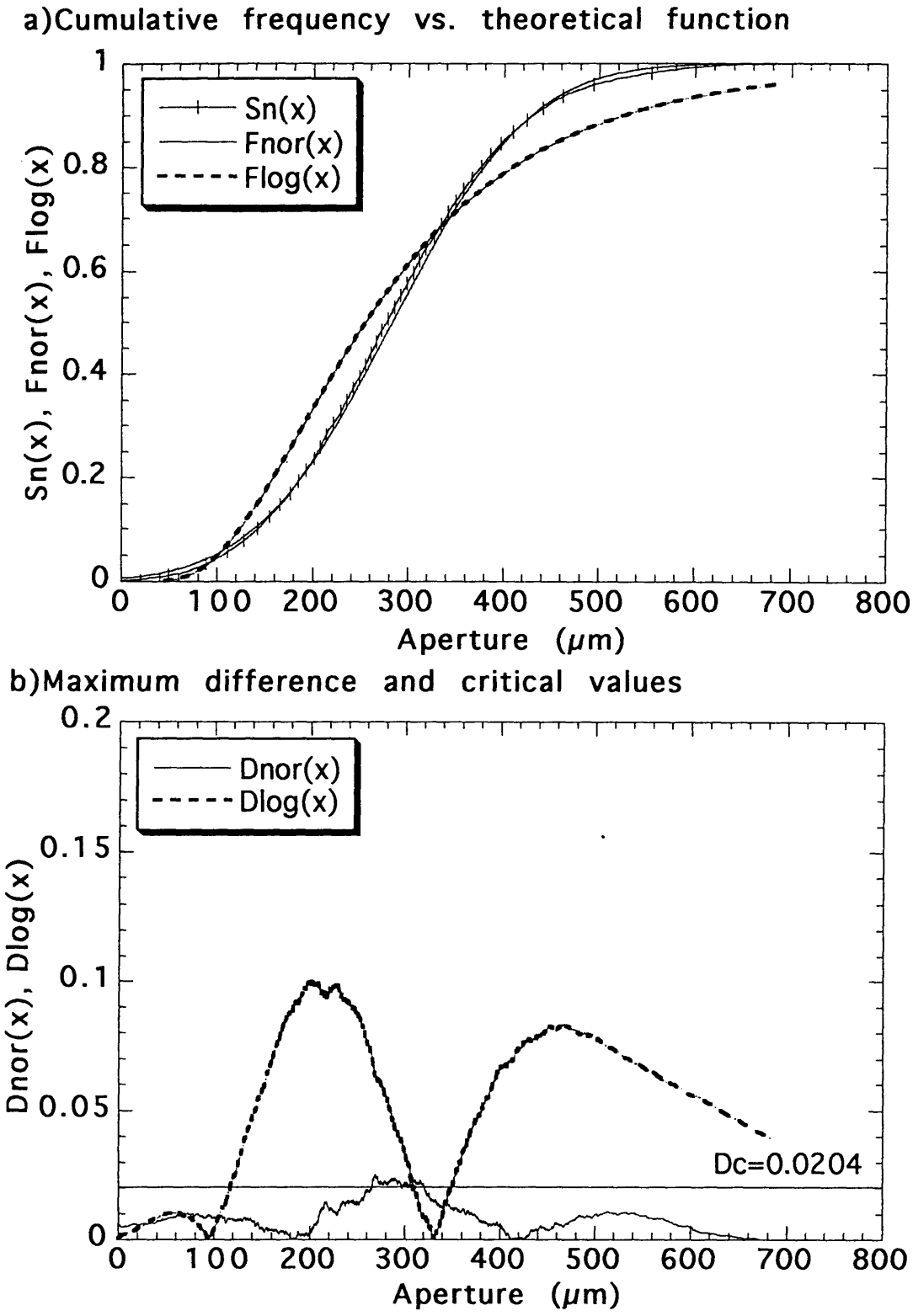

Fig. 3.12 Results of S-K goodness-of-fit test
(e) Tension joint in Chichibu schist

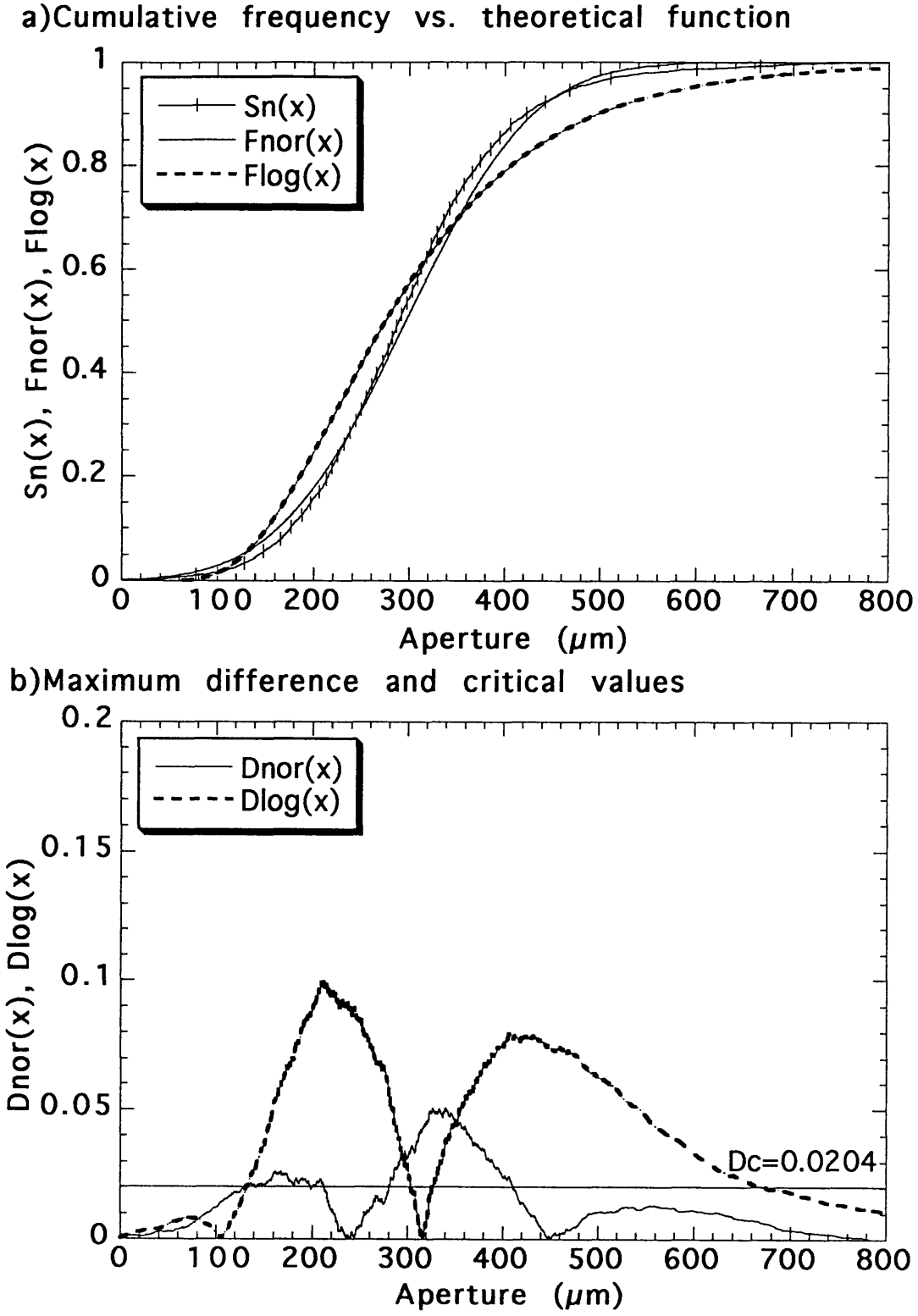

Fig. 3.12 Results of S-K goodness-of-fit test
(f) Tension joint in Kimachi sandstone

a)Correlation functions along four lines in a joint plane
(0, 30, 60, 90 degree oriented to the core axis)

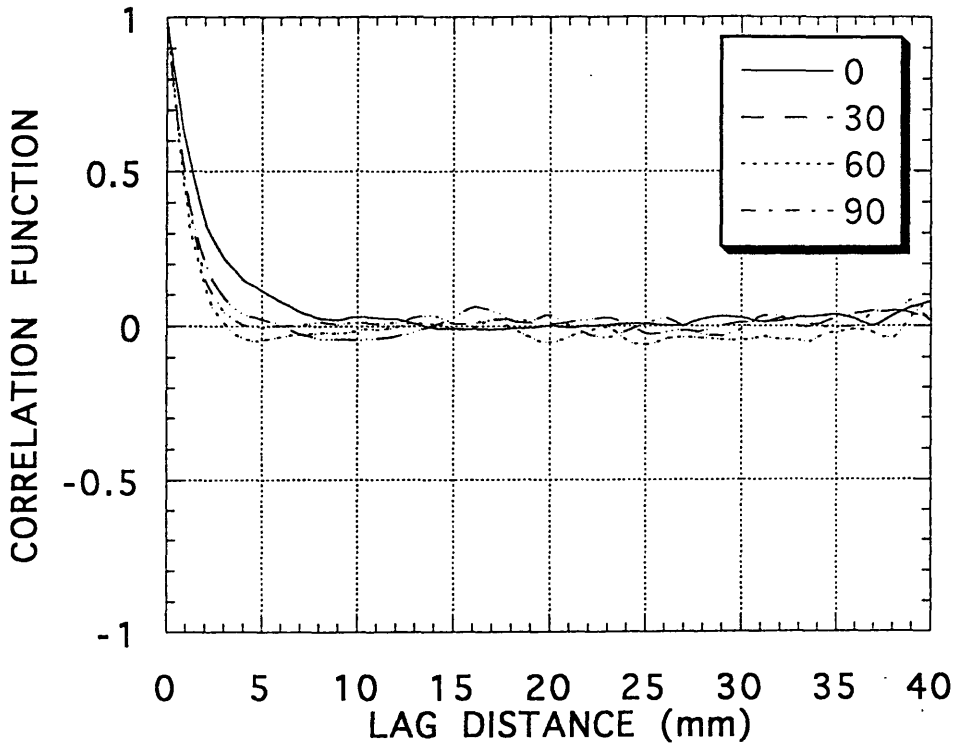

b)2-dimension correlation function in a joint plane

```
nx    =   198
ny    =    88
xmin  =  -99.000
xmax  =   99.000
ymin  =  -44.000
ymax  =   44.000
zmin  =   -0.299
zmax  =    1.000
```

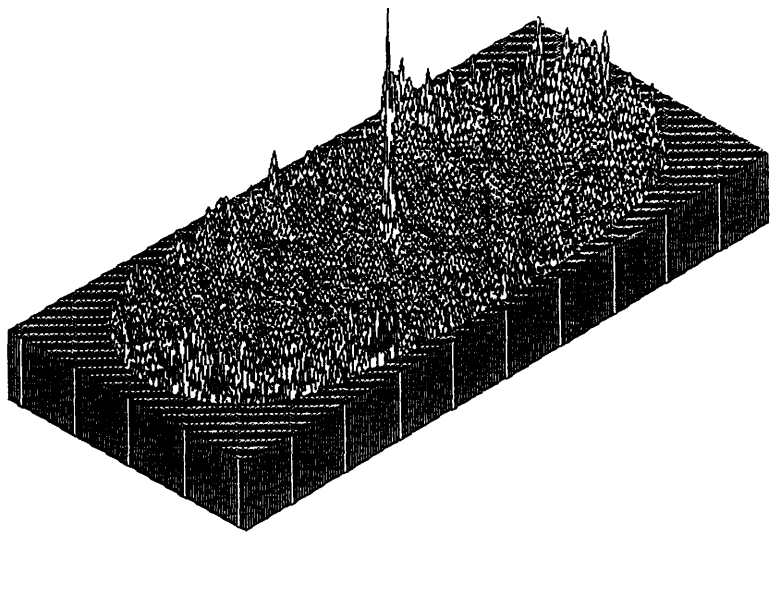

Fig. 3.13 Correlation function of aperture
(a) Natural joint in Kikuma granodiorite

a)Correlation functions along four lines in a joint plane
(0, 30, 60, 90 degree oriented to the core axis)

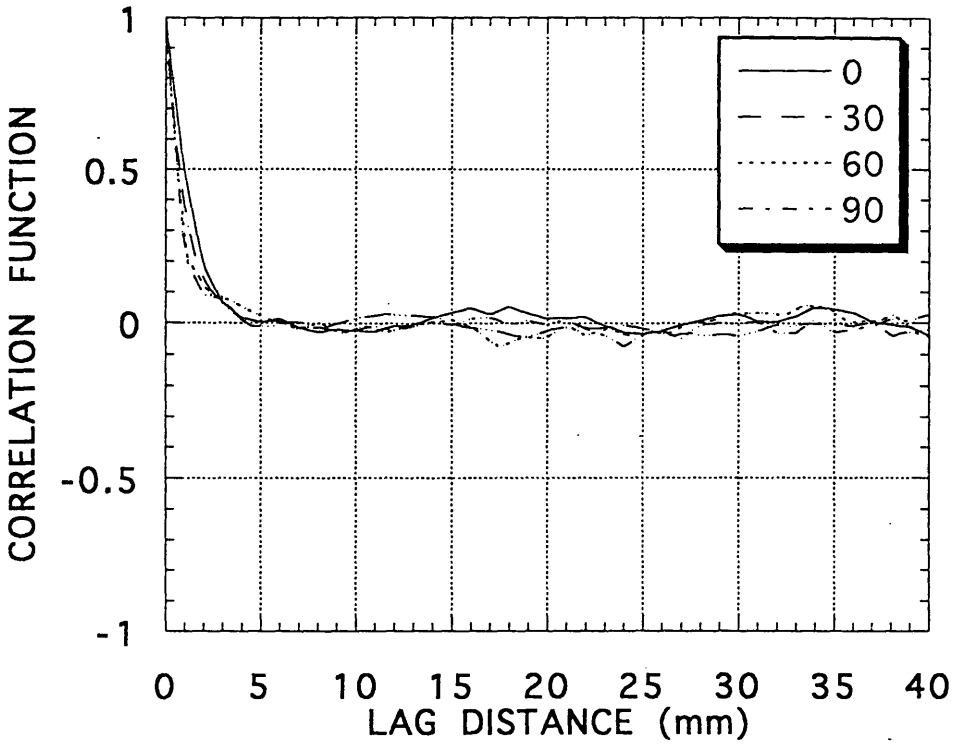

b)2-dimension correlation function in a joint plane

```
nx    =   196
ny    =    92
xmin  =  -98.000
xmax  =   98.000
ymin  =  -46.000
ymax  =   46.000
zmin  =   -0.302
zmax  =    1.000
```

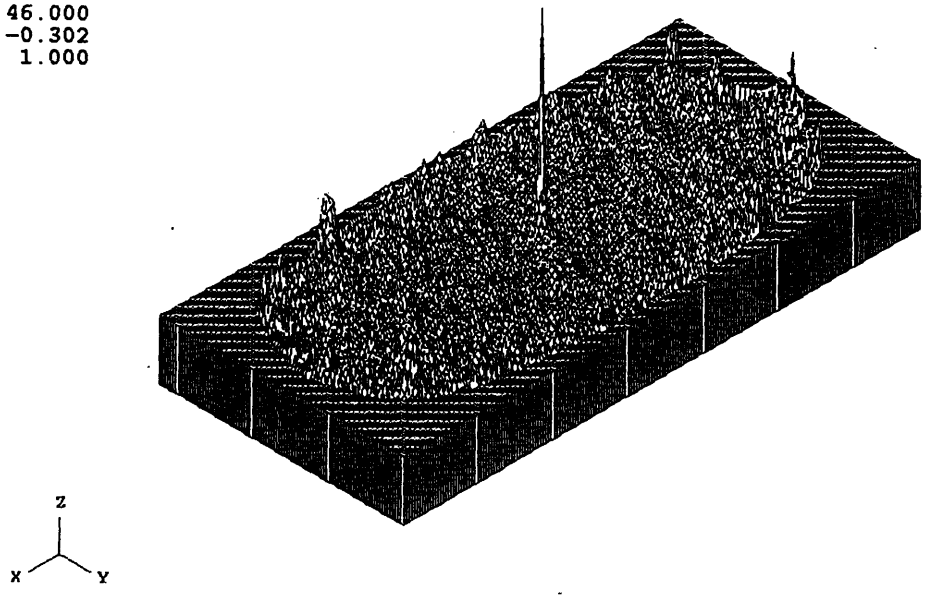

Fig. 3.13 Correlation function of aperture
(b) Tension joint in Kikuma granodiorite

a)Correlation functions along four lines in a joint plane
(0, 30, 60, 90 degree oriented to the core axis)

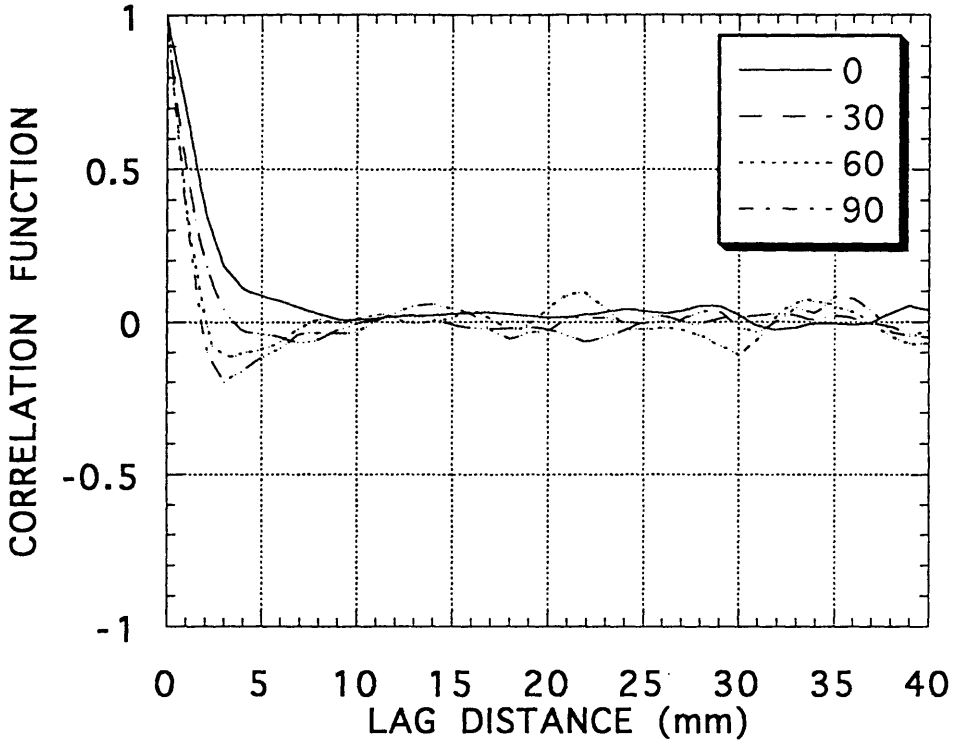

b)2-dimension correlation function in a joint plane

nx = 196
ny = 92
xmin = -98.000
xmax = 98.000
ymin = -46.000
ymax = 46.000
zmin = -0.306
zmax = 1.000

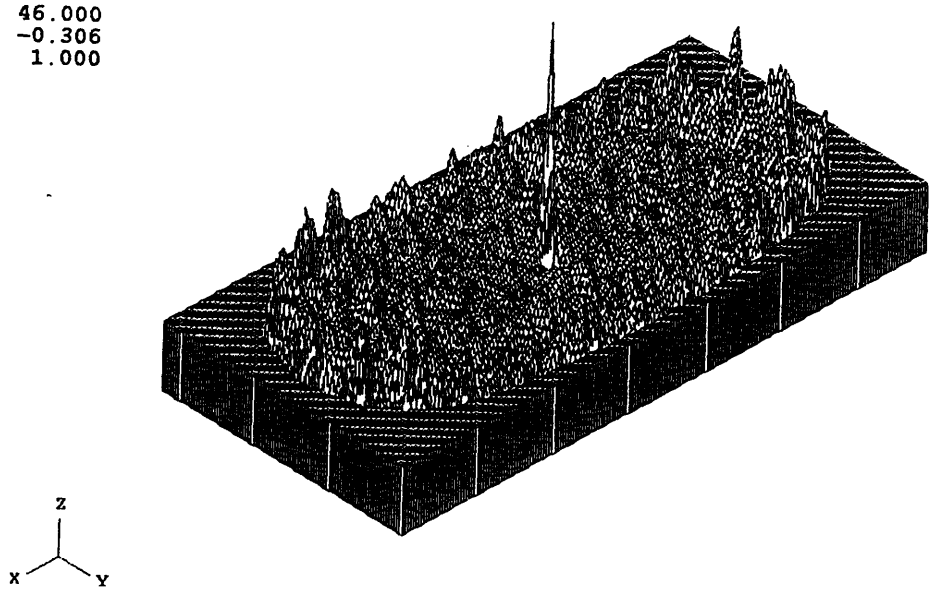

Fig. 3.13 Correlation function of aperture
(c) Sawed joint in Kikuma granodiorite

a)Correlation functions along four lines in a joint plane
(0, 30, 60, 90 degree oriented to the core axis)

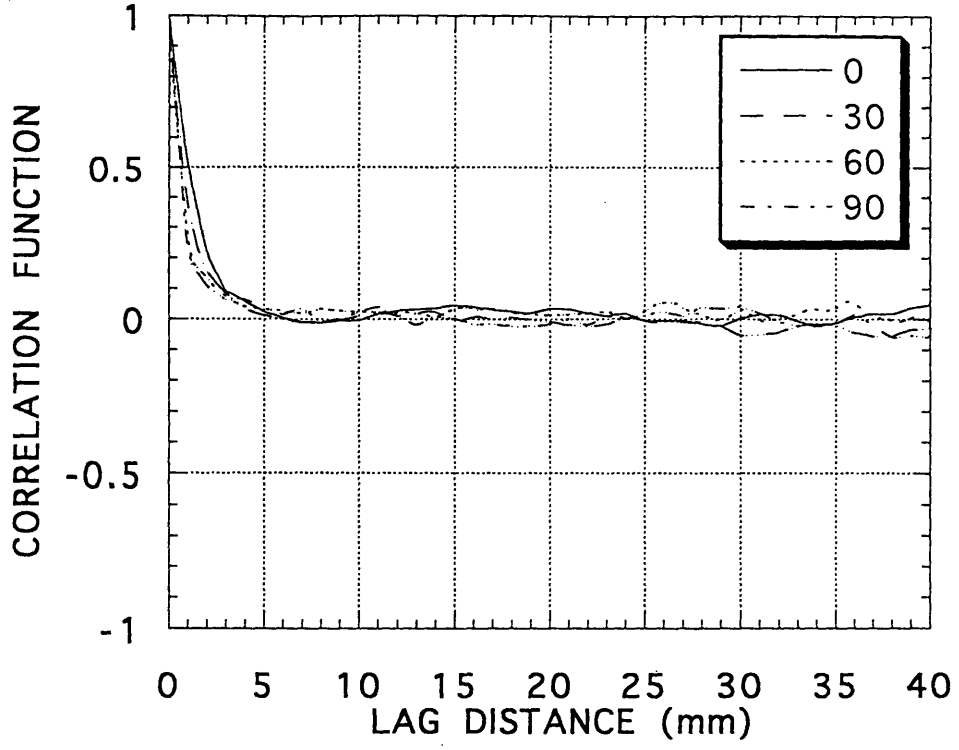

b)2-dimension correlation function in a joint plane

```
nx   =   193
ny   =    97
xmin =  -96.000
xmax =   96.000
ymin =  -48.000
ymax =   48.000
zmin =   -0.215
zmax =    1.000
```

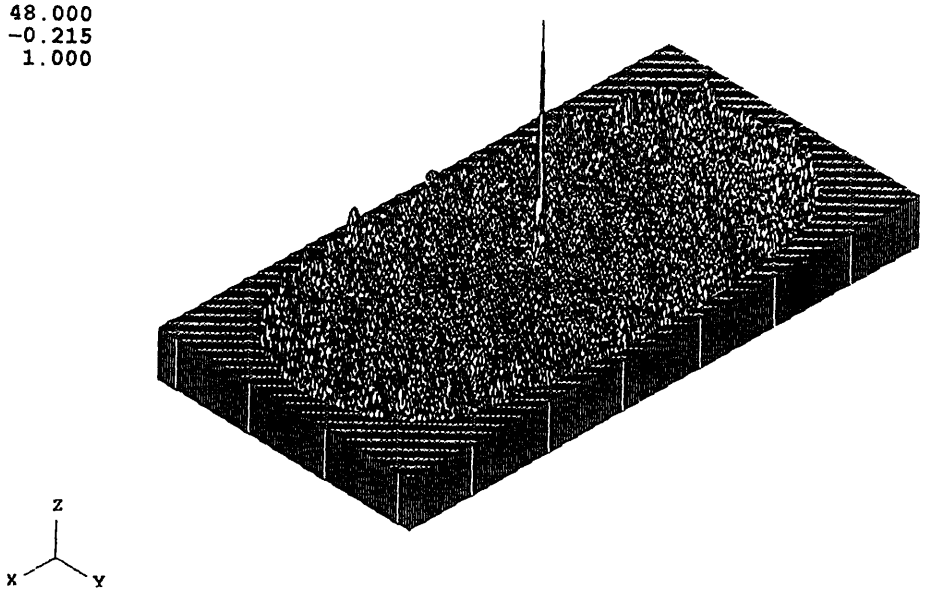

Fig. 3.13 Correlation function of aperture
(d) Tension joint in Inada granite

a)Correlation functions along four lines in a joint plane
(0, 30, 60, 90 degree oriented to the core axis)

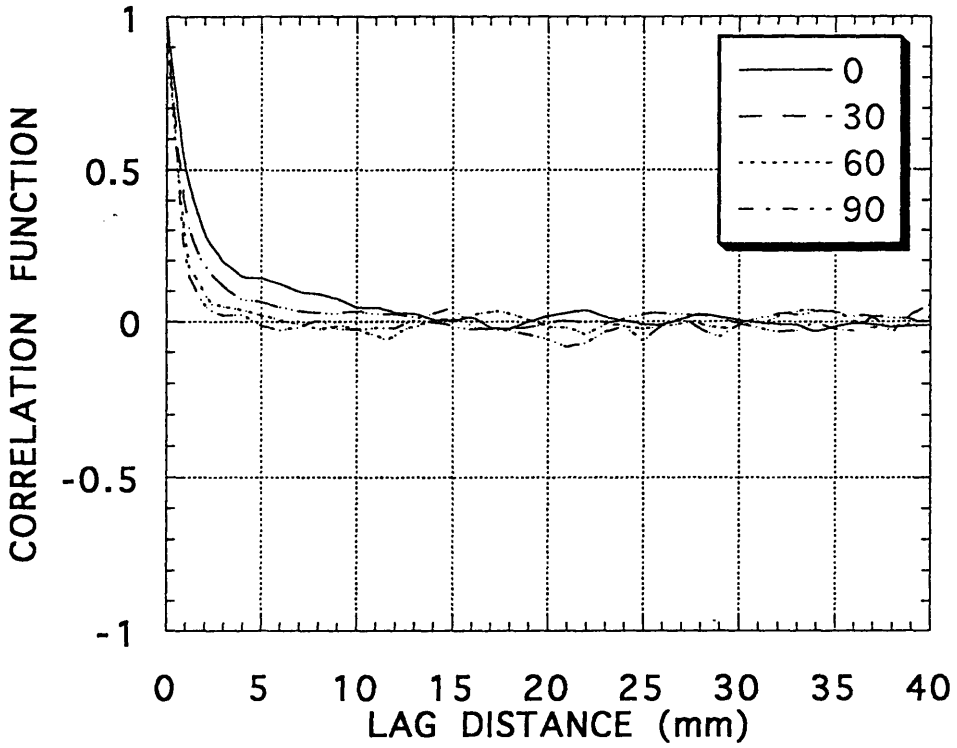

b)2-dimension correlation function in a joint plane

```
nx    =   192
ny    =    92
xmin  =  -96.000
xmax  =   96.000
ymin  =  -46.000
ymax  =   46.000
zmin  =   -0.257
zmax  =    1.000
```

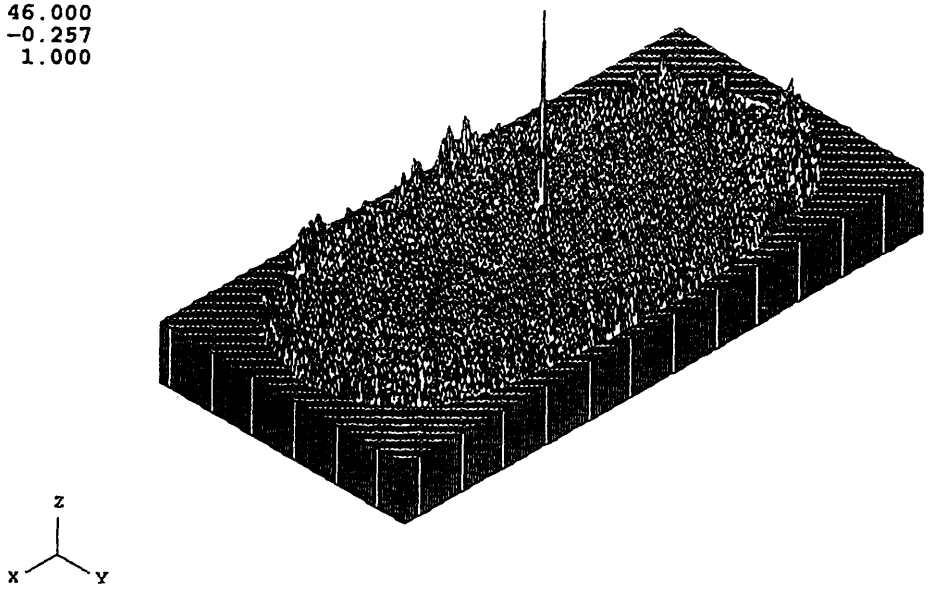

Fig. 3.13 Correlation function of aperture
(e) Tension joint in Chichibu schist

a)Correlation functions along four lines in a joint plane
(0, 30, 60, 90 degree oriented to the core axis)

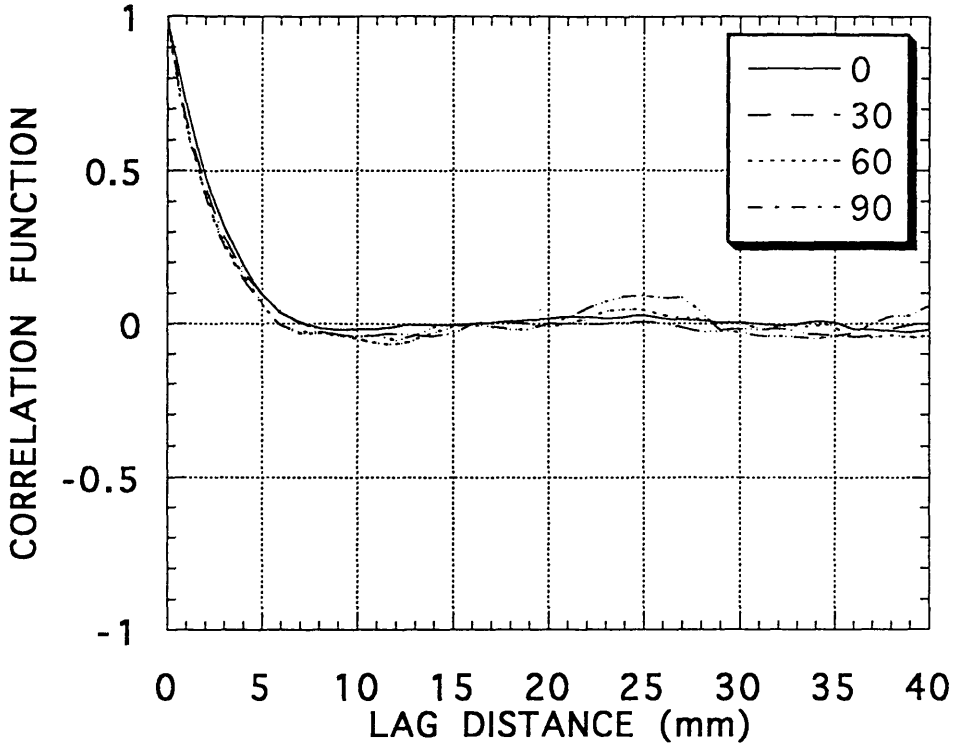

b)2-dimension correlation function in a joint plane

```
nx   =   192
ny   =    92
xmin =  -96.000
xmax =   96.000
ymin =  -46.000
ymax =   46.000
zmin =   -0.227
zmax =    1.000
```

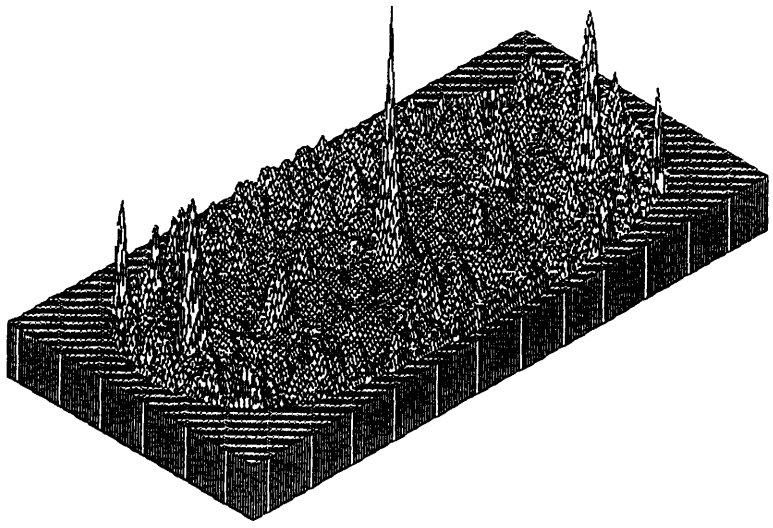

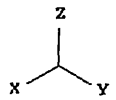

Fig. 3.13 Correlation function of aperture
(f) Tension joint in Kimachi sandstone

Chapter 4 Laboratory Experiments on Joint Conductivity Variation with Pressure

4.1 Introductory remarks

Individual joints are often visualized conceptually as parallel plates separated by some distance. The parallel plate representation, however, is too idealized since there are generally voids and contacts in the planes of real joints. The hydraulic properties of rock joints are governed by both the geometry of the void space and the distribution of contact areas between the two surfaces. The voids of a joint create a complex interconnected network which is a primary flow path in a joint. This geometry is very complex and its detailed nature is not well understood. When a joint is stressed, the joint void space deform and changes in the contact areas occur. These changes significantly affect the hydraulic properties of the joint. Increasing confining pressure reduces the hydraulic conductivity by progressively closing voids in a joint since the conductivity is primarily due to the interconnected network of voids in a joint..

On the other hand, pore pressure has an effect opposite to that of the confining pressure since increasing pore pressure tends to open the voids in a joint. The mechanical effect of pore pressure is usually incorporated into the analyses of crustal processes through the so-called "effective stress law". In general, the effect of confining pressure, P_c, and pore pressure, P_p, do not compensate for each other in rocks. That is, the pressure difference $P_d = P_c - P_p$ is not the effective pressure, as discussed by Skempton(1960) and Bernabe(1987). One can define the effective stress P_e in general form as follows (i.e.; Paterson 1987).

$$P_e = P_c - \alpha P_p \tag{4.1}$$

where α is called as the effective stress coefficient which is not necessarily constant but varies with the pressure.

In this study, since only hydrostatic stress is considered, i.e. ; confining pressure is an isotropic mean stress, the effective stress law is equivalent to the effective pressure law. In poroelasticity theory initiated by Biot(1941), α is expressed as a function of the bulk modulus of both of the macroscopic poroelastic material, B, and the solid part (i.e.; soil particle and rock grain), Bs, in the following form (see Paterson 1978).

$$\alpha = 1 - \frac{B}{Bs} \tag{4.2}$$

The alternative form using the incompressibility, C for the poroelastic material and Cs for the solid part, was also presented by Skempton(1960) as follows

$$\alpha = 1 - \frac{Cs}{C} \tag{4.3}$$

In soil mechanics, α is usually assumed to be a constant close to unity since the bulk modulus of solid part of soil is significantly large relative to the bulk modulus of soil skeleton. But in rock mechanics, both theoretical and experimental evidences show that a may be significantly lower than unity for intact rocks, which can be extremely important in practical cases. The representative values of α in typical rocks, concrete and soils were presented by Skempton(1960). For example, 0.54 in Quatzitic sandstone, 0.75 in Quincy granite, 0.92 in Vermont marble, 0.78 in concrete, 0.9985 in dense sand, 0.9997 in loose sand, 0.99975 in overconsolidated London clay and 0.99997 in normally-consolidated Gosport clay. This type of effective stress law has been commonly used and discussed by several investigators, i.e. ; Skempton(1960), Garg and Nur(1973), Jaegar and Cook(1976), Paterson(1978).

Using this type of the effective stress law, the volumetric change of poroelastic material can be expressed as follows

$$\varepsilon_v = \frac{P_c}{B} - \alpha\frac{P_p}{B} = \frac{1}{B}(P_c - \alpha P_p) = \frac{P_e}{B} \tag{4.4}$$

where ε_v is the volumetric strain of poroelastic material, i.e.; the volumetric change of the skeleton of soils per unit bulk volume.

The another type of volumetric change which is the change of pore volume space, must be considered for fluid flow problem since this type of change significantly affects the real flow path area. The volume change of pore space per unit bulk volume, ε_n, is defined as follows

$$\varepsilon_n = \frac{\Delta V_n}{V} \tag{4.5}$$

where ΔV_n is the volume change of pore space and V is the bulk volume of poroelastic material. ε_n is named as the porosity change by Peterson(1978).

There are tedious mathematical manipulations and the final form of en is expressed, according to Biot(1940), Jeager and Cook(1976) and Peterson(1978), as follows

$$\varepsilon_n = \left(\frac{1}{B} - \frac{1}{B_s}\right)\left[P_c - \left(1 - \frac{n}{\alpha}\frac{B}{B_s}\right)P_p\right] = \left(\frac{1}{B} - \frac{1}{B_s}\right)\left(P_c - \beta P_p\right) = \left(\frac{1}{B} - \frac{1}{B_s}\right)P_f \tag{4.6}$$

where n is initial porosity and α is given by Eq.(4.2). The coefficient β is newly introduced.

The coefficient β is a function of initial porosity, the bulk modules of both of the macroscopic poroelastic material, B, and the solid part , Bs, and is given in the following form

$$\beta = 1 - \frac{n}{\alpha}\frac{B}{B_s} = 1 - \frac{B}{B_s - B}n \tag{4.7}$$

Therefore the effective pressure for pore volume change, P_f, is determined using the coefficient β as follows

$$P_f = P_c - \beta P_p \tag{4.8}$$

When Bs is significantly large relative to B, the coefficient β also becomes unity and P_f becomes the conventional effective stress.

Note that the effective stress coefficients, α and β, are equal unity as far as failure behavior is concerned since failure behavior is deferent from the poroelastic deformation behavior. This fact has been confirmed by many researchers and different type of behavior can be governed by different type of effective stress law. Discussion on the effective stress law based on the poroelasticity theory is done in a short course on the poroelasticity in rock mechanics in the 34th U.S. symposium on rock mechanics hosted by Detournay(1993).

The effective stress coefficients, α and β, is not necessarily constant but varies with pressure. The correct measurements on these coefficients and their stress dependency are very complicated and relatively difficult. Zimmermann et al.(1986) presented an excellent

review on the effective stress law. Berryman (1992) also described the effective stress measurements on various physical properties of porous rocks. In his review, a few studies of the effective stress for fluid hydraulic conductivity of rocks are presented, such as Brace et al.(1968), Zoback(1975), Zoback and Byerlee(1975), Nur et al.(1980), Coyner(1984), Bernabe(1985,1986 and 1987) and Dey(1986), while many others are available for the behavior of hydraulic conductivity as a function of the confining pressure for fixed pore pressure.

Bernabe(1985) presented an empirical formulation yielding the effective stress coefficient, α, which was obtained by the response of hydraulic property due to the stress change. He was concerned on the stress effects on the hydraulic conductivity of rocks and has been carried out the extensive test series to measure the hydraulic conductivity of several crystalline rocks, i.e. ; hot-pressed calcite, Chelmsford granite, Barre granite, Westerly granite, Pigeon Cove granite and Pottsville sandstone (Bernabe 1982, 1986 and 1988).

In his definition, the effective stress coefficient, α, is given by

$$\alpha = -\frac{\partial k}{\partial P_c} / \frac{\partial k}{\partial P_p} \tag{4.9}$$

In order to evaluate these two partial derivatives, one can perform the following experiments successively. In the first one, one measures the variation in hydraulic conductivity corresponding to changing the confining pressure and pore pressure as follows.

The differential of the hydraulic conductivity can be written as

$$dk = \left(\frac{\partial k}{\partial P_c}\right) dP_c + \left(\frac{\partial k}{\partial P_p}\right) dP_p \tag{4.10}$$

In this case, dP_c=dP and dP_p=0 (dP can be either positive and negative corresponding loading and unloading). Using Eq.4.10, one find

$$\delta k_c = \left(\frac{dk}{dP_c}\right) \delta P \tag{4.11}$$

In the second experiment, one measures δk_p corresponding to dP_c=0 and dP_p=dP. δk_p

can be written as

$$\delta k_p = \left(\frac{dk}{dP_p}\right)\delta P \tag{4.12}$$

Combining Eq.4.9, Eq.4.11 and Eq.4.12, one obtains

$$\alpha = -\left(\frac{\delta k_p}{\delta k_c}\right) \tag{4.13}$$

where δk_p is the variation of hydraulic conductivity due to shifting the pore pressure, P_p, by dP while the confining pressure, P_c, is kept unchanged. Similar definition applies to δk_c with the subscription c and p interchanged.

In practice, these two partial derivatives can be evaluated by measuring the variations of hydraulic conductivity caused by changing P_c and P_p independently.

Kranz et al.(1979) presented the following definition similar to Eq.4.10 to examine the simple proportionality of hydraulic conductivity to the conventional effective pressure, P_c - P_p, and the stress history dependence of the hydraulic conductivity. In his study, supposing the hydraulic conductivity to be a function only of P_c and P_p, α is defined as follows.

$$\begin{aligned} dk &= \left[\frac{\partial k}{\partial(P_c - P_p)}\right]_{P_p} d(P_c - P_p) + \left[\frac{\partial k}{\partial(P_c - P_p)}\right]_{Pc} d(P_c - P_p) \\ &= \left[\frac{\partial k}{\partial(P_c - P_p)}\right]_{P_p} dP_c - \left[\frac{\partial k}{\partial(P_c - P_p)}\right]_{P_c} dP_p \\ &= -adP_c + bdP_p \end{aligned} \tag{4.14}$$

$$\alpha = b / a \tag{4.15}$$

where the coefficients a and b give the relative effect of confining pressure and pore pressure changes on the joint hydraulic conductivity. They are the slopes of equal P_p and equal P_c lines on the hydraulic conductivity vs P_c - P_p graph.

When P_c and P_p are changed by equal amounts, the value of (b - a) is proportional to the change in k. If dk is positive, the coefficient of b is greater than the coefficient of a and internal pore pressure is evidently of greater importance than the confining pressure.

Little is known about the variations of α for both intact rocks and jointed rock. The common observation that α for intact rocks is constant with pressure, is probably not valid for α for rock joints. Brace et al.(1968) implied that the conventional effective stress law held for Westerly granite, which is equivalent to having α =1. Zoback(1975) presented $2.2<\alpha<4.0$ for several unjointed sandstone. Bernabe(1986) found that a decrease of α with increasing P_c on Chelmsford granite and Barre granite.

In this study, however, the following modified definition of the coefficients a and b, in which the transformed permeability (lnk) instead of permeability (k) is used, since the joint permebility can change more rapidly with pressure than the permebility of intact rock.

$$\begin{aligned} d(\ln k) &= \left[\frac{\partial(\ln k)}{\partial(P_c - P_p)}\right]_{P_p} d(P_c - P_p) + \left[\frac{\partial(\ln k)}{\partial(P_c - P_p)}\right]_{Pc} d(P_c - P_p) \\ &= \left[\frac{\partial(\ln k)}{\partial(P_c - P_p)}\right]_{P_p} dP_c - \left[\frac{\partial(\ln k)}{\partial(P_c - P_p)}\right]_{P_c} dP_p \\ &= -a_{\ln k} dP_c + b_{\ln k} dP_p \end{aligned} \tag{4.16}$$

$$\alpha = b_{\ln k} / a_{\ln k} \tag{4.17}$$

This definition was also used in existing study (Takahashi et al. 1990). In this study, it is safe to drop the subscript and refer to a and b as simply the relative effect of confining pressure and pore pressure changes on the joint permeability.

When the sample is submitted to pressure cycling, one generally observes an irreversible variation of hydraulic conductivity due to irreversible changes in pore structure. This is a serious problem faced when one wishes to extrapolate laboratory data to in situ conditions. In the rock mechanics literature, the terms "stress history dependence" as well as "stress path dependence" refer to a dependence of rock properties on past state of stress. This behavior appears more clearly when rocks are submitted to a number of stress cycle. Haimson(1974), Zoback and Byerlee(1975) and Hadley(1976) studied the effect of such cycles on the dilatancy or the strength of rocks. Coyner et al.(1979), Kranz et al.(1979) and Bernabe et al.(1984) found that the hydraulic conductivity depended on the stress path. However, these studies were often restricted to the properties of intact rocks. The stress

history dependence as well as stress path dependence of the properties of rock joints are easily imagined to be much larger than those of intact rocks since their stress dependence may arise from the change of pores and cracks in rocks and rock joints due to stress changes. When a joint is stressed, the joint void space deforms and changes in contact area occur. Since void spaces in a rock joint play a predominant role in controlling the joint conductivity, the change of void spaces and their interconnectivity in a joint due to the external stress change on a joint changes the joint conductivity. Therefore the stress dependence of the joint conductivity can be explained by the change of geometry of void spaces in a joint. Joint conductivity is also supposed to be changed by internal pore pressure in a joint due to the same reason as the external stress.

In this study, the effects of confining pressure and pore pressure on the joint conductivity for three different joints in granodiorite were measured by means of transient pulse permeameter. Two important observations were focused on : the variations of both the coefficients a and b for joints with the conventional effective pressure and their relative sensitivity with the conventional effective pressure to those of intact rocks. In addition, the cyclic loading effects due to both the confining pressure cycle and pore pressure cycle on the joint hydraulic conductivity were also observed. Finally both the stress path dependence and the stress history dependence of joint hydraulic conductivity on the conventional effective pressure were analyzed and the applicability of the conventional effective pressure law to the joint hydraulic conductivity was examined.

4.2 Measurement of stress effect on joint hydraulic conductivity

4.2.1 Theory of transient pulse method

The measurement of very low hydraulic conductivity presents special problems such that the standard measuring techniques are generally impractical, inaccurate and difficult to be applied. Usual methods of measuring hydraulic conductivity in the laboratory have utilized steady flow. In the steady-state flow method, a constant water pressure gradient is applied across a sample and the volume of water flowing through it per unit time is measured. The hydraulic conductivity of sample is obtained by Darcy's law as follows.

$$K = \frac{Q}{AI} = \frac{Q}{A}\frac{L}{\Delta P_p} \tag{4.18}$$

where K is the hydraulic conductivity (cm/sec), Q is the water flow rate through a

specimen (cc/sec), A is the cross-sectional area of the specimens (cm^2), I is the hydraulic gradient, L is the specimen length in the flow direction (cm) and ΔP_p is water pressure head difference along the specimen (cm).

In practice, water flow volume through the specimen and the time interval are measured and then water flow rate can be calculated as water flow volume per unit time. The alternate expression for hydraulic conductivity is the intrinsic permeability, k (cm^2). In this study, it is safe to drop the subscript and refer to K as simply the hydraulic conductivity and k as the permeability. The permeability is expressed by using the hydraulic conductivity and the fluid viscosity as follows.

$$k = \frac{\mu}{\rho g} K = \frac{\nu}{g} K \qquad (4.19)$$

where μ is the fluid viscosity (dynamic viscosity), ρ is the fluid density, g is the gravitational acceleration and ν is the kinematic viscosity of fluid which is the ratio of the fluid viscosity to the fluid density.
For water, $\rho = 1.0 \ g/cm^3$, $\mu = 1.140 \ cP = 1.163 \times 10^{-7} \ g\,\mathrm{sec}/cm^2$ and
$\nu = 1.141 \ cSt = 1.141 \times 10^{-2} \ cm^2/\mathrm{sec}$ at $15.0\ ^\circ C$.

The density and viscosity of fluids are functions of temperature and pressure (Freeze and Cherry, 1979). In this study, water is used as the flowing fluid. In general, their variation is not so great in the range of pressures and temperatures that occur in practical applications. Since very small volumes of fluid are not easily measured in steady-state flow experiment, this conventional method is better for high conductivity, i.e.; greater than 10^{-6} cm/sec. If the conductivity is low, long periods of time are required to establish steady-state flow and these procedures are impractical. Also one needs to select the special material for the membrane to prevent the permeation of fluid through it.

Brace et al.(1968) introduced the transient pulse method (also called the pulse decay method) to measure the hydraulic conductivity of Westerly granite. The field equation given by Brace et al.(1968) is the one-dimensional transient flow equation. Brace' analysis is based on the theoretical consideration of a transient Laplace equation. The solution of this equation has been given in Carslaw and Jaeger (1959) in the form of an infinite series. They ignored the transient term by assuming that the porosity in rock is very small relative to the reservoir volumes and the compressibility of fluid is much larger than that of rock matrix. This assumption yields a linear pressure gradient along the specimen in the flow

direction at any time t. Because of its simplicity, their method has been used by many researchers to measure the hydraulic conductivity of rocks (Zoback and Byerlee, 1975 ; Coyner et al., 1979 ; Kranz et l., 1979). Lin(1977) took a more general approach to determine the permeabilities of crystalline rocks and argillite in an apparatus designed and developed by Trimmer et al.(1980). Also Lin(1982) examined the difference in hydraulic conductivity determined by both Brace's original method and his modified version of the transient pulse method. On the other hand, Hsieh et al.(1981) presented a general analytical solution for a transient pulse test for determining the hydraulic conductivity of rocks and Neuzil et al.(1981) applied their general analytical solution to obtain both the hydraulic conductivity and the specific storage of the Cretaceous Pierre Shale.

The transient pulse method is getting more frequently used to measure the hydraulic conductivity of rocks. There are, however, still many uncertainties in the transient pulse method to obtain the hydraulic conductivity much more correctly. It is not the purpose of this study to provide the more theoretical solutions and corrections to the measured hydraulic conductivity. Trimmer et al.(1980) and Ishijima et al.(1993) estimated errors in hydraulic conductivity when one uses Brace's method to determine the hydraulic conductivity of rocks. They concluded that the errors in hydraulic conductivity were relatively insignificant for practical applications. In conclusion, Brace's method can yield the reasonable representative value of hydraulic conductivity in practical usage. Therefore, in this study, Brace's method is adopted to determine the hydraulic conductivities of intact rocks and rock joints.

Fig.4.1 is a schematic view of the transient pulse method. Their experimental arrangement consists of a cylindrical rock specimen which is connected to fluid reservoirs at the both ends of specimens. In this method one starts with the fluid pressure in equilibrium in the whole system after applying the external confining pressure and the fluid pressure at the source on one side of specimen is instantaneously increased by pressure pulse, $\Delta P_{pi.}$ As a convention, this side is called the upstream side without considering in which direction the fluid actually flows. The pressure is then free to return to the equilibrium. The characteristics of this recovery yield the conductivity of the sample. Typical values of pressure in this study are also shown in Fig.4.1.

In this chapter, the term 'permeability' is used instead of the term 'hydraulic conductivity' since the term 'permeability' is more commonly used in the other existing relevant studies to this chapter.

Assuming the system geometry is known, the permeability can be computed from the decay time since the decay time inversely proportional to the permeability under certain conditions as shown by the following equations.

$$\Delta P_p = \Delta P_{pi} \exp(-\gamma t) \tag{4.20}$$

with

$$\gamma = \frac{kA(V_u + V_d)}{\beta \mu L V_u V_d} \tag{4.21}$$

where ΔP_p is the pressure difference between the upstream and downstream reservoirs, ΔP_{pi} is an initial pressure pulse, k is the permebility, A is the cross-sectional area of the specimen, β is the isothermal compressibility of the fluid, μ is the fluid viscosity, L is the specimen length and V_u and V_d are the volumes of fluid reservoirs at the upstream and downstream side of the specimen, respectively.

Derivations of Eq.4.20 and 4.21 were given by Brace et al.(1968). Once the value of γ is evaluated from the pulse decay curves, Eq.4.21 can be used to calculate the permeability for the rock sample. Isothermal compressibility of fluid is also a function of temperature and pressure. For water, β = 4.4 x 10-6 cm^2/N at 15.0 $^\circ C$.

The same procedure can be applied to a single rock joint by using split cylindrical specimens. This allows one to directly compare intact rocks and rocks with a joint but will not give an absolute value of the permeability for the joint itself because the assumptions made in deriving Eq.4.21 do not necessarily apply to single joints. If one simply applies Eq.4.21 to calculate the joint permeability, one can obtain the permeability of joint equivalent to that of the porous media which can conduct the same volume of fluid under the unit gradient during unit time. For rock with a joint, the effective cross sectional area to which fluid is exposed can be assumed to be a joint aperture alone since the permeability of surrounding host rock should be much lower than that of joint alone. In Eq.4.21, A for joint alone (A_j), the effective cross-sectional area of the joint, which can be defined by the joint width times the joint aperture, should be used. Therefore, to calculate the joint permeability alone, one needs to arrange the following equation and to obtain the other geometrical properties of the joint , i.e.; joint width and joint aperture.

$$k_j A_j = k_j \left(W_j b_j \right) = k_{eq} A_s \tag{4.22}$$

where kj is the joint permeability, A_j is the effective cross-sectional area of the joint, W_j is joint width and bj is joint aperture, k_{eq} is the equivalent permeability A_s is the cross-sectional area of the jointed sample.

k_{eq}, As and Wj can be measured with an appropriate precision even though one need to use the arithmetic mean of joint width along the length of a joint. The joint aperture cannot be evaluated with an appropriate precision under the changing external confining pressure and pore pressure even though one can estimate the initial average aperture with some uncertainties. Therefore the joint permeability itself cannot be calculated by Eq.4.22.

Kranz et al.(1979) encountered the similar difficulty to obtain the joint permeability alone and they used the quantity kA since the volume flow rate through a joint is proportional to kA and this quantity can be calculated using Eq.4.21 once γ is measured. As they mentioned, a direct comparison between the intact rock and the jointed rock sample can be made using kA rather than k or k_j. In fact this eliminates any questions about what value one should take for A for rock sample with a joint.

In this study, for convenience, both k_{eq}, based on the porous media equivalence, and kA , simple obtainable parameter from experimental result, are used to examine the effect of stress on the joint permeability since there are too many uncertainties and problems to directly estimate the joint permeability itself, i.e. ; the mode of deformation of rock sample with a joint, the validity of Darcy's law for a joint flow, the pressure distribution along a joint during transient condition and the problem regarding the specific storage of a joint as well as the measurement of geometrical properties of a joint. Kranz et al.(1979) used the following power law equation to analyze the stress dependence of permeability on the conventional effective confining pressure.

$$kA = [kA]_0 \left[P_c - P_p \right]^{-n} \tag{4.23}$$

where $[kA]_0$=kA at P_c-P_p=10MPa.

In this study, the same power law equation is also used to analyze the stress dependence of permeability on the conventional effective pressure. The reference effective pressure is changed from 10 MPa to 1 MPa since 10 MPa is too high and 1 MPa is more reasonable for practical applications. By plotting log[kA] vs log[P_c-P_p], one find the coefficients of $[kA]_0$ and n by fitting and choosing to produce the least variance. The exponent n, the coefficient of the negative power law, represents the degree of the stress dependence of the quantity of [kA].

4.2.2 Sample material and preparation

Four Kikuma granodiorite samples were used in this study for their homogeneous structure, relatively large grain size and low intact rock permeability. All samples are cored as solid cylinders with 50 mm diameter and were cut to 100 mm in length. The ends of each sample were polished so that the two opposing end planes were parallel and flat. One of these Kikuma granodiorite samples is an intact rock core and other three contain a natural joint, an artificially induced microcrack (micro-tension joint) and a sawed joint in each core specimen, respectively. The natural joint is a well matched joint and is almost parallel to the core axis. The microcrack was created along the core axis by loading the cylindrical specimen in compression from radial direction, in a Brazilian test manner as presented in Fig.3.1, under very slow controlled-strain-rate compressive loading. In this case, the test was stopped such that the specimen did not split apart but X-ray investigation showed that a persistent joint was induced. Therefore a joint is ideally matched. The sawed joint was cut along the axis of cylindrical rock specimen using a diamond saw and the joint surfaces were prepared with #120 grit. Basic properties of the Kikuma granodiorite were already presented in Table 3.1.

The X-ray CT scanner (Toscaner-23200, Toshiba Corporation) was used to ensure the degree of persistence of microcrack and its position in the core. The measurement and image analysis were conducted in five transverse cross sections of specimens which located from the top of specimen to bottom end and whose intervals between transverse cross sections were 2cm along the length of specimen. Also the measurement and image analysis in the longitudinal cross section which was parallel to core axis and was perpendicular to the joint plane were carried out. Fig.4.2 and Fig.4.3 present the examples of results of image analysis in the transverse cross section and the longitudinal cross section respectively. As shown in both figures, one can see that microcrack was induced and existed almost at the center of specimen.

After this check, the two rock specimens which contained the natural joint and microcrack were cut to each two specimens, whose lengths are about 50 mm, to be used for the transient pulse measurement. As a consequence, these specimens were finally about 50 mm in diameter and 50 mm in length. Next the joint ends at both sides in all specimens were sealed with the epoxy resin so as not to get rupture at the rubber membrane. Then the specimens were evacuated in the deionized water for more than 72 hours to saturate them with the deionized water. The specimens were stored in the deionized water until tested. The photographs of jointed specimens are shown in Appendix B.

4.2.3 Test apparatus setup

Schematic arrangement of the test apparatus is depicted in Fig.4.4. Its photograph is shown in Fig.4.5. The feature of the transient permeameter is summarized below.

Each specimen, which was precisely ground right cylinder, which was 50 mm in length and had a 19.63 cm2 in cross-sectional area, was placed in the cell. On the upper side it made contact with a stainless steel end cup. On the lower side it made contact with a stainless steel piston which can apply the axial pressure to specimens. The ultra-high pressure heavy-wall tubings (outer diameter 6.36 mm, inner diameter 1.53 mm, maximum working pressure 413 MPa) are used for all the line. Sno-Trik fittings and valves (maximum working pressure 413 MPa, Swagelok Company) are used. These make the system very rigid so as to minimize the effect of the deformations of the system (tube, fitting, connector, valve and pressure reservoir et al.) induced by water pressurization. 4-mm-thick porous disks (porosity 36%) made of 5 μ stainless steel beads which are of high rigidity, were placed on the both sides of specimen to separate specimen from both end cap and the piston since the applied water pressure needed to be distributed over the entire end surface of the specimen. Porous disk and specimen were enclosed in a 2 mm-thick fluoro-carbon rubber (known as Viton) for a membrane sleeve to reduce the fluid permeation. Both Silicon rubber and Neoprene rubber were not adequate to measure an ultra- low permeability of rock if more than a day was required to get to the steady-state flow condition. The tube connection must not be the weakest link in the system in the transient pulse permeameter. Therefore, to avoid the leakage from the system, the ultra-high pressure fittings (Sno-Trik), which use the pre-coned metal contact seal design, were used in all the line tubing for water pressure since the taper pipe thread type fittings with a Teflon sealing tape had a relatively lower reliability on the sealing under high pressure and it was very difficult to detect the very small leakage.

As shown in Fig.4.1, the system was almost completely enclosed in the stainless steel water pool to reduce the water temperature fluctuation in the system. Even though air temperature in a room was well controlled to $\pm$ 1 $^{\circ}C$ fluctuation, water temperature in the system was affected by out-door temperature fluctuation for a day long and had better be as small as possible. The water pool system was very effective and one day fluctuation of water temperature in the system was reduced to less than $\pm$ 0.1 $^{\circ}C$. Fig.4.6 shows an example of pressure change and temperature in the sequence of transient pulse test (A-test), in which the external confining pressure was increased from 3 MPa to 42 MPa step by step and decreased while pore pressure was remained to be constant (2MPa), a natural joint. This tests continued about for a month due to the relatively low conductivity and 2

cyclic incremental loading and unloading. As shown in this figure, maximum air temperature fluctuation was 0.8 $^{\circ}C$ and water temperature fluctuation was as high as 0.2 $^{\circ}C$. These temperature fluctuation arose because the temperature of the out-door air, which provided the cooling and warming to water, was not constant and changes in water temperature due to the cooling and warming by the air were only imperfectly compensated by the water pool. The longest duration for one test (A-test for intact rock sample at P_c=42 MPa) was about a week. But for almost of all tests for rocks with a joint except microcrack, it was required less than two hours to return equilibrium. Since the water temperature fluctuation for two hours seemed negligible small, the water pool was thought to be effective and adequate in this experiment.

Bernabe(1987) used the isothermal oven for the temperature control system. He reported that the water temperature fluctuations were also as high as 0.2 $^{\circ}C$. He also carried out several experiments in order to evaluate the effect of a known temperature change on the pulse decay curves. He concluded that one needed to use the segments of the pulse decay curves where the temperature was the relatively stable to obtain the permeability.

The fundamental specifications for the apparatus are listed in Table 4.1. In this system, the axial pressure and the lateral confining pressure can be applied individually to a specimen at to pressure up to 50 MPa. The maximum pore pressure is limited to 35 MPa due to the maximum working pressure of pore pressure transducers. The measurements of pore pressure in both up stream reservoir and down stream reservoir were carried out individually by using the pressure transducer (AB/HP 35 MPa) made by Data Instruments Co. LTD.. Axial pressure, lateral confining pressure and initial water pulse pressure are measured with the pressure transducers (PG-500KU 50 MPa) made by Kyowa Electronic Instruments Co. LTD.. The axial pressure, lateral confining pressure and pore pressures in both upper and lower stream reservoir, air temperature and water temperature are monitored simultaneously and digitized data are taken in by TDS-302 data logger (Tokyo Sokki Kenkyujo Co. LTD.) at the some specified sampling intervals during the test. Table 4.2 shows the sampling time in this study. Extensive preliminary tests show that this testing system can measure the hydraulic conductivity at the value to the order of 10^{-12} cm/sec (Aoki, et al., 1994).

4.2.4 Experimental methodology

Before carrying out the experiments using the three samples with different joints, the measurement of permeability of an intact sample was conducted. The following two types

of experiments were needed to observe the effects of external confining pressure and pore pressure on the permeability separately. The diagram outlining the cycling procedures of both A-test and B-test are schematically illustrated in Fig.4.7. These testing procedures are described below.

Note that pore pressure of at least 2 MPa is needed to ensure the sample saturation and this pressure is the back pressure. Therefore 2 MPa back pressure was used in this study. As noted in section 4.2.1, the transient pulse method is based on the assumption of Darcy's law. Several researchers have shown the validity of this assumption. Walder and Nur(1980) showed that the upper limit of pulse pressure for the validity of Darcy's law in transient pulse tests should be less than 1.5 MPa.

According to the results by Walder and Nur(1980) and Ishijima et al.(1993), 0.2 MPa for pulse pressure is used for all tests in this study, which is less than one tenth of back pressure (minimum pore pressure in this experiments). However, pulse pressures ranged from 0.2 MPa to 0.4 MPa. It was very hard to control pressure pulse at specified value, e.g.; 0.2 MPa, due to the usage of the hand pomp to set pore pressure and opening of ball valve, which is illustrated in Fig.4.4. Therefore some allowable variation of pressure pulse must be defined. Extensive preliminary experiments showed that the difference of pulse pressure ranging from 0.2 MPa to 0.4 MPa did not significantly affect the experimental results and yielded the same results in the permeability of rock.

1) A-test

After applying 3 MPa external confining pressure (the axial pressure and lateral pressure) to a specimen, water pressure in both up-stream and down-stream reservoir was increased to 2 MPa as a back pressure and then all ball valves (valves A, B and C shown in Fig. 4.4) were closed. 2 hours were required for initial equilibration. After opening valve C, increasing water pressure in the up-stream reservoir to 2.2 MPa (pressure pulse 0.2 MPa) and then closing again valve C, water pressure, axial pressure and lateral pressure were monitored to ensure that the fluctuations of pressures were getting to be negligible. Thus more 2 hours were required for this pressure set up. First transient pulse test was performed by opening valve B at this pressure condition. Subsequent measurements were carried out by increasing axial pressure and lateral pressure simultaneously 5 MPa steps up to 42 MPa. Thus effective confining pressure increases from 1 MPa to 40 MPa in this test series. Note that only first increment of external pressure is set to 4 MPa to get data at Pe=5 MPa just for convenience.

For three specimens with joints, the increment of external pressure is set to 2 MPa

for the natural joint and sawed joint to observe more minute change of their conductivity. For the microcrack, the increment of external pressure is set to 2 MPa steps up to 20 MPa and 5 MPa steps up to 40 MPa to save time since the conductivity of this sample is 3 orders of magnitude less than those of the other two jointed samples. Furthermore in the experiments on jointed samples, external pressure was decreased down to 3 MPa similar to the loading process to observe the change of joint permeability for unloading process. To observe the cyclic effect of external pressure on the joint conductivity, in addition, subsequent second loading and unloading have been carried out.

2) B-test

The B-test is a reversed version of the A-test. By decreasing the internal pore pressure, one can also increase the effective confining pressure. First the external confining pressure is increased up to 2 MPa and pore pressure is increased to 1 MPa to set the effective confining pressure 1 MPa. Next the external confining pressure and pore pressure are increased by 1 MPa step by step such that finally pressures were set to 38 MPa and 35 MPa respectively since the maximum working pressure for pressure transducers is 35 MPa. When increasing pressures, one needs to take care that the effective confining pressure should be less than 1 MPa in each intermediate step since the joints will deform according to the change of the effective confining pressure and their deformation are irrecoverable.

The first transient pulse test in the B-test was carried out by applying same pressure pulse (0.2 MPa) as in the A-test at this pressure condition. Subsequent measurements were carried out by decreasing pore pressure in 5 MPa steps down to 2 MPa. Thus effective confining pressure increases from 1 MPa to 36 MPa (loading process) in this test. Note that only the first decrement of water pressure was set to 4 MPa to get data at Pe=5 MPa and final decrement was set to 2 MPa. For three specimens with joints, the decrement of water pressure is set to 2 ~3 MPa to observe more minute change of their permeability. Also in the measurements for jointed samples in unloading process, pore pressure was increased up to 37 MPa with the same way in loading process to observe the change of joint conductivity in unloading process. To observe the effects of the cyclic incremental loading and unloading of pore pressure on the joint permeability, in addition, subsequent second loading and unloading have been carried out.

The A-test provides the effect of effective confining pressure on joint permeability due to the change of external confining pressure. On the other hand, the B-test produces the effect of effective confining pressure on joint permeability due to the change of internal

pore pressure cycles. By performing both tests, one can obtain the changes of joint permeability with respect to both external confining pressure and internal pore pressure. By comparing both results, the stress path dependency of joint conductivity can be observed. In addition, stress history dependence of joint conductivity as well as stress path dependence can be observed by performing both cyclic successive A-test and B-test. In this study, 2 successive cycles were performed in both A-test and B-test even though the number of pressure cycle was restricted to two. But it seems adequate to observe the presence of stress history dependence of joint conductivity with the conventional effective pressure as well as stress path dependence with it.

4.2.5 Experimental results

Fig.4.8 presents an example of results of both measurement and analysis using Brace's method (natural joint, A-test, Pe=40 MPa). Actual applied pressures are also described in Fig.4.8. In Fig.4.8(a), the vertical axis is a normalized pressure difference in water pressure between up-stream and down-stream reservoirs by the initial pulse pressure, which is the maximum pressure difference. One can see the very nice curves, in which upper curve is the water pressure in up-stream reservoir and lower curve is the water pressure in down-stream reservoir and both curves are free to return to the equilibrium condition which was almost half of the initial pulse pressure. In this case, about 500 sec was required to get to the equilibrium condition. In Fig.4.8(b), the vertical axis is the log of normalized pressure difference by the initial pulse pressure. A very linear behavior was obtained, which clearly shows the applicability of exponential decay theory (Brace's theory). The slope of this straight line is γ in Eq.4.21 and one can calculate the permeability once γ was obtained. In this study, the most linear part of this line was used to obtain γ. In this case, the portion of initial part, ranging from 60 sec to 160 sec, was used to obtain γ since the this part was most linear and the correlation coefficient of line fitting is 0.99975. In general, concave curves often appear both of the beginning and the end part of line. In the beginning part (0-60 sec in Fig.4.8(b)), some storage of water due to the deformation of joint is involved. In the final part (160-500 sec in Fig.4.8(b)), there is a resolution problem on transducer since the pressure difference becomes less than one tenth of the initial pulse pressure (0.2 MPa) in the end part of line. The same procedure was applied to all of test results to obtain the hydraulic conductivities. As mentioned in section 4.2.1, these conductivities are the equivalent conductivities for joints. In this study, all of the obtained conductivities are corrected to the conductivities at $15°C$ by multiplying the correction factor based on the temperature dependence of the kinematic viscosity of the

water (Cherry and Freeze 1984).

1) Intact sample

The changes of hydraulic conductivity of the intact sample due to the increase of the effective confining pressure are presented in Fig.4.9. The hydraulic conductivity of Kikuma granodiorite is very low and decreases from 4.64×10^{-11} to 5.52×10^{-12} cm/sec and from 7.71×10^{-11} to 8.36×10^{-12} cm/sec in A-test and B-test, respectively, up to 40 MPa effective confining stress. In terms of intrinsic permeability, from 5.40×10^{-8} to 6.43×10^{-12} darcy and from 8.35×10^{-11} to 9.73×10^{-12} darcy in A-test and B-test, respectively. Note that 1 cm/sec = 1164.2 darcy at $15°C$.

The linear relationships between the logalism of hydraulic conductivity and the effective confining pressure in both A-test and B-test are clearly observed. The local values of the coefficients of a and b, which are defined by Eq.4.16 and are obtained by A-test and B-teat, respectively, are calculated and are presented in Fig.4.10. Both coefficients are very close each other and decrease with the increase of the conventional effective confining stress, P_c-P_p. The change in the local values of α, the effective stress coefficient which can be calculated by b/a in Eq.4.17, with the conventional effective confining pressure are illustrated in Fig.4.11. The local value of a fluctuates somewhere around the value one but seems to be almost constant up to 40 MPa. Similar result, which is equivalent to having $\alpha=1$, was also observed by Brace et al.(1968) for Westerly granite. The exponent n and the reference value of kA, which are given by Eq.4.23, in both A-test and B-test are also obtained by the simple curve fitting and are tabulated in Table 4.3. For Kikuma granodiorite, the coefficients of n in both in A-test and B-test are very close and are defined as 0.58. Kranz et al.(1979) observed the exponent n for Barre granite. They reported n=0.9 at Pc=17 MPa and n=0.8 at Pc=100 MPa for Barre granite. The exponent n for Kikuma granodiorite is determined as 0.58 at the effective pressure up to 38 MPa, which is smaller than Barre granite. The stress dependence of permeability of the intact Kikuma granodiorite is less than that of Barre granite.

2) Jointed samples

The changes of equivalent joint conductivity of three different joints are presented in Fig.4.12 and the maximum values at the lowest effective confining pressure and the minimum values at the highest effective pressure in each loading and unloading cycle are listed in Table 4.4. In the A-test, the nonlinear behavior of conductivity is clearly observed

at pressure up to 20 MPa in a natural joint and microcrack. In particular, as the effective confining pressure is raised in 1st loading, the equivalent conductivities of joints decrease by two orders, two orders and one order of magnitude in a natural, microcrack and sawed joint, respectively. Relatively large irrecoverable conductivity changes for joints are also involved in 1st cycle even though the extents of hysteresis are different among samples and tests. The rates of recovery in 1st cycle (K_{eq} after 1st cycle / K_{eq} at initial) in A-test are about 44%, 9% and 58% for natural, microcrack and sawed joint, respectively. On the other hand, during 2nd cycle, changes in the joint conductivities are getting small. As a consequence, the permeability hysteresis is small.

In B-test, both the pressure dependence and the pressure cycling effect on the joint permeability are relatively smaller than those in A-test in all joints. In particular, no significant conductivity loss is observed in the sawed joint by pore pressure cycling under the constant confining pressure condition. The rates of recovery in 1st cycle (K_{eq} after 1st cycle / K_{eq} at initial) is 83 % for a sawed joint. The simple comparison of the equivalent conductivities of joints with the effective confining pressure in each cycle is made in Fig.4.13

The quantities of kA observed in experiments are presented in Fig.4.14. The results of power law fitting analysis are shown in Fig.4.15 for A-test and Fig.4.16 for B-test, respectively. These results are summarized and are listed in Table 4.3. The exponent n is an index which represents the dependence of joint permeability on the conventional effective confining pressure. The exponent n in three joints range from 0.671 to 2.234, whose values are very close to results in Barre granite by Kranz et al.(1979). Three things become immediately apparent. First, the exponent n for the jointed samples are greater than that of intact rock. Also, as mentioned previously, in 1st loading, the exponent n is the largest in all jointed samples and it decreases with successive cycle. These results show that the pressure effect on the joint permeability is most significant in 1st loading process and stress dependence is getting smaller by successive cyclic loading. The exponent n for all jointed samples in A-test are larger than those in B-test.

The exponent n describes the average dependence over the range of applied effective confining pressure. To observe the local changes of stress dependence of joint permeability on both the confining pressure and pore pressure, the coefficients a and b for three joints are calculated and are presented in Fig.4.17. As one can see in Fig.4.17, both coefficients a and b for a sawed joint is relatively smaller than those for natural joint and sawed joint. Therefore it can be concluded that the stress dependencies of a sawed joint on both the confining pressure and pore pressure are small. For natural joint and microcrack, the changes in the coefficients a and b look similar but the extents of the coefficient b is

smaller than that of the coefficient a. This results shows that the effect of confining pressure on the joint permeability is greater than that of pore pressure. The joint permeability is more sensitive to the external confining pressure. The larger variations of both the coefficients a and b with the effective confining pressure are observed in unloading process. It is not expected since the altered sheeting of the joint due to the crushing of the contact points or asperities can take place more during loading process than in unloading process. These geometrical changes strongly affect the hydraulic properties of joints. The differences in the coefficients a and b between jointed samples come from the differences of their geometrical properties in a joint such as surface roughness and aperture distribution. The relative small changes in the coefficients a and b for a sawed joint was expected since their surfaces were very smooth, but the relative large change for microcrack was not expected since this joint did not split apart and thus this joint was ideally matching. In this case, the changes in hydraulic conductivities with pressure may be the results of changes of interconnected networks of small void space in a microcrack. Small voids in a microcrack can deform and the new contact points can be created, which will disconnect the existing links between adjacent void spaces. But most significant observation is that the behaviors of hydraulic property of both a natural joint and microcrack are similar but of different magnitude.

4.3 Summary and discussion

When comparing changes in permeability of both an intact rock and joints, the permeability decreases more rapidly with pressure for jointed rock than for intact rock. In a porous rock, water flows through the interconnected pores and cracks. The mean cross sectional area along a flow path is much smaller than for a joint. Also the flow length is much greater in an intact rock. These two differences can account for the magnitude differences in the permeability, but not for the fact that the permeability decreases more rapidly with pressure in joints than in intact rock. It is, however, apparent that the compressibility of a joint is much greater than for that of intact rock. Therefore, the joint can close more rapidly under pressure than pores and cracks in an intact rock. Hence, the difference of the variation of the permeability with pressure between a joint and an intact rock is due to the differences of their compressibility.

The changes in confining pressure and pore pressure have significant effects on joint permeability, but confining pressure has a relatively greater effect on joint permeability than does pore pressure. In other words, the joint permeability is more sensitive to confining pressure than to pore pressure. The fact that the effects of both confining

pressure and pore pressure on joint permeability are different suggests that one should be cautious when applying the term "effective pressure" or "effective stress" to jointed rock. It follows that effective pressure is not the conventional effective pressure, which is defined as the pressure difference between confining pressure and pore pressure, at least for the hydraulic properties of jointed rock. Therefore one should not use the conventional effective pressure for the evaluation of joint permeability and for the estimation of the hydraulic behavior of jointed rock.

These results are consistent with the results observed by Kranz et al.(1979). At any particular confining pressure, one would expect more real area of contact the less rough the two opposing surfaces are. Asperities in contact affect the permeability in two ways. They change the path length or tortuosity of the flow path and they inhibit joint closure. Asperities are small so the joint closes rapidly at low pressures until enough of these asperities make contact with opposing surfaces to increase the flow tortuosity and to decrease the closure rate. Kranz et al.(1979) observed similar results in jointed Barre granite with ground joint surfaces. They considered the model of a part of joint sketched in Fig.4.18 and explain the difference of changes in contact area due to both confining pressure and pore pressure. They stated that equilibrium demands that

$$P_c A = N + P_p(A - A_r) \tag{4.24}$$

where P_c is confining pressure, P_p is pore pressure, A is the apparent joint surface, A_r is the real area of contact and N is the average normal load on an asperity.

They also assumed that the contact area increases linearly with normal load as follows.

$$A_r = \frac{N}{h} \tag{4.25}$$

where h is the indentation hardness for the asperity material.

Substituting for N from Eq.4.24 into Eq.4.25, one gets

$$\frac{A_r}{A} = \frac{P_c - P_p}{h - P_p} \tag{4.26}$$

To determine whether P_c or P_p have a greater effect on A_r, they compared the following

two quantities.

$$\frac{1}{A}\left[\frac{\partial A_r}{\partial P_c}\right]_{P_p} = \frac{1}{h - P_p} \quad and \quad \frac{1}{A}\left[\frac{\partial A_r}{\partial P_p}\right]_{P_c} = \frac{P_c - h}{\left(h - P_p\right)^2} \tag{4.27}$$

Finally they concluded that, whenever $P_c+P_P< 2h$,

$$\frac{1}{A}\left[\frac{\partial A_r}{\partial P_c}\right]_{P_p} > \frac{1}{A}\left[\frac{\partial A_r}{\partial P_p}\right]_{P_c} \tag{4.28}$$

This condition is certainly met for their experimental results and all the experiments reported in this thesis. Nevertheless, as one can imagine, real changes in joint surfaces topography with confining pressure and pore pressure may be much more complicated.

Other models regarding joint deformation and sliding can be applied to explain experimental observations. In the void asperity model proposed by Tsang and Witherspoon (1981), which has already been described in Chapter 2, with the number of contacts increasing, a single joint could be progressively transformed into an array of co-planar interconnected cracks with high aspect ratio, as shown in Fig.4.19. These small spheroid-like cracks are more resistant to pressure than the initial joint with an elongated shape. Therefore, an increase in mean crack aspect ratio due to the rugosity of the crack walls may explain the decrease in coefficients *a* and *b* with increasing confining pressure or decreasing pore pressure in the A-test and B-test, respectively, but of different magnitude. The decrease of the exponent *n* from the natural joint, to the microcrack, to the sawed joint and intact rock also support this interpretation.

There are many observations of hystereses. Most of them are related to intact rock dilatancy under uniaxial and triaxial loading (Walsh 1965 and Brace et al 1966). Under these conditions, large shear stresses can develop in the rock and friction seems to best explain the hystereses. Hystereses for joint closure were also observed by many researchers (Goodman 1976, Bandis et al. 1983, Scholz and Hickman 1983 and Brown and Scholz 1985) but mainly under the normal compressive stress. Hysteresis and stress history effects on the hydraulic properties of rocks were also observed under hydrostatic pressure (Kranz et al. 1979, Coyner et al.1979 and Bernabe 1986). This indicates that the stress is inhomogeneously distributed and that shear stress can be developed locally at places where joint surfaces are in contact. Since hysteresis may occur in joint closure with a considerable irrecoverable part, some asperities must be deforming plastically or are

crushed when the confining pressure is increased. Either plastic deformation or asperity crushing will increase the contact area and thus decrease the amount of surface area available for pore pressure to work against, in addition to increasing the flow tortuosity. Thus lowering the pore pressure apparently produces irrecoverable surface damage. The permeability can be recovered only if the joint aperture is increased. These facts were also observed by Witherspoon et al.(1977). They stated that flow rate showed a considerable difference between injection and withdrawal of fluid, but that the difference decreased with increasing normal stress. This fact indicates that the joint deforms differently during injection (joint extension) or withdrawal (joint compression) of fluid and this difference decreases under the higher normal stress since the change of fluid pressure in a joint due to injection or withdrawal of fluid is small relative to the higher normal stress.

Walsh (1965) clearly demonstrated the role of friction and suggested that, at stages in the unloading cycle, a rock sample was strongly vibrated while still loaded. This caused the strain in the sample to fall at constant stress to nearly the same value as obtained in the loading cycle. Apparently additional energy of the vibration was sufficient to overcome friction at crack surfaces. The usual hysteresis loop could be almost eliminated by this procedure. During loading, frictional sliding might have occurred at favorable configurations of cracks. During unloading, some of these sites remained blocked in the intermediate position, introducing residual shear stresses. Several models based on the sliding cracks exist (Stevens and Holcomb 1980, Holcomb and Stevens 1980 and Moss and Gupta 1982). Bernabe(1986) discussed the applicability of these models to explain his experimental results and suggested that models based on the sliding cracks were still controversial. Fig.4.20 illustrates examples of configurations where sliding can occur. Sliding cracks proposed by Brace et al.(1966), which configurations described in Fig.4.20(a), were very rarely observed (Tapponnier and Brace 1976), but sliding could easily occur in other configurations like en echelon cracks described in Fig.4.20(b), observed by Kranz (1979), or oblique contacts described in Fig.4.20(c), discussed by Sholz and Hickman (1983). Electron microscope measurements have been conducted to observe crack sliding with strong evidence of past shear motion by Kranz(1979) and Batzle et al. (1980). These microscopic observations are very powerful since one can observe directly the sliding of cracks and the crack propagation in rocks. The models proposed above can also be applied since a portion of void space in a joint does not re-open fully during unloading, causing permanent change in the permeability observed at the end of a pressure cycle. Finally, the reversible Griffith crack proposed as an alternative model by Holcomb and Stevens (1980) is very attractive to interpret the observed hydraulic behavior of the induced microcrack in granodiorite because this model requires a

perfect matching of the crack surfaces and the induced microcrack in this study was ideally matched.

Finally, once again, it is noted that one should not use the conventional effective pressure for the evaluation of joint permeability and for the estimation of the hydraulic behavior of jointed rock. Instead of the conventional effective pressure, one should use the effective pressure, P_e, in general form as follows.

$$P_e = P_c - \alpha P_p \tag{4.29}$$

where P_c is confining pressure, P_p is pore pressure and α is the effective stress coefficient.

To determine the effective stress coefficient for the joint permeability, the transient pulse method is recommended. In the transient pulse method, only a small amount of water flows through a joint during an experiment and the required time for each measurement is relatively short, e.g. ; a couple of hours. This is in contrast to the conventional steady-state flow tests in which relatively large amounts of water must flow and longer testing time is needed to get to the steady-state condition. For this reason, the transient pulse method seems to be more effective and practical, in particular for low permeability rocks and rock joints.

Table 4.1 Fundamental specification of transient pulse permeameter

Axial Pressure	Maximum : 50 MPa
Lateral Pressure	Maximum : 50 MPa
Pore Pressure	Maximum : 50 MPa
Up-stream Reservior	415 cc
Down-stream Reservior	415 cc
Sample Size	Diameter : 50 mm Length : less that 50 mm

Table 4.2 Sampling time for transient pulse test

Measurement Time (sec)	Duration Time (sec)	Sampling Time (sec)
0-100	100	1
100-400	300	5
400-1200	800	20
1200-3000	1800	60
3000-12000	9000	300
12000-30000	18000	1200
30000-end	-	3600

Table 4.3 Coefficient of negative power law and refference value of permeability times cross-sectional area (kA)

Name		Natural Joint			Microcrack		
Coefficient		[KA]0	n	R	[KA]0	n	R
A test	1st loading	6.598E-09	2.234	0.977	1.221E-13	1.404	0.886
	1st unloading	5.048E-11	1.224	0.977	6.285E-15	0.805	0.996
	2nd loading	1.010E-10	1.572	0.931	7.047E-15	0.815	0.970
	2nd unloading	5.551E-11	1.631	0.992	5.081E-15	0.850	0.999
B test	1st loading	1.907E-10	1.579	0.944	4.411E-14	0.967	0.948
	1st unloading	1.234E-11	0.998	0.999	1.045E-14	0.729	0.995
	2nd loading	2.671E-11	1.284	0.990	1.091E-14	0.802	0.982
	2nd unloading	8.662E-12	1.049	0.999	1.007E-14	0.822	0.995
Name		Sawed Joint			Intact		
Coefficient		[KA]0	n	R	[KA]0	n	R
A test	1st loading	1.018E-09	1.184	0.949	1.345E-15	0.584	0.932
	1st unloading	1.512E-10	0.671	0.943	-	-	-
	2nd loading	3.392E-10	0.914	0.960	-	-	-
	2nd unloading	1.386E-10	0.661	0.946	-	-	-
B test	1st loading	3.431E-10	0.939	0.980	2.190E-15	0.578	0.917
	1st unloading	2.587E-10	0.883	0.992	-	-	-
	2nd loading	4.245E-10	1.025	0.980	-	-	-
	2nd unloading	2.228E-10	0.849	0.981	-	-	-

Table 4.4 Maximum and minimum equivalent hydraulic conductivity of joints during cyclic loading

Name		Natural Joint			Microcrack		
		Kmax	Kmin	Kmin/Kmax	Kmax	Kmin	Kmin/Kmax
A test	1st loading	6.03E-06	3.11E-08	0.005	2.87E-09	1.73E-11	0.006
	1st unloading	2.64E-06	3.11E-08	0.012	2.67E-10	1.73E-11	0.065
	2nd loading	2.64E-06	8.06E-09	0.003	2.67E-10	1.32E-11	0.049
	2nd unloading	2.02E-06	8.06E-09	0.004	2.28E-10	1.32E-11	0.058
B test	1st loading	1.90E-06	1.66E-08	0.009	1.28E-09	3.32E-11	0.026
	1st unloading	3.14E-07	1.66E-08	0.053	4.54E-10	3.32E-11	0.073
	2nd loading	3.14E-07	1.08E-08	0.034	4.54E-10	2.19E-11	0.048
	2nd unloading	2.20E-07	1.08E-08	0.049	4.74E-10	2.19E-11	0.046
Name		Sawed Joint			Intact		
		Kmax	Kmin	Kmin/Kmax	Kmax	Kmin	Kmin/Kmax
A test	1st loading	8.77E-06	4.87E-07	0.056	4.64E-11	5.52E-12	0.119
	1st unloading	5.06E-06	4.87E-07	0.096	-	-	-
	2nd loading	5.06E-06	4.52E-07	0.089	-	-	-
	2nd unloading	4.84E-06	4.52E-07	0.093	-	-	-
B test	1st loading	4.47E-06	4.28E-07	0.096	7.17E-11	8.36E-12	0.117
	1st unloading	3.72E-06	4.28E-07	0.115	-	-	-
	2nd loading	3.72E-06	4.22E-07	0.113	-	-	-
	2nd unloading	3.24E-06	4.22E-07	0.130	-	-	-

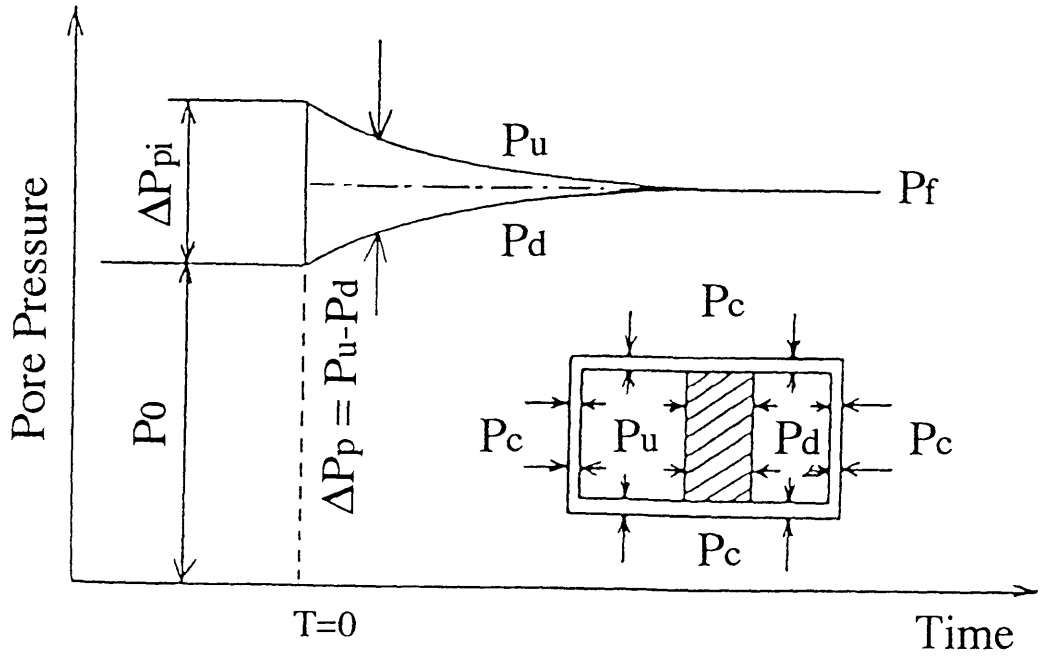

$$\Delta P_p = P_u - P_d = \Delta P_{pi}\, e^{-\gamma t} \quad \text{and} \quad \gamma = \frac{kA(V_u+V_d)}{\beta\mu L V_u V_d}$$

where
- P_0 : initial pore pressure
- P_u : upstream pore pressure
- P_d : downstream pore pressure
- P_f : final equilibrium pore pressure
- P_c : confining pressure
- ΔP_{pi} : initial pressure pulse
- k : permeability of sample
- β : isothermal compressibility of fluid
- μ : fluid viscosity
- A : cross-sectional area of sample
- L : length of sample
- V_u : volume of upstream reservior
- V_d : volume of downstream reservior

Fig. 4.1 Schematic view of transient pulse method

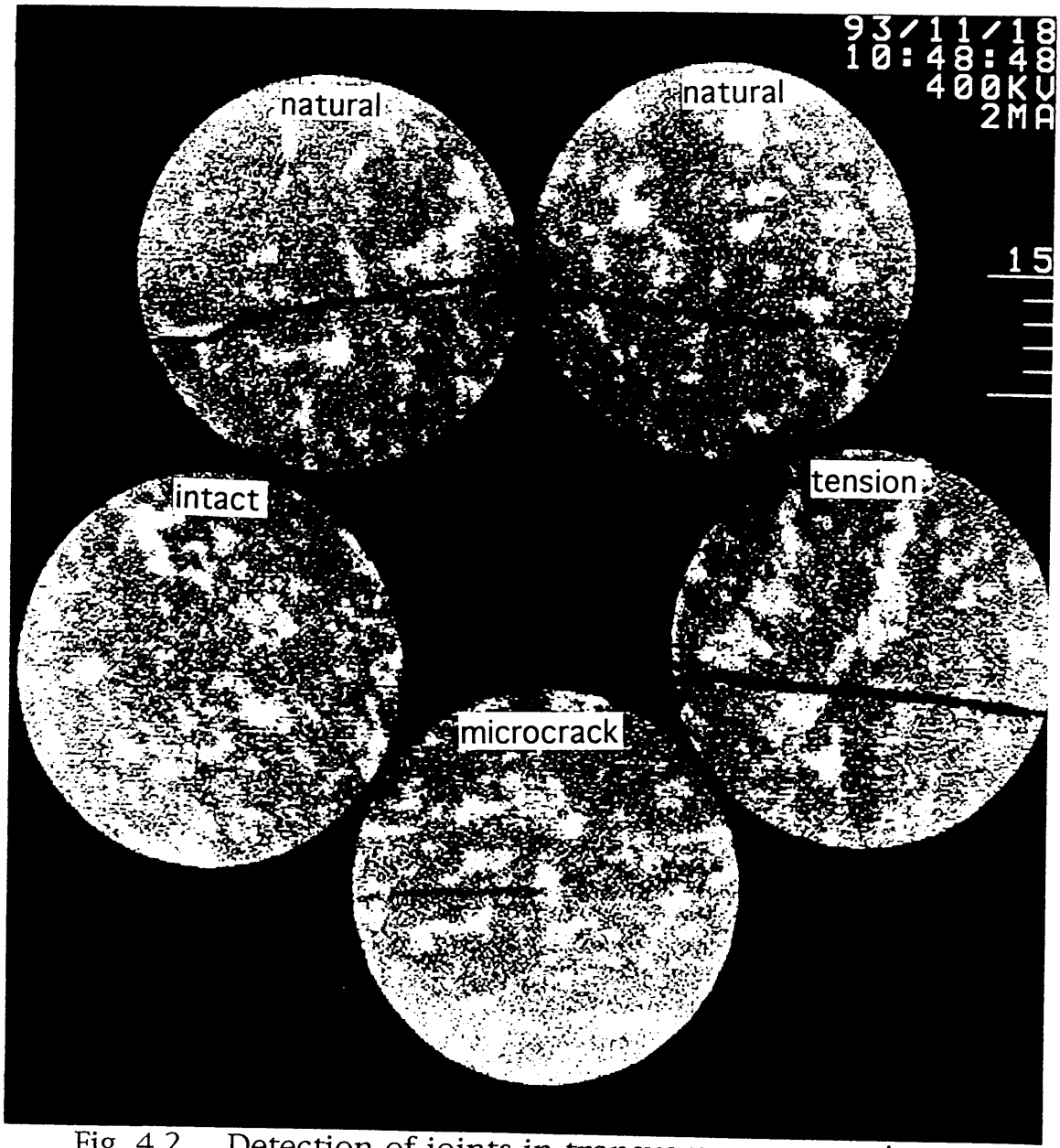

Fig. 4.2 Detection of joints in transverse cross section by X-ray CT scanner
(a)1cm from top end of sample

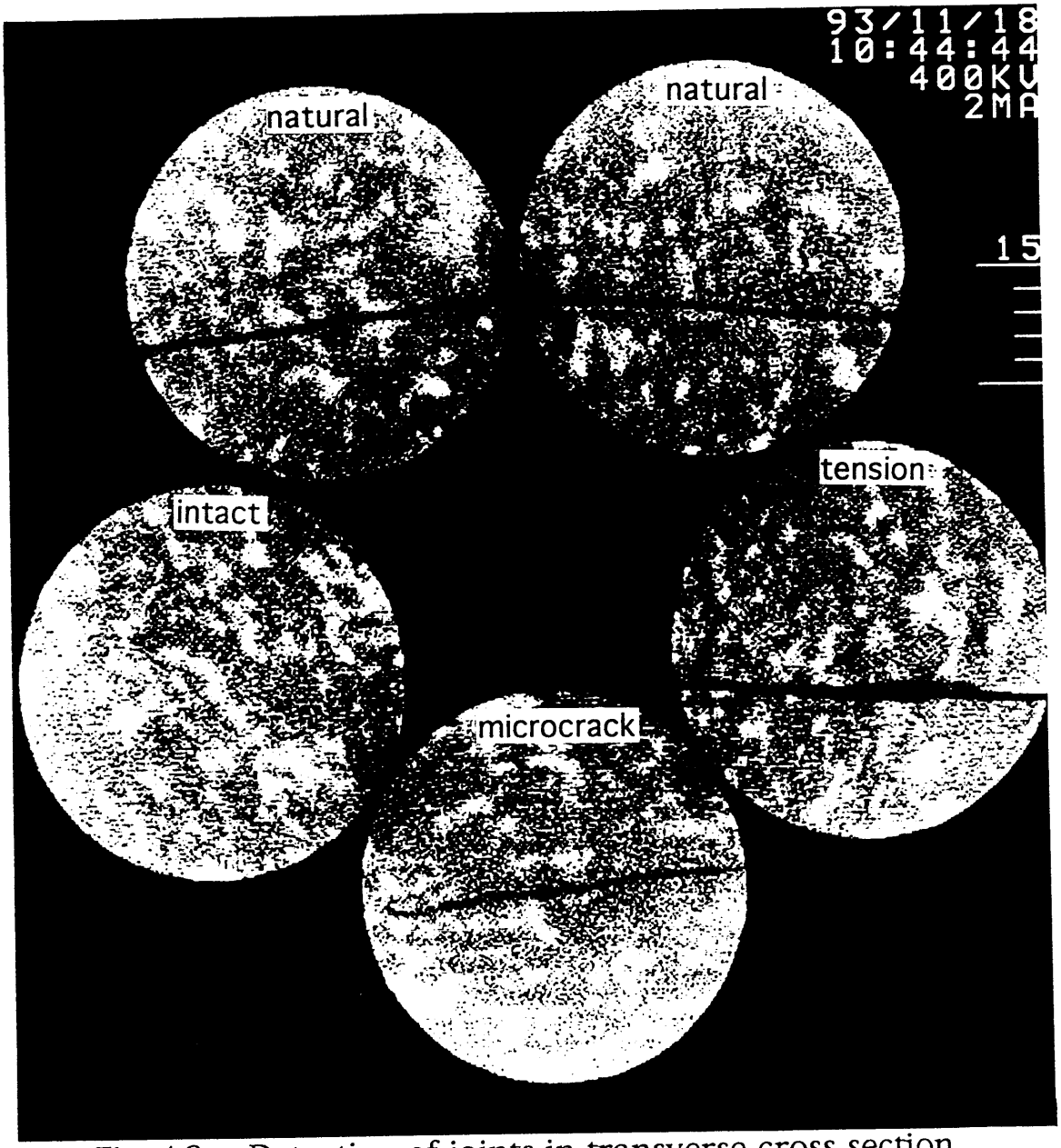

Fig. 4.2 Detection of joints in transverse cross section by X-ray CT scanner
(b)3cm from top end of sample

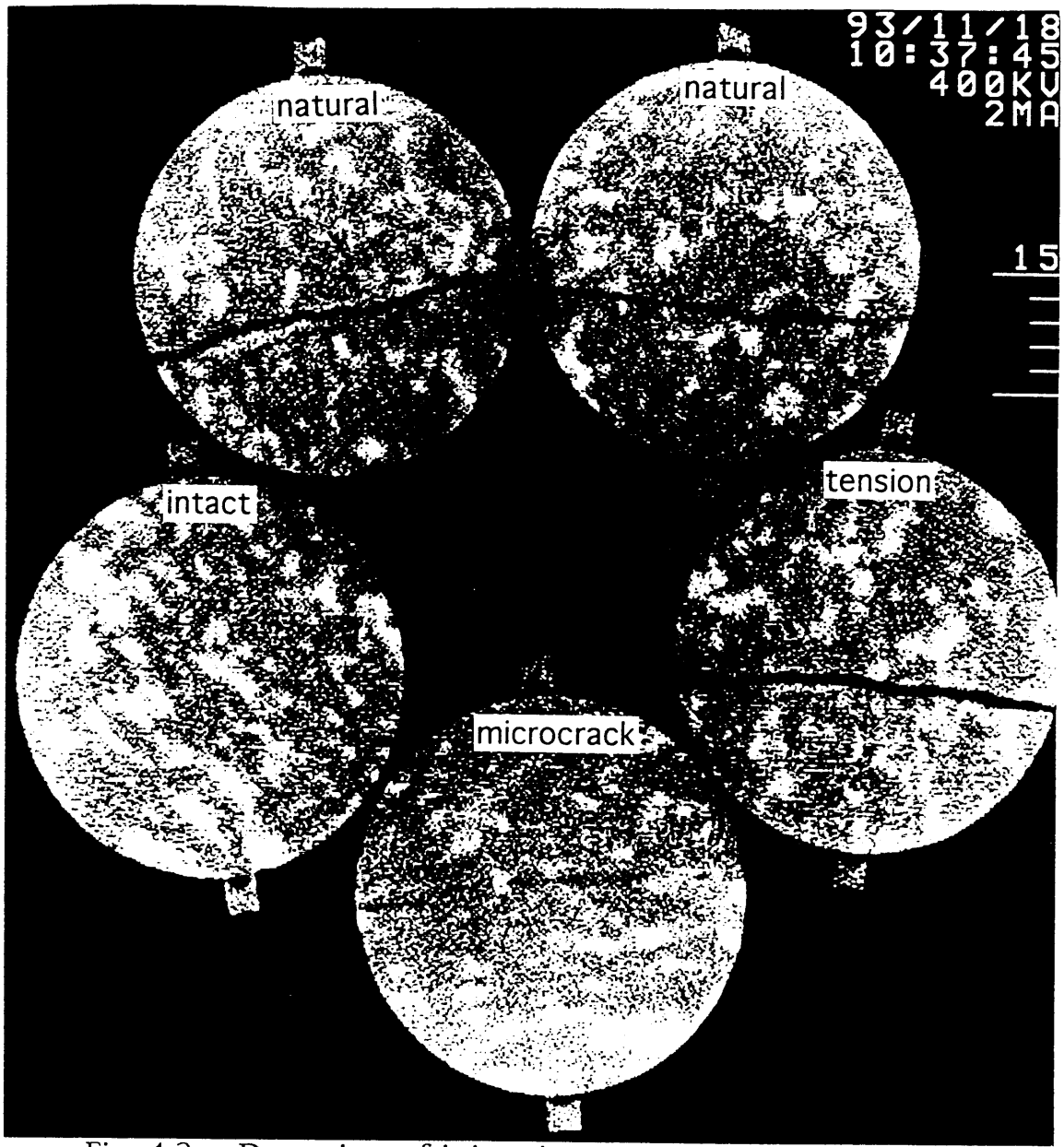

Fig. 4.2 Detection of joints in transverse cross section by X-ray CT scanner
(c)Center of sample

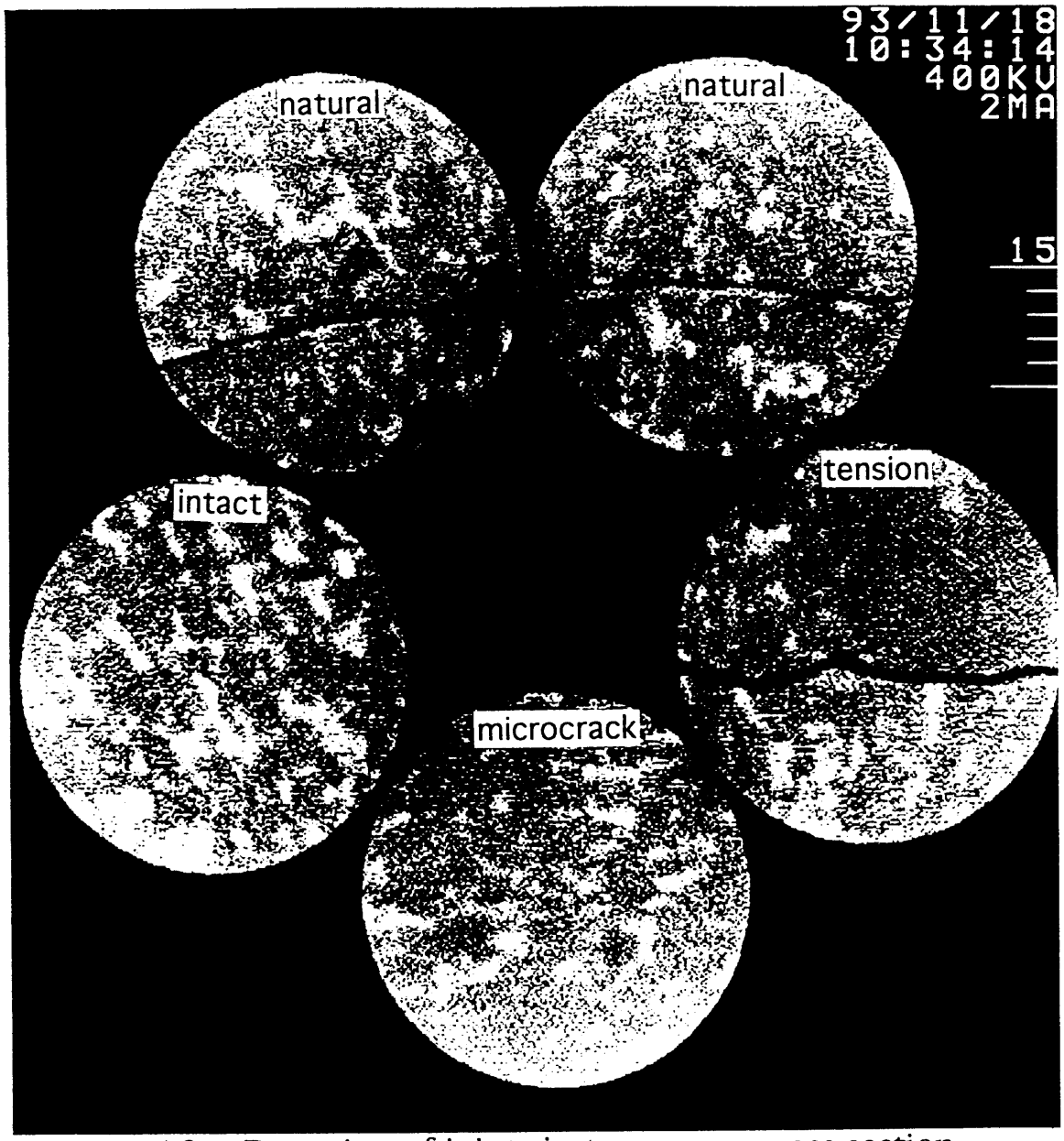

Fig. 4.2 Detection of joints in transverse cross section by X-ray CT scanner
(d)3cm from bottom end of sample

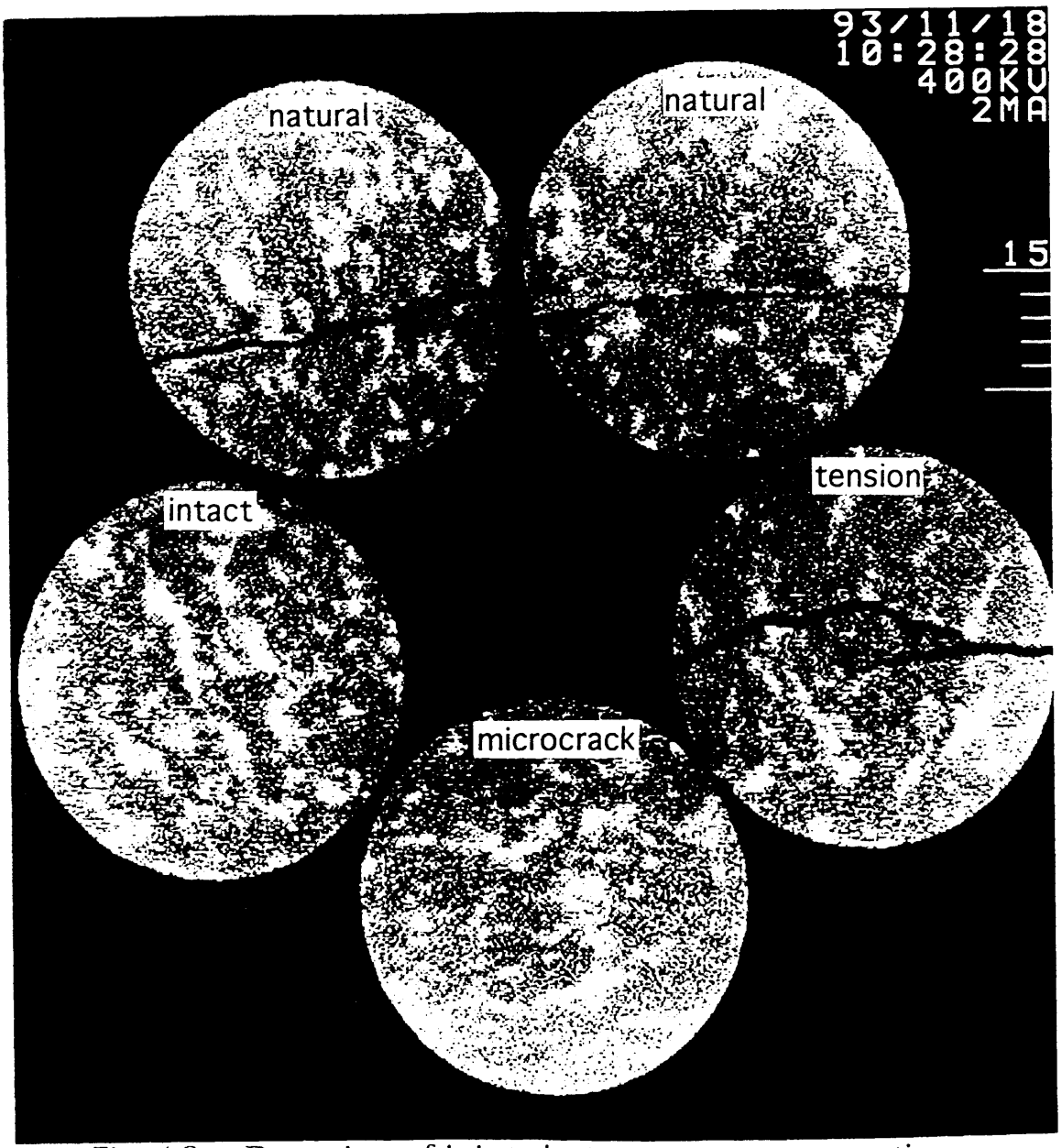

Fig. 4.2 Detection of joints in transverse cross section by X-ray CT scanner
(e)1cm from bottom end of sample

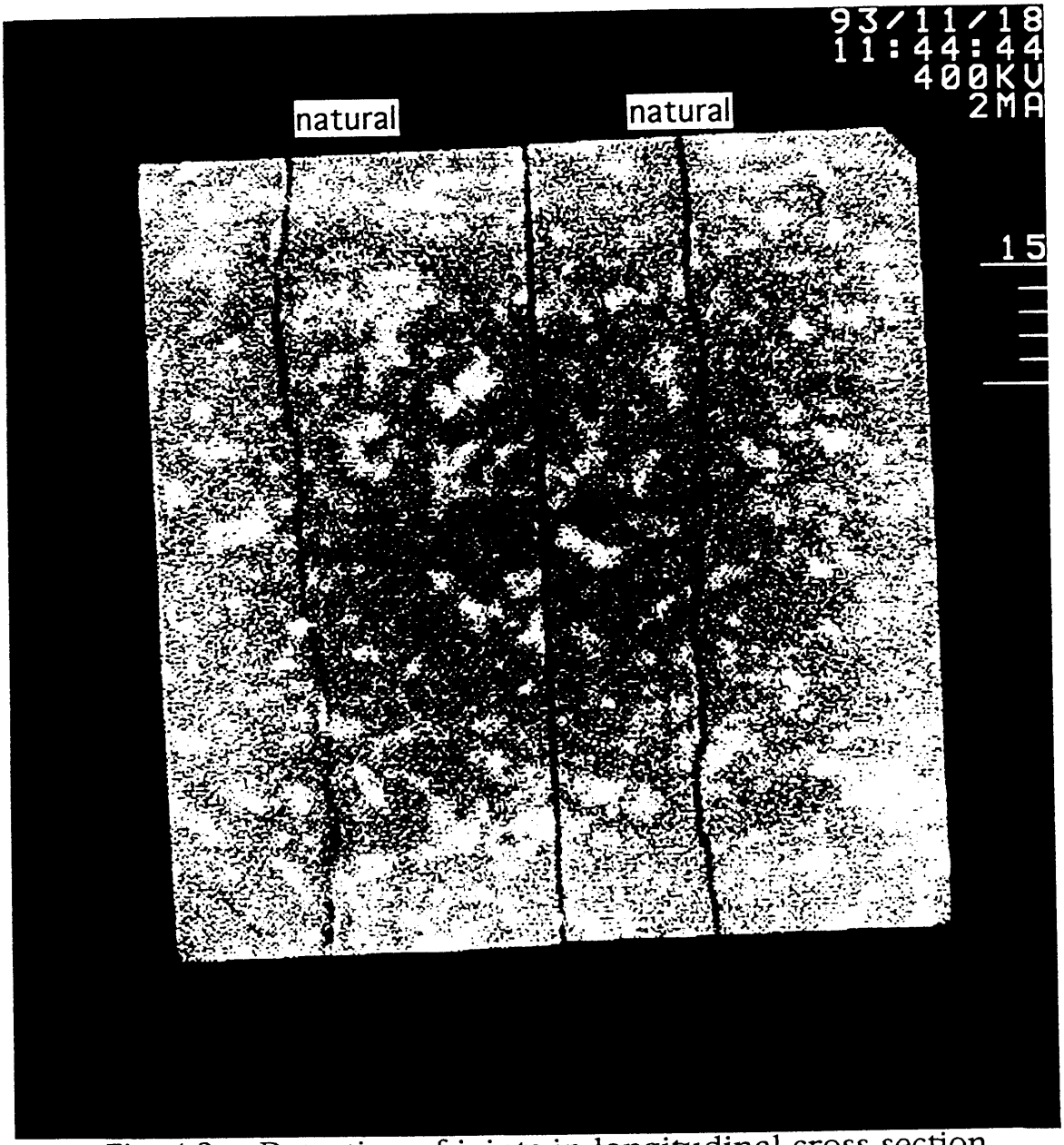

Fig. 4.3 Detection of joints in longitudinal cross section by X-ray CT scanner
(a)Natural joint (left and right)

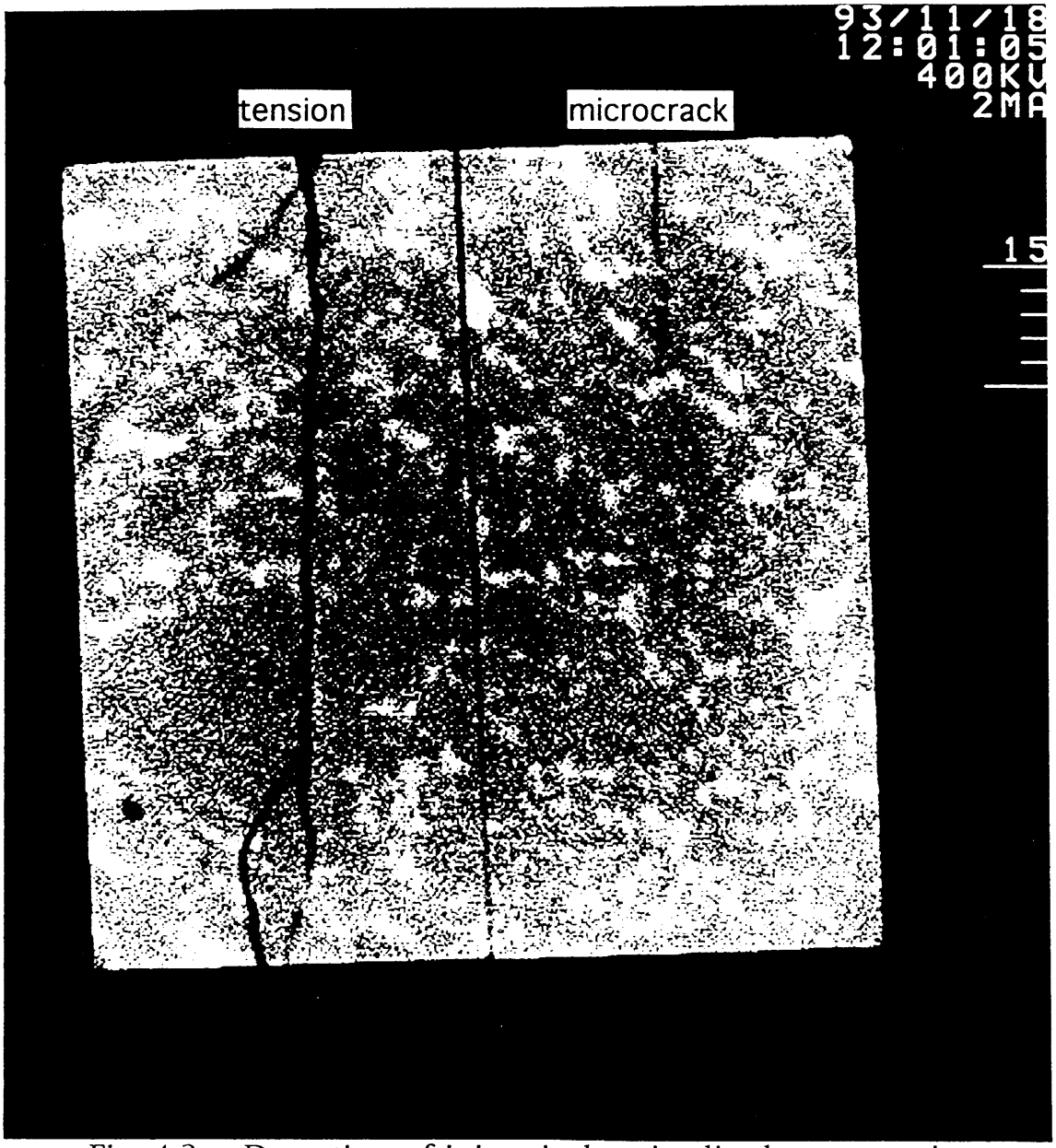

Fig. 4.3 Detection of joints in longitudinal cross section by X-ray CT scanner
(b)Tension joint (left) and Microcrack (right)

a) Schematic view of the transient pulse permeameter

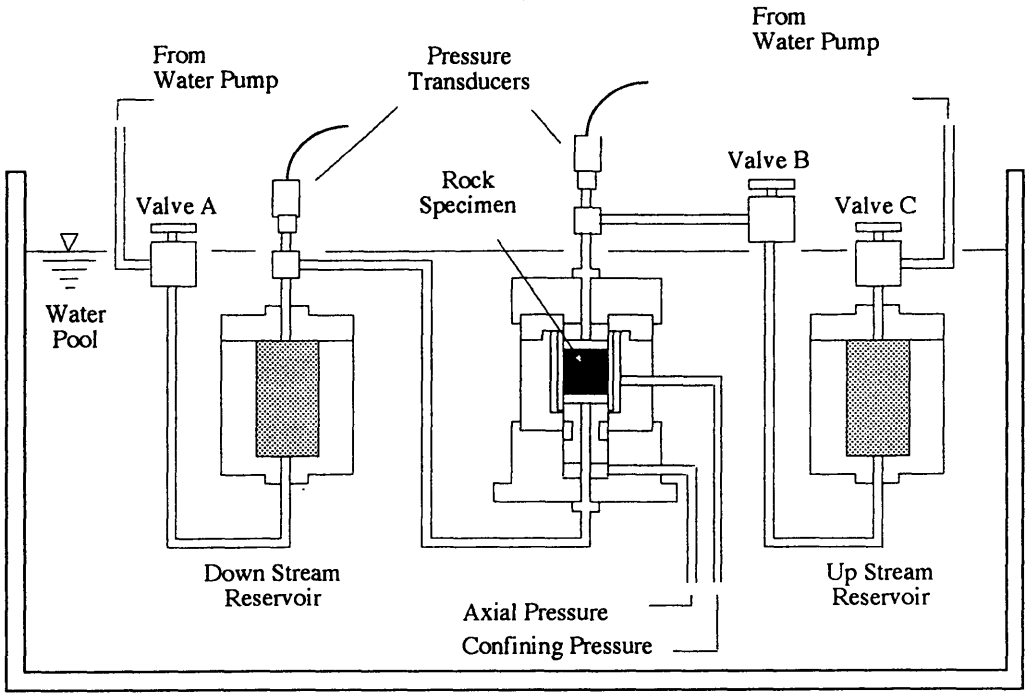

b) Pressure cell

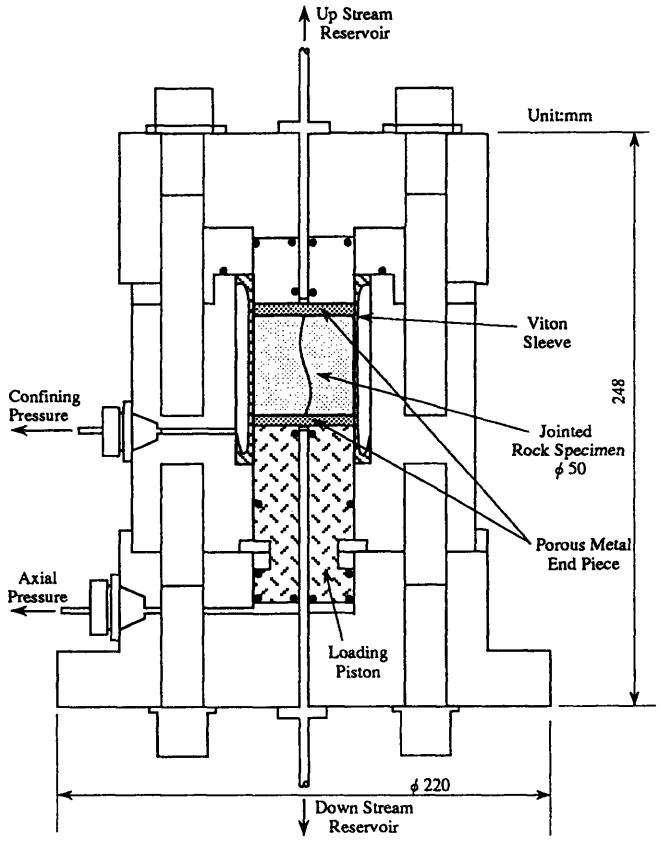

Fig. 4.4 Experimental arrangement of the transient pulse permeameter

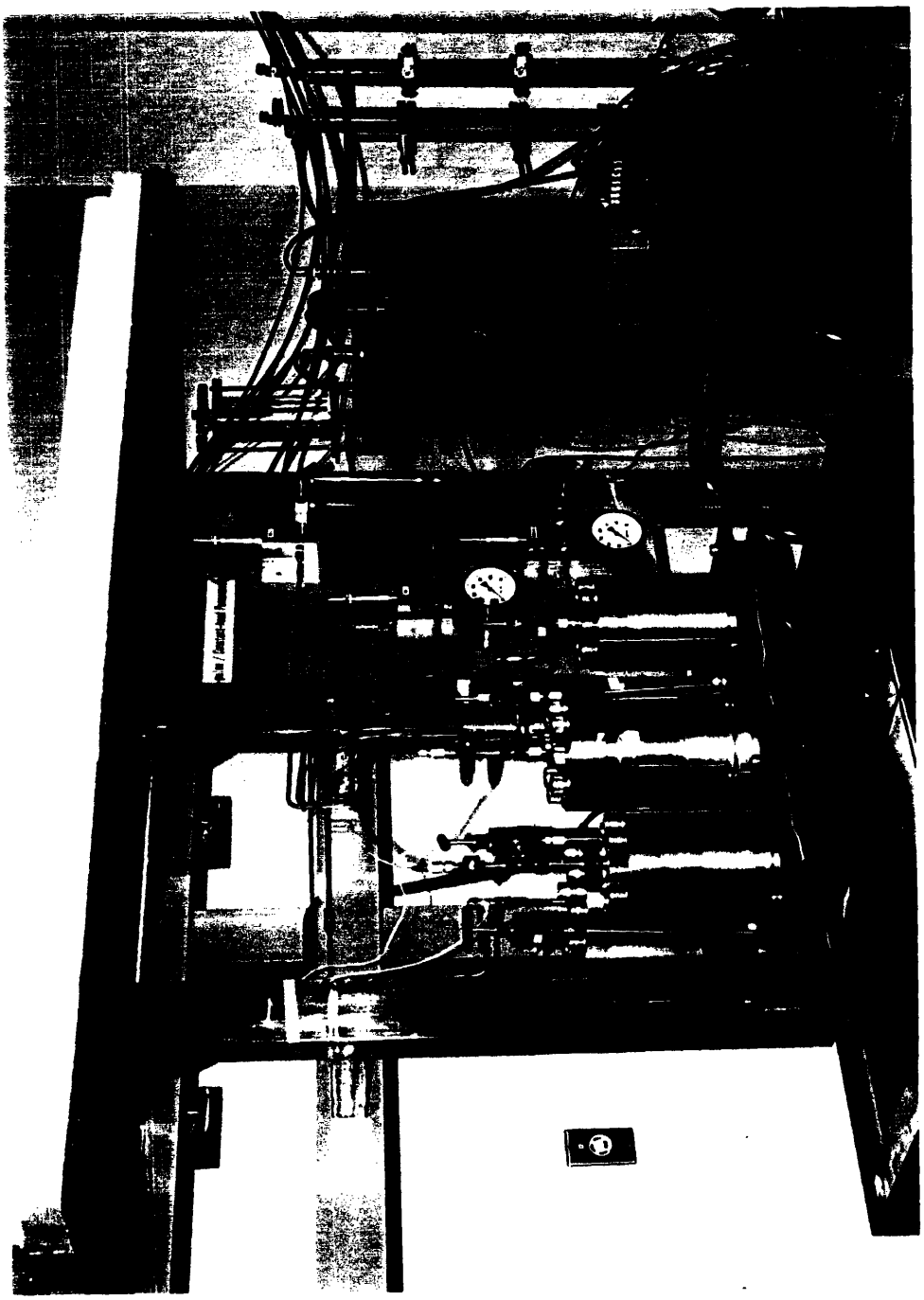

Fig. 4.5 A photograph of the transient pulse permeameter

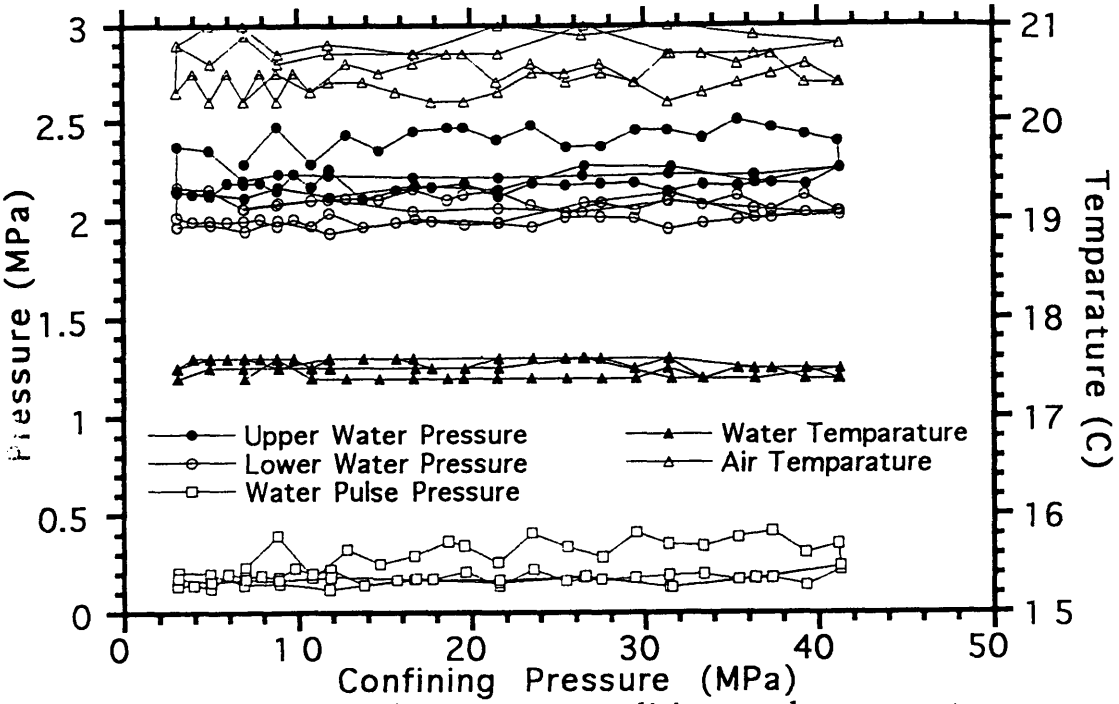

Fig. 4.6 Example of pressure condition and temperature fluctuation (natural joint : A-test)

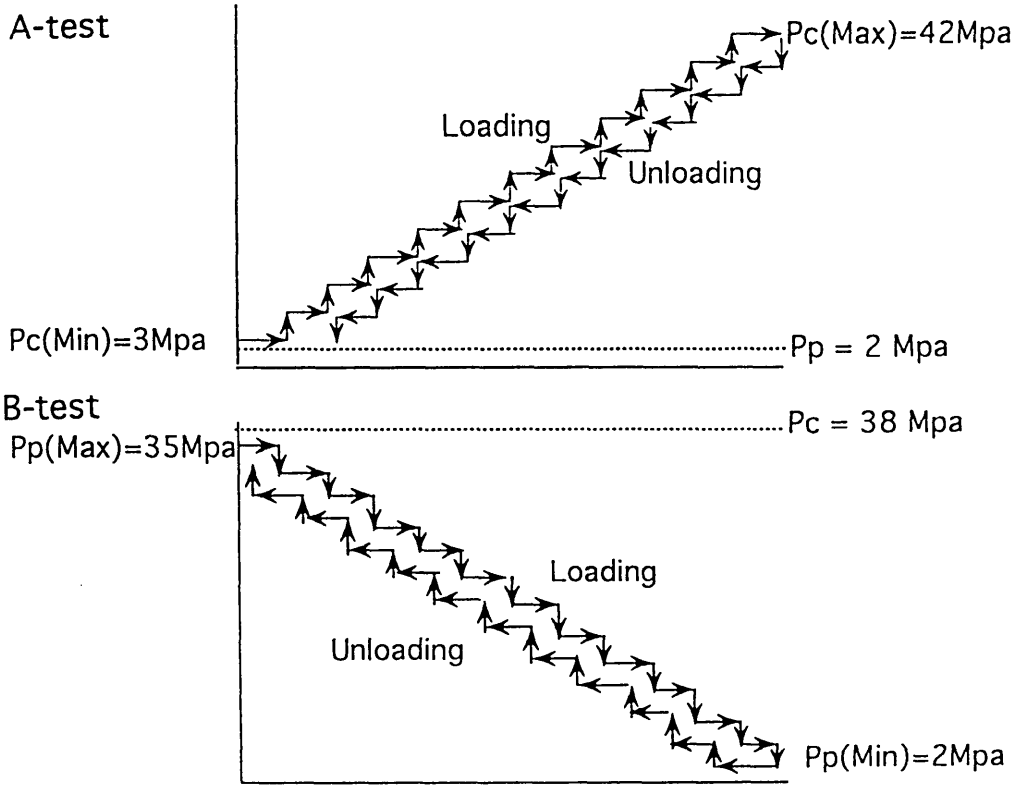

Fig. 4.7 Diagram outlining the cycling procedures of both A-test and B-test

a)Example of mesurement(Natural joint, A-test, Pc=42MPa)

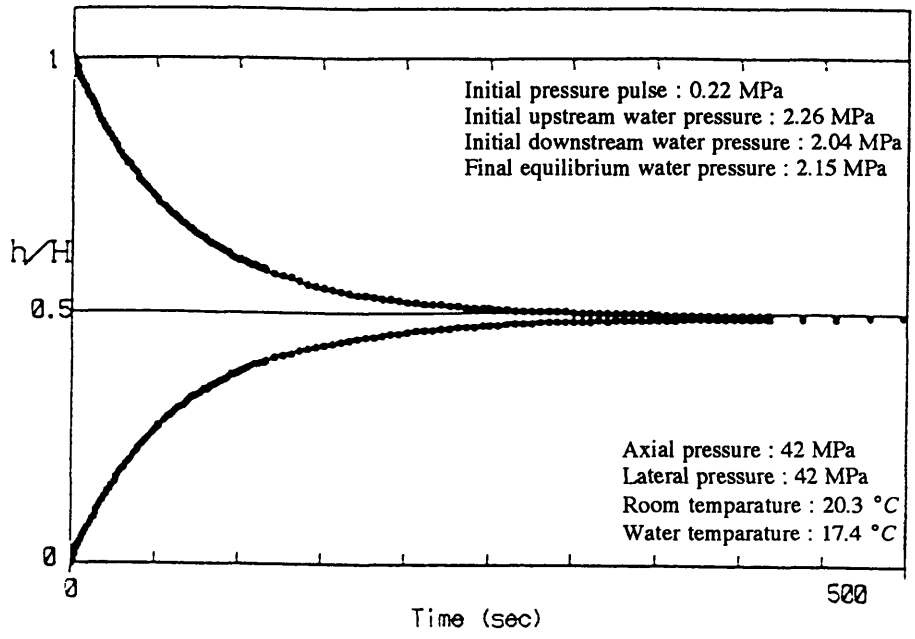

b)Result of analysis by Brace's method

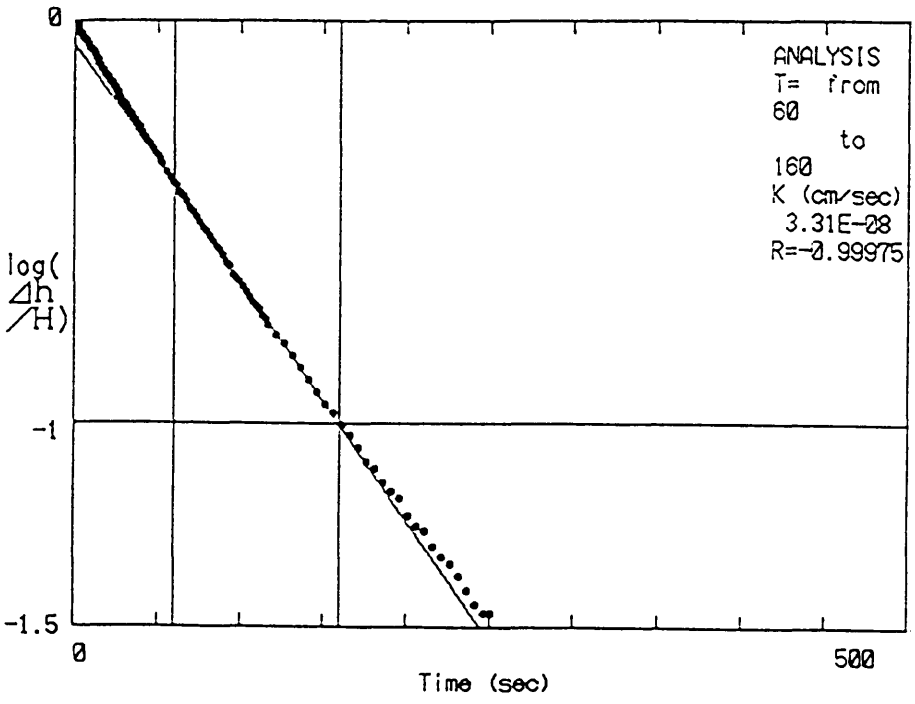

Fig. 4.8 Example of measurement and analysis by Brace's method

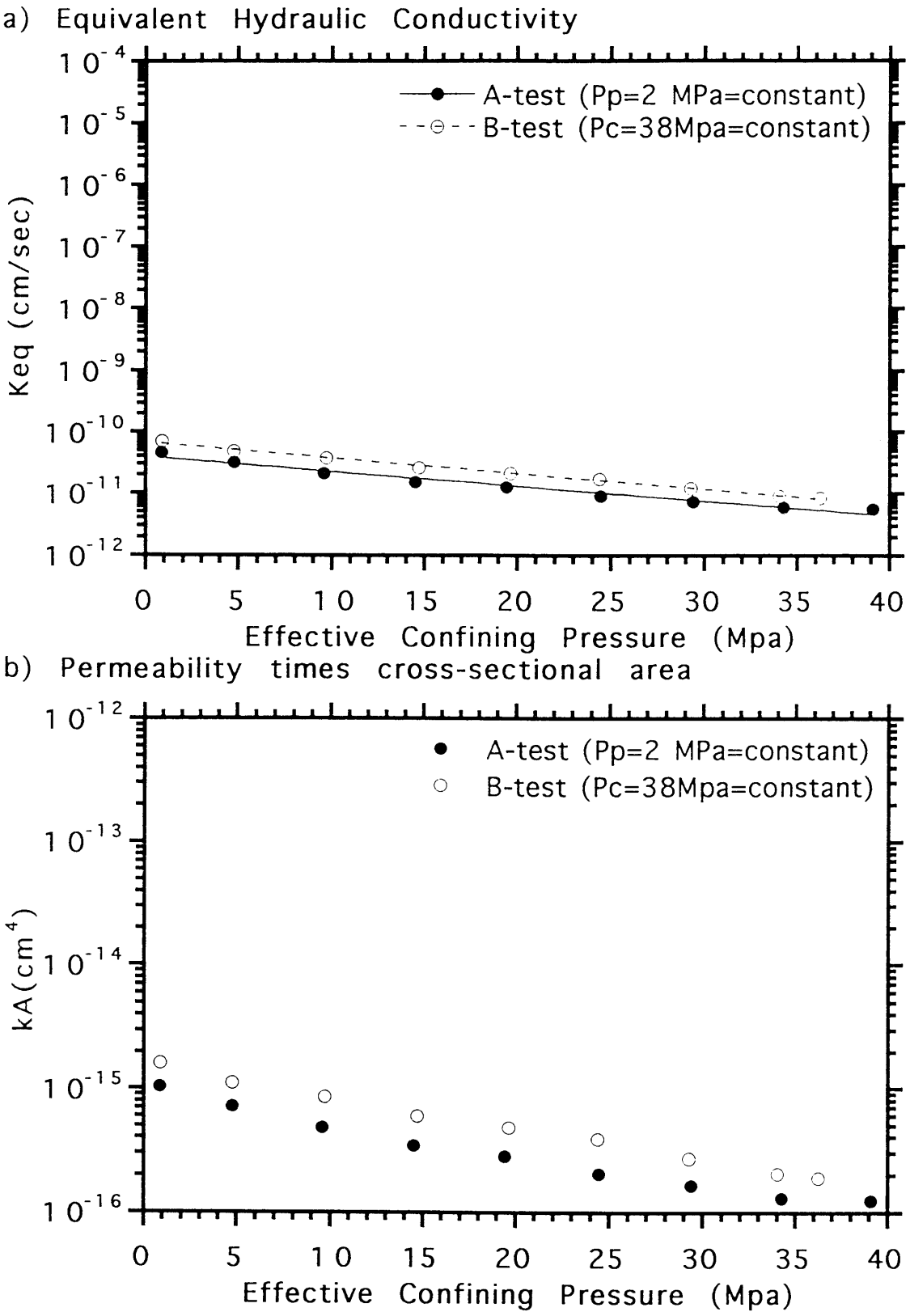

Fig. 4.9 Equivalent hydraulic conductivity and permeability times cross-sectional area (kA) vs Pc-Pp for Kikuma granodiorite

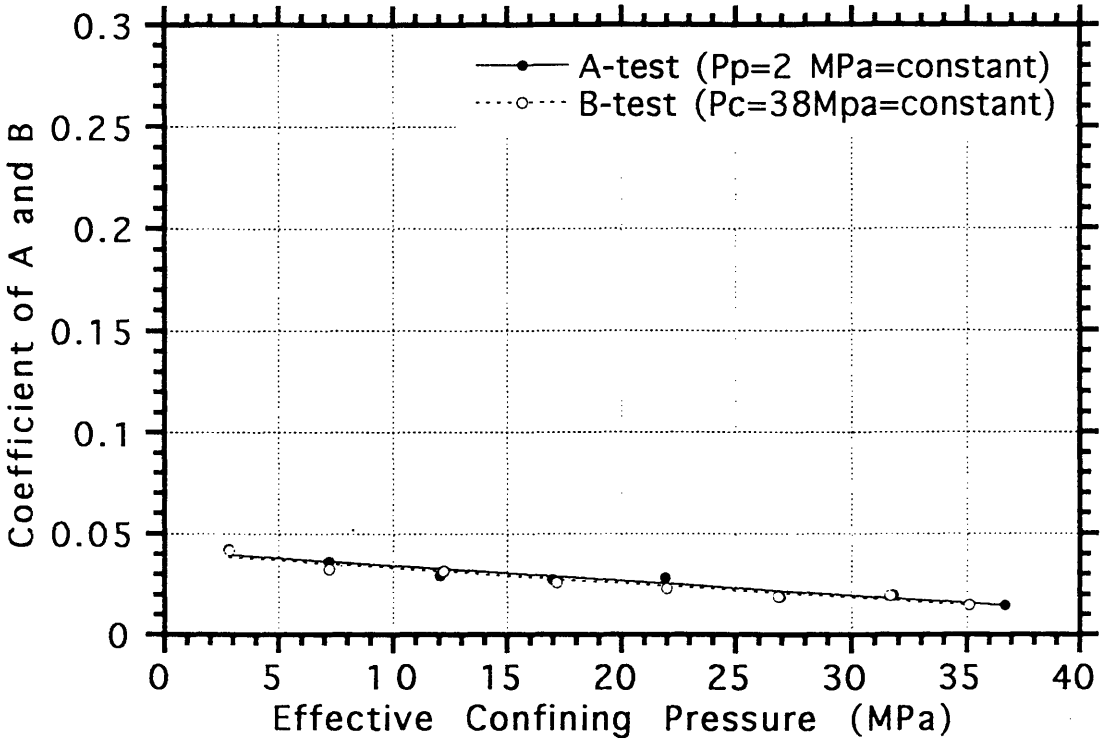

Fig.4.10 Coefficient of A and B vs effective confining pressure for Kikuma granodiorite

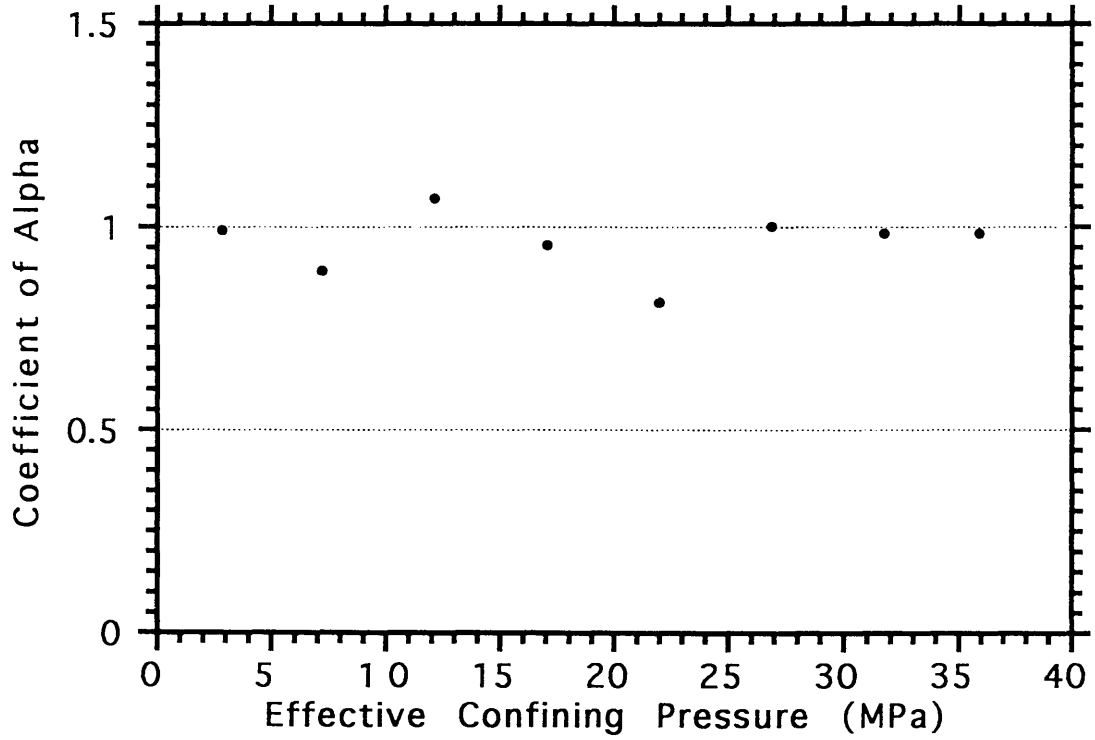

Fig.4.11 Coefficient of alpha vs effective confining pressure for Kikuma granodiorite

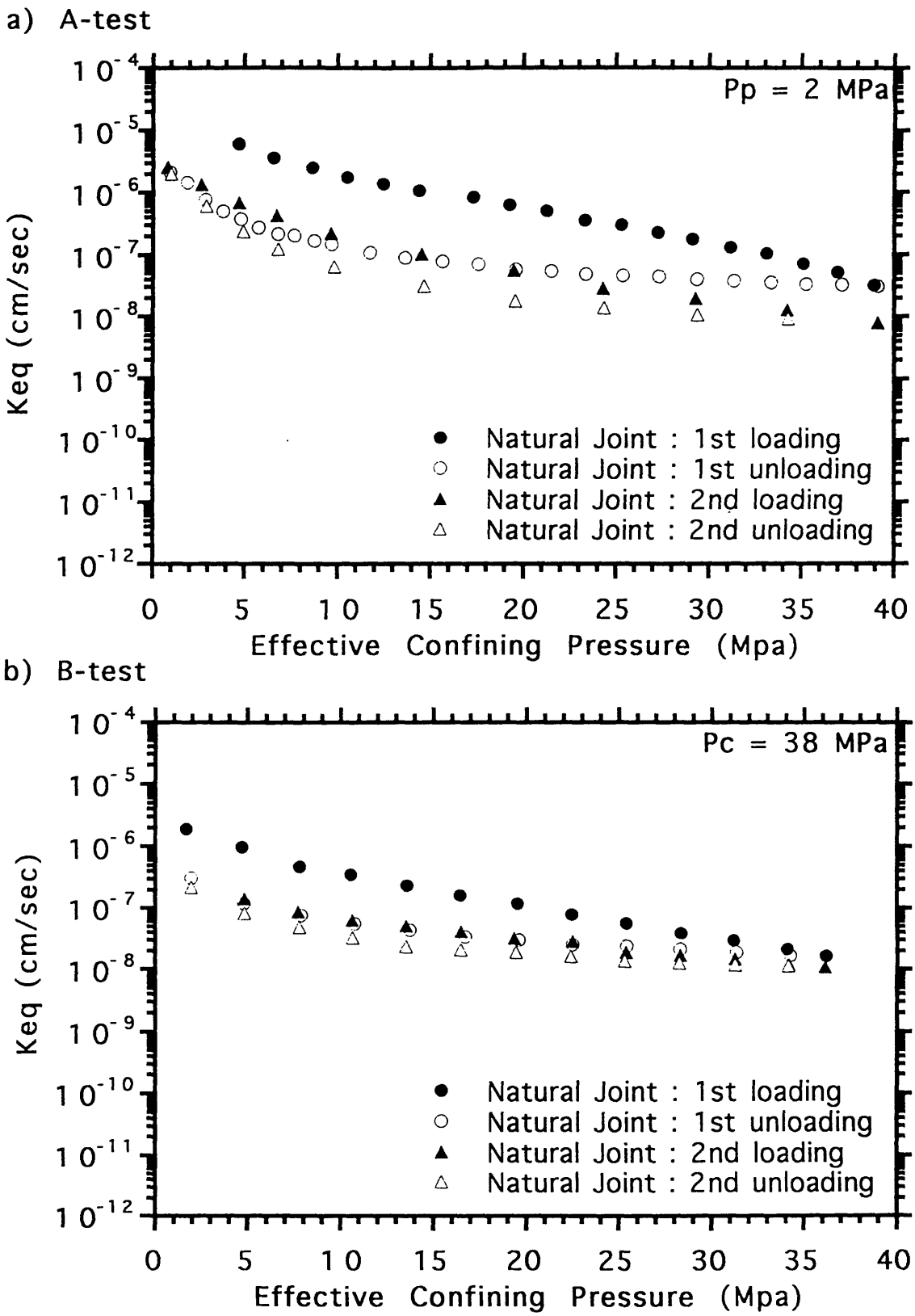

Fig. 4.12 Equivalent hydraulic conductivity vs Pc-Pp for joints
(A)Natural joint

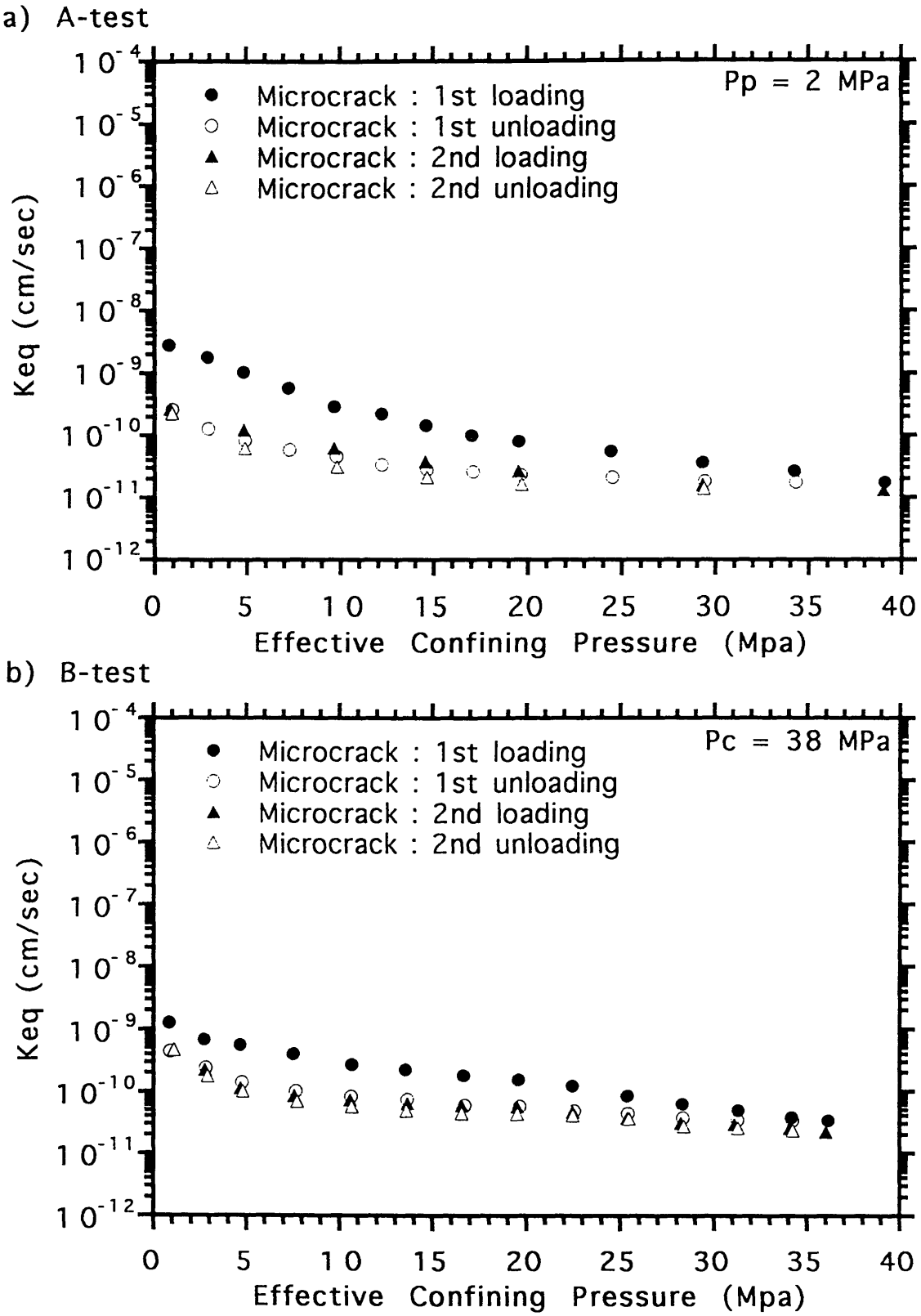

Fig. 4.12 Equivalent hydraulic conductivity vs Pc-Pp for joints (B)Microcrack

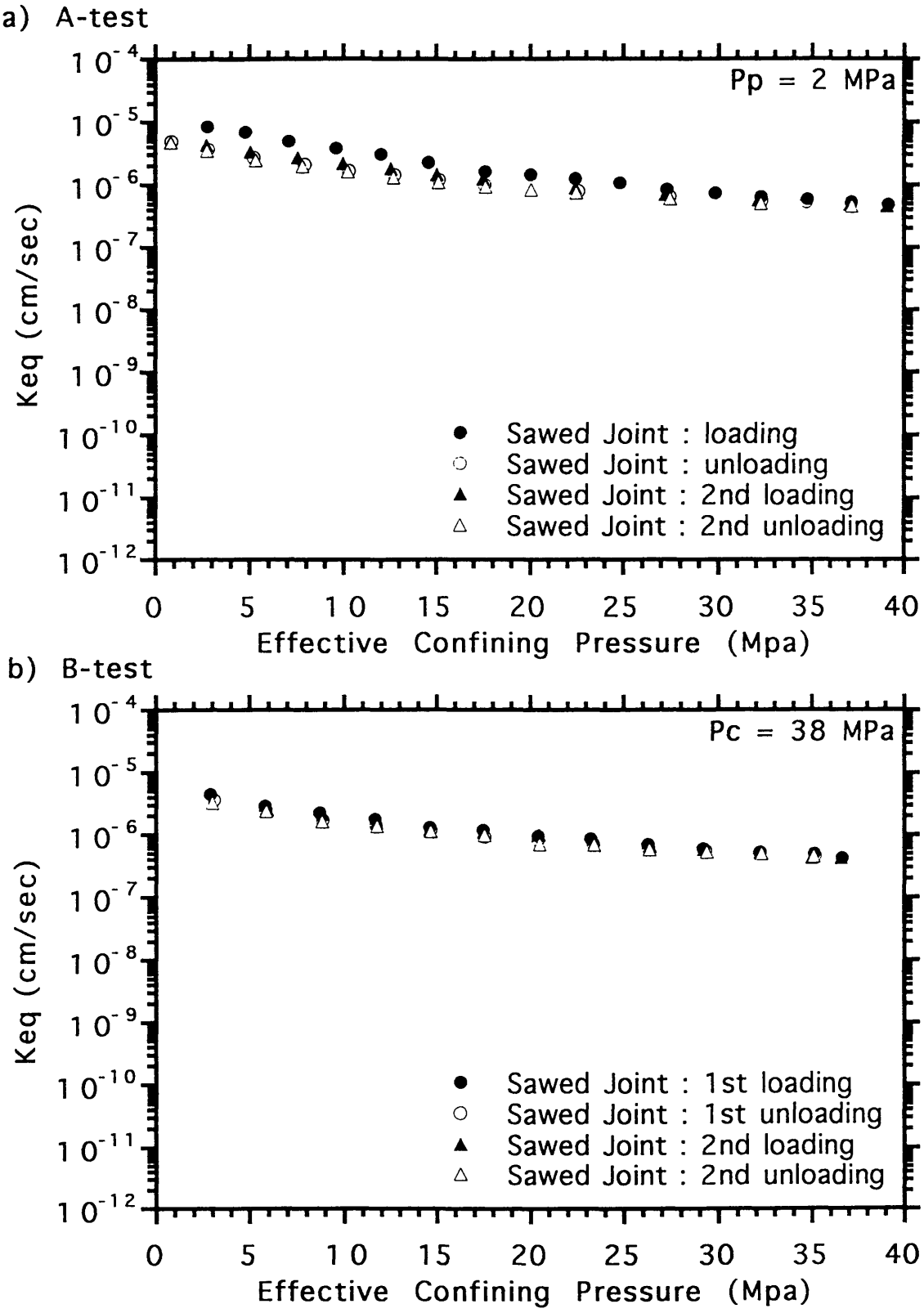

Fig. 4.12 Equivalent hydraulic conductivity vs Pc-Pp for joints (C)Sawed joint

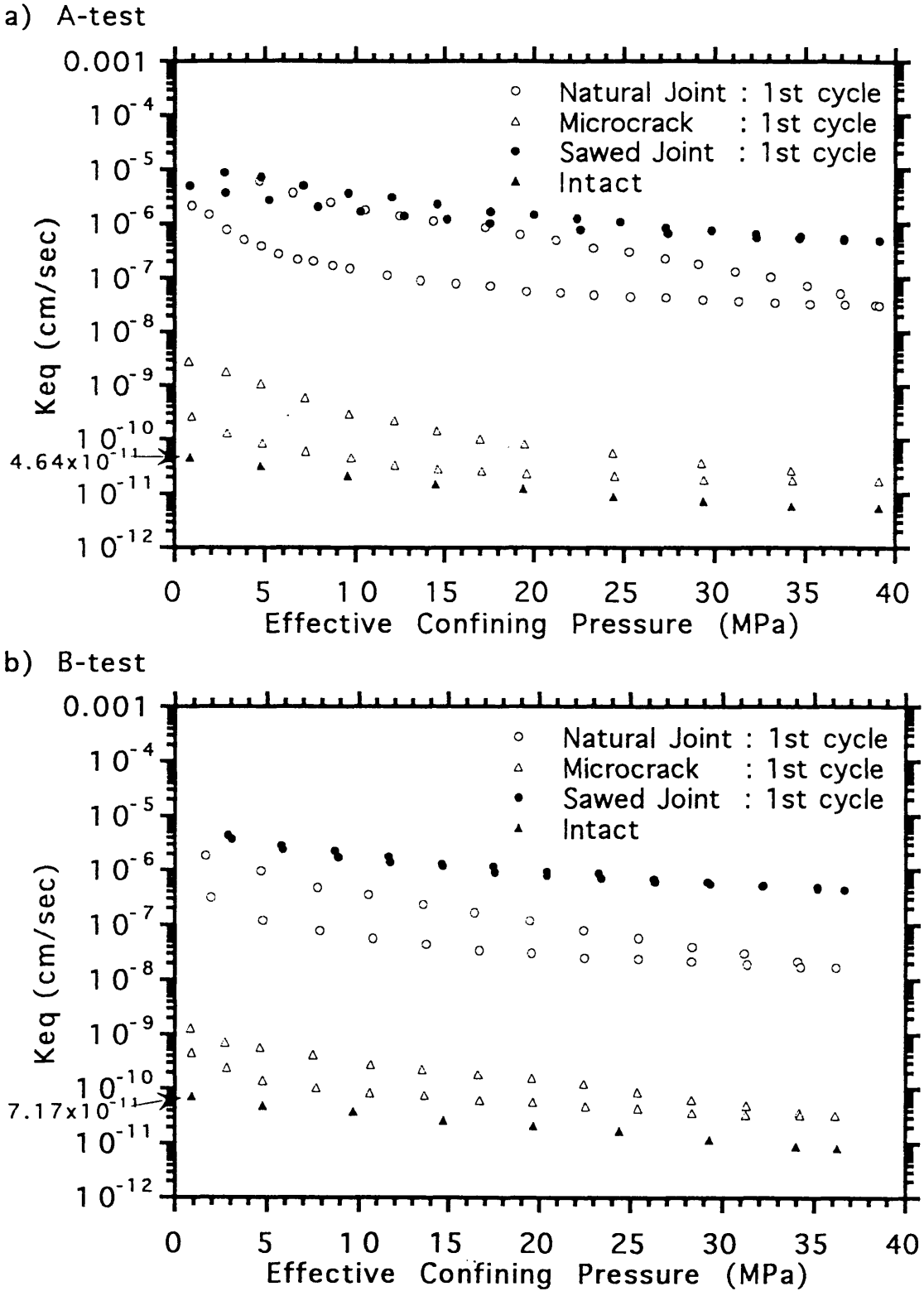

Fig. 4.13 Equivalent hydraulic conductivity vs Pc-Pp for joints (A)1st cycle

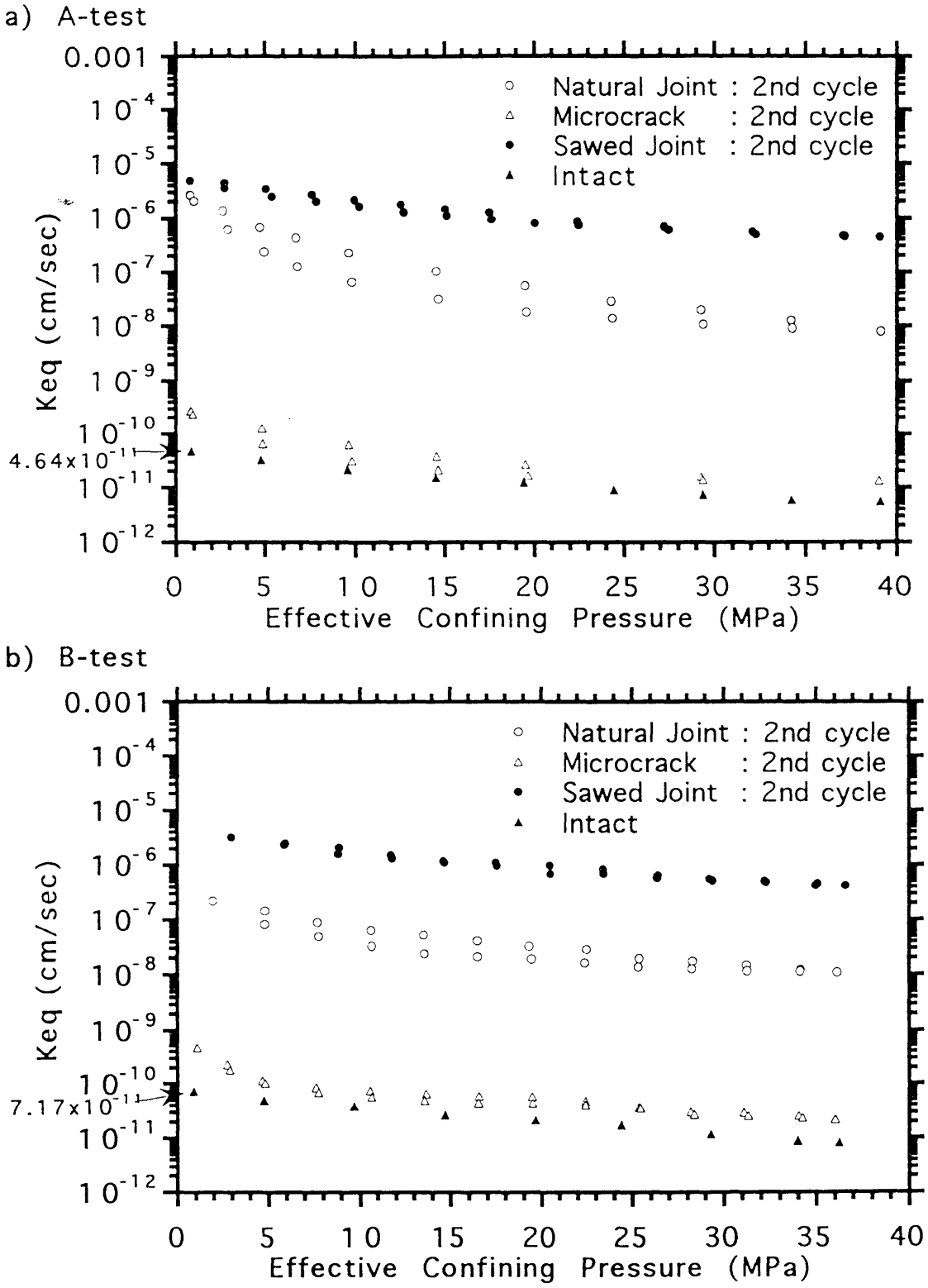

Fig. 4.13 Equivalent hydraulic conductivity vs Pc-Pp for joints (B)2nd cycle

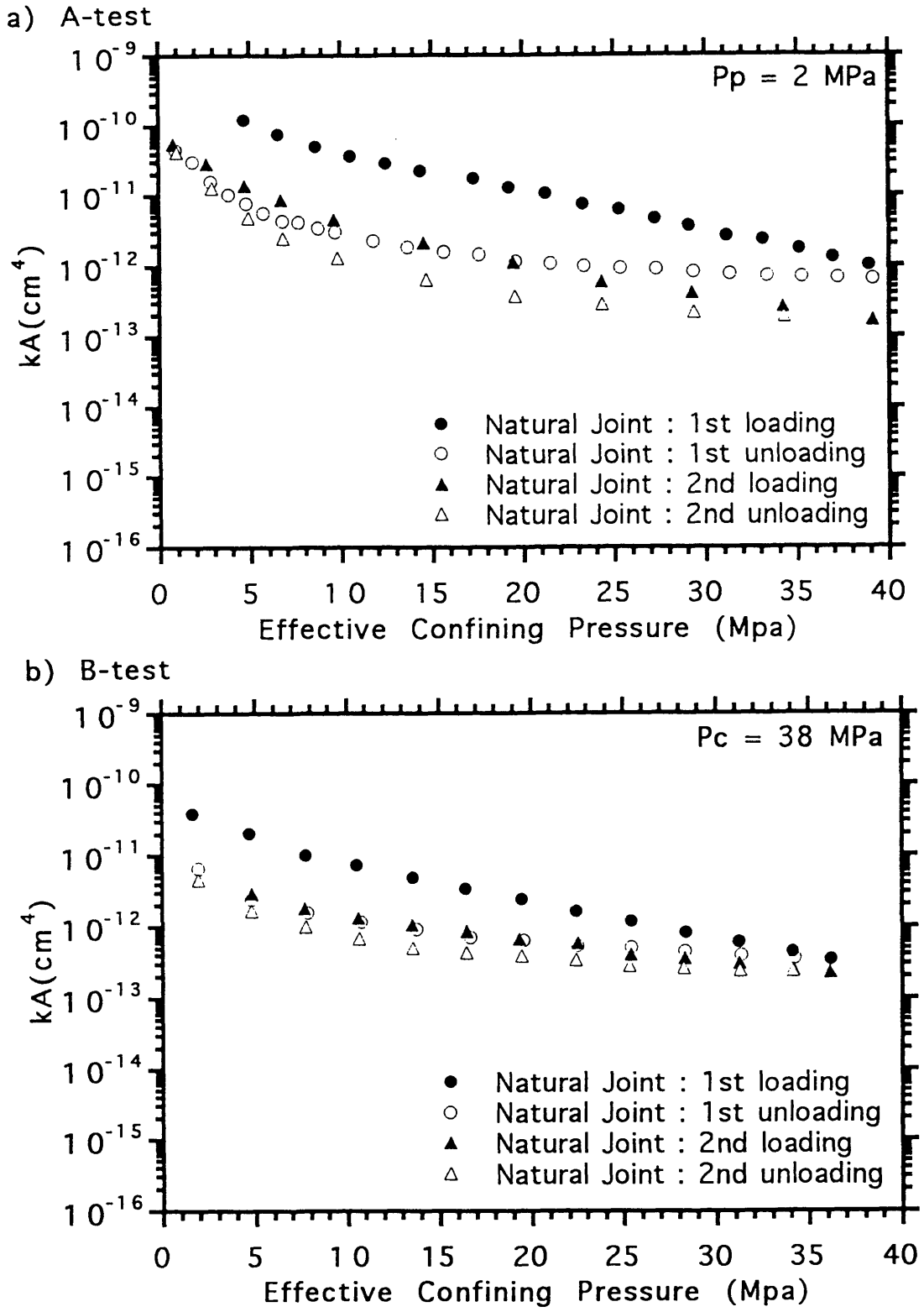

Fig. 4.14 Permeability times cross-sectional area vs Pc-Pp for joints (A)Natural joint

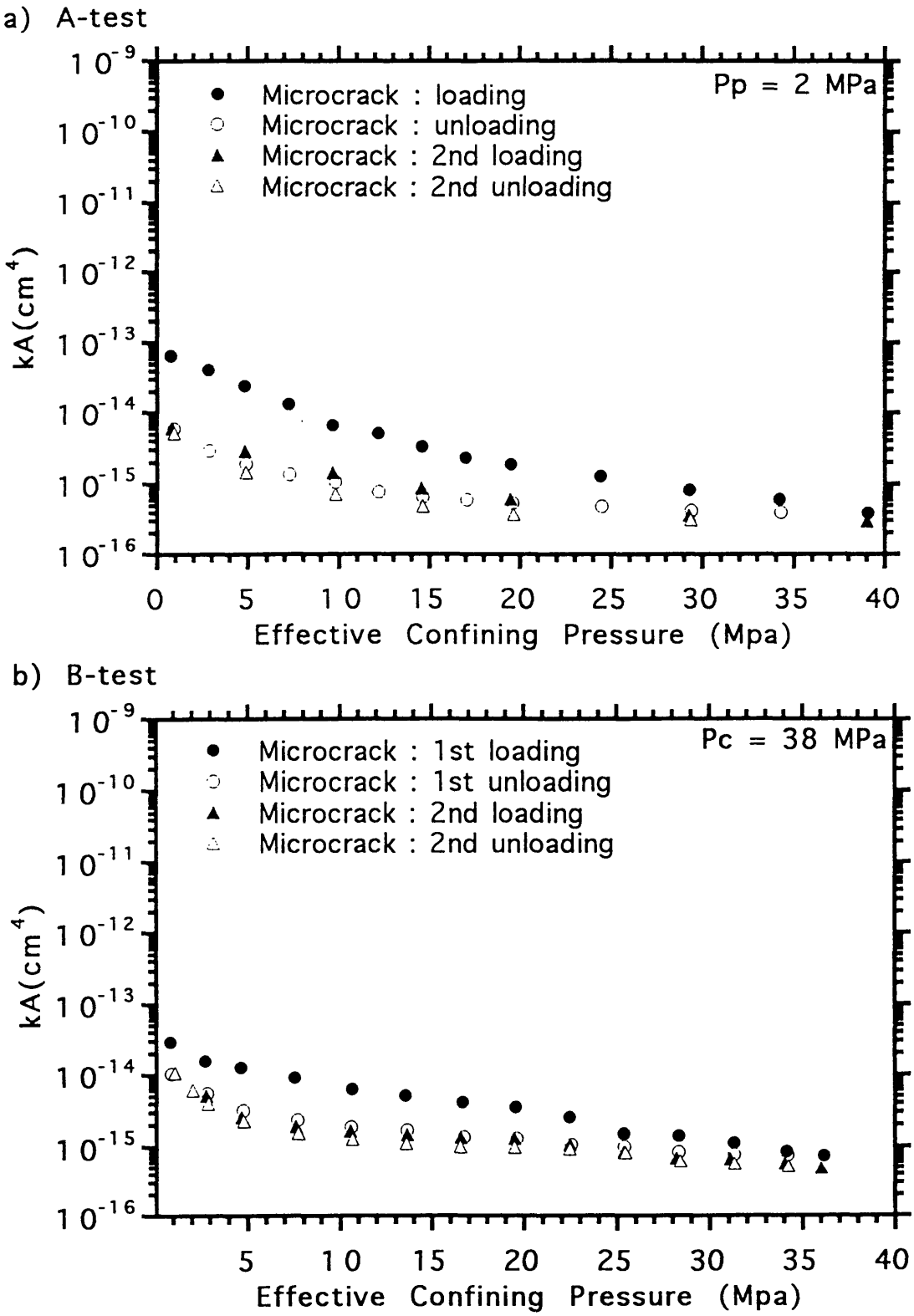

Fig. 4.14 Permeability times cross-sectional area vs Pc-Pp for joints (B)Microcrack

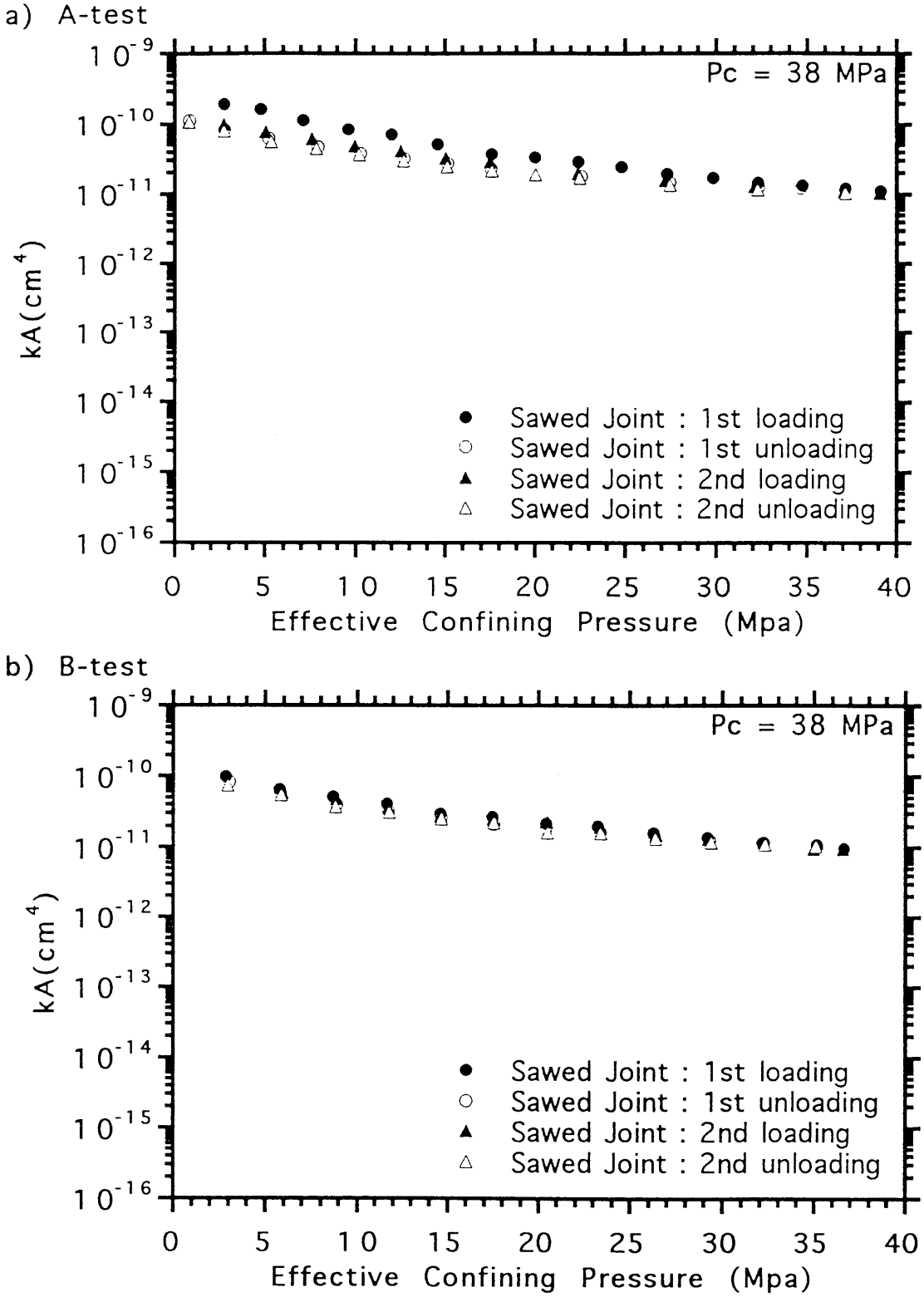

Fig. 4.14 Permeability times cross-sectional area vs Pc-Pp for joints (C)Sawed joint

a) A-test : 1st loading

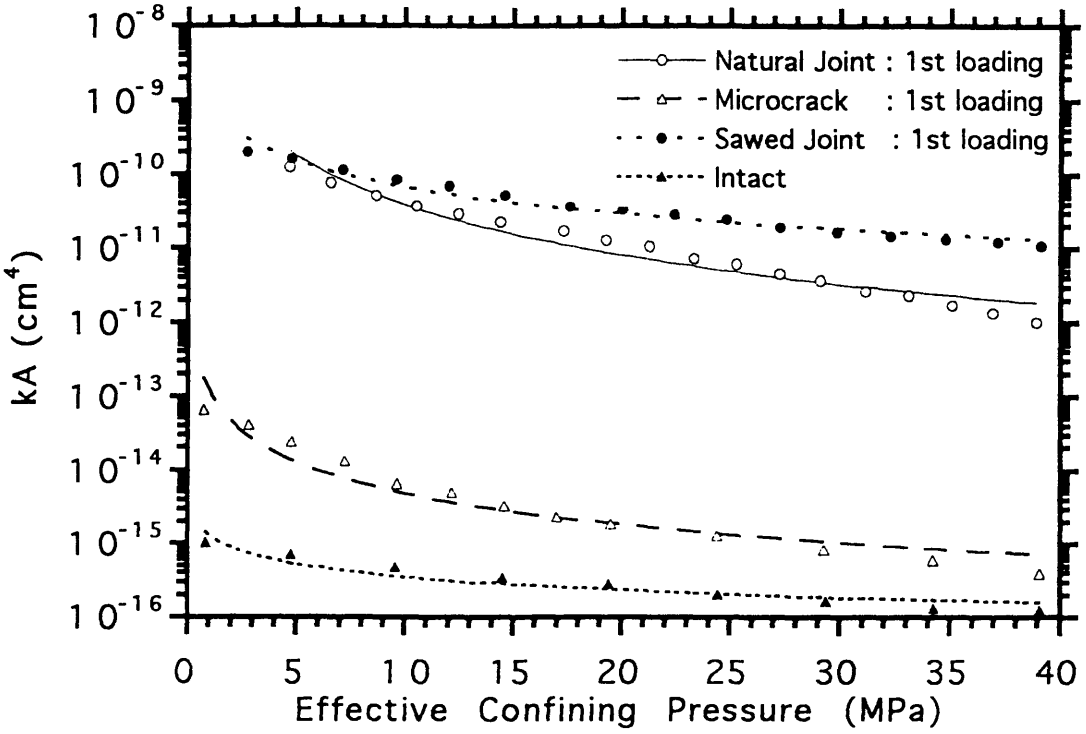

Natural Joint

$kA = [kA]_0 * [Pc-Pp]^{-n}$	
$[kA]_0$	6.5977e-09
n	2.2339
R	0.97748

Microcrack

$kA = [kA]_0 * [Pc-Pp]^{-n}$	
$[kA]_0$	1.2214e-13
n	1.404
R	0.88635

Sawed Joint

$kA = [kA]_0 * [Pc-Pp]^{-n}$	
$[kA]_0$	1.0185e-09
n	1.1841
R	0.94891

Intact

$kA = [kA]_0 * [Pc-Pp]^{-n}$	
$[kA]_0$	1.345e-15
n	0.58427
R	0.93205

Note : $[kA]_0$=kA at Pc-Pp=1 MPa

Fig. 4.15 Permeability times cross-sectional area vs Pc-Pp in A-test (A)1st loading

b) A-test : 1st unloading

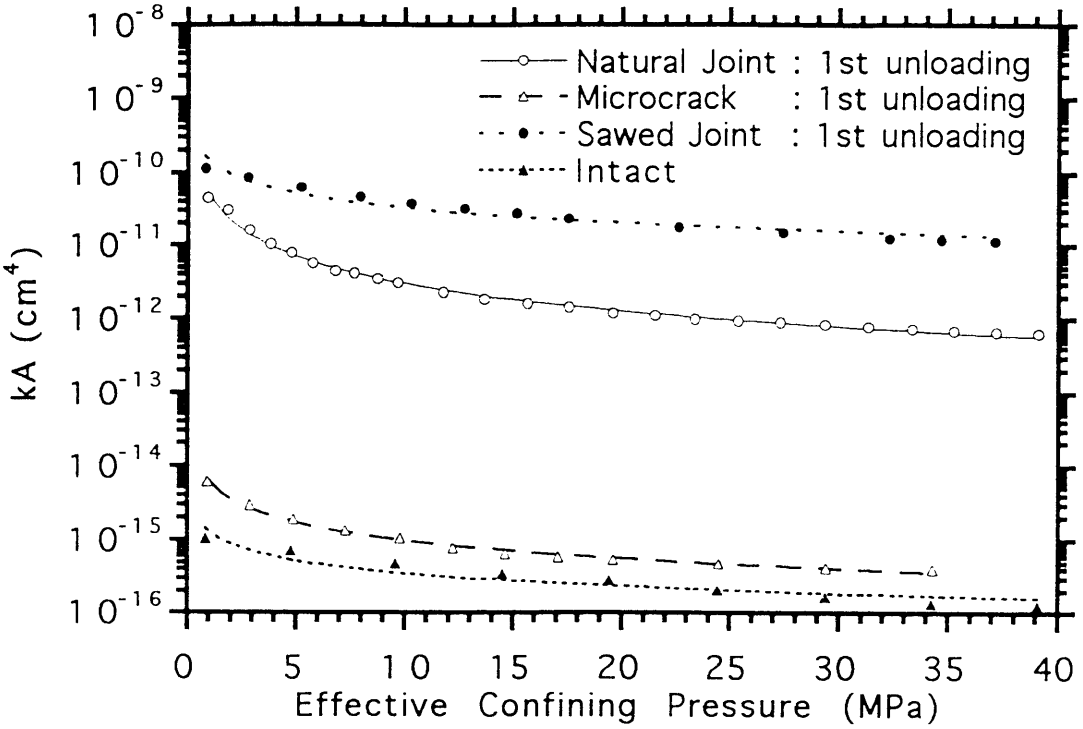

Natural Joint

$kA = [kA]_0 * [Pc-Pp]^{-n}$	
$[kA]_0$	5.0477e-11
n	1.2238
R	0.97671

Microcrack

$kA = [kA]_0 * [Pc-Pp]^{-n}$	
$[kA]_0$	6.2845e-15
n	0.80543
R	0.99594

Sawed Joint

$kA = [kA]_0 * [Pc-Pp]^{-n}$	
$[kA]_0$	1.5119e-10
n	0.67084
R	0.94287

Intact

$kA = [kA]_0 * [Pc-Pp]^{-n}$	
$[kA]_0$	1.345e-15
n	0.58427
R	0.93205

Note : $[kA]_0$=kA at Pc-Pp=1 MPa

Fig. 4.15 Permeability times cross-sectional area vs Pc-Pp in A-test (B)1st unloading

c) A-test : 2nd loading

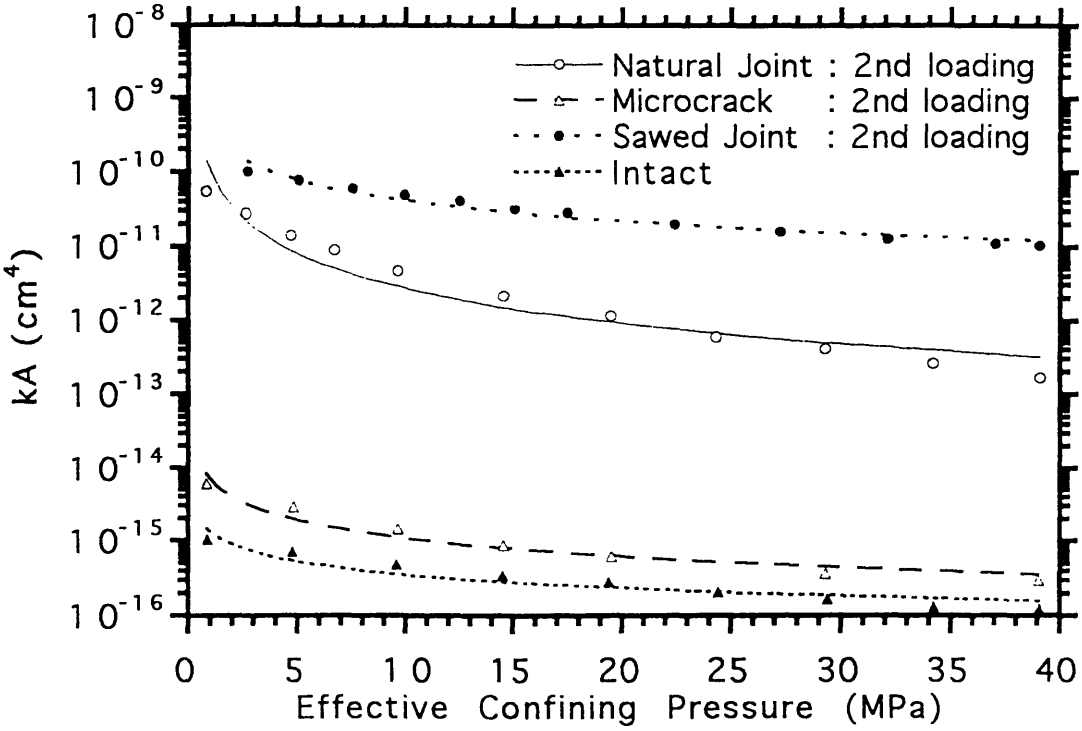

Natural Joint

$kA = [kA]_0 * [Pc-Pp]^{-n}$	
$[kA]_0$	1.0095e-10
n	1.5724
R	0.93128

Microcrack

$kA = [kA]_0 * [Pc-Pp]^{-n}$	
$[kA]_0$	7.0474e-15
n	0.81539
R	0.96962

Sawed Joint

$kA = [kA]_0 * [Pc-Pp]^{-n}$	
$[kA]_0$	3.3916e-10
n	0.91412
R	0.95921

Intact

$kA = [kA]_0 * [Pc-Pp]^{-n}$	
$[kA]_0$	1.345e-15
n	0.58427
R	0.93205

Note : $[kA]_0$=ka at Pc-Pp=1 MPa

Fig. 4.15 Permeability times cross-sectional area vs Pc-Pp in A-test (C)2nd loading

d) A-test : 2nd unloading

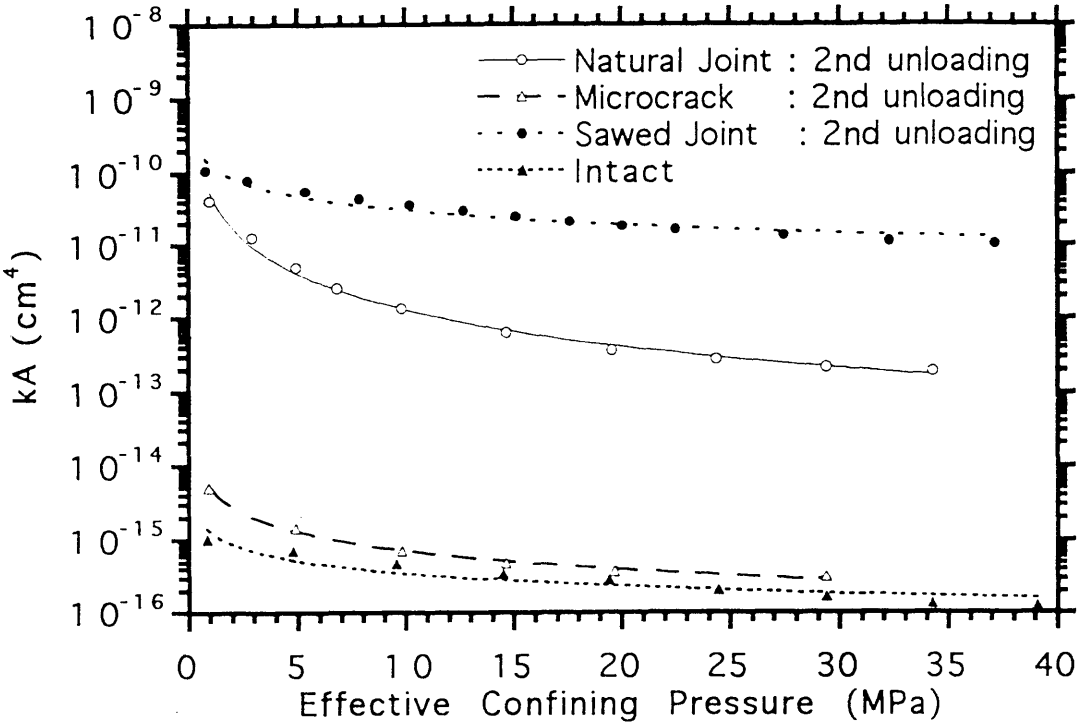

Natural Joint

$kA = [kA]_0 * [Pc-Pp]^{-n}$	
$[kA]_0$	5.5509e-11
n	1.6308
R	0.99245

Microcrack

$kA = [kA]_0 * [Pc-Pp]^{-n}$	
$[kA]_0$	5.0805e-15
n	0.85032
R	0.99934

Sawed Joint

$kA = [kA]_0 * [Pc-Pp]^{-n}$	
$[kA]_0$	1.386e-10
n	0.66146
R	0.94644

Intact

$kA = [kA]_0 * [Pc-Pp]^{-n}$	
$[kA]_0$	1.345e-15
n	0.58427
R	0.93205

Note : $[kA]_0$=kA at Pc-Pp=1 MPa

Fig. 4.15 Permeability times cross-sectional area vs Pc-Pp in A-test (D)2nd unloading

a) B-test : 1st loading

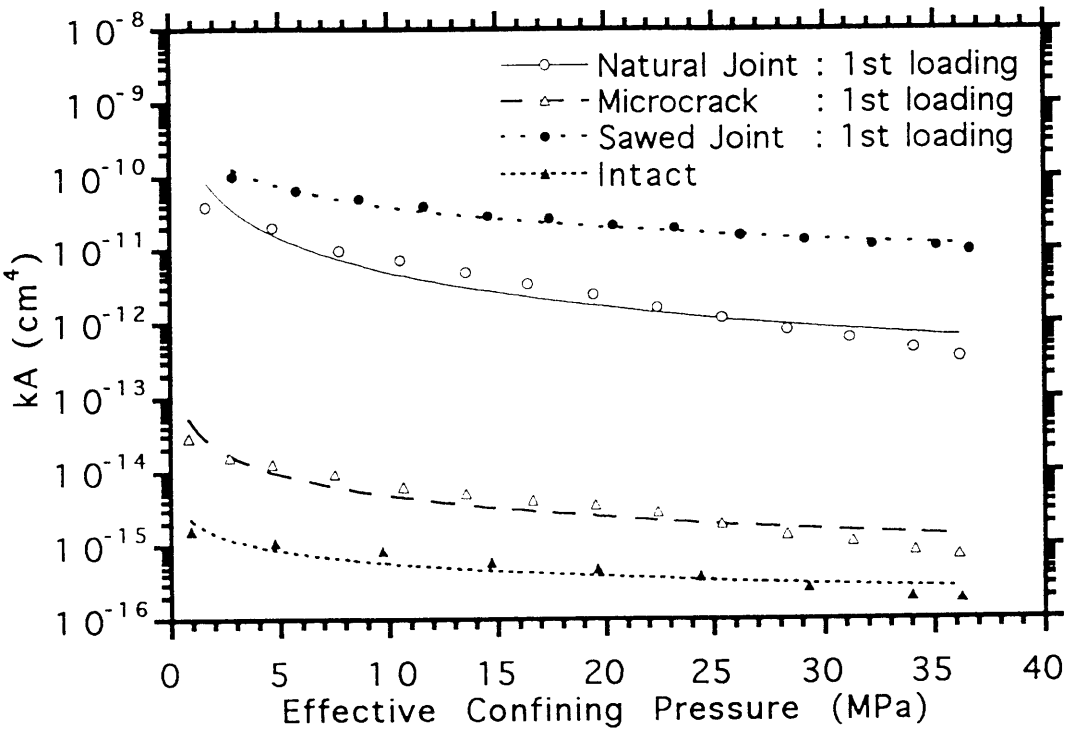

Natural Joint

$kA = [kA]_0 * [Pc-Pp]^{-n}$	
$[kA]_0$	1.907e-10
n	1.5788
R	0.94361

Microcrack

$kA = [kA]_0 * [Pc-Pp]^{-n}$	
$[kA]_0$	4.4107e-14
n	0.96659
R	0.94793

Sawed Joint

$kA = [kA]_0 * [Pc-Pp]^{-n}$	
$[kA]_0$	3.4313e-10
n	0.93878
R	0.97967

Intact

$kA = [kA]_0 * [Pc-Pp]^{-n}$	
$[kA]_0$	2.1896e-15
n	0.57808
R	0.9169

Note : $[kA]_0$=kA at Pc-Pp=1MPa

Fig. 4.16 Permeability times cross-sectional area vs Pc-Pp in B-test (A)1st loading

b) B-test : 1st unloading

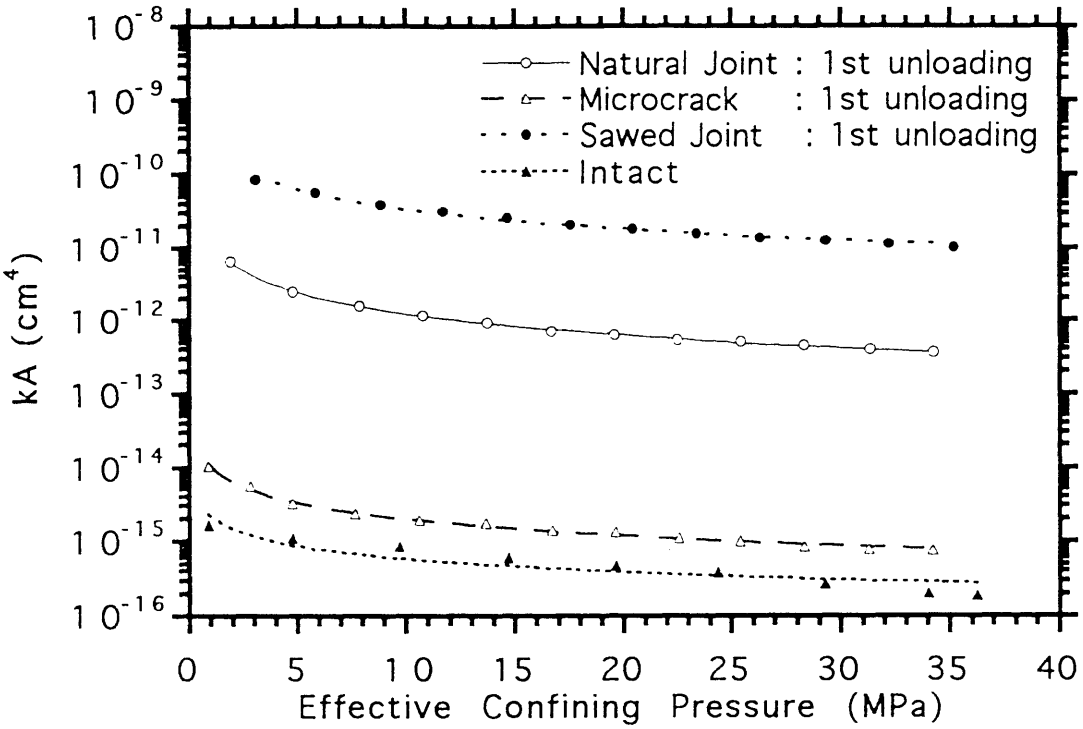

Natural Joint

$kA = [kA]_0 * [Pc-Pp]^{-n}$	
$[kA]_0$	1.2339e-11
n	0.99823
R	0.99964

Microcrack

$kA = [kA]_0 * [Pc-Pp]^{-n}$	
$[kA]_0$	1.0454e-14
n	0.72918
R	0.99461

Sawed Joint

$kA = [kA]_0 * [Pc-Pp]^{-n}$	
$[kA]_0$	2.5874e-10
n	0.88312
R	0.99171

Intact

$kA = [kA]_0 * [Pc-Pp]^{-n}$	
$[kA]_0$	2.1896e-15
n	0.57808
R	0.9169

Note : $[kA]_0$=ka at Pc-Pp=1 MPa

Fig. 4.16 Permeability times cross-sectional area vs Pc-Pp in B-test (B)1st unloading

c) B-test : 2nd loading

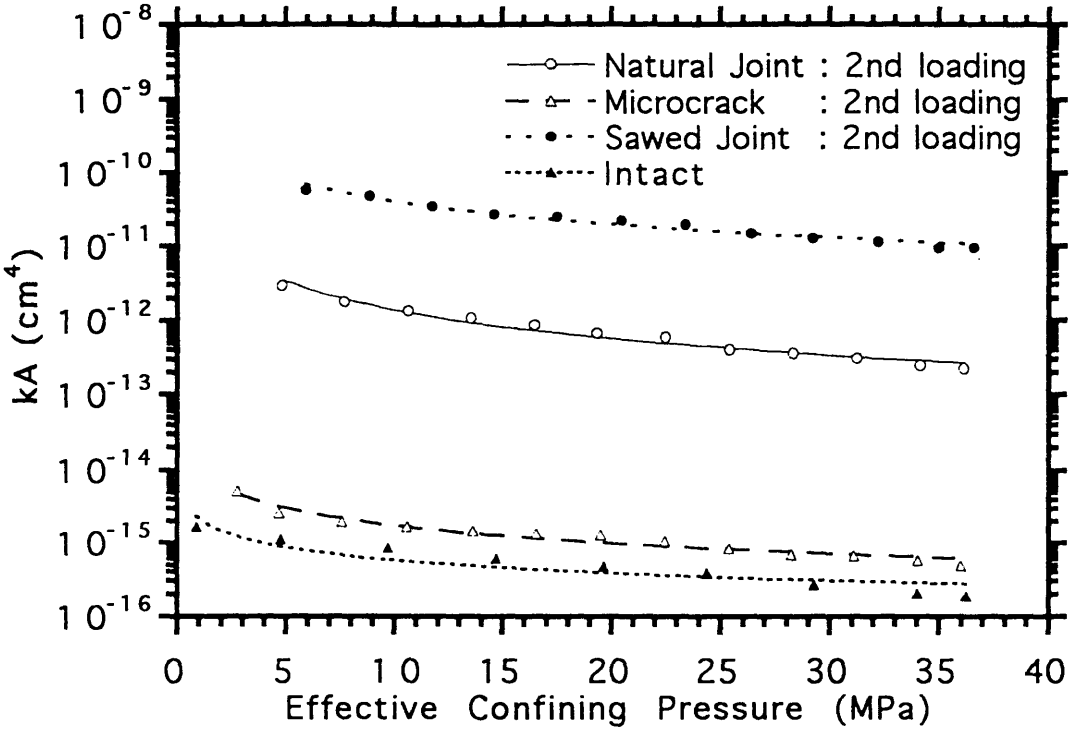

Natural Joint

$kA = [kA]_0 * [Pc-Pp]^{-n}$	
$[kA]_0$	2.6711e-11
n	1.2842
R	0.99015

Microcrack

$kA = [kA]_0 * [Pc-Pp]^{-n}$	
$[kA]_0$	1.0914e-14
n	0.80185
R	0.98217

Sawed Joint

$kA = [kA]_0 * [Pc-Pp]^{-n}$	
$[kA]_0$	4.2447e-10
n	1.025
R	0.98011

Intact

$kA = [kA]_0 * [Pc-Pp]^{-n}$	
$[kA]_0$	2.1896e-15
n	0.57808
R	0.9169

Note : $[kA]_0$=kA at Pc-Pp=1 MPa

Fig. 4.16 Permeability times cross-sectional area vs Pc-Pp in B-test (C)2nd loading

d) B-test : 2nd unloading

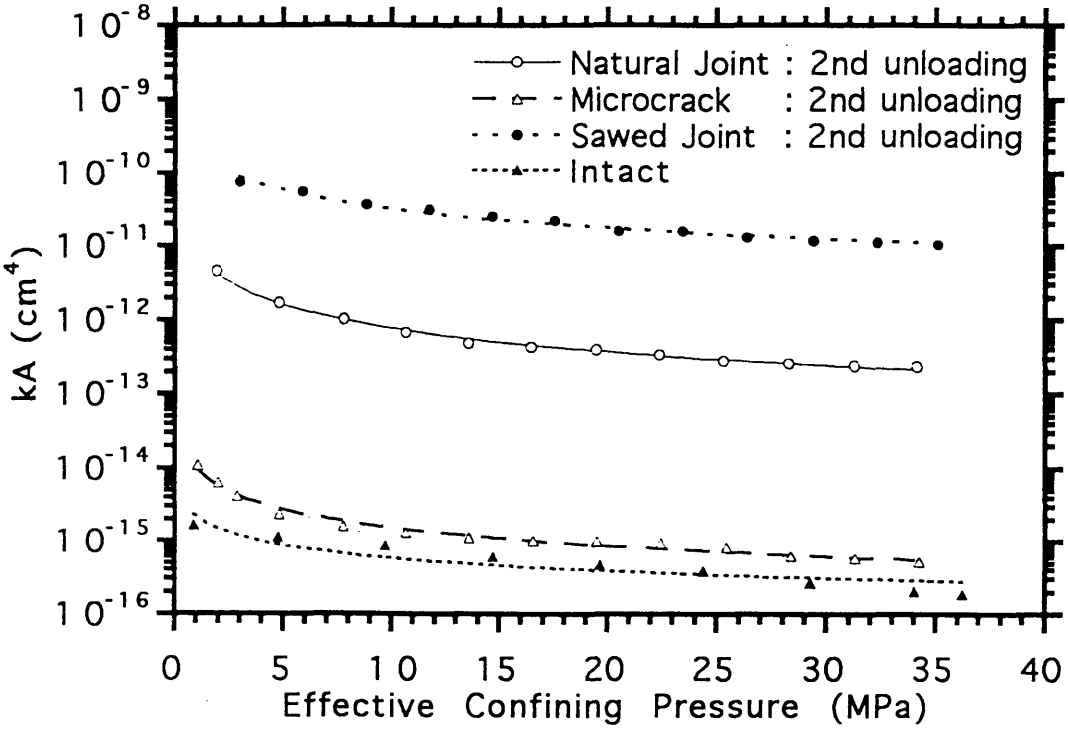

Natural Joint

$kA = [kA]_0 * [Pc-Pp]^{-n}$	
$[kA]_0$	8.6616e-12
n	1.0485
R	0.9996

Microcrack

$kA = [kA]_0 * [Pc-Pp]^{-n}$	
$[kA]_0$	1.0065e-14
n	0.82162
R	0.99511

Sawed Joint

$kA = [kA]_0 * [Pc-Pp]^{-n}$	
$[kA]_0$	2.2284e-10
n	0.84876
R	0.98086

Intact

$kA = [kA]_0 * [Pc-Pp]^{-n}$	
$[kA]_0$	2.1896e-15
n	0.57808
R	0.9169

Note : $[kA]_0$=kA at Pc-Pp=1 MPa

Fig. 4.16 Permeability times cross-sectional area vs Pc-Pp in B-test (D)2nd unloading

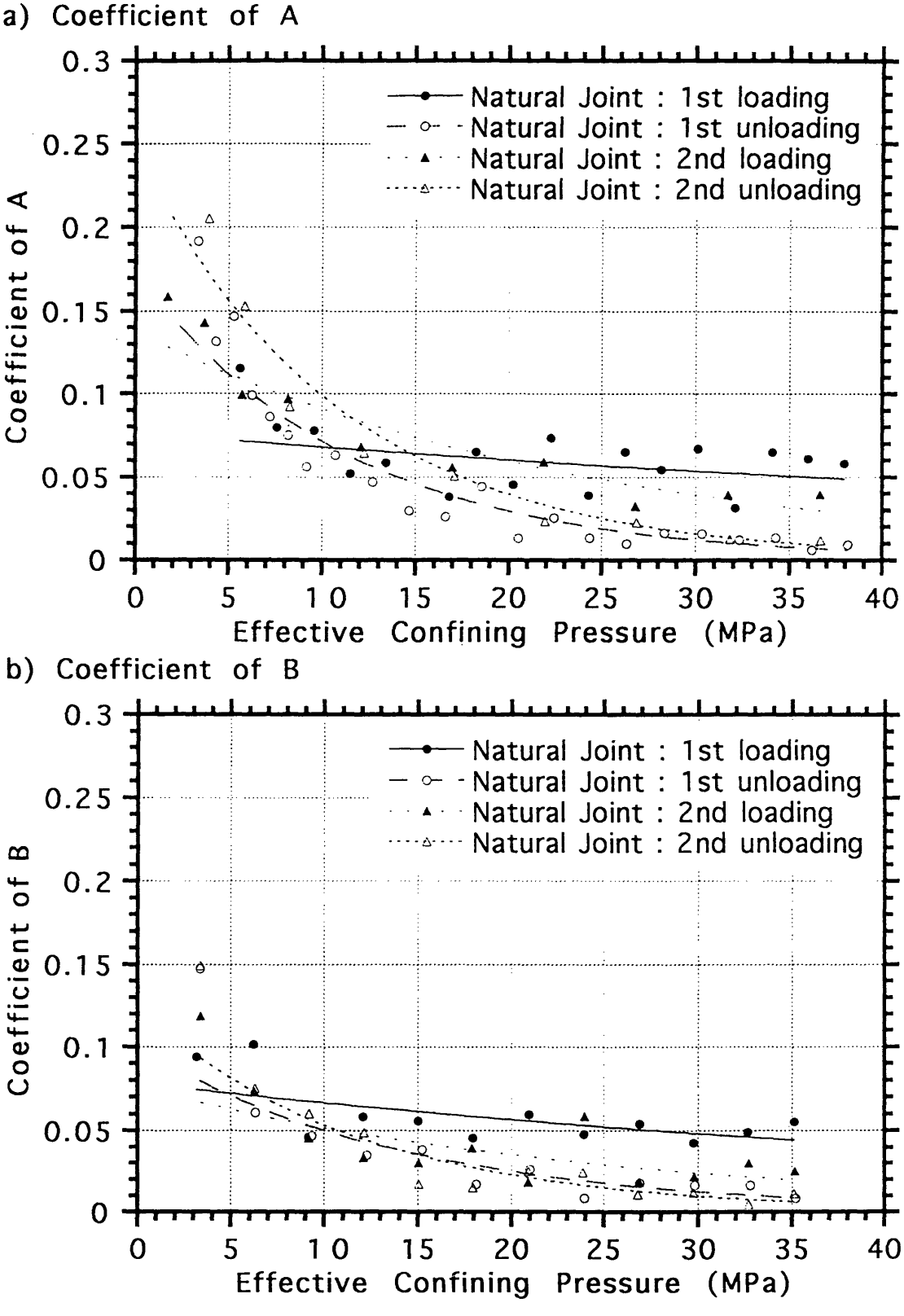

Fig. 4.17 Coefficient of A and B vs Pc-Pp for joints
(A)Natural joint

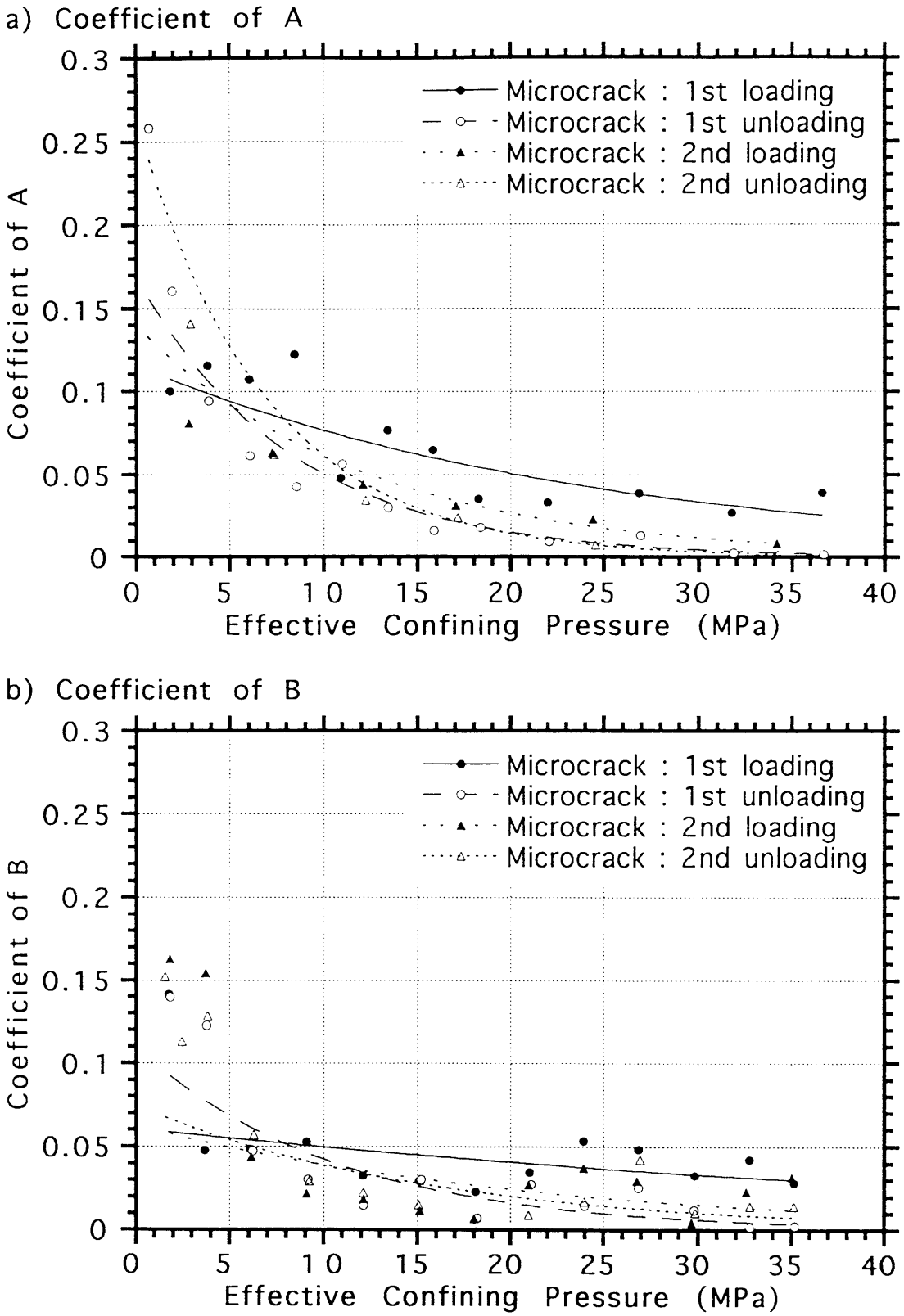

Fig. 4.17 Coefficient of A and B vs Pc-Pp for joints (B)Microcrack

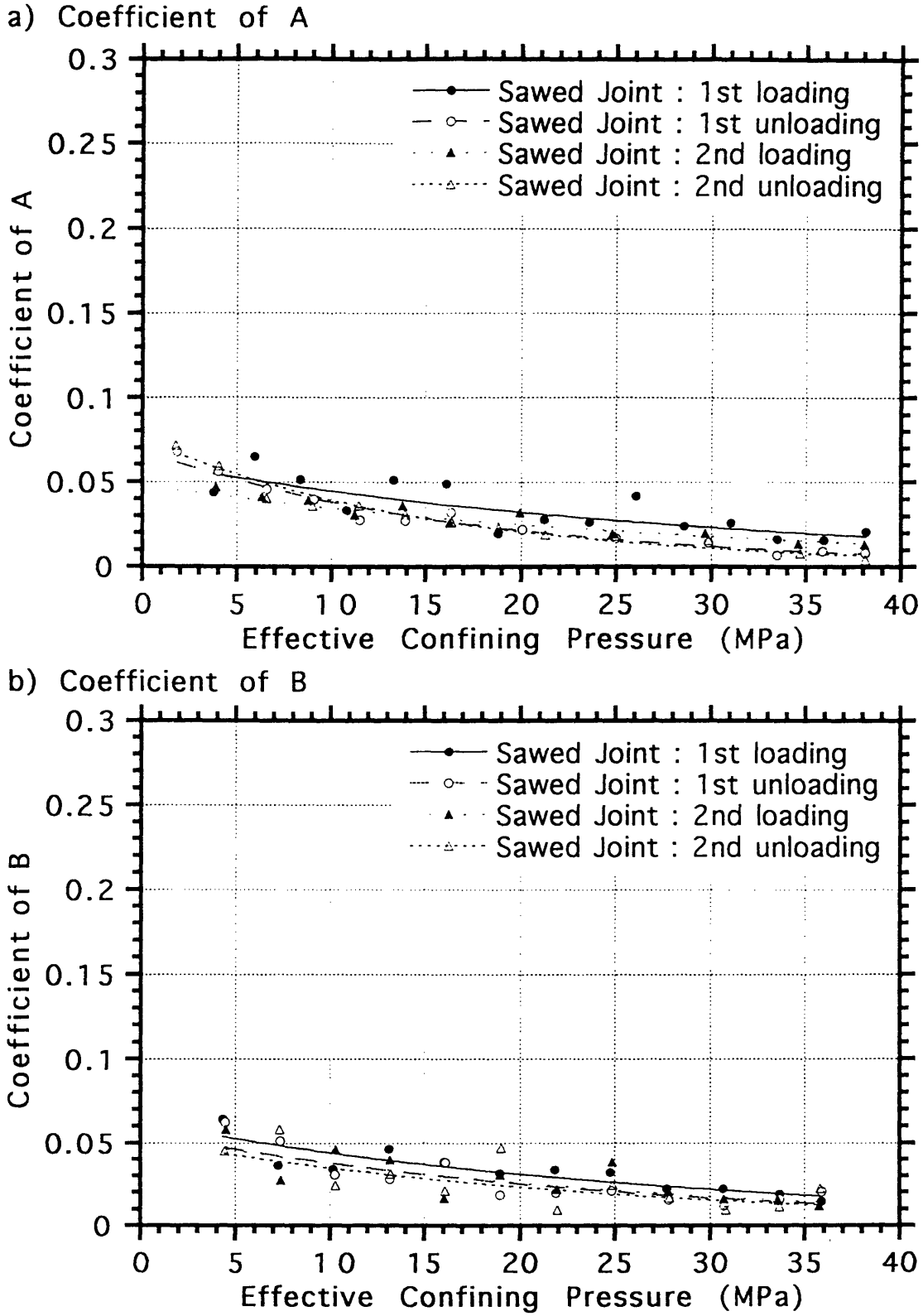

Fig. 4.17 Coefficient of A and B vs Pc-Pp for joints (C)Sawed joint

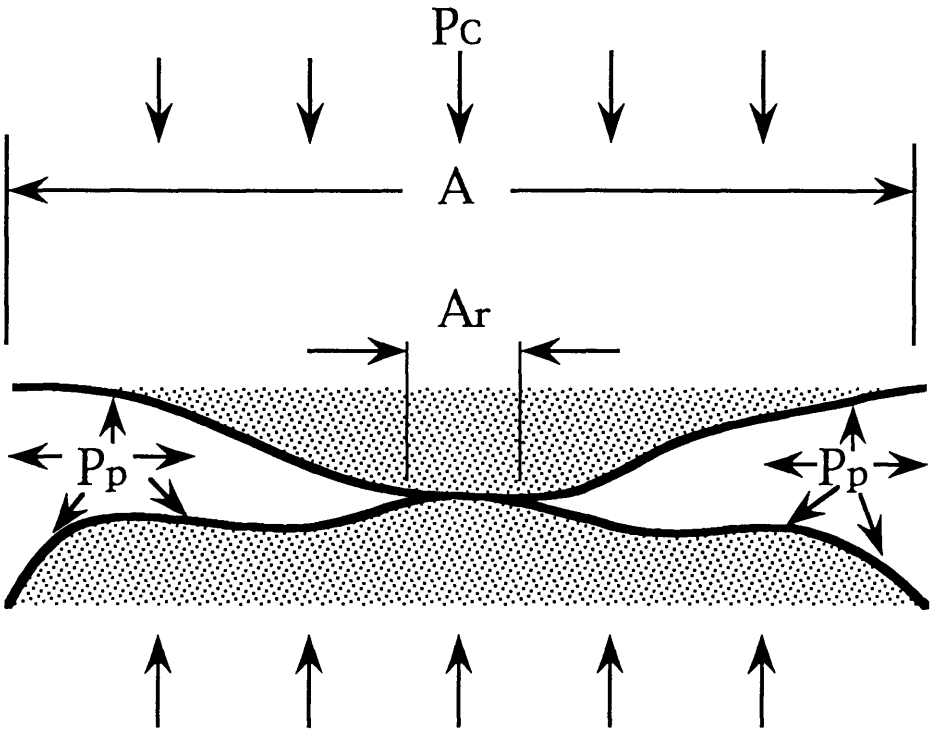

Pc : external confining pressure
Pp : internal pore pressure
A : aparent joint surface
Ar : real area of contact

Fig.4.18 An idealized joint section with an asperity subjected to external, Pc, and internal, Pp, pressures

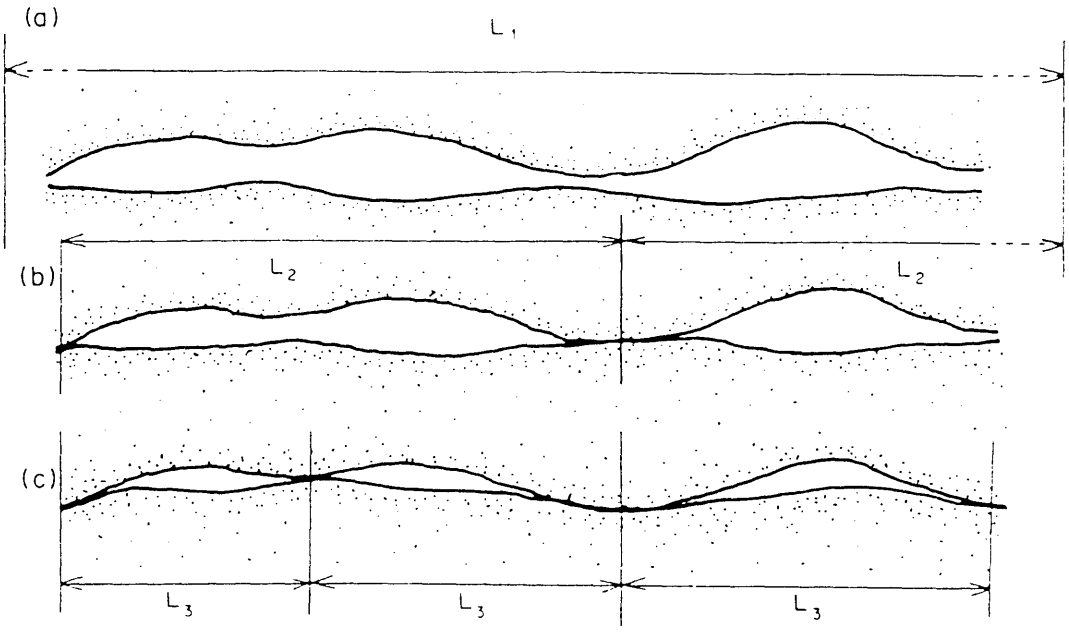

Fig.4.19 Model of crack closure (after Bernabe, 1986)

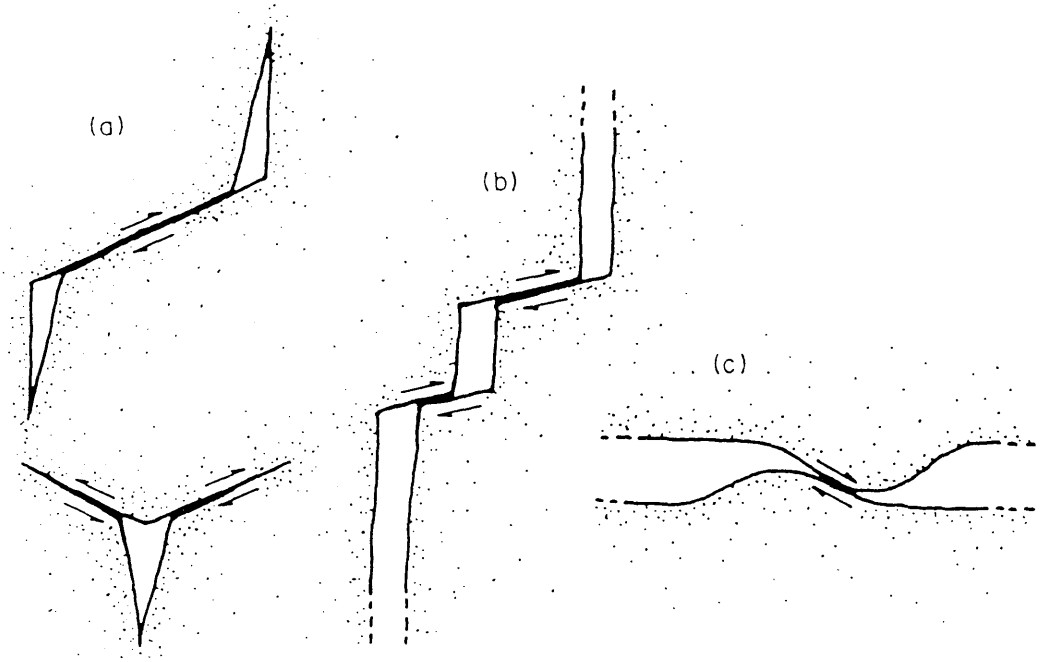

Fig.4.20 Examples of sliding in a joint (after Bernabe, 1986)

Chapter 5 Laboratory Experiments on Hydromechanical Behavior of a Single Joint

5.1 Introductory remarks

In most problems regarding the flow in jointed rocks, a rock joint is subject to some level of stresses. Therefore one needs to estimate the hydraulic conductivity of a joint under the specified stress conditions. When a joint is stressed, the joint void space deforms and changes in contact area occur. These changes significantly affect the hydraulic and mechanical properties of a joint. A considerable number of researchers have investigated the stress-deformation-flow characteristics of joints subject to different states of stress. Snow(1968) has discussed the effects of stress on the conductivity of jointed rocks in the water pressure tests at various dam sites. Jouanna(1972) performed both laboratory and small scale field tests on fissured mica schist. In his experiments, biaxial loads were applied to the specimens and flow rate was measured at each loading stage. He observed the significant non-recoverable changes in flow rate over repeated stress levels. Louis(1974) performed flow tests under uniaxial and biaxial loading conditions. He also stated that hysteresis would be the decisive factor in determining the hydraulic characteristics of joints. Pratt et al.(1977) have performed field permeability tests on a vertical joint under normal loading conditions as part of their in-situ rock mechanics test program. They observed a linear decrease in flow rate by increasing normal stress up to 2.5 MPa. Jones(1975) studied the effects of confining pressure on joint flow in carbonate rocks. He reported a linear relationship between the cube root of permeability and the logarithm of confining pressure. These observations clearly showed that the joint permeability is strongly dependent on states of stresses acting on a joint as well as on the stress history.

On the other hand, Sharp(1970) performed flow tests in the laboratory with a natural fracture in a hard granite porphyry. Sharp and Maini(1972) proposed an empirical flow law for natural joints that was based on effective aperture, which is the difference in the opening from the initial condition, and the net flow rate obtained from a calculation of the measured flow rate minus that observed under the initial closed conditions. They dispute the validity of the cubic law and have suggested that for their particular conditions the exponent in the relationship between the flow rate and aperture should be two. Gale(1975) reviewed their results and pointed out that the cubic law is still valid if one relates the flow rates corresponding to the apertures that were actually present.

However experiments by Sharp and Maini(1972) have been concerned with open

joints. One will encounter many situations in the field where the joints are not open. To test where the cubic law still holds under the closed conditions, extensive test series have been carried out by Iwai(1976) and Witherspoon et al.(1980) at Lawrence Berkeley Laboratory to verify the cubic law for closed joints.

Iwai (1976) studied flow through a joint as the functions of deformation, contact area and stresses up to 20 MPa. The results of his laboratory investigation on tension joints that were artificially induced in homogeneous specimens of granite, basalt, and marble have shown that the cubic law for flow in a joint was found to hold whether the joints are open or closed and whether the flow path geometry is straight or radial regardless of both the loading path and loading cycle. His experimental results were closely examined by Witherspoon et al.(1980). They used the following procedures to compare the experimental results and the theory based on the cubic law.

Fig.5.1 shows an example of flow rates as measured with the straight flow through a joint in a rectangular granite specimen with width=12.1 cm, length=20.7 cm and height=15.5 cm when normal stresses up to 17 MPa were employed in an attempt to close the joint. Witherspoon et al.(1980) reported that the effect of repeated loading cycles was to reduce the flow rate per unit head difference, $Q/\Delta H$, to a minimum of 5.33×10^{-10} m^2/s, but the joint could not be closed completely. When deformations across the joint were measured as a function of stress, a highly nonlinear behavior was observed. Fig.5.2 shows this behavior for the first loading cycle with the same straight flow granite specimen. The $\Delta V_{t,1}$ is the total deformation as measured on one side, and $\Delta V_{t,2}$ and $\Delta V_{t,3}$ were the total deformations as measured on the opposite side as shown in Fig.5.1. Knowing ΔVr which was measured on the intact specimen of granite, the net deformation of the joint was computed from

$$\Delta V = \frac{1}{2}\left[\Delta V_{t,1} + \frac{\Delta V_{t,2} + \Delta V_{t,3}}{2}\right] - \Delta V_r \qquad (5.1)$$

They determined the apparent aperture, b_d, at any stress level by reference to the maximum joint closure ΔV_m, which is shown in Fig.5.3, as follows.

$$b_d = \Delta V_m - \Delta V \qquad (5.2)$$

Also as shown in Fig.5.3, the true aperture, b, was determined as the sum of the apparent aperture, b_d, and residual aperture, b_r. They used the following equation for the flow rate per unit head by assuming both the steady-state flow condition and Darcy's law

in joint flow, which is the well known cubic law,

$$Q / \Delta H = Cb^3 \tag{5.3}$$

where C is a constant, which, in the case of straight flow, is given by

$$C = \frac{W}{L}\frac{g}{12\nu} \tag{5.4}$$

where W and L are the joint width and the joint length, respectively, as shown in Fig.5.1 and g is the acceleration of gravity and ν is kinematic viscosity of the fluid.

Eq.(5.4) can be applied to the ideal conditions, namely in the case of the smooth parallel plate model. In the case of rough surfaces, Eq.5.4 was slightly modified and the cubic law then became :

$$\frac{Q}{\Delta H} = \frac{C}{f}b^3 \tag{5.5}$$

where f is a factor that accounts for deviations from the ideal complete smooth condition. Therefore, for the parallel plate model to be valid, f should be unity. A value of f greater than unity may have a physical significance in the case of joints where contact between the surfaces tends to reduce the flow rate.

The apparent aperture could not be used directly in Eq.5.3 to check the validity of the cubic law because the measured flow rates depend on the true aperture, which could not be measured directly. One might wish to estimate the residual value using Eq.5.3, but this would assume that the cubic law holds for all apertures, especially as they become small at high stresses. To test the validity of the cubic law, Witherspoon et al.(1980) treated the residual aperture as an unknown parameter common to all data points. As a first approach, they assumed that the factor f could be set to unity and rearranged Eq.5.5 to

$$\frac{Q}{\Delta H} = C(b_a + b_r)^n \tag{5.6}$$

The unknown parameters n and b_r were then determined by the least squares fit for the data, which was done by minimizing the squares of the differences between the

experimental results and theoretically predicted values. They concluded that the cubic law seemed to hold regardless of the loading path and no matter how often the loading process is repeated. Permeability was uniquely defined by the joint aperture, and one could predict changes due to stress as long as there are no effects of shear movement or weathering. Therefore, Witherspoon et al.(1980) concluded that they were justified in adopting the exponent n =3 and one should reexamine the experimental data to determine the factor f. They rearranged Eq.(5.6) by setting the exponent n =3 in the form

$$\frac{Q}{\Delta H} = \frac{C}{f}(b_d + b_r)^3 \tag{5.7}$$

The unknown parameters f and b_r were also determined by the least squares fit for the data, which was done by minimizing the squares of the differences between the experimental results and predicted values by the theory. Parameters obtained by these two least squares fit analyses are reproduced in Table 5.1 and Table 5.2, respectively. The least squares results for the residual aperture presented in Table 5.2 are somewhat closer to the values that were calculated directly from Eq.5.3 than those in Table 5.1. Reasonable values are obtained for the factor f and they were all greater than unity. Having determined values for the residual aperture at maximum normal stress, it was then possible to examine how well the experimental data agree with the cubic law over the range of flow rates employed. Fig.5.4 shows the results for the granite specimen with straight flow and presents the data in accordance with Eq.5.5 where the solid line is for the special case of f=1.0. Witherspoon et al.(1980) also noted that the values of f in Table 5.2 generally decreased in progressing from the first cycle (run 1 in Table 5.2) to the third cycle (run 3 in Table 5.2). This may be an indication that the joints became progressively better mated during the cyclic loading. Witherspoon et al.(1980) concluded that the effects of deviations from the ideal parallel plate concept only cause an apparent reduction in flow and are taken care of by the factor f. In their investigation, f varies from 1.04 to 1.65.

To use the modified form of cubic law, a knowledge of joint aperture at any normal stress is required, but only joint-closure measurements are made. Therefore Witherspoon et al.(1980) assumed the validity of the cubic law at maximum normal stress in order to plot the experimental data and used a form of the cubic law to determine the residual aperture at the maximum normal stress. This assumption may not be valid as suggested by other studies (Kranz et al. 1979 and Engelder and Scholz 1981) particularly for rough-walled joints. This assumption was also discussed by Gale(1982). He showed that the degree of deviation from the cubic law or parallel plate model for joints could depend on

the choice of reference point in calculating joint apertures.

Sundaram et al.(1987) presented a modified form of the cubic law which used both the initial aperture at the start of the test series and the observed joint deformation in place of both the apparent aperture and residual aperture in Eq.5.7 as follows.

$$\frac{Q}{\Delta H} = \frac{C}{f}(b_0 - \Delta V)^3 \qquad (5.8)$$

where b_0 is an initial aperture at the start of the test series, ΔV is a joint deformation.

Sundaram et al.(1987) also used the regression analysis to obtain the initial aperture and the factor f. They obtained f=1.778 for a natural joint in a large specimen (91.4 cm in diameter) of granitic rock under divergent radial flow conditions and b_0 =78.22 μm. There are still uncertainties in estimation of both the residual aperture and initial aperture obtained by using the simple regression analysis since they did not check the accuracy of these properties resulting from the regression analysis and did not perform any direct measurements of these properties.

On the other hand, Raven and Gale(1985) studied the effect of changes in specimen size on the normal stress-permeability properties of natural joints. They used five granite cores (10.0, 15.0, 19.3, 24.5 and 29.4 cm diameter) which contained the part of the same natural joint oriented normal to the core axis. Each joint specimen was subjected to three uniaxial compressive loading and unloading cycles with maximum normal stresses up to 30 MPa. In each cycle, joint deformation and steady-state flow rate through a joint from a central borehole were measured for specified levels of normal stress. As shown in Fig.2.11, they found that their results did not follow the cubic law and the deviation between their results and the theory increased with the number of loading cycles and specimen size. They suggested that the main reason for these deviations is that the change in the contact area with stress plays a major role in decreasing the joint flow.

There are, thus, several inconsistencies, such as the applicability of the cubic law and the effect of contact area on flow in a joint. In addition, these existing studies have been concerned with joints that are deforming under normal stress, whereas the general situation in the field will involve both normal and shear deformation. The actual physical process that takes place during the deformation of joint surfaces and the effect of this behavior on the fluid flow process must be fully understood. Therefore, first of all in this study, the initial apertures for six joints have been measured before conducting cyclic stress-flow tests (SFT) with six jointed specimens, as shown in Chapter 3. Next cyclic stress-flow

(hydromechanical) tests are carried out to obtain both the joint deformation and the change of flow rate per unit head. In this study, the hydrostatic stress (uniform confining pressure) is applied to joints since this stress condition is much more realistic in the field than the simple normal stress condition. The change of the hydrostatic stress can induce the permanent deformation and hysteresis on the void geometry in a joint, which were observed by Kranz et al.(1979) and Coyner et al.(1979). This indicates that the stress is inhomogeneously distributed in the rock and rock joint and that shear stresses can develop locally at places where joints interact. Test results are compared with those presented by Iwai(1976), Witherspoon et al.(1979), Pratt et al.(1977) and Raven and Gale(1985) in terms of several commonly used parameters such as joint flow rate, transmissivity, permeability, maximum closure and mechanical aperture and their stress dependency. Finally, after cyclic stress-flow (hydromechanical) tests, the surface geometries of joints were again measured and the aperture geometries were derived. This made it possible to relate the observed hydromechanical performance to the joint aperture geometry.

5.2 Measurement of hydromechanical behavior of a single joint

5.2.1 Sample material and preparation

The six rock specimens used in this study, which were already presented in Chapter 3, were approximately 50 mm in diameter and 100 mm in length with a joint plane parallel to the core axis at the center of specimen. Photographs of the six jointed specimens were presented in Fig.3.3 (a natural joint in Kikuma granodiorite) and Appendix A. After measuring surface roughness of the joints, the cylindrical specimens were reassembled and the both intersections of the joints with specimen surface were sealed by epoxy resin (E380, Konishi Bond Corporation) as shown in Fig.5.5(a). Rock deformation across the joint plane and rock strains were measured with the Cantilever Radial Displacement Transducer (CRDT) and two strain gauges affixed to the jointed specimen. Fig.5.6 is a photograph of the CRDT and its final configuration attached to the jointed specimen. The original idea of the design of this CRDT was developed by Matsui and Kudo (1986) and the design was also similar to that presented by Dropek et al (1978). The CRDT is capable of recording deformations as small as 0.5 μm. The calibration of the CRDT has been carried out using dummy specimens made from brass and perspex under uniaxial compressive loading with strain gauges affixed to the dummy specimens at mid height.

Also uniaxial compression tests and preliminary triaxial tests under hydrostatic stress conditions using saturated intact rock specimens of Kikuma granodiorite have been

carried out to observe the Young's modulus and Poisson's ratio by using both the CRDT and strain gauges. These results showed that CRDT performs satisfactorily and its resolution is about 0.5 μm. Fig.5.7 and Fig.5.8 show the dummy specimen made from brass for uniaxial loading and the intact rock specimen of Kikuma granodiorite for triaxial hydrostatic compressive loading.

Before subjecting jointed specimens to vacuum in the deionized water to saturate them, two cross strain gauges affixed to the specimens were enclosed with silicon RTV rubber (KE-45RED, Shin-etsu Silicon Corporation), as shown in Fig.5.5(b). The jointed specimens were evacuated for more than 72 hours and were saturated with the deionized water. End caps with a center hole were placed on both ends of the specimens and the contacts between the specimens and end caps were also sealed by the epoxy resin as shown in Fig.5.5(c). The silicon RTV rubber was plastered on the jointed specimen by taking care that air was not entrapped in the silicon rubber coating. After the silicon RTV rubber has set, the CRDT is mounted so as to measure the combined deformation of the intact rock and the joint in the direction across the joint plane as shown in Fig.5.5(d). The final setup of the specimens is presented in Fig.5.5(d).

5.2.2 Test apparatus setup

Fig.5.9 is a photograph of the high-pressure triaxial testing apparatus which has been developed by Aoki et al.(1987) at the Technology Research Center of Taisei Corporation, Yokohama, Japan. Fig.5.10 is a schematic view of the test setup for stress-flow (hydromechanical) experiments. Fundamental specifications of the high pressure triaxial testing apparatus are given in Table 5.3. The features of the high-pressure triaxial testing apparatus are described below.

The main components are : (1) loading frame ; (2) triaxial pressure cell ; (3) axial loading and confining pressure control system ; (4) pore pressure control system ; (5) low-pressure regulation and fluid flow monitoring equipment ; (6) data acquisition system.

A 500 KN capacity servo-control system is used to apply the axial load. Confining pressures up to 50 MPa are applied by a servo-controlled booster system using hydraulic oil as a pressure fluid. The injection water pressure for the flow tests and back pressure are applied, via an interface, by air pressure which is controlled by precision pressure regulators (Kendall® Model 10, Fairchild Ltd.). The outflow volume from the jointed specimen is observed by capturing the outflow in a double-tube burette and measuring the water level change with a high-precision differential pressure transmitter (Teleperm Differential Pressure Transmitter, FFB 22WB2-100Y, pressure capacity : 25 mmH_2O

differential, 30kgf/cm2 working, Fuji Electric Co. Ltd.). Since the cross-sectional area of the internal measuring burette is known, the water level change can be converted to the volume of water. Since the range at applied injection pressure is as high as 0.4 MPa, this water head change at the burette would be negligible. A prescribed back pressure is applied to both the outer cylinder of the double-tube burette and the base pressure port of the differential pressure transmitter, in order to assist saturation of the rock specimen and conduits. Deformation of the intact rock is measured with the strain gauges attached to the specimen. The CRDT is used to measure the combined deformation of the intact rock and the joint ; the joint deformation is then obtained by subtracting the rock deformation measured with the strain gauges from the total deformation measured with the CRDT. The data acquisition system is shown in Fig.5.11; it consists of a multi channel strain amplifier, a digital data acquisition unit, a chart recorder, a printer, monitoring indicators and a personal computer.

5.2.3 Experimental methodology

Each specimen was subjected to three cycles of incremental loading and unloading of uniform compressive confining stresses which ranged from 0.4 MPa to 20 MPa. The test conditions for the six jointed specimens are listed in Table 5.4. Steady-state straight (axial) flow tests were performed by applying the injection water pressure ranging from 0.24 MPa to 0.4 MPa at each confining stress. In this study, 0.2 MPa back pressure was used for all the tests to ensure that the specimens were saturated and to control the hydraulic head on one end of specimen as the boundary condition in steady-state flow test. The injection water pressure was applied to the bottom end of the jointed specimens, which must be higher than the back pressure to make the straight flow along the jointed specimen. At least three tests have been carried out on each test condition by changing the injection water pressure while the back pressure maintained constant. These three test results were compared to check that the joint flow obeyed Darcy's law and average values were used in successive analysis.

After each flow test, flushing of the differential pressure transmitter and the lines for fluid application was conducted since some air could get trapped, which might come from water in the system and rock specimens during unloading stage even though the degasified water source was used for specimen saturation and flow experiments. The recurrence of reading of flow rate, fluid pressure, applied load, confining stress and displacement readings for three complete data scan intervals (20-30 min intervals between scans) constituted a completed testing sequence at a given load increment. One full testing cycle

(loading and unloading) was completed in 36 - 60 hours and thus it required 108 - 180 hours for three testing cycles (loading and unloading). After three successive cyclic stress-flow tests, one additional loading-unloading cycle of confining stress up to 20 MPa was applied to obtain the maximum closure of joints more accurately, but no flow test was conducted during this additional cycle. During each flow test, applied load, the deformation both with the strain gauge and the CRDT, the outflow volume and the injection- and back pressure were recorded.

5.2.4 Experimental Results

1) Hydraulic characteristics of the joints

Joint flow rate per unit head ($Q/\Delta H$), which can be obtained from the outflow and pressure measurements (Eq.5.3), is used to express the hydraulic joint characteristics and to relate them to the applied confining stress. Iwai(1976) and Raven and Gale(1985) also used this characteristic. The joint flow rates per unit head ($Q/\Delta H$) as a function of normal stress obtained by Iwai(1976) are reproduced in Fig.5.12. Fig.5.13 shows the joint flow rates per unit head ($Q/\Delta H$) as a function of confining stress for the six different joints. A large hysteresis of $Q/\Delta H$ during the 1st cycle can be seen, and this is consistent with several other experimental studies (Iwai,1976; Witherspoon et al.,1980; Pratt et al.,1977; Jones, 1975; Nelson and Handin, 1977; Kranz et al.,1979 and Raven and Gale,1985). The flow rate hystereses decreased with successive test cycles for all specimens. However, in the 2nd cycle, the granodiorite tension joint still showed a relatively large hysteresis while practically no hysteresis was observed in the sawed joint. This fact seems to be related to surface roughness and aperture since the tension joint has a relatively rough surface compared to the sawed joint. This and the general decrease of the hystereses with additional loading cycles indicate that crushing of contact points or asperities during loading may be the underlying cause.

$Q/\Delta H$ for three different joints in granodiorite are compared with those obtained for the tension joint in granite with straight flow by Iwai(1976) in Fig.5.14. $Q/\Delta H$ as a function of confining stress are similar but the observed hystereses of flow rate in the three joints in granodiorite are relatively larger than that obtained by Iwai(1976), in particular during the 1st cycle. The effects of surface roughness on the hydromechanical behavior of a joint are also clearly observed in the deformation characteristics of joints, which will be discussed later.

Also$Q/\Delta H$ for three tension joints in three different rocks, granite, schist and

sandstone, are compared with that for a tension joint in granite with straight flow obtained by Iwai(1976) in Fig.5.15. The relations $Q/\Delta H$ versus confining stress are similar in granite and schist but there is significant reduction in $Q/\Delta H$ for a tension joint in sandstone.

To compare the results in this study with the previously published data summarized by Witherspoon et al.(1979) and Raven and Gale(1985), it is assumed initially that the parallel plate model is valid and that hydraulic aperture, b_h, can be defined by taking the cubic root in Eq.5.3, in the following form.

$$b_h = \sqrt[3]{\frac{Q}{\Delta HC}} \tag{5.9}$$

where C is a constant as defined in Eq.5.4.

As one can see from Eq.5.9, the hydraulic aperture, b_h, is defined as the joint width, backcalculated from flow experiments assuming that a joint is an ideal parallel plate. Correspondingly, the joint hydraulic conductivity, K_j, can be calculated as

$$K_j = \frac{g}{12\nu} b_h^2 \tag{5.10}$$

where ν is the kinematic viscosity, g the acceleration of gravity.

The calculated joint hydraulic conductivities during 1st loading for the three different joints in granodiorite and analogously calculated conductivities from other studies are shown in Fig.5.16. One should note that the 5 x 10 cm joint specimens used in this study are smaller in size than the specimens in the other studies. Witherspoon et al(1979) concluded that the minimum values of the joint hydraulic conductivity were not the same for each specimen at the maximum stress levels (10-20 MPa) and these minimum values increased with specimen size but the net change of joint hydraulic conductivity with normal stress decreased with specimen size. On the other hand, the results by Raven and Gale(1985) on the effect of specimen size were the opposite in terms of minimum joint hydraulic conductivity and the net change in the joint hydraulic conductivity as a function of stress. They suggested that this discrepancy was probably attributable to the different rock types, joint types and flow boundary conditions in the experiments. The reader is referred to Witherspoon et al.(1979) and Raven and Gale(1985) for comments on size effects. As Fig.5.16 shows, the results obtained in this study are similar to those obtained in the studies by others. Most important, however, is the fact that three different joints have

curves which are similar to each other in shape but different in magnitude. This corresponds well to the observed apertures, which are smallest for the sawed joint, intermediate for the natural joint and largest for the tension joint.

If the parallel plate model for flow in deformable joints is not valid, as it will be discussed in the next section under 'Mechanical joint characteristics', the effective aperture for flow and joint hydraulic conductivity cannot be calculated using Eq.5.9 and Eq.5.10. In this case one can use joint transmissivity (T_j) (see e.g. Raven and Gale,1985) to hydraulically characterize joints and relate this to confining stress.

The joint transmissivity can be directly obtained from the steady-state flow rate per unit head, which is proportional to the joint flow rate per unit head ($Q/\Delta H$) as follows.

$$T_j = \frac{Q}{\Delta H}\frac{L_j}{W_j} \tag{5.11}$$

where L_j is a joint length and W_j is a joint width. These two parameters can be obtained in jointed specimens.

Raven and Gale(1985) have related joint transmissivity (T_j) and normal stress (σ_n) with a negative power law :

$$T_j = T_{j0}\sigma_n^{-n} \tag{5.12}$$

where T_{j0} is the value of T_j at normal stress equal to 1.0 MPa.

The joint transmissivity (T_j) is also defined by joint hydraulic conductivity times joint aperture as follows.

$$T_j = K_j b_j = K_j \frac{A_j}{W_j} \tag{5.13}$$

where b_j is a joint aperture, A_j is cross-sectional area of a joint and W_j is a joint width. In this equation, b_j and A_j is unknown parameters.

Thus the joint transmissivity is also proportional to $[K_jA_j]$ which was already discussed in Chapter 4. Determining the joint hydraulic conductivity is not simple as was mentioned in Chapter 4. One possible approximation is Eq.5.10 which is derived by assuming the

validity of cubic law. Kranz et al.(1979) encountered the same difficulty to obtain the joint hydraulic conductivity or the joint permeability. Thus they also used $[K_jA_j]$ since the volume flow rate through a joint is proportional to $[K_jA_j]$.

In addition, Eq.5.12 used by Raven and Gale(1985) is analogous to Eq.4.11 used by Kranz et al.(1979). Thus in this study, the joint transmissivity is calculated using Eq.5.11 and a power law equation similar to Eq.5.12 is also used to express the dependence of transmissivity, but on confining stress :

$$T_j = T_{j0}(P_c)^{-n} \tag{5.14}$$

where T_{j0} is the value of T_j at a confining stress (P_c) equal to 1.0 MPa.

By plotting $\log[T_j]$ vs $\log[P_c]$ and through regression analysis, one can find the coefficients T_{j0} and n. The results of the regression analysis are presented in Fig.5.17 and the summary of all analyses is presented in Fig.5.18 and in Table 5.4.

For all data except Kimachi sandstone in unloading, regression analysis on the joint transmissivity showed strong correlation coefficients, R, between 0.940 and 1.0. As shown in Fig.5.18(a), the intercept T_{j0} decreased with successive cycles for all jointed specimens. These results indicate a general trend in joint transmissivity at a given confining stress with successive cycles. As shown in Fig.5.18(b), the effect on the exponent n is similar, but less pronounced. Moreover the values of the exponent n in unloading cycles are smaller that those in loading cycles. Therefore it can be concluded that the stress dependency of joint transmissivity in the loading process is larger than that in the unloading process. This result comes from the difference of joint deformability between compression (loading process) and extension (unloading process).

2) Mechanical characteristics of the joints

As shown in Fig.5.1, Iwai(1976) measured combined total deformation (ΔV_t) of a jointed specimen across the joint plane of joint deformation (ΔV) and intact rock deformation (ΔV_r) using three LVDTs. Intact rock deformation (ΔV_r) also was measured by strain gauges which have been affixed on the upper block of rectangular specimen. Then he obtained the joint deformation (ΔV), which could not be measured directly, by subtracting intact rock deformation (ΔV_r) from total deformation (ΔV_t).

In my experiments, total deformation across the joint plane (ΔV_t) is observed with the CRDT halfway along the core length and intact rock deformation ($\Delta V_{r,1}$ and $\Delta V_{r,2}$) are

measured on two opposing sides across the joint plane. Knowing $\Delta V_{r,1}$ and $\Delta V_{r,2}$ which are measured on the intact part of the jointed specimen, the net deformation of the joint (ΔV) is computed by the following equation analogous to Eq.5.1.

$$\Delta V = \Delta V_t - \left[\frac{\Delta V_{r,1} + \Delta V_{r,2}}{2}\right] \tag{5.15}$$

Experimental results regarding total deformation (ΔV_t), intact rock deformation (ΔV_r) and joint deformation (ΔV) during the 1st cycle for the six jointed specimens are presented in Fig.5.19.

To obtain the maximum joint deformation (closure) of joint (ΔV_m) as shown in Fig.5.3, one additional loading-unloading cycle of confining stress is applied to the jointed specimen after three successive cyclic stress-flow (hydromechanical) tests, but no flow test is conducted during this additional cycle. The joint deformation (ΔV) for all cycles and the resulting maximum closure for joints are presented in Fig.5.20. As shown in Fig.5.20, the most notable feature of the joint deformation curve during loading and unloading is the highly non-linear behavior with pronounced hysteresis. Non-linear behavior is compatible with the trends in non-linearity and hysteresis in joint flow rate. This reflects the close relation between joint deformation and joint flow rate. As load is applied across the joint plane, the joint closes, increases flow-path tortuosity and decreases closure rate. Permanent joint deformation is clearly observed for each test cycle and specimen. The permanent deformation decreases with successive test cycles for all jointed specimens. An approximate measure of the permanent joint deformation imparted with successive loading cycles is evident in the change in average joint closure at maximum confining stress between test cycles. The change of joint closure for all specimens is greater between the 1st and 2nd cycles than between the 2nd and 3rd cycles indicating that most of the irrecoverable joint deformation occurred during the 1st loading cycle. No significant irrecoverable joint deformations are observed during the 3rd cycle. The fact that the first test cycle also exhibited the largest flow rate hysteresis is suggesting that the extent of the hysteresis is related to the amount of permanent joint deformation or crushing of joint asperities and altered joint seating. This will be closely examined in the next section by comparing the differences of the geometrical properties such as surface roughness, aperture distribution and correlation function before and after the stress-flow test. The obtained maximum closures of joints are the maximum possible closures of joints from the initial state of stress (confining pressure P_{c0} =0.4 MPa in this test). It is one of the commonly used properties to model the joint deformation behavior (Goodman, 1976 and

Bandis et al., 1983).

Note that the joint may have been closed to some extent at the initial state of stress (confining pressure P_{c0} =0.4 MPa) in this experiments since the confining pressure have been increased from the initial setup at zero up to 0.4 MPa. This initial state of stress is also called as the seating pressure (Goodman, 1979), defining the initial condition for measuring the joint closure.

Since the joint deformation before starting stress-flow (hydromechanical) tests, which involved increasing the confining pressure from the initial setup at zero to 0.4 MPa, could not be measured, the real absolute closures of joints are larger than the observed maximum closure of joints (ΔV_m). Also in existing studies with respect to the normal deformation of joint, the weight of the upper block of the joint specimen in the laboratory was not zero at the start of the test and it was assumed that the weight of the upper block of the joint specimen was in general negligible compared to the applied normal stresses. The maximum closures of joints must be less than the "thickness" of joints which is denoted as the mean initial aperture (or the initial deformable aperture or the initial mechanical aperture), (b_o), in this study. As shown in Table 5.5 and Table 5.7, the comparison between the maximum closure of joints (ΔV_m) and the mean initial aperture (b_o) estimated with roughness measurements in Chapter 3 clearly shows that the maximum closure of joints (ΔV_m) is less than the mean initial aperture (b_o). To obtain the mean initial aperture from the observed stress-deformation curves, one needs to extrapolate the stress-deformation curves.

In general the following parabolic form is commonly used for the normal stress-deformation curves in rock mechanics. (Goodman, 1976)

$$\frac{\sigma_n - \sigma_{n0}}{\sigma_{n0}} = D\left(\frac{\Delta V}{V_m - \Delta V}\right)^t \tag{5.16}$$

where $\sigma_{n0,}$ is the sheeting pressure and D and t are constants.

A schematic view of this parabolic equation is presented in Fig.5.21. As one sees in Fig.5.21, the proposed curve becomes asymptotic to a horizontal line, which is the zero confining stress, and thus this curve does not give any values of joint deformation at zero normal stress. It is physically incorrect since a joint must have some physical thickness at zero normal stress.

Bandis et al.(1983) proposed a hyperbolic model to describe the normal load-displacement behavior of a rock joint. The normal stress, $\sigma_{n,}$ and joint deformation, ΔV,

are related as follows.

$$\sigma_n = \frac{k_{ni} \cdot \Delta V_m}{\Delta V_m - \Delta V} \Delta V \tag{5.17}$$

or

$$\Delta V = \frac{\Delta V_m \sigma_n}{k_{ni} \cdot \Delta V_m + \sigma_n} \tag{5.18}$$

where k_{ni} is the initial normal stiffness of the joint.

The hyperbolic models accounts for two basic physical constraints on the normal deformations of a joint. First, the joint has a negligible tensile strength. Secondly, there is a limit to the amount of possible closure, a maximum closure, which must be less than or equal to the joint thickness. This maximum closure is also defined with respect to a zero initial normal stress level and can be determined by subjecting a jointed specimen in the laboratory to an increasing normal stress. Bandis et al.(1983) stated that the hyperbolic model could describe the normal deformability of mated rock joints quite well. However, they recommended using a logarithmic relationship for unmated joints. Thus, as one can see in Eq.5.18, in the hyperbolic model, the joint deformation curve will start from zero at a zero initial normal stress level. Therefore this hyperbolic model also cannot give a realistic initial aperture at zero confining stress.

Saeb and Amadei(1992) proposed a slightly modified version of the hyperbolic model as follows

$$\Delta V = u\left(1 + \frac{\sigma_n}{\sigma_T}\right)^t \tan i_0 + \frac{\sigma_n \Delta V_m}{k_{ni} \cdot \Delta V_m + \sigma_n} \tag{5.19}$$

where u is the shear displacement, σ_T is the tensile strength of joint, t is a constant and i_0 is the dilation angle.

They simply combined the hyperbolic model by Bandis et al.(1983) and the joint dilatancy model by Goodman and St. John(1977) to take into account for both the degree of matching of joint at initial condition and the effect of shear dilation on the normal joint deformation. Gerrard(1985) mentioned that a "fresh" joint is a joint on which each asperity, on one of its surfaces, has a peak that matches a depression on the other. The term "mated" implies that there is full interlocking and juxtaposition between all peaks and

their corresponding depressions. In this study, five newly created tension joints were fresh joints and a natural joint in Kikuma granodiorite was a well matched joint. In these experiments, five tension joints (fresh joints) were subject to first normal compression due to the initial setup and became mated joints. But under a mated condition (u=0 in Eq.5.19), Eq.5.19 becomes Eq.5.18. Therefore Eq.5.19 also does not work to give any value of initial aperture at zero normal stress. In conclusion, existing models do not give any reasonable answers for the estimation of initial value at zero confining stress.

3) Hydromechanical joint characteristics

It is particularly interesting to compare the flow - confining stress relations to aperture - confining stress relations. At different stages of joint deformation, several parameters or terms are used to indicate the condition of joint aperture and its change due to applied stress, which are "initial aperture", "apparent aperture (named mechanical aperture in this study)", "maximum closure" and "residual aperture". But it is noted that the obtainable parameters in the stress-flow experiments are maximum closure (at some reasonable high stress level) and apparent aperture (maximum closure minus joint deformation). There are still uncertainties in the estimation of initial aperture and residual aperture (see Witherspoon et al.(1980)). Also there is some confusion in the definitions of these terms due to the similarity of the parameters used by different researchers.

In this study, an additional cycle up to 20 MPa confining stress after three successive cyclic stress-flow tests was applied to joints to obtain more accurate maximum closure than those obtained just after three successive stress-flow tests since joint closure behavior is cumulative in general. One difficulty which was briefly mentioned earlier is the definition and measurement of joint aperture. Thus "mechanical aperture" is defined and is measured as : mechanical aperture = maximum joint deformation (closure) at a very high confining stress minus joint deformation at a particular confining stress. (our "mechanical aperture" corresponds to Witherspoon's et al. (1980) "apparent aperture). The minimum of mechanical aperture during three cycles, which is mostly observed at 20 MPa in 3rd cycle, is also found. This minimum mechanical aperture can be thought as a kind of residual aperture, which is named the mechanical residual aperture in this study. Therefore to completely describe the change of joint aperture during cyclic stress-flow experiments, the following quantities are used : the mechanical aperture (apparent aperture by Witherspoon et al.(1980)), the maximum closure (the initial mechanical aperture), the minimum mechanical aperture (residual mechanical aperture at 20 MPa confining stress) and final mechanical aperture after the cyclic stress-flow test. These values and the change of

mechanical apertures for six jointed specimens during three cyclic stress-flow tests are presented in Fig. 5.22.

As shown in Fig.5.22, non-linear behavior and the large hysteresis of mechanical aperture in the 1st loading is compatible with the trends in joint deformation (Fig.5.20) and joint flow rate (Fig.5.13). The irrecoverable deformation in the mechanical aperture increases with successive cycles for all joints. The observed maximum closure, mechanical residual aperture, final mechanical aperture and the permanent joint closure are listed in Table 5.5. Tension joints in Kimachi sandstone seem to be most deformable and most inelastic since maximum closure and permanent deformation of this joint are largest. Residual mechanical aperture at 20 MPa confining stress ranges from 2.5 to 7.4 μm and final mechanical aperture after the stress-flow (hydromechanical) tests ranges from 25 μm to 103 μm at 0.4 MPa confining stress.

To investigate the difference between the mechanical aperture and the hydraulic aperture as defined earlier, changes in both apertures during the stress-flow tests are compared and presented in Fig.5.23. The hydraulic aperture, which is backcalculated from the flow rate using Eq.5.9, does plot, as expected, as a straight line in the log-log plot with a slope equal to one third. This is so since Eq.5.9 assumes the validity of the cubic law for parallel plate flow. The difference between hydraulic aperture and mechanical aperture describes the deviation from the behavior predicted by the parallel plate model. Gale (1982) suggested that the degree of deviation from the cubic law model for joints could be an artifact caused by the choice of reference point in calculating aperture. For this reason, a maximum closure at 20 MPa confining stress is chosen as a reference point since maximum closure is a directly obtainable parameter in the experiments and any change of mechanical aperture can be related to this reference value as a straight line on a log-log plot with a slope equal to one third. Several trends evident in these figures suggest the existence of both cyclic loading effect and aperture variation effects on the joint transmissivity.

In Fig.5.23, a natural joint in Kikuma granodiorite plots closest to the line defining the cubic law while a tension joint in Kimachi sandstone plots farthest from this line. At low confining stress in the 1st cycle, the relation between joint aperture and transmissivity for tension joints in Kikuma granodiorite, Inada granite and Kimachi sandstone are characterized by slopes less than one third, suggesting a reduction in transmissivity greater than that attributable simply to joint closure. Such additional reductions are probably due to increasing contact area and associating flow path tortuosity with increasing confining stress. At intermediate to high confining stress in 1st cycle, joint aperture and transmissivity for all six joints show slopes that are greater than one third. This suggests that the parallel plate model may not be valid for the rough-walled joints at intermediate to

high confining stress levels.

In the 2nd and 3rd cycles, relatively small hystereses are obtained in a natural joint and a sawed joint in Kikuma granodiorite and their slopes are close to one third. Therefore, these two joints most closely resemble a parallel plate. Asperities in these two joints are relatively small so that the joints close rapidly at low stress until enough of these asperities make contact with the opposing surfaces to increase the flow tortuosity and to decrease the joint closure rate. The contrasts between these with Fig.5.23 (c), (d) and (f) where the asperities are larger, diminishing the rate of transmissivity declines as confining stress and promoting the hesteresis in joint aperture, are clear. Hysteresis in joint aperture is probably a result of irrecoverable damage of asperities due to increasing confining stress. Plastic deformation or asperity crushing will increase the contact area and thus decrease the joint transmissivity. At high confining stress, particularly in the 2nd and 3rd cycles, slopes for all joints are greater than one third and are close to unity.

It is noted that one of the reasons for these discrepancies between measurements and the cubic law is the uncertainty in the estimation of an initial reference values for mechanical apertures at the starting points of the experiments. The other reason is clogging. The redistribution of rock fragments crushed during initial loading may be capable of altering the available flow channels. This non-stress related change in joint transmissivity was observed during experiments, in particular in the 2nd and 3rd cycles for a tension joint in sandstone.

5.3 Change of geometrical properties

After cyclic stress-flow (hydromechanical) tests, the surface geometries of the joints were again measured and the aperture geometry derived. The changes of these geometrical properties due to the compressive loading cycles are obtained and are closely examined by comparing joint deformations in stress-flow experiments. Fig.5.24 shows the two digitized surfaces of six joints after the stress-flow test and their histograms are presented in Fig.5.25. Comparing these figures with Fig.3.7 and Fig.3.8, one cannot observe the significant changes of surface roughness distributions, but small changes can be observed. As shown in Fig.5.26, a comparison in the cumulative plot of asperity height before and after the hydromechanical tests also confirms this small changes. The observed statistical values for the six joints are compared with those before stress-flow test and are listed in Table 5.6.

A comparison of the aperture distributions before and after the hydromechanical experiments is presented in Fig.5.27. Also their histograms are compared in Fig.5.28.

These figures show small changes. As one can see, the average apertures of all joints decreased and the variations of aperture distributions also decreased. Statistics of aperture distributions before and after the stress-flow (hydromechanical) tests are summarized in Table 5.7. All statistical parameters such as maximum aperture, mean aperture, standard deviation and geometric mean aperture decreased after stress-flow test. From these results, one can conclude that the joint with the greatest variation in aperture is the tension joint in Kimachi sandstone and the "most constant" one is the sawed joint in Kikuma granodiorite in terms of the coefficient of variation. The means of the apertures range from 78 to 495 μm, the coefficients of variation range from 0.350 to 0.511 and the maximum apertures from 186 to 1585 μm.

Comparisons in the correlation functions of the six apertures before and after the stress-flow (hydromechanical) tests are presented in Fig.5.29. The calculations are performed along four lines in the x-y plane whose directions range from 0 degree (x direction) to 90 degrees (y direction) in 30 degree steps. The correlation functions are plotted with respect to the lag distance which is the separation length for calculating the covariance of two corresponding points. To clearly visualize these features, comparisons in the 2-dimensional correlation functions of the six joint apertures are also presented in Fig.5.30. These comparisons of the aperture correlation functions for the six joints before and after the stress flow tests shows practically no change.

In conclusion, these results suggest that the change of aperture distribution (decrease in aperture and aperture variation) due to the hydromechanical experiments, in which the jointed specimens were subjected to three loading and unloading cycles, may have been caused by the crushing of contact points or asperities during loading. However, this seems to have no effect on aperture correlation. The effect of crushing of asperities on the roughness distribution could not be clearly observed by means of histograms since few asperities at contact points actually were broken, but histograms could not represent the changes in a few sample points. However it was clearly observed that all joint apertures shrank by different magnitudes and that their distributions became sharper due to the hydrostatic cyclic loading.

5.4 Summary and discussion

Previous experimental work does not provide a consistent answer regarding the applicability of the cubic law and the effect of contact area on flow in a joint. In addition, these existing studies have been concerned with joints that are subjected to normal stress, while the general situation in the field involves both normal and shear deformation. These unresolved problems led to the research reported in this chapter which consists of three steps: (1) Measurement of surface geometry and derivation of aperture geometry before stress-flow (hydromechanical) tests (described in Chapter 3), (2) Cyclic stress-flow (hydromechanical) tests, (3) Repetition of the surface geometry measurements and aperture derivations to relate the observed hydromechanical performance to the joint aperture geometry. This made it possible to relate the observed hydromechanical performance to the joint aperture geometry. The three different joint types, which were all in Kikuma granodiorite, one being a natural joint, one an artificially induced tension joint and one an artificially induced sawed joint, were examined. Also three tension joints in different rocks, one being in Inada granite, one being in Chichibu schist, one being in Kimachi sandstone, were also studied.

In all jointed specimens, the large hystereses of joint flow rate ($Q/\Delta H$) were clearly observed during the 1st cycle and these results are consistent with several other experimental studies [Iwai(1976), Witherspoon et al(1980), Pratt et al.(1977), Jones(1975), Nelson and Handin(1977), Kranz et al.(1979) and Raven and Gale(1985)]. The flow rate hystereses decreased with successive test cycles for all specimens, especially for a joint in sandstone. The non-linear behavior and the large hysteresis of mechanical aperture under increasing and decreasing confining stress compares well to the observed joint flow behavior. The irrecoverable deformation in mechanical aperture in the each current cycle decreased with successive cycles for all joints. These results also indicate that the cubic law or the parallel plate flow assumption may not be valid at intermediate to high confining stresses. The decreasing hydraulic aperture and joint transmissivity indicate that permanent changes of the joint geometry occur. When comparing our testing procedure and results to those of others, it did not seem to make a difference if the external stresses were applied in form of stresses normal to the joint plane or in form of confining stresses.

Increasing the confining stress leads to a reduction of hydraulic aperture and of joint transmissivity which is similar to what has been observed by others [Kranz et al. (1979), Coyner et al.(1979) and Bernabe (1986)]. What is more interesting is the fact that these hydraulic characteristics decreased with the number of load-unload cycles and that the initially very large hystereses related to loading and unloading decreased with the number

of cycles. This indicates that the stress is inhomogeneously distributed in rock and a joint and that shear stress can be developed locally at places where joint surfaces are contact. Therefore, these hystereses of hydromechanical properties of joints may be the result of altered seating of the joint due to the crushing of the contact points or asperities during loading, but it will be less by the hydrostatic cyclic loading than by the normal compressive loading. Also, by a comparison in experimental results on three different joints in Kikuma granodiorite, the joint type seems to have an effect on the hydromechanical joint characteristics in that the hysteresis for the sawed joint was most strongly reduced.

The regression analysis on joint transmissivity vs confining stress showed that the stress dependency of joint transmissivity in the loading process was larger than that in unloading process. This difference might come from the difference of joint deformability between compression (loading process) and extension (unloading process), which was already explained in Section 2.6 .

The aperture distributions showed a decrease in mean aperture and a "sharpening" (decreasing variability) after the hydromechanical tests. One can, therefore, conclude that the changes in joint conductivity and transmissivity are indeed related to the permanent changes in joint geometry. However, the geometric changes, at least so far, were less dramatic than expected. These results suggest that the change of aperture distribution (decrease in aperture and aperture variation) due to the hydromechanical experiments, in which the jointed specimens were subjected to three loading and unloading cycles, may have been caused by the crushing of contact points or asperities during loading. However, this seems to have no effect on aperture correlation.

More work, particularly the gathering of data from careful experimental investigations, is needed to provide a solid basis for joint stress-flow theory. It is hoped that this study may help provide a rational framework for such investigations.

In addition, there are potential problems regarding size effect that have been observed in determining the hydraulic properties of joints in rock specimens of different dimensions. Witherspoon et al.(1979) suggested that there could be an effect of size on the hydraulic flow characteristics of a rock joint, as is the case for strength-deformation characteristics of rock joints. One of the significant controlling parameters is the scale of roughness which can contribute to the joint closure, the geometry of interconnecting void in a joint and contact area. The different scales of surface roughness first received attention in terms of their role in defining shear strength between two rough contacting surfaces. Variations in height and spacing of asperities have received considerable attention from workers who have attempted to develop models for joint closure under normal stress

conditions [Greenwood and Williamson(1966), Walsh and Grosenbaugh(1979), Swan(1983) and Brown and Scholz(1984)].

On the other hand, there are a few investigations on the scale effect of joint hydraulic properties (Witherspoon et al. 1979, Brace 1984, Raven and Gale 1985, Gale 1993). The results obtained in this study are relatively similar to those obtained by Witherspoon et al.(1979) since the change in the joint hydraulic conductivity are relatively large and the minimum hydraulic conductivity is relatively small even though the 5 x 10 cm jointed specimens used in this study are smaller in size than the specimens in the other studies. But the most important result is the fact that three different joints in granodiorite have curves which are similar to each other in slope but different in magnitude. This corresponds to the observed aperture, which are smallest for the sawed joint, intermediate for the natural joint and largest for the tension joint in granodiorite.

The results of this study suggest that where laboratory experiments are deemed necessary, more work on the measurement of joint aperture in combination with stress-flow (hydromechanical) tests on varying size specimens of joint planes is needed to confirm the existing trends and to determine the scale effect on joint hydraulic properties so that reliable results on flow in a joint under stress will become available.

Table 5.1 Results of least squares fit for parameters n and b_r (after Witherspoon et al, 1980)

Sample	Run	Fitted n	Residual Aperture	
			Fitted, μm	Calculated,* μm
Granite†	1	3.04	9.0	7.9
	2	3.03	6.7	6.7
	3	3.01	11.6	11.4
Granite‡	1	3.07	5.1	4.4
	2	3.04	4.0	3.2
	3	3.06	13.1	10.9
Basalt‡	1	3.08	10.5	10.0
	2	3.10	10.8	10.4
	3	3.02	9.1	9.8
Marble‡	1	3.06	2.5	4.0
	2	3.06	2.2	4.0
	3	3.01	18.2	18.1

* Calculated from E.q.5.3
† With straight flow.
‡ With radial flow.

Table 5.2 Results of least squares fit for parameters f and b_r (after Witherspoon et al, 1980)

Sample	Run	Fitted f	Residual Aperture	
			Fitted, μm	Calculated,* μm
Granite†	1	1.21	8.8	7.9
	2	1.15	6.6	6.7
	3	1.04	11.6	11.4
Granite‡	1	1.49	4.8	4.4
	2	1.29	3.8	3.2
	3	1.32	12.4	10.9
Basalt‡	1	1.45	9.8	10.0
	2	1.65	9.9	10.4
	3	1.10	8.7	9.8
Marble‡	1	1.36	2.2	4.0
	2	1.36	1.8	4.0
	3	1.05	18.2	18.1

* Calculated from equation E.q.5.3
† With straight flow.
‡ With radial flow.

Table 5.3 Fundamental specification of high pressure triaxial testing apparatus

Loading System		Maximum Load/Pressure
Axial Load	Actuator	500 KN
Confining Pressure	Hydraulic Oil	50 MPa
Pore Pressure	Degasified Water	50 MPa

Specimen Size	Diameter : 50 mm
	Height : 100mm

Table 5.4 Stress conditions for the hydromechanical experiments

	NKGD	SKGD	TKGD	TIGN	TCSC	TKSS
	0.44	0.53	0.59	0.53	0.42	0.42
	1.06	1.11	1.06	1.05		1.05
	2.38	2.53	2.55	2.57	2.39	2.53
	4.80	4.99	5.02	5.01	4.72	5.03
	7.29	7.46	7.47	7.21	7.33	7.50
	9.76	9.92	9.87	9.66	9.68	9.88
	12.19	12.30	12.37	12.20	12.20	12.32
	14.60	14.83	14.80	14.73	14.68	14.79
	17.11	17.24	17.25	16.97	17.06	17.22
1st Cycle	19.58	19.67	19.69	19.64	19.56	19.75
	17.45	17.28	17.25	17.48	17.47	
	15.02	14.81	14.82	14.85	14.99	14.84
	12.52	12.35	12.38	12.64	12.55	
	10.11	9.87	9.90	9.96	10.17	9.94
	7.59	7.44	7.48	7.72	7.61	7.48
	5.18	5.03	5.02	5.32	5.19	5.02
	2.79	2.53	2.58	2.60	2.58	2.57
	1.26	1.09	1.13	1.07		1.07
	0.57	0.58	0.56	0.63	0.57	0.54
	1.06		1.09			1.00
	2.43	2.55	2.58	2.50	2.37	2.52
	4.76	5.03	5.02	4.96	4.98	5.00
	7.29		7.45			7.46
	9.74	9.90	9.93	9.65	9.79	9.88
	12.53		12.37			
	14.61	14.75	14.80	14.52	14.66	14.84
			17.29			
2nd Cycle	19.71	19.64	19.69	19.62	19.54	19.68
			17.29			
	15.00	14.90	14.83	15.05	14.97	14.85
			12.35			
	10.11	9.90	9.92	10.19	9.99	9.96
	7.61		7.45			7.46
	5.20	5.01	4.98	5.30	5.16	5.00
	2.57	2.61	2.53	2.60	2.53	2.53
	1.14		1.09			1.07
	0.52	0.56	0.57	0.71	0.50	0.53
	1.01		1.06			
	2.50	2.55	2.55	2.39	2.53	2.57
	4.83	5.01	5.02	4.81	4.82	4.96
	7.43		7.47			
	9.84	9.87	9.87	9.58	9.68	9.89
			12.37			
	14.97	14.76	14.80	14.78	14.56	14.75
			17.25			
3rd Cycle	19.52	19.71	19.69	19.46	19.53	19.68
			17.25			
	15.03	14.80	14.82	15.06	14.86	14.84
	12.55		12.38			
	10.06	9.92	9.90	9.91	10.07	9.96
	7.64		7.48			
	5.20	5.03	5.02	5.25	5.03	5.05
	2.70	2.58	2.58	2.73	2.41	2.58
	1.08		1.13			1.10
	0.54	0.60	0.56	0.69	0.57	0.51

Unit(MPa)

NKGD : Natural joint in Kikuma granodiorite
SKGD : Sawed joint in Kikuma granodiorite
TKGD : Tension joint in Kikuma granodiorite
TIGN : Tension joint in Inada granite
TCSC : Tension joint in Chichibu schist
TKSS : Tension joint in Kimachi sandstone

Table 5.5 Results of least squares fit for parameters *n* and reference value of joint transmissivity

Name	Natural Joint in Kikuma Granodioritre			Sawed Joint in Kikuma Granodioritre		
Coefficient	Tj0	n	R	Tj0	n	R
1st loading	2.520E-04	1.7026	0.96666	9.153E-05	1.4609	0.99336
1st unloading	3.465E-05	1.4609	0.98511	4.666E-06	0.68249	0.97129
2nd loading	5.593E-05	1.6	0.99011	5.090E-06	1.06	1.000
2nd unloading	2.165E-05	1.4363	0.98978	3.589E-06	0.989	0.99844
3rd loading	2.746E-05	1.5283	0.99214	3.637E-06	1.0019	0.99919
3rs unloading	1.393E-05	1.3437	0.99434	2.633E-06	0.90747	0.99617
Name	Tension Joint in Kikuma Granodioritre			Tension Joint in Inada Granite		
Coefficient	Tj0	n	R	Tj0	n	R
1st loading	5.167E-04	1.3656	0.99908	2.287E-04	1.3005	0.99266
1st unloading	4.896E-05	0.83958	0.99566	5.280E-06	0.41761	0.93895
2nd loading	7.190E-05	1.3649	0.971	1.339E-05	0.8263	0.992
2nd unloading	2.404E-05	1.2479	0.99595	3.024E-06	0.80038	0.98488
3rd loading	3.489E-05	1.2557	0.996	6.783E-06	0.68928	0.988
3rd unloading	1.819E-05	1.2917	0.98715	2.482E-06	0.74399	0.98749
Name	Tension Joint in Chichibu Schist			Tension Joint in Kimachi Sandstone		
Coefficient	Tj0	n	R	Tj0	n	R
1st loading	1.744E-04	1.3379	0.97887	1.772E-05	2.1287	0.99561
1st unloading	8.624E-06	0.67235	0.98616	1.492E-07	0.4697	0.8318
2nd loading	8.358E-06	1.2459	0.99986	1.961E-07	0.6402	0.944
2nd unloading	1.907E-06	0.82614	0.9984	6.011E-08	0.242	0.82387
3rd loading	2.396E-06	0.87635	0.9676	7.189E-08	0.34148	0.96633
3rs unloading	1.644E-06	0.87502	0.99853	5.026E-08	0.21883	0.83258

Table 5.6 Maximum closure, mechanical aperture and permanent joint closure due to stress-flow test

		Maximum Closure (μm)	Mechanical Aperture (μm)		Permanent Joint Closure due to Cyclic Loading (μm)
			Residual	Final	
Kikuma Granodiorite	Natural Joint	161.4	4.2	45.4	116.0
	Tension Joint	220.1	7.4	103.3	116.8
	Sawed Joint	125.4	4.0	25.0	100.4
Inada Granite	Tension Joint	227.5	4.2	77.6	149.9
Chichibu Shist	Tension Joint	132.6	2.5	31.3	101.5
Kimachi Sandstone	Tension Joint	370.6	5.5	73.9	296.7

Table 5.7 Comparison of statistics of asperity heights of surfaces in six joints

Before Stress-flow Test

			Mean (μm)	Standard Deviation (μm)	Maximum Asperity Height (μm)	Minimum Asperity Height (μm)	Double Amplitude (μm)
Kikuma Granodiorite	Natural Joint	Upper Surface	0.0	983	1860	-3488	5348
		Lower Surface	0.0	980	1849	-3476	5325
	Tension Joint	Upper Surface	0.0	1326	4449	-3416	7865
		Lower Surface	0.0	1334	5079	-3242	8321
	Sawed Joint	Upper Surface	0.0	21	77	-84	161
		Lower Surface	0.0	19	91	-81	172
Inada Granite	Tension Joint	Upper Surface	0.0	743	2265	-2496	4761
		Lower Surface	0.0	735	2548	-2358	4906
Chichibu Shist	Tension Joint	Upper Surface	0.0	398	1367	-1310	2677
		Lower Surface	0.0	395	1316	-1250	2566
Kimachi Sandstone	Tension Joint	Upper Surface	0.0	561	1844	-1508	3352
		Lower Surface	0.0	560	1851	-1495	3346

After Stress-flow Test

			Mean (μm)	Standard Deviation (μm)	Maximum Asperity Height (μm)	Minimum Asperity Height (μm)	Double Amplitude (μm)
Kikuma Granodiorite	Natural Joint	Upper Surface	0.0	1001	1843	-3992	5835
		Lower Surface	0.0	986	2096	-3690	5786
	Tension Joint	Upper Surface	0.0	1316	4451	-3878	8329
		Lower Surface	0.0	1315	4835	-3299	8134
	Sawed Joint	Upper Surface	0.0	25	90	-102	191
		Lower Surface	0.0	27	127	-97	224
Inada Granite	Tension Joint	Upper Surface	0.0	758	2053	-2521	4574
		Lower Surface	0.0	739	2750	-2392	5142
Chichibu Shist	Tension Joint	Upper Surface	0.0	403	1348	-1756	2644
		Lower Surface	0.0	392	1310	-1334	3104
Kimachi Sandstone	Tension Joint	Upper Surface	0.0	558	1825	-1569	3394
		Lower Surface	0.0	560	1855	-1515	3370

Table 5.8 Comparison of statistics of apertures in six joints

a)before stress-flow test

Joint	Points	Minimum (μm)	Maximum (μm)	Mean (μm)	Geometric mean(μm)	Standard Devi.(μm)	C.O.V.	Standard Error(μm)	Skewness	Kurtosis
NKGD	4500	0	691	262	238	105	0.402	1.57	0.792	1.191
SKGD	4653	0	243	101	93	30	0.297	0.45	0.285	0.284
TKGD	4656	0	1874	627	536	311	0.497	4.56	0.767	0.855
TIGN	4462	0	1990	650	539	350	0.539	5.24	0.761	0.600
TCSH	4462	0	683	283	255	113	0.400	1.69	0.332	0.136
TKSS	4462	0	798	296	275	104	0.352	1.56	0.733	1.866

b)after stress-flow test

Joint	Points	Minimum (μm)	Maximum (μm)	Mean (μm)	Geometric mean(μm)	Standard Devi.(μm)	C.O.V.	Standard Error(μm)	Skewness	Kurtosis
NKGD	4455	0	657	239	224	89	0.374	1.33	0.956	2.052
SKGD	4653	0	186	78	74	27	0.350	0.40	0.117	0.282
TKGD	4653	0	1585	495	441	253	0.511	3.71	0.852	1.026
TIGN	4753	0	1531	457	412	221	0.484	3.21	0.957	1.733
TCSH	4559	0	597	252	218	101	0.393	1.50	0.127	0.084
TKSS	4559	0	644	164	151	72	0.437	1.07	1.537	5.634

Table 5.9 Changes of apertures due to stress-flow test

Joint	Change of mean aperture due to stress-flow test (μm)	Change of maximum aperture due to stress-flow test (μm)	Change of geometric mean aperture due to stress-flow test (μm)
NKGD	23	34	14
SKGD	23	57	19
TKGD	132	289	95
TIGN	193	459	127
TCSH	31	86	37
TKSS	132	154	124

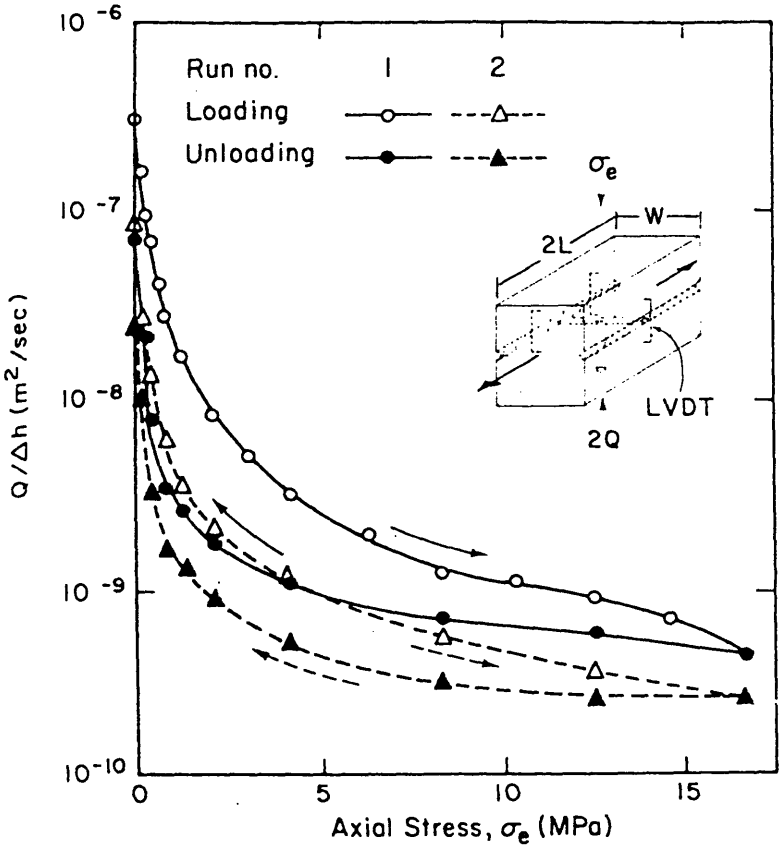

Fig.5.1 Effect of cyclic loading on flow rate of tension joint in granite with straight flow (after Iwai, 1976)

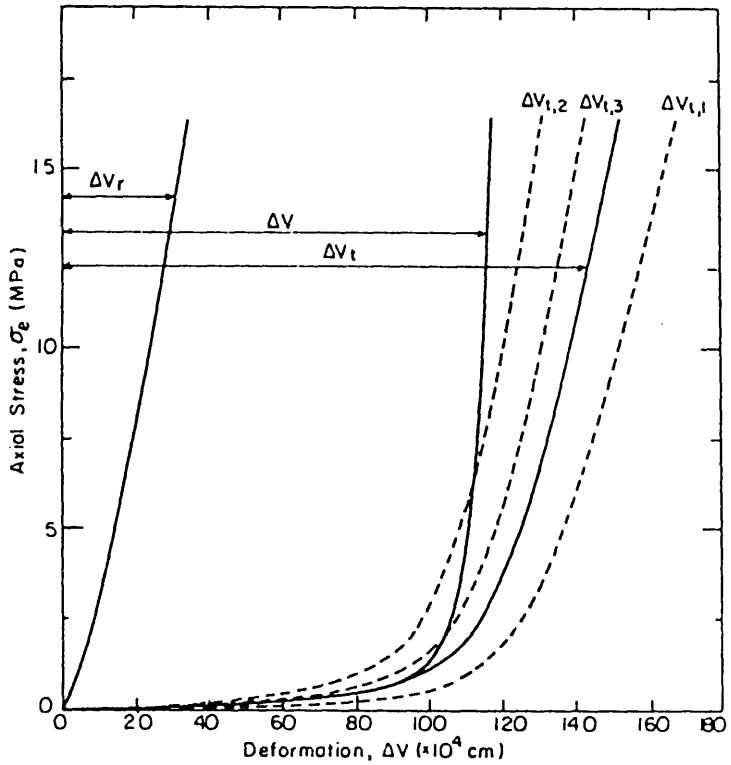

Fig.5.2 Mechanical properties of jointed granite sample used in straight flow model (after Iwai, 1976)

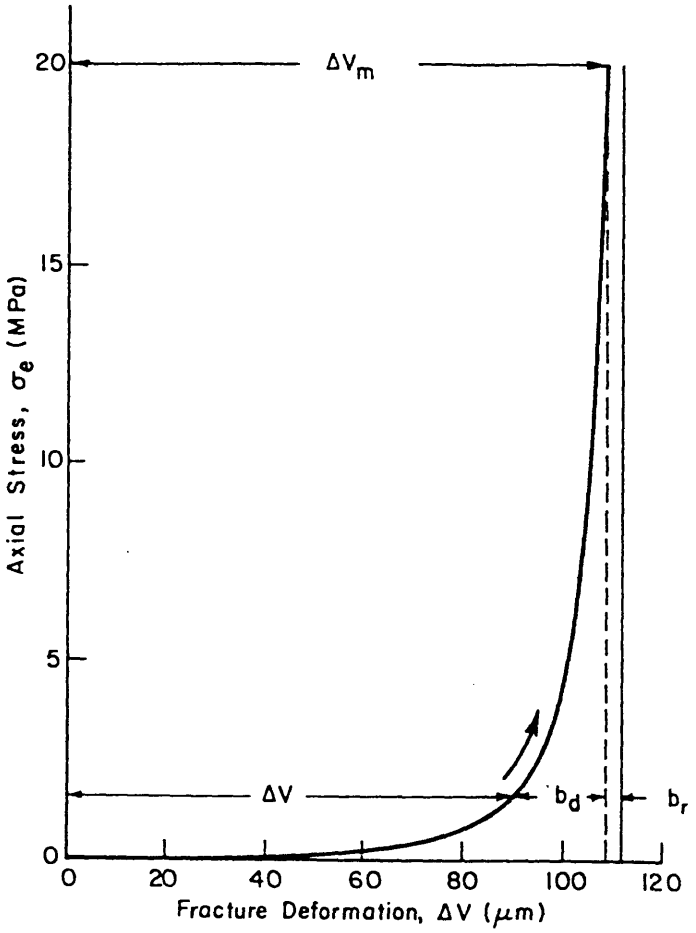

Fig.5.3 Mechanical properties of joint used in determining changes in aperture (after Witherspoon et al., 1980)

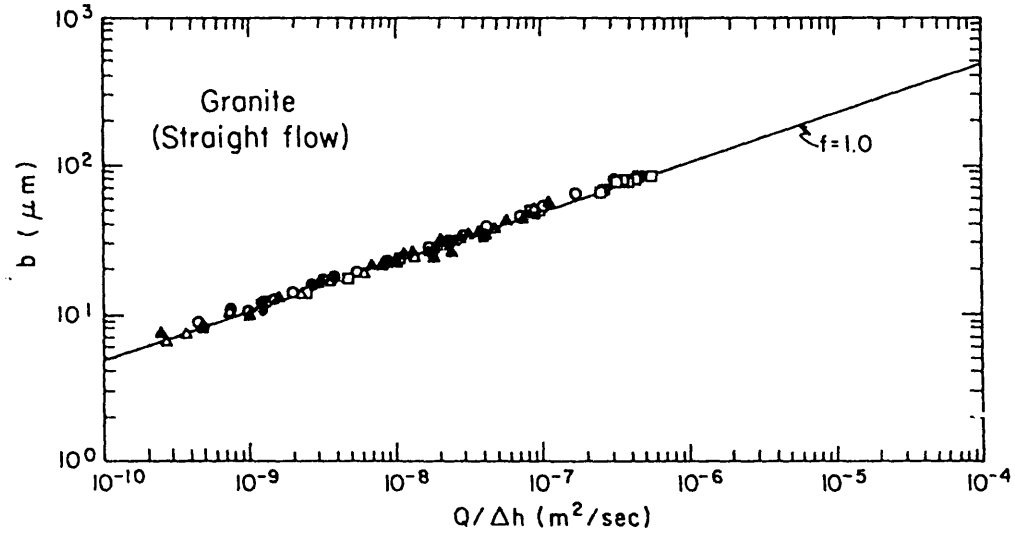

Fig.5.4 Comparison of experimental results for straight flow through tension joint in granite with cubic law (after Iwai, 1976)

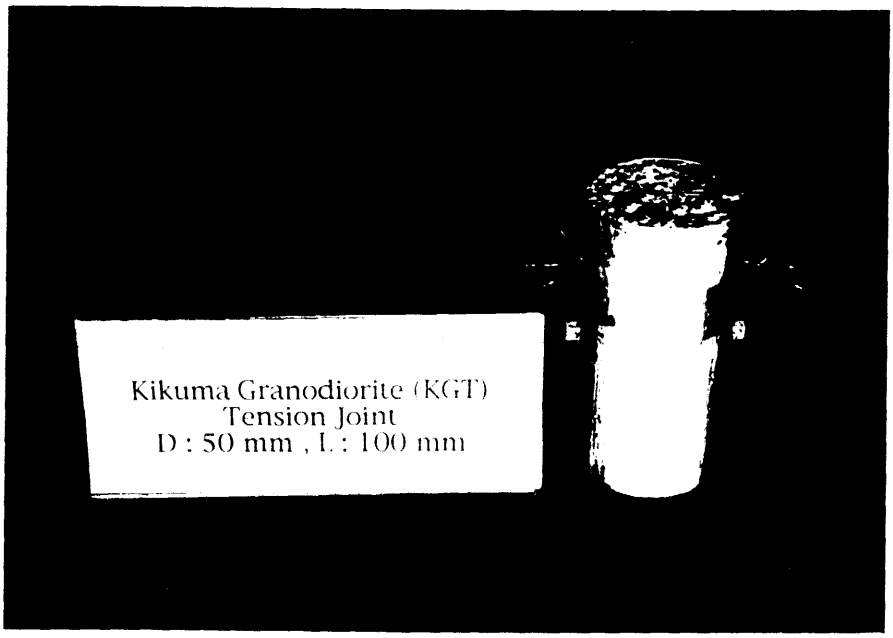

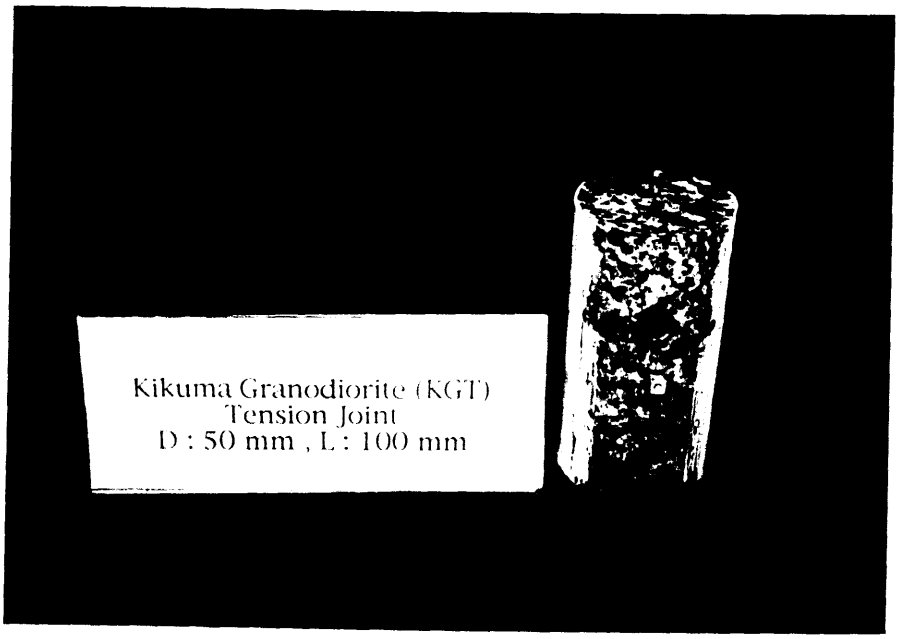

Fig.5.5 Photographs on the procedure for the sample preparation
(a) Sealing both side ends of a joint with epoxy

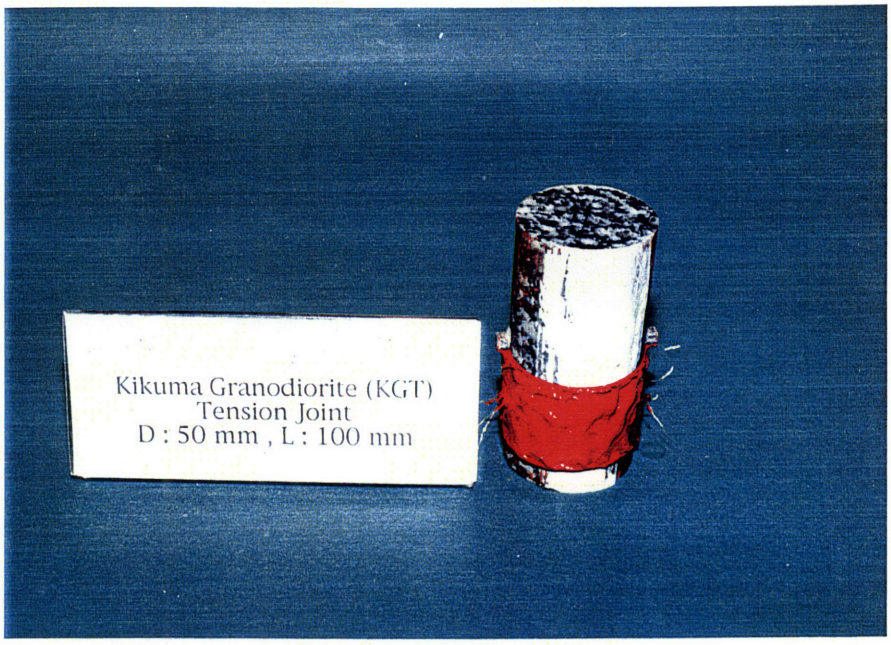

Fig.5.5 Photographs on the procedure for the sample preparation
(b) Enclosing the affixed strain gauges with silicon rubber

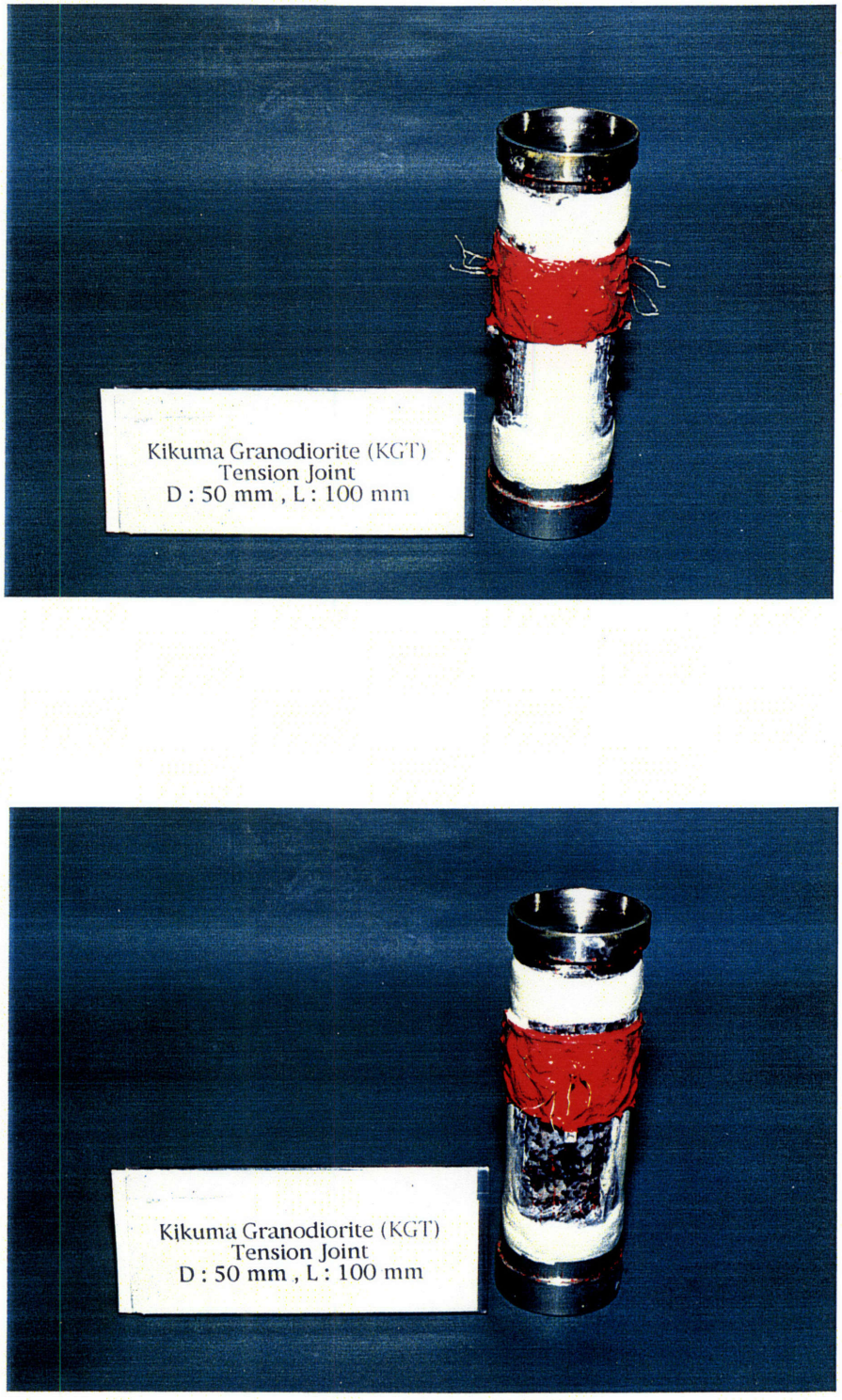

Fig.5.5 Photographs on the procedure for the sample preparation
(c) Sealing both ends of a specimen with epoxy

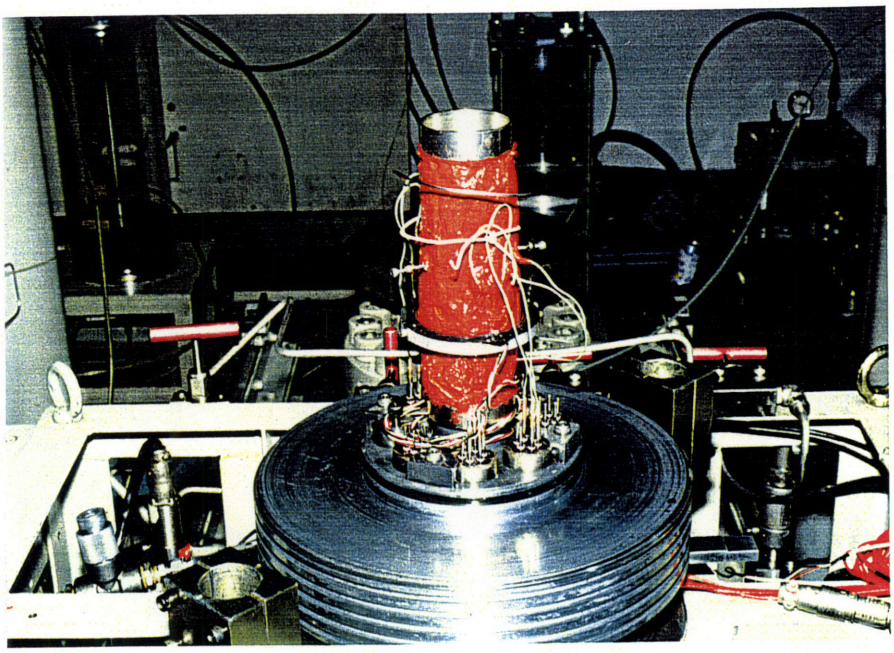

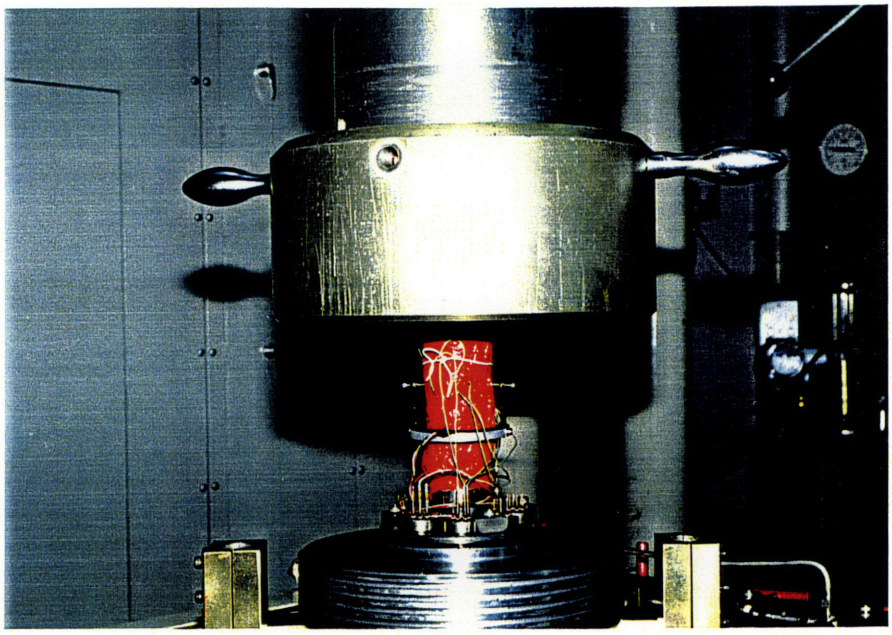

Fig.5.5 Photographs on the procedure for the sample preparation
(d) Final setup of a specimen

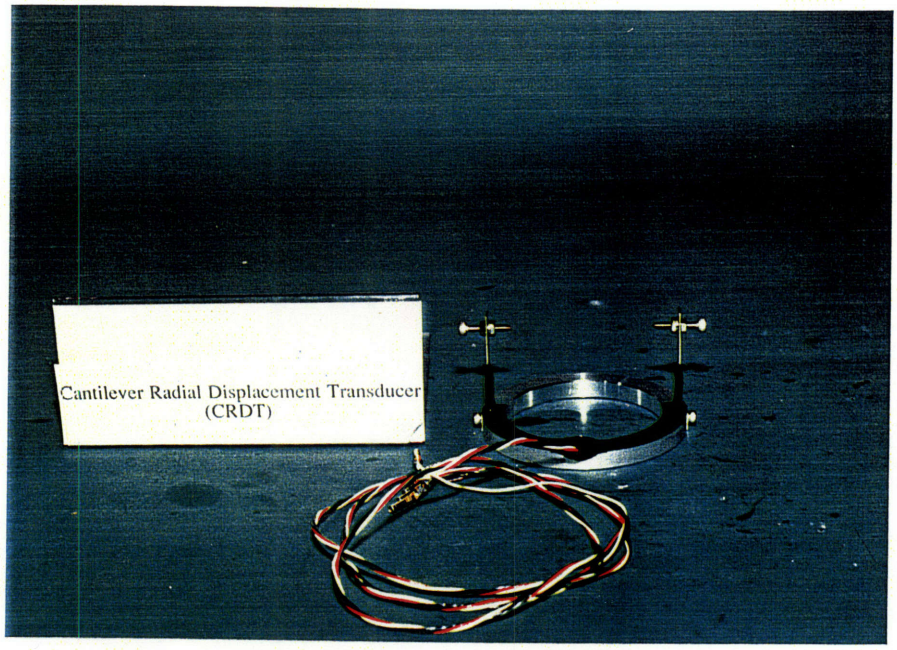

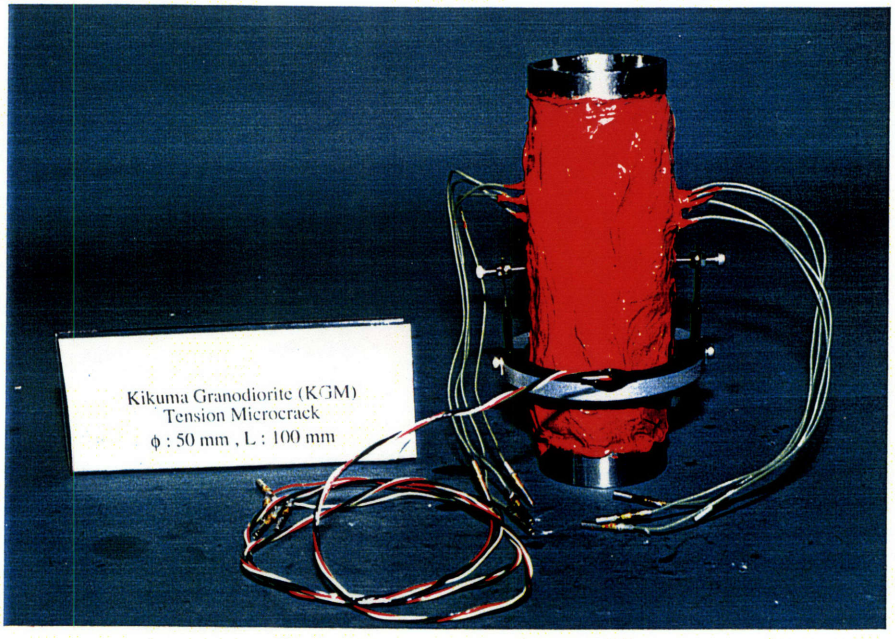

Fig.5.6 A photograph of the cantilever radial displacement transducer (CRDT)

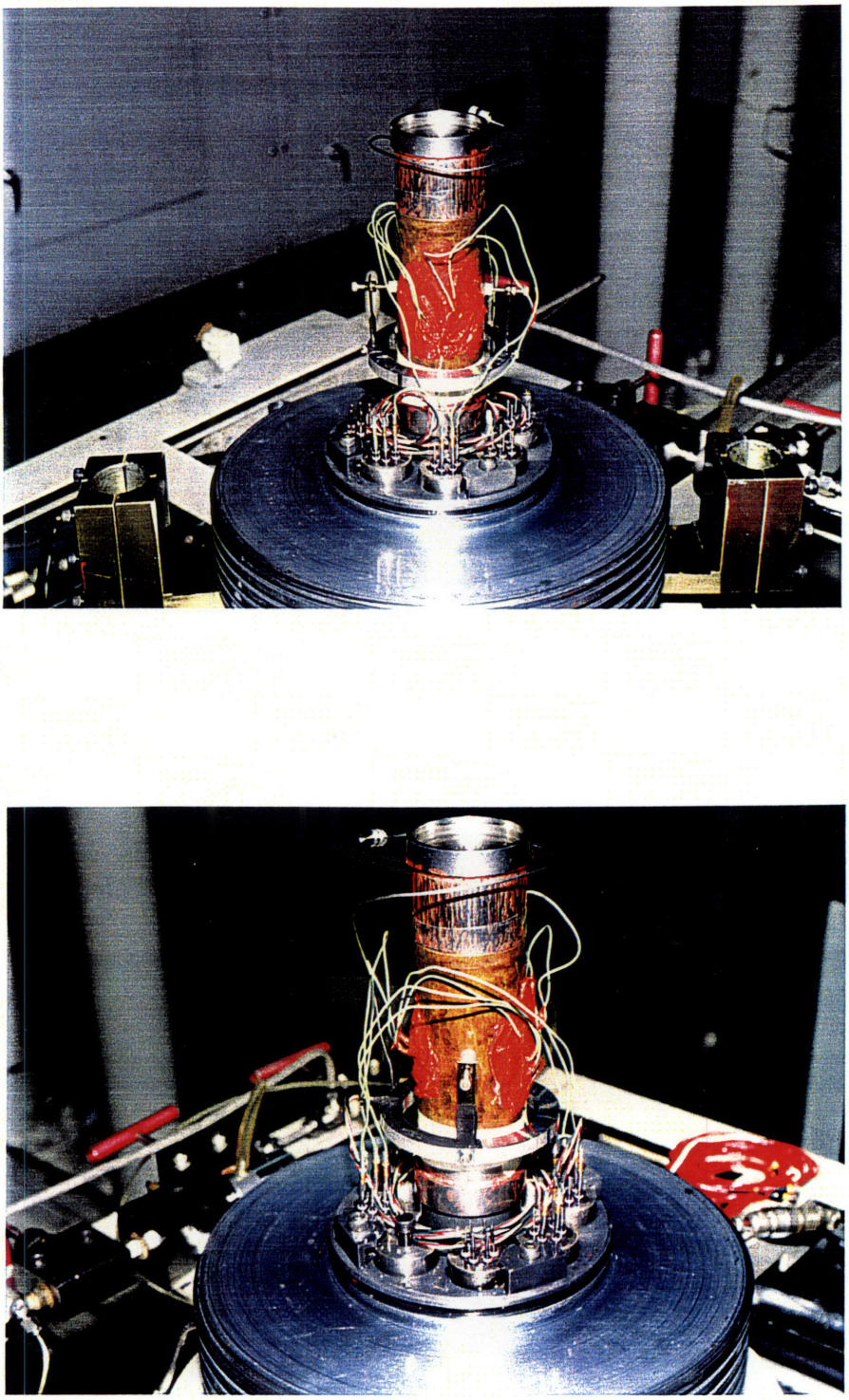

Fig.5.7 A photograph of the calibration test of CRDT using a brass specimen

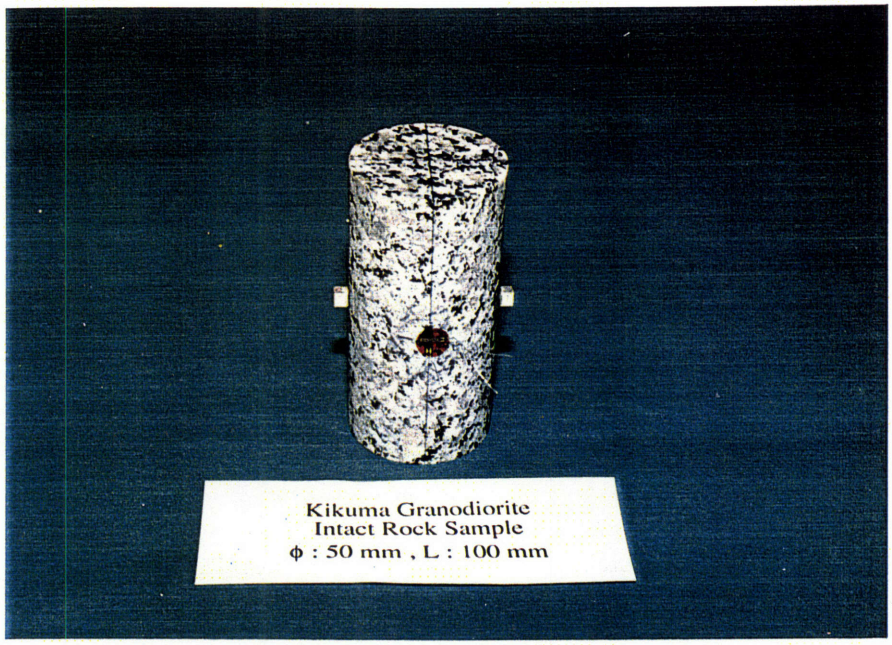

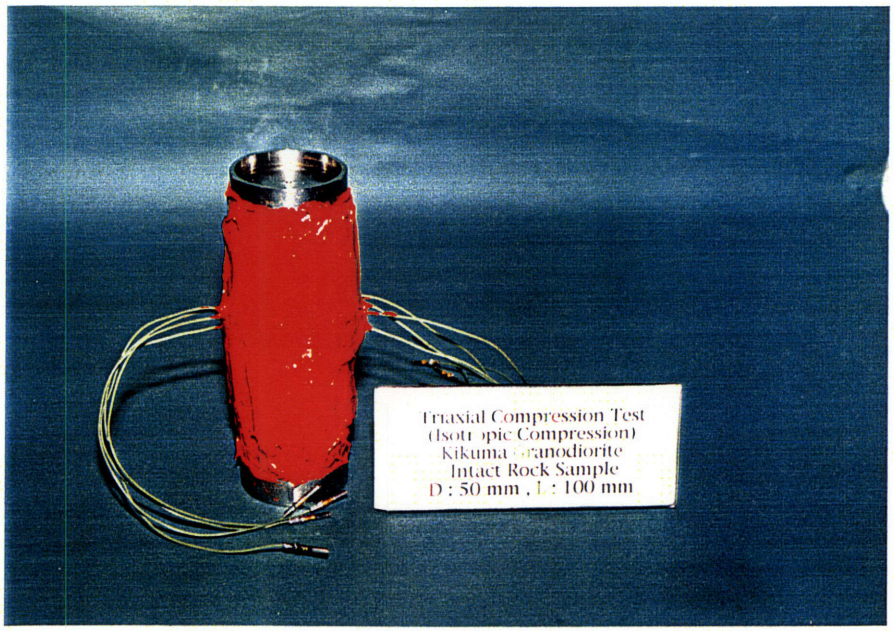

Fig.5.8 A photograph of calibration test of CRDT using intact rock specimen

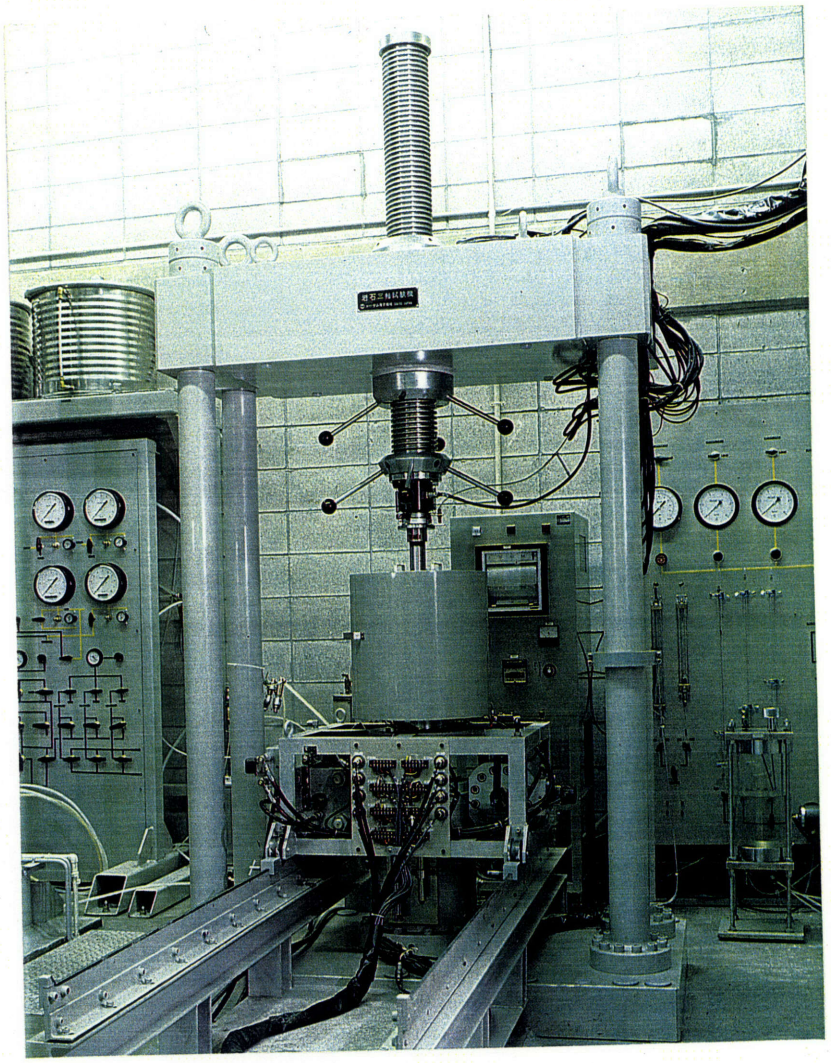

Fig.5.9 A photograph of the high pressure triaxial testing apparatus

a) The high pressure triaxial testing apparatus

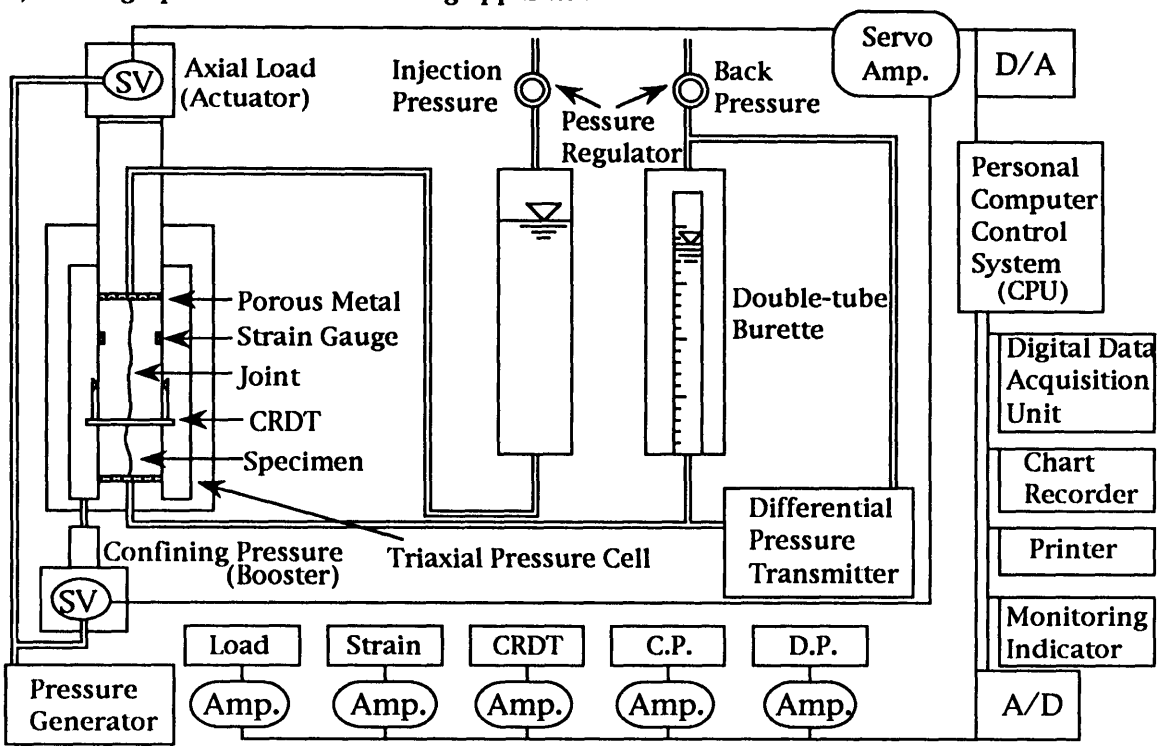

b) The CRDT and final configuration attached to the jointed specimen

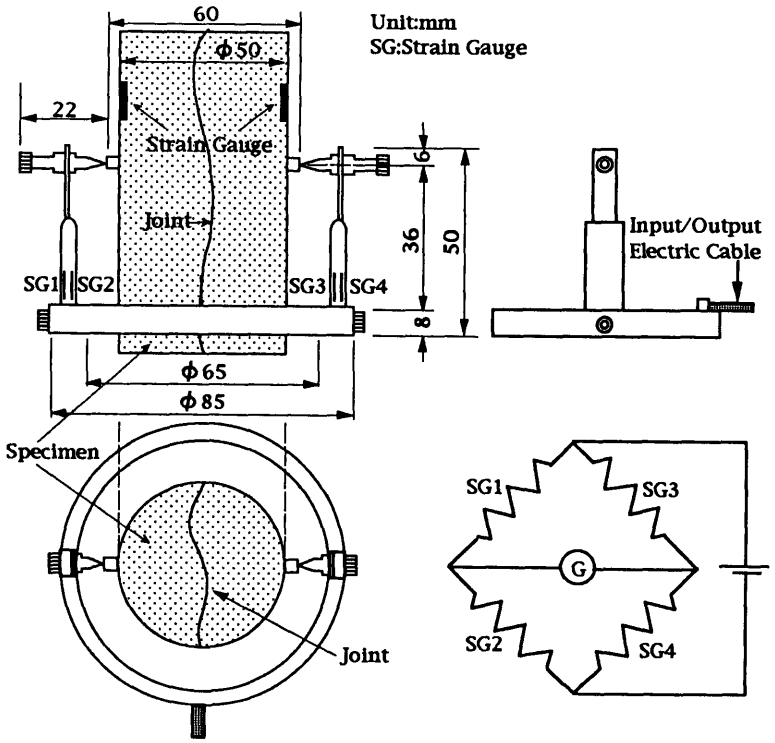

Fig.5.10 Schematic view of the setup for stress-flow (hydromechanical) experiments using the high pressure triaxial testing apparatus

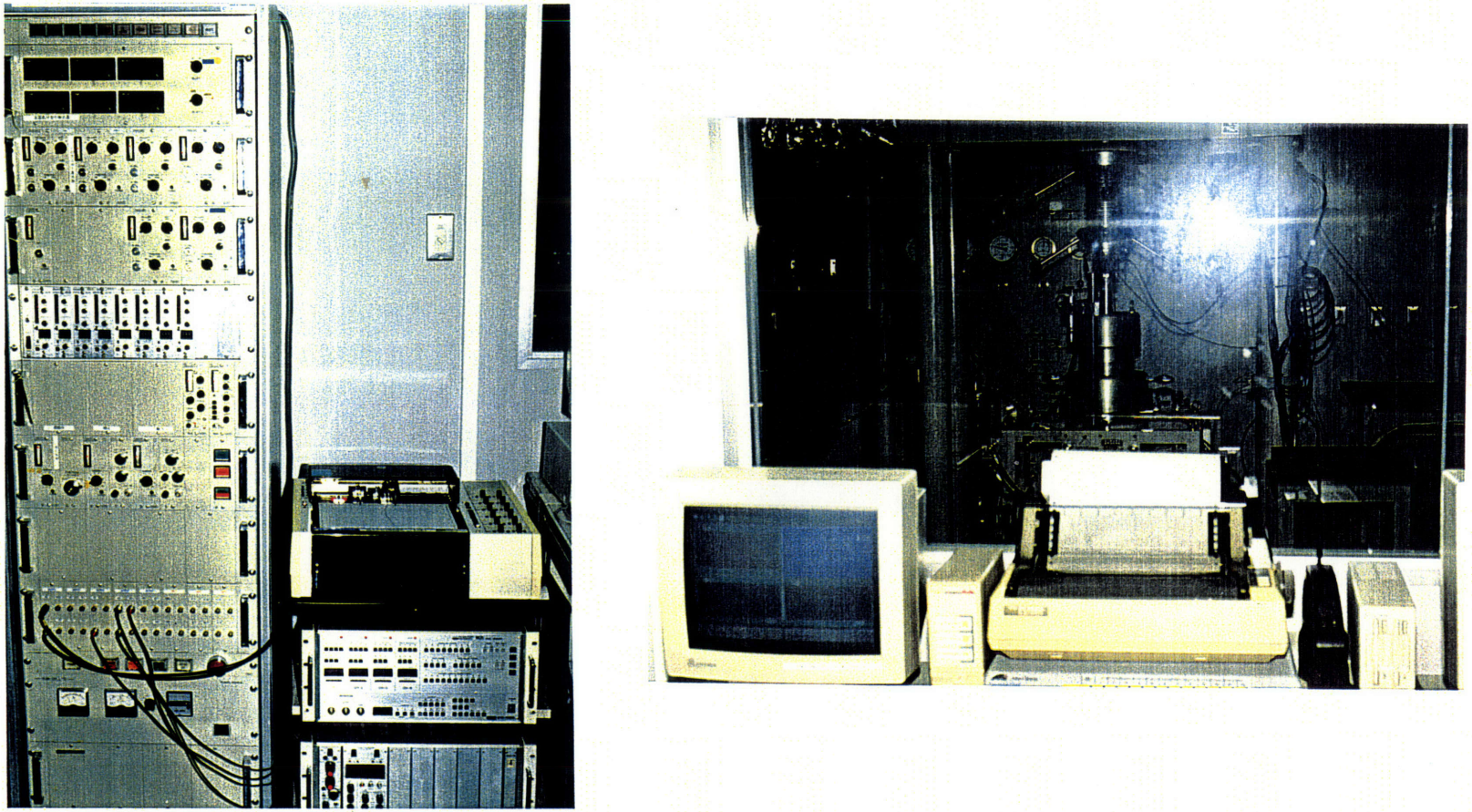

Fig.5.11 A photograph of the data acquisition system for the high pressure triaxial testing apparatus

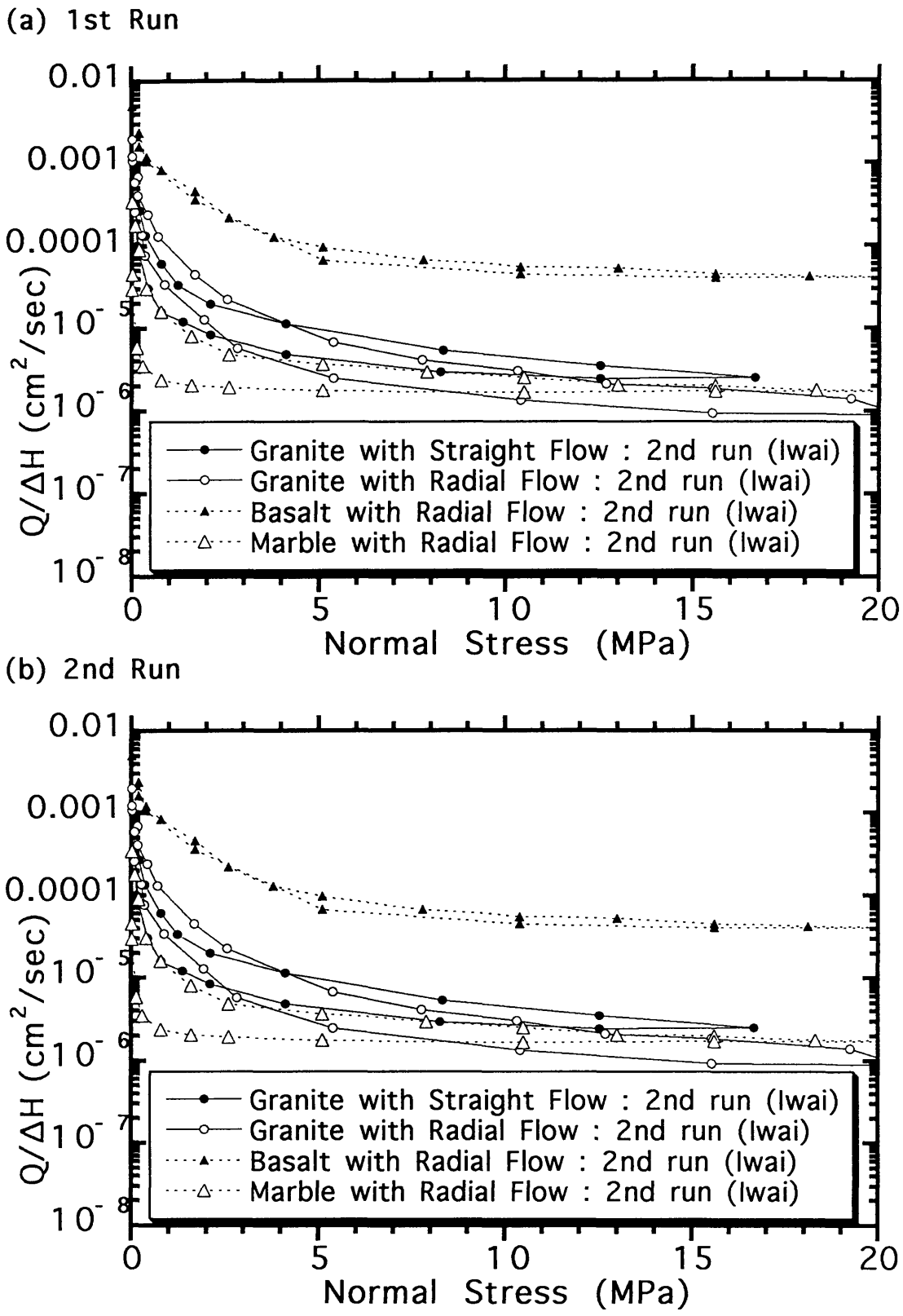

Fig.5.12 Joint flow rate versus normal stress obtained by Iwai(1976)

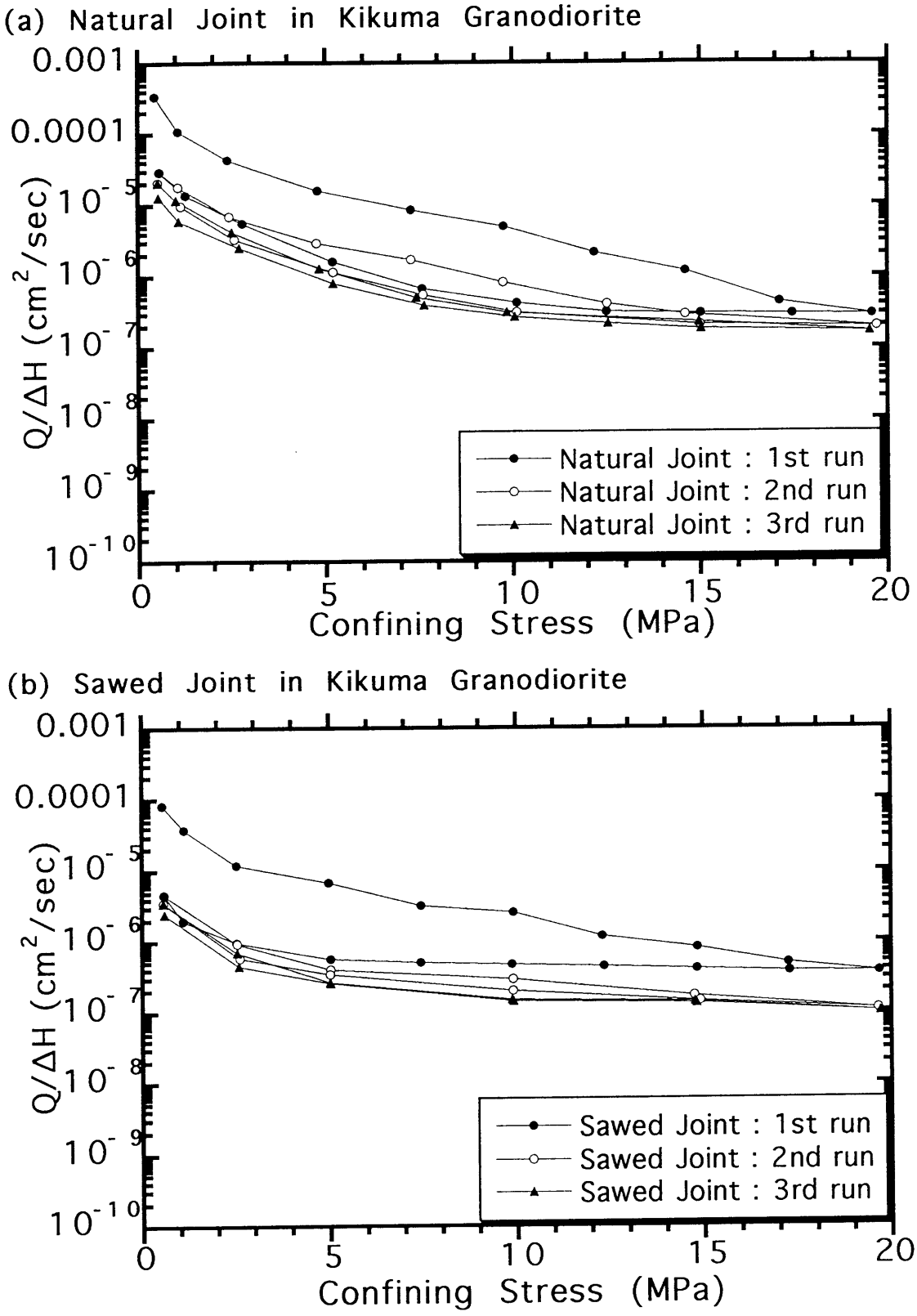

Fig.5.13 Joint flow rate per unit head as a function of confining stress

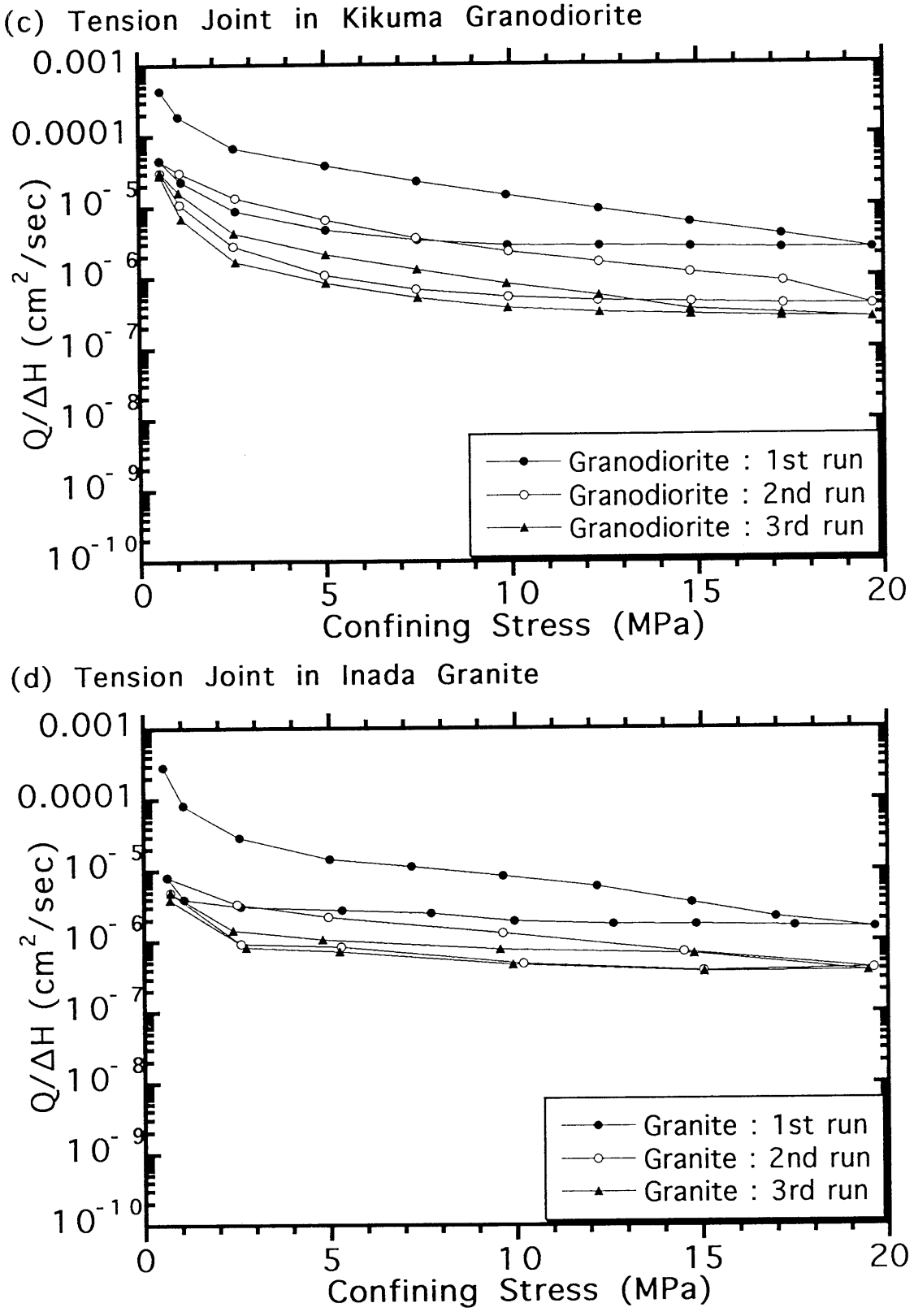

Fig.5.13 Joint flow rate per unit head as a function of confining stress

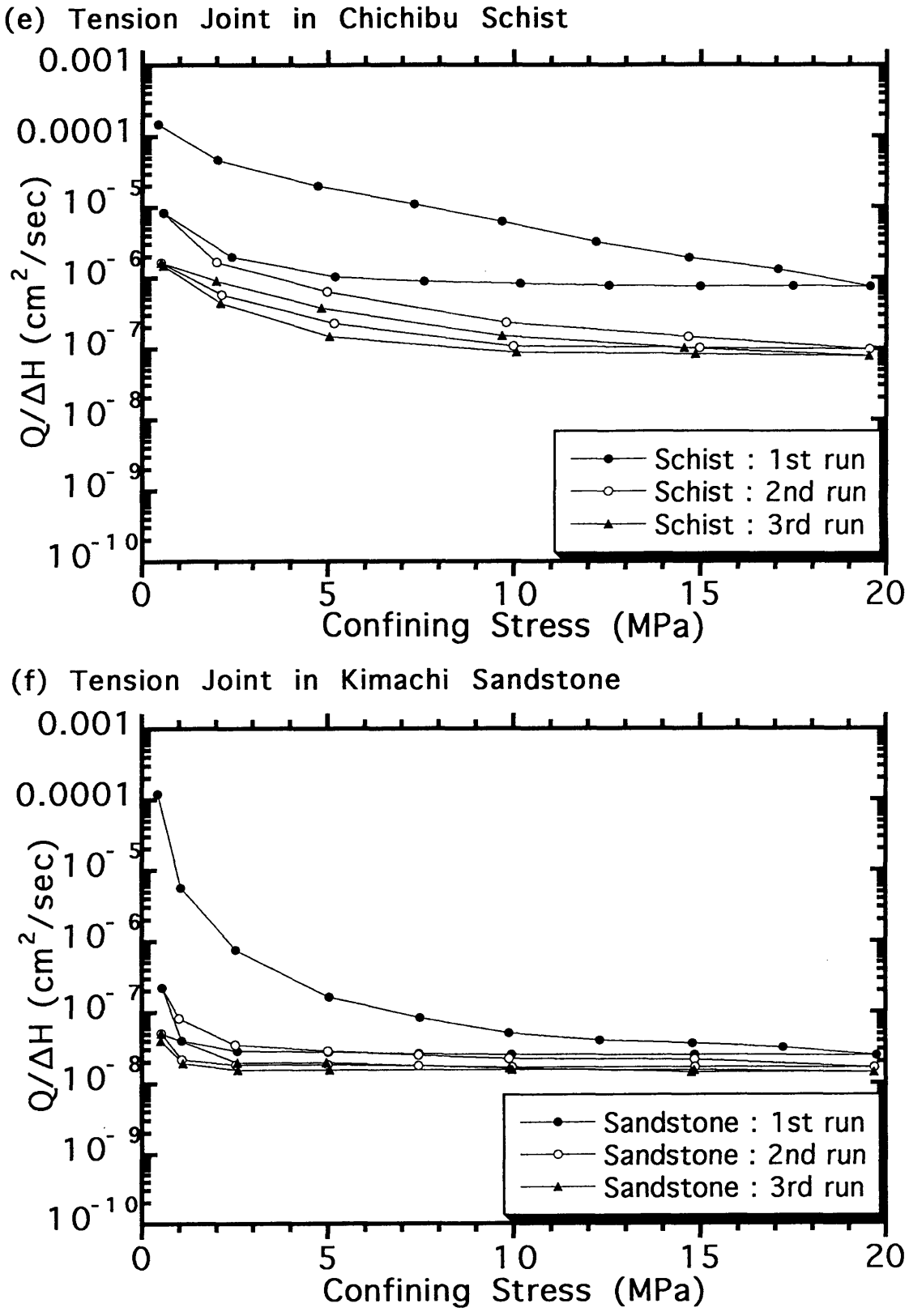

Fig.5.13 Joint flow rate per unit head as a function of confining stress

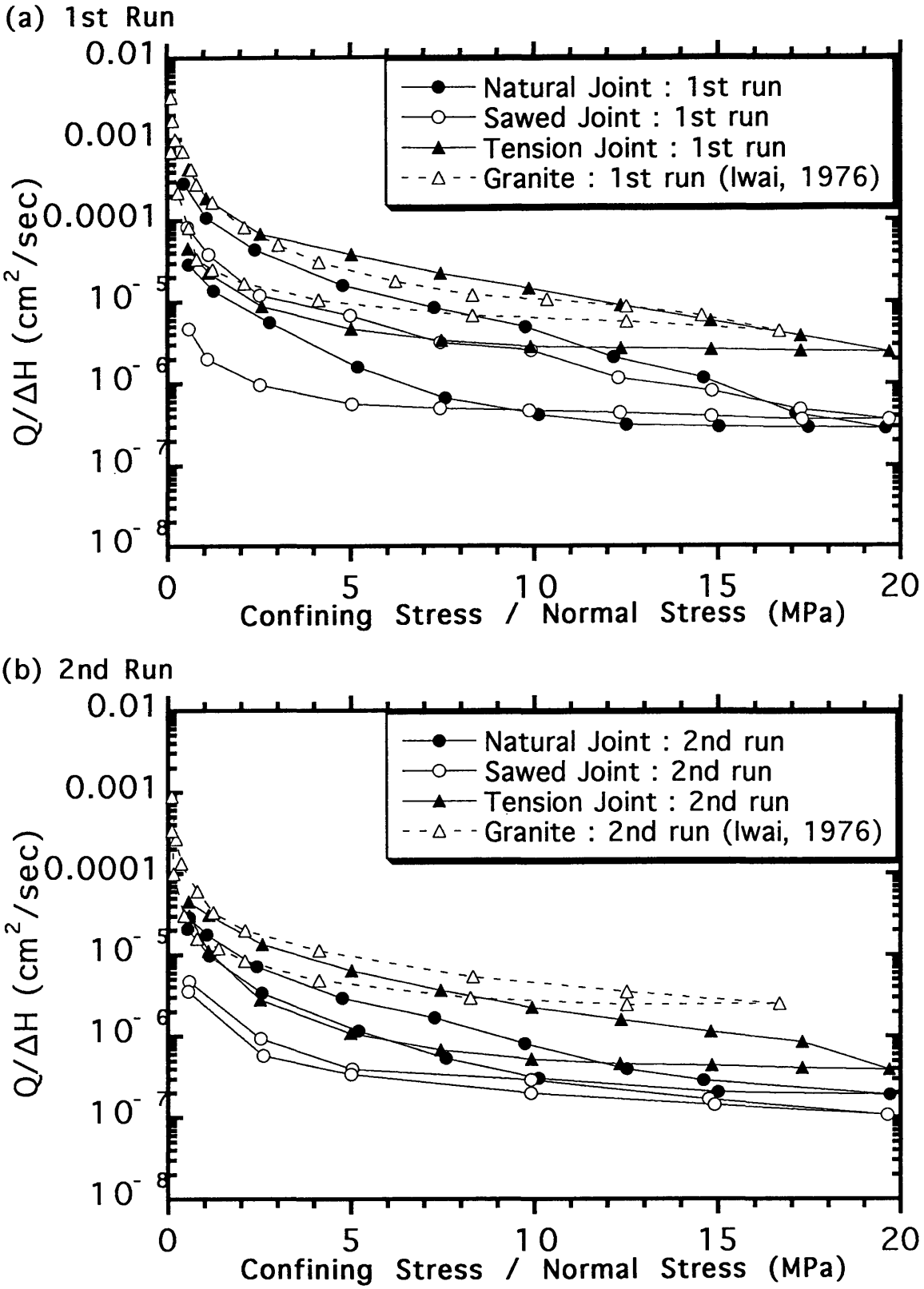

Fig.5.14 Comparison of flow rate per unit head of joints in Kikuma Granodiorite with Iwai's experimental result on a tension joint in granite with straight flow (a)1st run (b)2nd run

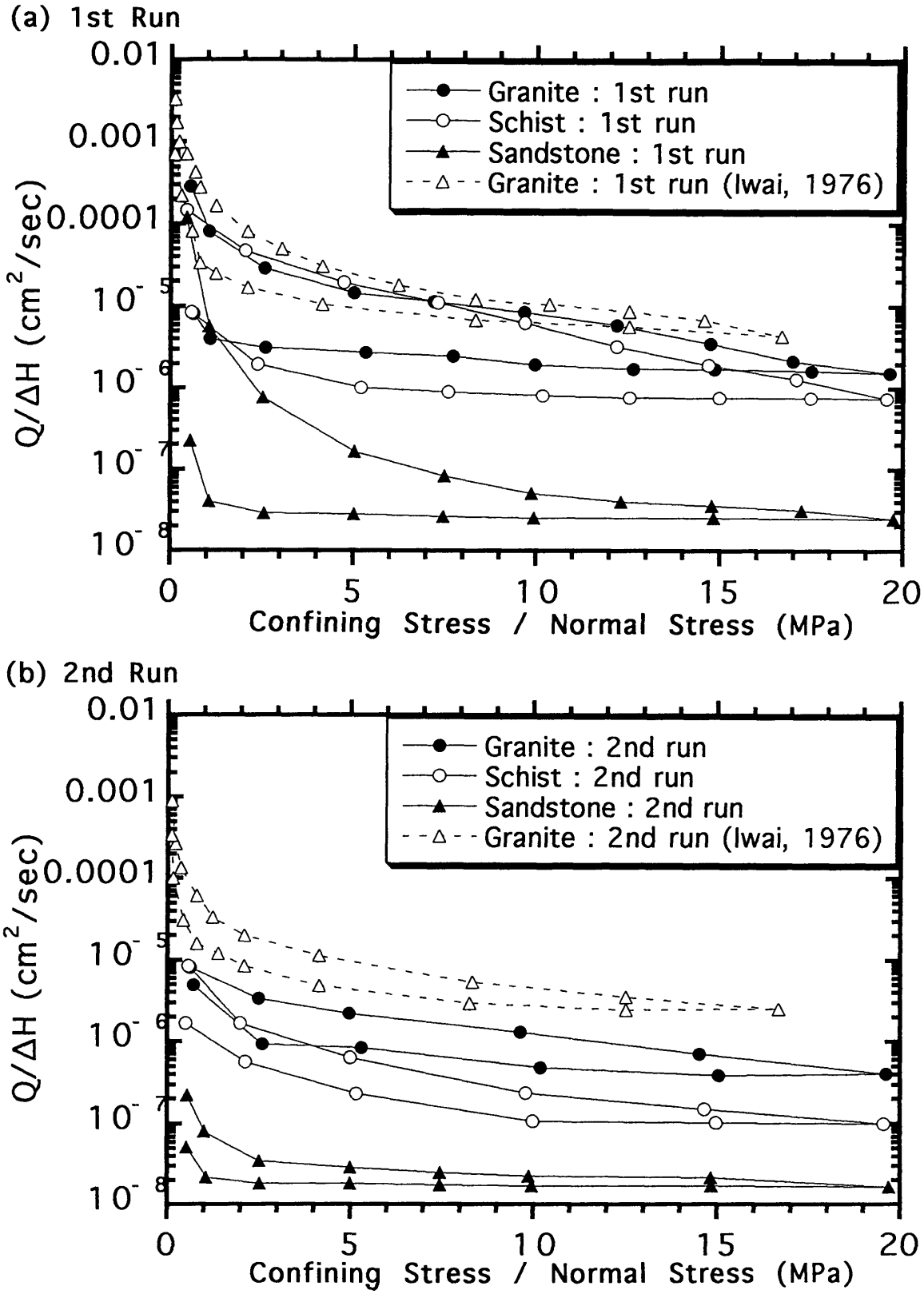

Fig.5.15 Comparison of flow rate per unit head of joints in three different rocks with Iwai's experimental result on a tension joint in granite with straight flow (a)1st run (b)2nd run

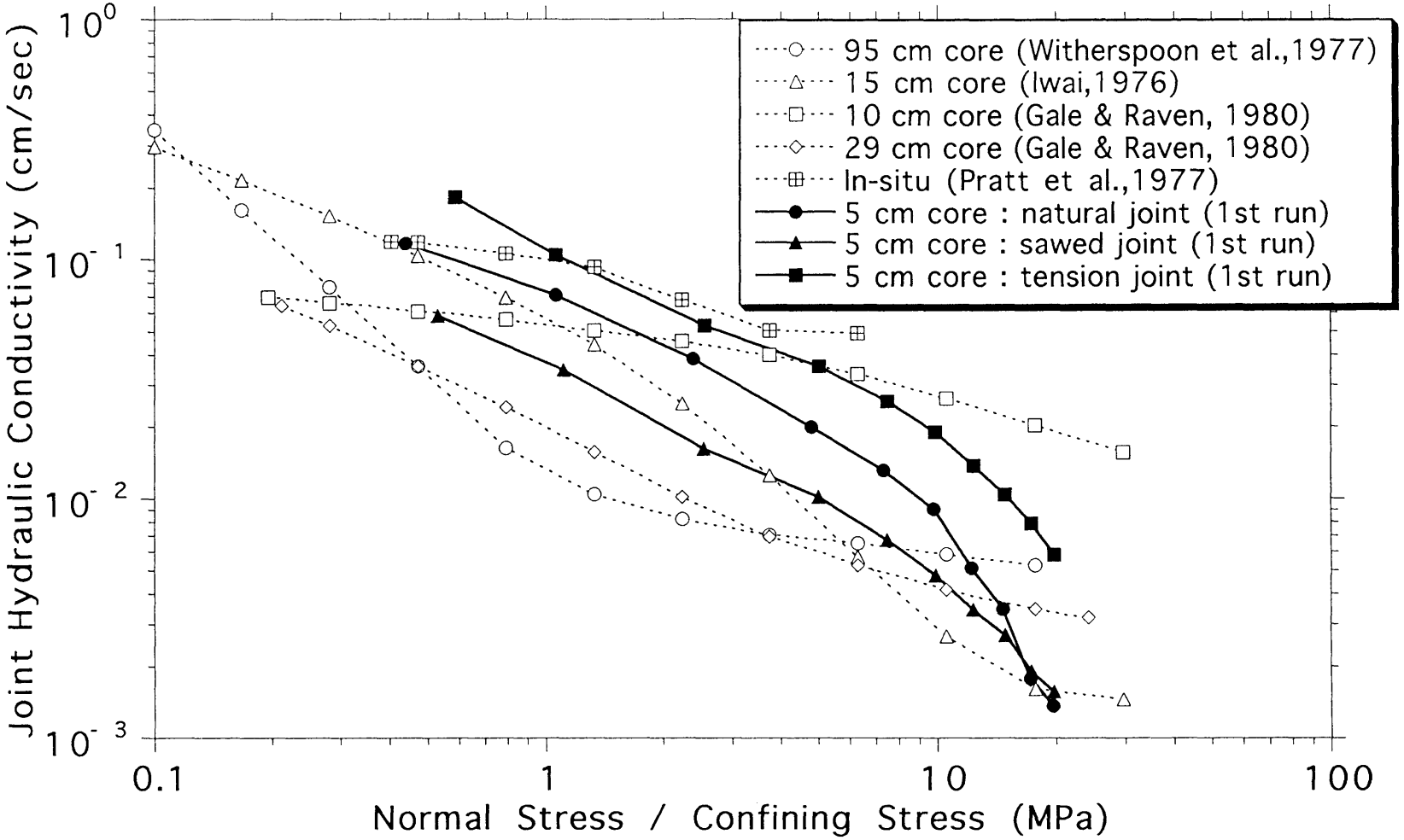

Fig.5.16 Comparison of the variation of joint hydraulic conductivity with stress using published data and data from this study
(after Witherspoon et al., 1979 and Raven and Gale, 1985)

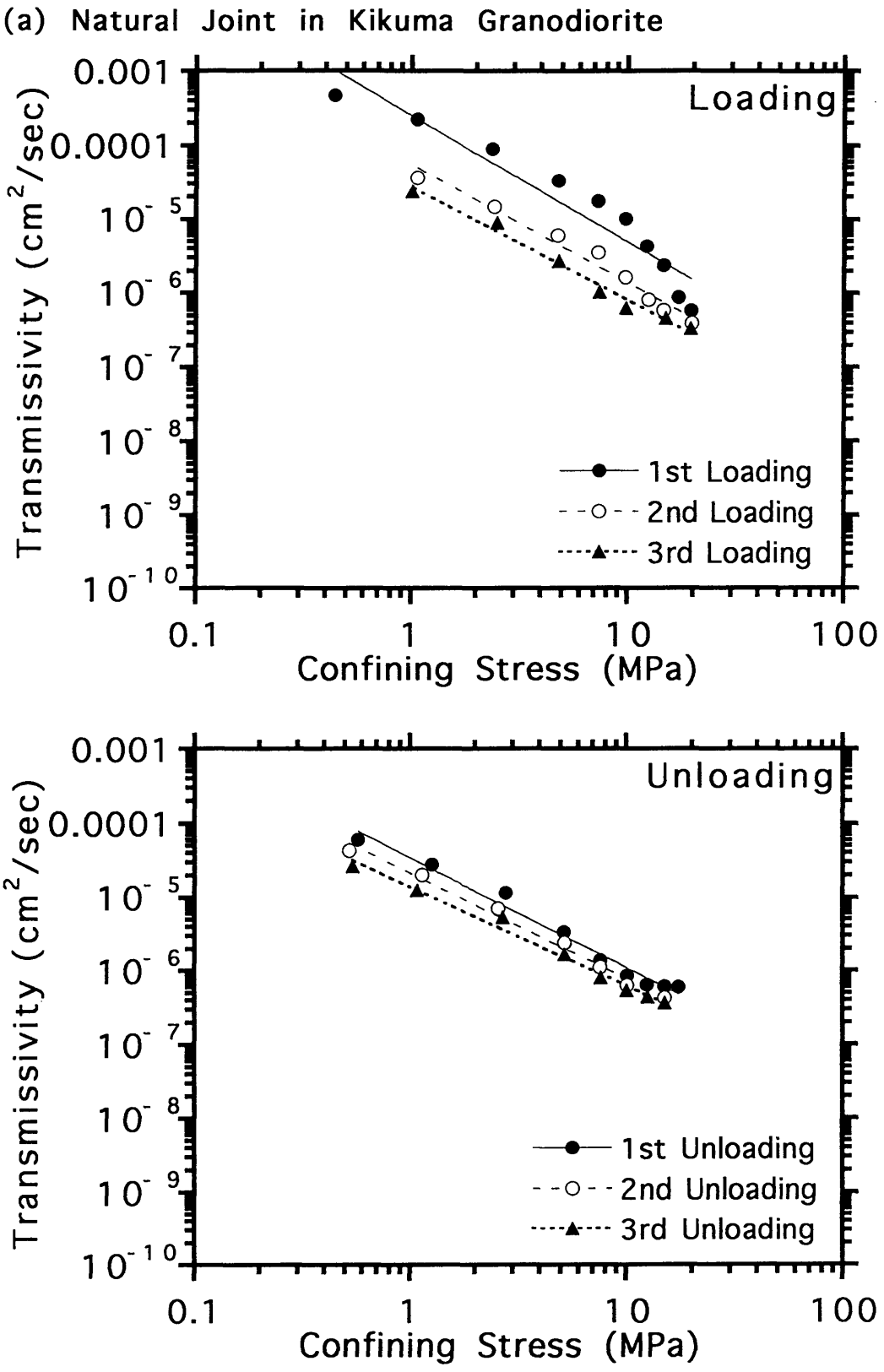

Fig.5.17 Joint transmissivity vs confining stress and results of regression analysis (a)Natural joint in granodiorite

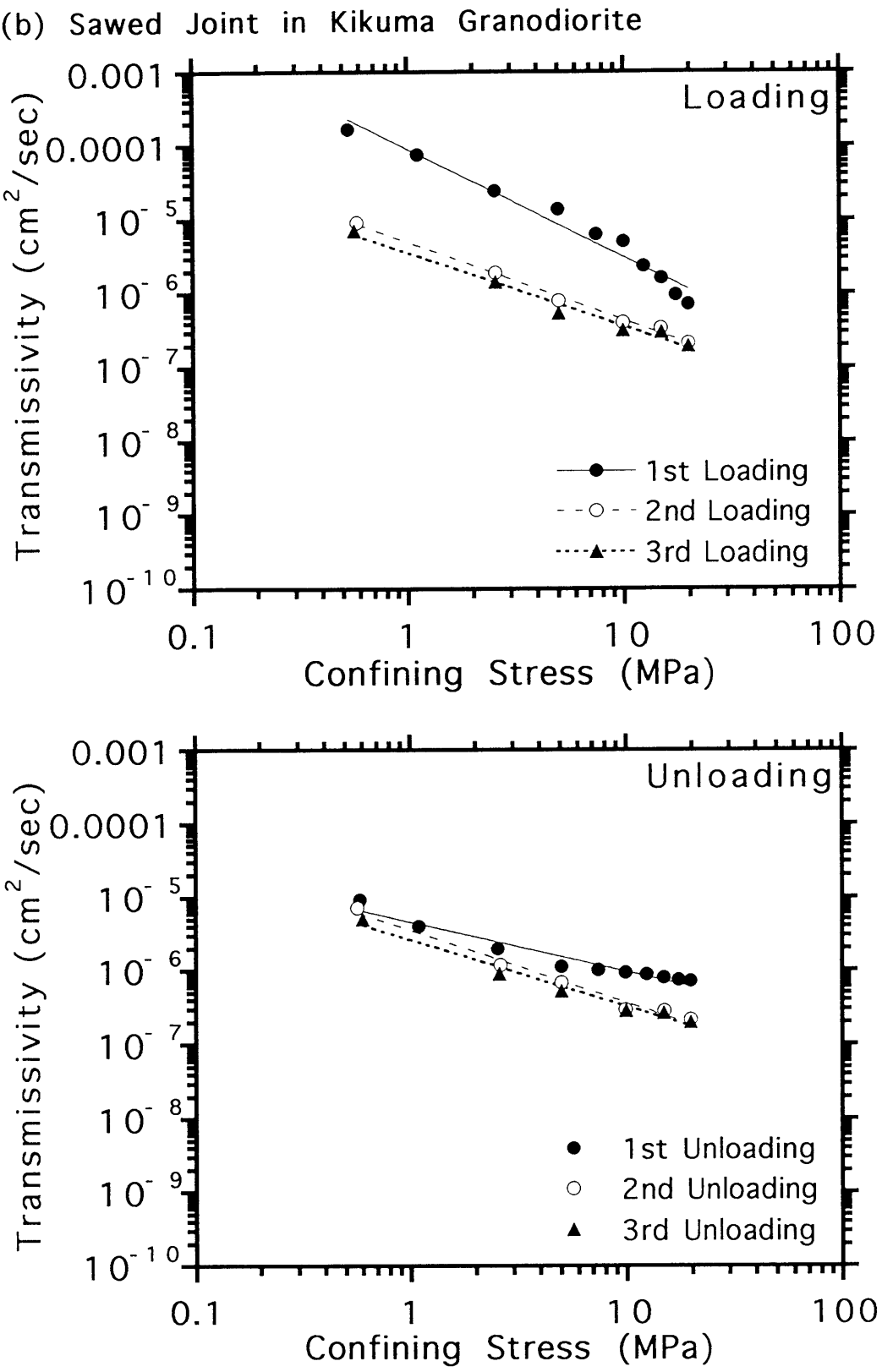

Fig.5.17 Joint transmissivity vs confining stress and results of regression analysis (b)Sawed joint in granodiorite

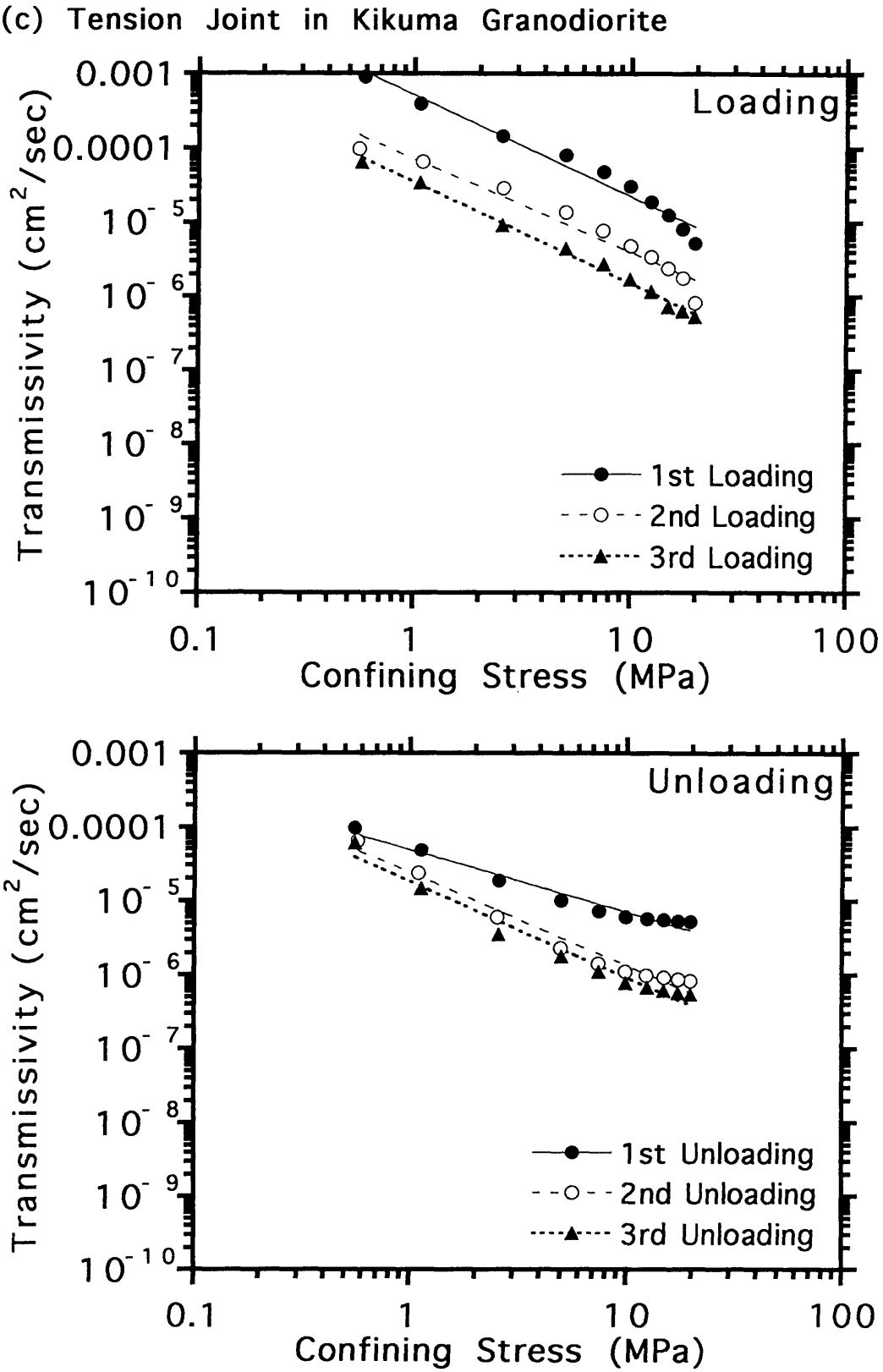

Fig.5.17 Joint transmissivity vs confining stress and results of regression analysis (c)Tension joint in granodiorite

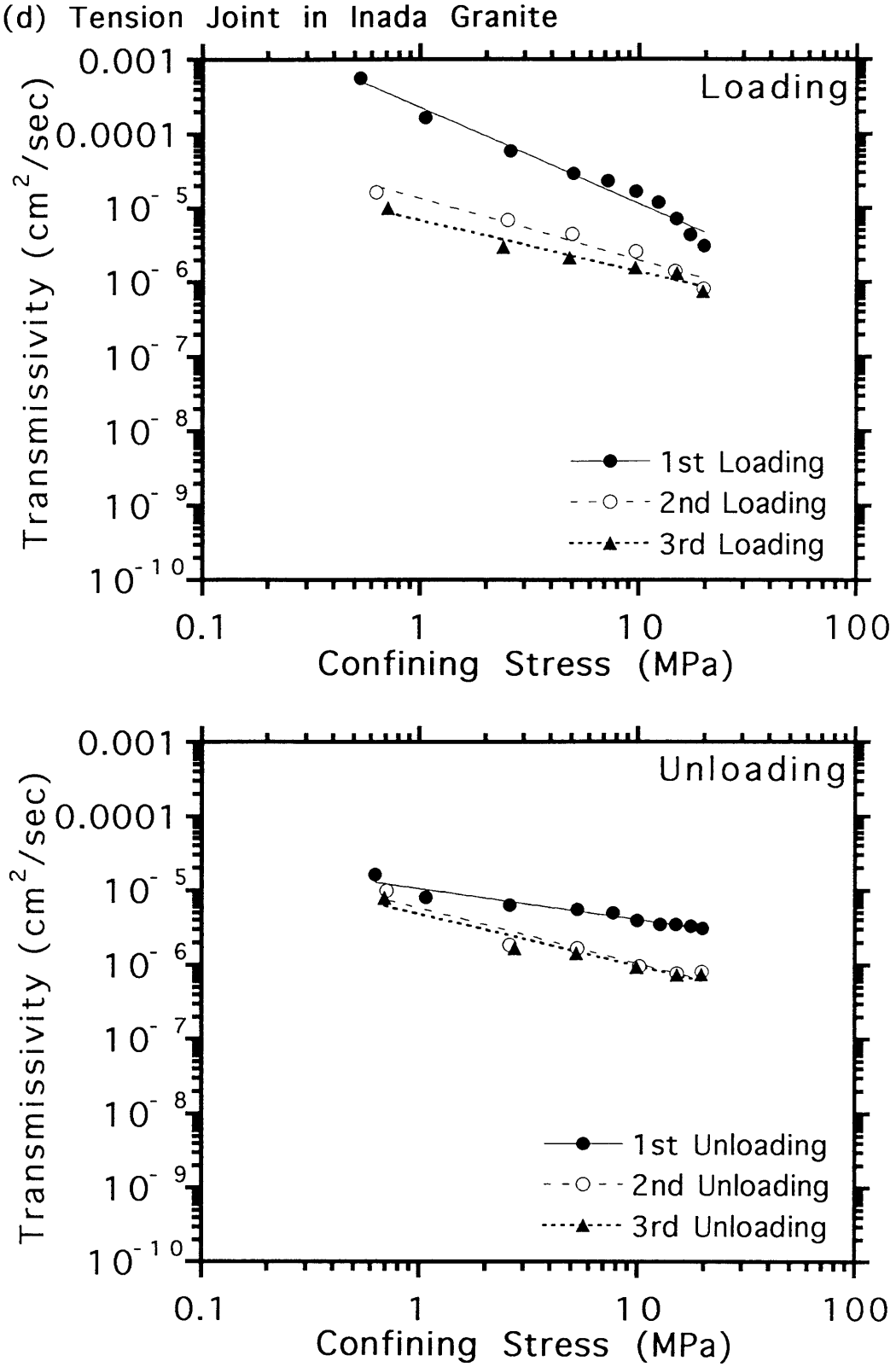

Fig.5.17 Joint transmissivity vs confining stress and results of regression analysis (d)Tension joint in granite

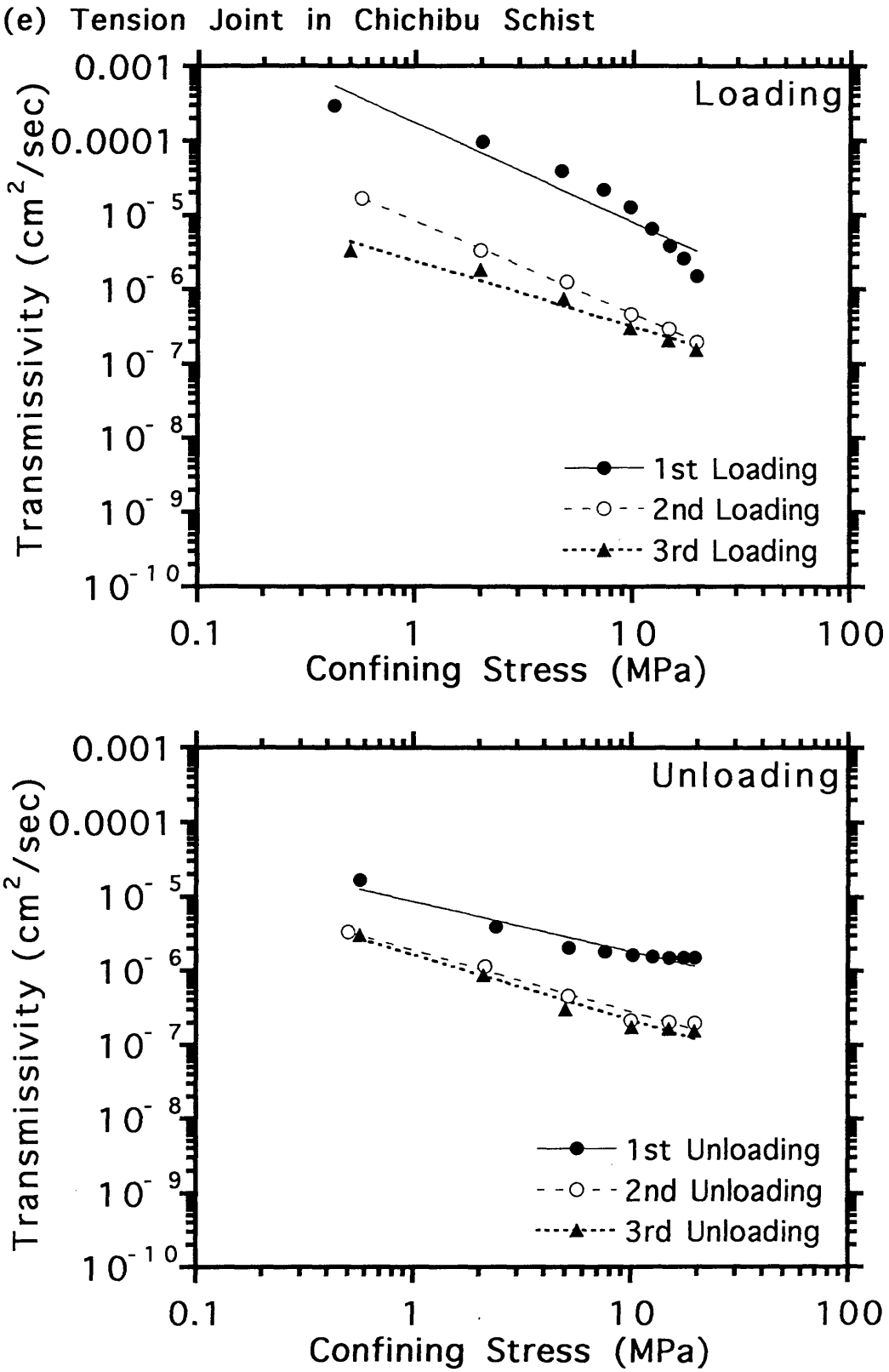

Fig.5.17 Joint transmissivity vs confining stress and results of regression analysis (e)Tension joint in schist

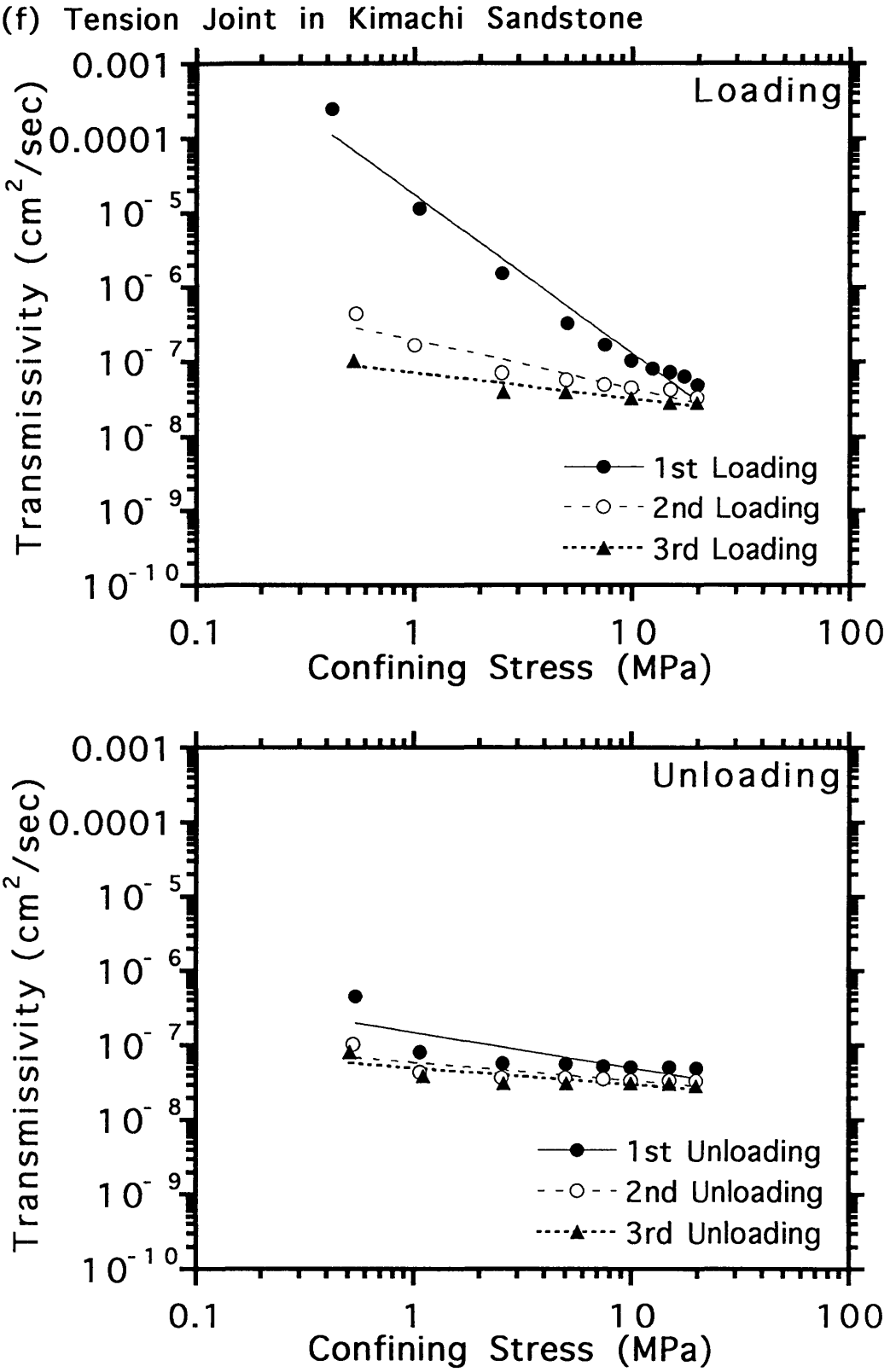

Fig.5.17 Joint transmissivity vs confining stress and results of regression analysis (f)Tension joint in sandstone

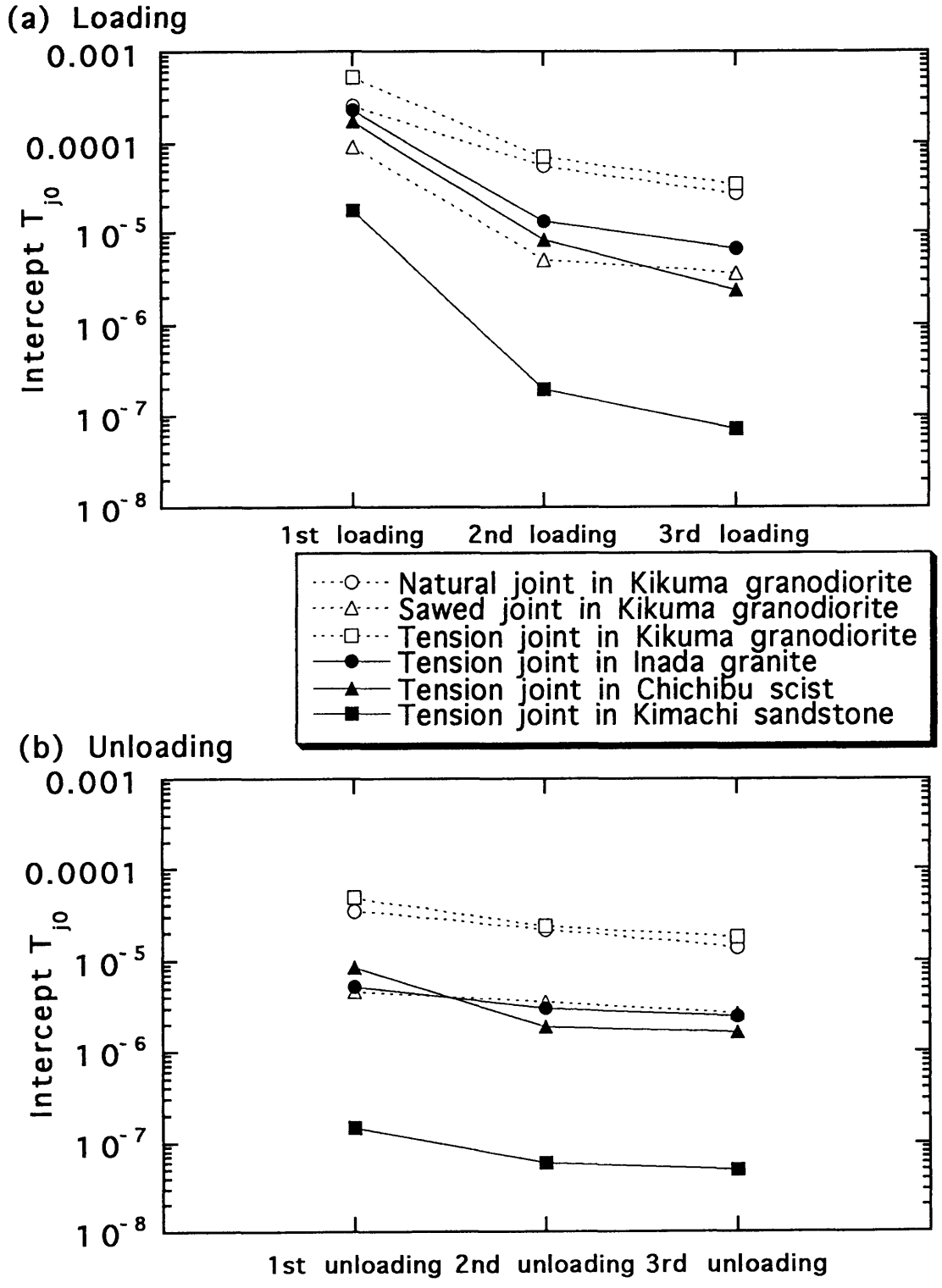

Fig.5.18 Variation of the derived parameters by the regression analysis of joint transmissivity
(a)Intercept T_{j0}

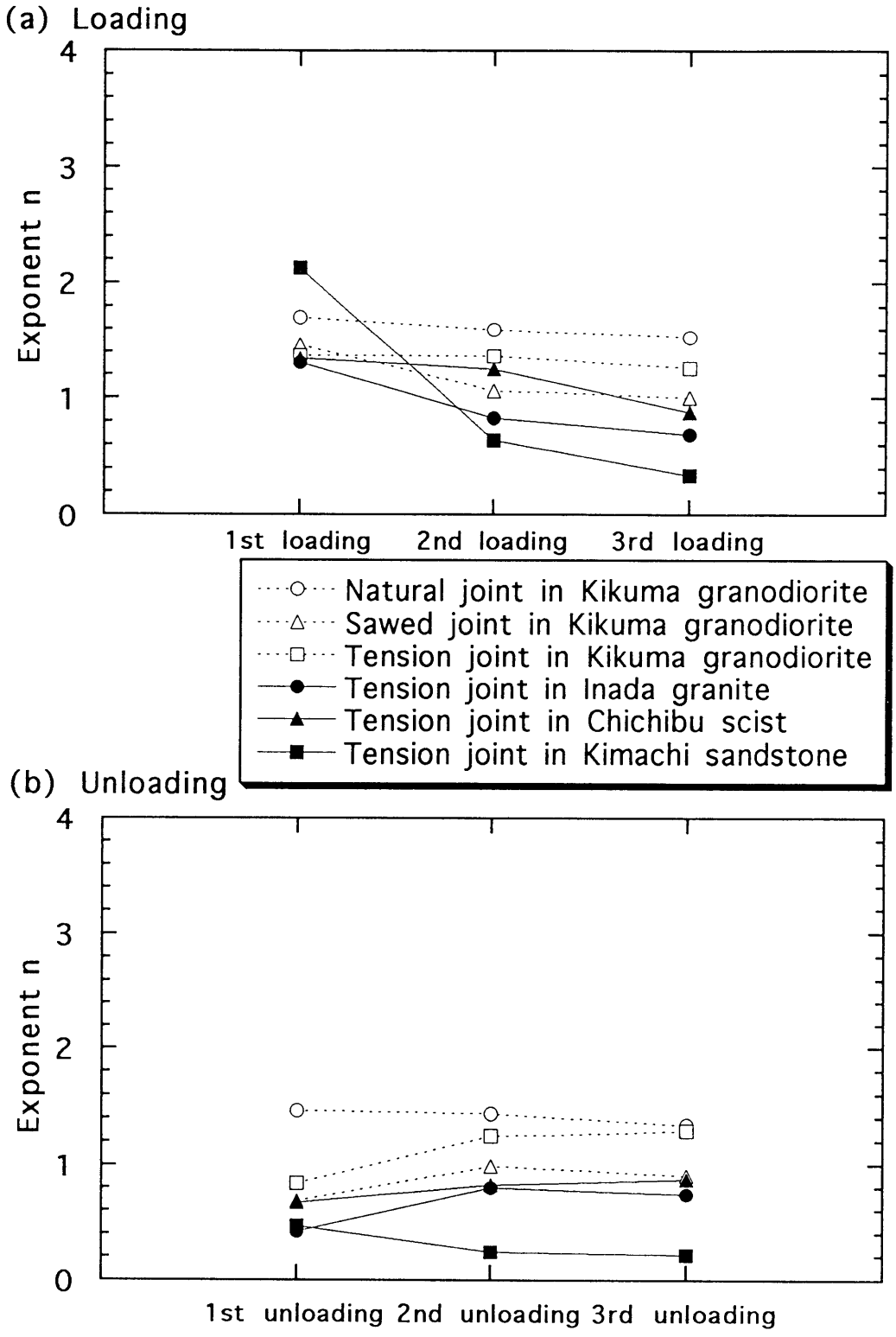

Fig.5.18 Variation of the derived parameters by the regression analysis of joint transmissivity
(b)Exponent n

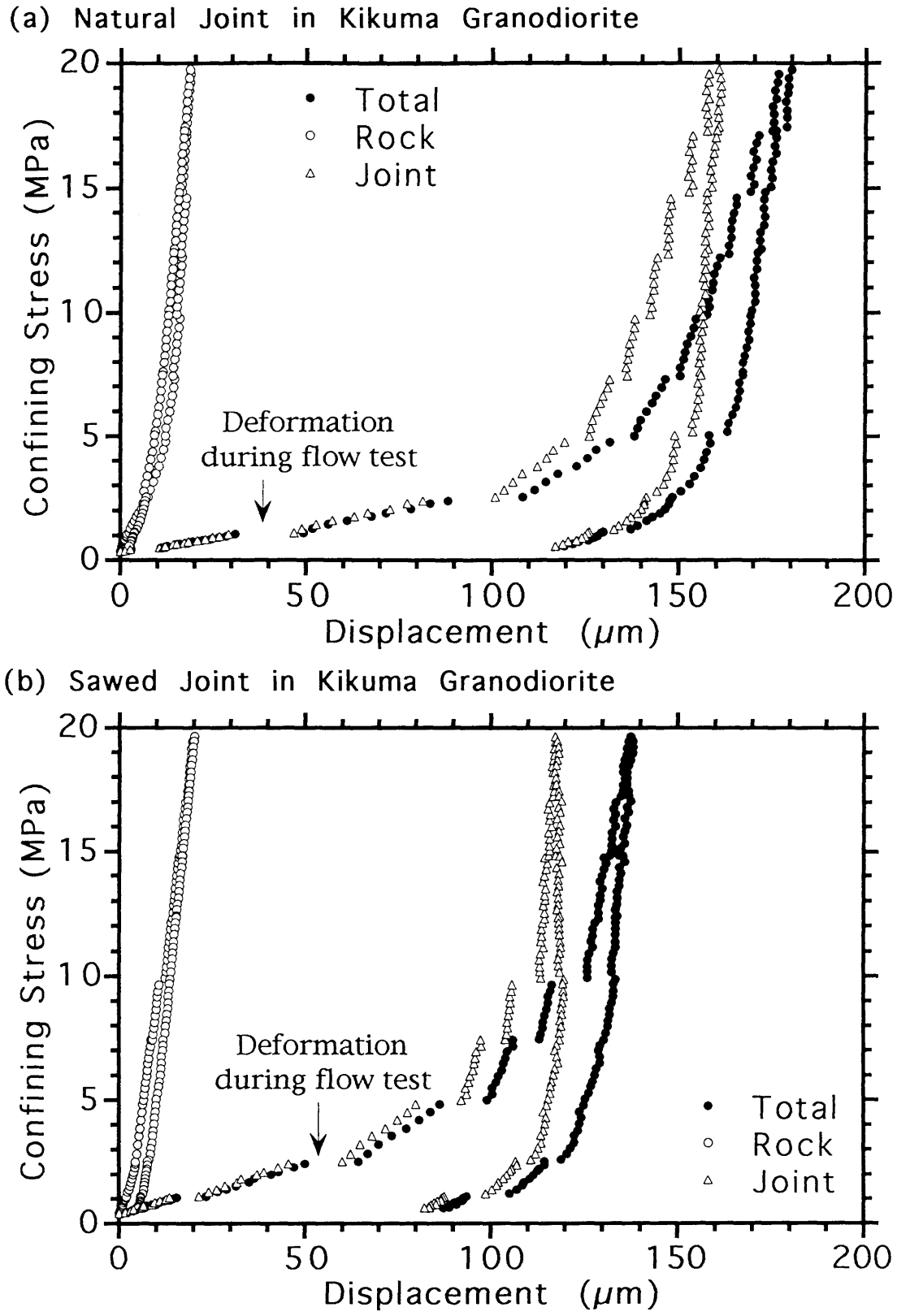

Fig.5.19 Deformation of jointed rock specimen during 1st cyclic

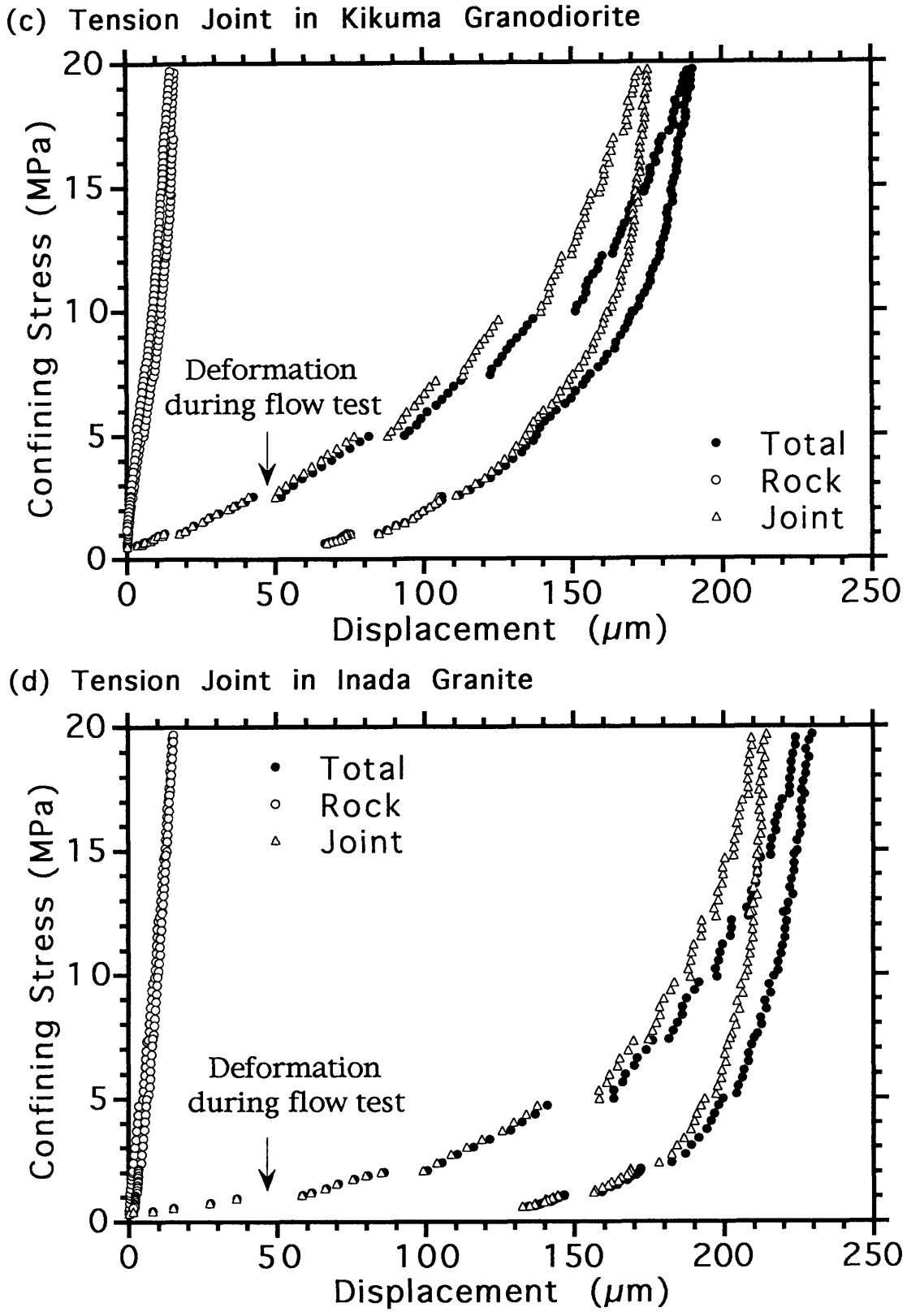

Fig.5.19 Deformation of jointed rock specimen during 1st cyclic

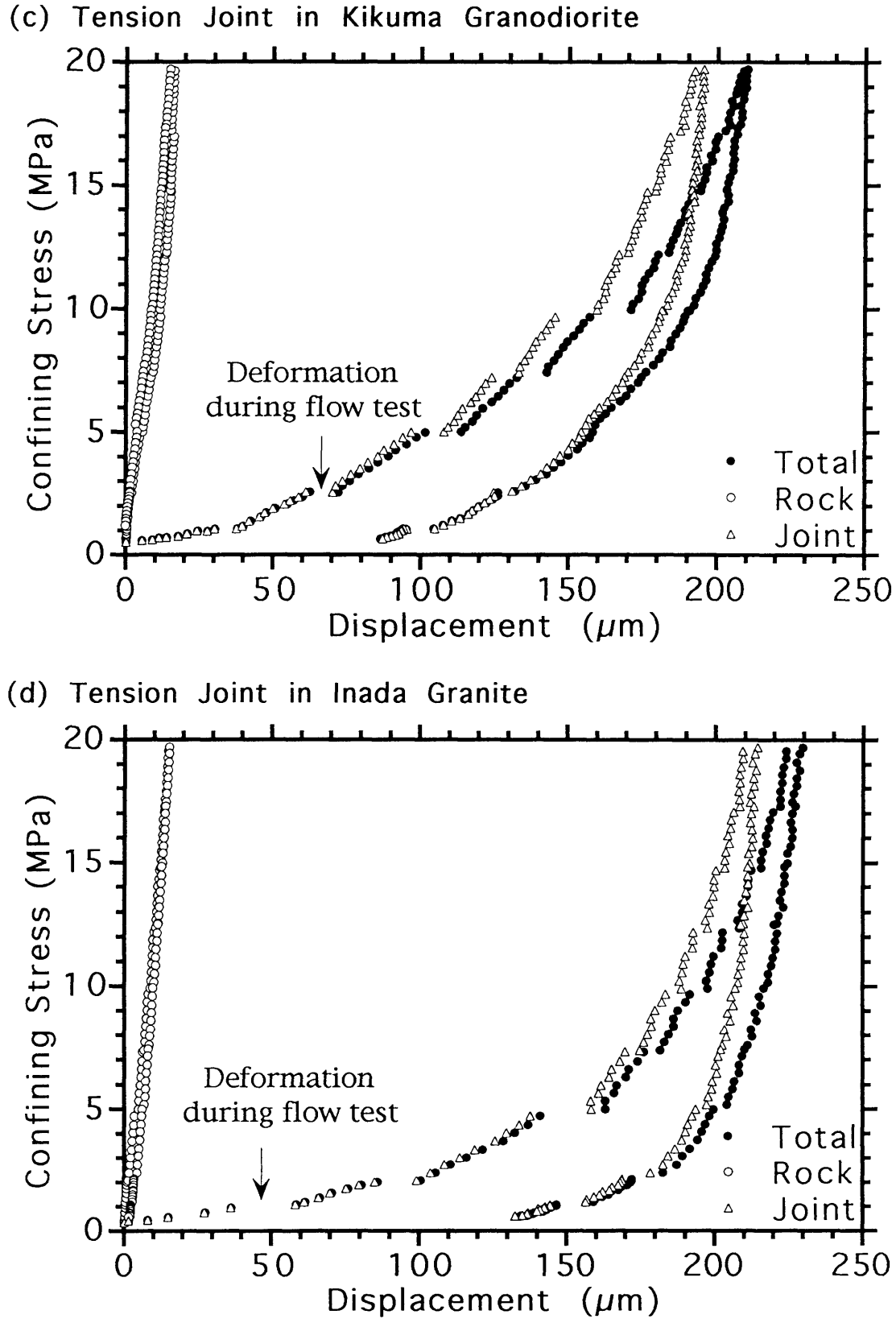

Fig.5.19 Deformation of jointed rock specimen during 1st cyclic

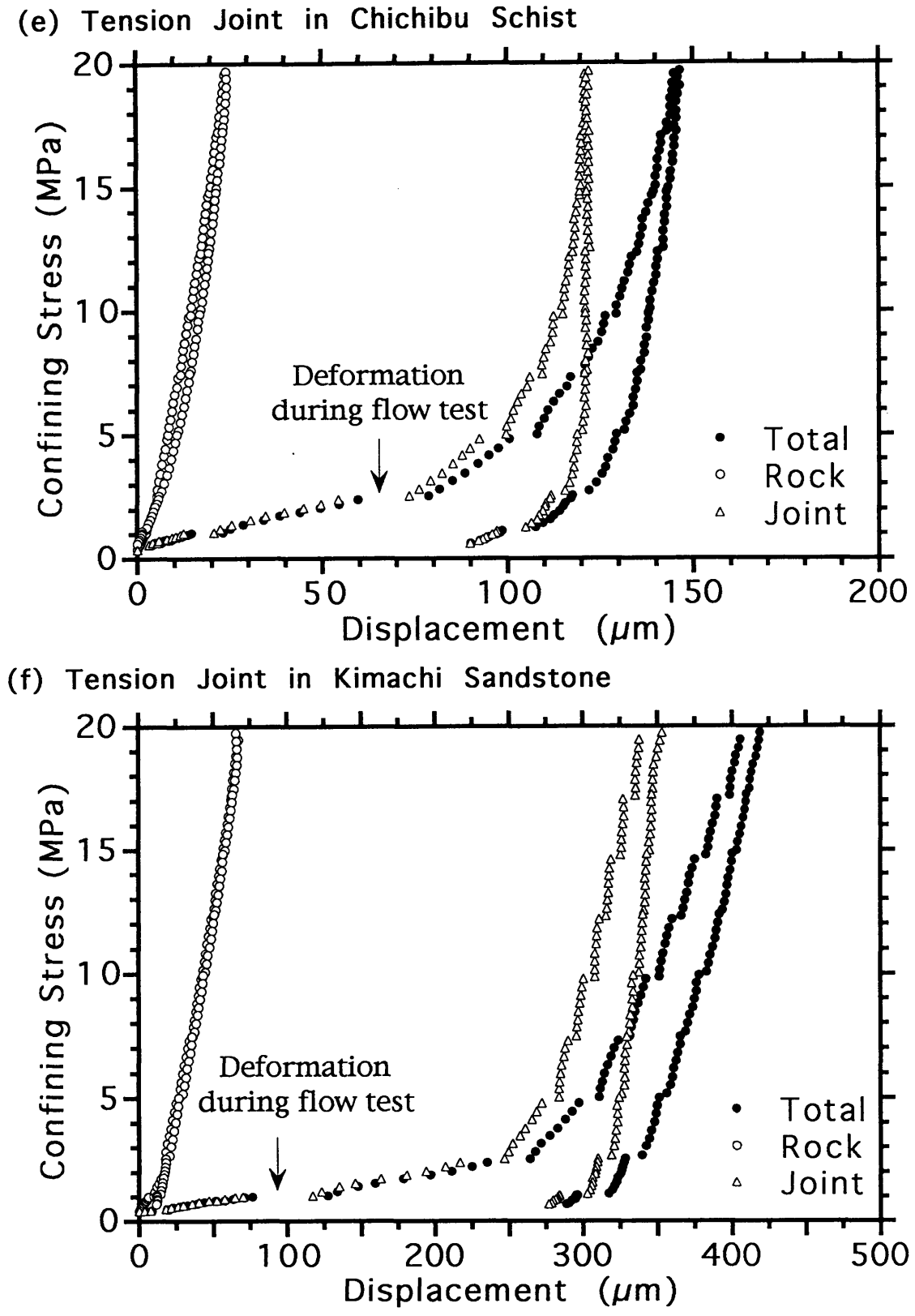

Fig.5.19 Deformation of jointed rock specimen during 1st cyclic

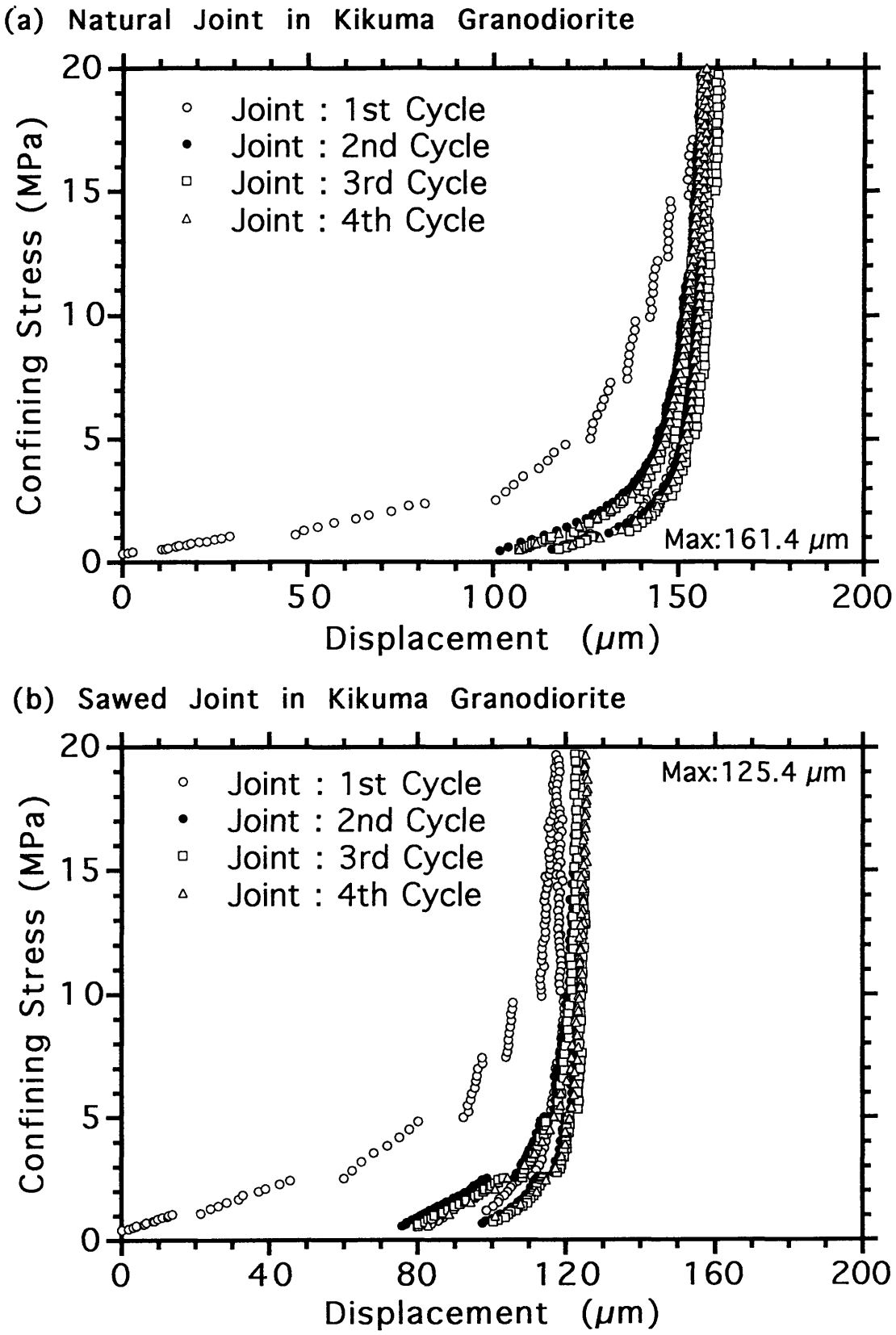

Fig.5.20 Joint deformation during successive cyclic loading and maximum closure

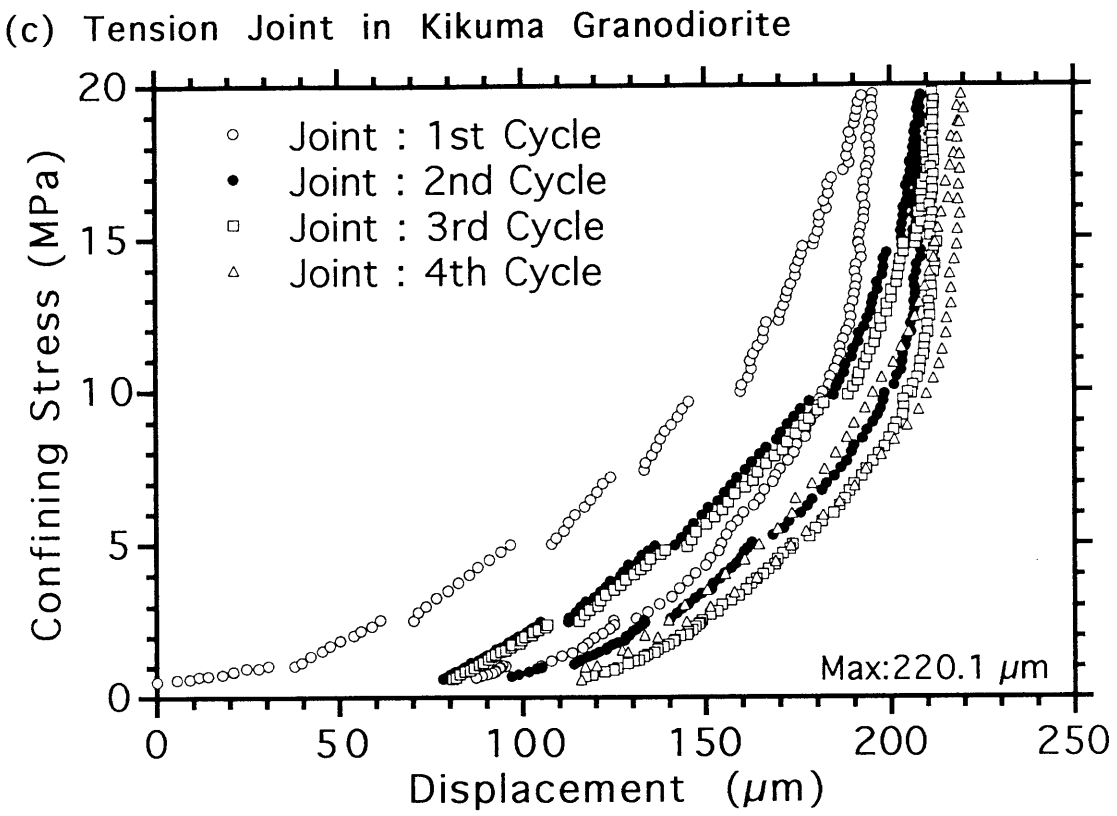

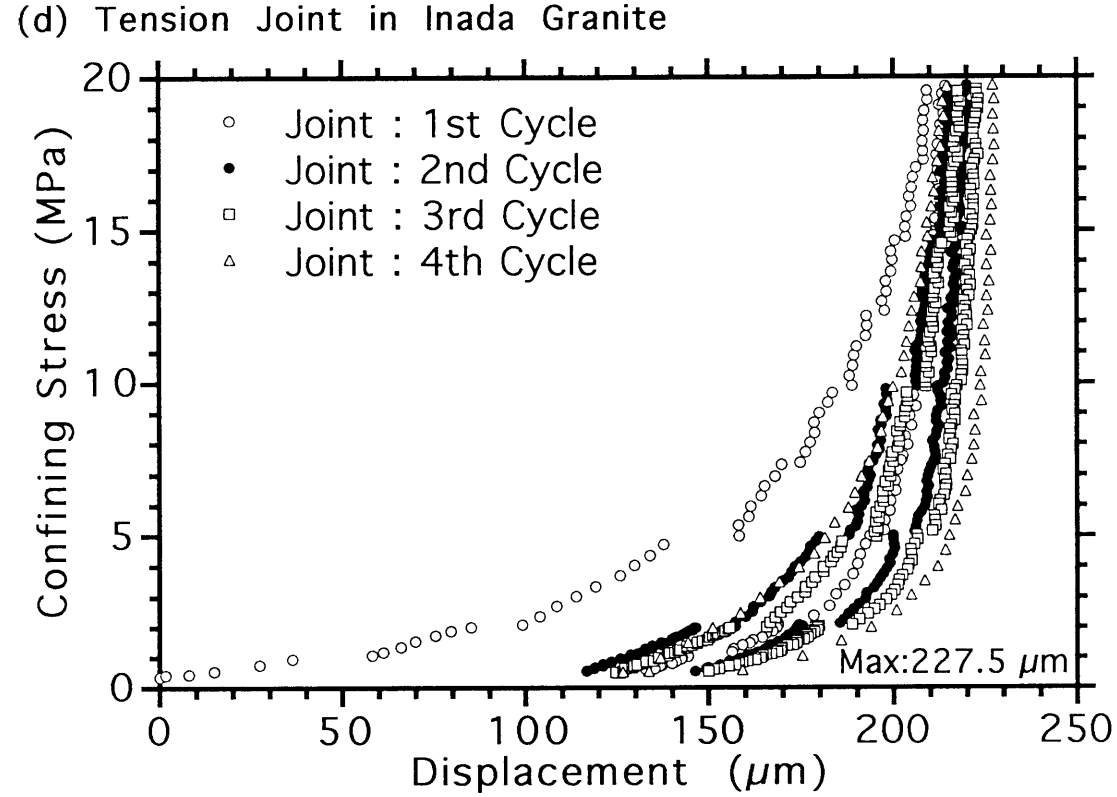

Fig.5.20 Joint deformation during successive cyclic loading and maximum closure

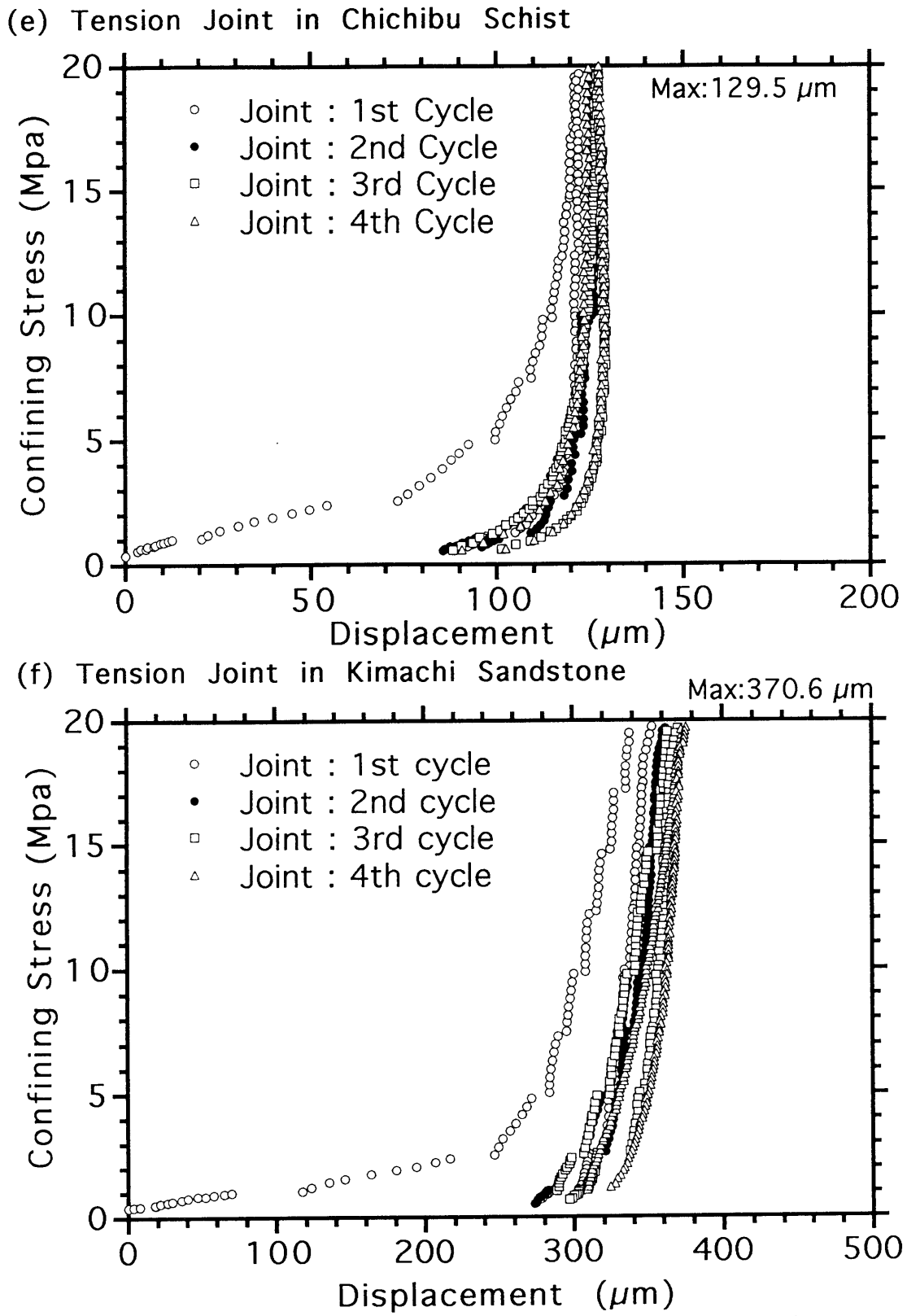

Fig.5.20 Joint deformation during successive cyclic loading and maximum closure

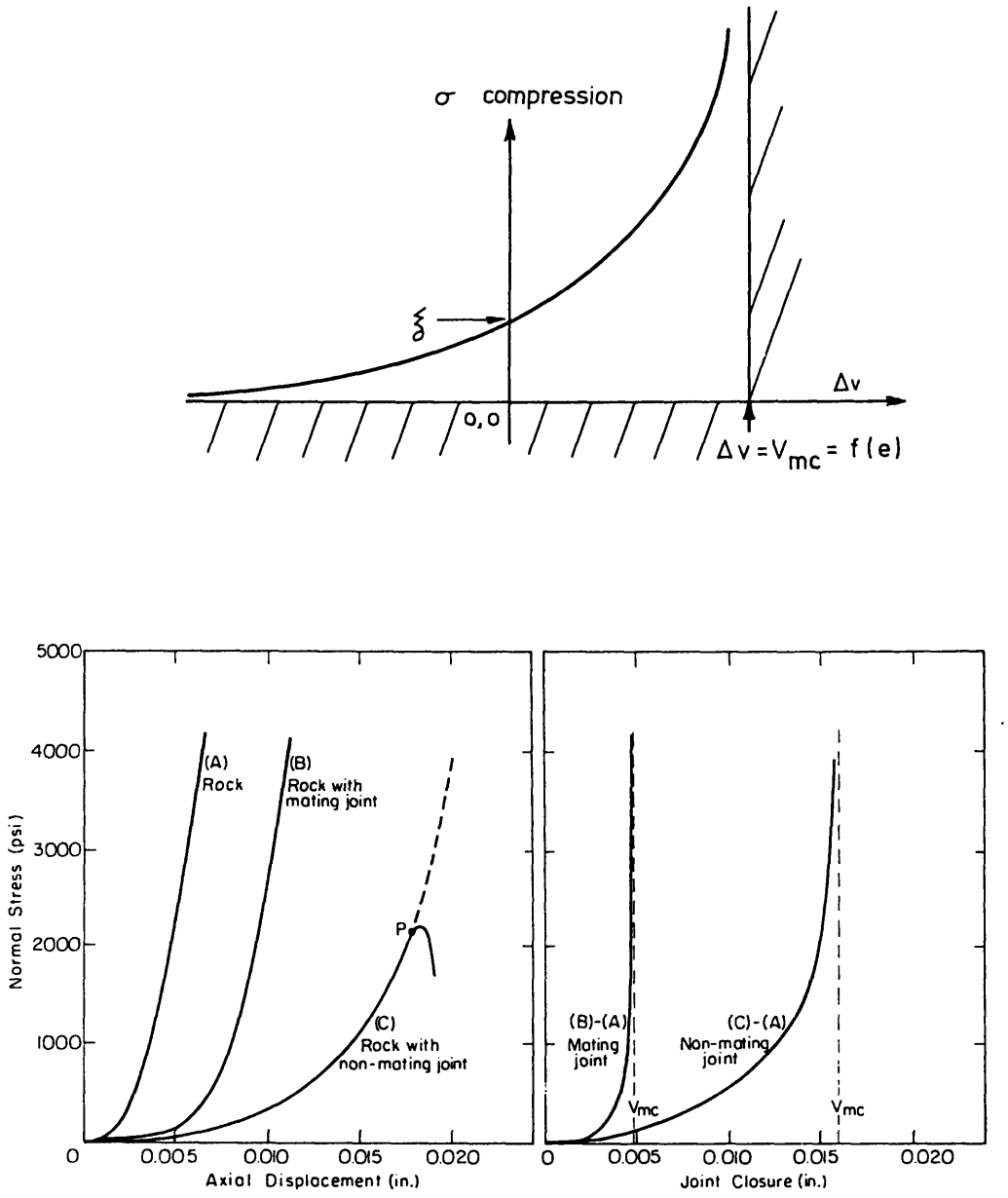

Fig.5.21 Schematic view of joint deformation in compression and normal compression of an extension joint in a granodiorite specimen (after Goodman, 1976)

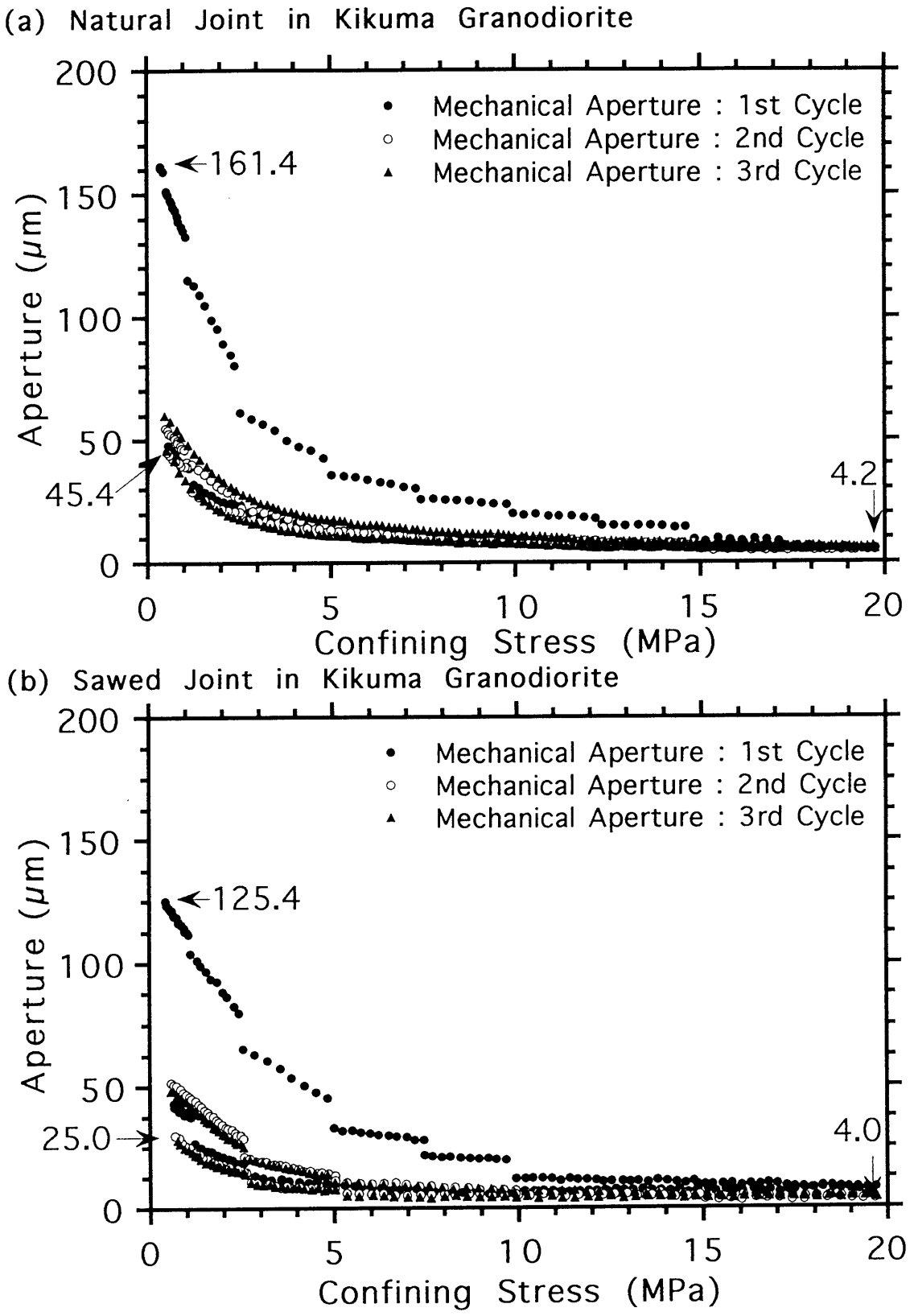

Fig.5.22 Variation of mechanical aperture with confining stress during cyclic loading

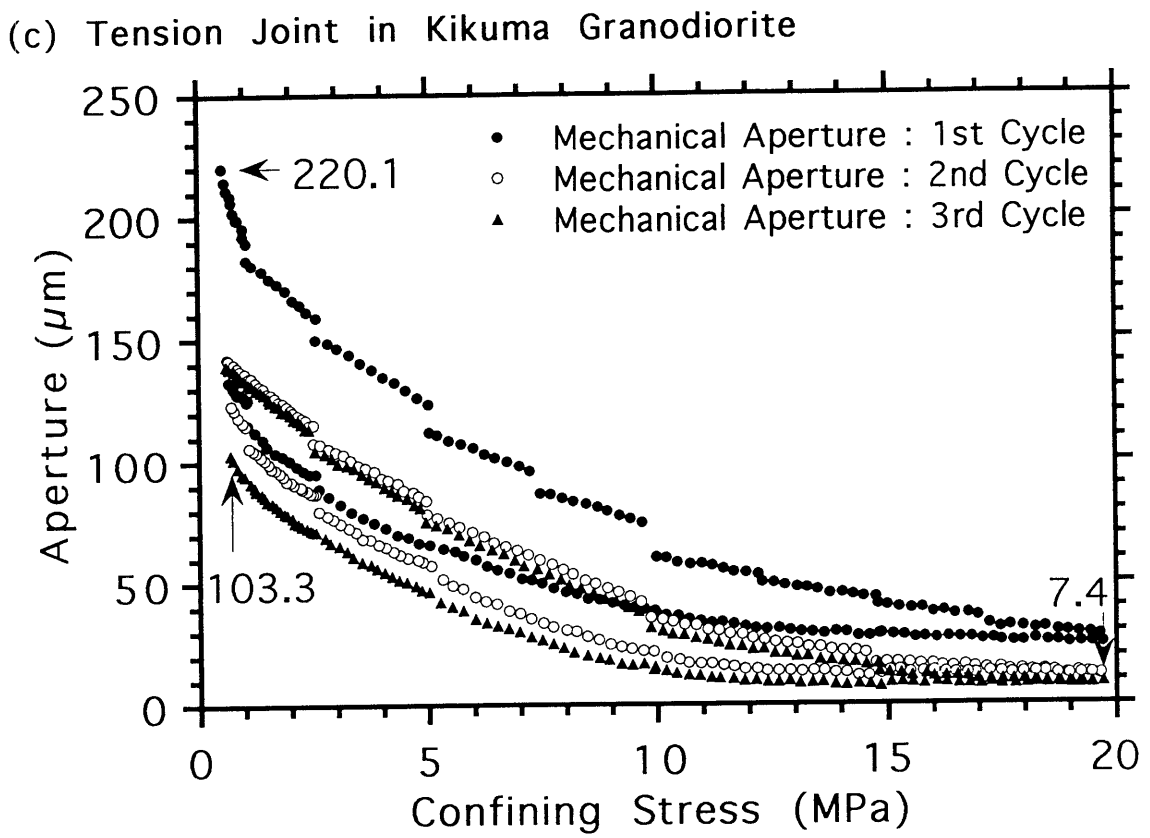

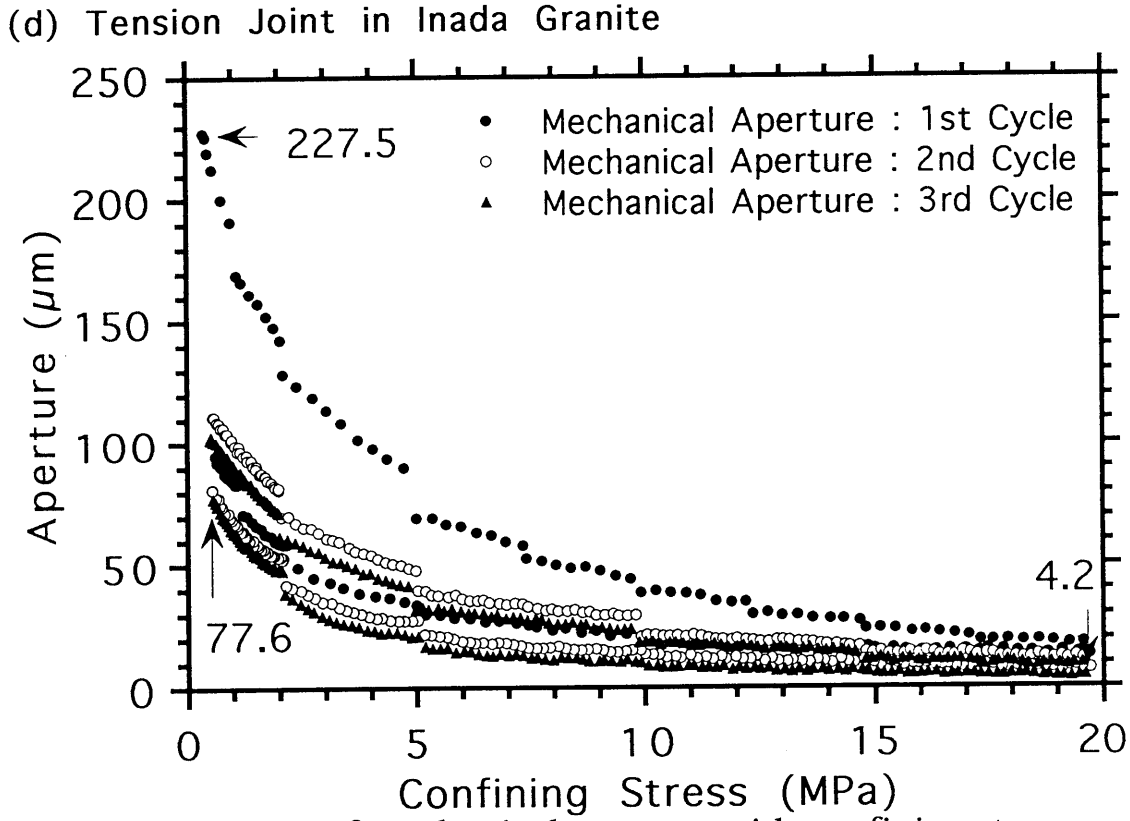

Fig.5.22 Variation of mechanical aperture with confining stress during cyclic loading

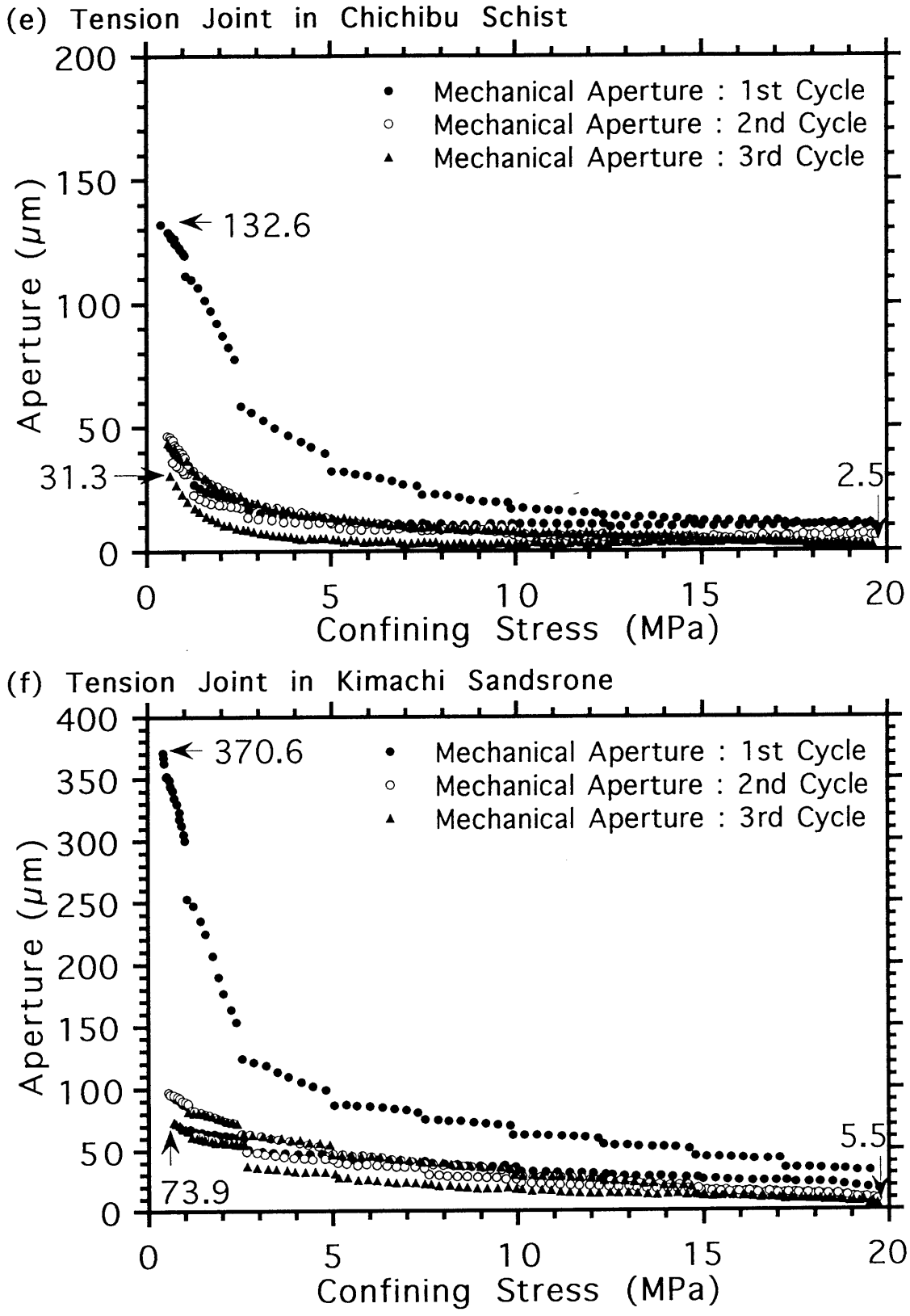

Fig.5.22 Variation of mechanical aperture with confining stress during cyclic loading

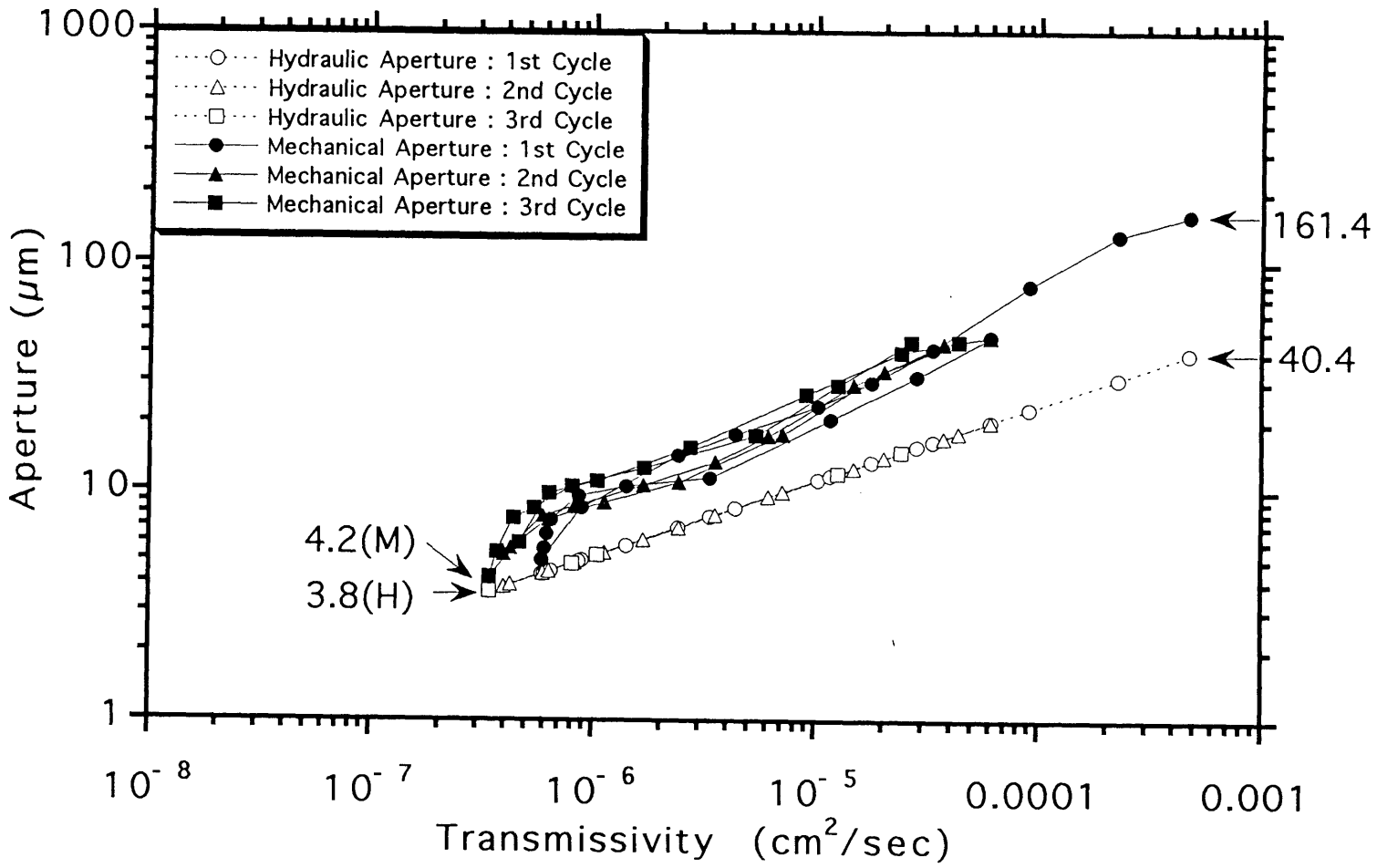

Fig.5.23 Joint aperture versus joint transmissivity
(a) Natural Joint in Kikuma Granodiorite

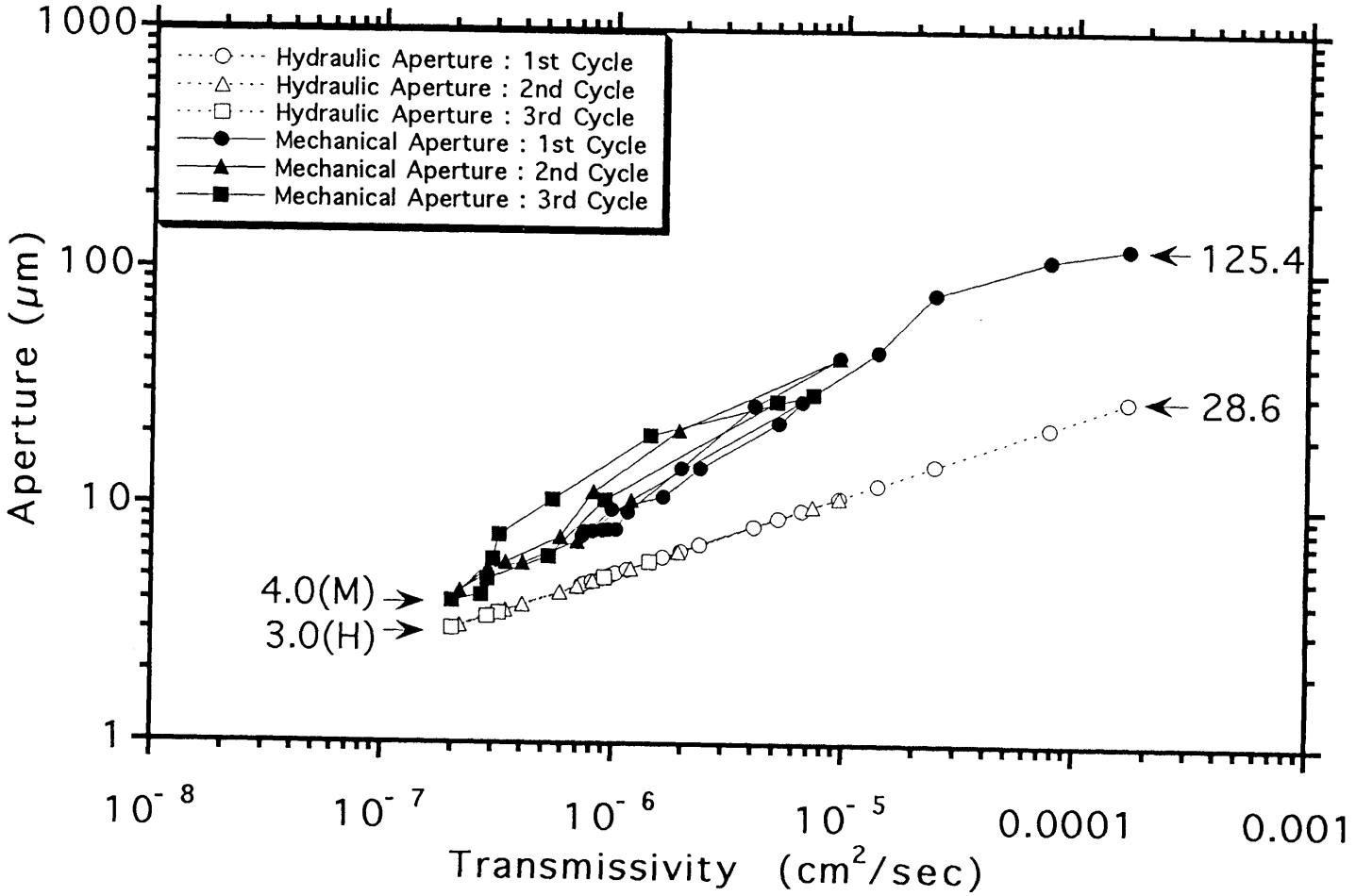

Fig.5.23 Joint aperture versus joint transmissivity
(b) Sawed Joint in Kikuma Granodiorite

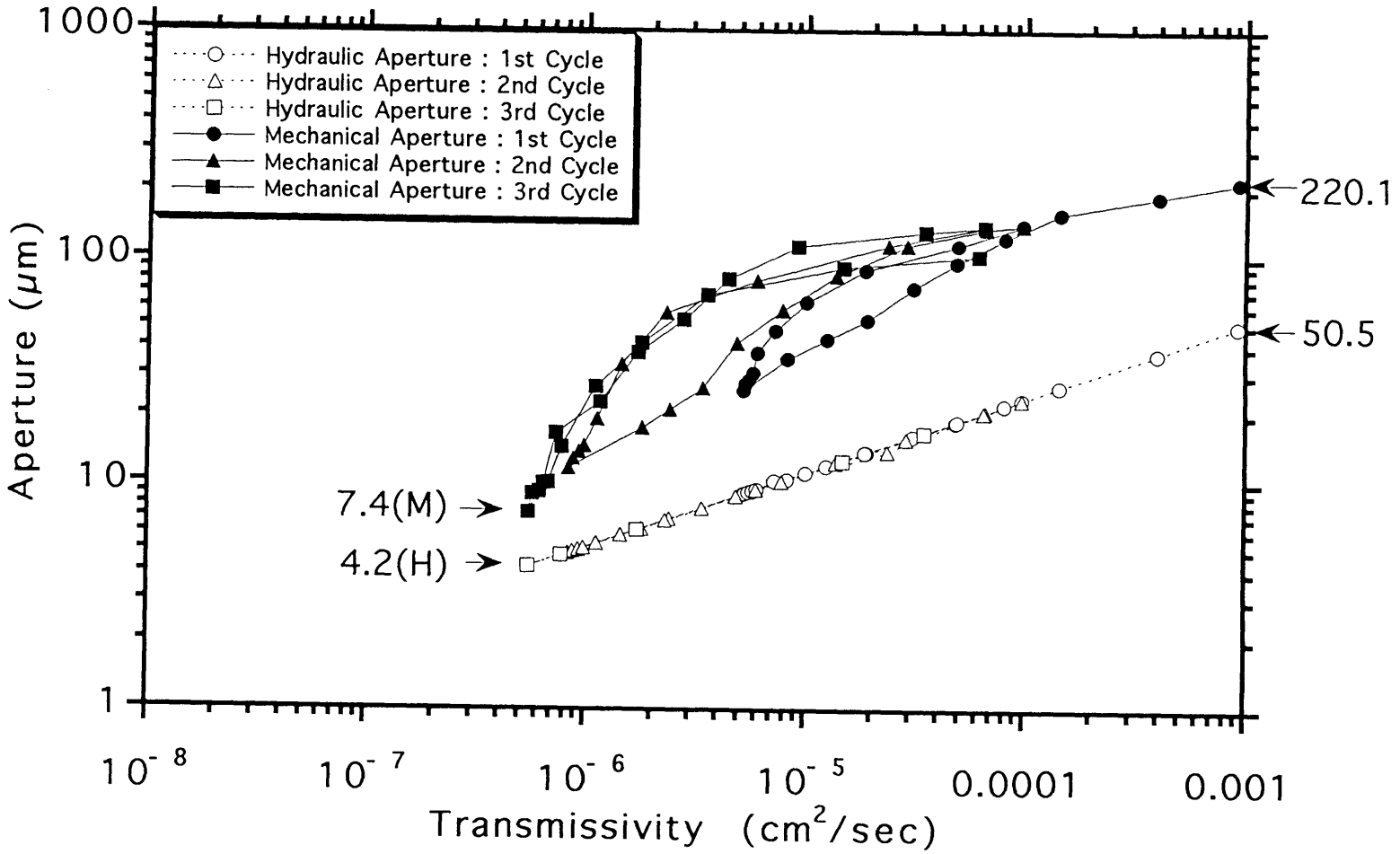

Fig.5.23 Joint aperture versus joint transmissivity
(c) Tension Joint in Kikuma Granodiorite

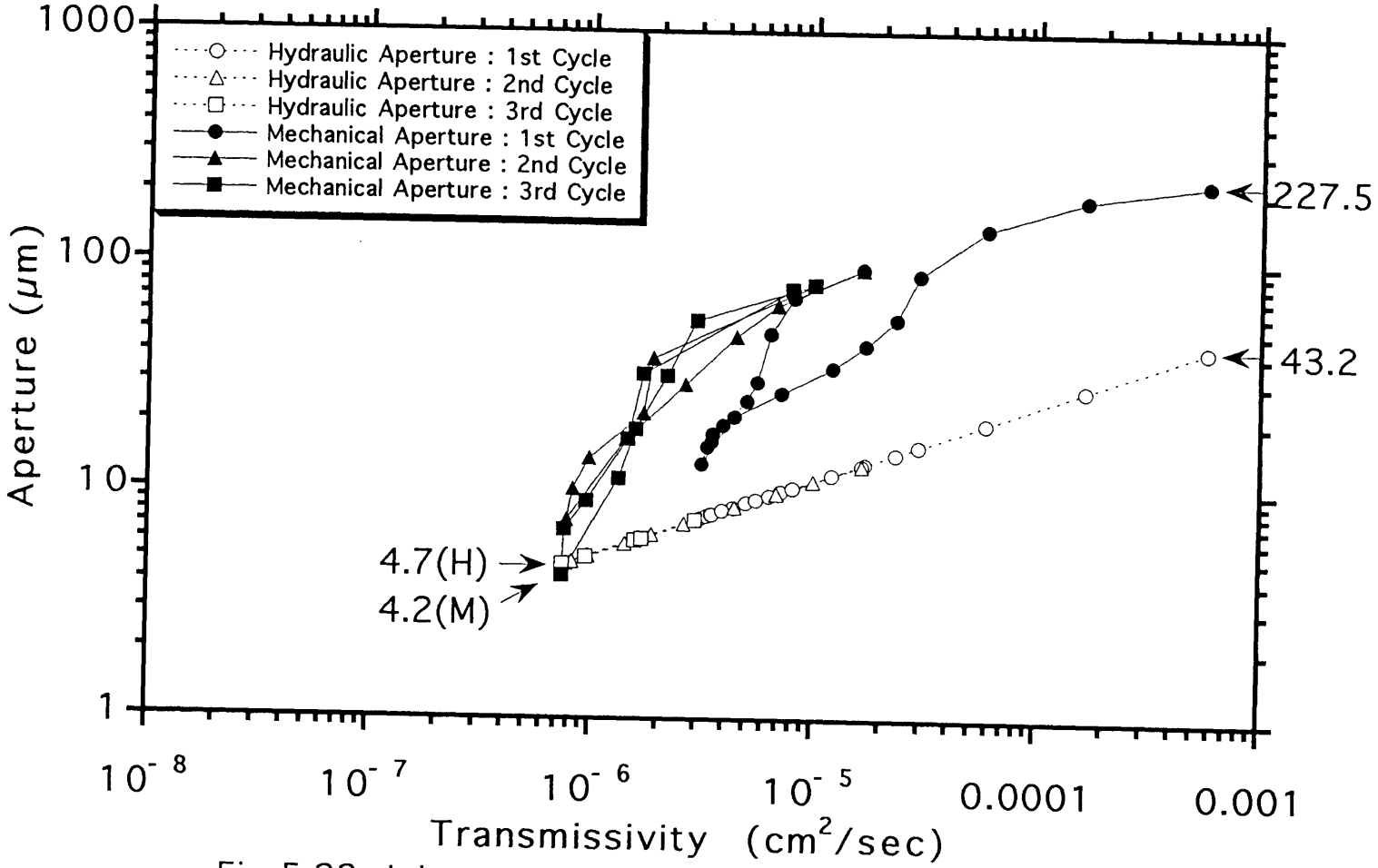

Fig.5.23 Joint aperture versus joint transmissivity
(d) Tension Joint in Inada Granite

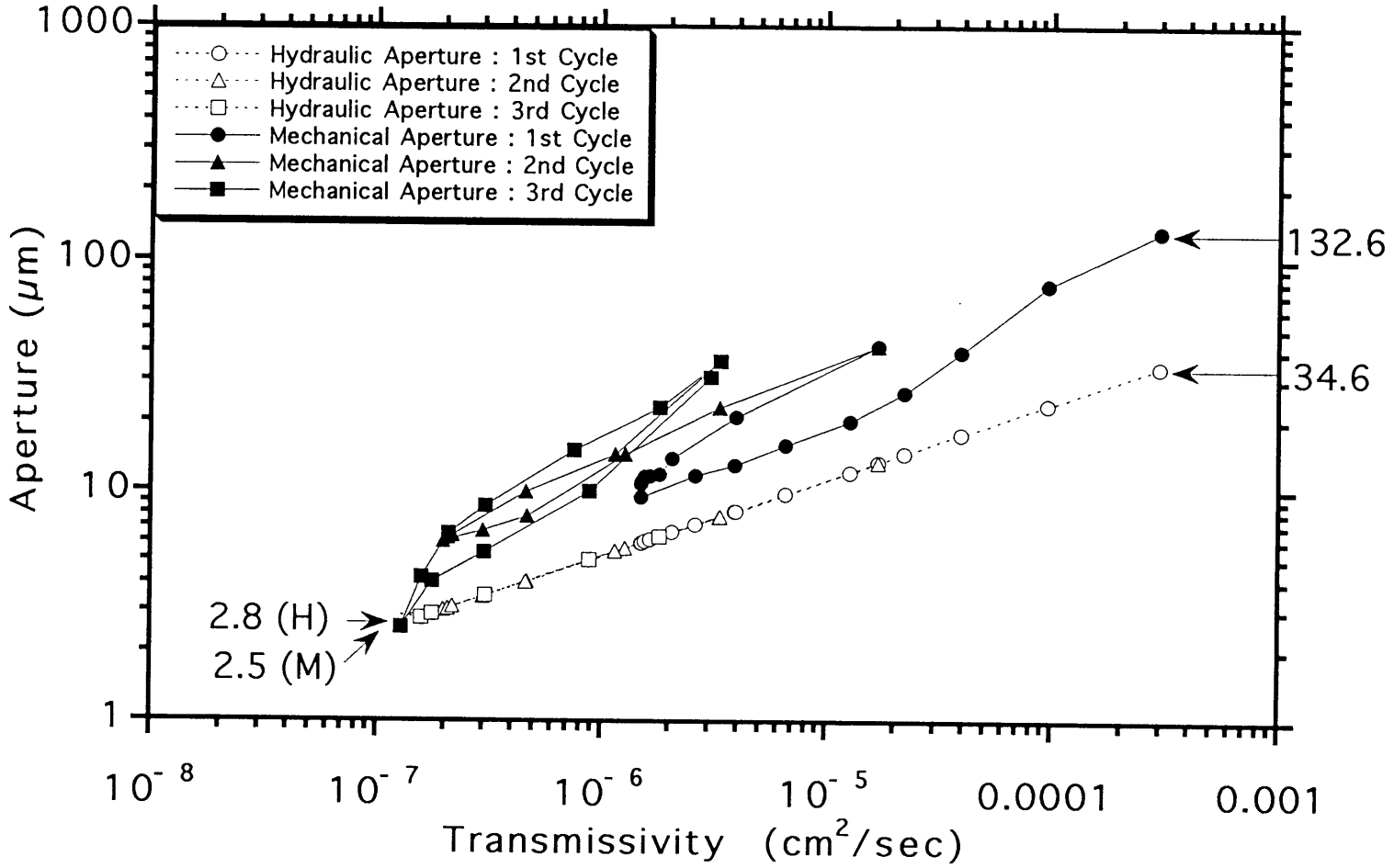

Fig.5.23 Joint aperture versus joint transmissivity
(e) Tension Joint in Chichibu Schist

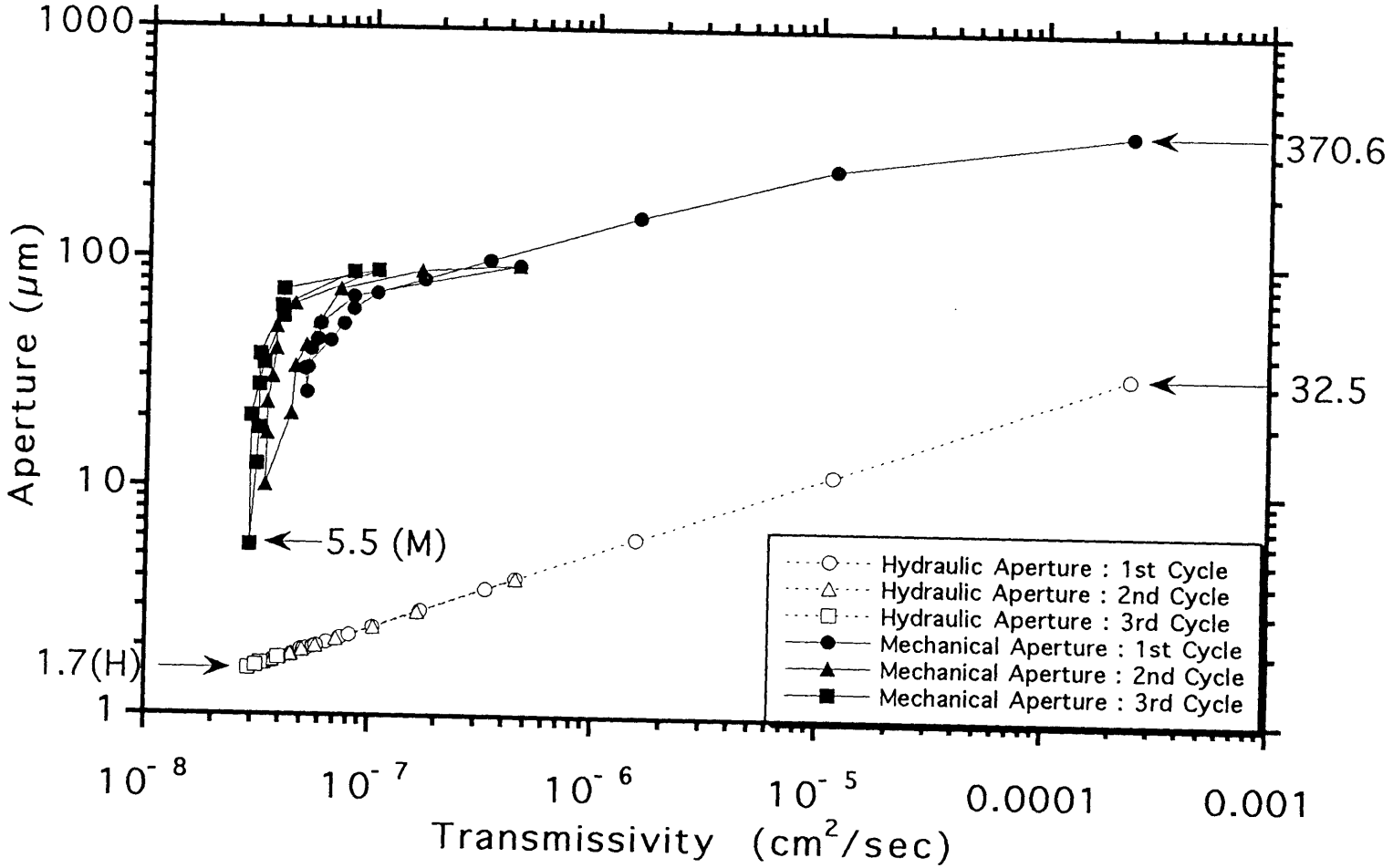

Fig.5.23 Joint aperture versus joint transmissivity
(f) Tension Joint in Kimachi Sandstone

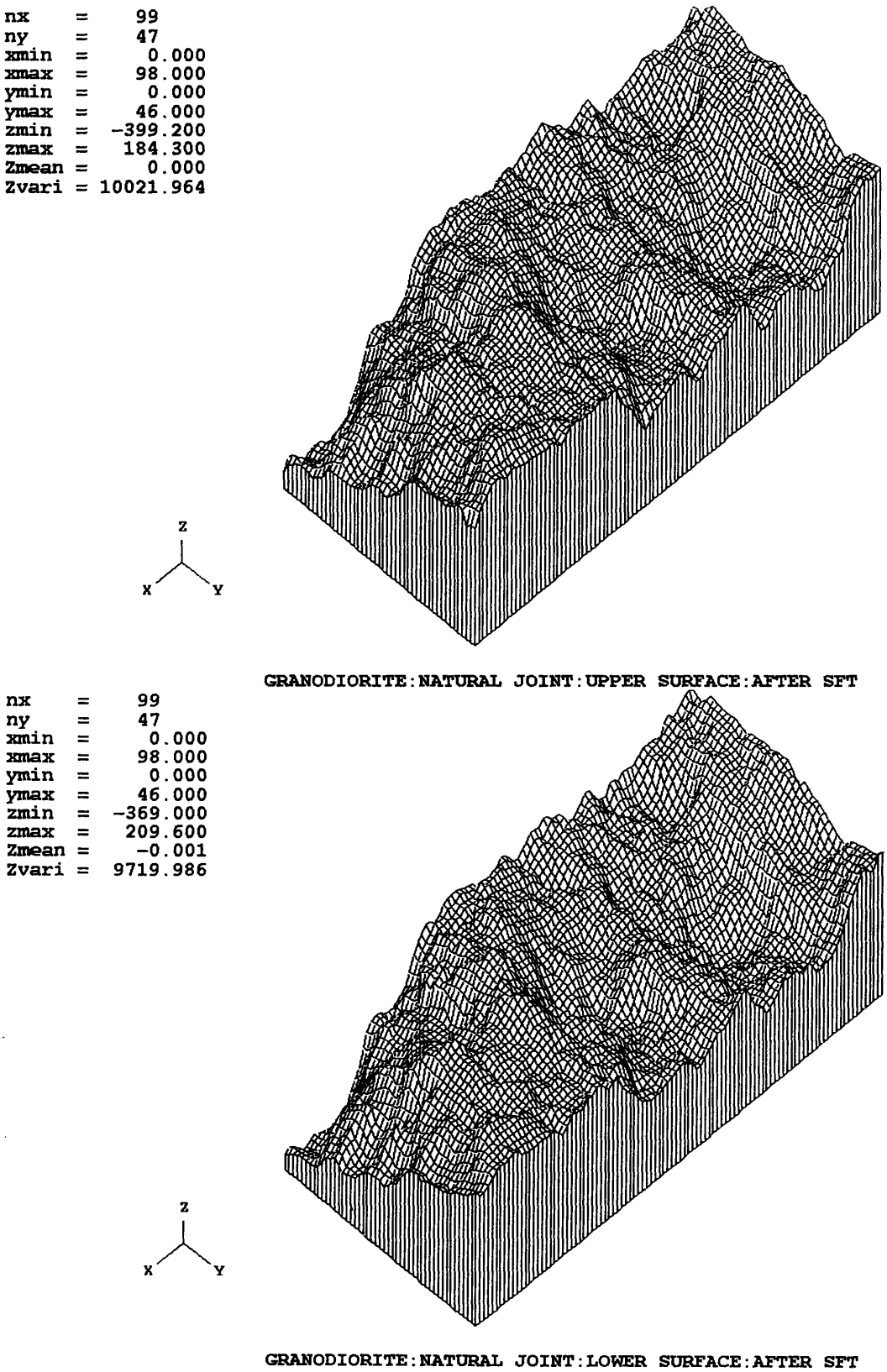

Fig. 5.24 Two digitized surfaces of a joint after stress-flow test
(a) Natural joint in Kikuma granodiorite

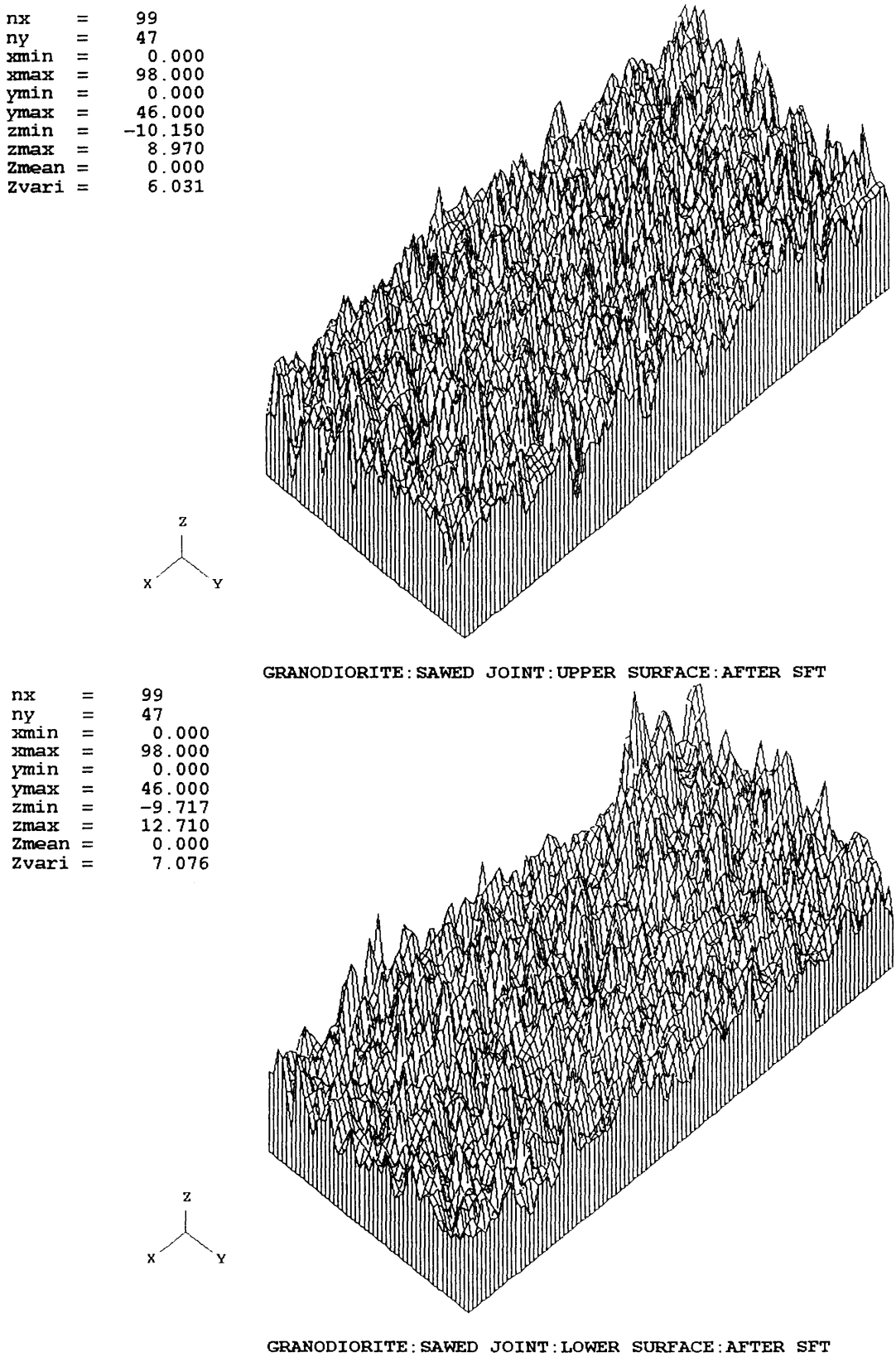

Fig. 5.24 Two digitized surfaces of a joint after stress-flow test
(b) Sawed joint in Kikuma granodiorite

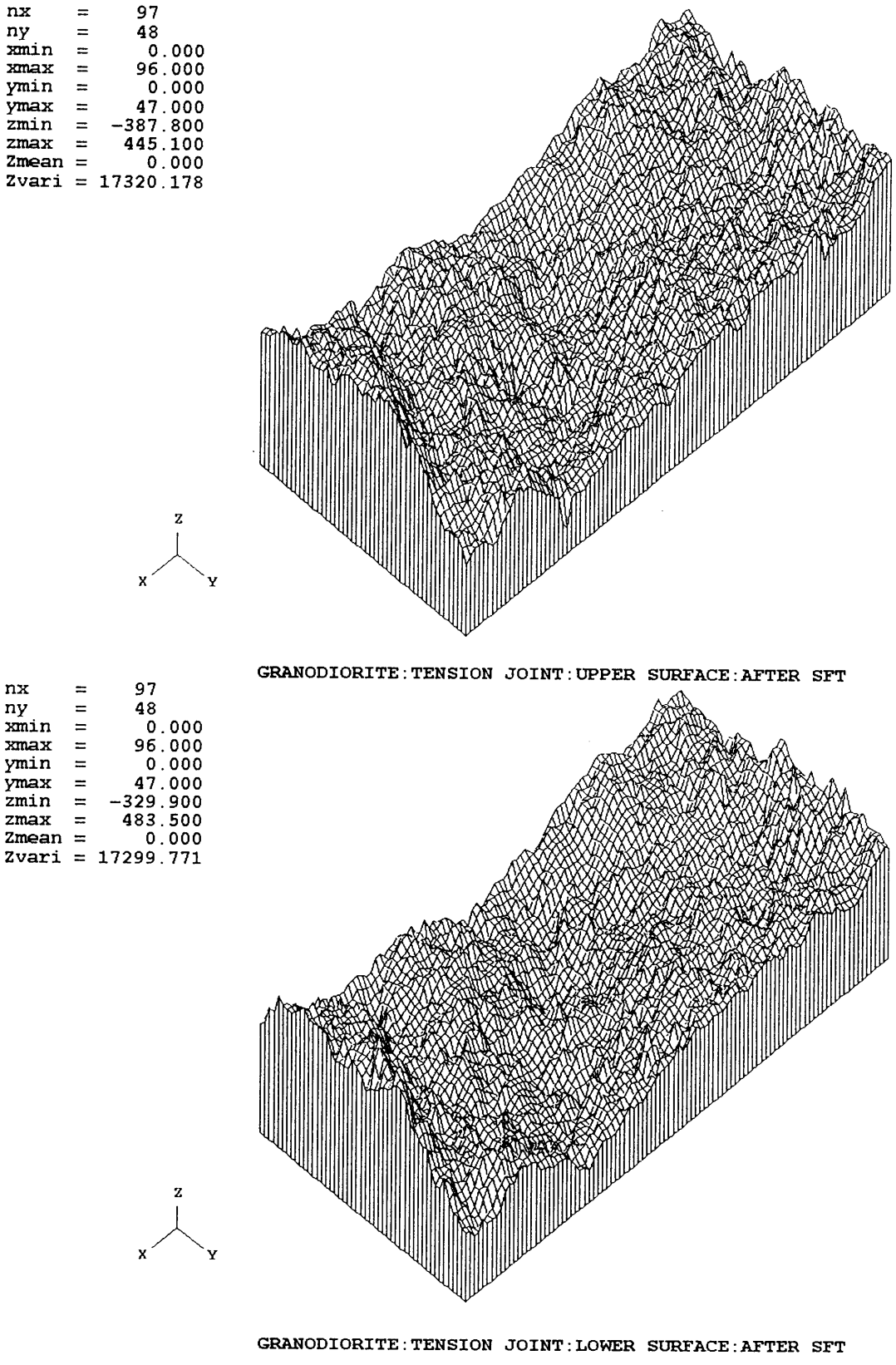

Fig. 5.24 Two digitized surfaces of a joint after stress-flow test
(c) Tension joint in Kikuma granodiorite

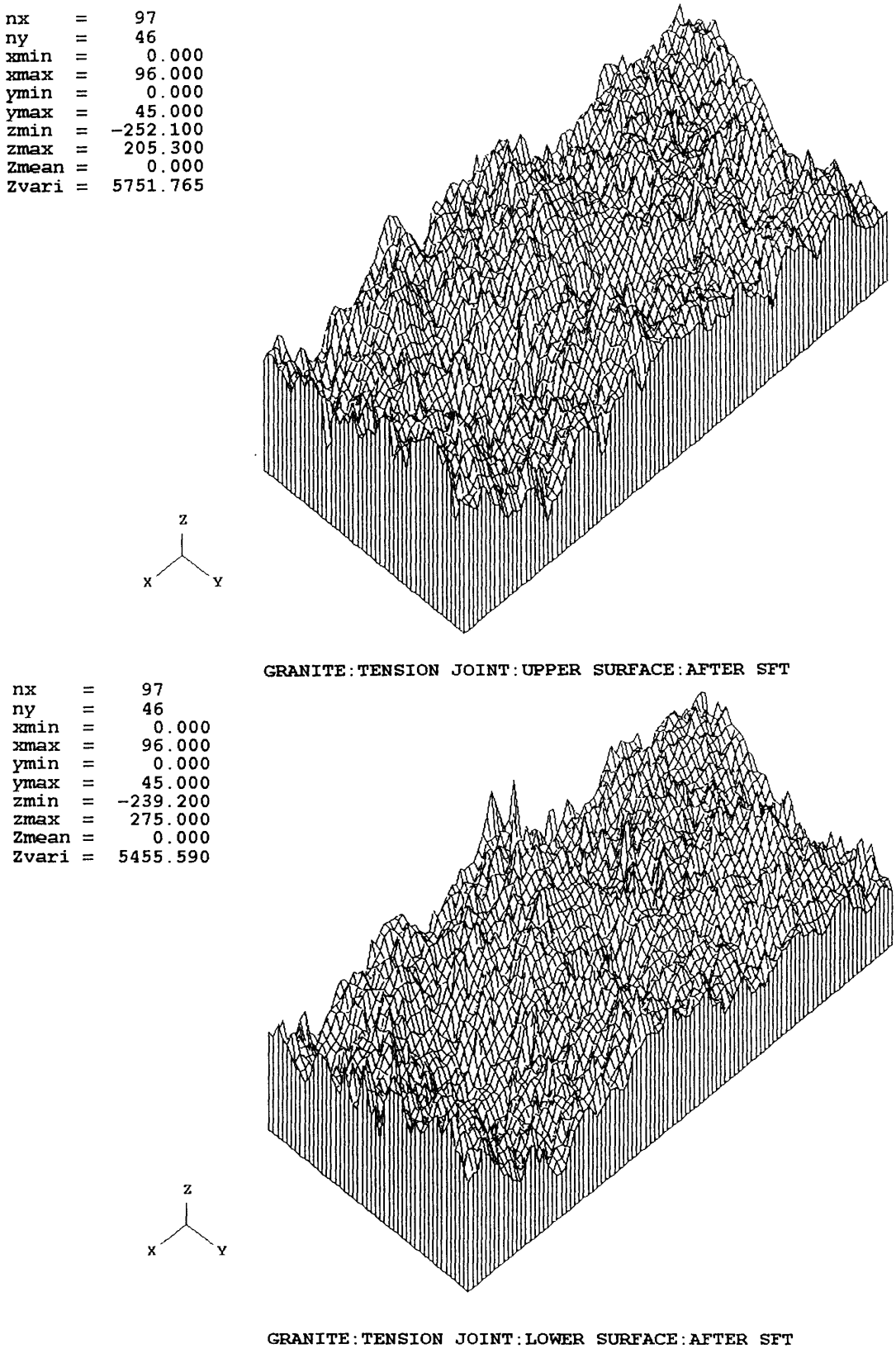

Fig. 5.24 Two digitized surfaces of a joint after stress-flow test
(d) Tension joint in Inada granite

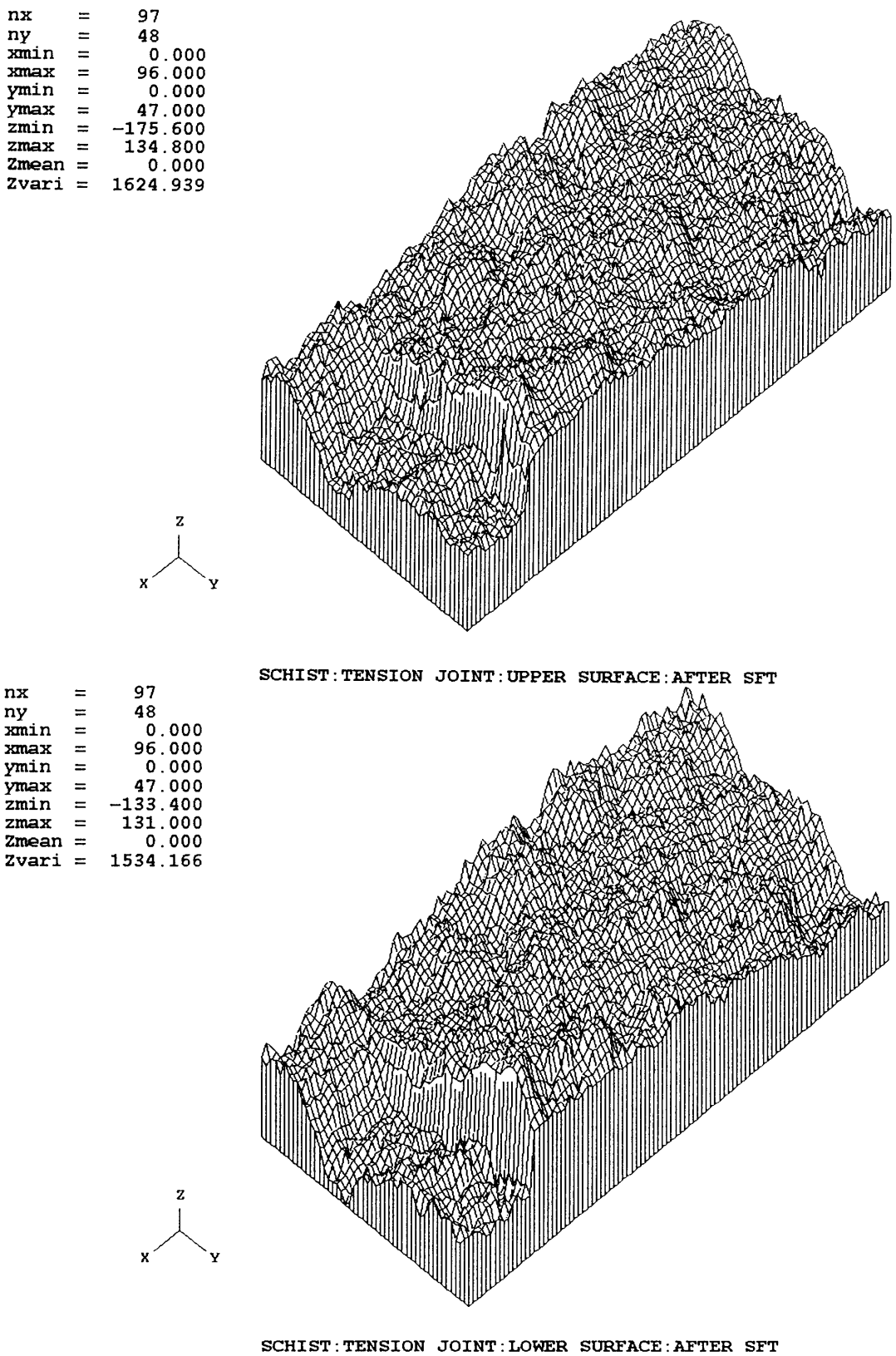

Fig. 5.24 Two digitized surfaces of a joint after stress-flow test
(e) Tension joint in Chichibu schist

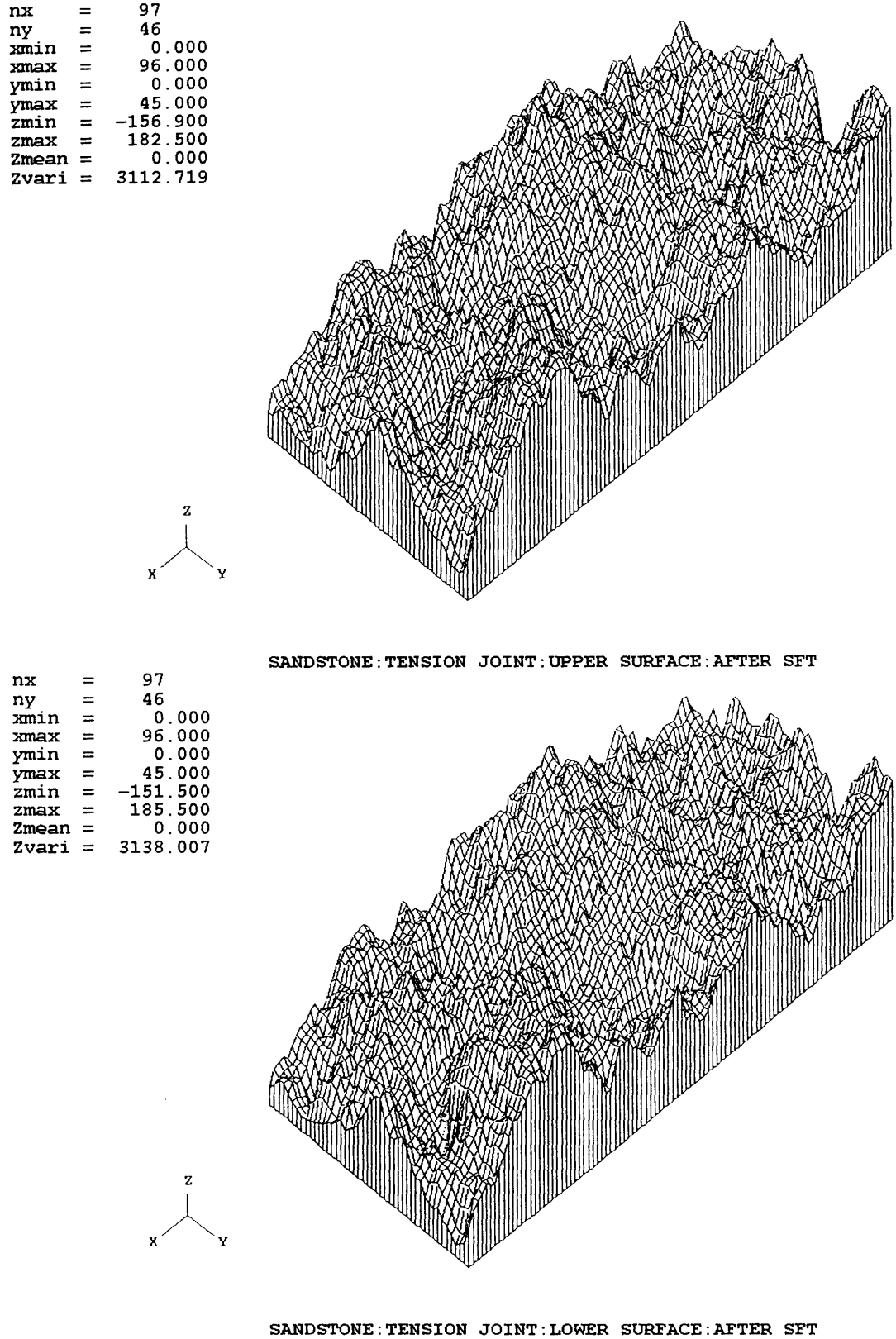

Fig. 5.24 Two digitized surfaces of a joint after stress-flow test
(f) Tension joint in Kimachi sandstone

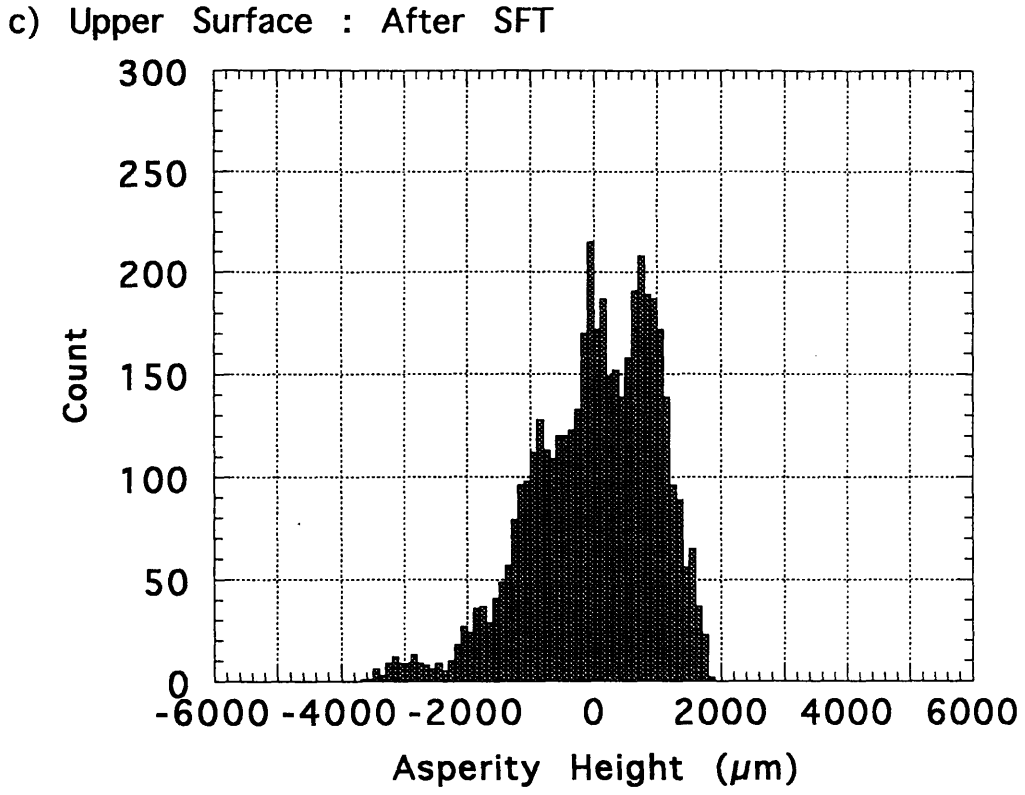

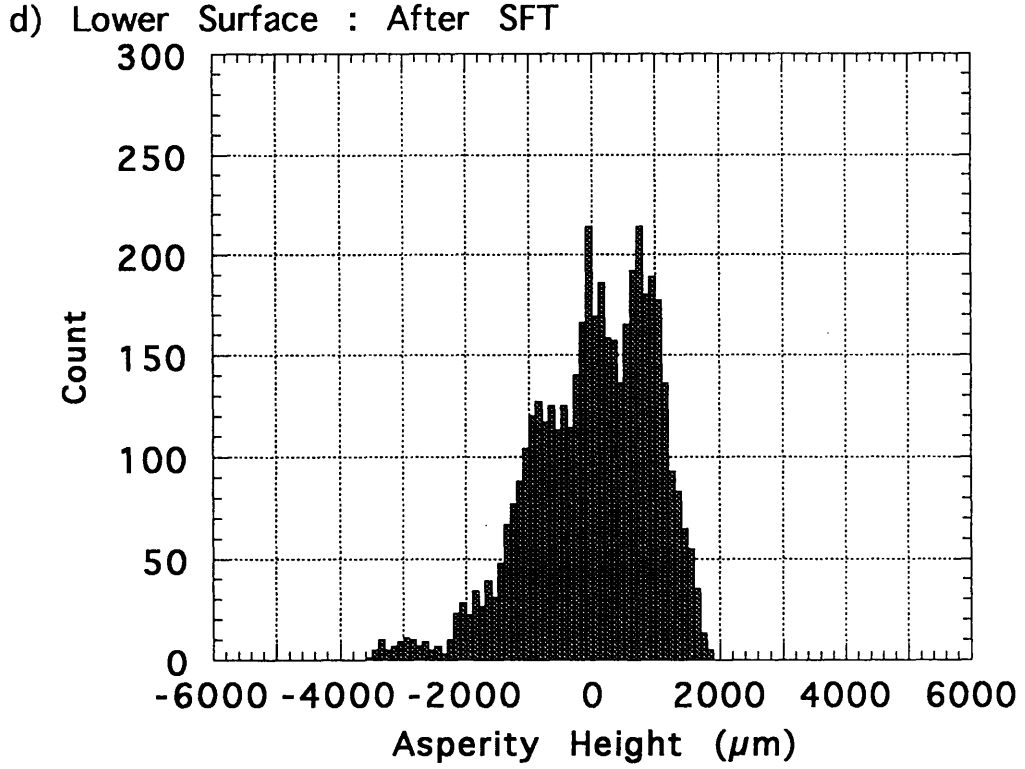

Fig.5.25 Histogram plot for asperities of two digitized surfaces after stress-flow test
(a) Natural joint in Kikuma granodiorite

c) Upper Surface : After SFT

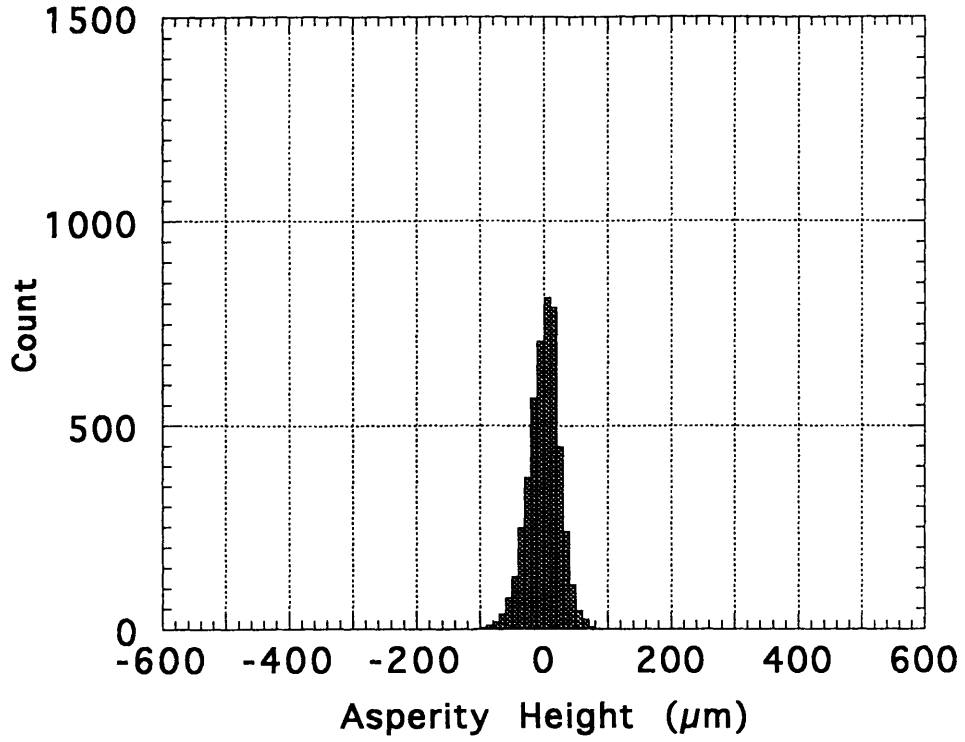

d) Lower Surface : After SFT

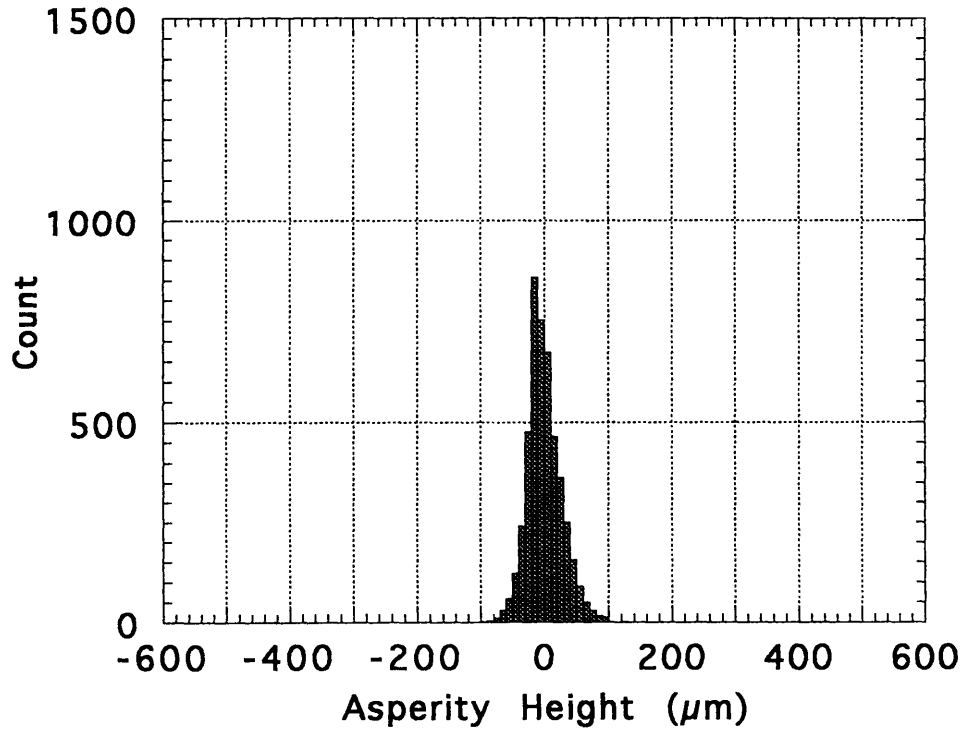

Fig.5.25 Histogram plot for asperities of two digitized surfaces after stress-flow test
(b) Sawed joint in Kikuma granodiorite

c) Upper Surface : After SFT

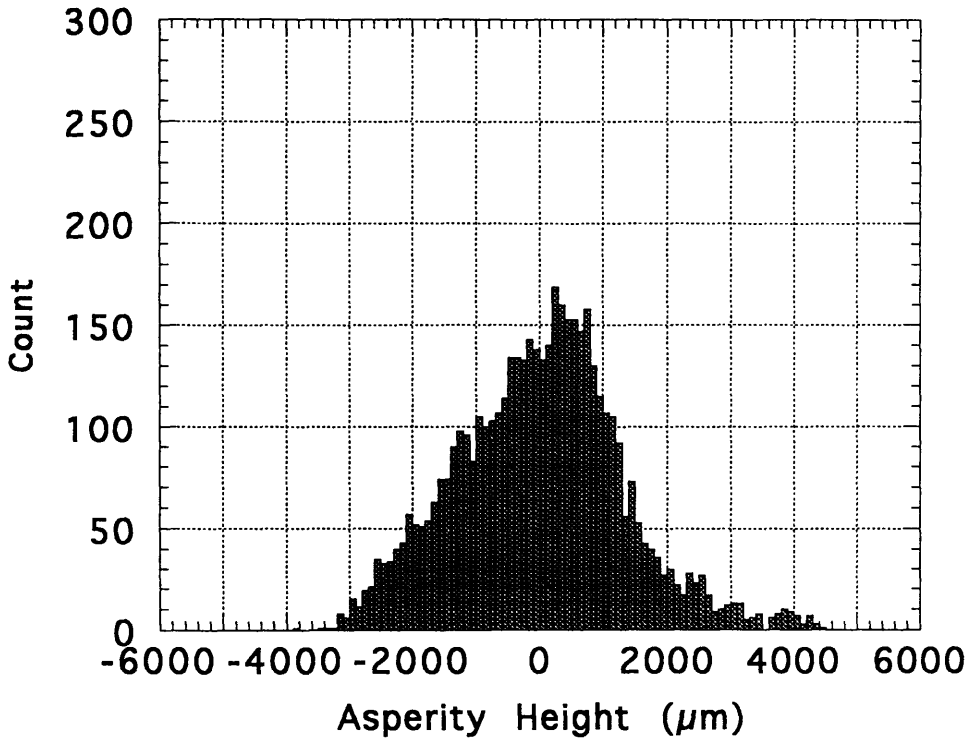

d) Lower Surface : After SFT

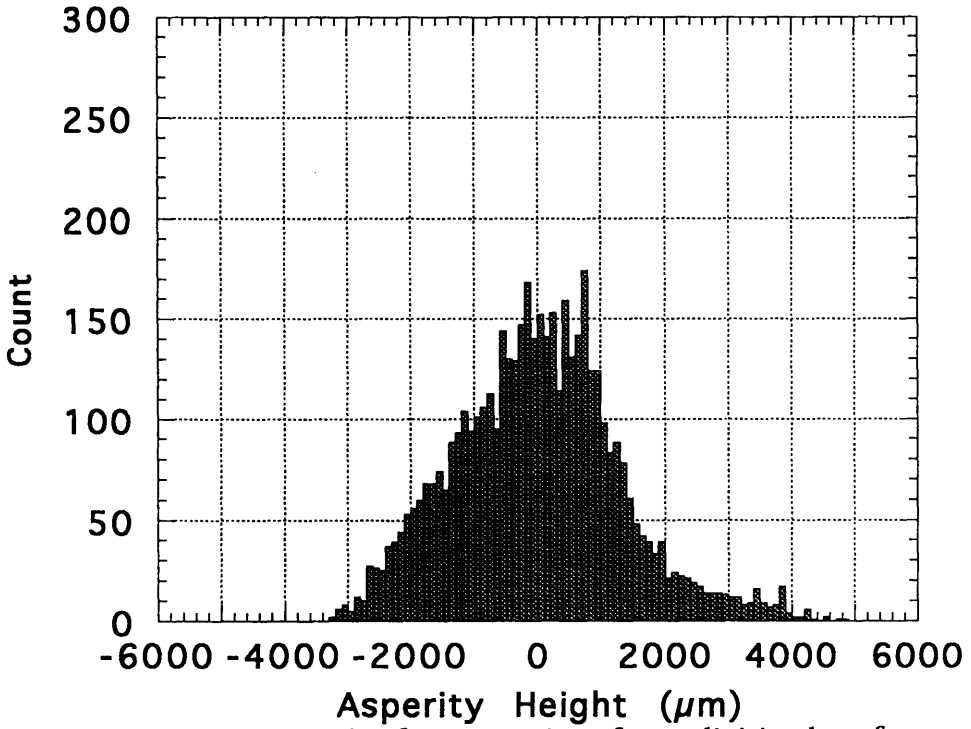

Fig.5.25 Histogram plot for asperities of two digitized surfaces after stress-flow test
(c) Tension joint in Kikuma granodiorite

c) Upper Surface : After SFT

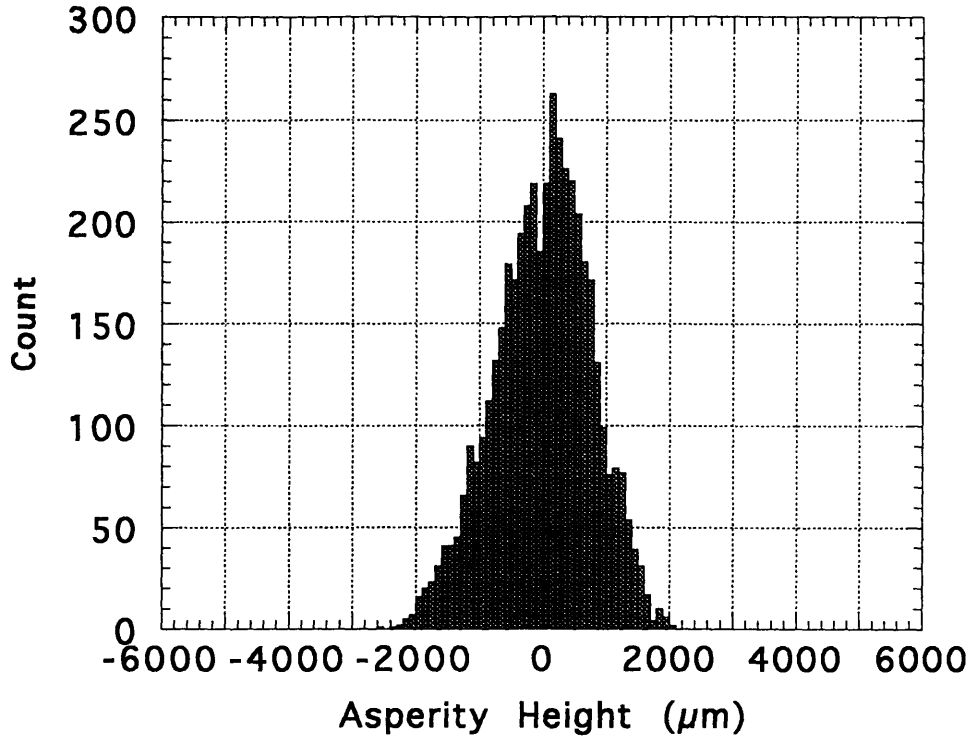

d) Lower Surface : After SFT

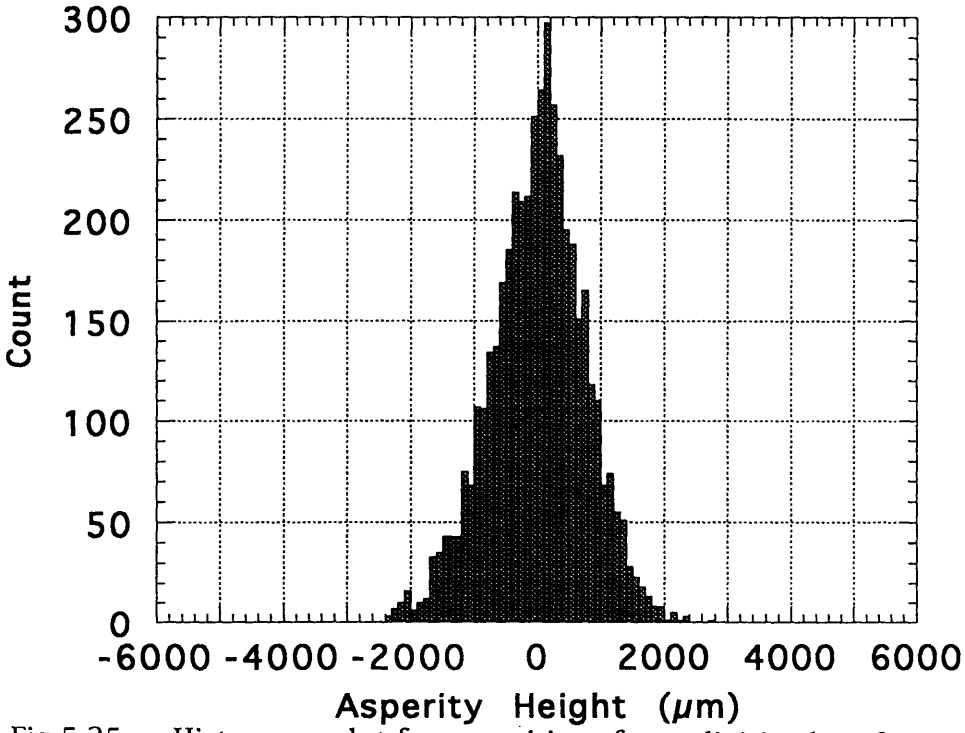

Fig.5.25 Histogram plot for asperities of two digitized surfaces after stress-flow test
(d) Tension joint in Inada granite

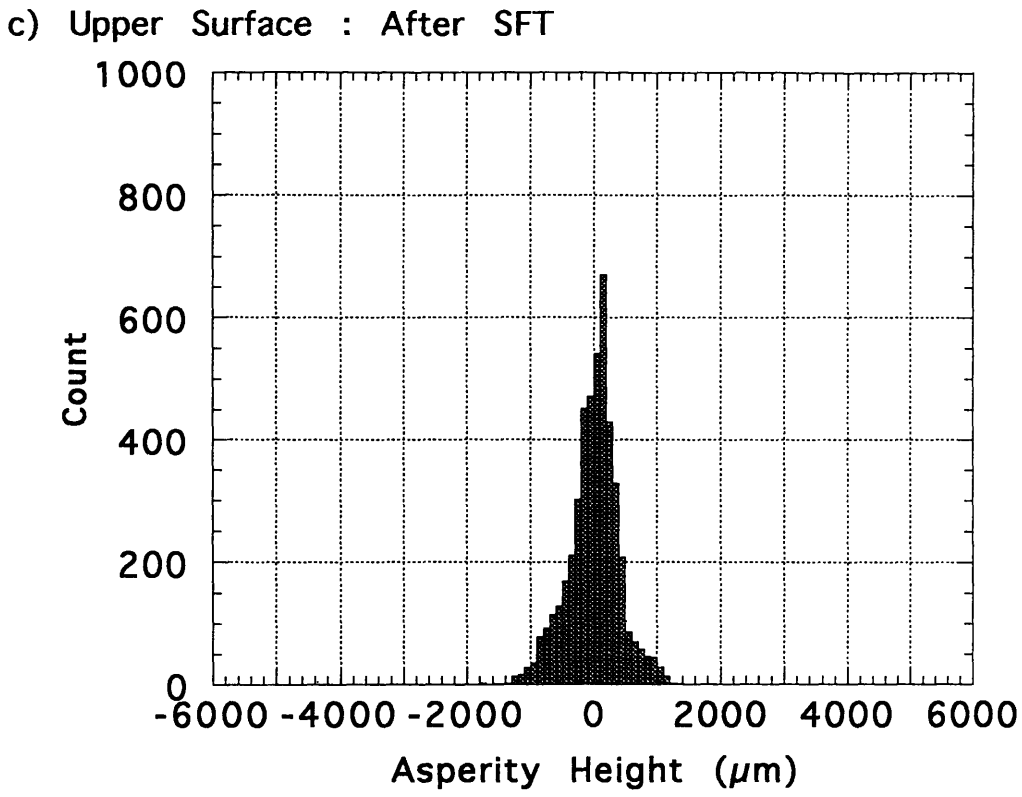

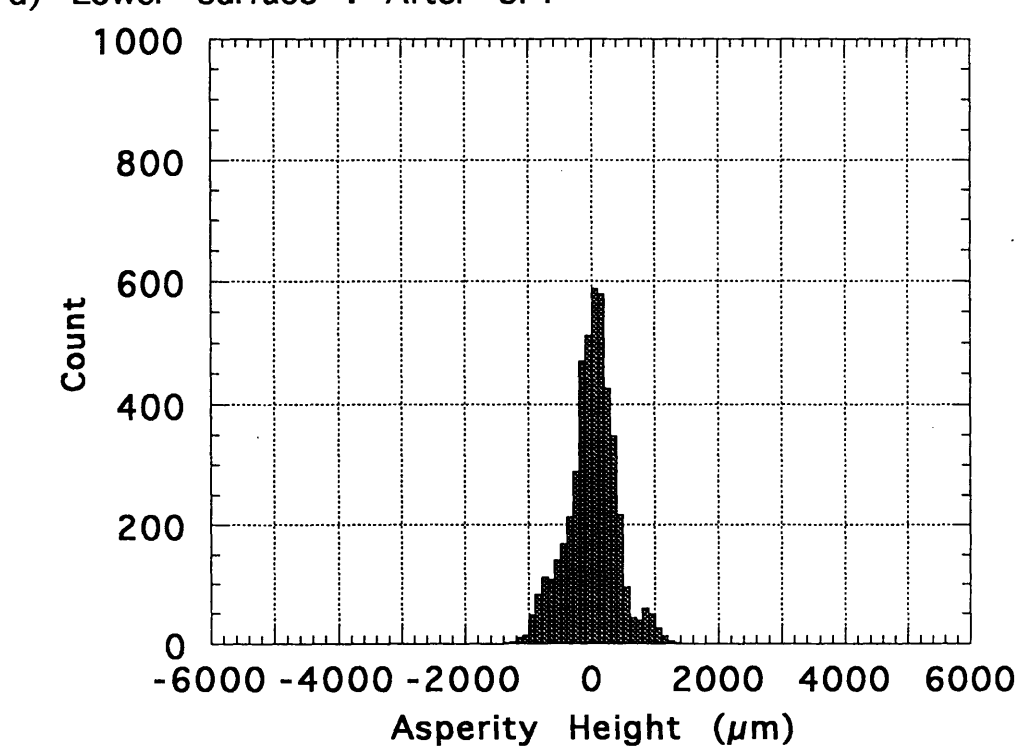

Fig.5.25 Histogram plot for asperities of two digitized surfaces after stress-flow test
(e) Tension joint in Chichibu schist

c) Upper Surface : After SFT

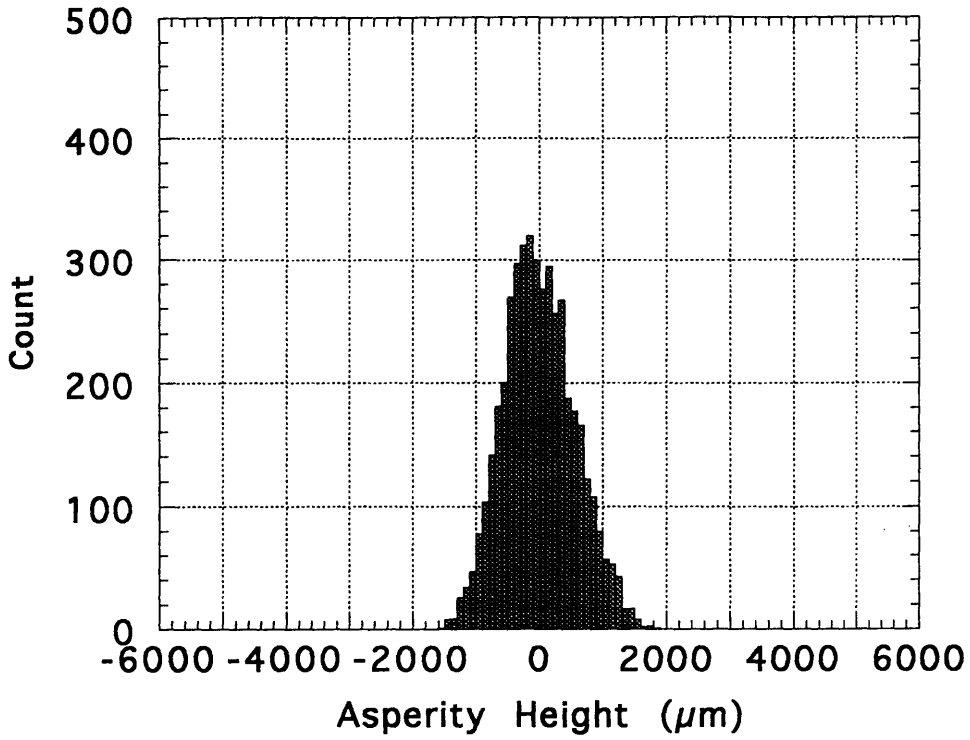

d) Lower Surface : After SFT

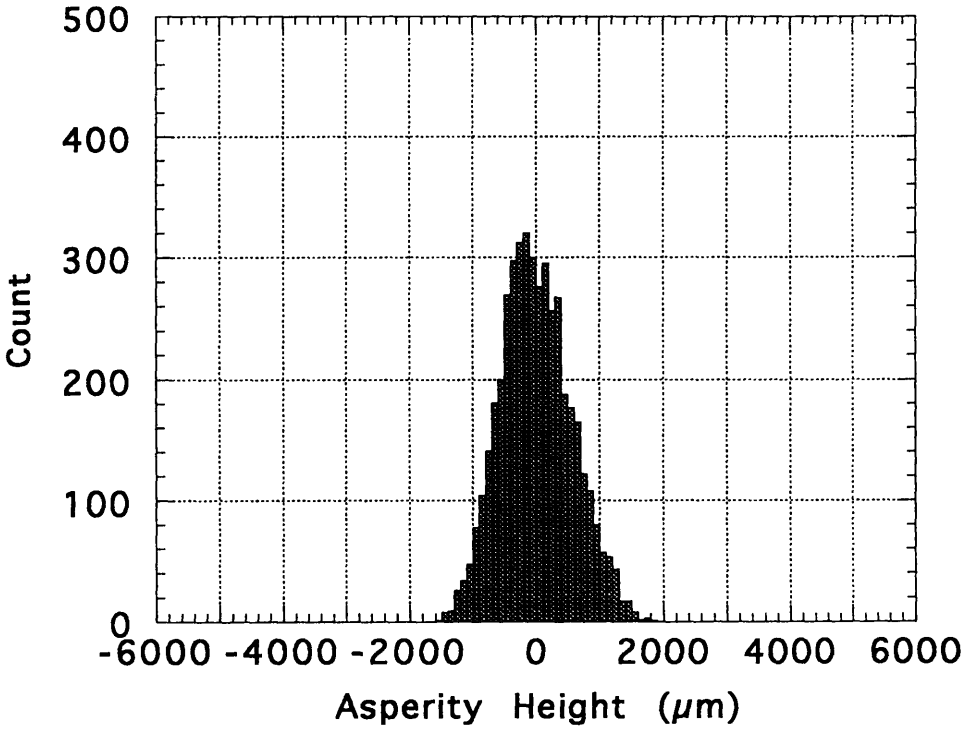

Fig.5.25 Histogram plot for asperities of two digitized surfaces after stress-flow test
(f) Tension joint in Kimachi sandstone

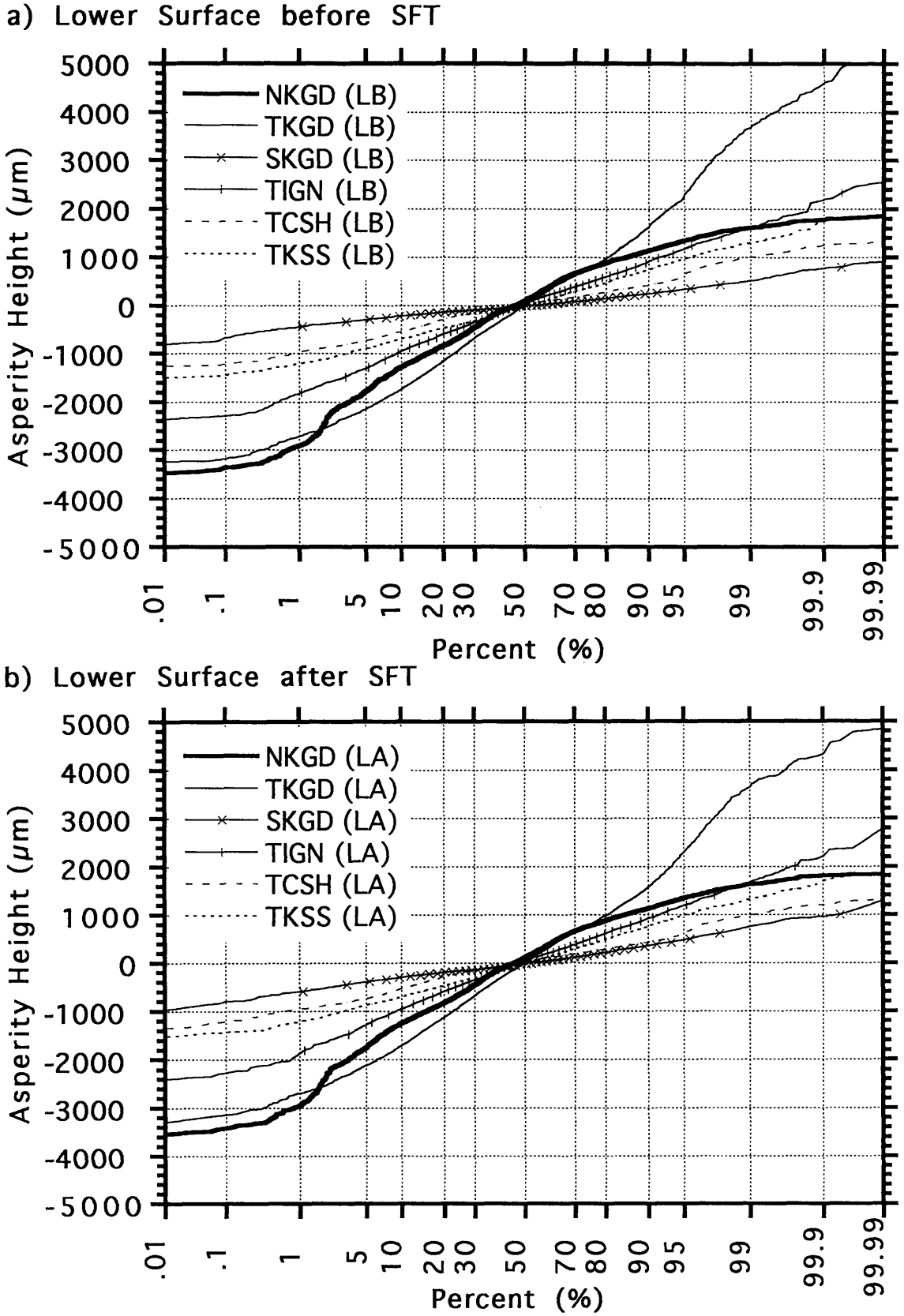

Fig.5.26 Comparison of cumulative probability plot of asperity height before and after stress-flow test (a) lawer surface

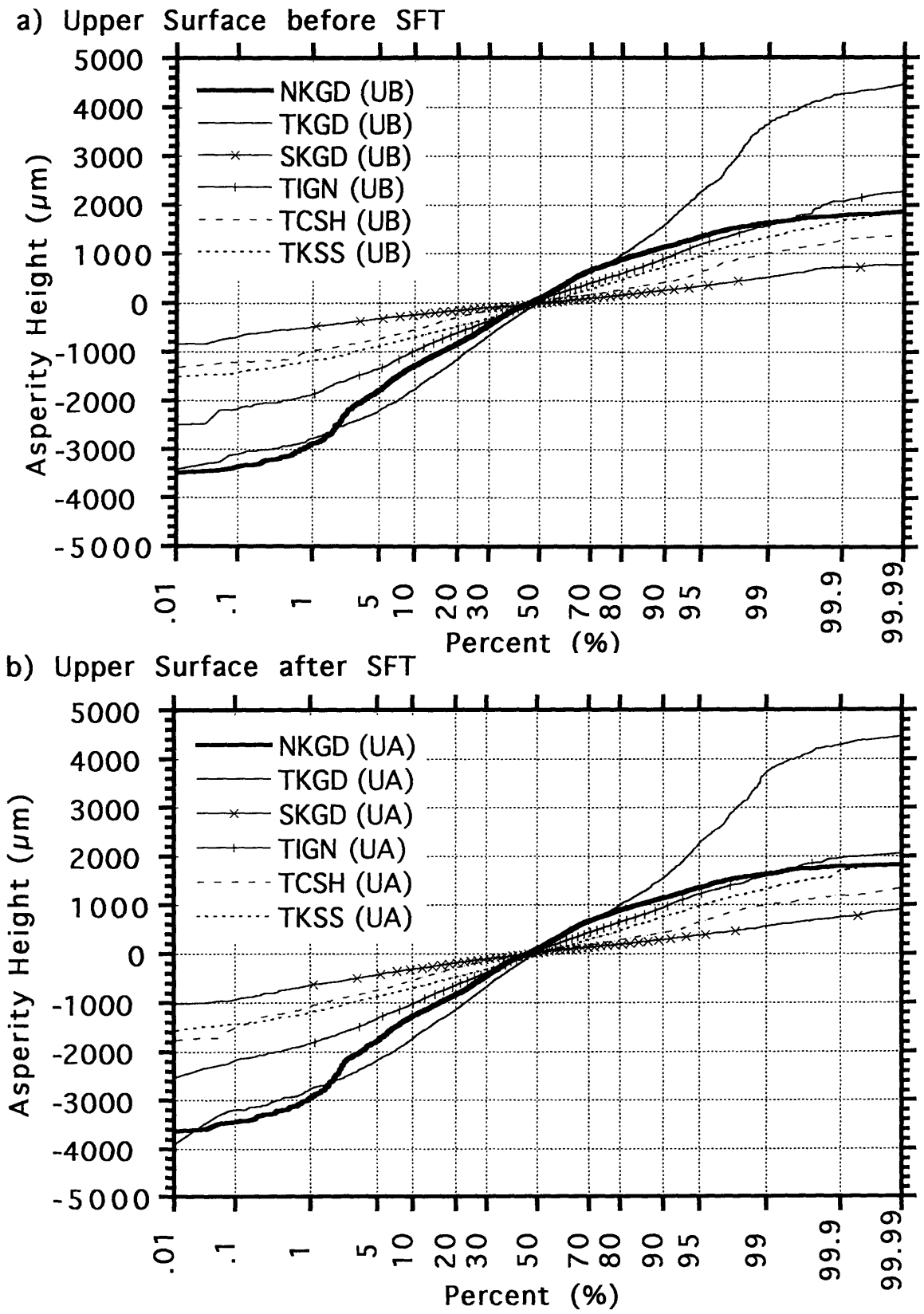

Fig.5.26 Comparison of cumulative probability plot of asperity height before and after stress-flow test (b) upper surface

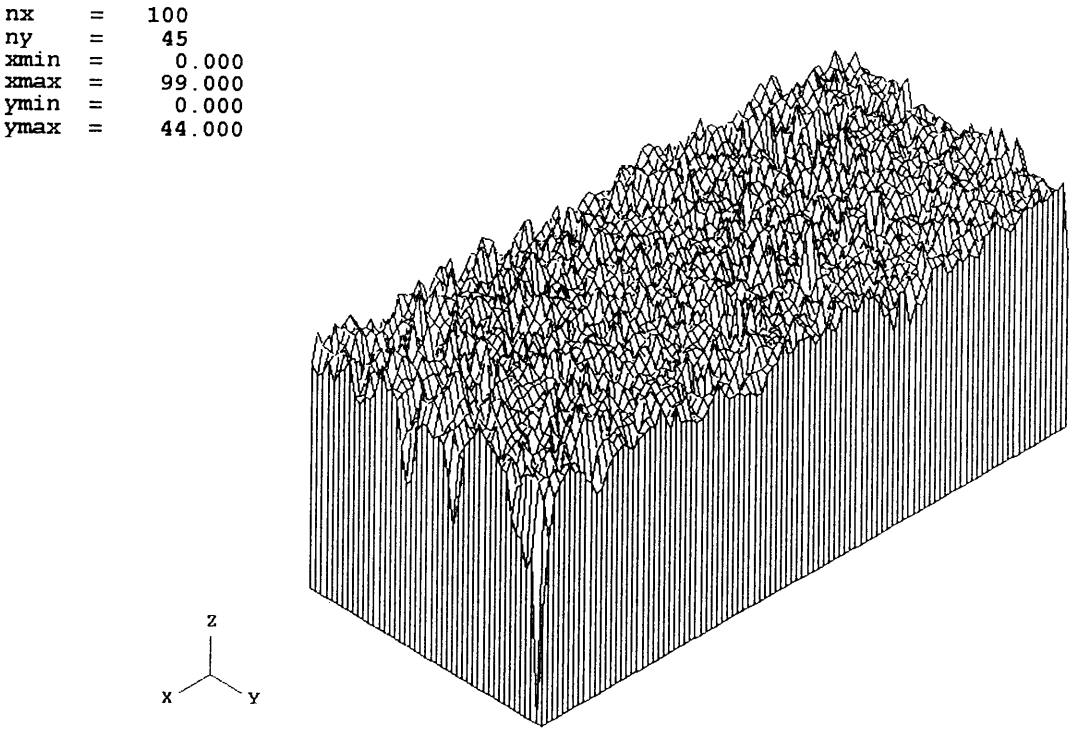

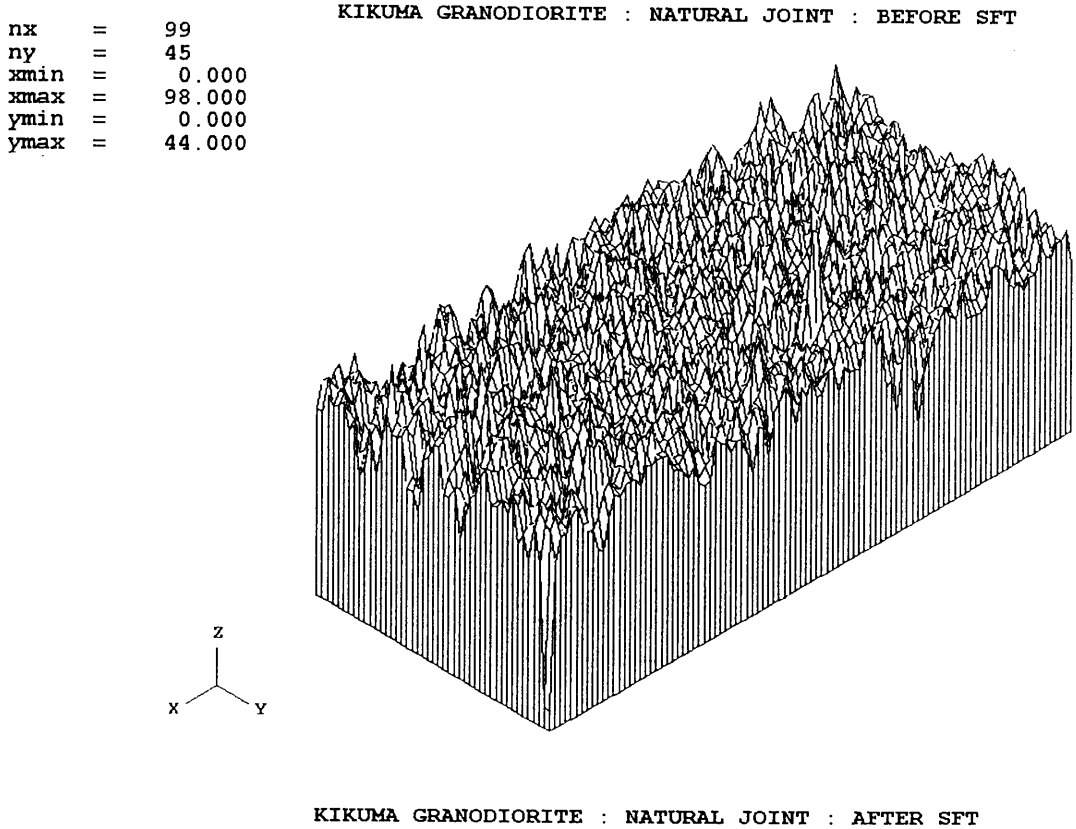

Fig.5.27 Comparison of aperture distribution before and after stress-flow test
(a) Natural joint in Kikuma granodiorite

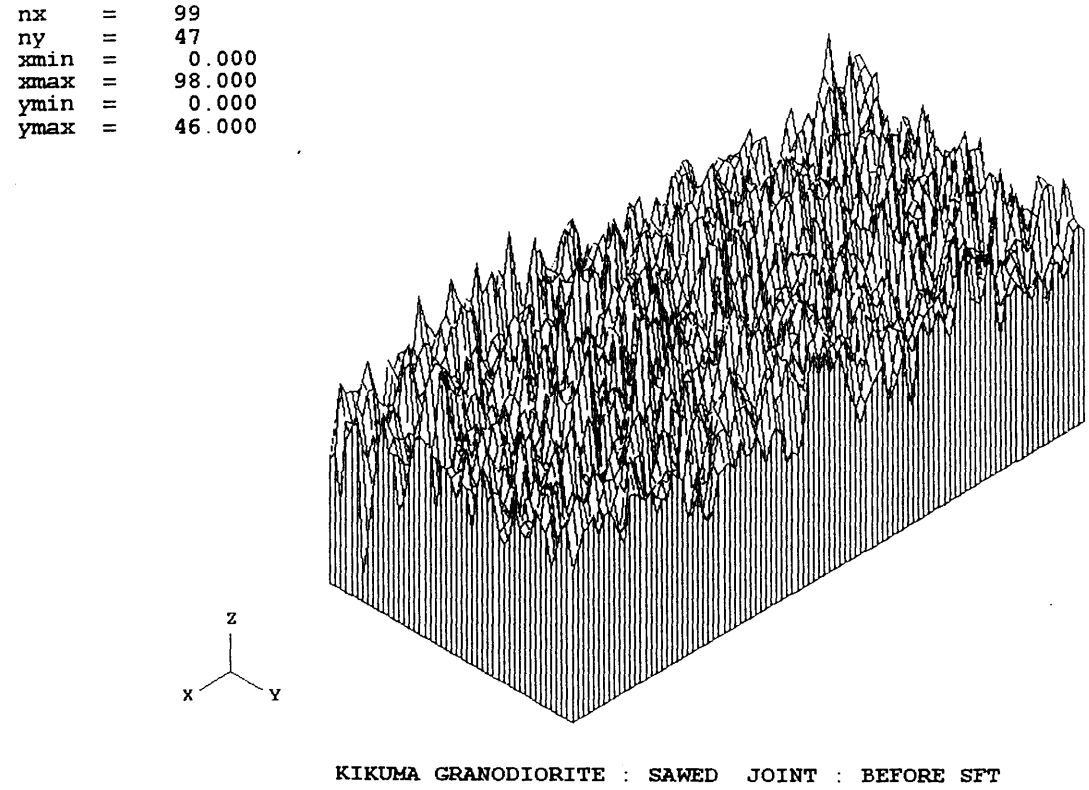

Fig.5.27 Comparison of aperture distribution before and after stress-flow test (b) Sawed joint in Kikuma granodiorite

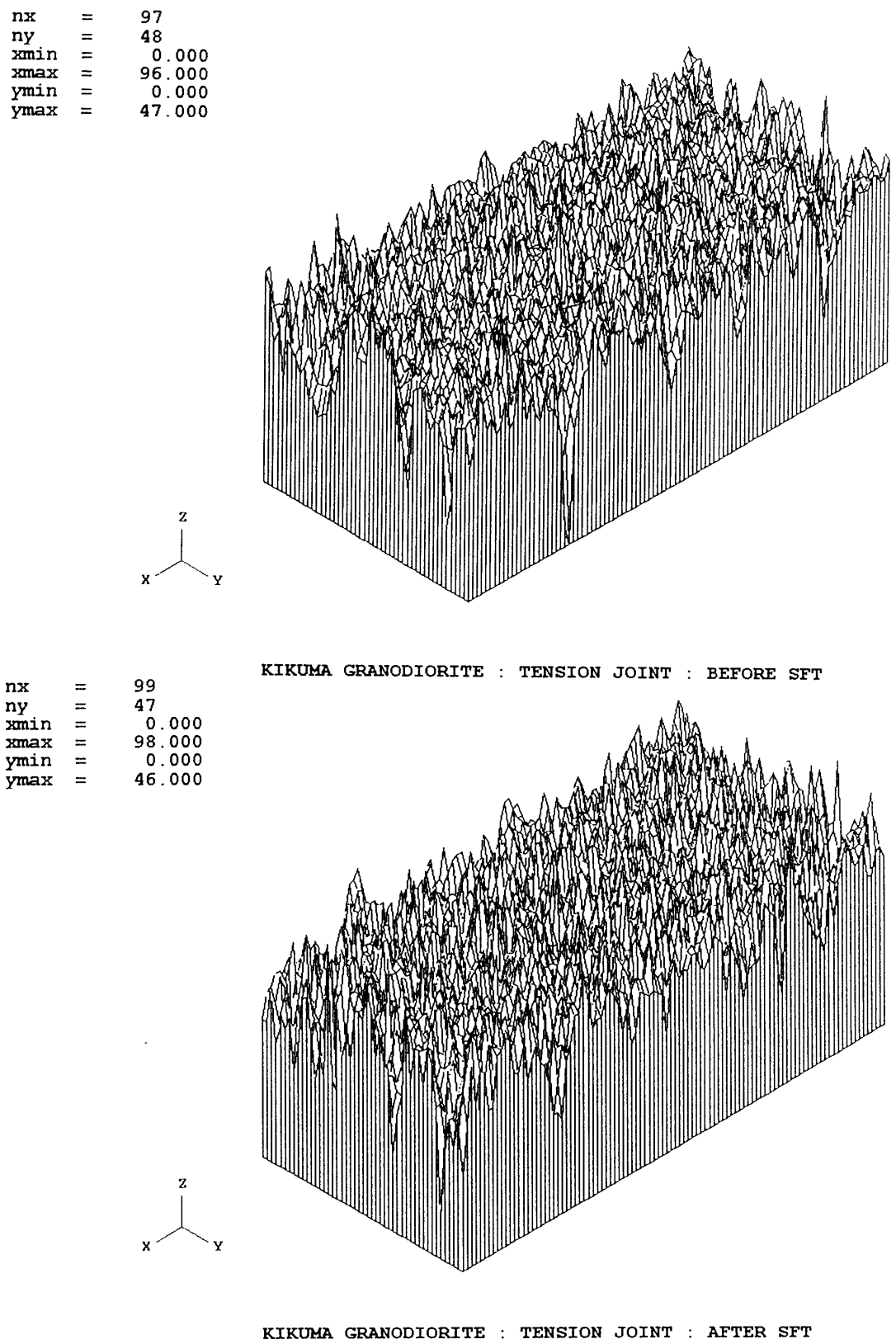

Fig.5.27 Comparison of aperture distribution before and after stress-flow test
(c) Tension joint in Kikuma granodiorite

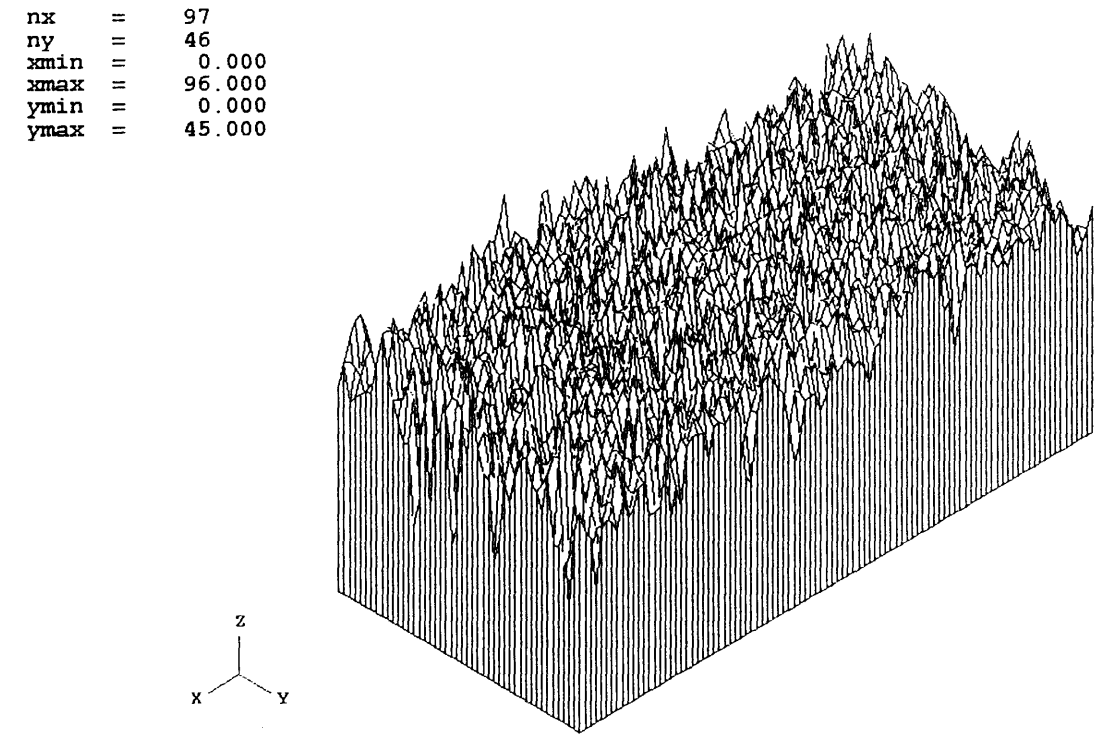

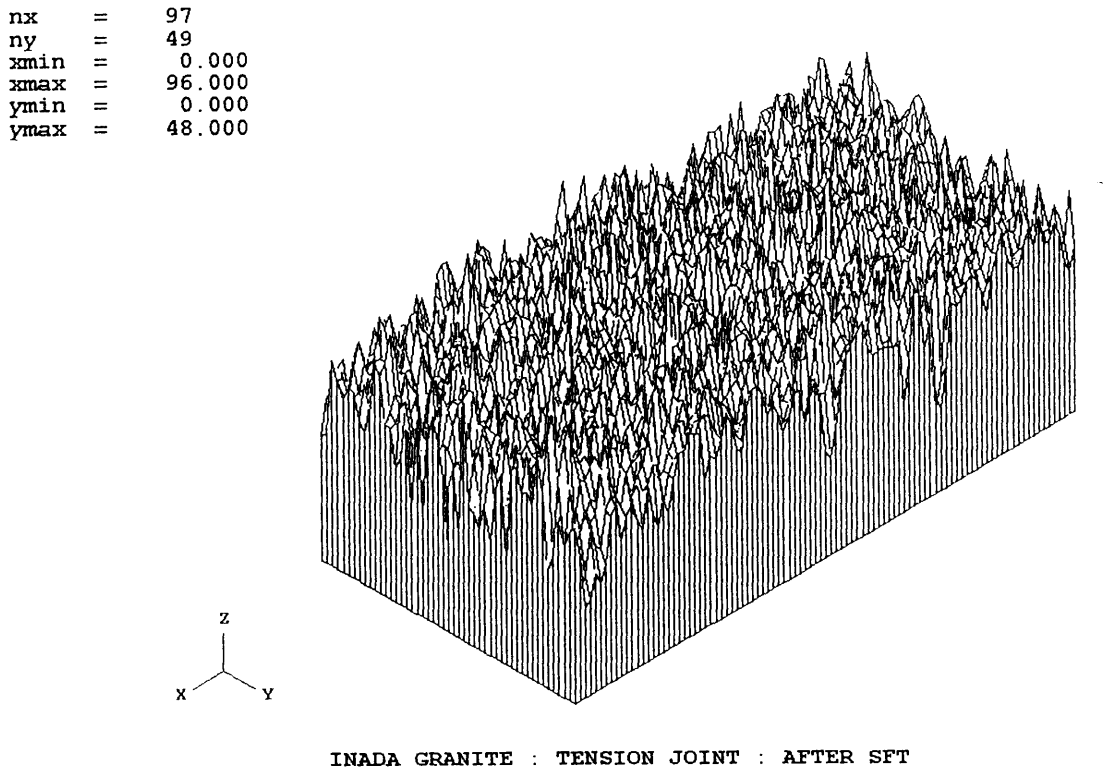

Fig.5.27 Comparison of aperture distribution before and after stress-flow test (d) Tension joint in Inada granite

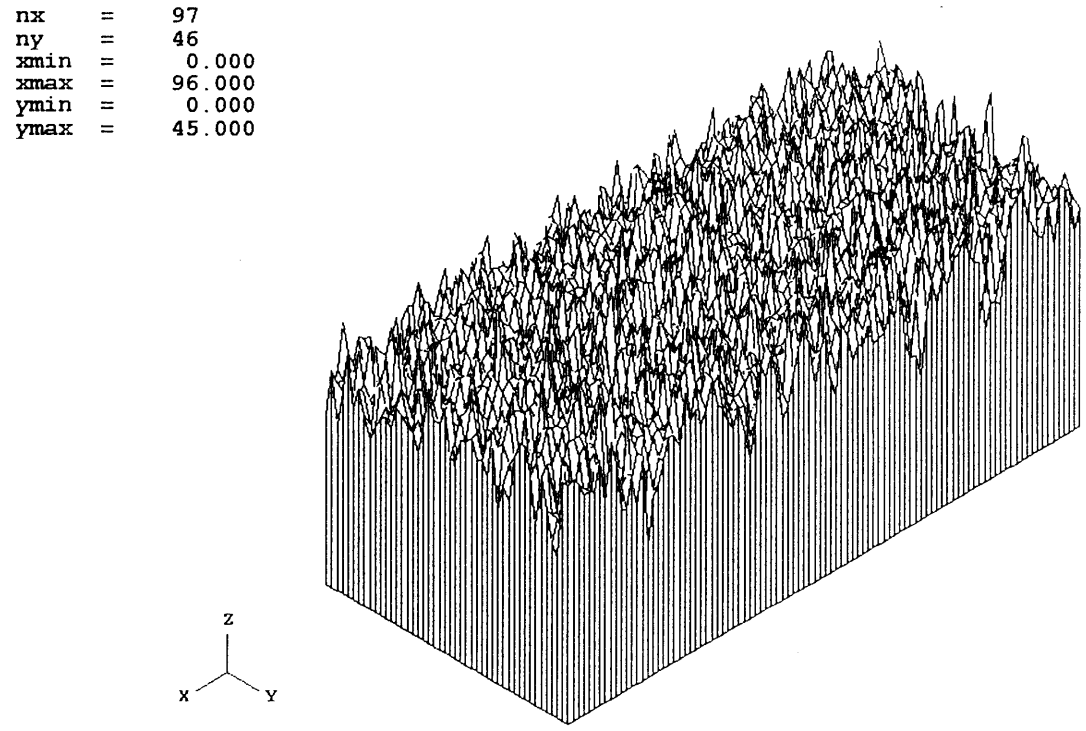

Fig.5.27 Comparison of aperture distribution before and after stress-flow test (e) Tension joint in Chichibu schist

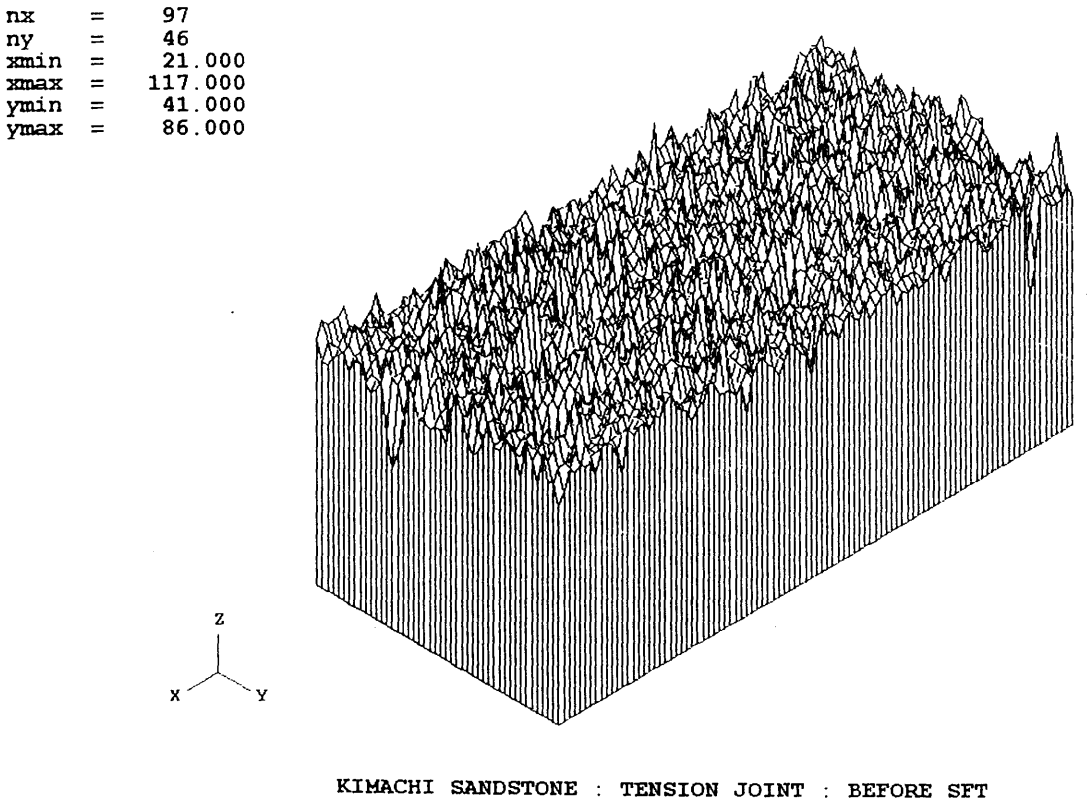

Fig.5.27 Comparison of aperture distribution before and after stress-flow test
(f) Tension joint in Kimachi sandstone

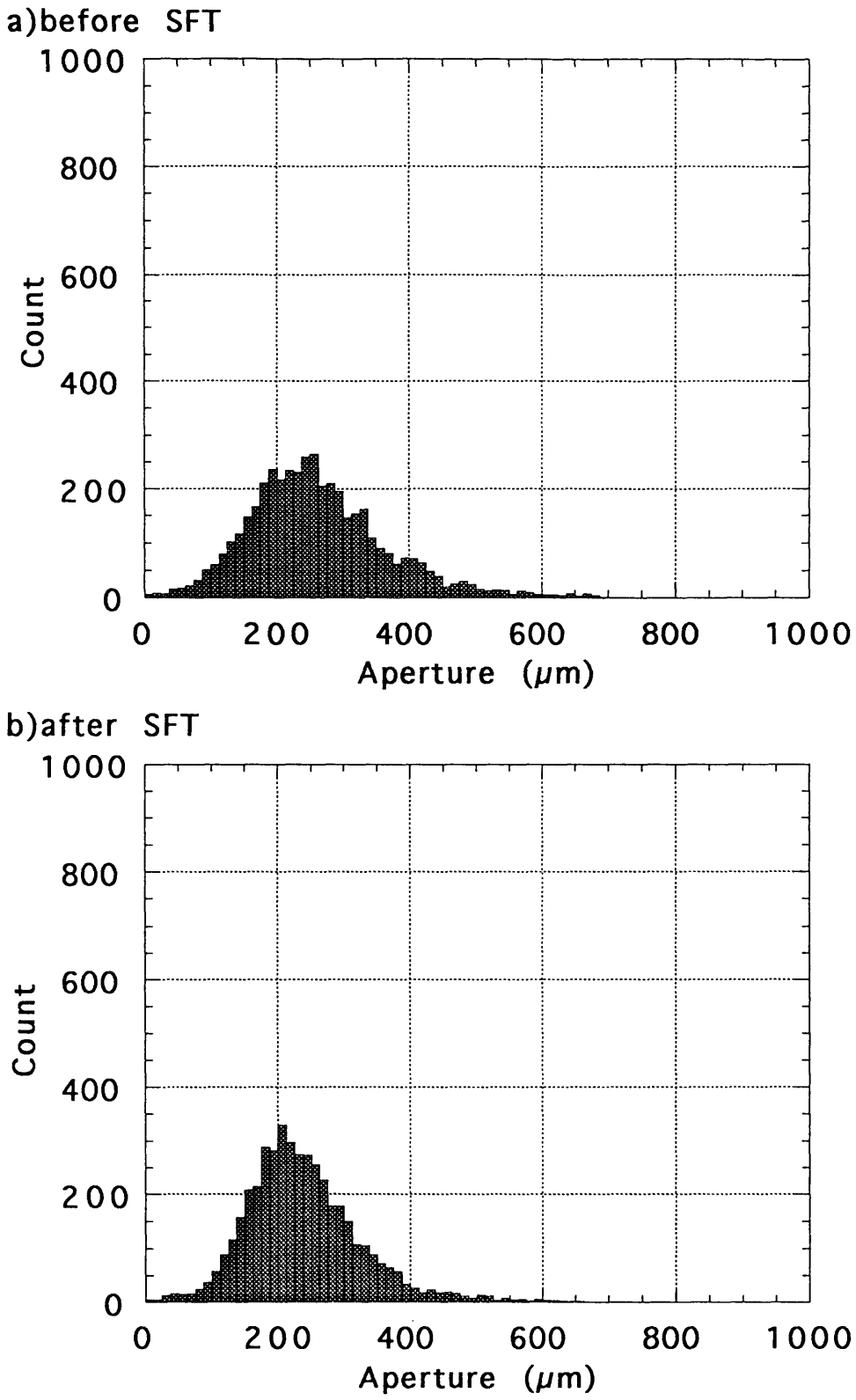

Fig.5.28 Comparison of histogram plot for aperture distribution before and after stress-flow test
(a) Natural joint in Kikuma granodiorite

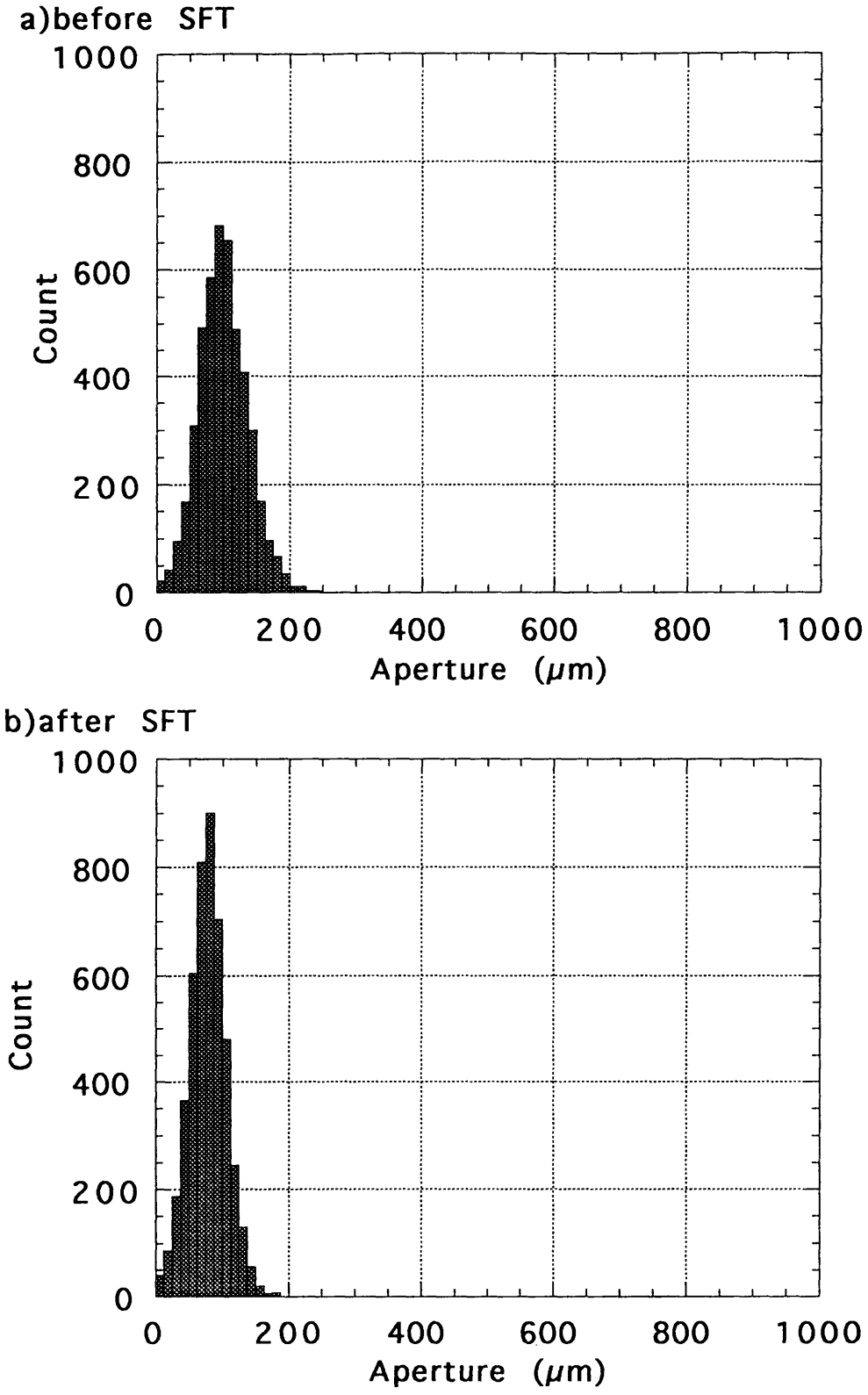

Fig.5.28 Comparison of histogram plot for aperture distribution before and after stress-flow test
(b) Sawed joint in Kikuma granodiorite

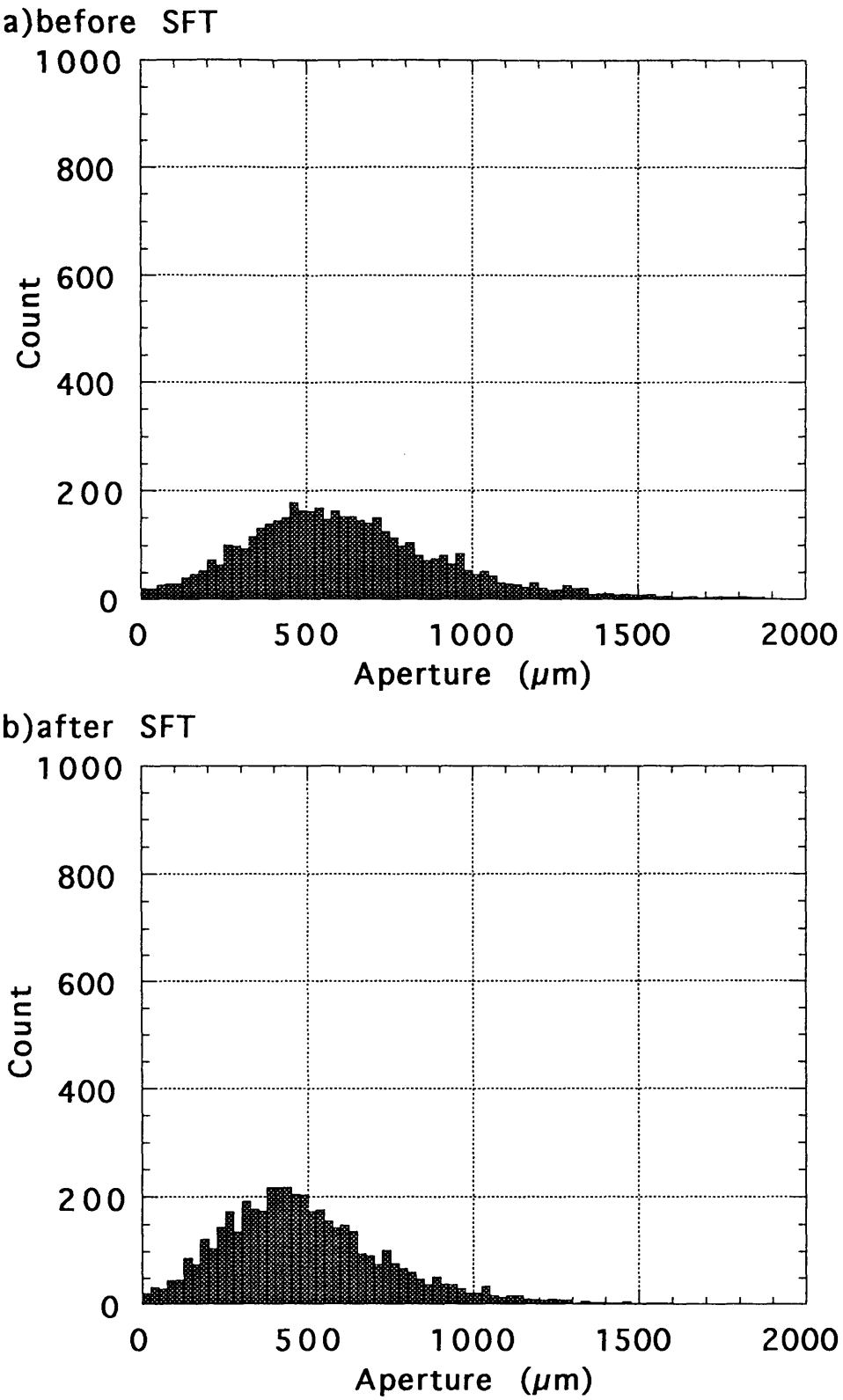

Fig.5.28 Comparison of histogram plot for aperture distribution before and after stress-flow test
(c) Tension joint in Kikuma granodiorite

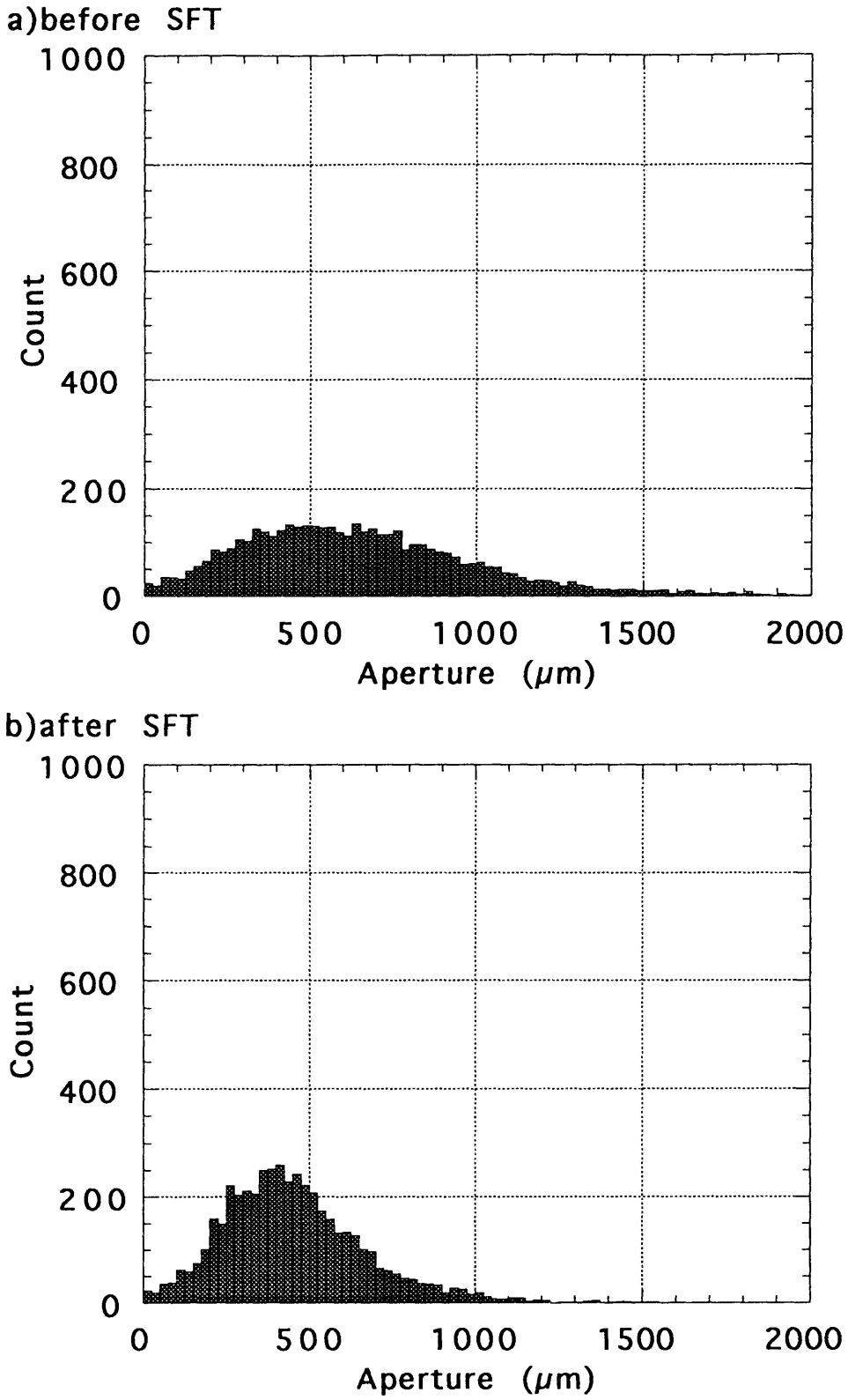

Fig.5.28 Comparison of histogram plot for aperture distribution before and after stress-flow test
(d) Tension joint in Inada granite

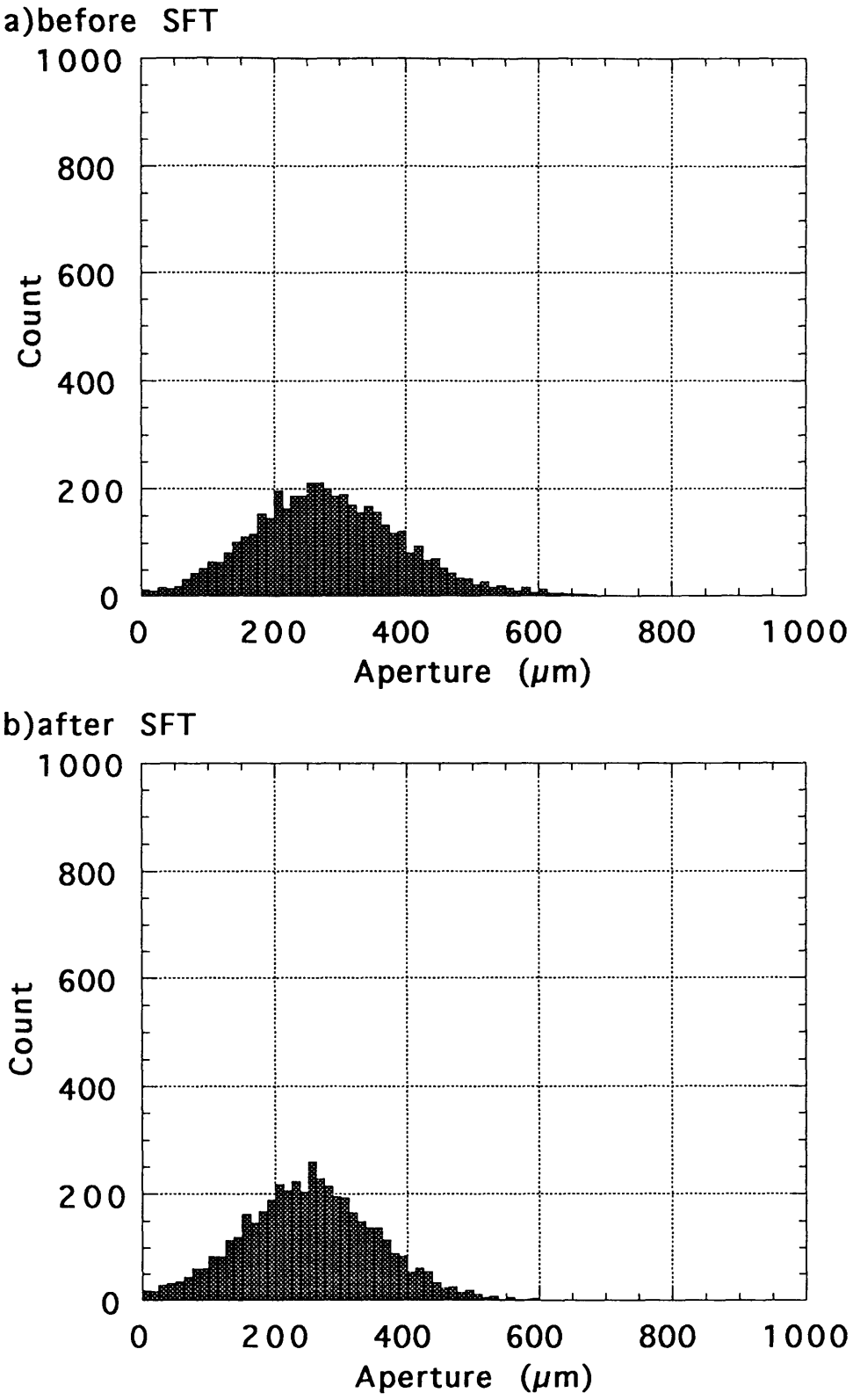

Fig.5.28 Comparison of histogram plot for aperture distribution before and after stress-flow test
(e) Tension joint in Chichibu schist

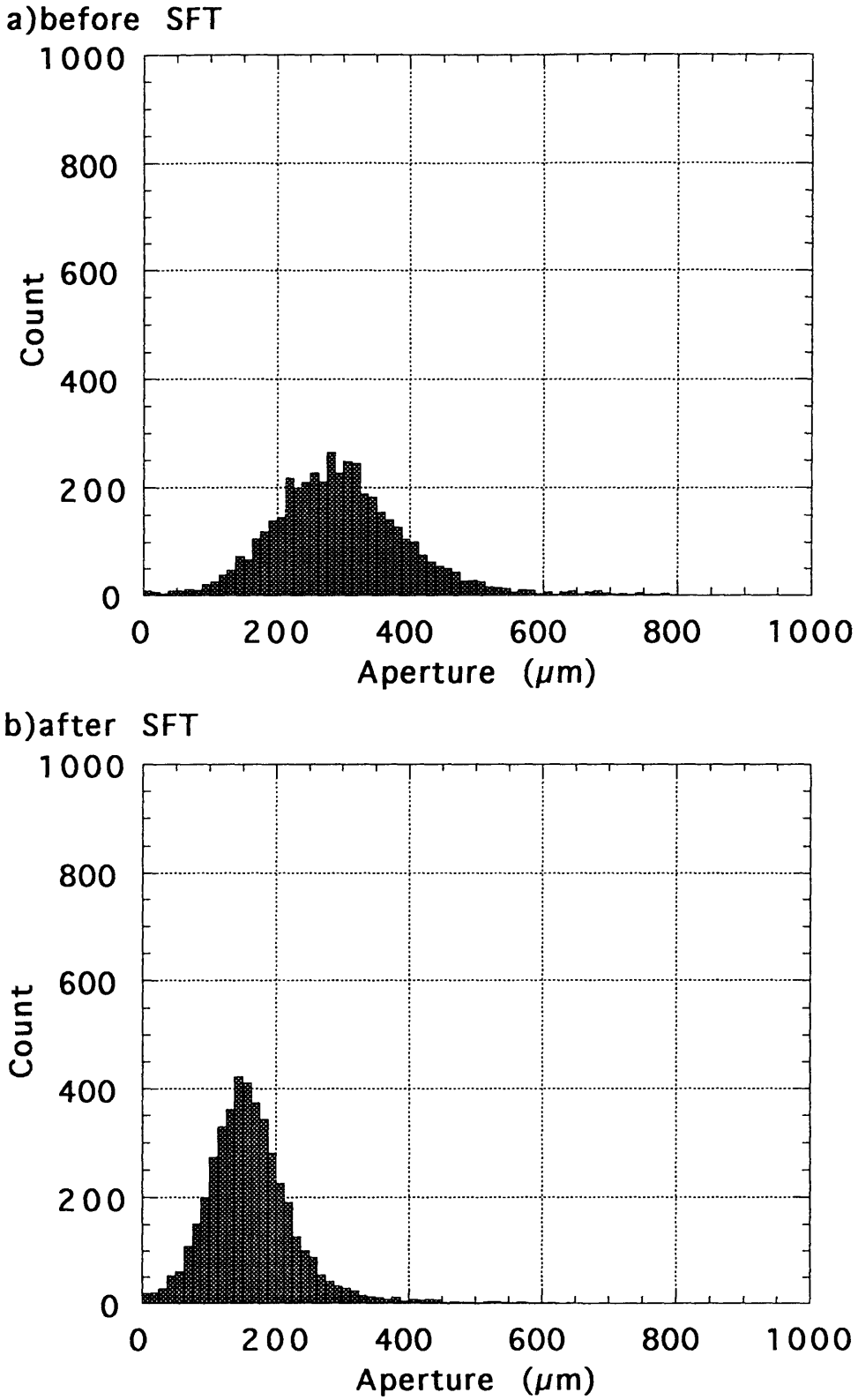

Fig.5.28 Comparison of histogram plot for aperture distribution before and after stress-flow test
(f) Tension joint in Kimachi sandstone

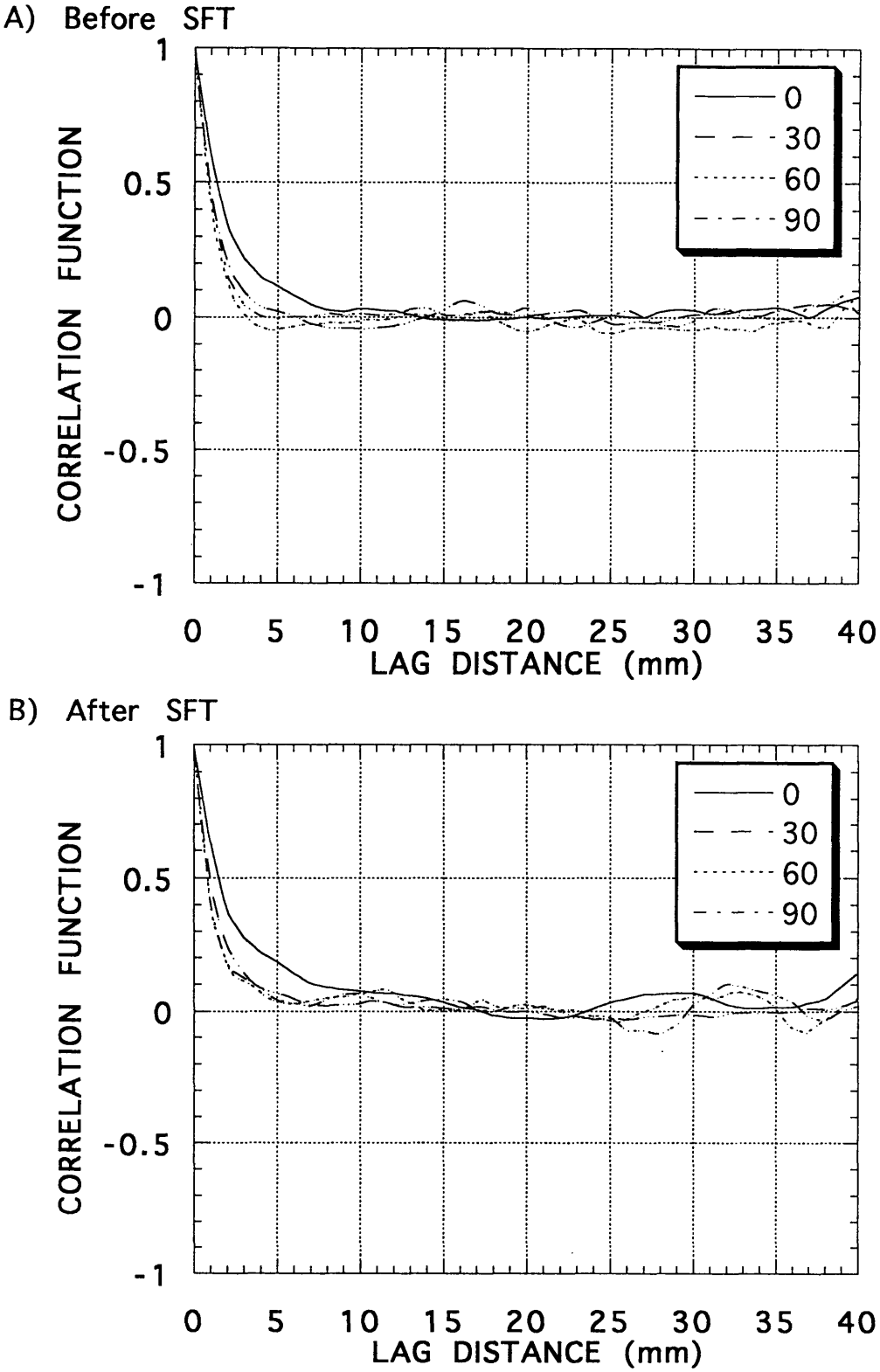

Fig.5.29 Comparison of the correlation function of aperture along four lines on the joint plane before and after stress-flow test
(a) Natural joint in Kikuma granodiorite

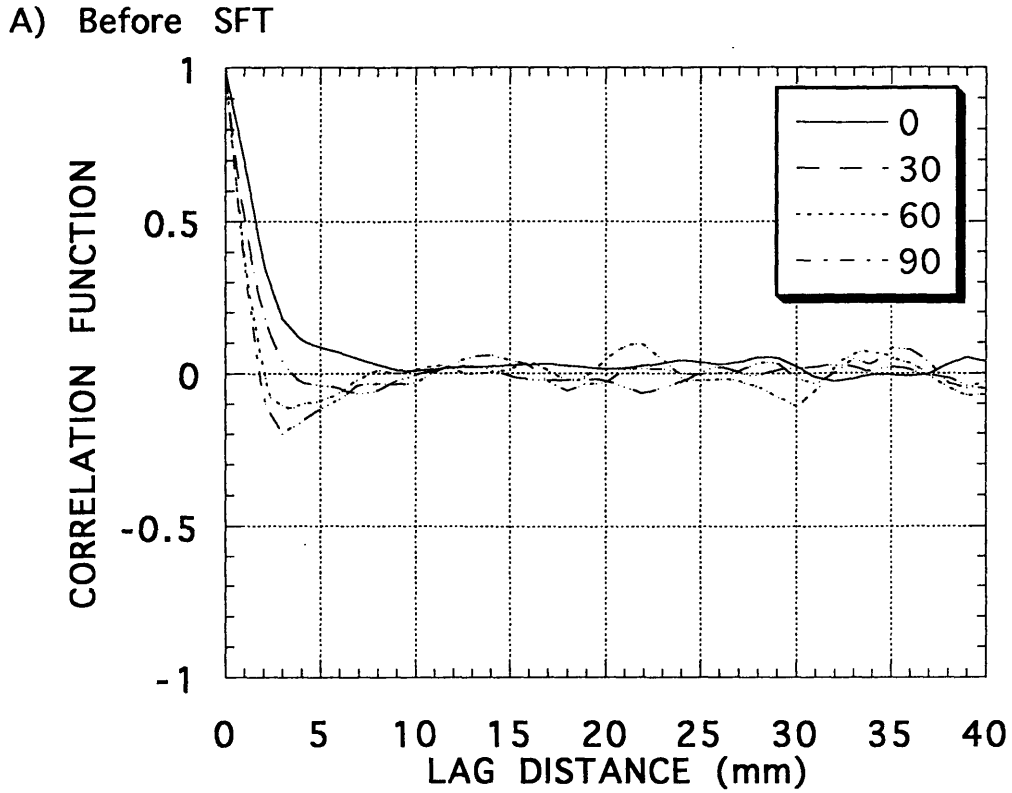

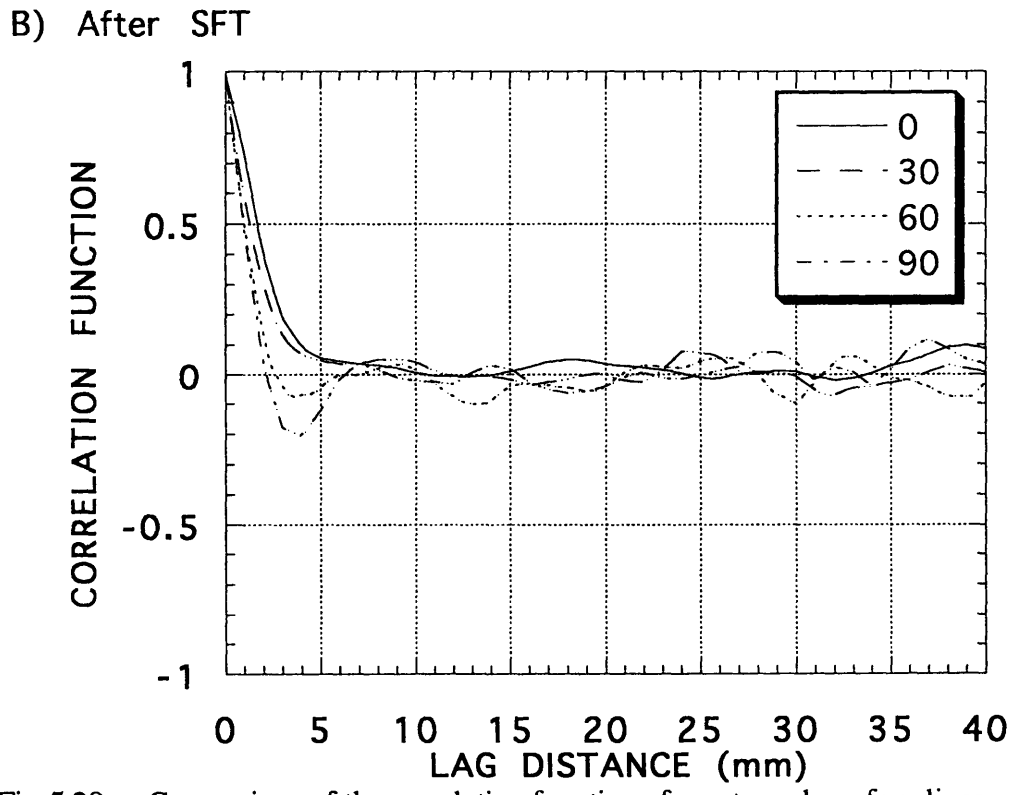

Fig.5.29 Comparison of the correlation function of aperture along four lines on the joint plane before and after stress-flow test
(b) Sawed joint in Kikuma granodiorite

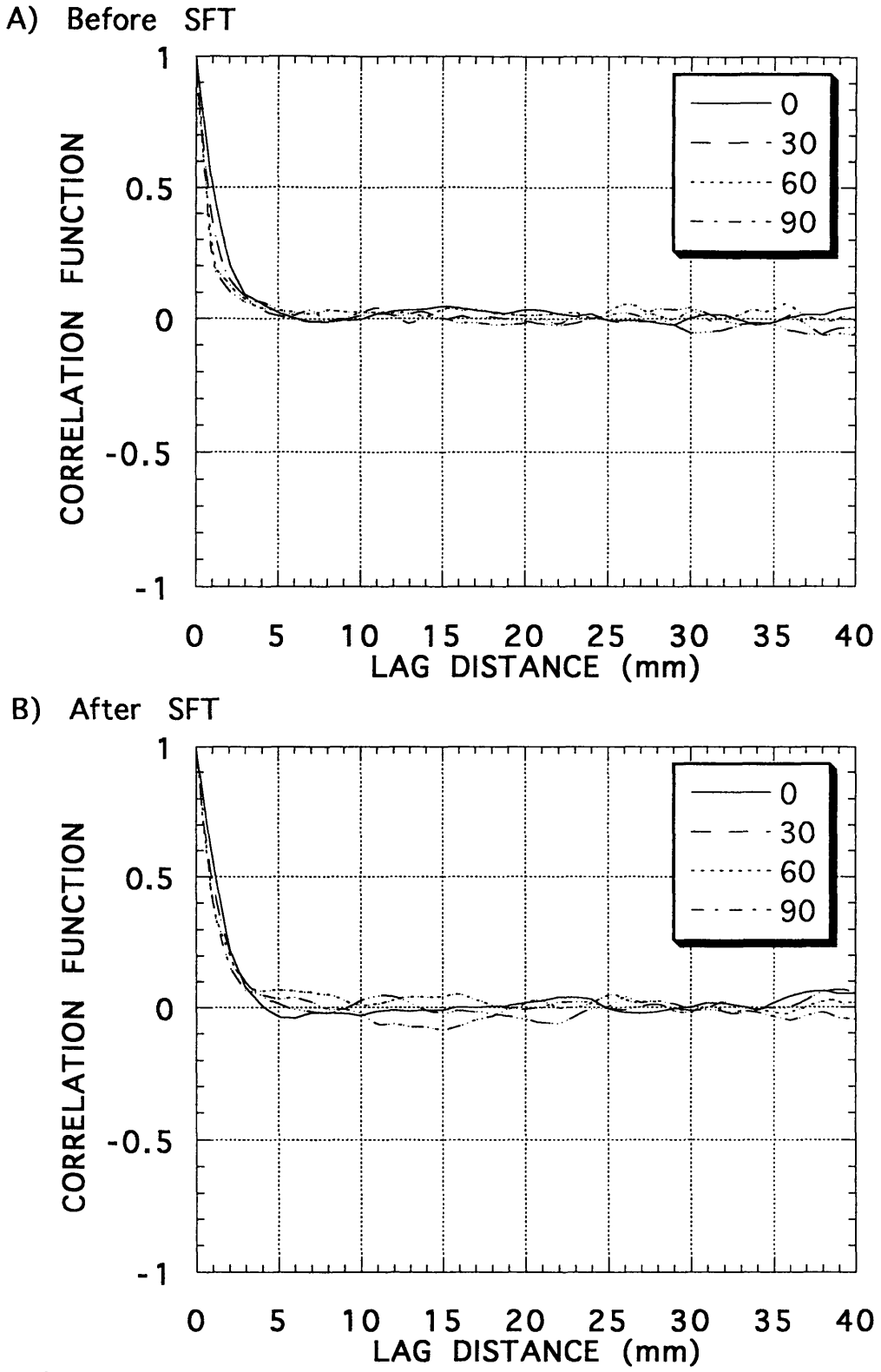

Fig.5.29 Comparison of the correlation function of aperture along four lines on the joint plane before and after stress-flow test
(c) Tension joint in Kikuma granodiorite

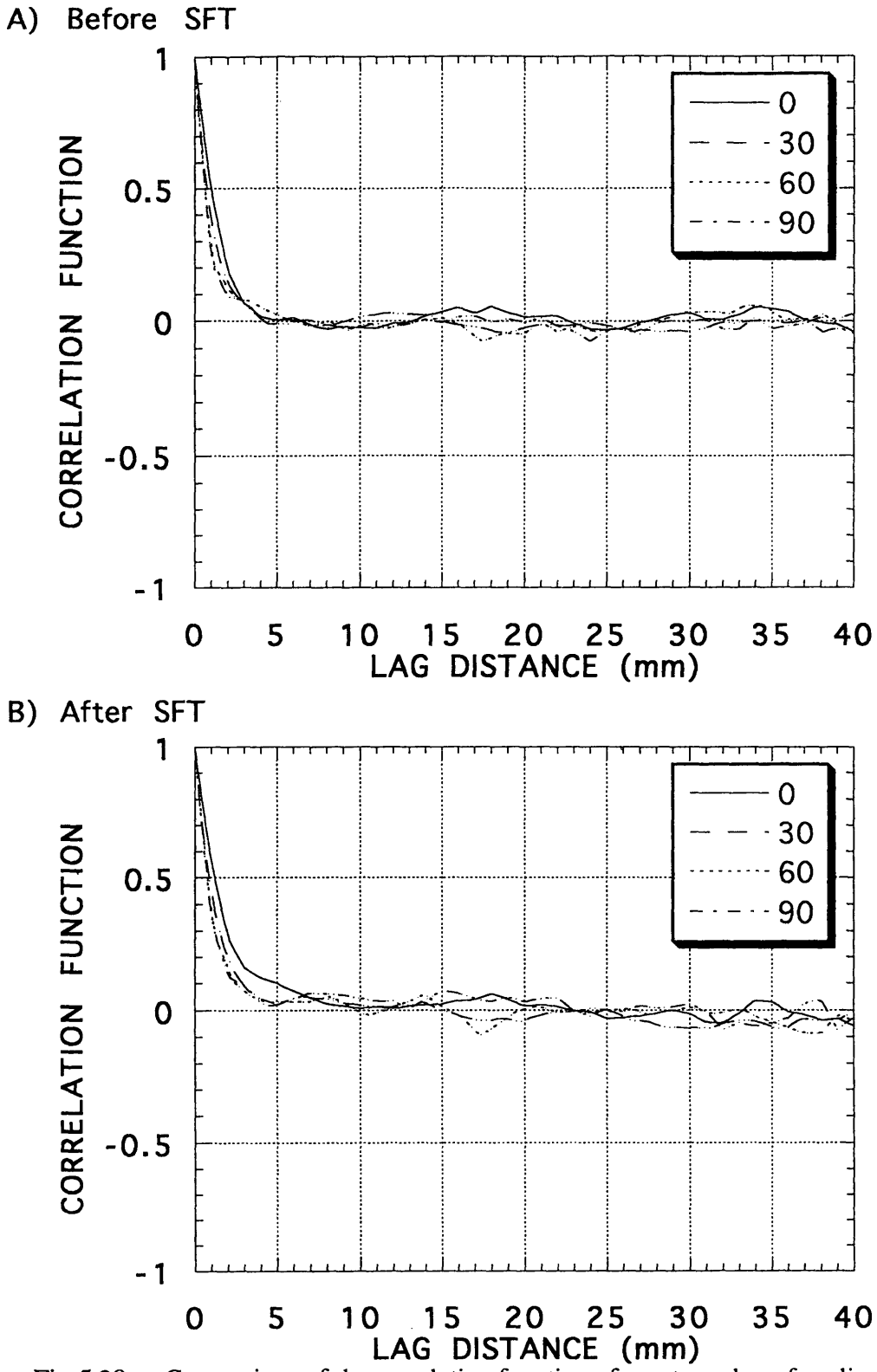

Fig.5.29 Comparison of the correlation function of aperture along four lines on the joint plane before and after stress-flow test
(d) Tension joint in Inada granite

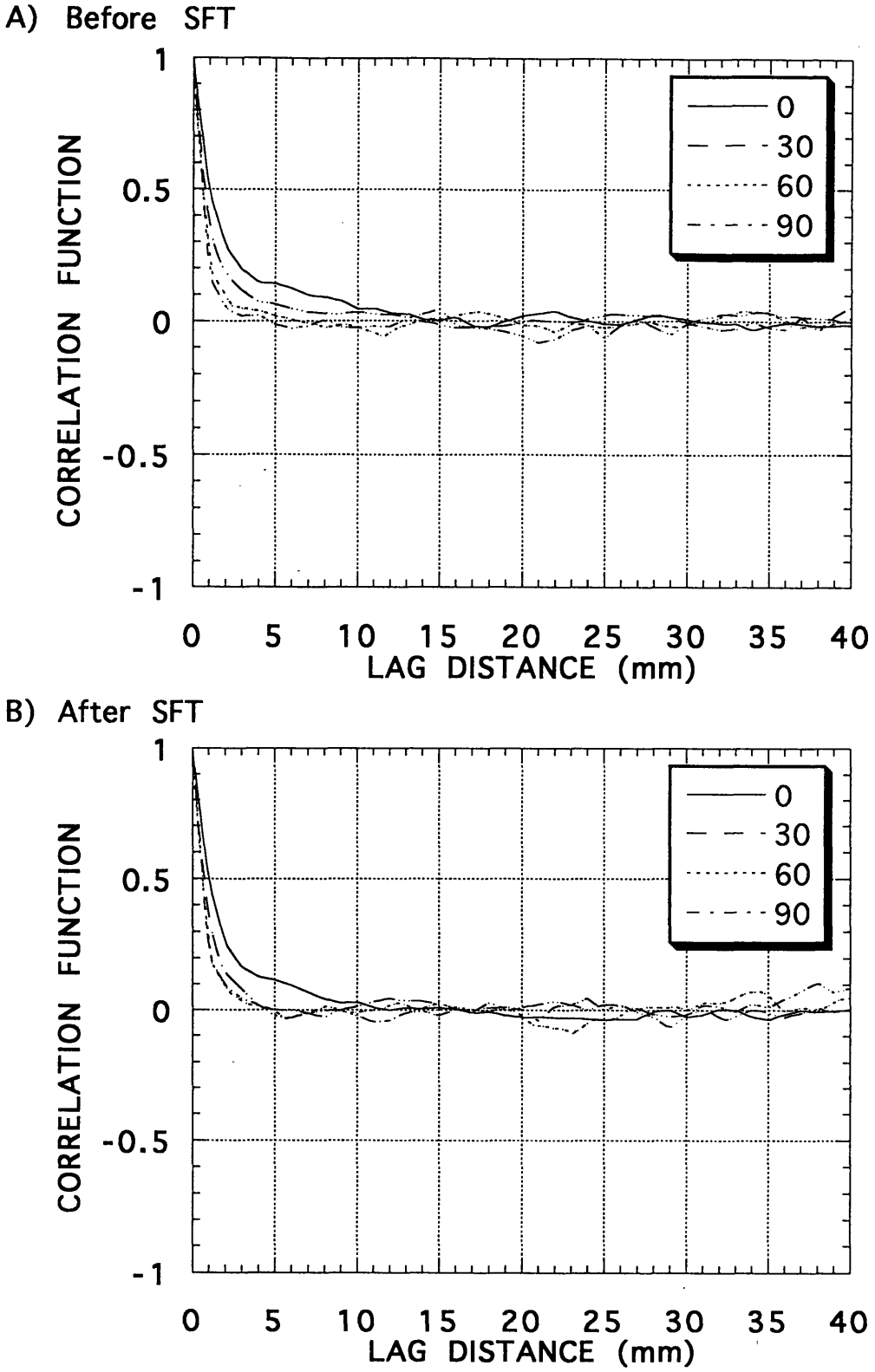

Fig.5.29 Comparison of the correlation function of aperture along four lines on the joint plane before and after stress-flow test
(e) Tension joint in Chichibu schist

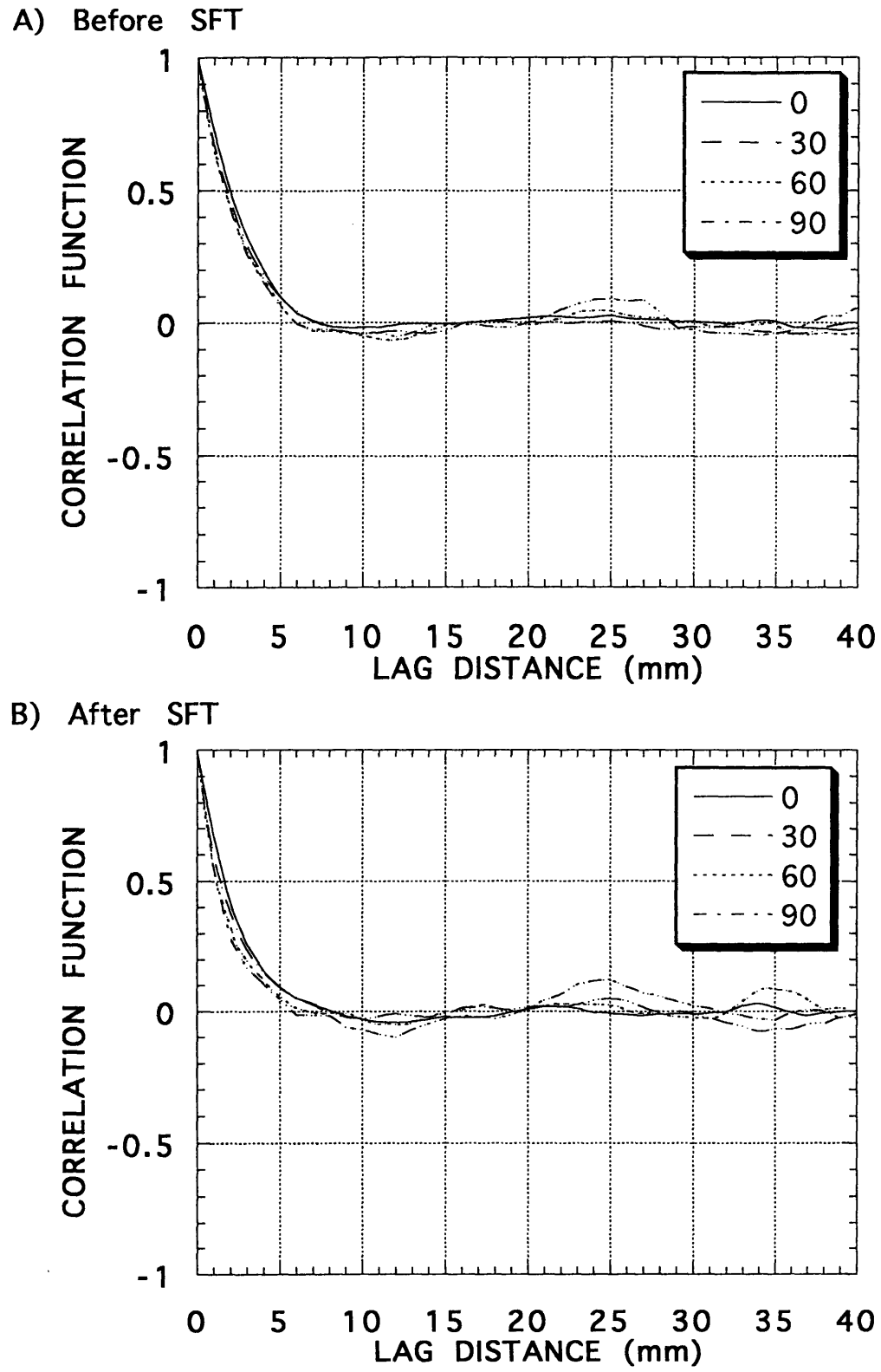

Fig.5.29 Comparison of the correlation function of aperture along four lines on the joint plane before and after stress-flow test
(f) Tension joint in Kimachi sandstone

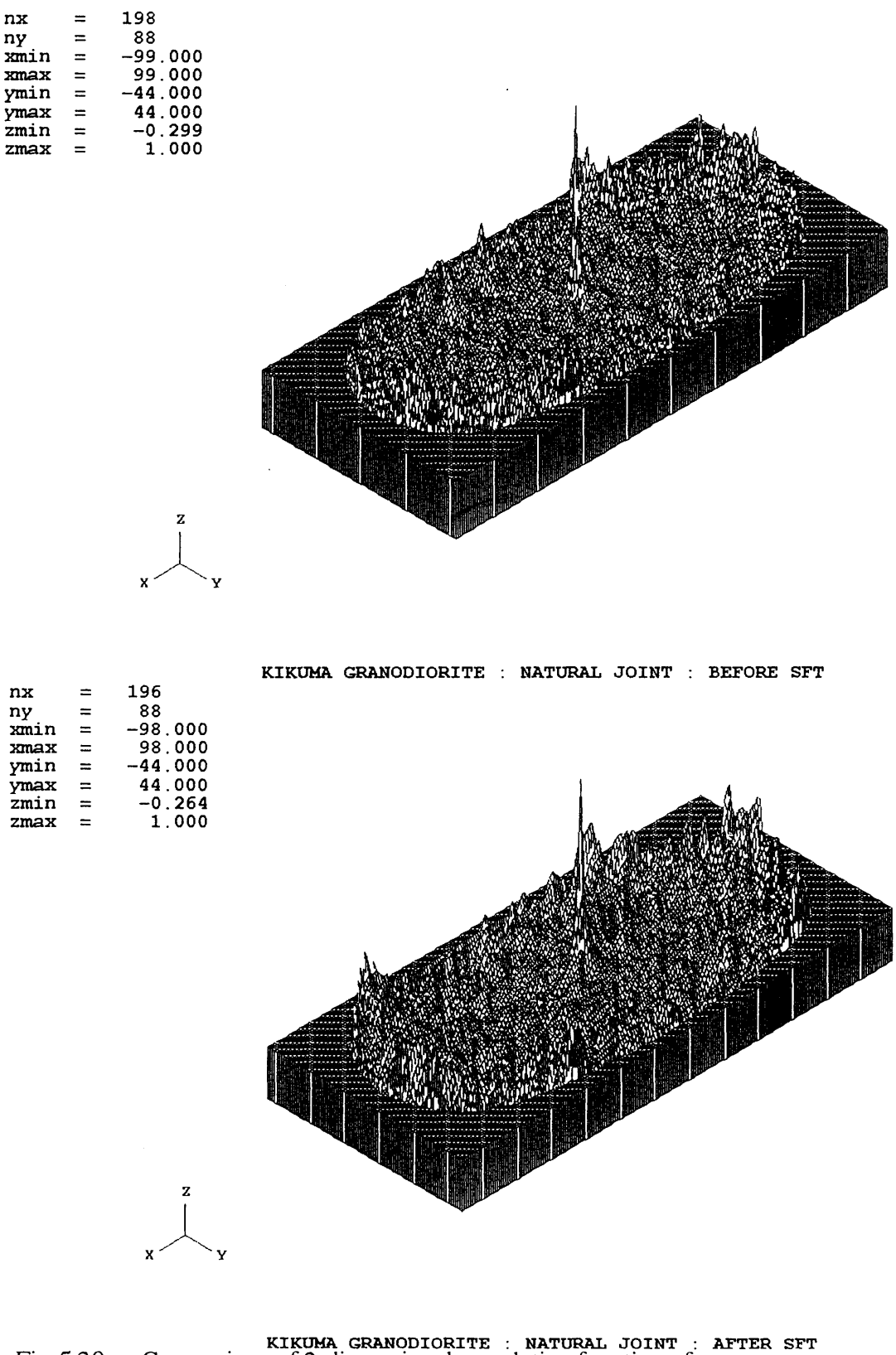

Fig.5.30 Comparison of 2-dimensional correlation function of aperture before and after stress-flow test
(a) Natural joint in Kikuma granodiorite

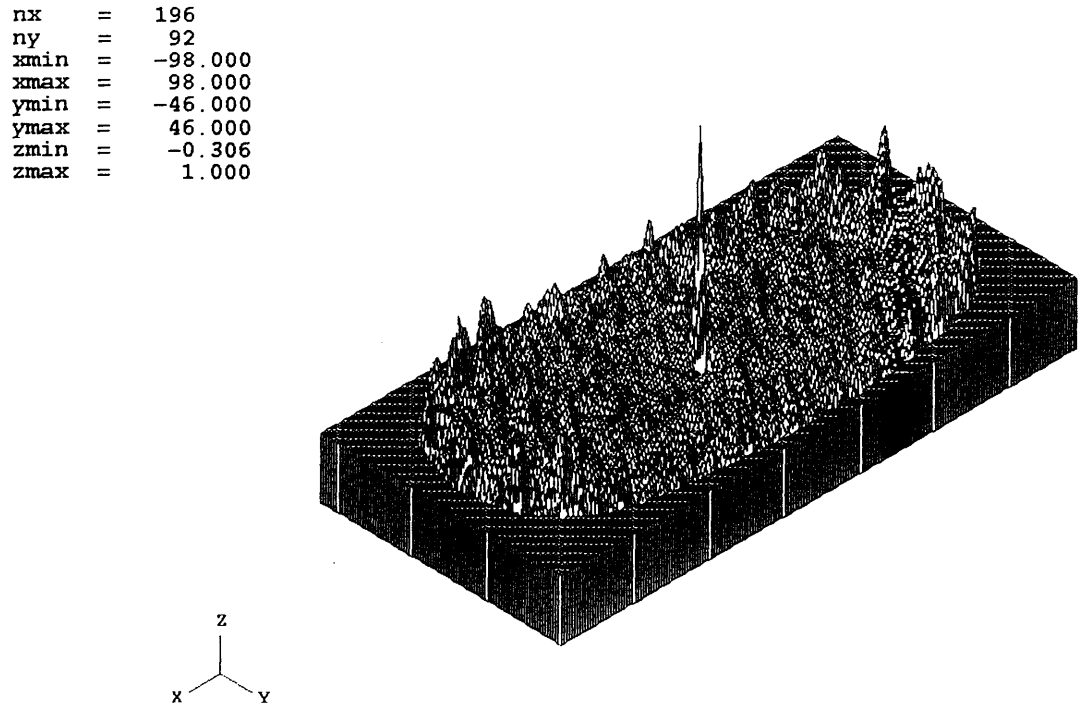

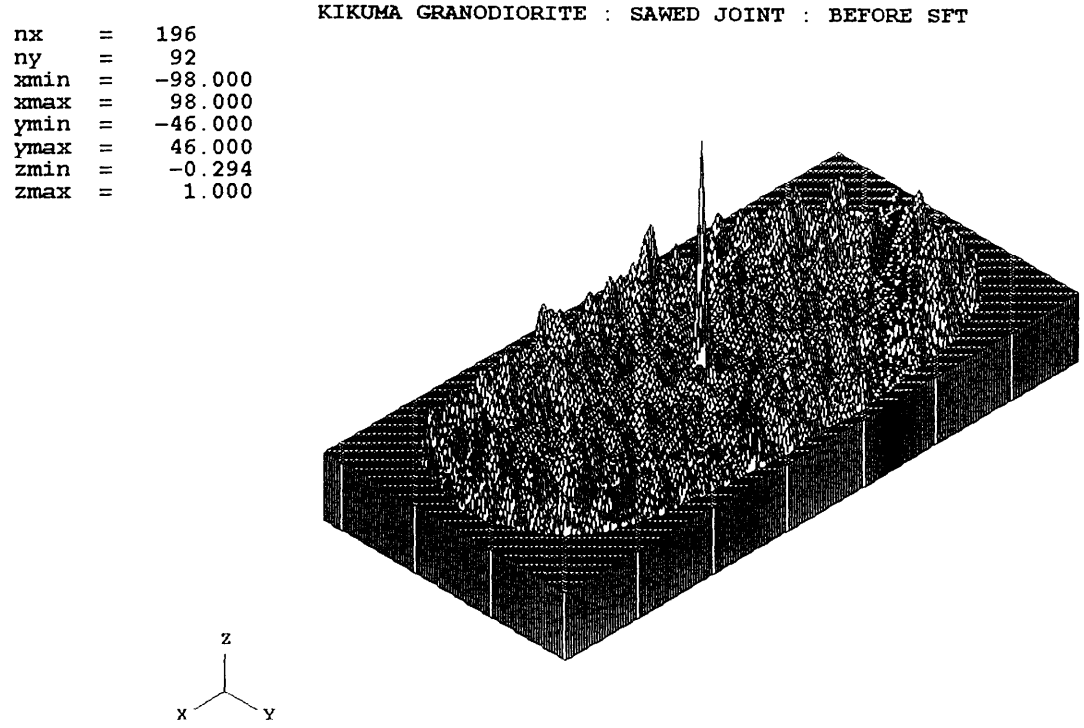

Fig.5.30 Comparison of 2-dimensional correlation function of aperture before and after stress-flow test
(b) Sawed joint in Kikuma granodiorite

nx = 196
ny = 92
xmin = -98.000
xmax = 98.000
ymin = -46.000
ymax = 46.000
zmin = -0.302
zmax = 1.000

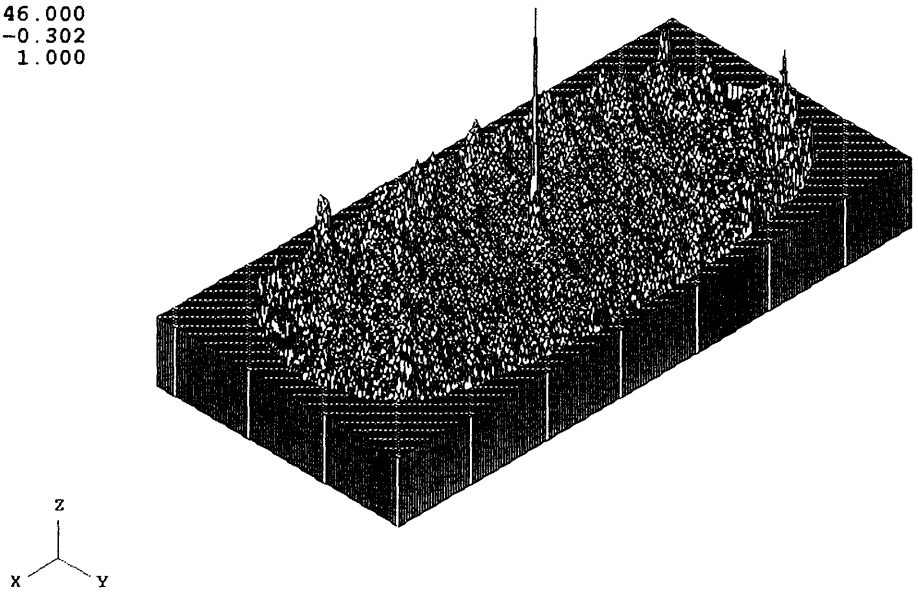

KIKUMA GRANODIORITE : TENSION JOINT : BEFORE SFT

nx = 192
ny = 94
xmin = -96.000
xmax = 96.000
ymin = -47.000
ymax = 47.000
zmin = -0.276
zmax = 1.000

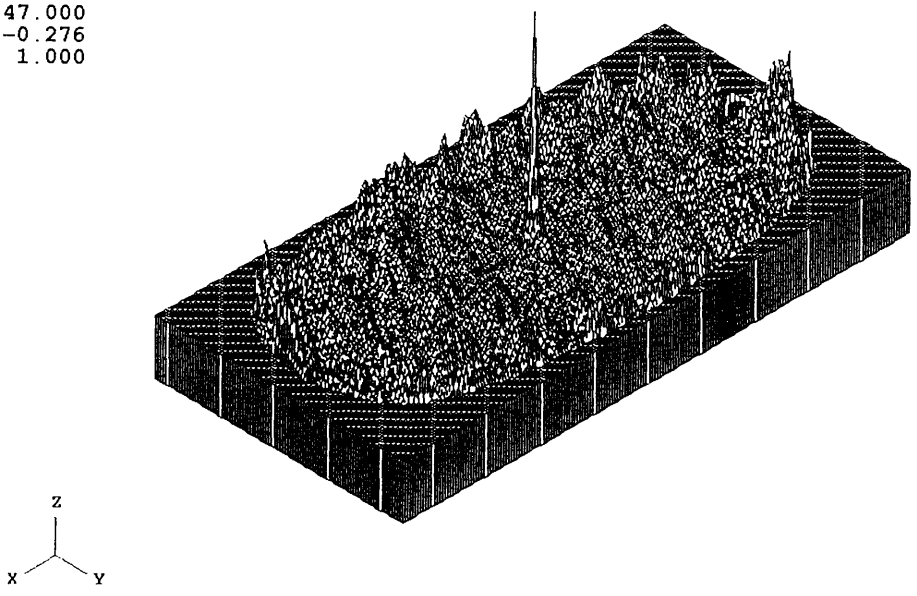

KIKUMA GRANODIORITE : TENSION JOINT : AFTER SFT

Fig.5.30 Comparison of 2-dimensional correlation function of aperture before and after stress-flow test
(c) Tension joint in Kikuma granodiorite

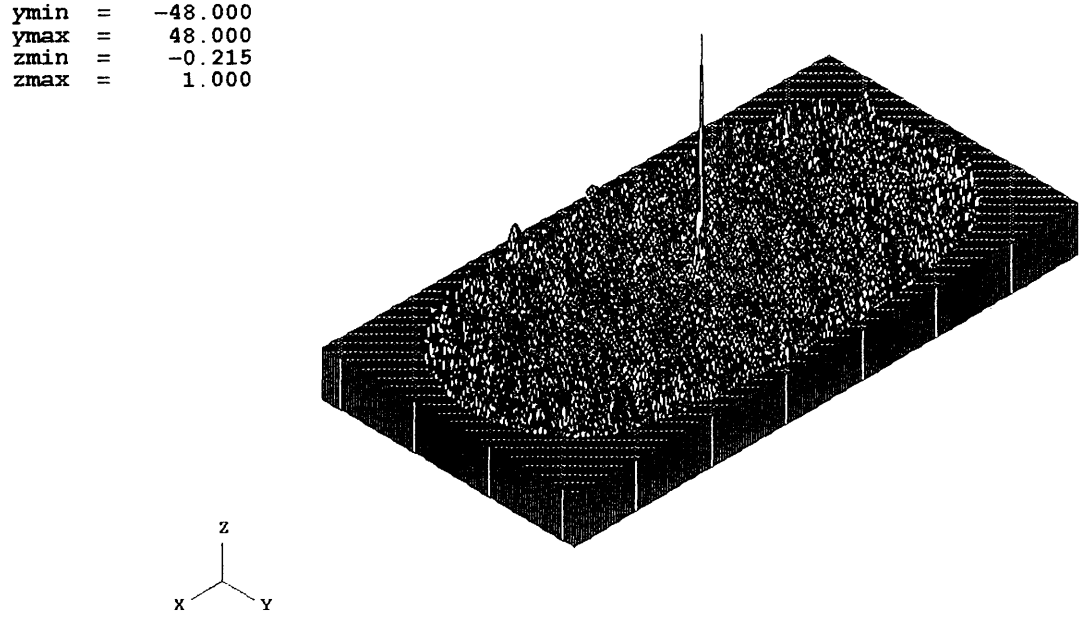

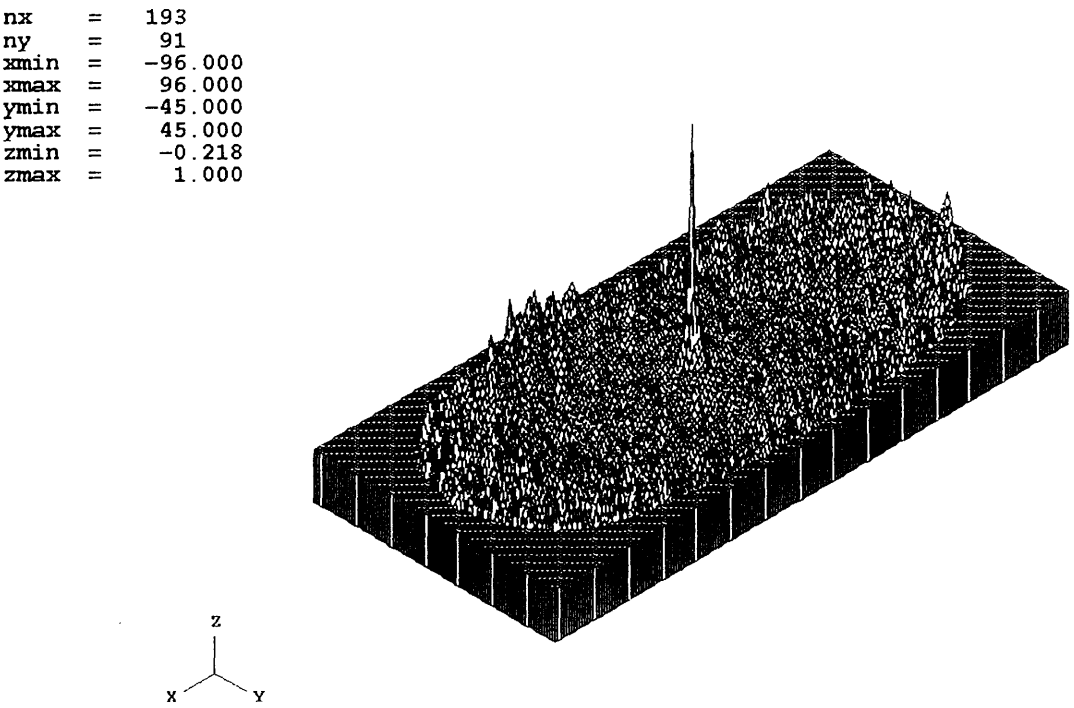

Fig.5.30 Comparison of 2-dimensional correlation function of aperture before and after stress-flow test
(d) Tension joint in Inada granite

nx = 192
ny = 92
xmin = -96.000
xmax = 96.000
ymin = -46.000
ymax = 46.000
zmin = -0.257
zmax = 1.000

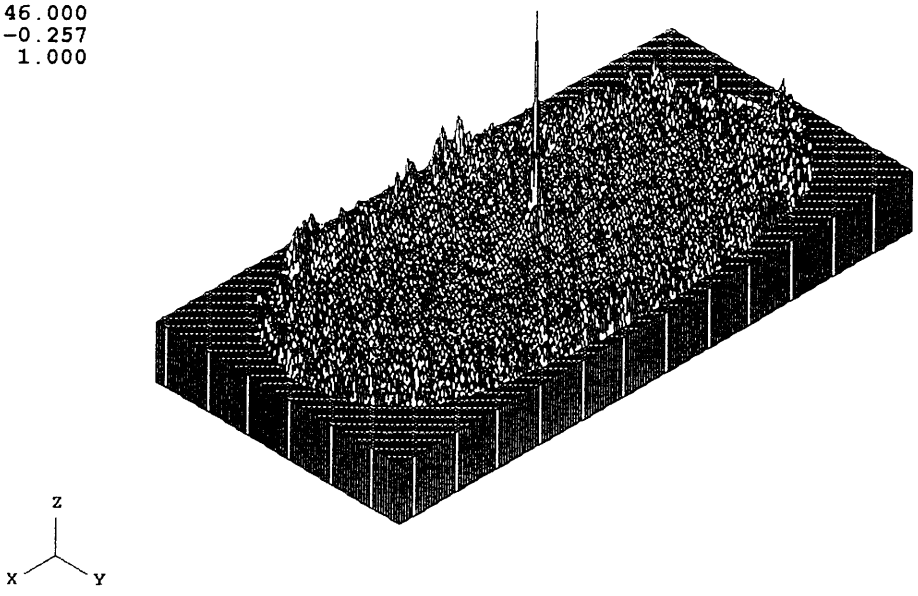

CHICHIBU SCHIST : TENSION JOINT : BEFORE SFT

nx = 192
ny = 90
xmin = -96.000
xmax = 96.000
ymin = -45.000
ymax = 45.000
zmin = -0.264
zmax = 1.000

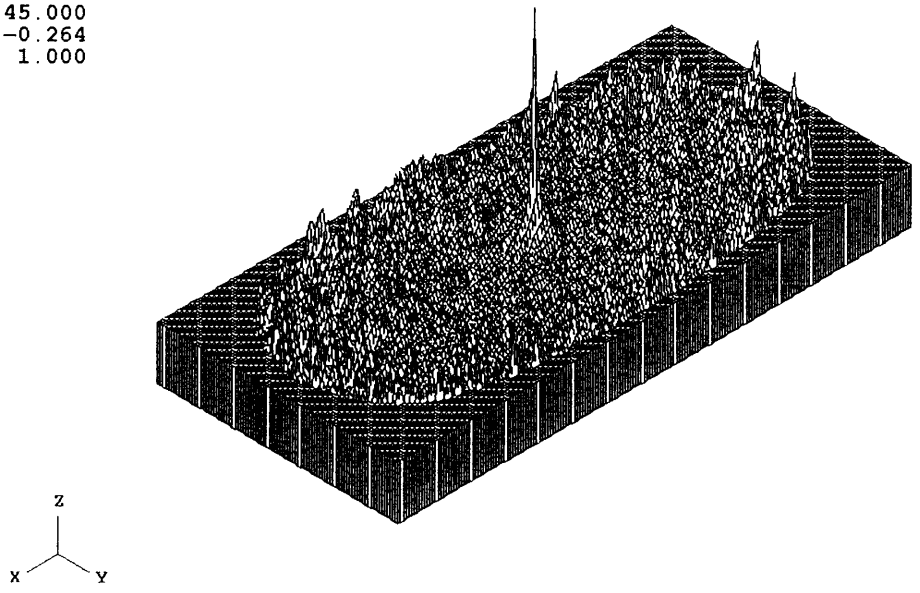

CHICHIBU SCHIST : TENSION JOINT : AFTER SFT

Fig.5.30 Comparison of 2-dimensional correlation function of aperture before and after stress-flow test
(e) Tension joint in Chichibu schist

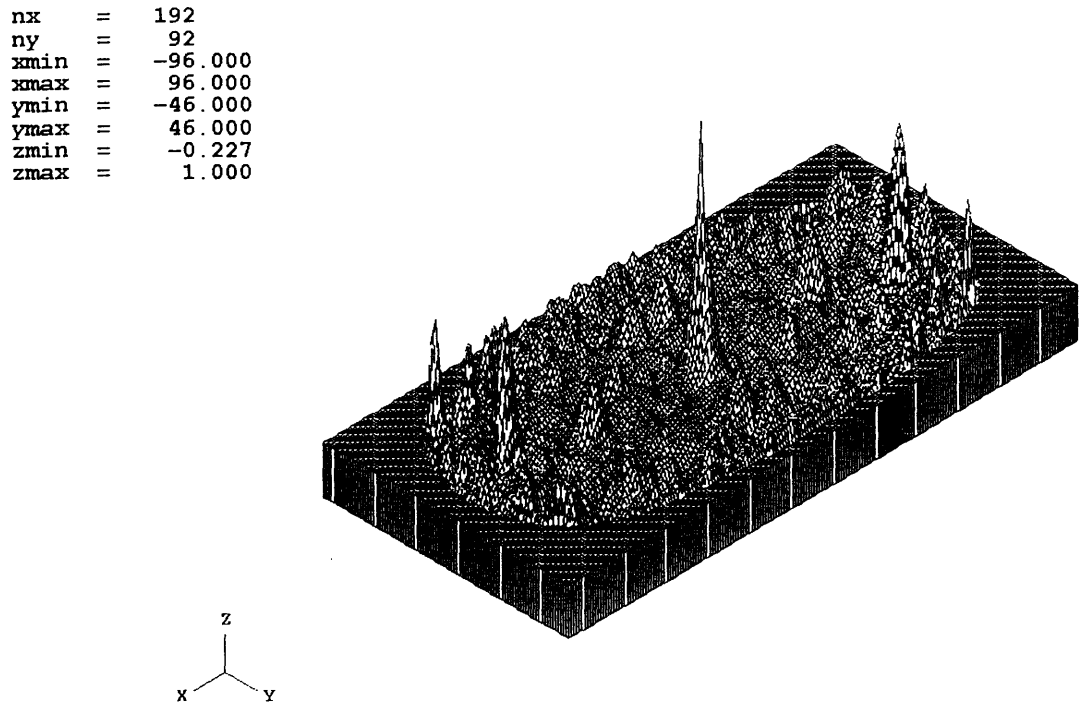

Fig.5.30 Comparison of 2-dimensional correlation function of aperture before and after stress-flow test
(f) Tension joint in Kimachi sandstone

Chapter 6 Conclusions and Recommendations

The objective of this research is to observe both the surface roughness and aperture of joints together with the hydromechanical behavior of a single joint and to draw conclusions from these observations. For these purposes, three different experiments have been conducted. In this chapter, the major results and contributions of this research are summarized. Also other potential applications and related future topics are identified.

6.1 Summary and contributions

The described method for measuring the surface roughness is relatively simple and produces results with sufficient accuracy. From the observed statistical values and distributions for the six joints, the aperture distributions seem to widen with increasing average aperture. Positive skewness is observed for all aperture distributions. These results are consistent with those reported by Hakami (1988) and Hakami and Barton (1990). All of the histograms seem to have either a normal or a lognormal form. However, based on the Kolmogorov-Smirnov test, neither form fits the aperture distributions and this for all six joints. This contradicts observations made by others which state that aperture distributions are usually lognormal (Gentier, 1986 ; Gale, 1987 ; Hakami, 1988). However, since we have only a limited set of observations, one cannot draw any conclusions at this stage. The aperture correlation in the six joints is limited to very small distances (less than 1 cm); in addition, these correlations are almost isotropic.

In this study, the effects of confining pressure and pore pressure on joint permeability for three different joints in granodiorite were measured using a transient pulse method. Two important contributions were made : the determination of both the coefficients a and b for joints, which describe the relative effect both of confining pressure and of pore pressure on joint permeability, respectively, and the observations of the stress history dependence of the joint permeability both due to the confining pressure cycle and due to the pore pressure cycle.

When comparing changes in permeability of both an intact rock and joints, the permeability decreases more rapidly with pressure for jointed rock than for intact rock. In a porous rock, water flows through the interconnected pores and cracks. The mean cross sectional area along a flow path is much smaller than for a joint. Also the flow length is much greater in an intact rock. These two differences can account for the magnitude differences in the permeability, but not for the fact that the permeability decreases more rapidly with pressure for a joint than for intact rock. It is, however, apparent that the

compressibility of a joint is much greater than that of intact rock. Therefore, a joint can close more rapidly under pressure than pores and cracks in an intact rock. Hence, the difference of the change of permeability with pressure between a joint and an intact rock is due to the differences in their compressibility.

The changes in confining pressure and pore pressure have significant effects on the joint permeability, but the confining pressure has a relatively greater effect on joint permeability than the internal pore pressure. In other words, the joint permeability is more sensitive to the external confining pressure than to the internal pore pressure. The fact that the effects of both the confining pressure and pore pressure on joint permeability are different suggests that one should be cautious when applying the term "effective pressure" or "effective stress" to jointed rock. It follows that effective pressure in jointed rock is not the conventional effective pressure, which is defined as the pressure difference between confining pressure and pore pressure and one should not use the conventional effective pressure for the evaluation of joint permeability and for the estimation of the hydraulic behavior of jointed rock. Instead of the conventional effective pressure, one should use the effective pressure, P_e, in general form as follows.

$$P_e = P_c - \alpha P_p \tag{6.1}$$

where P_c is confining pressure, P_p is pore pressure and α is the effective stress coefficient.

To determine the effective stress coefficient for the joint permeability, the transient pulse method is recommended. In the transient pulse method, only a small amount of water flows through a joint during an experiment and the required time for each measurement is relatively short, e.g. ; a couple of hours. This is in contrast to the conventional steady-state flow tests in which relatively large amounts of water must flow and longer testing time is needed to get to the steady-state condition. Therefore, for permeability measurements of rocks in the laboratory, the transient pulse method seems to be more effective and practical, in particular for low permeability rocks and rock joints.

The experimental results in this thesis are consistent with results observed by Kranz et al.(1979). At any particular confining pressure, one would expect more real area of contact the less rough the two opposing surfaces are. Asperities in contact affect the permeability in two ways. They change the path length or tortuosity of the flow path and they inhibit joint closure. Asperities are small so that the joint closes rapidly at low pressures until enough of these asperities make contact with opposing surfaces to increase the flow tortuosity and to decrease the closure rate.

An extensive series of stress-flow experiments using jointed specimens were conducted by applying external stress in form of uniform confining pressures. These tests show large hystereses of joint flow rate ($Q/\Delta H$) during the 1st cycle in all jointed specimens, which are consistent with several other experimental studies in which external stress was applied in form of normal stress to the joint plane [Iwai(1976), Witherspoon et al(1980), Pratt et al.(1977), Jones(1975) and Raven and Gale(1985)]. Also increasing the confining pressure leads to a reduction of hydraulic aperture and of joint transmissivity which is similar to what was observed by others [Kranz et al. (1979), Coyner et al.(1979) and Bernabe (1986)]. The decreasing hydraulic aperture and joint transmissivity indicate that permanent changes of the joint geometry occur. Regression analyses on joint transmissivity vs confining pressure show that the stress dependency of joint transmissivity in the loading process is larger than that in unloading. This difference may come from the difference of joint deformability in compression (loading process) and extension (unloading process).

What is more interesting is the fact that these hydraulic characteristics decrease with the number of loading-unloading cycles and that the initially very large hystereses related to loading and unloading decrease with the number of cycles. The non-linear behavior and the large hysteresis of mechanical aperture under increasing and decreasing confining pressure compare well to the observed joint flow behavior. The irrecoverable deformation in joint aperture also decreases with successive cycles for all joints. This indicates that the stress is inhomogeneously distributed and that shear stress can be developed locally at places where joint surfaces are contact. Therefore, these hystereses of the hydromechanical properties of joints may be the result of altered seating of the joint due to the crushing of the contact points or asperities during loading. Also, a comparison of experimental results on the six different joints indicates that the joint type seems to have an effect on the hydromechanical joint characteristics.

From experimental results in this thesis, the cubic law may not be valid under uniform confining stress, in particular at higher confining stress since the number of asperities in contact increase rapidly at higher confining stress, causing a decrease in the average void length in a joint and a resulting rapid decrease in the joint flow. From a comparison of the results in existing studies and in this study, it is concluded that the cubic law may be valid when the joint is far from being 'closed' (roughly when the average aperture is greater than 20 μm) under low normal stress or low uniform confining stress since surface roughness does not greatly influence the joint flow, and the degree of contact area across the joint seems to be small under these conditions. Also, the law is limited to the laminar flow region. However, the applicability strongly depends on the geometry of

joint aperture and on the mated condition of joint surfaces.

Aperture distributions show a decrease in mean aperture and a "sharpening" (decreasing variability) after the hydromechanical tests. One can, therefore, conclude that the changes in joint conductivity and transmissivity are indeed related to the permanent changes in joint geometry, and the change of aperture distribution (decrease in aperture and aperture variation) due to the hydromechanical experiments, in which the jointed specimens are subjected to three loading-unloading cycles, may be caused by the crushing of contact points or asperities during loading. However, the geometric changes in joint aperture, at least so far, are less dramatic than expected. Also, this seems to have no effect on aperture correlation. The research objectives, the experiments, the main results and the conclusions are schematically summarized in Fig.6.1.

6.2 Future research

In order to draw general conclusions on geometric joint aperture characteristics, more precise measurements and interpretations regarding joint apertures in the laboratory are required involving a wide variety of rock types, joint types and sizes, especially using natural joints. From an engineering point of view, however, these observations on the geometrical properties of joint aperture on small size joints (laboratory scale, i.e. ; less than 10 cm), cannot to be extrapolated to those on large size joints (e.g., in site scale) since in-situ joints may have both more large scale variations and more anisotropic correlation of apertures due to either their size or the multitude of joint genesis processes or both. Also, the described methods for the aperture measurements are all intended for research purposes. As Hakami et al. (1995) mention, one objective of future research on joint aperture characterization is the development of quick and simple methods for joint characterization. Further studies on size effect of the geometrical properties such as roughness and aperture are also highly recommended.

When a rock specimen is submitted to pressure cycling, one generally observes an irreversible variation of hydraulic conductivity due to irreversible changes in pore structure. This is a serious problem when one wishes to extrapolate laboratory data to in situ conditions. In the rock mechanics literature, the terms "stress history dependence" as well as "stress path dependence" refer to a dependence of rock properties on past state of stress. This behavior appears more clearly when rocks are submitted to a number of stress cycles. Haimson(1974), Zoback and Byerlee(1975) and Hadley(1976) studied the effect of such cycles on the dilatancy or the strength of rocks. Coyner et al.(1979), Kranz et al.(1979) and Bernabe et al.(1984) found that the hydraulic conductivity depended on the

stress path. However, these studies were often restricted to the properties of intact rocks. When a joint is stressed, the joint void space deforms, changes in contact area occur and so does the joint conductivity. The stress history dependence as well as stress path dependence of the hydraulic properties of rock joints are probably much greater than those of intact rocks since their stress dependence may arise from the changes of pores and cracks in rocks and in rock joints. To describe the void changes in rock joints with stress, one needs to develop an effective stress law for rock joints since the conventional effective stress law cannot be applied to rock joints. Little is known, however, about the effective stress coefficient, α, for rock joints. The common observation that α for intact rocks is constant with pressure, is probably not valid for rock joints. The experimental results in this thesis show that the effective stress coefficient for rock joints is more highly dependent on the stress path and the stress history than that for an intact rock. More theoretical and experimental work is needed to clarify the effects of external confining pressure and internal pore pressure on the hydraulic properties of joints and to develop an effective stress law for jointed rocks.

To characterize hydromechanical behavior of joints and to provide a solid basis for joint stress-flow theory, more work, particularly gathering of data from careful experimental investigations, is needed involving a wide variety of rock types, joint types and sizes. In particular, there are problems regarding scale effect that has been observed in determining the hydraulic properties of joints in rock specimens of different dimensions. From the experimental results in this thesis, one of the significant controlling parameters is joint roughness which can contribute to the joint closure, to the geometry of interconnecting voids in a joint and to contact area. The different scales of surface roughness first received attention in terms of their role in defining shear strength between two rough contacting surfaces. Variations in height and spacing of asperities have received considerable attention from workers who have attempted to develop models for joint closure under normal stress conditions. On the other hand, there are a few investigations on the scale effect of joint hydraulic properties (Witherspoon et al. 1979, Brace 1984, Raven and Gale 1985, Gale 1993). The results of these studies and this study suggest that more work on the measurement of joint aperture in combination with stress-flow (hydromechanical) tests on different size joints is needed.

It is hoped that this study may help to provide a rational framework for such future investigations and will provide some aid to other researchers in this field.

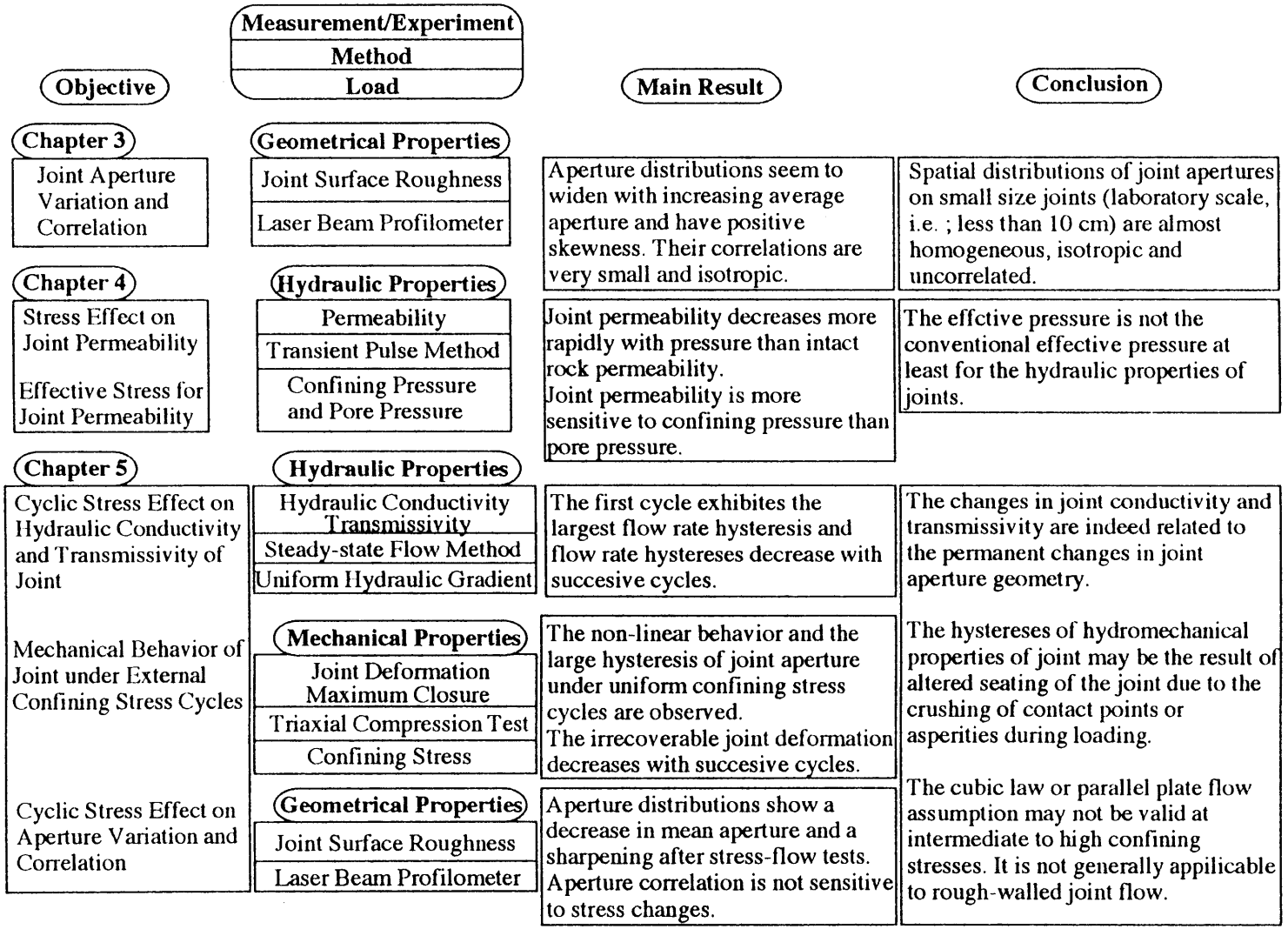

Fig.6.1 Summary of research

Bibliography

Abelin H., I. Neretnieks, S. Tunbrant and L. Moreno (1985), Final Report of the Migration in a Single Fracture - Experimental Results and Evaluation, SKB Technical Report, TR 85 - 03, SKB, Stockholm, Sweden.

Amadei B. and S. Saeb (1990), Constitutive Models of Rock Joints, Proceedings of the International Symposium on Rock Joints, Loen, Norway, pp.581-594.

Amadei B. and T. Illangasekare (1992), Analytical Solutions for Steady and Transient Flow in Non-homogeneous and Anisotropic Rock Joints, International Journal of Rock Mechanics and Mining Sciences and Geomechanics Abstracts, Vol.29, No.6, pp.561-572.

Amadei B. and T. Illangasekare (1994), A Mathematical Model for Flow and Solute Transport in Non-homogeneous Rock Fractures, International Journal of Rock Mechanics and Mining Sciences and Geomechanics Abstracts, Vol.31, No.6, pp.719-731.

Aoki, T., M. Sato and K. Kamemura (1987), The Triaxial Testing Apparatus for Rock Relating to High Temparature, High Stress and High Pore Pressure Conditions, Taisei Technical Research Report, Technical Research Center, Taisei Corporation, No.19, pp.235-243 (written in Japanese with Englist Abstract).

Aoki, T., C.P. Tan and W.E. Bamford (1993), Effects of Deformation and Strength Anisotropy on Borehole Stability in Saturated Shales, International Journal of Rock Mechanics and Mining Sciences and Geomechanics Abstracts, Vol.30, No.6.

Aoki, T., Y. Ijiri and M. Shimo (1994), A Development of High Performance Transient Pulse Test Machine, Annual Conference of Japanese Society of Civil Engineering, Sapporo, III-43, pp.80-81 (written in Japanese).

Bandis S. C., A.C. Lumsden and N. Barton (1981), Experimental Studies of Scale Effects on the Shear Behavior of Rock Joints, International Journal of Rock Mechanics and Mining Sciences and Geomechanics Abstracts, Vol.18, pp.1-21.

Bandis S. C., A.C. Lumsden and N. Barton (1983), Fundamentals of Rock Joint Deformation, International Journal of Rock Mechanics and Mining Sciences and Geomechanics Abstracts, Vol.20, No.6, pp.249-268.

Barton N.(1971), A Relationship between Joint Roughness and Joint Shear Strength, Proceedings of International Symposium on Rock Fracture, Paper I-8, Nancy, France.

Barton N.(1972), A Model Study of Rock-Joint Deformation, International Journal of Rock Mechanics and Mining Sciences, Vol. 9, pp.579-602.

Barton N.(1973), Review of a New Shear-Strength Criterion for Rock Joints, Engineering Geology, Vol. 7, pp.287-332.

Barton N., R. Lien and J. Lunde (1974), Engineering Classification of Rock Masses for the Design of Tunnel Support, Rock Mechanics, Vol. 6, pp.189-236.

Barton N. and V. Choubey (1976), The Shear Strength of Rock Joints in Theory and Practice, Rock Mechanics, Vol. 10, pp.1-54.

Barton N.(1977), The Shear Strength of Rock and Rock Joints, International Journal of Rock Mechanics and Mining Sciences and Geomechanics Abstracts, Vol. 13, pp.255-279.

Barton N., Bandis S. C. (1980), Some Effects of Scale on the Shear Strength of Joints, International Journal of Rock Mechanics and Mining Sciences and Geomechanics Abstracts, Vol.17, pp.69-73.

Barton N., S.C. Bandis and C. Bakhtar (1985), Strength Deformation and Conductivity Coupling of Rock Joints, International Journal of Rock Mechanics and Mining Sciences and Geomechanics Abstracts, Vol. 22, No.3, pp.121-140.

Barton N. (1986), Deformation Phenomena in Jointed Rock, Geotechnique, Vol.36, No.2, pp.147-167.

Batzle, M.L., G. Simmons and W. Siegfried (1980), Microcrack Closure in Rocks under stress; Direct Observation, Journal of Geophysical Research, Vol.85, No.B12, pp.7072-7090.

Bernabe, Y., W.F. Brace and B. Evans (1982), Permeability, Porosity and Pore Geometry of Hot-Pressed Calcite, Mechanics of Materials, Vol.1, pp.173-183.

Bernabe, Y. (1985), Permeability and Pore Structure of Rock Under Pressure, Ph.D. Dissertation, Massachusetts Institute of Technology, Cambridge, Massachusetts.

Bernabe, Y. (1986), The Effective Pressure Law for Permeability in Chelmsford Granite and Barre Granite, International Journal of Rock Mechanics and Mining Sciences and Geomechanics Abstracts, Vol.23, No.3, pp.267-275.

Bernabe, Y. (1986), Pore Volume and Transport Properties Changes During Pressure Cycling of Several Crystalline Rocks, Mechanics of Materials, Vol.5, pp.235-249.

Bernabe, Y. (1987), A Wide Range Permeameter for Use in Rock Physics, International Journal of Rock Mechanics and Mining Sciences and Geomechanics Abstracts, Vol.24, No.5, pp.309-315.

Bernabe, Y. (1988), Comparison of the Effective Pressure Law for Permeability and Resistivity Formation Factor on Chelmsford Granite, Pageoph, Vol.127, No.4, pp.607-625.

Berryman, J.G. (1992), Effective Stress for Transport Properties of Inhomogeneous Porous Rock, Journal of Geophysical Research, Vol.97, No.B12, pp.17,409-17,424.

Benjamin J.R. and C.A. Cornell(1970), Probability, Statistics, and Decision for Civil Engineers, McGraw-Hill, Inc., New York.

Bianchi, L. and D.T. Snow (1968), Permeability of Crystalline Rock Interpreted from Measured Orientation and Apertures of Fracture, Annals of Arid Zone, Vol.8, pp.231-245.

Brace, W.F., A.S. Orange and T.R. Madden (1965), The Effect of Pressure on the Electrical Resistivity of Water-Saturated Crystalline Rocks, Journal of Geophysical Research, Vol.70, No.22, pp.5,669-5,678.

Brace, W.F. (1965), Relation of Elastic Properties of Rocks to Fabric, Journal of Geophysical Research, Vol.70, No.22, pp.5,657-5,667.

Brace, W.F., B.W. Paulding and C.H. Scholz (1966), Dilatancy in the Fracture of Crystalline Rocks, Journal of Geophysical Research, Vol.71, No.16, pp.3,939-3,953.

Brace, W.F., J.B. Walsh, and W.T. Frangos (1968), Permeability of Granite under High Pressure, Journal of Geophysical Research, Vol.73, No.6, pp.2,225-2,236.

Brace, W.F. (1977), Permeability from Resistivity and Pore Shape, Journal of Geophysical Research, Vol.82, No.23, pp.3,343-3,349.

Brace, W.F. (1980), Permeability of Crystalline and Argillaceous Rocks, International Journal of Rock Mechanics and Mining Sciences and Geomechanics Abstracts, Vol. 17, pp.241-251.

Brace, W.F. (1984), Permeability of Crystalline Rocks: New In-situ Measurements, Journal of Geophysical Research, Vol.89, No.B6, pp.4,327-4,330.

Brown, D.M. (1984), Stochastic Analysis of Flow and Solute Transport in a Variable-Aperture Rock Fracture, M.S. Thesis, Massachusetts Institute of Technology, Cambridge, Massachusetts.

Brown, S.R. (1984), Fundamental Study of the Closure Property of Joints, Ph.D Dissertation, Columbia University, New York.

Brown, S.R. and C.H. Scholz (1985), Closure of Random Elastic Surfaces in Contact, Journal of Geophysical Research, Vol.90, No.B7, pp.5,531-5,545.

Brown, S.R. and C.H. Scholz (1985), Broad Bandwidth Study of the Topography of Natural Rock Surfaces, Journal of Geophysical Research, Vol.90, No.B14, pp.12,575-12,582.

Brown, S.R. and C.H. Scholz (1986), Closure of Rock Joints, Journal of Geophysical Research, Vol.91, No.B5, pp.4,939-4,948.

Brown, S.R., R.L. Kranz and B.P. Bonner (1986), Correlation between the Surfaces of Natural Rock Joints, Geophysical Research Letters, Vol.13, pp.1,430-1,433.

Brown, S.R. (1987), A Note on The Description of Surface Roughness Using Factual Dimension, Geophysical Research Letters, Vol.14, No.11, pp.1,095-1,098.

Brown, S.R. (1987), Fluid Flow through Rock Joints ; The Effect of Surface Roughness, Journal of Geophysical Research, Vol.92, No.B2, pp.1,337-1,347.

Brown, S.R. (1989), Transport of Fluid and Electric Current Through a Single Fracture, Journal of Geophysical Research, Vol.94, No.B7, pp.9,429-9,438.

Carslaw, H.S. and J.C. Jaeger (1959), Conduction of Heat in Solids, Oxford Univ. Press, London.

Carrol, M.M. (1979), An Effective Stress Law for Anisotropic Elastic Deformation, Journal of Geophysical Research, Vol.84, No.B13, pp.7,510-7,512.

Caruso, L., G. Simmons and R. Wilkens (1985), The Physical Properties of a Set of Sandstones-Part I. The Samples, International Journal of Rock Mechanics and Mining Sciences, and Geomechanics Abstracts, Vol. 22, No.6, pp.381-392.

Clauser, C. (1992), Permeability of Crystalline Rocks, EOS, Trans. AGU, Vol.73, No.21, P.233.

Coyner, K.B., W.F. Brace and J.B. Walsh (1979), EOS, Trans. AGU, Vol.60, No.46, P.943.

David, C. and M. Darot (1989), Permeability and Conductivity of Sandstones, Proceedings of the International Symposium on Rock at Great Depth, pp.203-209, Pau, France.

Daw, G.P. (1974), The Effect of Applied Stress upon The Permeability of Some Permian and Triassic Sandstone of Northern England, Proceedings of the 3rd International Congress on Rock Mechanics, Denver, Colorado, pp.537-542.

Dey, T.D. (1986), Permeability and Electrical Conductivity Changes due to Hydrostatic Stress Cycling of Berea and Muddy J Sandstone, Journal of Geophysical Research, Vol.91, pp.763-766.

Dropec, R.K., J.N. Johnson and J.B. Walsh (1978), The Influence of Pore Pressure on the Mechanical Properties of Kayenta Sandstone, Journal of Geophysical Research, Vol.83, No.B6, pp.763-766.

Douglass, P.M. and B. Voight (1969), Anisotropy of Granites ; A Reflection of Microscopic Fabric, Geotechnique, Vol.19, No.3, pp.376-398.

Dullien, F. A. C. (1979), Porous Media, Fluid Transport and Pore Structure, Academic Press, New York.

Elsworth D. and R.E. Goodman (1986), Characterization of Rock Fissure Hydraulic Conductivity Using Idealized Wall Roughness Profiles, International Journal of Rock Mechanics and Mining Sciences and Geomechanics Abstracts, Vol. 23, No.3, pp.233-243.

Elsworth D. and C.R. Mase (1993), Groundwater in Rock Engineering, Comprehensive Rock Engineering, Vol.1, pp.201-226.

Engelder, T and C. Scholz(1981), Fluid Flow along Very Smooth Joints at Effective Pressure up to 200 Megapascals. In Mechanical Behavior of Crustal Rocks, Am. Geophys. Un. Monogr., Vol.24, PP.147-152.

Feves, M. and G. Simmons (1976), Effect of Stress on Cracks in Westerly Granite, Bulletin of the Seismological Society of America, Vol.66, No.5, pp.1,755-1,765.

Freeze, R.A. and J.A. Cherry (1979), Groundwater, Prentice-Hall, Inc., New Jersey.

Gale, J.E. (1980), Effects of Fracture Type on Permeability, Proceedings of the 23rd U.S. Symposium on Rock Mechanics, Berkeley, California, pp.291-298.

Gale, J.E. (1982), The Effects of Fracture Type (Induced versus Natural) on the Stress-fracture Closure-fracture Permeability Relationships, Proceedings of the 23th U.S. Symposium on Rock Mechanics, Univ. of California, Berkeley, California, pp.290-298.

Gale, J.E. (1987), Comparison of Coupled Fracture Deformation and Fluid Flow Models with Direct Measurements of Fracture Pore Structure and Stress-flow Properties, Proceedings of the 28th U.S. Symposium on Rock Mechanics, Tucson, Arizona, pp.1,213-1,222.

Gale, J.E. (1993), Fracture Properties from Laboratory and Large Scale Field Tests : Evidence of Scale Effects, Proceeding of the 2nd International Workshop on Scale Effects in Rock Masses - Scale Effect in Rock Masses 93, Lisbon, Portugal, pp.341-352.

Gangi, A.F. (1978), Variation of Whole and Fractured Porous Rock Permeability with Confining Pressure, International Journal of Rock Mechanics and Mining Sciences and Geomechanics Abstracts, Vol. 15, pp.249-257.

Garg, S.K. and A. Nur (1973), Effective Stress Laws for Fluid-Saturated Porous Rocks, Journal of Geophysical Research, Vol.78, No.26, pp.5,911-5,921.

Gaviglio P. and Y. Glard (1971), Study of a Jointed Dolomitic Limestone, Proceedings of the International Symposium on Rock Fracture, Paper I-8, Nancy, France.

Gerrard, C. (1985), Formulation for the Mechanical Properties of Rock Joints, Proceedings of the International Symposium on Fundamentals of Rock Joints, Björkliden, Lapland, Sweden, pp.405-422.

Gelhar, L. W. and C.L. Axness (1986), Three Dimensional Stochastic Analysis of Macrodispersion in Aquifer, Water Resources Research, Vol.19, No.1, pp.161-180.

Gelhar, L. W. (1986), Stochastic Subsurface Hydrology: : From Theory to Application, Water Resources Research, Vol.22, No.9, pp.135S-145S.

Gelhar, L.W. (1987), Appications of Stochastic Models to Solute Transport in Fractured Rocks, SKB Technical Report, TR 87-05, SKB, Stockholm, Sweden.

Gentier, S. (1986), Morphologie et comportement hydromecanique d'une fracture naturelle dans un granite sous contrainte normale, Ph.D Dissertation, Université d'Orleans, Orléans, France.

Gentier, S., D. (1987), Comportement hydromécanique d'une fracture naturelle sous contraine normale, Proceedings of the 6th International Congress on Rock Mechanics, Montréal, Canada, pp.105-108.

Gentier, S., D. Billaux and L. Vliet (1989), Laboratory Testing of the Voids of a Fracture, Rock Mechanics and Rock Engineering, Vol.22, No.3, pp.149-157.
Goodman, R. (1976), Methods of Geological Engineering in Discontinuous Rocks, West Publishing Company, New York.

Goodman, R. and C. St. John (1977), Finite Element Analysis for Discontiuous Rocks, International Journal for Numerical and Analytical Methods in Geomechanics, Vol.1., pp.148-175.

Guéguen, Y. and V. Palciauskas (1994), Introduction to the Physics of Rocks, Princeton University Press, New Jersey.

Greenwood, J. A. and J.B.P. Williamson (1966), Contact of Nominally Flat Surfaces, Proc. Royal Society of London, Ser. A295, pp.300-319.

Handin, J., R.V. Hager, Jr., M. Friedman and J.N. Feather (1963), Experimental Deformation of Sedimentary Rocks under Confining Pressure, Bulletin of the American Association of Petroleum Geologists, Vol.47, No.5, pp.717-755.

Hakami, E. (1988), Water Flow in Single Rock Joints, Licentiate Thesis, Luleå University of Technology, Luleå, Sweden.

Hakami, E. and N. Braton (1990), Aperture Measurements and Flow Experiments using Transparent Replicas of Rock Joints, Proceedings of the International Symposium on Rock Joints, Loen, Norway, pp.383-390.

Hakami, E. (1992), Joint Aperture Measurements - An Experimental Technique, Proceedings of the International Symposium on Fractured and Jointed Rock Masses, Lake Tahoe, California, pp.463-467.

Hakami, E. and O. Stephansson (1993), Experimental Technique for Aperture Studies of Intersecting Joints, Eurock '93, Lisbon, Portugal, pp.301-308.

Hakami, E., H.H. Einstein, S. Gentier and M. Iwano (1995), Characterization of Fracture Apertures - Methods and Parameters, Proceedings of the 8th International Congress on Rock Mechanics, Tokyo, Japan (to be published).

Holcomb D.J. and J.L. Stevens (1980), The Reversible Griffith Crack : A Viable Model for Dilatancy, Journal of Geophysical Research, Vol.85, No.12, pp.7,101-7,107.

Hsieh, P.A., J.V. Tracy, C.E. Neuzil, J.D. Bredehoeft and S.E. Silliman (1981), A Transient Laboratory Method for Determining the Hydraulic Properties of 'Tight' Rocks - 1. Theory, International Journal of Rock Mechanics and Mining Sciences and Geomechanics Abstracts, Vol. 18, pp.245-252.

Hsieh P. A. and Neuman S. P.(1985), Field Determination of the Three-Dimensional Hydraulic Conductivity Tensor of Anisotropic Media - 1. Theory, Water Resources Research, Vol.21, No.11, pp.1,655-1,665.

Hsieh P. A., Neuman S. P., Stiles G. K. and Simpson E. S.(1985), Field Determination of the Three-Dimensional Hydraulic Conductivity Tensor of Anisotropic Media - 2. Methodology and Application to Fractured Rocks, Water Resources Research, Vol.21, No.11, pp.1,667-1,676.

Hustrulid, W.A. and G.A. Johnson (1990), Rock Mechanics Contributions and Challenges, Proceedings of the 31st U.S. Symposium on Rock Mechanics, Boulder, Colorado, pp.269-276.

Ishijima Y., Z. Xue and M. Takahashi (1993), Some Basic Problems on Measurement of Hydraulic Properties of Rock by the Transient Pulse Method, Shigen-to-Sozai, Vol.109, pp.511-516 (written in Japanese with English abstract).

Iwai, K. (1976), Fundamental Studies of the Fluid Flow through a Single Fracture, Ph.D Dissertation, Univ. of California, Berkeley, California.

Iwano M. (1990), Probabilistic Modelling of a Single Fracture, M.S. Thesis, Massachusetts Institute of Technology, Cambridge, Massachusetts.

Iwano M. and H.H. Einstein (1993), Stochastic Analysis of Surface Roughness, Aperture and Flow in a Single Fracture, Eurock '93, Lisbon, Portugal, pp.135-141.

Iwano M. and H.H. Einstein (1995), Laboratory Experiments on Geometric and Hydromechanical Characteristics of Three Different Fractures in Granodiorite, Proceedings of the 8th International Congress on Rock Mechanics, Tokyo, Japan (to be published).

Jones, F.O., Jr. (1975), A Laboratory Study of the Effects of Confining Pressure on Fracture Flow and Storage Capacity in Carbonate Rocks, Journal of Petroleum Technology, pp.21-27.

Jouanna, P. (1972), Laboratory Tests on the Permeability of Micaschist Samples under Applied Stresses, Proceedings of International Symposium on Percolation through Fissured Rock, I.S.R.M., T2-F, Stuttgart, Germany.

Kimura, T. and T. Esaki (1992), Surface Roughness and Apertures of a Fractured Rock and Its Hydraulic Properties, Journal of the Japanese Society of Engineering Geology, Vol.33, No.2, pp.61-70 (written in Japanese with English abstract).

Kranz, R.L. and C.H. Scholz (1977), Critical Dilatant Volume of Rocks at the Onset of Tertiary Creep, Journal of Geophysical Research, Vol.82, No.30, pp.4,893-4,898.

Kranz, R.L. (1979), Crack Growth and development during Creep of Barre Granite, International Journal of Rock Mechanics and Mining Sciences and Geomechanics Abstracts, Vol.16, pp.23-35.

Kranz, R.L. (1979), Crack-crack and Crack-pore Interactions in Stressed Granite, International Journal of Rock Mechanics and Mining Sciences and Geomechanics Abstracts, Vol.16, pp.37-47.

Kranz, R.L., A.D. Frankel, T. Engelder and C.H. Scholz (1979), The Permeability of Whole and Jointed Barre Granite, International Journal of Rock Mechanics and Mining Sciences and Geomechanics Abstracts, Vol.16, pp.225-234.

Kulhawy, F.H. (1975), Stress Deformation Properties of Rock and Rock Discontinuities, Engineering Geology, Vo.9, pp.327-390.

Lee, C. and I. Farmer (1993), Fluid Flow in Discontinuous Rocks, Chapman & Hall Inc., London.

Lin, W. (1982), Parametric Analysis of the Transient Method of Measuring Permeability, Journal of Geophysical Research, Vol.87, No.B2, pp.1,055-1,060.

Long, J.C.S. (1983), Investigation of Equivalent Porous Medium Permebility in Networks of Discontinuous Fractures, Ph.D Dissertation, Univ. of California, Berkeley, California.

Louis, C. (1969), A Study of Ground Water Flow in jointed Rock and Its Influence on the Stability of Rock Masses, Rock Mechanics Report, No.10, Imperial College, London.

Louis, C. (1974), Rock Hydraulics, Bureau de Recherches Geologiques et Minieres.

Lumley, J. L. and H.A. Panofsky (1964), The Structure of Atmospheric Turbulence, John Wiley & Sons Inc., New York.

Mantoglou, A. and J.L. Wilson (1981), Simulation of Random Fields with the Turning Bands Method, R.M. Parsons Laboratory Report, No.264, Massachusetts Institute of Technology, Cambridge, Massachusetts.

Mantoglou, A. and J.L. Wilson (1982), The Turning Bands Method for Simulation of Random Fields Using Line Generation by a Spectral Method, Water Resources Research, Vol.18, No.5, pp.1,379-1,394.

Matheron, G. (1973), The Intrinsic Random Functions and Their Application, Adv. Appl. Prob., Vol.5, pp.439-468.

Matsuki, K. and H. Kudo, Cyclic Fatigue Characteristics of Unsaturated Rocks under Confining Pressure, Journal of the Mining and Metallurgy Institute of Japan, Vol.102, No.1186, pp.849-854 (written in Japanese).

Maurice, A.B. (1941), General Theory of Three-Dimensional Consolidation, Journal of Applied Physics, Vol.12, pp.155-164.

Mejia, J. and I. Rodriguez-Iturbe (1974), On the Synthesis of Random Fields from the Spectrum : An Application to the Generation of Hydrologic Spatial Processes, Water Resources Research, Vol.10, No.4, pp.705-711.

Miller, S.M., P.C. McWilliams and J.C. Kerkering (1990), Ambiguities in Estimating Fractal Dimensions of Rock Fracture, Proceedings of the 31st U.S. Symposium on Rock Mechanics, Boulder, Colorado, pp.471-478.

Mizell, S. A., A.L. Gutjahr and L.W. Gelhar (1982), Stochastic Analysis of Spatial Variability in Two-dimensional Steady Ground Flow Assuming Stationary and Non-stationary Heads, Water Resources Research, Vol.18, No.4, pp.1,053-1,067.

Moreno L., I. Neretnieks and T. Eriksen (1985), Analysis of Some Laboratory Tracer Runs in Natural Fissures, Water Resources Research, Vol. 21, No.7, pp.951-958.

Moreno, L., Y.W. Tsang, C.F. Tsang, F.V. Hale and I. Neretnieks (1988), Flow and Transport in a Single Fracture : A Stochastic Model and Its Relation with Field Observations, Water Resources Research, Vol.24, No.12, pp.2,033-2,048.

Moreno, L., C.F. Tsang, Y. Tsang and I. Neretnieks (1990), Some Anomalous Features of Flow and Solute Transport Arising from Fracture Aperture Variability, Water Resources Research, Vol.26, No.10, pp.2,377-2,391.

Moss W.C. and Y.H.A. Gupta (1982), A Constitutive Model Describing Dilatancy and Cracking in Brittle Rocks, Journal of Geophysical Research, Vol.87, pp.2,985-2,998.

Nelson R.A. and J. Handin (1977), Experimental Study of Fracture Permeability in Porous Rock, Bulletin of the American Association of Petroleum Geologists, Vol.61, No.2, pp.227-236.

Neuman, S.P. (1990), Universal Scaling of Hydraulic Conductivities and Dispersivities in Geologic Media, Water Resources Research, Vol.26, No.8, pp.1,749-1,758.

Neuzil, C. E. and J.V. Tracy (1981), Flow through Fractures, Water Resources Research, Vol.17, No.1, pp.191-199.

Neuzil C.E., C. Cooley, S.E. Silliman, J.D. Bredehoeft and P.A. Hsieh (1981), A Transient Laboratory Method for Determining the Hydraulic Properties of 'Tight' Rocks - 2. Application, International Journal of Rock Mechanics and Mining Sciences and Geomechanics Abstracts, Vol. 18, pp.253-258.

Nishiyama T. and H. Kusuda (1994), Identification of Pore Spaces and Microcracks Using Fluorescent Resins, International Journal of Rock Mechanics and Mining Sciences and Geomechanics Abstracts, Vol. 31, No.4, pp.253-258.

Nur, A. and J.D. Byerlee (1971), An Exact Effective Stress Law for Elastic Deformation of Rocks with Fluids, Journal of Geophysical Research, Vol.76, No.26, pp.6,414-6,419.

Nur, A. (1974), Matsushiro, Japan, Earthquake Swarm ; Confirmation of the Dilatancy-Fluid Diffusion Model, Geology, pp.217-221.

Olsson, W.A. (1992), The Effect of Slip on the Flow of Fluid through a Fracture, Geophysical Research Letters, Vol.19, No.6, pp.541-543.

Paterson, M.S. (1978), Experimental Rock Deformation - The Brittle Field, Springer-Verlag, New York.

Paterson, M.S. (1983), The Equivalent Channel Model for Permeability and Resistivity in Fluid-Saturated Rock-A Re-Appraisal, Mechanics of Materials, Vol.2, pp.345-352.

Pratt, H.R., H.S. Swolfs, W.F. Brace, A.D. Black and J.W. Handin (1977), Elastic and Transfort Properties of an In Situ Jointed Granite, International Journal of Rock Mechanics and Mining Sciences and Geomechanics Abstracts, Vol.14, pp.35-45.

Pyrak-Nolte, L.J., L.R. Myer, N.G.W. Cook and P.A. Witherspoon (1987), Hydraulic and Mechanical Properties of Natural Fractures in Low Permeability Rock, Proceedings of the 6th International Congress on Rock Mechanics, Vancouver, Canada, Vol.1, pp.225-231.

Pyrak-Nolte L. J. and N.G.W. Cook (1988), Fluid Percolation through Single Fractures, Geophysical Research Letters, Vol.15, No.11, PP.1,247-1,250.

Raven, K. G. and J.E. Gale (1985), Water Flow in a Natural Rock Fracture as a Function of Stress and Sample Size, International Journal of Rock Mechanics and Mining Sciences and Geomechanics Abstracts, Vol.22, No.4, pp.251-261.

Roberds, W.J. (1979), Numerical Modelling of Jointed Rock, Sc.D. Dessertation, Massachusetts Institute of Technology, Cambridge, Massachusetts.

Roberds, W.J., M. Iwano and H.H. Einstein (1990), Probabilistic Mapping of Rock Joint Surfaces, Proceedings of the International Symposium on Rock Joints, Loen, Norway, pp.681-691.

Robin, P.Y.F. (1973), Note on Effective Pressure, Journal of Geophysical Research, Vol.78, No.14, pp.2,434-2,437.

Rouleau A. and Gale J. E. (1985), Statistical Characterization of the Fracture System in the Stripa Granite, Sweden, International Journal of Rock Mechanics and Mining Sciences and Geomechanics Abstracts, Vol.22, No.6, pp.353-367.

Rouleau A. and Gale J. E. (1987), Stochastic Discrete Fracture Simulation of Groundwater Flow into an Underground Excavation in Granite, International Journal of Rock Mechanics and Mining Sciences and Geomechanics Abstracts, Vol.24, No.2, pp.99-112.

Saeb, S. and B. Amadei (1992), Modelling Rock Joints under Shear and Normal Loading, International Journal of Rock Mechanics and Mining Sciences and Geomechanics Abstracts, Vol.29, No.3, pp.267-278.

Scheidegger, A. E. (1974), The Physics of Flow Through Porous Media, University of Toronto Press, Toronto, Canada.

Scholz, C.H. (1974), Post-Earthquake Dilatancy Recovery, Geology, pp.551-554.

Scholz, C.H. and S.H. Hickman (1983), Hysteresis in the Closure of a Nominally Flat Crack, Journal of Geophysical Research, Vol.88, No.B8, pp.6,501-6,504.

Schrauf, T. W. and D.D. Evans (1986), Laboratory Studies of Gas Flow through a Single Natural Fracture, Water Resources Research, Vol.22, No.7, pp.1,038-1,050.

Sharp, J.C. (1970), Fluid Flow through Fissured Media, Ph.D. Dissertation, University of London, Imperial College of Science and Technology, London.

Sharp, J.C. and Y.N.T. Maini (1972), Fundamental Considerations on the Hydraulic Characteristics of Joints in Rock, Proceedings of International Symposium on Percolation through Fissured Rock, I.S.R.M., T1-F, Stuttgart, Germany.

Shinozuka, M. and C.M. Jan (1972), Digital Simulation of Random Processes and Its Applications, Journal of Sound and Vibration, Vol.25, No.1, PP.111-128.

Silliman, S. E. (1989), An Interpretation of the Difference between Aperture Estimates Derived from Hydraulic and Tracer Tests in a Single Fracture, Water Resources Research, Vol.25, No.10, pp.2,275-2,283.

Skempton, A.W. (1960), Effective Stress in Soils, Concrete and Rocks, Proceedings of the International Conference on Pore Pressure and Suction in Soils, London, United Kingdom, pp.4-16.

Smith L. and F.W. Schwartz (1984), An Analysis of the Influence of Fracture Geometry on Mass Transport in Fractured Media, Water Resources Research, Vol. 20, No.9, pp.1,241-1,252.

Snow, D.T. (1965), A Parallel Plate Model of Fractured Permeable Media, Ph.D. Dissertation, Univ. of California, Berkeley, California.

Snow D. T. (1968), Rock Fracture Spacings, Openings, and Porosities, Journal of the Soil Mechanics and Foundations Division, ASCE, pp.73-91.

Snow D. T. (1969), Anisotropic Permeability of Fractured Media, Water Resources Research, Vol.5, No.6, pp.1,273-1,289.

Snow D. T. (1970), The Frequency and Apertures of Fractures in Rock, International Journal of Rock Mechanics and Mining Sciences and Geomechanics Abstracts, Vol.7, pp.23-40.

Sprunt, E. and W.F. Brace (1974), Some Permanent Structural Changes in Rocks due to Pressure and Temperature, Proceedings of the 3rd International Congress on Rock Mechanics, Denver, Colorado, pp.524-529.

Sprunt, E. and W.F. Brace (1974), Direct Observation of Microcavities in Crystalline Rocks, International Journal of Rock Mechanics and Mining Sciences and Geomechanics Abstracts, Vol.11, pp.139-150.

Stevens J.L. and D.J. Holcomb (1980), A Theoretical Investigation of the Sliding Crack Model of Dilatancy, Journal of Geophysical Research, Vol.85, No.12, pp.7,091-7,100.

Summers, R., Winkler, K. and Byerlee, J.D. (1978), Permeability Changes During the Flow of Water through Westerly Granite at Temperatures of 100° - 400°C, Journal of Geophysical Research, Vol. 83, No.B1, pp.339-344.

Sundaram P.N., D.J. Watkins and W.E. Ralph (1987), Laboratory Investigations of Coupled Stress-Deformation-Hydraulic Flow in a Natural Rock Fracture, Proceedings of the 28th U.S. Symposium on Rock Mechanics, Tucson, Arizona, pp.585-592.

Swan, G. (1981), Tribology and the Characterization of Rock Joints, Proceedings of the 22nd U.S. Symposium on Rock Mechanics, Cambridge, Massachusetts, pp.402-407.

Swan, G. (1983), Determination of Stiffness and Other Joint Properties from Roughness Measurements, Rock Mechanics and Rock Engineering, Vol.16, pp.19-38.

Tapponnier P. and W.F. Brace (1976), Development of Stress-induced Microcracks in westerly Granite, International Journal of Rock Mechanics and Mining Sciences and Geomechanics Abstracts, Vol. 13, pp.103-112.

Takahashi M., A. Hirata and H. Koide (1990), Effect of Confining Pressure and Pore Pressure on Permeability of Inada Granite, Journal of the Japanese Society of Engineering Geology, Vol.31, No.3, pp.1-10 (written in Japanese with English abstract).

Thompson, M.E. and S.R. Brown (1991), The Effect of Anisotropic Surface Roughness on Flow and Transport on Fractures, Journal of Geophysical Research, Vol.96, No.B13, pp.21,923-21,932.

Todd, T. and G. Simmons (1972), Effect of Pore Pressure on the Velocity of Compressional Waves on Low-Porosity Rocks, Journal of Geophysical Research, Vol.77, No.20, pp.3,731-3,743.

Trimmer, D., B. Bonner, H.C. Heard. and A. Duba (1980), Effect of Pressure and Stress on Water Transport in Intact and Fractured Gabbro and Granite, Journal of Geophysical Research, Vol.85, No.B12, pp.7,059-7,071.

Tsang Y. W. and P.A. Witherspoon (1981), Hydromechanical Behavior of a Deformable Rock Fracture Subject to Normal Stress, Journal of Geophysical Research, Vol.86, No.B10, pp.9,287-9,298.

Tsang Y. W. and P.A. Witherspoon (1983), The Dependence of Fracture Mechanical and Fluid Flow Properties on Fracture Roughness and Sample Size, Journal of Geophysical Research, Vol.88, No.B3, pp.2,359-2,366.

Tsang Y. W. (1984), The Effect of Tortuosity on Fluid Flow Through a Single Fracture, Water Resources Research, Vol.20, No.9, pp.1,209-1,215.

Tsang Y. W. and C.F. Tsang (1987), Channel Flow through Fractured Media, Water Resources Research, Vol.23, No.3, pp.467-479.

Tsang Y. W., C.F. Tsang, I. Neretnieks and L. Moreno (1988), Flow and Transport in Fractured Media: A Variable Aperture Channel Model and Its Properties, Water Resources Research, Vol.24, No.12, pp.2,049-2,060.

Tsang Y. W. and C.F. Tsang (1988), Flow and Tracer Transport in Fractured Media: A Variable Aperture Channel Model and Its Properties, Water Resources Research, Vol.24, No.12, pp.2,049-2,060

Tsang, Y.W. and C.F. Tsang (1989), Flow Channeling in a Single Fracture as a Two-dimensional Strongly Heterogeneous Permeable Medium, Water Resources Research, Vol.25, No.9, pp.2,076-2,080.

Tsang Y. W.(1992), Usage of "Equivalent Apertures" for Rock Fractures as Derived From Hydraulic and Tracer Tests, Water Resources Research, Vol.28, No.5, pp.1451-1455.

Walsh, J.B. (1965), The Effect of Cracks on the Compressibility of Rock, Journal of Geophysical Research, Vol. 70, No.2, pp.381-389.

Walsh, J.B. and W.F. Brace (1966), Cracks and pores in rocks, Proceedings of the 1st International Congress on Rock Mechanics, Lisbon, Portugal, pp.643-646.

Walsh, J.B. and M.A. Grosenbaugh (1979), A New Model for Analyzing the Effect of Fractures on Compressibility, Journal of Geophysical Research, Vol. 84, No.B7, pp.3,532-3,536.

Walsh, J.B. (1981), Effect of Pore Pressure and Confining Pressure on Fracture Permeability, International Journal of Rock Mechanics and Mining Sciences and Geomechanics Abstracts, Vol. 18, pp.429-435.

Walsh, J.B. and W.F. Brace (1984), The Effect of Pressure on Porosity and the Transport Properties of Rock, Journal of Geophysical Research, Vol. 89, No.B11, pp.9,425-9,431.

Wang, H.F. and D.J. Hart (1993), Experimental Error for Permeability and Specific Storage from Pulse decay Measurements, International Journal of Rock Mechanics and Mining Sciences and Geomechanics Abstracts, Vol. 30, No.7, pp.1,173-1,176.

Wissler, T.M. and G. Simmons (1985), The Physical Properties of a Set of Sandstones - Part II. Permanent and Elastic Strains During Hydrostatic Compression to 200 MPa, International Journal of Rock Mechanics and Mining Sciences and Geomechanics Abstracts, Vol. 22, No.6, pp.393-406.

Witherspoon P. A., C.H. Amick, J.E. Gale, K. Iwai (1979), Observations of a Potential Size Effect in Experimental determination of the Hydraulic Properties of Fractures, Water Resources Research, Vol.15, No.5, pp.1,142-1,146.

Witherspoon P. A., J.S.Y. Wang, K. Iwai and J.E. Gale (1980), Validity of Cubic Law for Fluid Flow in a Deformable Rock Fracture, Water Resources Research, Vol.16, No.6, pp.1,016-1,024.

Yamada, S.F. and A.H. Jones (1980), A Review of a Pulse Technique for Permeability Measurement, SPEJ Forum, pp.357-358.

Zimmerman, R.W., W.H. Somerton and M.K. King (1986), Compressibility of Porous Rock, Journal of Geophysical Research, Vol.91, No.B12, pp.12,765-12,777.

Zimmerman, R.W., S. Kumar and G.S. Bodvarsson (1991), International Journal of Rock Mechanics and Mining Sciences and Geomechanics Abstracts, Vol. 28, pp.325-331.

Zimmerman, R.W., D. Chen and N.G.W. Cook (1992), The Effect of Contact Area on the Permeability of Fractures, Journal of Hydrology, Vol.139, pp.79-96.

Zimmerman, R.W., L.R. Myer and N.G.W. Cook (1994), Grain and Void Compression in fractured and Porous Rocks, International Journal of Rock Mechanics and Mining Sciences and Geomechanics Abstracts, Vol. 31, No.2, pp.179-184.

Zoback, M. D. and J.D. Byerlee (1975), The Effect of Microcrack Dilatancy on the Permeability of Westerly Granite, Journal of Geophysical Research, Vol. 80, No.5, pp.752-755.

Zoback, M. D. and J.D. Byerlee, J.D. (1975), The Effect of Cyclic Differential Stress on Dilatancy in Westerly Granite Under Uniaxial and Triaxial Conditions, Journal of Geophysical Research, Vol. 80, No.11, pp.1,526-1,530.

Zoback, M. D. and J.D. Byerlee, J.D. (1975), Permeability and Effective Stress, Bulletin of the American Association of Petroleum Geologists, Vol.59, No.1, pp.154-158.

Appendices

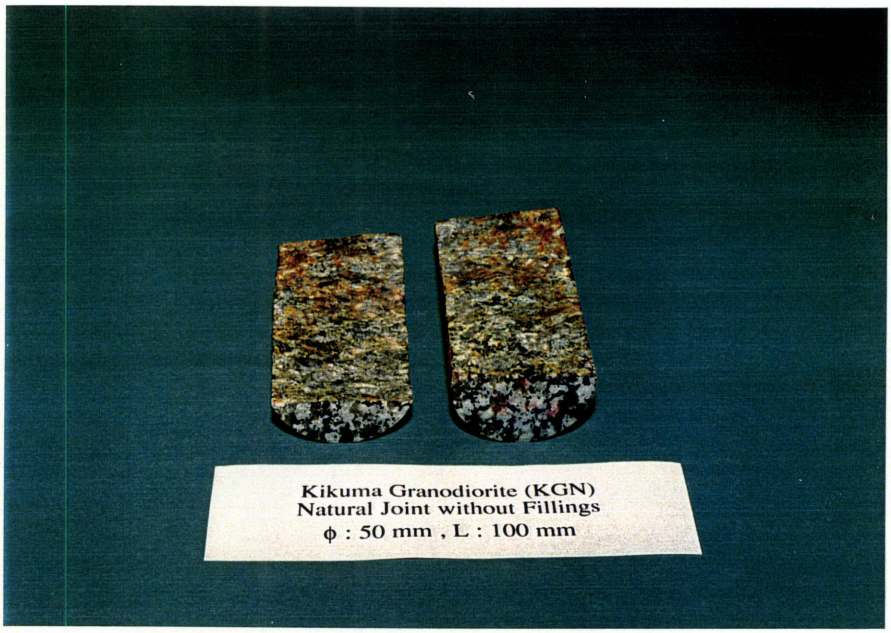

A.1 A photograph of a natural joint in Kikuma granodiorite (NKGD, L=10 cm)

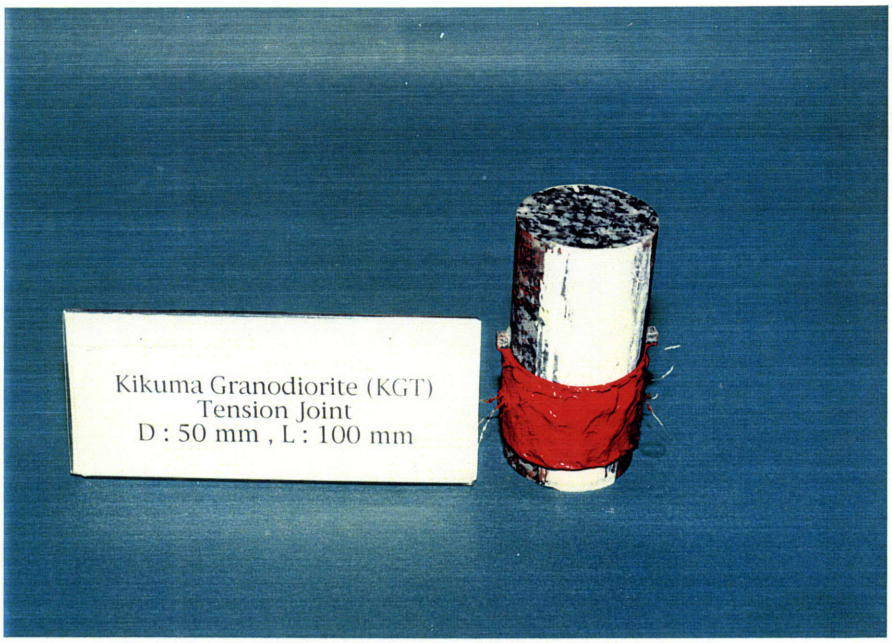

A 2 A photograph of a tension joint in Kikuma granodiorite (TKGD, L=10 cm)

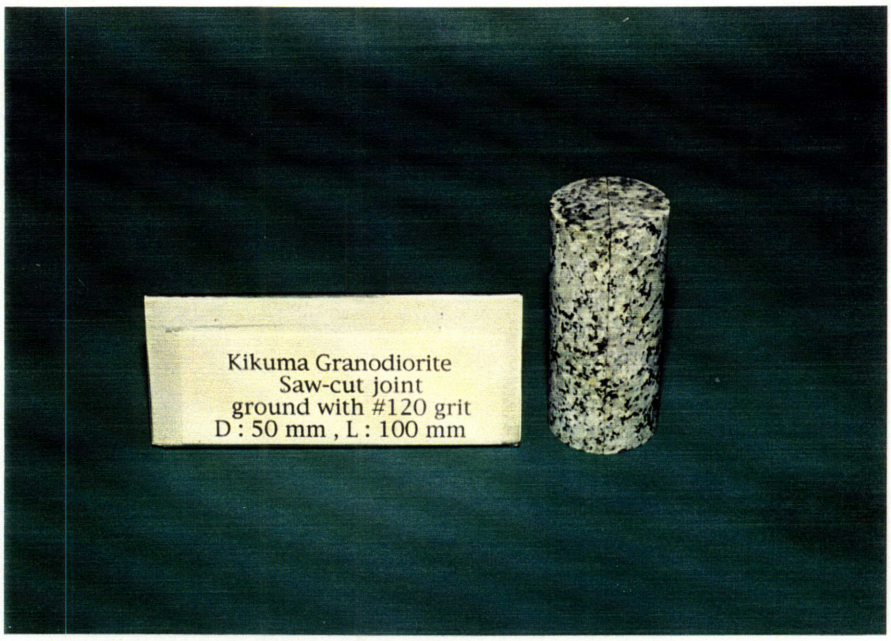

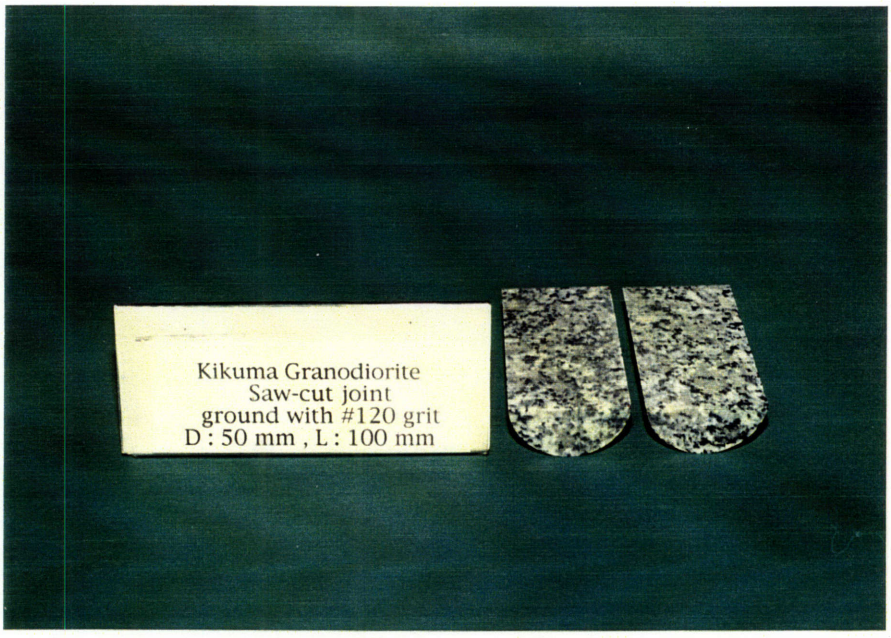

A.3 A photograph of a sawed joint in Kikuma granodiorite (SKGD, L=10 cm)

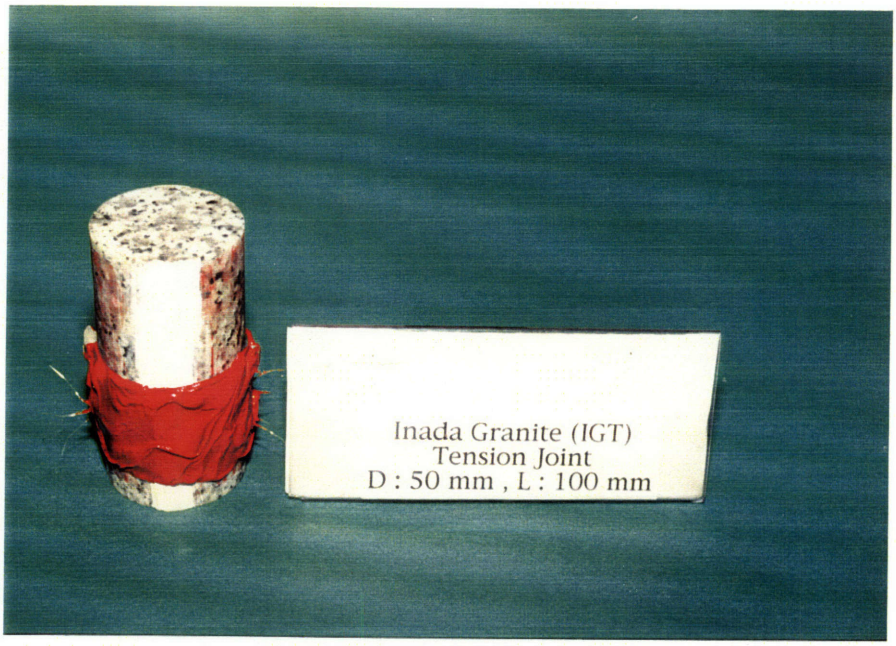

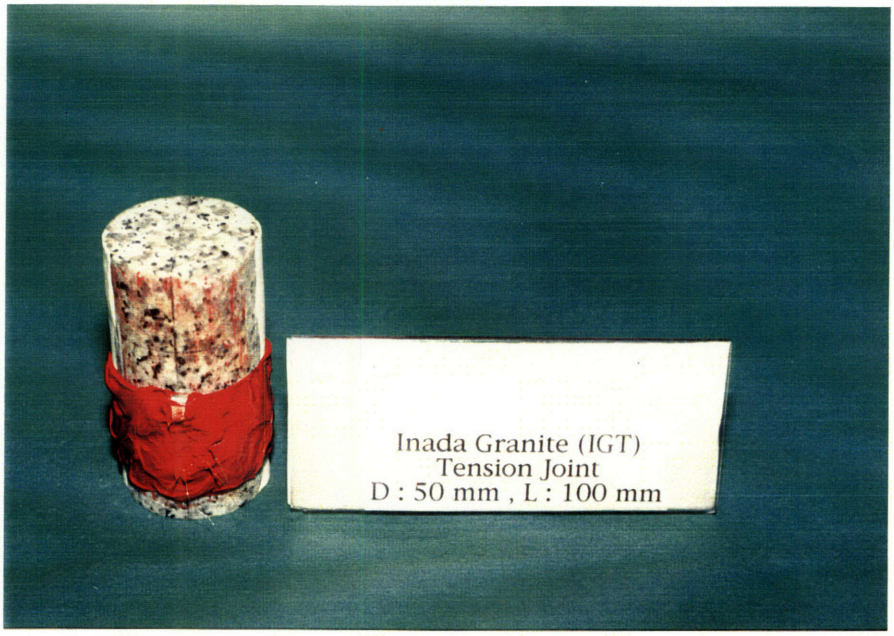

A 4 A photograph of a tension joint in Inada granite (TIGN, L=10 cm)

A 5 A photograph of a tension joint in Chichibu schist (TCSH, L=10 cm)

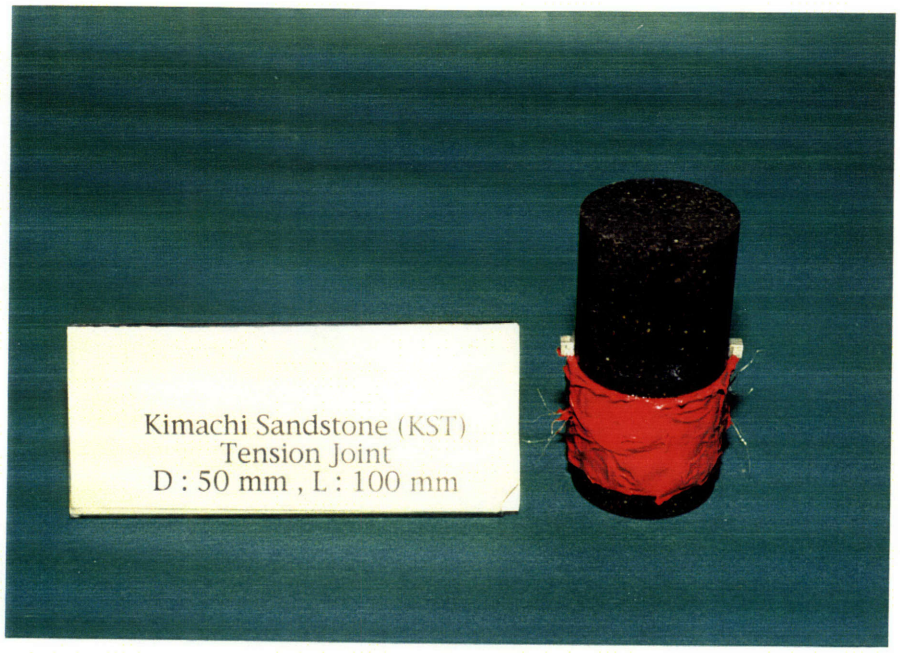

A 6 A photograph of a tension joint in Kikachi sandstone (TKSS, L=10 cm)

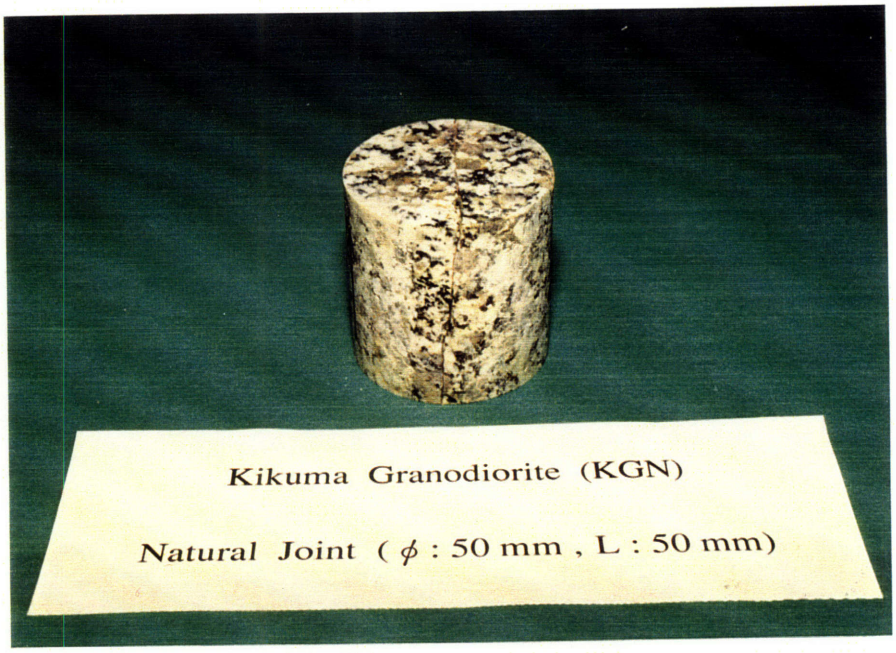

B.1 A photograph of a natural joint in Kikuma granodiorite (L=5 cm)

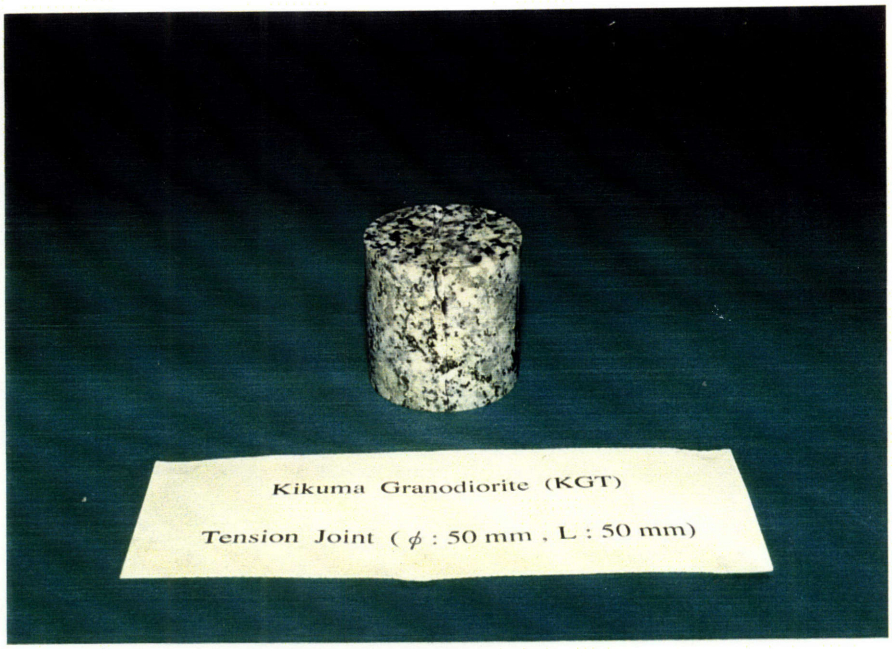

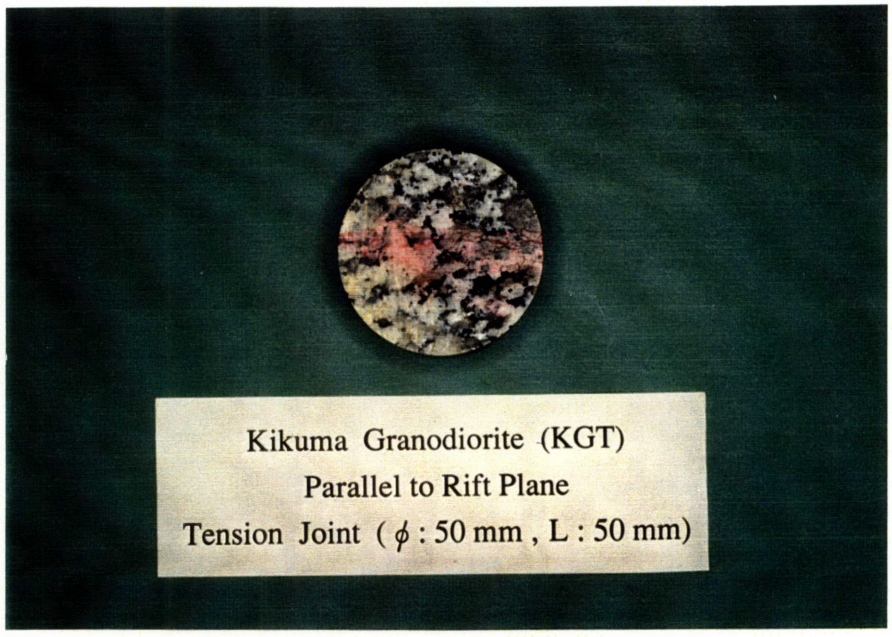

B.2 A photograph of a microcrack in Kikuma granodiorite (L=5 cm)

B.3 A photograph of a sawed joint in Kikuma granodiorite (L=5 cm)